Universität zu Köln
Mathematisch-Naturwissenschaftliche Fakultät
Geographisches Institut

Coasts at risk

–

Improving flood hazard and relative sea-level rise impact assessments in data-sparse coastal lowlands

---

Dissertation
zur
Erlangung des Doktorgrades
der Mathematisch-Naturwissenschaftlichen Fakultät
der Universität zu Köln

vorgelegt von Katharina Seeger
aus Köln

Köln, 2025

Gutachter: PD Dr. Dominik Brill

Prof. Dr. Torbjörn Törnqvist

Summary

Coastal lowlands such as river deltas and low-lying coastal plains are highly vital environments, offering a wide range of ecosystem services that have attracted human settlement and economic development ever since, making them critical hubs of economic productivity and global trade. Today, almost 40 % of the world's population live within 100 km distance from the coast and projections indicate global coastal population to increase by 60 % to 70 % by 2050 with highest growths being observed in Asian and African low-lying coastal areas of less than 10 m elevation above sea level – trends that are expected to continue in the future. With ongoing climate change, consequently rising sea level and shifting patterns in atmospheric circulation and extreme weather events, coastal lowlands face an increased exposure to flooding and sea-level rise. Densely populated river deltas, many of them located in tropical Southeast Asia, are particularly vulnerable as human activities have significantly altered deltaic dynamics and thereby increased the risk of flooding and permanent inundation.

Comprehensive hazard exposure and impact assessments are needed to understand hazards and estimate the area, population and assets at risk, which will inform risk assessments and support the development of risk-sensitive coping strategies. Acknowledging the complex interactions of natural drivers and human pressures that shape the coastal-deltaic system helps to achieve a more holistic understanding and to design sustainable coastal management. For many coasts and deltas such as in Southeast Asia and Africa, however, the absence or unavailability of high-quality data often challenges to gain a complete understanding of processes, interactions and impacts in the context of flooding and to generate detailed and reliable information about flood hazards and exposure. Especially as both sea-level rise impact and flood inundation are closely related to land elevation, the quality of these assessments largely relies on vertical accuracy and proper datum referencing of the elevation data used. This thesis aims at improving the understanding of flood hazards and impacts and solving challenges in their assessments in the world's data-sparse coastal-deltaic lowlands to guide disaster risk reduction and coping strategies in the view of future flood risk and relative sea-level rise. To achieve this overarching goal, the thesis addresses data-sparse coastal lowlands at various spatial scales, ranging from local (delta) scale by showcasing the Ayeyarwady Delta (Myanmar) and Mekong Delta (Vietnam), to regional (including five Asian megadeltas in South- and Southeast Asia), to global scale (the world's coasts). The thesis entails four core sections that (i) assess the state-of-the-art of coastal hazards, including drivers and pressures as well as data and modelling

requirements to improve the understanding; (ii) evaluate flood hazards in data-sparse coastal lowlands; (iii) highlight the need of proper handling of coastal land elevation and sea-level data and showing ways to reduce uncertainty in elevation assessments by elevation models; and (iv) unravel land elevation change and potential driving mechanisms and their relevance for future relative sea-level rise and flood exposure.

Coastal flooding in the five Asian megadeltas of the Ganges-Brahmaputra-Meghna, Ayeyarwady, Chao Phraya, Mekong and Red River is controlled by geophysical drivers of monsoon and river discharge, tides, tropical cyclones, storm surges and wind-waves, as well as sea-level change, vertical land motion and land elevation dynamics, and sediment, shoreline and deltaic landform changes. Main human pressures include population growth and deltaic land-use land cover changes due to urbanisation, mangrove loss due to the expansion of agriculture and aquaculture, groundwater extraction, sand mining and upstream interventions (due to dam construction and impacts on river flow and sediment dynamics). Coastal flooding shows various interlinkages between direct and indirect societal, economic, technical, socio-technical, physical and ecological impacts as well as beneficial effects of ecosystem services but can often cause significant setbacks in socio-economic development and exacerbate poverty in these densely populated and highly resource-dependent lowlands. The Ayeyarwady and Red River deltas constitute the least studied deltas out of the five assessed while data collection and monitoring needs to be improved in all five megadeltas with regard to discharge and sediment gauges, sea- and water-level monitoring and tide gauges, near-shore and channel bathymetry measurements, subsidence monitoring as well as regular updates of elevation data.

A standardised, integrative workflow was developed to perform first-order assessments of flood hazard exposure with respect to single flood types as well as multiple ones at low computational capacities. The highly flexible approach allows to evaluate flood-prone areas on regional and local scale, integrating local, high-quality data and, in its absence, regional or global substitutes, while it is independent of index values that are related to a specific unit of area or administrative boundaries. The workflow was demonstrated in the Ayeyarwady Delta to assess its exposure to monsoon and storm-surge flooding as well as relative sea-level rise and attribute flood components. In its design, the approach allows to complement index-based vulnerability and risk assessments while cloud-computed flood frequency maps serve as a fast-processed data product to validate existing global flood mappings and modelling studies.

To investigate the impact of elevation data on sea-level rise impact assessments, the new, local AD-DEM was generated for the Ayeyarwady Delta and used to assess the performance of 10

commonly used global, space-borne elevation models after all datasets were referenced to local mean sea level. Local elevation data indicates the average elevation of the delta plain at ~1.3 m above local mean sea level which is overestimated by global elevation models by several metres. Best performing global elevation models differ by ~2 m RMSE from local data. Using latest IPCC sea-level rise scenarios, the consequences of inaccuracy of global elevation models were quantified in terms of area and population falling below sea level. Referring to best performing elevation models allowed to narrow down the range of area and population as was estimated by most inaccurate elevation models.

As the proper alignment of coastal land elevation and sea-level data is critical for reliable sea-level rise and coastal hazard impact assessments, a systematic evaluation of the scientific literature was combined with quantifications of the most prominent errors on global and regional scale. >99 % of the evaluated assessments handled sea-level and land elevation data improperly and the most prominent error (25 % of the studies) was the neglection of datum conversion, followed by incomplete datum conversion (7 %). Consequently, actual sea-level height is underestimated by 0.2–0.5 m on average in coastal hazard assessments globally, regionally exceeding 1 m such as in Southeast Asia. The use of properly aligned sea-level and elevation data reveals worldwide 37 % more area and 67 % more people (i.e. increase of 88 million to 132 million people) to fall below sea-level following 1 m relative sea-level rise than estimated by existing scientific assessments.

Works on the accuracy of the elevation data (case study on the Ayeyarwady Delta) and vertical datum offset (global assessment) were detailed by including also elevation change since data acquisition into account. As coastal-deltaic landscapes are often experiencing high rates of relative sea-level rise that sediment accretion cannot compensate for, thus resulting in elevation loss, elevation as indicated by old elevation models (some are 25 years old) may be completely off. A globally applicable approach was established and allows to quantify and attribute uncertainties in elevation assessment for data-sparse coastal lowlands using global elevation models to sources such as inaccuracy, vertical datum offset and elevation change since data acquisition. Applying the approach to the Mekong Delta not only reveals the best performing elevation model but also pinpoints errors in processing steps and indicates how much model performance (and its applicability) can be improved if certain processing steps are prioritised and properly applied.

To move from (static) elevation to elevation dynamics to strengthen coastal hazard and impact assessments, first delta-wide InSAR-derived information on land elevation change in the

Ayeyarwady Delta was estimated. Elevation change reveals a heterogenous pattern with moderate negative (e.g. elevation loss/subsidence) and positive elevation change (e.g. elevation gain/uplift) spread over the entire delta. Delta-wide average elevation change is -4 mm/yr, while areas of maximal elevation loss include the hotspot of Yangon City, where rates reach -100 mm/yr, as well as the northeastern delta and southern coastal range. Our findings are in line with previous studies for Yangon City, whereas the coastal pattern of elevation loss resembles that of other deltas in the world, suggesting potentially similar driving mechanisms. Limited by data scarcity and the final post-processing of the InSAR data still ongoing, relations between land elevation change and potential drivers were only tentatively determined. Implications on the delta's exposure to relative sea-level rise and flooding highlighted the increased susceptibility especially in low-lying parts of the southern deltaic area, which already suffers from highest exposure and vulnerability.

The works of this research constitute first steps in improving the understanding of flood hazards and impacts as well as solving challenges in their assessment in the world's data-sparse coastal-deltaic lowlands. However, the outcomes of this reveal fundamental insights into the exposure of some of the least studied megadeltas, (i.e. the Ayeyarwady) while providing globally applicable workflows of flood hazard exposure and elevation uncertainty assessment that contribute to unravel the unknowns of flooding and relative sea-level rise in any data-sparse coastal lowland in the world.

Kurzzusammenfassung

Küstentiefländer wie Flussdeltas und niedrig gelegene Küstenebenen sind äußerst wichtige Lebensräume, die eine Vielzahl von Ökosystemleistungen bieten und seit jeher Anziehungspunkt für menschliche Besiedlung und wirtschaftliche Entwicklung sind, was sie zu wichtigen Zentren für wirtschaftliche Produktivität und globalen Handel macht. Heutzutage leben fast 40 % der Weltbevölkerung in weniger als 100 km von der Küste entfernt, und Prognosen gehen davon aus, dass die globale Küstenbevölkerung bis 2050 um 60 % bis 70 % zunehmen wird, wobei die stärksten Zuwächse in den tief liegenden Küstengebieten Asiens und Afrikas mit einer Höhe von weniger als 10 m über dem Meeresspiegel zu verzeichnen sind – ein Trend, der sich auch in Zukunft fortsetzen dürfte. Angesichts des fortschreitenden Klimawandels, des damit einhergehenden Anstiegs des Meeresspiegels und der sich verändernden Muster der atmosphärischen Zirkulation sowie extremer Wetterereignisse sind die Küstentiefländer verstärkt Überschwemmungen und dem Meerespiegelanstieg ausgesetzt. Dicht besiedelte Flussdeltas, von denen viele im tropischen Südostasien liegen, sind besonders gefährdet, da menschliche Aktivitäten die Deltadynamik erheblich verändert und damit das Risiko von Überschwemmungen und dauerhafter Überflutung erhöht haben.

Umfassende Bewertungen der Gefährdung und der Auswirkungen sind erforderlich, um die Gefahren zu verstehen und das Gebiet, die Bevölkerung und die gefährdeten Sachwerte abzuschätzen, was eine Grundlage für Risikobewertungen bildet und die Entwicklung risikosensibler Bewältigungsstrategien unterstützt. Die Berücksichtigung der komplexen Wechselwirkungen zwischen natürlichen Faktoren und menschlichen Einflüssen, die das Küsten-Deltasystem prägen, trägt zu einem ganzheitlicheren Verständnis und zur Gestaltung eines nachhaltigen Küstenmanagements bei. Für viele Küsten und Deltas, wie z. B. in Südostasien und Afrika, stellt das Fehlen oder die Nichtverfügbarkeit qualitativ hochwertiger Daten jedoch häufig eine Herausforderung dar, um ein vollständiges Verständnis der Prozesse, Wechselwirkungen und Auswirkungen im Zusammenhang mit Überschwemmungen zu erlangen und detaillierte und zuverlässige Informationen über Hochwassergefahren und -exposition zu generieren. Da sowohl die Auswirkungen des Meeresspiegelanstiegs als auch der Überflutungen eng mit der Geländehöhe zusammenhängen, hängt die Qualität dieser Bewertungen weitgehend von der vertikalen Genauigkeit und der korrekten Referenzierung der verwendeten Höhendaten ab. Diese Arbeit zielt darauf ab, das Verständnis der Überflutungsgefahren und -auswirkungen zu verbessern und die Herausforderungen bei deren

Bewertung in den datenarmen Küsten-Delta-artigen Tiefländern der Welt zu lösen, um die Katastrophenvorsorge und die Anpassungsstrategien im Hinblick auf das zukünftige Überflutungsrisiko und den relativen Meeresspiegelanstieg zu unterstützen. Um dieses übergeordnete Ziel zu erreichen, befasst sich die Arbeit mit datenarmen Küstentiefländern auf unterschiedlichen räumlichen Ebenen, angefangen von der lokalen Ebene (Delta) mit dem Ayeyarwady-Delta (Myanmar) und dem Mekong-Delta (Vietnam) über die regionale Ebene (einschließlich fünf asiatischer Megadeltas in Süd- und Südostasien) bis hin zur globalen Ebene (die Küsten der Welt). Die Dissertation umfasst vier Kernabschnitte, die (i) den aktuellen Stand der Küstengefahren, einschließlich der treibenden Kräfte und der Belastungsfaktoren, sowie die Daten- und Modellierungsanforderungen zur Verbesserung des Verständnisses bewerten; (ii) die Flutgefahren in datenarmen Küstentieflandgebieten bewerten; (iii) die Notwendigkeit eines angemessenen Umgangs mit Küstenlandhöhen- und Meeresspiegeldaten hervorheben und Wege zur Reduzierung der Unsicherheiten bei Höheneinschätzungen durch Höhenmodelle aufzeigen; und (iv) die Landhöhenveränderungen und die potenziellen treibenden Mechanismen sowie deren Bedeutung für den künftigen relativen Meeresspiegelanstieg und die Überflutungsgefahr aufzeigen.

Küstenüberflutungen in den fünf asiatischen Megadeltas Ganges-Brahmaputra-Meghna, Ayeyarwady, Chao Phraya, Mekong und Roter Fluss werden durch geophysikalische Faktoren wie Monsun und Flussabfluss, Gezeiten, tropische Wirbelstürme, Sturmfluten und Windwellen sowie durch Veränderungen des Meeresspiegels, vertikale Landbewegungen und Landhöhendynamiken sowie durch Veränderungen von Sedimentablagerungen, Küstenlinien und Deltalandschaften gesteuert. Zu den Hauptbelastungen durch den Menschen gehören das Bevölkerungswachstum und die Veränderung der Landnutzung im Delta aufgrund der Verstädterung, der Verlust von Mangroven durch die Ausdehnung von Landwirtschaft und Aquakultur, die Grundwasserentnahme, der Sandabbau und flussaufwärts gerichtete Eingriffe (durch den Bau von Staudämmen und die Auswirkungen auf den Flusslauf und die Sedimentdynamik).

Küstenüberflutungen haben vielfältige Wechselwirkungen zwischen direkten und indirekten gesellschaftlichen, wirtschaftlichen, technischen, sozio-technischen, physischen und ökologischen Auswirkungen sowie positiven Effekten von Ökosystemleistungen, können aber oft zu erheblichen Rückschlägen in der sozioökonomischen Entwicklung führen und die Armut in diesen dicht besiedelten und stark von Ressourcen abhängigen Tiefländern verschärfen. Die Deltas des Ayeyarwady und des Roten Flusses sind die am wenigsten erforschten der fünf

untersuchten Deltas, während die Datenerfassung und -überwachung in allen fünf Megadeltas verbessert werden muss, was Abfluss- und Sedimentpegel, die Überwachung des Meeresspiegels und des Wasserstands sowie Gezeitenpegel, küstennahe und kanalbezogene bathymetrische Messungen, die Überwachung von Landsenkung sowie die regelmäßige Aktualisierung von Höhendaten angeht.

Es wurde ein standardisierter, integrativer Arbeitsablauf entwickelt, um erste Bewertungen der Hochwassergefährdung sowohl für einzelne als auch für mehrere Fluttypen bei geringer Rechenkapazität durchzuführen. Der hochflexible Ansatz ermöglicht es, hochwassergefährdete Gebiete auf regionaler und lokaler Ebene zu bewerten, indem lokale, qualitativ hochwertige Daten und, falls diese fehlen, regionale oder globale Ersatzdaten integriert werden. Der Arbeitsablauf wurde am Beispiel des Ayeyarwady-Deltas vorgestellt, um dessen Gefährdung durch Monsun- und Sturmfluten sowie den relativen Anstieg des Meeresspiegels zu bewerten und Überflutungskomponenten zuzuschreiben. Der Ansatz ermöglicht es, indexbasierte Anfälligkeits- und Risikobewertungen zu ergänzen, während cloudbasierte Hochwasserhäufigkeitskarten als schnell zu erstellendes Datenprodukt zur Validierung bestehender globaler Hochwasserkartierungen und Modellierungsstudien eingesetzt werden können.

Um den Einfluss von Höhendaten auf die Einschätzung der Auswirkungen des Meeresspiegelanstiegs zu untersuchen, wurde das neue, lokale AD-DEM für das Ayeyarwady-Delta erstellt und verwendet, um die Leistung von 10 häufig verwendeten globalen, satellitengestützten Höhenmodellen zu bewerten, nachdem alle Datensätze auf den lokalen mittleren Meeresspiegel referenziert worden waren. Lokale Höhendaten geben die durchschnittliche Höhe der Deltaebene mit ~1,3 m über dem lokalen mittleren Meeresspiegel an, was von globalen Höhenmodellen um mehrere Meter überschätzt wird. Die besten globalen Höhenmodelle weichen um ~2 m RMSE von den lokalen Daten ab. Anhand der neuesten IPCC-Meeresspiegelanstiegsszenarien wurden die Folgen der Ungenauigkeit globaler Höhenmodelle in Bezug auf die unter den Meeresspiegel fallende Fläche und Bevölkerung quantifiziert. Durch den Rückgriff auf die leistungsfähigsten Höhenmodelle konnte der Bereich der Fläche und der Bevölkerung eingegrenzt werden, der durch die ungenauesten Höhenmodelle geschätzt wurde.

Da die korrekte Angleichung von Küstenlandhöhen- und Meeresspiegeldaten für zuverlässige Bewertungen des Meeresspiegelanstiegs und der Auswirkungen von Küstengefahren von entscheidender Bedeutung ist, wurde eine systematische Auswertung der wissenschaftlichen Literatur mit Quantifizierungen der auffälligsten Fehler auf globaler und regionaler Ebene

kombiniert. In mehr als 99 % der ausgewerteten Studien wurden Meeresspiegel- und Geländehöhendaten unsachgemäß gehandhabt, wobei der auffälligste Fehler (25 % der Studien) die Vernachlässigung der Datumsumrechnung war, gefolgt von unvollständiger Datumsumrechnung (7 %). Infolgedessen wird die tatsächliche Höhe des Meeresspiegels bei der Bewertung von Küstengefahren weltweit im Durchschnitt um 0,2-0,5 m unterschätzt, regional sogar um mehr als 1 m, z. B. in Südostasien. Die Verwendung korrekt angepasster Meeresspiegel- und Höhendaten zeigt, dass weltweit 37 % mehr Fläche und 67 % mehr Menschen (d. h. ein Anstieg von 88 Mio. auf 132 Mio. Menschen) bei einem relativen Meeresspiegelanstieg von 1 m unter den Meeresspiegel fallen werden als in den bisherigen wissenschaftlichen Bewertungen angenommen.

Die Arbeiten zur Genauigkeit der Höhendaten (Fallstudie zum Ayeyarwady-Delta) und zum vertikalen Datumsversatz (globale Bewertung) wurden vertieft, indem auch die Höhenveränderung seit der Datenerfassung berücksichtigt wurde. Da Küstenlandschaften wie Deltas oft einen hohen relativen Meeresspiegelanstieg erleben, der durch die Sedimentanlagerung nicht kompensiert werden kann, was zu einem Höhenverlust führt, können die Höhenangaben in alten Höhenmodellen (einige sind 25 Jahre alt) vollkommen unzutreffend sein. Es wurde ein global anwendbarer Ansatz entwickelt, der es ermöglicht, Unsicherheiten bei der Höhenbestimmung für datenarme Küstentiefländer unter Verwendung globaler Höhenmodelle zu quantifizieren und auf Quellen wie Ungenauigkeit, Versatz der vertikalen Bezugssysteme und Höhenänderungen seit der Datenerfassung zurückzuführen. Durch die Anwendung des Ansatzes auf das Mekong-Delta wurde nicht nur das leistungsfähigste Höhenmodell ermittelt, sondern es wurden auch Fehler in den Verarbeitungsschritten lokalisiert und es wurde aufgezeigt, wie sehr die Modellleistung (und seine Anwendbarkeit) verbessert werden kann, wenn bestimmte Verarbeitungsschritte priorisiert und richtig ausgeführt werden.

Um von der (statischen) Geländehöhe zur Geländehöhendynamik überzugehen und so die Bewertung von Küstenrisiken und -auswirkungen zu verbessern, wurden erstmals deltaweite InSAR-gestützte Informationen über Geländehöhenänderungen im Ayeyarwady-Delta geschätzt. Die Höhenveränderung zeigt ein heterogenes Muster mit mäßig negativen (z.B. Höhenverluste/-senkungen) und positiven Höhenveränderungen (z.B. Höhengewinn/-erhöhung) über das gesamte Delta verteilt. Die durchschnittliche deltaweite Höhenänderung beträgt -4 mm/Jahr, während die Gebiete mit maximalem Höhenverlust den Hotspot von Yangon City umfassen, wo Raten von -100 mm/Jahr erreicht werden, sowie das nordöstliche Delta und der südliche Küstenbereich. Unsere Ergebnisse stimmen mit früheren Studien für

Yangon City überein, während das Muster des Höhenverlusts an der Küste dem anderer Deltas in der Welt ähnelt, was auf möglicherweise ähnliche Antriebsmechanismen hindeutet. Da nur wenige Daten zur Verfügung stehen und die abschließende Nachbearbeitung der InSAR-Daten noch nicht beendet ist, konnten die Zusammenhänge zwischen der Veränderung der Landhöhe und den potenziellen Antriebsfaktoren nur vorläufig ermittelt werden. Die Auswirkungen auf die Gefährdung des Deltas durch den relativen Meeresspiegelanstieg und Überflutungen zeigten die erhöhte Anfälligkeit vor allem in den tief liegenden Teilen des südlichen Deltagebiets, das bereits jetzt am stärksten gefährdet und vulnerabel ist.

Die Arbeiten dieser Forschung sind erste Schritte zur Verbesserung des Verständnisses von Überflutungsgefahren und -auswirkungen sowie zur Lösung von Problemen bei deren Einschätzung in den datenarmen deltaartigen Küstentiefländern der Welt. Die Ergebnisse geben jedoch grundlegende Einblicke in die Gefährdung einiger der am wenigsten untersuchten Megadeltas (d.h. des Ayeyarwady) und stellen gleichzeitig global anwendbare Arbeitsverfahren für die Bewertung von Überflutungsgefahren und der Unsicherheit in Bezug auf die Geländehöhe bereit, die dazu beitragen, die Unbekannten von Überflutungen und relativem Meeresspiegelanstieg in jedem datenarmen Küstentiefland der Welt zu enträtseln.

Acknowledgements

This dissertation was conducted under the project *Driving factors for and societal effects of sea-level rise and delta flooding in the Ayeyarwady Delta (Myanmar) – Lessons from the past for disaster governance in the future* (continued by the follow-up project *Rising sea and sinking land: Determining spatially resolved subsidence rates for the Ayeyarwady Delta (Myanmar) and developing dynamic adaptation scenarios for the increased risk of flooding*) funded by the German Research Foundation (DFG). This dissertation is the outcome of an intense working process and an adventurous (unexpected) journey of studying coastal lowlands, hazard and impact exposure. From the very beginning on, this thesis involved ups and downs that often felt like navigating mountainous terrain rather than a delta landscape – with steep climbs, sometimes easier, sometimes more difficult descents, interspersed with moments offering sweeping, beautiful views of the path ahead. What started with a day, where the world turned upside down, requiring the creativity and flexibility to find a way, improvise and re-design an entire project where the *field* could suddenly not be accessed anymore, for me turned from isolation into new windows of opportunities where the experiences from diving into the deep fundamentals, building new networks with experts and peers from all over the world, have led to fill blank maps with insights from *remote*.

Looking back, I can only say that this journey would not have been possible without those people who have accompanied me all along the way, standing by my side in challenging, difficult times and enriching this journey with wonderful, memorable moments and fascinating discoveries, both personally and scientifically. I am deeply grateful for their trust and support throughout my PhD and beyond.

I thank my supervisors PD Dr. Dominik Brill, Prof. Dr. Helmut Brückner and Assoc. Prof. Dr. Philip S.J. Minderhoud for their overall support in the last years and letting me scientifically grow. Without your trust in all the past years, starting in my bachelors and continuing throughout my studies and PhD, I wouldn't have made it that far. Thank you, Dominik, for encouraging my curiosity about Earth, sparking my enthusiasm about coastal (hazard) research and being key in my development towards a scientist – by the way how you taught and supervised my bachelor and master theses and letting me collect experiences in your research projects, always having an open ear and giving me the right amount of freedom and guidance when I needed. I always enjoyed working together with you, our conversations (also apart from

work), and don't want to miss a single moment of that time. Thank you for your advice and belief in me from the very beginning and especially when I struggled the most. Thank you both, Dominik and Helmut, for giving me the opportunity to be part of your research project in which this dissertation is embedded and giving me the freedom to shape this project with my ideas, initiatives and collaborations. You introduced me into research project management and proposal writing, all of which is valuable for the next steps in academic research life. Thank you, Helmut, for all your trust and openness towards the ideas I proposed and your support to make these ideas become real. Without this, it would not have been possible to visit other research institutions, attend several international conferences and connect to experts from all over the world to exchange knowledge and experiences in coastal-lowland research. My special thanks to you, Philip, for crossing my way and becoming my PhD supervisor. With things going the other way round, me asking whether you would like to supervise my thesis, I truly appreciate that you agreed without knowing me or my work. Thank you for opening doors and all your advice and support in finding a way and climbing the mountains – I learned a lot from you over the last years, not only for my PhD but for my life. Your previous work on delta elevation was a kick-off and a huge inspiration for my research. I always enjoyed our inspiring brainstorming sessions about the loads of exciting ideas we have and after which we often came up with even more. I don't want to forget our golden writing hours, open and deep discussions, all the research visits, conference and field travels you enabled – and along with which came of course also a lot of fun time enriching my life, including, for example, my first visit at a rooftop bar, my first whiskey tasting and karaoke. You have not only sparked the inquisitive paper tiger and let it grow into a graceful lion but have been a mentor in my work–life. I thank the coincidence and Dr. Kim Cohen for connecting Philip and me by sending him a screenshot of my presentation's title slide that got stuck in the video conferencing software during an online workshop in times of the Covid-19 pandemic.

What made the time of my PhD also special, is the close collaboration with Anissa Vogel from the human-geographical counterpart of this project. Working and teaching together was always a pleasure – we could rely on each other blindly, translating the bridge between physical and human-geographical disciplines into practice and therewith truly addressing the core of geography. Thank you, Anissa, for being my PhD twin – I don't know whether I would have managed all the way without you. You became a very good friend, who accompanied me all along, especially in times that were not simple, and have enriched my life with great memories and a lot of fun – may it be hiking tours, city trips or going out for concerts and drinks. I look

very much forward to call you doctor soon and am very proud of how you navigated all the challenges in your thesis and our project. I also thank Prof. Dr. Frauke Kraas, PI of the human-geographical part of the project, for her advice from her longstanding working experience in Myanmar, which offered me the opportunity to see my work and the academic landscape through different lenses.

Thanks to all experts for the fruitful discussions, sharing experiences from which I could learn, and to all colleagues who supported me in my work. Prof. Dr. Torbjörn E. Törnqvist examined this thesis and I thank you for your critical feedback and your clarity in our exchange on river deltas, coastal land elevation and elevation change, which motivated me even more to understand to what extent the complexities of delta dynamics and environments are captured by the measurements and models we have, and how we can account for them. All computations and processings of my PhD research would not have been possible without Dr. Andreas Bolten, Dr. Luc Steinbuch and Dr. Marijn van der Meij. Thank you, Andreas, for all your support in enabling the computational resources and storage capacities I needed, making the impossible possible, your always immediate response and help if I faced problems, and your patience with my numerous questions. Thank you, Marijn and Luc, for giving me additional computation capacities in Cologne and Wageningen, and for your support, Luc, in getting the global datasets published and always helping when I had questions. Many thanks to Dr. Mélanie Becker for opening me doors to get in touch with experts from coastal and delta research, for our inspiring discussions and brainstormings and your overall support to navigate the academic pathway. Likewise, I thank Prof. Dr. Manoochehr Shirzaei and Prof. Dr. Susanna Werth for hosting me at Virginia Tech University, introducing me to InSAR processing and postprocessing, for all your patience with my numerous questions and the fun time we had in the lab and wherever we meet at conferences. Many thanks also to Andreas Peffeköver who assisted in the project as a student assistant during the first project phase. Thanks for your thorough work, the great collaboration and that I could always rely on you. Knowing you since your bachelor thesis, I am very proud of your achievements and wish you all the best for your ongoing PhD and look forward to your next steps. I would like to thank my coauthors for their collaboration, contributing to the research of this thesis, and all who supported me by taking time to exchange. Many thanks to Dr. Sinem Ince and Dr. Saskia Esselborn for the exchange on geodetic aspects of my research. I look forward to continuing our exchange to further strengthening the bridge between geography and geodesy in coastal research. Thank you, Prof. Dr. Georg Bareth and Dr. Christoph Hütt, for your support in questions concerning computational infrastructure, your

advice regarding flood mapping for large areas of interest, and offering support in proposals to request remote sensing data of restricted access. It helped me to identify some starting points in the beginning of my thesis, which I could then explore further. In this sense, I also thank you, Prof. Dr. Holger Schüttrumpf and Dr. Jan Oetjen from the Institute of Hydraulic Engineering and Water Resources Management at RWTH Aachen University, for exploring possibilities with me to set up a hydrodynamic model for the Ayeyarwady Delta. Although the modelling turned out to be too challenging given the thesis' timeline and the conditions of data sparsity and scarcity in the delta, I hope it will be possible in the future, with this thesis providing some valuable ingredients.

My special thanks to all the working groups with which I have had the pleasure to connect to. Thanks to the Geomorphology & Geochronology group at the University of Cologne, and especially Dr. Lucas Ageby, Linda Maßon and Arindam Biswas for the great time in our office, exchanging on our research and beyond while having a full, hot cup of tea from our huge tea selection. Thank you, Dr. Anja Zander, for always having an open ear in times of struggles and moments of joy. Thanks to the beach volleyball team for the wonderful active lunch breaks and all the fun moments we shared. I consider myself as part of a large international working group on sinking deltas and wish to express my special thanks to the Soil Geography and Landscape Group at Wageningen University & Research, the Earth Observation and Innovation Lab at Virginia Tech and the Hydrology and Hydraulic Engineering working group at the University of Padova for being part of my PhD journey and beyond, your company and creating an enjoyable working atmosphere. Thank you, Assoc. Prof. Dr. Pietro Teatini, for giving me the room to focus on and finish my thesis, for all your trust in my work and your advice in challenging times. Thank you, Dr. Claudia Zoccarato, for the great time together in the office and on our conference trips. My PhD journey would not have been the same without Assistant Prof. Dr. Artur Guzy. Reading about your research already before starting my PhD thesis, it has been a great pleasure to get to know you in person, meeting you on field and conference travels. I appreciate your unwavering commitment and thoroughness in work, your perceptive and empathetic character with a genuine concern for others and thank you for our numerous conversations about work and life, your advice in difficult times, all the laughs and joyful moments in our German-Polish friendship. You have been an academic big brother to me on my scientific journey and I look forward to work together with you, exploring our research ideas, and to our tradition of making a hiking tour wherever we meet.

I am deeply thankful to those who by their enthusiasm and commitment impressed me, laying the foundations in my excitement about geography and scientific work. My special thanks to Johannes Pernack not only for teaching me in geography but for sparking my curiosity about Earth. I will never forget your creative, unconventional way of teaching and your tireless dedication to your students. I would probably never have taken geography as a major subject at school or at university without you. Your clarity in teaching combined with your detailed feedback laid the cornerstone for my academic work. My special thanks also to PD Dr. Bodo Maria Möseler. Without you, I probably would not have had the confidence to start navigating the mountainous path of my PhD project. Thank you for your advice as a fatherly friend, knowing me better than I did. Sharing your enthusiasm about plants and biodiversity, I appreciate I could join your courses in agricultural sciences, learning a lot from your well-prepared lectures, all of which has fostered my excitement about Earth, botany and nature conservation and being a huge inspiration when I teach.

My deep gratitude goes to my friends and family who accompanied me all the way of my PhD journey and in my life. Thank you, Laura, for our, meanwhile over 20 years of friendship, that you have always been there for me and understand me, no matter where we are or how much time has passed since we last met. I am curious what the next 20 years hold for us. Thank you, Michael, for enriching my PhD time with a lot of fun, music, iced coffee and tea. Wherever our ways cross, there is a lot of laughter and something to drink or ice cream (or both). Thank you, Martin, for your constant friendship, always being up for a call, and your uncomplicated way of seeing life, which offered me a perspective when I saw things too complicated. Thank you, Anna-Maartje, for being my PhD mate in Wageningen and becoming a very good friend. I have always enjoyed our chats about (the role and responsibility of) science and life while sitting on our bikes cycling in the Netherlands, in a café or on a roof terrace in Italy. Thank you, Svenja, for being a friend always with a helping hand. To plan our meetups, we don't need more than saying 'as always' and we have a great evening with great conversations. Thanks to the Unlimited Voice Company and Gerald Meier for enriching my life with music and joy. Singing and spending time together with you means a lot to me and wherever I am in the world, I try to make it to our Monday evening rehearsals and join our concerts. My warmest thanks to my family. Mama and Papa, thank you for your unconditional support. Thank you, Mama, for always being excited about my scientific adventures and joining my long-distance travels virtually. Thank you for all the efforts you took for me, our family, for others. Without you, I would not have made it where I am today. Thank you, Papa, for your thoughtful, prudent but

also spontaneous nature and sharing some of your perfectionism with me, making me try to understand phenomena to the utmost detail, which has helped me to make some of the major discoveries in my thesis. Many thanks to my twin sister Friederike and my brothers Friedemann and Paul and their families. Thank you for encouraging me when the path was steep and rocky and for sharing with me the joy of every rewarding view along the way. My heartfelt thanks to my grandparents. Grandma and grandpa from Berlin, I wish I could share this moment with you and will carry you with me in this achievement and beyond. Grandma, thank you for joining me in all the ups and downs of my PhD journey. You were often the first to hear about any news I had and I will always remember the sparkle in your eyes in those moments. Thank you for the wonderful time we had together and know that you will be with me wherever I am.

My deep gratitude to all of you who patiently stood by my side, encouraged me, and always believed in me.

"*the world should be a little better because a man has lived — even ever so little better*"

Little Lord Fauntleroy (1886), Frances Hodgson Burnett

May this thesis contribute to better-informed decisions in data-sparse coastal lowlands at risk and thereby help to making this world a little bit better.

For all those whose voices are not heard.

Content

Summary ..... **I**

Kurzzusammenfassung ..... **V**

Acknowledgements ..... **X**

Figures ..... **XXII**

Tables ..... **XXIX**

1 Introduction **1**

1.1 Coastal lowlands in times of human impact and environmental change 1

1.2 Flood-related hazards in coastal lowlands and challenges of data sparsity 3

1.3 Research motivation 6

1.4 Research hypotheses and goals 8

References 14

2 Coastal flooding in Asian megadeltas: Recent advances, persistent challenges, and call for actions amidst local and global changes **20**

3 Evaluating flood hazards in data-sparse coastal lowlands: highlighting the Ayeyarwady Delta (Myanmar) **21**

3.1 Introduction 22

3.2 Material and methods 26

3.3 Results and discussion 28

3.3.1 Flood exposure of the Ayeyarwady Delta 28

3.3.1.1 Exposure to single flood-type hazards 28

3.3.1.2 Exposure to multiple flood-type hazards 32

3.3.2 Implications for coping with flood hazards in the Ayeyarwady Delta 36

3.3.3 Implications for generating first-order flood hazard assessments in data-sparse coastal lowlands of the world ... 37

3.4 Conclusions ... 38

References ... 40

4 Land elevation is key – On the proper handling of elevation and sea-level data for improving assessments of relative sea-level rise impact ... 49

4.1 Assessing land elevation in the Ayeyarwady Delta (Myanmar) and its relevance for studying sea level rise and delta flooding ... 49

4.1.1 Introduction ... 51

4.1.2 Study area ... 54

4.1.3 Material and methods ... 57

4.1.3.1 Generation of an elevation model for the Ayeyarwady Delta based on geodetic data ... 57

4.1.3.2 Processing of global DEMs and determination of local mean sea level (MSL) ... 58

4.1.3.3 Mapping of areas prone to monsoon flooding ... 61

4.1.3.4 Mapping of areas prone to future RSLR ... 61

4.1.4 Results ... 62

4.1.4.1 Performance and accuracy of the AD-DEM ... 62

4.1.4.2 Performance and accuracy of global satellite-based DEMs ... 63

4.1.4.2.1 Performance of global DEMs based on visual inspection ... 63

4.1.4.2.2 Direct validation with spot heights from topographic maps ... 65

4.1.4.2.3 Direct validation of global DEMs with AD-DEM ... 67

4.1.4.2.4 Indirect validation of DEMs by comparison with areas drowned during recent flood events ... 69

4.1.4.3 Estimation of coastal area at risk of future sea level rise ... 72

4.1.5 Discussion ... 76

4.1.5.1 Suitability of DEMs for studying flood risk in the Ayeyarwady Delta ... 76

4.1.5.2 Implications for assessing flood risk in the Ayeyarwady Delta ... 78

4.1.6 Conclusions ... 81

References ... 84

4.2 Sea level much higher than assumed in most coastal hazard assessments ... 96

4.2.1 Introduction ... 96

4.2.2 Methods 98

4.2.2.1 Conduction of literature research and evaluation 98

4.2.2.2 Vertical datum conversion and processing of digital elevation models ... 99

4.2.2.3 Assessment of coastal land elevation and sea-level height, sea-level rise impact and low-elevation coastal zone from global digital elevation models 101

4.2.3 Majority of coastal hazard assessments contains errors or is not reproducible 102

4.2.4 Sea level higher than previously assumed in most coastal hazard assessments 106

4.2.5 Conclusions and outlook 109

References 111

4.3 Attributing uncertainties in elevation assessments for data-sparse coastal lowlands using global elevation models: A globally applicable approach showcasing the Vietnamese Mekong Delta 117

4.3.1 Introduction 118

4.3.2 Methods 123

4.3.2.1 Processing of local elevation data: Generation of Topo DEM v2 123

4.3.2.2 Assessment of global elevation model performance 126

4.3.2.3 Quantification of vertical datum offsets 128

4.3.3 Results and interpretation 128

4.3.3.1 Converting vertical datum to actual continuous local sea level 128

4.3.3.2 Performance of digital elevation models in the Vietnamese Mekong Delta 131

4.3.3.2.1 Revisiting local elevation data in the Vietnamese Mekong Delta 131

4.3.3.2.2 Which one is the best? – On the local validation of global satellite-based digital elevation models 132

4.3.4 Discussion, conclusions and outlook 136

References 142

5 Understanding land elevation dynamics for strengthening coastal hazard and impact assessments in the Ayeyarwady Delta (Myanmar) 151

5.1 Introduction 152

5.2 Methods 155

5.2.1 SAR interferometric analysis for determining land elevation change 155

5.2.2 Seasonal signal component filtering for unravelling the impact of water load on spatio-temporal InSAR pattern 156

5.2.3 Integrating InSAR and existing data to identify local drivers of land elevation change and implications on relative SLR and flood exposure 157

5.3 Preliminary results, interpretation and discussion 158

5.3.1 Land elevation change in the Ayeyarwady Delta 158

5.3.2 Seasonality in water load and signal decomposition 162

5.3.3 Unravelling potential drivers of land elevation change based on comparison with existing data 163

5.3.3.1 Potential natural drivers 164

5.3.3.2 Potential anthropogenic drivers 167

5.3.4 Implications of land elevation change on present and future relative sea-level rise and flood exposure 171

5.4 Conclusions and outlook 174

References 176

6 Synthesis 184

6.1 Improving the understanding of flood hazards and impacts in data-sparse coastal lowlands 185

6.2 Improving the understanding of coastal land elevation and vertical datums for reliable relative sea-level rise and flood impact and exposure assessments in data-sparse coastal lowlands 188

6.2.1 Bridging from geodesy to geography to overcome vertical reference issues in coastal lowlands 189

6.2.2 Accounting for uncertainties in coastal land elevation for reliable relative sea-level rise and flood impact assessments 192

6.3 Paving the way for risk-sensitive development in the view of future flood risk and relative sea-level rise 195

6.4 Recommendations for further research 198

References 200

Appendix A – Supplement to Chapter 2 202

Appendix B – Supplement to Chapter 3 203

Appendix C – Supplement to Chapter 4.1 234

Appendix D – Supplement to Chapter 4.2 284

Appendix E – Supplement to Chapter 4.3 306

Appendix F – Supplement to Chapter 5 317

Own contribution 320

Figures

Figure 3.1 | Workflow to perform flood hazard mapping and exposure analysis in data-sparse coastal lowlands such as the Ayeyarwady Delta in Myanmar (GEE = Google Earth Engine, GIS = Geographic Information System). 27

Figure 3.2 | Exposure of the Ayeyarwady Delta in Myanmar to single types of flooding. 29

Figure 3.3 | Exposure of area, population, and land-use properties to single-type flooding and relative sea-level rise (RSLR). 30

Figure 3.4 | Exposure of the Ayeyarwady Delta in Myanmar to multiple types of flooding and relative sea-level rise (SL = sea level). 33

Figure 3.5 | Exposure of area, population, and land-use properties to multiple flooding from monsoon and storm surge. Note that numbers on the y axis indicate months of monsoon flooding. 34

Figure 3.6 | Exposure of area, population, and land-use properties to multiple flooding and relative sea-level rise. Note that numbers on the y axis indicate months of monsoon flooding (SL = sea level). 35

Figure 4.1 | Local digital elevation model for the Ayeyarwady Delta in Myanmar (AD-DEM; Seeger et al., 2023a) based on the interpolation of digitised spot and contour heights from topographic maps (see also Figure C1). 55

Figure 4.2 | Workflow of datum conversions conducted in this study to reference the Mean Dynamic Topography (i.e. $MDT_{GOCO05s}$) and digital elevation models to a common reference geoid first (i.e. to the EGM96 geoid (MDT_{EGM96} in a); datum conversion I in b). 60

Figure 4.3 | The new, local AD-DEM (a) in comparison to global digital elevation models in the Ayeyarwady Delta (b–i). 64

Figure 4.4 | Differences between global DEMs and the AD-DEM together with frequency distributions of height residuals (in m). 68

Figure 4.5 | Delta elevation along longitudinal (a) and cross sections (b–f) in deltaic areas affected by flooding during the monsoon seasons of 2015 and 2020 (Base map: EsriWorld Imagery, 2017). 70

Figure 4.6 | Area below future mean sea level according to local and global DEMs following median sea level rise projections for Yangon for 2100 (compared to the baseline period 1995–2014) from the Sea Level Projection Tool of the IPCC Sixth Assessment Report (Fox-Kemper et al., 2021; Garner et al., 2021, 2022). Note that in case of higher RSLR, these scenarios will be reached sooner than 2100. 73

Figure 4.7 | Area (a) and people (b) affected by sea level rise of 1.229 m as projected by SSP5-8.5 (83rd percentile) for 2100 for each administrative district of the Ayeyarwady Delta and the entire delta. 75

Figure 4.8 | Evaluation of sea-level and coastal elevation data documentation and their proper use and alignment in coastal hazard assessments. 104

Figure 4.9 | Discrepancy between coastal sea-level and most-used geoid height across the globe. 106

Figure 4.10 | Discrepancy between commonly assumed coastal sea-level height in hazard assessments with actual local sea-level height. 107

Figure 4.11 | Differences in population falling below sea level following 1m relative sea-level rise (RSLR) with proper alignment of land and sea-level height. 108

Figure 4.12 | Local topographical elevation model of the Vietnamese Mekong Delta, updated from Minderhoud et al. (2019a) by referencing to actual local, continuous mean sea level indicated by mean dynamic topography (Jousset et al., 2023). 123

Figure 4.13 | Vertical datums of elevation and sea-level datasets used for the example of the Mekong Delta together with steps of datum conversion for local (1–3) and global elevation data (a–b) and sources of uncertainty associated with global elevation data (A–E). 125

Figure 4.14 | Offsets between commonly used geoid models (EGM96 (a); EGM2008 (b)) as well as an example of incomplete datum conversion (c) and local mean sea level as indicated by mean dynamic topography of Jousset et al. (2023) in the Vietnamese Mekong Delta. 129

Figure 4.15 | Digital elevation models included in this study, all referenced to actual, local continuous mean sea level as indicated by mean dynamic topography (Jousset et al., 2023). 133

Figure 4.16 | Height residuals of DEMs referenced to mean sea level compared to Topo DEM v2. 136

Figure 4.17 | Quantification and attribution of uncertainties associated with global DEMs in their performance to correctly quantify the elevation of the Vietnamese Mekong Delta. 138

Figure 5.1 | InSAR-derived displacement velocities along line-of-sight (LOS) for the Ayeyarwady Delta (a) and Yangon City (b). 158

Figure 5.2 | Timeseries of land elevation change based on InSAR-estimated displacement along line-of-sight (LOS) for selected locations in the Ayeyarwady Delta over the investigation period of March 2017 to October 2023. 161

Figure 5.3 | Monthly measurements of the Earth's surface mass and water changes (blue), 6-month running average (red), as well as the harmonic model (grey) fitted to decompose annual signal components and trend (orange). 163

Figure 5.4 | Overview of potential natural drivers of land elevation change in the Ayeyarwady Delta in Myanmar. 165

Figure 5.5 | Overview of potential anthropogenic drivers of land elevation change in the Ayeyarwady Delta in Myanmar. 169

Figure 5.6 | Outline of how land elevation change information can be used to improve assessments of relative sea-level rise impact (Seeger et al., 2023) and update coastal assessments of coastal exposure, multiple flood hazards (Seeger et al., 2024), vulnerability and risk (Vogel et al., 2024). Land elevation change can be either directly integrated into exposure assessments or used to create scenarios of future land elevation (1) that serve as a basis for relative sea-level rise impact assessment (2) which will then

update previous coastal hazard and exposure assessments (3), thereby providing better informed vulnerability (4) and risk assessments (5). 171

Figure 6.1 | Relations between vertical reference systems in the coastal landscape. 190

Figure B1 | Precipitation (a) and runoff patterns (b) in Myanmar and the Ayeyarwady Delta in 2015 based on the GPM_3IMERGM_ v06 product (0.1°; Huffman et al., 2019) and River and Reservoir Watch Version 4.5 (Brakenridge et al., 2023a, 2023b, 2023c). Locations of RiverWatch 4.5 sites 25, 29, and 30 are shown in (a)..... 209

Figure B2 | Precipitation (a) and runoff patterns (b) in Myanmar and the Ayeyarwady Delta in 2016 based on the GPM_3IMERGM_ v06 product (0.1°; Huffman et al., 2019) and River and Reservoir Watch Version 4.5 (Brakenridge et al., 2023a, 2023b, 2023c). Locations of RiverWatch 4.5 sites 25, 29, and 30 are shown in (a)..... 210

Figure B3 | Precipitation (a) and runoff patterns (b) in Myanmar and the Ayeyarwady Delta in 2017 based on the GPM_3IMERGM_ v06 product (0.1°; Huffman et al., 2019) and River and Reservoir Watch Version 4.5 (Brakenridge et al., 2023a, 2023b, 2023c). Locations of RiverWatch 4.5 sites 25, 29, and 30 are shown in (a)..... 211

Figure B4 | Precipitation (a) and runoff patterns (b) in Myanmar and the Ayeyarwady Delta in 2018 based on the GPM_3IMERGM_ v06 product (0.1°; Huffman et al., 2019) and River and Reservoir Watch Version 4.5 (Brakenridge et al., 2023a, 2023b, 2023c). Locations of RiverWatch 4.5 sites 25, 29, and 30 are shown in (a)..... 212

Figure B5 | Precipitation (a) and runoff patterns (b) in Myanmar and the Ayeyarwady Delta in 2019 based on the GPM_3IMERGM_ v06 product (0.1°; Huffman et al., 2019) and River and Reservoir Watch Version 4.5 (Brakenridge et al., 2023a, 2023b, 2023c). Locations of RiverWatch 4.5 sites 25, 29, and 30 are shown in (a)..... 213

Figure B6 | Precipitation (a) and runoff patterns (b) in Myanmar and the Ayeyarwady Delta in 2020 based on the GPM_3IMERGM_ v06 product (0.1°; Huffman et al., 2019) and River and Reservoir Watch Version 4.5 (Brakenridge et al., 2023a, 2023b, 2023c). Locations of RiverWatch 4.5 sites 25, 29, and 30 are shown in (a)..... 214

Figure B7 | Precipitation (a) and runoff patterns (b) in Myanmar and the Ayeyarwady Delta in 2021 based on the GPM_3IMERGM_ v06 product (0.1°; Huffman et al., 2019) and River and Reservoir Watch Version 4.5 (Brakenridge et al., 2023a, 2023b, 2023c). Locations of RiverWatch 4.5 sites 25, 29, and 30 are shown in (a)..... 215

Figure B8 | Runoff patterns in the lower Ayeyarwady River and the delta for the year 2022 based on River and Reservoir Watch Version 4.5 (Brakenridge et al., 2023a, 2023b, 2023c). 216

Figure B9 | Runoff patterns in the lower Ayeyarwady River and the delta for the year 2023 based on River and Reservoir Watch Version 4.5 (Brakenridge et al., 2023a, 2023b, 2023c). 216

Figure B10 | Flood frequency pattern during the monsoon season for every year of the investigated time period 2015–2023 217

Figure B11 | Flood frequency pattern for every month of the monsoon season of the investigated time period 2015–2023 218

Figure B12 | Flood frequency pattern for each administrative district for every month of the monsoon season of the investigated time period 2015–2023. 219

Figure B13 | Monsoon flooding in selected areas of the Ayeyarwady Delta. 220

Figure B14 | Exposure of delta districts to monsoon flooding. 221

Figure B15 | Exposure of delta districts to storm surge flooding based on the flood extent of TC Nargis 2008. 222

Figure B16 | Exposure of delta districts to relative sea-level rise based on area falling below sea level assuming relative sea-level rise of 1 m. 223

Figure B17 | Exposure to multiple flooding differentiated into individual components. 224

Figure B18 | Exposure of delta districts to both monsoon and storm surge flooding. 224

Figure B19 | Exposure to multiple flooding and relative sea-level rise differentiated into individual components. 225

Figure B20 | Exposure of delta districts to both monsoon and storm surge flooding as well as relative sea-level rise. 226

Figure B21 | Linkages between zones exposed to multiple flooding and relative sea-level rise, elevation and land-use land cover. 227

Figure B22 | Linkages between zones exposed to multiple flooding and relative sea-level rise, elevation and land-use land cover. 228

Figure B23 | Linkages between zones exposed to multiple flooding and relative sea-level rise, elevation and land-use land cover. 229

Figure B24 | Linkages between zones exposed to multiple flooding and relative sea-level rise, elevation and land-use land cover. 230

Figure C1 | Spot heights from topographic maps used for interpolation of the AD-DEM (a; contour data are not shown). 243

Figure C2 | Regional setting of geoids (a–c) relevant to transpose MDT data from GOCO05s to EGM96 geoid (d). Height anomalies of GOCO05s and EGM96 compared to WGS84 ellipsoid (a and b) and compared to each other along a shoreline profile (black line; a–c). Processing of the MDT resulted in a MDT dataset, which is referenced to EGM96 geoid and resampled to a spatial resolution of 750 m (d). The black dot at the Tanintharyi coast shows the location of Kyaikkhami, where the original vertical basis of Myanmar elevation data is located. 245

Figure C3 | Relations between Mean Dynamic Topography (MDT) and EGM96 and GOCO05s geoids with respect to WGS84 ellipsoid for the coastal area of Kyaikkhami in Myanmar (distances are not to scale). 247

Figure C4 | The new local AD-DEM (a and b) in comparison to global digital elevation models in the Ayeyarwady Delta, which were excluded from the main text (c and d). 250

Figure C5 | Frequency distribution of elevation counts (in m) for each DEM (based on versions resampled to 750 m). 251

Figure C6 | Frequency distribution of elevation counts (in m) for spot heights inside the ROI of the Ayeyarwady Delta. 252

Figure C7 | Spot height residuals for global DEMs classified by standard deviation. 253

Figure C8 | Spot height residuals for global DEMs classified by standard deviation. 254

Figure C9 | 2D density plots for global DEMs in comparison with spot heights in relation to the 1:1 line. 255

Figure C10 | 2D density plots for global DEMs in comparison with spot heights in relation to the 1:1 line. 256

Figure C11 | 2D density plots for global DEMs in comparison with spot heights of less than 10 m above MSL in relation to the 1:1 line. 257

Figure C12 | 2D density plots for global DEMs in comparison with spot heights of less than 10 m above MSL in relation to the 1:1 line. 258

Figure C13 | Differences between global DEMs and the AD-DEM together with frequency distributions of height residuals (in m). 258

Figure C14 | Monthly accumulated precipitation in Myanmar (a) and the Ayeyarwady Delta (b) for the monsoon season 2015 together with locations of microwave discharge measurement sites (Brakenridge et al., 2022) based on Esri World Imagery (2017). 260

Figure C15 | Discharge pattern of the monsoon season 2015. 261

Figure C16 | Monthly accumulated precipitation in Myanmar (a) and the Ayeyarwady Delta (b) for the monsoon season 2020 together with locations of microwave discharge measurement sites (Brakenridge et al., 2022) based on Esri World Imagery (2017). 262

Figure C17 | Discharge pattern of the monsoon season 2020. 262

Figure C18 | Frequency distribution of elevation counts (in m) for DEMs inside areas affected by flooding during the monsoon season of 2015 (dark blue) and 2020 (light blue). 263

Figure C19 | Delta elevation along longitudinal (a) and cross sections (b–f) in deltaic areas affected by flooding during the monsoon seasons 2015 and 2020 (Base map: Esri World Imagery, 2017). 264

Figure C20 | Area below future mean sea level according to local and global DEMs following median sea level rise projections for Yangon for 2150 (compared to the baseline period 1995–2014) from the Sea Level Projection Tool of the IPCC 6th Assessment Report (Fox-Kemper et al., 2021; Garner et al., 2021, 2022). 265

Figure C21 | Area below future mean sea level according to global DEMs, which were excluded from the main text, following median sea level rise projections for Yangon for 2100 (a and b) and 2150 (c and d) (compared to the baseline period 1995–2014) from the Sea Level Projection Tool of the IPCC 6th Assessment Report (Fox-Kemper et al., 2021; Garner et al., 2021, 2022). 266

Figure C22 | Area and people that will fall below future sea level by 2100 (a) and 2150 (b) following median sea level rise projections for Yangon (compared to the baseline period 1995–2014) from the Sea Level Projection Tool of the IPCC 6th Assessment Report (Fox-Kemper et al., 2021; Garner et al., 2021, 2022). 268

Figure C23 | Area (a) and people (b) affected by sea level rise of 1.229 m as projected by SSP5-8.5 (83rd percentile) for 2100 for each administrative district of the Ayeyarwady Delta and the entire delta. 269

Figure C24 | Area (a) and people (b) affected by sea level rise of 2.210 m as projected by SSP5-8.5 (83rd percentile) for 2150 for each administrative district of the Ayeyarwady Delta and the entire delta. 270

Figure C25 | Estimated percentage of administrative district area and inhabitants affected by sea level rise according to projections of the IPCC 6th Assessment Report for the years 2100 (a) and 2150 (b) based on AD-DEM, FABDEM, and CoastalDEM v2.1, respectively. 271

Figure C26 | Population density in the Ayeyarwady Delta (a) and in Myanmar (b; based on LandScan Global 2020 population data (Rose et al., 2021)) together with the location of major cities and urban settlements that will be most affected by future sea level rise. 272

Figure C27 | Performance of selected DEMs in sea level rise impact assessments for 2150 in relation to land cover based on Esri World Imagery (2017). 273

Figure C28 | Discrepancies in delta shape between boundaries of administrative units (MIMU, 2021) and the ROI used in this study (Tessler et al., 2015). 274

Figure D1 | Overview of publications searched and screened for their suitability to be included in the literature evaluation of this study. 284

Figure D2 | Overview of publications included in the literature evaluation of this study. 285

Figure D3 | Vertical datum types used by the literature evaluated. 285

Figure D4 | Evaluation of the usage of digital elevation models (DEMs) in the literature investigated in this study. 286

Figure D5 | Relations between vertical reference systems and processing workflow of vertical datum conversion of elevation data. 287

Figure D6 | Global coastal elevation and discrepancy between geoid-based and sea-level-based elevation for CoastalDEM v2.1. 288

Figure D7 | Global coastal elevation and discrepancy between geoid-based and sea-level-based elevation for FABDEM v1.0. 289

Figure D8 | Global coastal elevation and discrepancy between sea-level-based elevation for GLL-DTM v2 after Vernimmen and Hooijer (2023), Vernimmen and Hooijer (2022), Rio et al. (2014) and following this study. 290

Figure D9 | Global coastal elevation and discrepancy between geoid-based and sea-level-based elevation for DeltaDTM v1. 291

Figure D10 | Differences in area falling below sea level following 1m relative sea-level rise (RSLR) with proper alignment of land and sea-level height. 292

Figure D11 | Area impacted by 1 m RSLR and within the LECZ for CoastalDEM v2.1. 293

Figure D12 | Area impacted by 1 m RSLR and within the LECZ for FABDEM v1.0. 294

Figure D13 | Area impacted by 1m RSLR and within the LECZ for GLL-DTM v2 295

Figure D14 | Area impacted by 1 m RSLR and within the LECZ for DeltaDTM v1. 296

Figure D15 | Study areas referred to in this study. 297

Figure E1 | Offsets between commonly used geoid models and local mean sea level as indicated by mean dynamic topography of Jousset et al. (2023) in the Vietnamese Mekong Delta and its adjacent provinces. 310

Figure E2 | Digital elevation models for the Vietnamese Mekong Delta and its adjacent provinces, all referenced to actual, local continuous mean sea level as indicated by mean dynamic topography (Jousset et al., 2023). 311

Figure E3 | Height residuals of DEMs referenced to mean sea level compared to Topo DEM v2 for the Vietnamese Mekong Delta and its adjacent provinces. 312

Figure F1 | Standard deviations for InSAR-derived displacement velocities along line-of-sight (LOS) for the Ayeyarwady Delta (a) and Yangon City (b). 317

Figure F2 | Data record of GPS station IGL1 (network operator's station ID: IGLE) situated outside the Ayeyarwady Delta but providing the highest data density and showing – apart from seasonal variations – a comparably stable vertical movement component, especially over the investigation period from March 2017 to October 2023 (Blewitt et al., 2018; Nevada Geodetic Laboratory, without date). Note that last data of IGL1 was obtained on 31st December 2020. 318

Tables

Table 4.1 | Statistics for DEMs minus spot height elevation at spot height location. 66

Table 4.2 | Statistics for DEMs minus spot height elevation at spot height location for the low-lying delta plain (spot heights <10 m above MSL). 67

Table 4.3 | Offsets between commonly used geoid models as well as an example of incomplete datum conversion and local mean sea level as indicated by mean dynamic topography of Jousset et al. (2023) in the Vietnamese Mekong Delta. 129

Table 4.4 | Performance of local and global DEMs in the Vietnamese Mekong Delta validated by the local Topo DEM v2 and DEM-specific vertical datum offsets quantified as differences in RMSE and discrepancies from RMSE of DEMs referenced to mean dynamic topography (MDT). 134

Table 5.1 | Radar satellite data processed to investigate land elevation change in the Ayeyarwady Delta. 155

Table 5.2 | Average, minimum and maximum values of land elevation change (LEC), and standard deviation (SD) for the Ayeyarwady Delta and Yangon City based on InSAR-estimated LOS displacement velocities. 159

Table B1 | Overview of flood events that impacted Myanmar in the last ~20 years. 203

Table B2 | Time frames of Sentinel-1 data acquired for determining monthly flood extents during the monsoon season from 2015 to 2023. 206

Table C1 | Overview of all elevation models used in this study. 235

Table C2 | Summary of cross validation measures for all nine versions of the AD-DEM from the Empirical Bayesian Kriging algorithm. 249

Table C3 | Raster statistics for DEMs of this study. 249

Table C4 | Statistics for DEMs minus spot height elevation at spot height location. 252

Table C5 | Statistics for DEMs minus spot height elevation at spot height location for the low-lying delta plain (spot heights <10 m above MSL). 256

Table C6 | Statistics for DEM minus AD-DEM. Best performances are shown in italics. 259

Table C7 | Area and population below sea level for selected relative sea level rise scenarios taken from projections of the IPCC 6th Assessment Report for the years of 2100 and 2150, respectively. 266

Table D1 | Search term and screening used to collect and select scientific literature for evaluation. 297

Table D2 | Code description of evaluation categories used to evaluate scientific literature. 300

Table E1 | Performance of local and global DEMs in the Vietnamese Mekong Delta validated by local point elevations for versions referenced to mean dynamic topography (MDT) and their original vertical reference..... 307

Table E2 | Performance of local and global DEMs in the Vietnamese Mekong Delta validated by local point elevations ≤10 m for versions referenced to mean dynamic topography (MDT) and their original vertical reference..... 309

Table E3 | Offsets between commonly used geoid models and local mean sea level as indicated by mean dynamic topography of Jousset et al. (2023) in the Vietnamese Mekong Delta and its adjacent provinces. 310

Table E4 | Performance of local and global DEMs in the Vietnamese Mekong Delta and its adjacent provinces validated by the local Topo DEM v2 and DEM-specific vertical datum offsets quantified as differences in RMSE and discrepancies from RMSE of DEMs referenced to mean dynamic topography (MDT)..... 312

Table E5 | Performance of local and global DEMs in the Vietnamese Mekong Delta and its adjacent provinces validated by local point elevations for versions referenced to mean dynamic topography (MDT) and their original vertical reference. 313

Table E6 | Simulated, non-linear, extraction-induced land subsidence (Minderhoud et al., 2017; B1 scenario of Minderhoud et al., 2020), and annual rates of local, delta-average sea-level rise estimated from PSMSL data of Vung Tau tide-gauge observations (1979–2010) and IPCC AR6 total rates of sea-level change (PSMSL, 2025; Fox-Kemper et al., 2021; Garner et al., 2021; Garner et al., 2022) used to obtain tentative estimates of non-linear impact of elevation change due to vertical land motion (e.g. extraction-induced land subsidence) and sea-level change affecting DEM actuality. 314

1 Introduction

1.1 Coastal lowlands in times of human impact and environmental change

Coasts are dynamic landscapes at the interface of land, sea and atmosphere, being shaped by the interaction of processes of these three systems (Davidson-Arnott, 2019). Geological and tectonic factors, sea-level evolution, climatic setting as well as wave climate, ocean currents and tides are major controls over coastal formation, in which morphological changes become effective over short (seconds to days; e.g. ripple formation/migration due to waves and tides) to seasonal (days to years; e.g. beach position/migration due to seasonal to annual storm events and shifts in tidal cycles and wave climate) to long-term time scales (years/decades to centuries/millennia; e.g. shoreline position/migration, due to changes in sediment supply, climate and sea-level change and long-term tectonic movements) (Carter and Woodroffe, 2010). The characteristics of those determinants and the interplay of coastal processes have resulted in a variety of coast types and coastal landforms, of which this thesis focusses on sedimentary coasts, paying special attention to low-lying, coastal-deltaic landscapes.

Coastal lowlands are low-lying areas along the coast, whose elevations mount only to a few metres above sea level. While some studies and reports refer to a specific elevation threshold, for example, of 100 m (Small and Nicholls, 2003) or 10 m (e.g., Lichter et al., 2011; IPCC, 2023), the application of a threshold may be highly subjective and should be made with respect to the research context and the characteristics of the coastal lowland under study. In contrast, the particularly low-lying areas are commonly delineated by applying the 10-m elevation threshold to determine the low-elevation coastal zone (LECZ), while the 5-m elevation threshold serves for assessing the lowest-lying elevation coastal zone (LLEZ). It is these two zones (and particularly the LECZ), for which coastal exposure and impact assessments as well as projections of future coastal development are performed (especially on global scale) (e.g., McGranahan et al., 2007; Neumann et al., 2015; Merkens et al., 2016; Kulp and Strauss, 2019). In this work, the term coastal lowlands is – unless specified – not connotated with a specific max. elevation but refers to those coastal regions that are relatively low-lying compared to their surroundings and therefore relatively more exposed to relative-sea level rise and flooding.

Coastal lowlands include various landforms, all of which are typically at or near to sea level. Among these are beaches, salt marshes, mangrove swamps, estuaries, coastal plains and deltas. However, due to the focus on coastal-deltaic landscapes, the following sections provide information on deltaic landforms or refer to coastal lowlands in general, without detailing other typical landforms of coastal lowlands.

Coastal deltas are landforms that evolve where rivers flow into the sea, and deposit fluvial sediments that allow the shoreline to prograde, usually forming flat alluvial cones of only a few metres elevation above sea level. With their low-lying, flat topography, they are typical landforms of coastal lowlands. The most prominent delta is the Nile Delta whose shape resembles the Greek letter *delta* (*Δ*) and gave the landform its name (Herodotus in *Histories*, ca. 430BC; Celoria, 1966). However, the morphology of deltas is subject to the interplay of aforementioned physical factors and processes in which the typical delta shape may vary depending on the relative intensities of fluvial, tide and wave dynamics (Galloway, 1975).

Modern coasts are comparably young and have evolved considerably within the last 8000–6000 years, when post-glacial sea-level rise stabilised (e.g., Bird, 2008). Almost at the same time, humans started to settle and cultivate the coastal landscapes, particularly deltas, thereby acknowledging the range of ecosystem services that these landforms provide by their constant supply of freshwater and nutrient-rich sediments (Adger et al., 2018; Stanley and Warne, 1997; Becker et al., 2024; Best et al., 2024). In addition to agricultural, aquacultural and fishery production, coastal regions such as deltas are strategically favourable and with the provision of access to both inland and ocean waters, resources such as hydrocarbon and brines have served for benefits in travelling, transportation, trading, promoting rapid urban development. Consequently, deltas have become critical hubs of economic productivity, ensuring millions of livelihoods, global food security and, accompanied with mega- and/or metropolitan cities, serve as centres of global commerce and innovation (e.g., Scown et al., 2023). The prospects of coastal development have resulted in disproportionally high population growth and population densities, where at present (as of 2018) 2.86 billion people, i.e. 38.1 % of the world's population, are estimated to live within 100 km distance from the coast (Cosby et al., 2024). Globally, more than 500 million people, i.e. 7 % of the global population (Ericson et al., 2006; Nicholls et al., 2020) live in deltas while projections indicate the global coastal population to grow by 58 % to 71 % by 2050 (Merkens et al., 2016). Africa faces highest relative growths whereas highest absolute growths are expected for Asia (Merkens et al., 2016), in which already the majority of the world's delta population live (Small et al., 2018). About 50 % of the deltaic

population has been documented to live at an elevation of less than ~7 m (Edmonds et al., 2020), which on regional scale mounts to more than 174 million people in Asia (Small et al., 2018), and future projections indicate further population increase in low-lying coastal areas of less than 10 m elevation (Neumann et al., 2015; Small et al., 2018).

In line with population increasing in low-lying coastal areas such as deltas, so have human interventions on the natural landscape and modified the pristine coastal-deltaic conditions by substantial land-use land cover changes, thereby affecting the coast's/delta's natural balance and its resilience towards environmental impacts such as those caused by climate change, relative sea-level rise, or flooding (e.g., Renaud et al., 2013; Loucks, 2019). Under pristine conditions, deltas, which are naturally subsiding due to natural compaction and eventually tectonic/isostatic effects, could keep up with sea-level rise as the deposition of fluvial sediments would be sufficient to outpace natural compaction and gain elevation. However, human activities such as groundwater or hydrocarbon extraction as well as surface loading due to buildings and infrastructure have exaggerated natural rates of subsidence, resulting in rates of relative sea-level rise up to four times higher than global, climate-driven sea-level rise (Nicholls et al., 2021). In addition, human interventions in form of sediment mining and upstream dam construction have resulted in substantial reductions of fluvial sediment loads and thus sediment supply to the delta necessary to gain elevation and keep up with relative sea-level rise (e.g., Tessler et al., 2018). Further effects include shifts in hydrological regimes that affect channel dynamics, estuarine turbidity and coastal wetland state (van de Vijsel et al., 2024). The magnitudes at which local human interventions lead to far-reaching impacts on deltaic coastal lowlands, nowadays dominates large-scale contemporary natural and/or climate-related changes and shifts (Eslami et al., 2025). Against this background of natural and anthropogenic stressors, sustainable management actions are required to be effective across multiple scales (Schmitt and Minderhoud, 2023), taking a systems perspective that considers environmental and human compartments equally.

1.2 Flood-related hazards in coastal lowlands and challenges of data sparsity

With their low elevation above sea level, on average often only a few metres or even only decimetres (e.g., Minderhoud et al., 2019; Edmonds et al., 2020), coastal lowlands face an

increased susceptibility to hazards such as relative sea-level rise and flooding, and large, densely populated river deltas in Southeast Asia are among the most threatened (Woodruff et al., 2013; Tessler et al., 2015; Hill et al., 2020; Hooijer and Vernimmen, 2021). Comprehensive assessments of flood hazards and exposure are essential in order to identify hazards risks and develop effective mitigation and adaptation strategies.

Hazards are defined as (natural) events or (human-induced) processes that have the potential to create loss and therefore constitute a general source of future danger (UNDRR, 2017a; Smith et al., 2023). For example, a flood itself constitutes an event, however, it becomes a hazard with respect to people and assets exposed in coastal areas. Exposure refers to the presence of people and assets within hazardous areas (de Brito et al., 2017; UNDRR, 2017b). Combining quantifications of exposed population and types of assets with their specific vulnerability and capacity to a certain hazard consequently allows to estimate hazard risk (UNDRR, 2017b). Vulnerability is defined as the conditions shaped by physical, social, economic and environmental factors that increase the susceptibility to the effects of hazards, while capacity refers to the positive connotation of vulnerability (UNDRR, 2017c).

Coastal flood hazards that need to be assessed in coastal-deltaic settings include episodic/occasional to frequent/annual/seasonal storm surge flooding and other cyclone-induced impacts, especially in tropical areas, where 89 % of the global delta population are exposed to pronounced tropical cyclone activity (Edmonds et al., 2020). Relative sea-level rise adds on this exposure. Though it is a slow, long-term hazard if compared with (extreme) wave events, it constitutes a particular risk for densely populated lowlands where human-induced subsidence exaggerates global sea-level rise. In this sense, latest IPCC AR6 global sea-level rise projections of 32 to 101 cm (SSP1-2.6 to SSP5-8.5; IPCC, 2023) could be reached already decades sooner than projected for the year 2100. Further coastal hazards include high tides that are linked to frequently recurring high tides of the tidal cycles but also due interannual to decadal long-term tidal cycles (Enríquez et al., 2022). In flat, low-lying landscapes, high tides can reach several kilometres inland and add to elevated water levels from surges and waves (e.g., Kuenzer et al., 2013). In contrast to these hazards, tsunamis are high-energy wave events that occur on much larger recurrencies, i.e. in the range of centuries (e.g., Brill et al., 2011). Being hydrologically connected to the hinterland, deltas are also exposed to inland (fluvial) flooding, when precipitation or snow melt lead to high river discharges and increased flooding on the inner delta plain. As the majority of South- and Southeast-Asian river systems are influenced by the tropical monsoon climate where high annual discharge variabilities follow

seasonal monsoon precipitation and result in frequent pluvial and fluvial flooding, so are livelihoods of 60 % of the world's population, of which most concentrate along these rivers (Plink-Björklund, 2015; Hansford et al., 2020). Although not a flood hazard per se, coastal-deltaic land subsidence constitutes a 'hidden' hazard of comparably slow onset and delayed response that contributes to relative sea-level rise and increasing flood exposure. It might be included by relative sea-level rise impact assessments, however projecting non-linear future vertical land motion is not straightforward yet and challenges to adequately integrate vertical land motion with sea-level rise rates (Kopp et al., 2014; IPCC, 2023). In order to address root causes of relative sea-level rise impact and flood exposure in coastal lowlands, it is of utmost important to assess the hazard of land subsidence and unravel its drivers. Still, land subsidence constitutes a large unknown for many coastal lowlands and has only recently been addressed by global-scale works (Wu et al., 2022; Ohenhen et al., 2025).

In order to gain a comprehensive understanding of flood hazards and exposure, vulnerability and risk, assessments need to acknowledge the systems perspective, be as inclusive as possible and address the multitude of hazards, where events may occur simultaneously (i.e. as compound floods), cascadingly or cumulatively over time, hence defined as multiple hazards (UNDRR, 2017a). Likewise, quality checks of the input data used ensure the reliability of hazard assessments (e.g., UNISDR, 2017; Government of Canada, 2025). However, the generation of local reliable hazard assessments remains challenging for coastal areas that are hardly accessible or inaccessible and/or suffer from the absence or unavailability of high-resolution and high-accuracy data. Global data products may serve as substitutes, however are, due to their limited scalability, only of limited reliability and require validation (e.g., Jongman et al., 2012; Ward et al., 2018). Sometimes, also global-scale hazard and impact assessments exclude those data-sparse regions as these are not covered by the input data used (e.g., Eilander et al., 2020). Consequently, these regions often constitute 'blank maps' as hazard exposure and impact assessments are not openly available or do not exist.

Data sparsity is rather a continuum than a sharply defined term and similarly, there is no clear indication of data-sparse vs. data-rich coastal regions. Data sparsity can be described with respect to spatial, temporal, spatio-temporal, non-spatio-temporal and thematical sparsity. Spatial data sparsity refers to the absence of data/information for a certain location while temporal sparsity addresses inadequate time coverage due to insufficiently long time periods or discontinuous/irregular timeseries (Hamdi et al., 2021). Consequently, spatio-temporal sparsity denotes a combination of both components while non-spatio-temporal sparsity refers to

information such as attributes or metadata that are not related to the spatio-temporal components but provide further information (Hamdi et al., 2021). The absence of any contextual information, for example certain monitoring data, is categorised as thematical data sparsity. Globally, data-sparse coasts largely coincide with regions from the Global South where high-quality data either does not exist due to technical limitations in data acquisition or lack of capacity, or is treated highly confidentially where high-quality data exists but is not shared openly or with the scientific community. Especially for regions which are not only characterised by poor data coverage and availability, but which are hardly accessible or inaccessible, it is a major challenge to overcome the state of data sparsity and therefore move out of a locked-in status. However, recently launched satellite missions offering a plethora of freely-available data have the great potential to serve as a starting point to study flood hazard and relative sea-level rise impact and to explore open-data approaches that allow to conduct first-order coastal exposure and impact assessments and include quality assessments, all of which allow to be applied in any other data-sparse coastal region in the world.

1.3 Research motivation

One of the least studied coastal lowlands is the Ayeyarwady Delta in Myanmar although it is one of the main Southeast-Asian river systems, home to one third of the country's population (ca. 13 million people) and as the core of agricultural production serves as the 'rice bowl' of Myanmar, making the country the sixth largest rice producer in the world (Schneider and Asch, 2020). At the same time, the Ayeyarwady Delta is highly prone to flooding (Phongsapan et al., 2019). In 2008, category-4 tropical cyclone Nargis in 2008 caused disastrous storm surge flooding with >138,000 fatalities (Webster et al., 2008; Fritz et al., 2009). In 2015, exceptionally strong monsoon flooding affected >530 000 ha land used for agricultural and aquacultural production, resulting in substantial crop losses (Government of the Union of Myanmar, 2015). Except of a few emergency mappings from international initiatives (ITHACA et al., 2008; Copernicus Emergency Management Service, 2015; UNOSAT, 2015) and national institutions (Myanmar Information Management Unit (MIMU), 2015, 2020) in the aftermath of those events, information on flood exposure and risk has been very scarce and not openly available. Similarly, (relative) sea-level rise impact has not been studied before although increasing human activities such as upstream interventions and potential groundwater

extraction in the delta have been reported to challenge the environmental stability of the delta system and its capacity to withstand drowning from relative sea-level rise (Syvitski et al., 2009; Anthony et al., 2019; Chen et al., 2020).

The research project *Driving factors for and societal effects of sea-level rise and delta flooding in the Ayeyarwady Delta (Myanmar) – Lessons from the past for disaster governance in the future* (continued by the follow-up project *Rising sea and sinking land: Determining spatially resolved subsidence rates for the Ayeyarwady Delta (Myanmar) and developing dynamic adaptation scenarios for the increased risk of flooding*), into which this thesis is embedded, aimed to understand the interplay between sea-level rise, delta flooding and societal activities in the understudied Ayeyarwady Delta, including sea-level rise and flood impacts on population dynamics as well as the impact of societal activity in form of land use and water management on physical parameters. It is the project's ultimate goal to provide information that serves for improved risk assessment and mitigation strategies. The research project was funded by the German Research Foundation (DFG Project Number 411257639) and research in form of this thesis was conducted between February 2021 and July 2025. The design of this research project is unique in that as physical-geographical investigations (this work) and human-geographical investigations are closely integrated and aim to create synergies, thereby acknowledging the need to study relative sea-level rise and flooding in the Ayeyarwady Delta through a systems perspective and forming a sound base to provide reliable information for effective risk-sensitive development strategies in the Ayeyarwady Delta.

Although the Covid-19 pandemic and the military takeover in February 2021 challenged the conduction of the research project and has made field work impossible, important insights into flood hazards, exposure, vulnerability and risk of the Ayeyarwady Delta were achieved by using open and freely available remote sensing data. The advancements made not only include (in the absence of ground-truthing possibilities) first-order assessments of flood hazards and exposure in the data-sparse Ayeyarwady Delta. Rather, workflows were established that have the potential to perform those assessments solely based on open data and improve them by integrating land elevation data, for which uncertainties in land elevation assessment have been quantified and attributed. As these approaches are applicable to any data-sparse coastal lowlands in the world, the scope of this thesis was extended beyond the Ayeyarwady Delta and includes also research from the Vietnamese Mekong Delta and other Asian deltas, ultimately moving to the global scale.

1.4 Research hypotheses and goals

This research aims to improve the understanding of flood hazards and impacts in coastal-deltaic lowlands in the world that are particularly sparse in data. Therefore, this thesis envisages to unravel exposure to coastal and inland flood hazards as well as long-term effective relative sea-level rise impact for large, densely populated river deltas in Southeast Asia, highlighting the particularly data-sparse Ayeyarwady Delta in Myanmar. Given the limited availability/absence of high-quality local data, this work seeks to introduce open-data workflows that allow for first-order coastal exposure assessments and for increasing the reliability of globally available data on coastal elevation which are fundamental to relative sea-level rise and flood impact assessment. While the latter includes building bridges between geodetical and geographical disciplines, this thesis also aims to demonstrate the potential to form a fundamental base and/or complement vulnerability and risk assessments, ultimately informing disaster risk reduction and coping strategies in data-sparse coastal lowlands.

The overarching goal of this thesis is:

Improving the understanding of flood hazards and impacts and solving challenges in their assessments in the world's data-sparse coastal-deltaic lowlands to guide disaster risk reduction and coping strategies in the view of future flood risk and relative sea-level rise.

Implicit to this overarching goal are the three following hypotheses which are evaluated by meeting the respective subordinate goals.

Hypothesis 1 | Coastal hazards, their geophysical drivers and human pressures can be successfully assessed in data-sparse coastal lowlands through using state-of the-art space-borne observation and numerical analyses.

Goal 1.1 | Providing a state-of-the-art understanding of coastal flooding in five selected Asian megadeltas through a systems perspective and learning from state-of-the-art monitoring and modelling approaches.

To generate a thorough understanding of coastal hazards, their drivers and pressures for data-sparse coastal-deltaic lowlands, many of which are globally important hotspots of settlement and economic productivity, an extensive literature review was conducted for some of the most densely populated and rapidly growing, flood-prone and climate-vulnerable Asian megadeltas, namely the Ganges-Brahmaputra-Meghna, Ayeyarwady,

Chao Phraya, Mekong and Red River. The literature review included state-or-the-art monitoring and modelling works and covered geophysical drivers from climate influence, hydrology, oceanography, geomorphology and geophysical processes and their interactions as well as human disturbances to the deltaic landscape due to pressuring, dynamic land-use land cover changes and upstream interventions along with rapid population and economic growth. Taking a systems perspective, that considers environmental and human compartments equally, the interconnectedness between drivers and pressures is highlighted and allows for insights in order to target drivers of flood risk and increase the deltas' resilience.

Goal 1.2 | Defining data and modelling requirements for addressing urgent scientific and policy-relevant questions in the context of coastal flooding in five selected Asian megadeltas.

The methodological/technical advances in quantifying and understanding driving mechanisms were reviewed for the Ganges-Brahmaputra-Meghna, Ayeyarwady, Chao Phraya, Mekong and Red River deltas. In combination with the current knowledge of coastal hazards, drivers and pressures, this review allowed to elaborate key gaps and requirements for advancing the quantification of processes as well as to highlight the potential of transferability of methodologies and approaches across the deltas.

Goal 1.3 | Evaluating flood hazards in data-sparse coastal lowlands.

To overcome challenges in flood-prone data-sparse coastal lowlands where information about flood hazards, their potential impact and characteristics of areas, population and assets at risk is, in the limitation/absence of high-quality data, not existing or not accessible, a standardised, integrative open-data workflow was developed to perform first-order assessments of flood hazard exposure. The approach was showcased in the data-sparse Ayeyarwady Delta in Myanmar but with its highly flexible design offers the potential to be applied to other data-sparse coastal lowlands at various spatial scales.

Hypothesis 2 | Coastal land elevation is one of the main uncertainties in relative sea-level rise and flood impact assessments.

Goal 2.1 | Assessing land elevation in the Ayeyarwady Delta (Myanmar) and quantifying related data-driven uncertainties in sea-level rise impact assessment.

To unravel the elevation with respect to local sea level in a data-sparse coastal lowland such as the Ayeyarwady Delta, available local and space-borne elevation datasets were compiled and converted to a consistent sea level datum, using an improved vertical datum conversion approach based on open-available geoid and sea-level information. Space-borne elevation datasets were validated directly against local spot heights and a local elevation model as well as indirectly by comparison with flood maps. Estimating areas and population at risk of sea-level rise allowed for the first delta-wide sea-level rise impact assessment, and, in view of the range of elevation data used, to quantify data-driven uncertainties.

Goal 2.2 | Evaluating shortcomings and errors in handling of coastal elevation and sea-level data in the vast majority of contemporary sea-level rise and coastal hazard impact assessments.

Based on the complexity involved into the alignment of coastal elevation and sea-level data, where incorrect handling may introduce errors into assessments of sea-level rise and flood impact, a systematic literature evaluation was conducted to infer whether and to what extent impact assessments of sea level rise and coastal flood hazards used elevation and sea-level data properly. The dimensions of incorrect vertical datum alignment were quantified using an updated open-data approach of vertical datum conversion from previous works. To demonstrate the potential magnitude of errors, the impacts of the most frequently witnessed errors on global relative sea-level rise impact and exposure in the low-elevation coastal zone were quantified.

Goal 2.3 | Quantifying and attributing uncertainties in land elevation assessment to vertical datum offset, data-inherent inaccuracy and elevation change since data acquisition.

To improve the understanding of land elevation and the performance of elevation data in coastal-deltaic lowlands, where elevation is not static but subject to change due to vertical land motion and sediment accretion/erosion, uncertainties in estimating land elevation were

quantified by revisiting land elevation in the Vietnamese Mekong Delta. While assessing elevation models referenced to actual local sea level and in their original vertical reference allowed to attribute elevation assessment uncertainty to vertical datum offset, the consideration of non-linear rates land subsidence and sea-level rise allowed for tentative attribution of uncertainty to time since elevation data acquisition, whereas remaining uncertainties reflect inaccuracy due to elevation data acquisition and processing.

Hypothesis 3 | The alignment of coastal land elevation, with integrated vertical land motion, and coastal sea level data is of paramount importance to conduct thorough coastal hazard and impact assessments.

Goal 3.1 | Understanding land elevation dynamics for strengthening coastal hazard and impact assessments in the Ayeyarwady Delta (Myanmar).

In coastal-deltaic lowlands, where human-induced land subsidence and reduced sediment aggradation often result in net elevation loss and accelerating relative sea-level rise, land elevation change needs to be integrated with land elevation and sea-level information in order to substantiate impact assessments of relative sea-level rise and flood hazard exposure. For the data-sparse Ayeyarwady Delta, where this information was so far only available for Yangon City, delta-wide land elevation change was unravelled for the first time while potential natural and human drivers were discussed to derive implications for effective mitigation and adaptation strategies in view of present and future relative sea-level rise and flood risk.

Goal 3.2 | Bridging from geodesy to geography to overcome vertical datum issues in coastal lowlands.

To solve the considerations and processing steps that are required to be made in order to integrate data on sea level, coastal land elevation and elevation dynamics properly, users of the coastal research and practice community have to cross disciplines to become familiar with different types and models of vertical reference systems and how to properly convert between them. Linking the coexistence of vertical datums together with the relevance of aligning them when combining datasets that use different vertical reference systems to the coastal-deltaic landscape not only bridges between geodetical and geographical disciplines but also highlights how inadequate consideration of vertical datum alignment affects impact and exposure studies of relative sea-level rise and flooding.

Goal 3.3 | Paving the way for complementing coastal vulnerability and risk assessments to guide disaster risk reduction and coping strategies in the view of future flood risk and relative sea-level rise.

Establishing novel approaches that allow to assess coastal-related flood hazards and to quantify the uncertainties introduced by elevation data into relative sea-level rise impact assessments in data-sparse coastal lowlands allowed for unprecedented insights into coastal hazard exposure of these regions. The enhanced database of quality-assessed elevation, unravelled elevation dynamics, relative sea-level rise impact and flood exposure, together with the workflows' independency of index values shows high potential to feed and detail index-based vulnerability and risk studies with spatially resolved information.

To address all goals and hypotheses, this thesis includes four core sections. The first core section (*Chapter 2*) focuses on the state-of-the-art overview of coastal flood-related hazards and pressures in the five Asian megadeltas of the Ganges-Brahmaputra-Meghna, Ayeyarwady, Chao Phraya, Mekong and Red River, including a summary of the current knowledge and recent advances in quantifying and understanding natural and anthropogenic drivers. The second core section (*Chapter 3*) constitutes the establishment of the standardised, integrative approach for conducting first-order flood hazard assessments and exemplifies its applicability by using the data-sparse Ayeyarwady Delta in Myanmar to unravel its exposure to frequent (annual) monsoon flooding, episodic (occasional) storm surge flooding and long-term relative sea-level rise. The third core section (*Chapter 4*) focuses on the proper handling of coastal land elevation and sea-level data as aligning them to the same vertical datum is not straightforward and especially challenging in data-sparse coastal lowlands where local, high-resolution and high-accuracy data is absent and only global datasets suffering from large uncertainties can be used. The fourth core section (*Chapter 5*) moves from (static) land elevation to land elevation dynamics, for the first time providing delta-wide estimates of land elevation change for the Ayeyarwady Delta and tentatively discussing potential driving mechanisms of elevation loss as well as its implications for future relative sea-level rise and flood exposure.

The outcomes of this research addressing individual goals and hypotheses are synthesised in the concluding section (*Chapter 6*) of this thesis in order to highlight how those four core sections contribute to an improved understanding of flood hazards and relative sea-level rise impact in data-sparse coastal lowlands (*i*), making use of new standardised, integrative open-data workflows to unravel those hazards and by quantifying and accounting for uncertainties related to coastal elevation data improving previous coastal impact assessments (*ii and iii*),

finally allowing to establish/improve the fundamental basis of coastal vulnerability and risk assessments and to inform effective risk adaptation and mitigation strategies (*iv*).

References

Adger, W. N., Adams, H., Kay, S., Nicholls, R. J., Hutton, C. W., Hanson, S. E., Rahman, Md.M., & Salehin, M. (2018). Ecosystem services, well-being and deltas: Current knowledge and understanding. In: Nicholls, R., Hutton, C., Adger, W., Hanson, S., Rahman, M., Salehin, M. (eds) Ecosystem Services for Well-Being in Deltas. Palgrave Macmillan, Cham, 3–27. https://doi.org/10.1007/978-3-319-71093-8_1.

Anthony, E. J., Besset, M., Dussouillez, P., Goichot, M., & Loisel, H. (2019). Overview of the Monsoon-influenced Ayeyarwady River delta, and delta shoreline mobility in response to changing fluvial sediment supply. *Marine Geology*, *417*, 106038. https://doi.org/10.1016/j.margeo.2019.106038

Becker, M., Seeger, K., Paszkowski, A., Marcos, M., Almar, R., Bates, P., France-Lanord, C., Hossain, Md S., Khan, J., Karegar, M., Karpytchev, M., Long, N., Minderhoud, P. S. J., Neal, J., Nicholls, R. J., & Syvitski, J. (2024). Coastal flooding in Asian Megadeltas: Recent advances, persistent challenges, and call for actions admidst local and global changes. *Reviews of Geophysics*, *62*(4), e2024RG00846. https://doi.org/10.1029/2024RG000846.

Best, J., Darby, S., Esteves, L., Wilson, C. (2024). The world Atlas of rivers, estuaries, and deltas. Princeton University Press. https://doi.org/10.1515/9780691244846.

Bird, E. C. (2008). Coastal geomorphology: an introduction. John Wiley & Sons, 448 pp.

Brill, D., Brückner, H., Jankaew, K., Kelletat, D., Scheffers, A., & Scheffers, S. (2011). Potential predecessors of the 2004 Indian Ocean Tsunami – Sedimentary evidence of extreme wave events at Ban Bang Sak, SW Thailand. *Sedimentary Geology*, *239*(3–4), 146–161. https://doi.org/10.1016/j.sedgeo.2011.06.008.

Carter, R.W.G., Woodroffe, C.D., 2010. Coastal Evolution – Late Quaternary Shoreline Morphodynamics. Cambridge University Press. https://doi.org/10.1017/CBO9780511564420.

Celoria, F. (1966). Delta as a geographical concept in Greek literature. *Isis*, *57*(3), 385–388.

Chen, D., Li, X., Saito, Y., Liu, J. P., Duan, Y., Liu, S. A., & Zhang, L. (2020). Recent evolution of the Irrawaddy (Ayeyarwady) Delta and the impacts of anthropogenic activities: A review and remote sensing survey. *Geomorphology*, *365*, 107231. https://doi.org/10.1016/j.geomorph.2020.107231.

Copernicus Emergency Management Service (© 2015 European Union) (2015). [EMSR130] Irrawaddy Delta: Delineation Map, Monitoring 1.

Cosby, A. G., Lebakula, V., Smith, C. N., Wanik, D. W., Bergene, K., Rose, A. N., Swanson, D., & Bloom, D. E. (2024). Accelerating growth of human coastal populations at the global and continent levels: 2000–2018. *Scientific Reports*, *14*(1), 22489. https://doi.org/10.1038/s41598-024-73287-x.

Davidson-Arnott, R., Bauer, B., Houser, C. (2019). Introduction to coastal processes and geomorphology. Cambridge University Press.

de Brito, M. M., Evers, M., & Höllermann, B. (2017). Prioritization of flood vulnerability, coping capacity and exposure indicators through the Delphi technique: A case study in Taquari-Antas basin, Brazil. *International Journal of Disaster Risk Reduction*, *24*, 119–128. https://doi.org/10.1016/j.ijdrr.2017.05.027.

Edmonds, D. A., Caldwell, R. L., Brondizio, E. S., & Siani, S. M. O. (2020). Coastal flooding will disproportionately impact people on river deltas. *Nature Communications*, *11*, 4741. https://doi.org/10.1038/s41467-020-18531-4.

Eilander, D., Couasnon, A., Ikeuchi, H., Muis, S., Yamazaki, D., Winsemius, H. C., & Ward, P. (2020). The effect of surge on riverine flood hazard and impact in deltas globally. *Environmental Research Letters*, *15*(10), 104007. https://doi.org/10.1088/1748-9326/ab8ca6.

Enríquez, A. R., Wahl, T., Baranes, H. E., Talke, S. A., Orton, P. M., Booth, J. F., & Haigh, I. D. (2022). Predictable changes in extreme sea levels and coastal flood risk due to long-term tidal cycles. *Journal of Geophysical Research: Oceans*, *127*(4), e2021JC018157. https://doi.org/10.1029/2021JC018157.

Ericson, J. P., Vörösmarty, C. J., Dingman, S. L., Ward, L. G., & Meybeck, M. (2006). Effective sea-level rise and deltas: Causes of change and human dimension implications. *Global and Planetary Change*, *50*(1-2), 63–82. https://doi.org/10.1016/j.gloplacha.2005.07.004.

Eslami, S., Oude Essink, G., Paszkowski, A., Seeger, K., Minderhoud, P.S.J., Sloff, K., & Nicholls, R.J. (2025). A systems perspective for climate adaptation in deltas. *Nature Climate Change*, *15*, 687–691. https://doi.org/10.1038/s41558-025-02368-0.

Fritz, H., Blount, C., Swe Thwin, Moe Kyaw Thu, & Nyein Chan (2009). Cyclone Nargis storm surge in Myanmar. *Nature Geoscience*, *2*, 448–449. https://doi.org/10.1038/ngeo558.

Galloway, W. E. (1975). Process framework for describing the morphologic and stratigraphic evolution of deltaic depositional systems.

Government of Canada, 2025. Coastal Flood Hazard Assessment for Risk-Based Analysis on Canada's Marine Coasts. https://natural-resources.canada.ca/coastal-flood-hazard-assessment-risk-based-analysis-canada-s-marine-coasts (last access: 7 July 2025)

Government of the Union of Myanmar (2015). Myanmar – Post-disaster needs assessment of floods and landslides July–September 2015, Government of the Union of Myanmar, https://documents1.worldbank.org/curated/en/646661467990966084/pdf/103631-WP-P157276-PUBLIC-PFLNA-Report-2016.pdf (last access: 7 July 2025)

Hamdi, A., Shaban, K., Erradi, A., Mohamed, A., Rumi, S. K., & Salim, F. D. (2022). Spatiotemporal data mining: a survey on challenges and open problems. *Artificial Intelligence Review*, 1–48. https://doi.org/10.1007/s10462-021-09994-y.

Hansford, M. R., Plink-Björklund, P., & Jones, E. R. (2020). Global quantitative analyses of river discharge variability and hydrograph shape with respect to climate types. *Earth-Science Reviews*, *200*, 102977. https://doi.org/10.1016/j.earscirev.2019.102977.

Hill, C., Dunn, F., Haque, A., Amoako-Johnson, F., Nicholls, R. J., Raju, P. V., & Appeaning Addo, K. (2020). Hotspots of Present and Future Risk Within Deltas: Hazards, Exposure and Vulnerability. In: Nicholls, R., Adger, W., Hutton, C., & Hanson, S. (2020). Deltas in the Anthropocene. Palgrave Macmillan, Cham, 127–151. https://doi.org/10.1007/978-3-030-23517-8_6.

Hooijer, A., & Vernimmen, R. (2021). Global LiDAR land elevation data reveal greatest sea-level rise vulnerability in the tropics. *Nature Communications*, *12*, 3592. https://doi.org/10.1038/s41467-021-23810-9.

IPCC, "Climate Change 2023: Synthesis Report. Contribution of Working Groups I, II and III to the Sixth Assessment Report of the Intergovernmental Panel on Climate Change" (IPCC, 2023); https://doi.org/10.59327/IPCC/AR6-9789291691647.

ITHACA, WFP, & DLR (2008). Myanmar: Tropical Cyclone Nargis – TerraSAR-X acquisition footprints (scheduled for May, 8th 2008). https://reliefweb.int/attachments/bcdcc378-7f8c-31df-8e66-c1d06be843de/BDA65B02003DDE36C1257442003F3724-ithaca_TC_mmr080507.pdf (last access: 7 July 2025)

Jongman, B., Ward, P. J., & Aerts, J. C. J. H. (2012). Global exposure to river and coastal flooding: Long term trends and changes. Global Environmental Change, 22(4), 823–835. https://doi.org/10.1016/j.gloenvcha.2012.07.004.

Kopp, R. E., Horton, R. M., Little, C. M., Mitrovica, J. X., Oppenheimer, M., Rasmussen, D. J., Strauss, B.H., & Tebaldi, C. (2014). Probabilistic 21st and 22nd century sea-level projections at a global network of tide-gauge sites. *Earth's Future*, *2*(8), 383–406. https://doi.org/10.1002/2014EF000239.

Kuenzer, C., Guo, H., Huth, J., Leinenkugel, P., Li, X., & Dech, S. (2013). Flood Mapping and Flood Dynamics of the Mekong Delta: ENVISAT-ASAR-WSM Based Time Series Analyses. *Remote Sensing*, *5*(2), 687–715. https://doi.org/10.3390/rs5020687.

Kulp, S. A., & Strauss, B. H. (2019). New elevation data triple estimates of global vulnerability to sea-level rise and coastal flooding. *Nature Communications*, *10*, 4844. https://doi.org/10.1038/s41467-019-12808-z.

Lichter, M., Vafeidis, A. T., Nicholls, R. J., & Kaiser, G. (2011). Exploring data-related uncertainties in analyses of land area and population in the "Low-Elevation Coastal Zone" (LECZ). *Journal of Coastal Research*, *27*(4), 757–768. https://doi.org/10.2112/JCOASTRES-D-10-00072.1.

Loucks, D. P. (2019). Developed river deltas: are they sustainable?. *Environmental Research Letters*, *14*(11), 113004. https://doi.org/10.1088/1748-9326/ab4165.

McGranahan, G., Balk, D., & Anderson, B. (2007). The rising tide: assessing the risks of climate change and human settlements in low elevation coastal zones. *Environment and Urbanization*, *19*(1), 17–37. https://doi.org/10.1177/0956247807076960.

Merkens, J. L., Reimann, L., Hinkel, J., & Vafeidis, A. T. (2016). Gridded population projections for the coastal zone under the Shared Socioeconomic Pathways. *Global and Planetary Change*, *145*, 57–66. https://doi.org/10.1016/j.gloplacha.2016.08.009.

Minderhoud, P. S. J., Coumou, L., Erkens, G., Middelkoop, H., & Stouthamer, E. (2019). Mekong delta much lower than previously assumed in sea-level rise impact assessments. *Nature Communications*, *10*(1), 3847. https://doi.org/10.1038/s41467-019-11602-1.

Myanmar Information Management Unit (MIMU) (2015). Probable Affected Village Tracts in Ayeyarwady Region. MIMU, MIMU1324v01. https://documents.themimu.info/downloads/QhCT0Hd/Map_Flood%20Affected%20Village%20Tracts-Ayeyarwady%20Reg_MIMU1324v01%2007Sep2015%20A1.pdf (last access: 22 February 2024)

Myanmar Information Management Unit (MIMU) (2020). Probable Flood Inundated Ayeyarwady and Bago (West) Region (as of 1st September 2020). MIMU, MIMU1515v01. https://documents.themimu.info/downloads/p1wVEsI/Map_Flood-Area%20in%20Ayeyarwady%20and%20Bago%20(As%20of%2001Sep)%20MIMU1515v01%2002Sep2020%20A3_ENG.pdf (last access: 22 February 2024)

Neumann, B., Vafeidis, A. T., Zimmermann, & Nicholls, R. J. (2015). Future Coastal Population Growth and Exposure to Sea-Level Rise and Coastal Flooding – A Global Assessment. *PLoS ONE*, *10*(3), e0118571. https://doi.org/10.1371/journal.pone.0118571.

Nicholls, R. J., Adger, W. N., Hutton, C. W., & Hanson, S. E. (Eds.) (2020). Deltas in the Anthropocene, Palgrave Macmillan, Cham, Switzerland, 282 pp., https://doi.org/10.1007/978-3-030-23517-8.

Nicholls, R. J., Lincke, D., Hinkel, J., Brown, S., Vafeidis, A. T., Meyssignac, B., Hanson, S. E., Merkens, JL., & Fang, J. (2021). A global analysis of subsidence, relative sea-level change and coastal flood exposure, *Nature Climate Change*, *11*, 338–342. https://doi.org/10.1038/s41558-021-00993-z.

Ohenhen, L., Shirzaei, M., Davis, J.L., Tiwari, A., Nicholls, R.J., Dasho, O., Sadhasivam, N., Seeger, K., Werth, S., Chadwick, A.J., Onyike, F., Lucy, J., Atkins, C., Daramola, S., Ankamah, A., Minderhoud, P.S.J., Yemele, G.C., in review. The Global Threat of Sinking Deltas, 07 April 2025, PREPRINT (Version 1) available at Research Square [https://doi.org/10.21203/rs.3.rs-6223150/v1].

Phongsaphan, K., Chishtie, F., Poortinga, A., Bhandari, B., Chinaporn Meechaiya, Thannarot Kunlamai, Khun San Aung, Saah, D., Anderson, E., Markert, K., Markert, A., & Peeranan Towashiraporn (2019). Operational Flood Risk Index Mapping for Disaster Risk Reduction Using Earth Observations and Cloud Computing Technologies: A Case Study on Myanmar. Frontiers in Environmental Science, 7, 191. https://doi.org/10.3389/fenvs.2019.00191.

Plink-Björklund, P. (2015). Morphodynamics of rivers strongly affected by monsoon precipitation: Review of depositional style and forcing factors. *Sedimentary Geology*, *323*, 110–147. https://doi.org/10.1016/j.sedgeo.2015.04.004.

Renaud, F. G., Syvitski, J. P., Sebesvari, Z., Werners, S. E., Kremer, H., Kuenzer, C., Ramesh, R., Jeuken, A., & Friedrich, J. (2013). Tipping from the Holocene to the Anthropocene: How threatened are major world deltas?. *Current Opinion in Environmental Sustainability*, *5*(6), 644–654. https://doi.org/10.1016/j.cosust.2013.11.007.

Schmitt, R. J. P., & Minderhoud, P. S. J. (2023). Data, knowledge, and modeling challenges for science-informed management of river deltas. *One Earth*, *6*(3), 216–235. https://doi.org/10.1016/j.oneear.2023.02.010.

Schneider, P., & Asch, F. (2020). Rice production and food security in Asian Mega deltas—A review on characteristics, vulnerabilities and agricultural adaptation options to cope with climate change. *Journal of Agronomy and Crop Science*, *206*(4), 491–503. https://doi.org/10.1111/jac.12415.

Scown, M. W., Dunn, F. E., Dekker, S. C., van Vuuren, D. P., Karabil, S., Sutanudjaja, E. H., Santos, M.J., Minderhoud, P.S.J., Garmestani, A.S., & Middelkoop, H. (2023). Global change scenarios in coastal river deltas and their sustainable development implications. *Global Environmental Change*, *82*, 102736. https://doi.org/10.1016/j.gloenvcha.2023.102736.

Small, C., & Nicholls, R. J. (2003). A global analysis of human settlement in coastal zones. *Journal of Coastal Research*, 584–599. https://www.jstor.org/stable/4299200.

Small, C., Sousa, D., Yetman, G., Elvidge, C., & MacManus, K. (2018). Decades of urban growth and development on the Asian megadeltas. *Global and Planetary Change*, *165*, 62–89. https://doi.org/10.1016/j.gloplacha.2018.03.005.

Smith, K., Fearnley, C.J., Dixon, D., Bird, D.K., & Kelman, I. (2023). Environmental Hazards: Assessing Risk and Reducing Disaster (7th ed.). Routledge. https://doi.org/10.4324/9781351261647.

Stanley, D. J., & Warne, A. G. (1997). Holocene sea-level change and early human utilization of deltas. *GSA Today*.

Syvitski, J. P., Kettner, A. J., Overeem, I., Hutton, E. W., Hannon, M. T., Brakenridge, G. R., Day, J., Vörösmarty, C., Saito, Y., Giosan, L., & Nicholls, R. J. (2009). Sinking deltas due to human activities. *Nature Geoscience*, *2*(10), 681–686. https://doi.org/10.1038/ngeo629.

Tessler, Z. D., Vörösmarty, J., Grossberg, M., Gladkova, I., Aizenman, H., Syvitski, J. P. M., & Foufoula-Georgiou, E. (2015). Profiling risk and sustainability in coastal deltas of the world. *Science*, *349*(6248), 638–643. https://doi.org/10.1126/science.aab3574.

Tessler, Z. D., Vörösmarty, C. J., Overeem, I., & Syvitski, J. P. (2018). A model of water and sediment balance as determinants of relative sea level rise in contemporary and future deltas. *Geomorphology*, *305*, 209–220. https://doi.org/10.1016/j.geomorph.2017.09.040.

United Nations Office for Disaster Risk (UNISDR), 2017. Coastal Erosion Hazard and Risk Assessment. https://www.preventionweb.net/files/52828_07coastalerosionhazardandriskassess.pdf (last access: 7 July 2025)

United Nations Office for Disaster Risk Reduction (UNDRR). 2017a. The Sendai Framework Terminology on Disaster Risk Reduction. "Hazard". https://www.undrr.org/terminology/hazard. (last access: 7 July 2025)

United Nations Office for Disaster Risk Reduction (UNDRR). 2017b. The Sendai Framework Terminology on Disaster Risk Reduction. "Exposure". https://www.undrr.org/terminology/exposure. (last access: 7 July 2025)

United Nations Office for Disaster Risk Reduction (UNDRR). 2017c. The Sendai Framework Terminology on Disaster Risk Reduction. "Vulnerability". https://www.undrr.org/terminology/vulnerability. (last access: 7 July 2025)

UNOSAT (2015). Flood Waters Near City of Yangon, Myanmar (10 Aug 2015). https://reliefweb.int/attachments/9b42a7be-91b8-39e5-a59f-0e602863dd7a/UNOSAT_A3_20150703MMR_Portrait_Yangon_South.pdf (last access: 22 February 2024)

van de Vijsel, R. C., Scheffer, M., & Hoitink, A. J. (2024). Tipping points in river deltas. *Nature Reviews Earth & Environment*, 1–16. https://doi.org/10.1038/s43017-024-00610-5.

Ward, P. J., de Perez, E. C., Dottori, F., Jongman, B., Luo, T., Safaie, S., & Uhlemann-Elmer, S. (2018). The Need for Mapping, Modeling, and Predicting Flood Hazard and Risk at the Global Scale. In: Schumann, G. JP., Bates, P. D., Apel, H., & Aronica, G. T. (2018). Global Flood Hazard – Applications in Modeling, Mapping, and Forecasting. American Geophysical Union, Washington D.C., 1–18. https://doi.org/10.1002/9781119217886.ch1.

Webster, P. J. (2008). Myanmar's deadly daffodil. *Nature Geoscience*, *1*, 488–490. https://doi.org/10.1038/ngeo257.

Woodruff, J. D., Irish, J. L., & Camargo, S. J. (2013). Coastal flooding by tropical cyclones and sea-level rise. *Nature*, *504*(7478), 44–52. https://doi.org/10.1038/nature12855.

Wu, P. C., Wei, M., & D'Hondt, S. (2022). Subsidence in coastal cities throughout the world observed by InSAR. *Geophysical Research Letters*, *49*(7), e2022GL098477. https://doi.org/10.1029/2022GL098477.

2 Coastal flooding in Asian megadeltas: Recent advances, persistent challenges, and call for actions amidst local and global changes

Chapter 2 is related to: Becker, M., **Seeger, K.**, Paszkowski, A., Marcos, M., Papa, F., Almar, R., Bates, P., France-Lanord, C., Hossain, Md S., Khan, Md J.U., Karegar, M.A., Karpytchev, M., Long, N., Minderhoud, P.S.J., Neal, J., Nicholls, R.J., Syvitski, J., 2024. *Coastal Flooding in Asian Megadeltas: Recent Advances, Persistent Challenges, and Call for Actions Amidst Local and Global Changes*. Reviews of Geophysics, 62 (4), e2024RG000846. https://doi.org/10.1029/2024RG000846.

The scientific article is published under a CC-BY-NC-ND 4.0 Attribution-NonCommercial-NoDerivatives 4.0 International licence (https://creativecommons.org/licenses/by-nc-nd/4.0/) and is therefore not included as a chapter in the thesis publication. The reader is referred to access the content of this chapter via the article doi provided above. Throughout this thesis, any references to headings, figures and tables of this chapter/article are prefixed with ‘2’.

Data availability statement: No new data was created or used for this research.

3 Evaluating flood hazards in data-sparse coastal lowlands: highlighting the Ayeyarwady Delta (Myanmar)

Abstract: Coastal lowlands and river deltas worldwide are increasingly exposed to coastal, pluvial and fluvial flooding as well as relative sea-level rise (RSLR). However, information about both single and multiple flood-type hazards, their potential impact and the characteristics of areas, population and assets at risk is often still limited as high-quality data either does not exist or is not accessible. This often constitutes a main barrier for generating sound assessments, especially for scientific and public communities in the so-called Global South. We provide a standardised, integrative approach for the first-order assessment of these single and multiple flood-type hazards and show how this can be conducted for data-sparse, hardly accessible and inaccessible coastal lowlands such as the Ayeyarwady Delta in Myanmar by using only open accessible and freely available datasets of satellite imagery, global precipitation estimates, satellite-based river discharge measurements, elevation, land use, and population data. More than 70 % of the delta, mainly used for agriculture, and about 40 % of its present population are prone to flooding due to either monsoon precipitation and runoff, storm surge, and RSLR, or their combination, jeopardising food security and economic development in the region. The approach allows for the integration and combination of various datasets, combined in a highly flexible workflow that performs at low computational capacities, supporting the evaluation of flood-prone areas on regional and local scale for data-sparse coastal lowlands worldwide. It thereby allows to attribute different types of flood hazards, complements concepts of vulnerability and risk, and supports risk-informed decision making and development of effective multi-flooding adaptation strategies.

Keywords: flooding, coastal lowlands, river deltas, monsoon, relative sea-level rise, storm surge

Chapter 3 is related to: **Seeger, K.**, Peffeköver, A., Minderhoud, P.S.J., Vogel, A., Brückner, H., Kraas, F., Nay Win Oo, Brill, D., 2024. *Evaluating flood hazards in data-sparse coastal*

lowlands: highlighting the Ayeyarwady Delta (Myanmar). Environmental Research Letters, 19 (8), 084007. https://doi.org/10.1088/1748-9326/ad5b07.

The scientific article is published under a CC-BY 4.0 Attribution 4.0 International licence (http://creativecommons.org/licenses/by/4.0/). The reader can access the content of this chapter also via the article doi provided above. The article material was not modified; only the thesis layout was adopted.

3.1 Introduction

With ongoing climate change, consequently rising sea level and shifting patterns of atmospheric circulation and extreme weather events, coastal lowlands are increasingly exposed to flood hazards. Globally, 2.23 million km^2 and up to 290 million people were affected by floods between 2000 and 2018 (Tellman et al., 2021). Especially large and densely populated river deltas, many of them located in tropical Southeast Asia, are among the most threatened and constitute areas of high exposure and vulnerability (Woodruff et al., 2013; Tessler et al., 2015; Hill et al., 2020; Hooijer and Vernimmen, 2021). According to Edmonds et al. (2020), 89 % of the global delta population (estimated to 302 million of in total 340 million of 2017 population) lives in regions with tropical cyclone (TC) activity and from the 76 million people which would be directly affected by a 100 year flood, 41 % (~31 million) live in deltas (Edmonds et al., 2020). These numbers reflect lower-end estimates as estimations of global delta populations count to ~500 million or even more (Syvitski et al., 2022; Schmitt and Minderhoud, 2023; Becker et al., 2024). Relative sea-level rise (RSLR) adds on this exposure, driving and increasing coastal flood frequency and shoreline retreat also in areas where cyclone activity is comparably low (Woodruff et al., 2013). As already moderate RSLR of 1 m would increase the present global population at risk to 410 million, ~60 % living in tropical Asia (Hooijer and Vernimmen, 2021), Kulp and Strauss (2019) estimate up to 630 million people (of 2010) to be affected by flooding by 2100 due to extreme water levels on top of SLR scenarios of high representative concentration pathways. However, as population growth is projected for many coastal lowlands in the world, particularly in Asia and Africa, these numbers provide only minimum estimates and might be exceeded already by the mid of the 21st century (Neumann et al., 2015). This holds especially true as these studies did not account for the contribution of

vertical land motion, while land subsidence currently affects~20 % of the world's population (Herrera-García et al., 2021), many of them living in densely populated deltaic areas where highest RSLR occurs (Nicholls et al., 2021). Unlike extreme water levels due to storm surge and RSLR that—in terms of cyclones—may occur on annual time scales, or—in terms of RSLR—will become effective over decades, tides constitute a coastal flood type of daily frequency. High tides in coastal lowlands regularly lead to flooding, often up to several kilometres inland (e.g. Marfai and King, 2008; Kuenzer et al., 2013), and dominate many of the world's deltas (Goodbred and Saito, 2012), where they add on elevated water levels from surges and waves while their constituents being altered by RSLR (Pickering et al., 2017). Furthermore, tsunamis also pose a coastal hazard as they constitute high-energy wave events caused by submarine earthquakes, submarine failures or flank collapses, or meteorological forces (Röbke and Vött, 2017). However, their timing occurs on much larger recurrencies, i.e. in the range of centuries (e.g. Brill et al., 2011), and their assessment involves large uncertainties stemming from uncertainties in underlying scenario parameters (e.g. moment magnitudes of such low-frequency events; Davies et al., 2018 and references therein).

Besides these coastal flood hazards, river deltas are exposed to flooding from the hinterland, which is induced by high discharges, thereby increasing inundation extents in case these inland floods occur simultaneously to other flood types. Particularly river basins characterised by a tropical monsoon climate show high annual discharge variabilities that follow the seasonal monsoon precipitation pattern (Hansford et al., 2020) and have experienced serious flooding (e.g. Islam et al., 2010; Syvitski and Brakenridge, 2013). Livelihoods of 60 % of the world's population are directly affected by the Asian monsoon (Plink-Björklund, 2015). In this region, most of the population concentrates along large South- and Southeast-Asian rivers and their deltas, such as the Ganges–Brahmaputra–Meghna, the Chao Phraya, Mekong and Ayeyarwady (WorldPop and CIESIN, 2018), and all of them were affected by catastrophic flooding in the recent past (Cosslett and Cosslett, 2014; Liew et al., 2016; Brakenridge et al., 2017; Krien et al., 2017).

The Ayeyarwady Delta in Myanmar was severely affected by the storm surge of category-4 TC Nargis in 2008 that caused >138 000 fatalities (Webster, 2008; Fritz et al., 2009), and the exceptional monsoon flooding in 2015 that affected >530 000 ha agricultural and aquacultural land (Government of the Union of Myanmar, 2015). However, information on flood exposure and hazards is still limited (e.g. Table B1; Brakenridge et al., 2017; Phongsaphan et al., 2019) and spatio-temporal patterns of floods have been only addressed by emergency mappings from

international initiatives (ITHACA et al., 2008; Copernicus Emergency Management Service, 2015; UNOSAT, 2015) or national institutions (e.g. Myanmar Information Management Unit (MIMU), 2015, 2020), rather than being systematically studied by scientific endeavours and other efforts using decentralised information and following standardised data organisation pathways. So far, flood hazard and risk maps only exist on township level but do not provide information on local-scale characteristics, nor distinguish different types of flood hazards (Phongsaphan et al., 2019) or they only delineate zones in specific urbanised areas that will be inundated in case of a 'Nargis'-like flood and a 100 yr probability (ICHARM et al., 2016a, 2016b, 2016c, 2016d). Similarly, areas, people, and assets at risk of both inland and coastal flooding have been only partially addressed so far (Brakenridge et al., 2017; Heinkel et al., 2022), mainly by large-scale models (Dottori et al., 2016; Tierolf et al., 2021), while on local scale, RSLR has been shown to cause major parts of the delta to fall below sea level in the coming decades (Seeger et al., 2023a) and thus constitutes a substantial determinant of future flood risk.

For other data-sparse coastal lowlands, where comparably more information is available, some regional-scale flood hazard and risk assessments were generated for entire river basins. For example, Sriariyawat et al. (2022) identified areas at risk of flooding from rainfall and runoff in the Chao Phraya Basin based on simulated flood inundation and duration while Shakti et al. (2020) addressed pluvial flooding in the Chao Phraya Basin based on 100 yr, 200 yr, and 500 yr return periods estimated from rain gauge measurements. Although indicating a flood risk assessment, neither societal nor socio-economic variables were considered, thereby underscoring the wide range of how exposure, hazard, vulnerability, and risk are defined and consequently handled in related research and assessments. For the Ganges–Brahmaputra–Meghna Delta, efforts have been undertaken to investigate the impact of multiple flood hazards on the delta as Rahman et al. (2019) modelled storm surge inundation in combination with SLR scenarios to report the effects on population and the Sundarban mangroves. Still for several local to regional hazard assessments in data-sparse coastal lowlands, the linkages between flood exposure and environmental characteristics such as local elevation and geomorphological features have not been adequately addressed. These physical characteristics have rarely been quantified or qualitatively assessed, which is partly due to the insufficient spatial resolution and focus of those assessments.

The above examples show that existing flood hazard assessments in data-sparse coastal lowlands are often incomplete as they (1) do not distinguish different flood types and their

combination in terms of compound flooding, (2) do not cover entire, hydrologically-connected low-lying landscapes (such as deltas), (3) are not sufficiently spatially resolved, (4) are not up to date and miss new available information and data, or (5) require measurement data for validation (e.g. ICHARM, 2016a, 2016b, 2016c, 2016d; Hein Min Htet et al., 2017; Ikeuchi et al., 2017). Global flood hazard assessments cannot fill these gaps as they are comparably coarse and typically involve data processing that, if applied on smaller scales, would introduce substantial errors and therefore should not be applied on regional or local scale (Jongman et al., 2012) but requires validation with observational data (e.g. Ward et al., 2018; Maranzoni et al., 2023). They also tend to exclude data-sparse coastal lowlands since these are often not covered by the input datasets used (Eilander et al., 2020). As a result, information on flood exposure and hazards is limited in many densely populated coastal areas in the world. Here, high-quality data either does not exist or is not accessible which often constitutes a main barrier for generating sound assessments and developing risk mitigation strategies, especially for scientific and public communities in the so-called Global South.

In this study, we present a standardised, integrative approach to generate a first-order assessment of both single and multiple flood-type hazards for data-sparse, poorly accessible and inaccessible coastal lowlands by combining various open and publicly available datasets and software. The approach yields information on spatial patterns as well as population and assets at risk. It thereby forms the basis for follow-up focus studies and enables stakeholders from all fields of action to generate flood hazard assessments as a basis for risk mitigation strategies. We highlight the applicability of our approach by using the example of the Ayeyarwady Delta in Myanmar as this region suffers from data paucity and severe difficulties in accessibility due to political restrictions and recent conflicts. We demonstrate the generation of a thorough understanding of the exposure of areas and population to flood hazards by (a) unravelling monthly flooding activity in the Ayeyarwady Delta in the era of Sentinel-1 imagery; (b) investigating single-type flood hazards in the delta such as monsoon and storm surge flooding, and RSLR; (c) identifying and characterising areas prone to both inland and coastal flooding, as well as RSLR; and (d) placing the findings from (a) to (c) into the broader context with implications for other data-sparse coastal areas. Therewith, our workflow proves successful in attributing different types of flood hazards, ranking exposed areas, and offers valuable insights for vulnerability and risk assessments as base for risk-informed management decisions.

3.2 Material and methods

The extents of recent flood events were mapped using free-available Sentinel-1 data which offers actively sensed earth observation imagery at high spatiotemporal resolution, being highly proficient to capture flood events independent of daylight and weather conditions. Flooding in the Ayeyarwady Delta during the last ~10 years was mainly associated with monsoon precipitation and river discharge. For this reason, our investigations focused on months of the monsoon season, i.e. from May to October. Monthly flood extents were mapped for the years of 2015–2023 using the cloud computing platform of Google Earth Engine (GEE; Gorelick et al., 2017) and a pixel-based image rationing approach following the open accessible GEE script of the United Nations Platform for Space-based Information for Disaster Management and Emergency Response (UN-SPIDER) program (UN-SPIDER, no date). A detailed description of the applied GEE script settings and data processing to obtain monthly flood extents in the Ayeyarwady Delta is given in Appendix B.

The individual monthly flood maps were summed (i) for all months of individual years of the investigation period (2015–2023), (ii) for individual months of all years, and (iii) for all months of the entire investigation period (2015–2023). To better understand the spatio-temporal pattern of the floodings mapped, we supplemented our investigations by open-source freely available precipitation data from the GPM IMERG Final Precipitation L3 v.6.0 product (0.1° × 0.1°) and runoff data from River and Reservoir Watch version 4.5 (Figures 3.1 and B1–B9; Huffman et al., 2019; Brakenridge et al., 2023a, 2023b, 2023c).

To exemplify the suitability of the approach for assessing the hazard of multiple flood types and providing a glimpse towards their impacts in the future, we studied both storm surge flooding and RSLR in the Ayeyarwady Delta separately and investigated their combination with monsoon flooding. To determine areas at risk of storm surge, we used the flooding extent of the storm surge of TC Nargis 2008 which directly hit the delta. The related data was obtained via the freely accessible global flood database from Tellman et al. (2021). To consider RSLR in the hazard assessment, we used a RSLR scenario of 1 m to map areas falling below sea level based on a locally improved FABDEM from Seeger et al. (2023b). The exposure to multiple flooding was assessed through two scenarios: The short-term scenario included monsoon flood frequency and storm surge flooding while the mid- to long-term scenario also integrated the impact of RSLR. To characterise assets that nowadays would be affected by those hazards, we used the local land-use land cover (LULC) dataset of Vogel et al. (2022) for the year 2021.

Latest available WorldPop data (i.e. for the year 2020; Bondarenko et al., 2020) was used to estimate population exposed to flooding. All post-processing investigations were performed in GIS on all single-type flood maps (i.e. monsoon flood frequencies, storm surge, and RSLR) and two scenarios of multiple flood hazards (i.e. the combination of monsoon and storm surge, and the combination of monsoon, storm surge and RSLR; Figure 3.1).

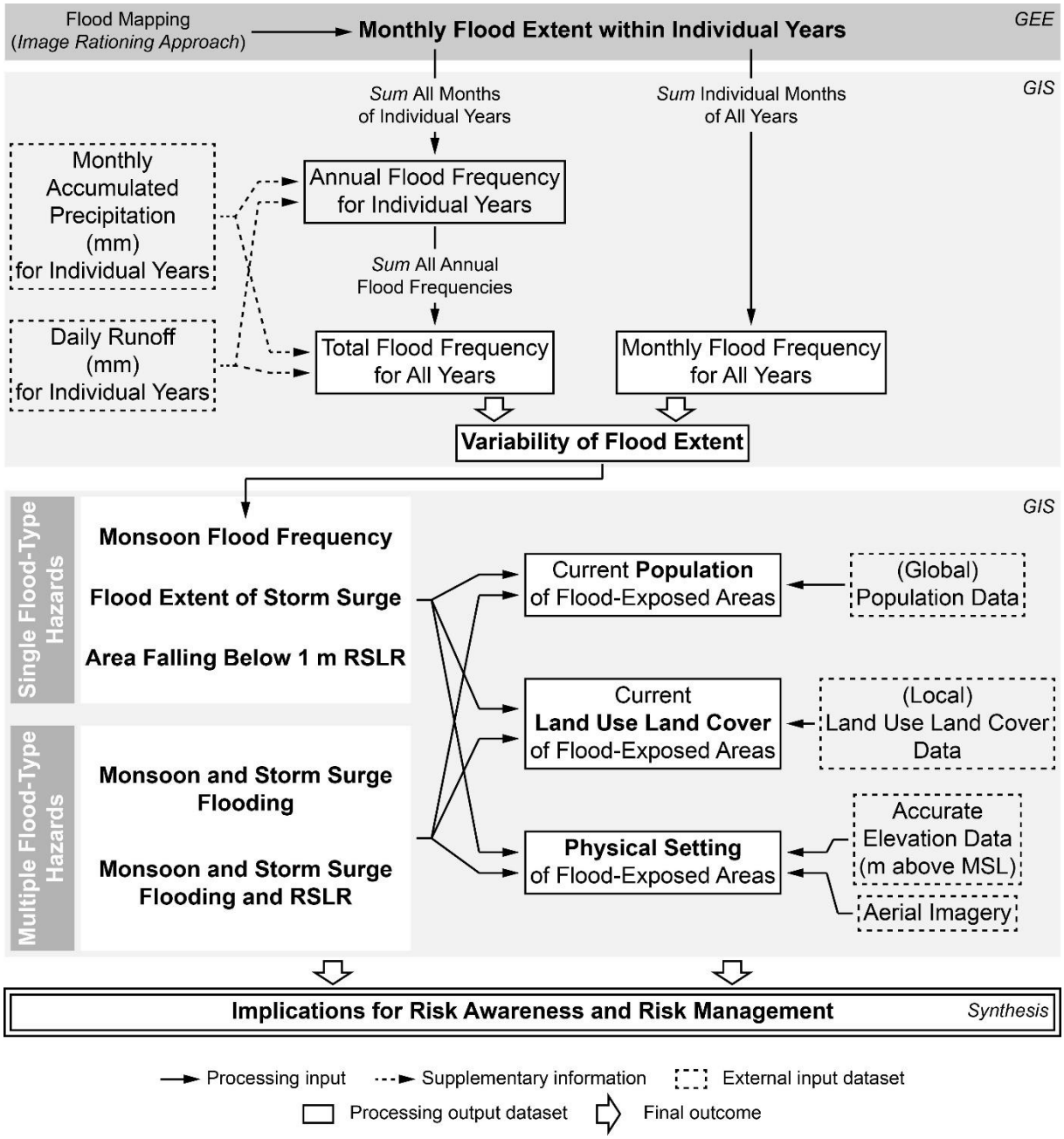


***Figure 3.1** | Workflow to perform flood hazard mapping and exposure analysis in data-sparse coastal lowlands such as the Ayeyarwady Delta in Myanmar (GEE = Google Earth Engine, GIS = Geographic Information System).*

3.3 Results and discussion

3.3.1 Flood exposure of the Ayeyarwady Delta

Our systematic mapping approach delivers detailed information about the flooding history of the last ~10 years and characterises areas in the delta that are frequently flooded in terms of their exposure by today's population and land use. Except of few outcrops and parts in the western and eastern delta margins, the entire delta is prone to (regular) flooding.

3.3.1.1 Exposure to single flood-type hazards

Monsoon flooding constitutes the most frequent flood hazard in the Ayeyarwady Delta, affecting ~60 % of the delta where ~43 % (~5.4 million people) of the current delta population live (Figures 3.2, 3.3 and B1–B12). Flood frequency is highest in Pathein District as more than 5 250 people of~786 000 people exposed in the district are prone to flooding every month of the monsoon season (Figure B14). Especially Hinthada, Thayarwady, and Ma-ubin Districts in the upper and central delta as well as Pyapon District are among the most frequently and extensively flooded (~64 %–71 %) whereas population counts indicate that the majority is not exposed (Figure B14).

Though ~73 %–77 % of the population in the districts of Yangon seem to be unaffected by monsoon flooding, generally higher population densities in these districts compared to other deltaic ones result in substantially higher absolute population amounts of ~1.8 million people, most of them being based in Yangon North. However, relatively, the administrative districts of Labutta and Myaungmya show the highest exposure as most people live in areas being flooded several months a year (Figures 3.2 and B14).

Assets at risk are mainly agricultural crops (Figure 3.3). With increasing flood frequency, mainly irrigated areas are flooded. However, as our mapping approach does not allow for the differentiation between intended vs. unintended flooding, and cropping seasons and patterns vary annually, we cannot further characterise whether the exposed irrigated crops are assets with potential loss due to flooding. To a lesser extent, monsoon flooding also affects other economic sectors such as aquaculture and mineral extraction through brine ponds as well as shrubland (Figures 3.3 and B14).

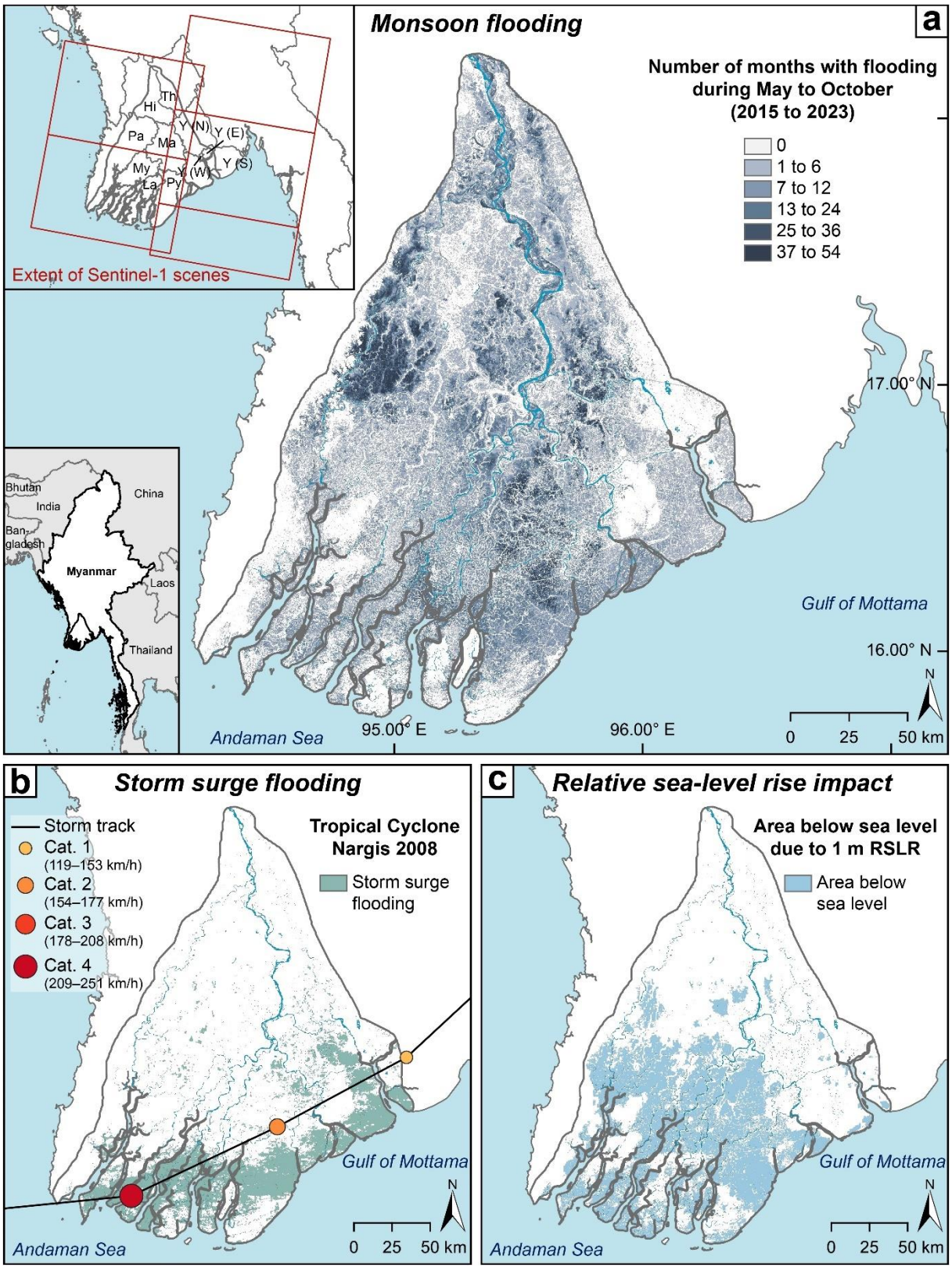


Figure 3.2 | *Exposure of the Ayeyarwady Delta in Myanmar to single types of flooding. Flood hazards include (a) monsoon flooding, which was mapped over the entire Sentinel period from 2015 to 2023 based on scene extents shown in the inset, (b) storm surge flooding by using the extent of the disastrous flood of tropical cyclone Nargis in 2008 (track and intensity data as well as flood extent information obtained from the Joint Typhoon Warning Center (2023) and Tellman et al. (2021)), and (c) a scenario of 1 m relative sea-level rise (RSLR) based on the locally adjusted FABDEM (Seeger et al., 2023b). Administrative districts are abbreviated by their first two letters (Hi = Hinthada, La = Labutta, Ma = Ma-ubin, My = Myaungmya, Pa = Pathein, Py =*

Pyapon, Th = Thayarwady, Y (E) = Yangon East, Y (N) = Yangon North, Y (S) = Yangon South, Y (W) = Yangon West).

Given only ~2 % of the entire delta are covered by urbanised areas, and several small settlements in the delta are located outside areas flooded during the monsoon season (Figure B13(e)), they are relatively less exposed. However, built-up areas are particularly at risk in Yangon East and West where they constitute up to ~50 % of frequently flooded areas (Figure B14).

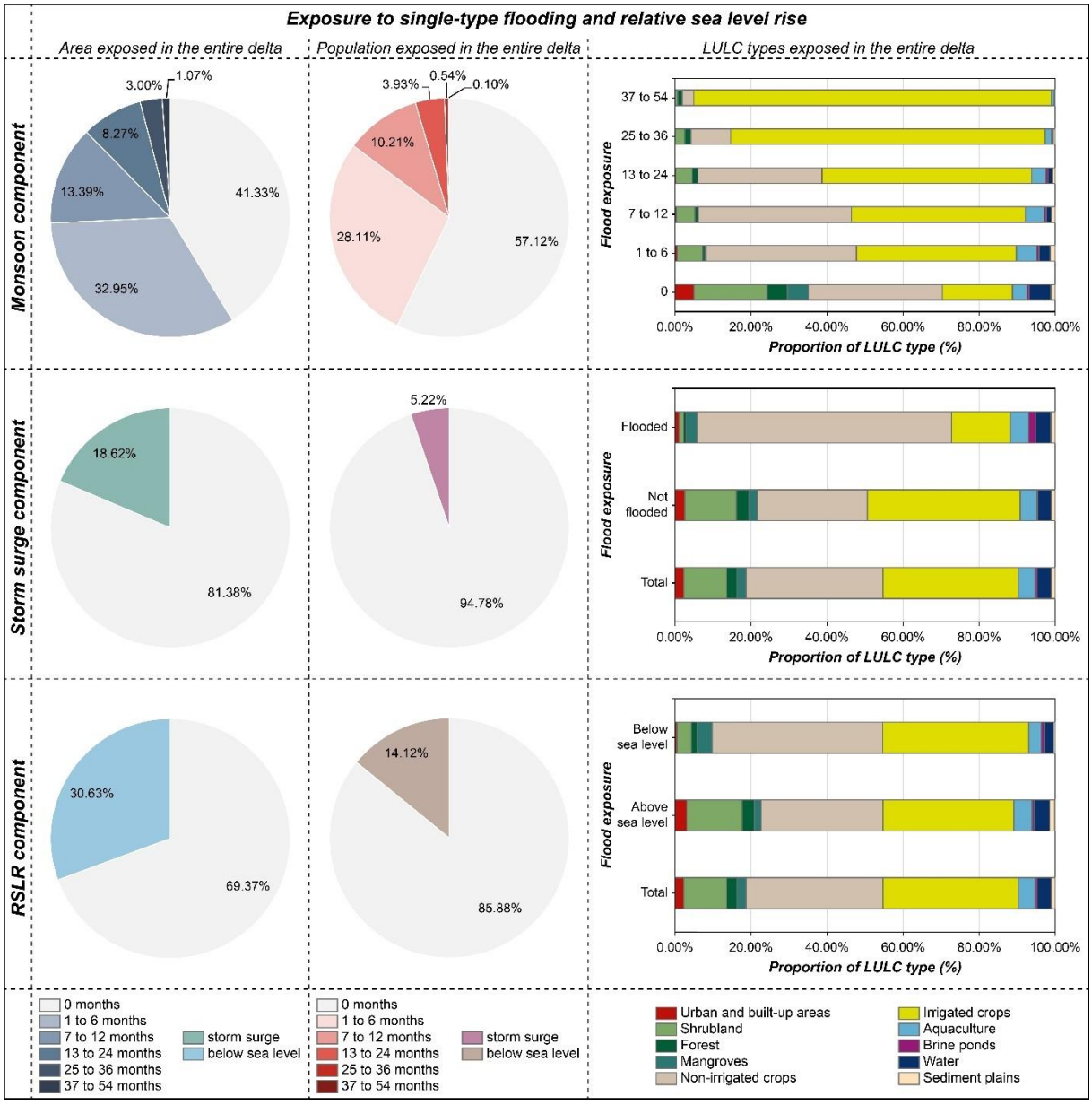


Figure 3.3 *| Exposure of area, population, and land-use properties to single-type flooding and relative sea-level rise (RSLR).*
Population counts are based on WorldPop data from 2020 (Bondarenko et al., 2020) and information on land-use land cover (LULC) was obtained from Vogel et al. (2022). Note that numbers on the y axis of LULC graphs indicate months of monsoon flooding.

Monthly and interannual flood frequency and duration vary, ranging from water-saturated soils to extensively flooded depressions and reactivated cut-off meanders, being subject to precipitation amount and intensity, runoff and discharge as well as infiltration capability of the soils (Figure B13; Brakenridge et al., 2017). Between years, variability in flood duration and/or frequency depend on the combination of onset, intensity, and duration of the monsoon season whereas the spatial flood pattern varies less being dominated by the effects of local topography where depressions are longer/more often flooded (Figure B13), and properties of underlying soils (mainly gleysols and fluvisols that will be waterlogged; FAO and UNESCO, 1976). In contrast, exposure to monsoon flooding also varies within the monsoon season due to a shift of control from a precipitation-dominated pattern in the first months (May to July), affecting the entire delta and causing delta-wide flooding and water saturation of soils, to a runoff-dominated pattern (July to October) where water flow results in flooding of particular areas such as topographic depressions (Figures B1–B13). Consequently, this dynamic variability of flooding needs to be taken into account when considering the annually occurring, and therefore well-assessable monsoonal hazard in flood risk assessments.

Compared to monsoon flooding, affecting both inland and coastal areas, storm surge and RSLR are coastal hazards that may propagate inland depending—in case of storm surge—on incidence angle during landfall, wind direction, surge and wave heights, and—especially in terms of RSLR—on land elevation with respect to the sea. In this sense, the storm surge of TC Nargis constitutes a worst-case scenario as the 5 m surge compounded with 2 m storm waves led, together with tides, up to 50 km inland propagation of water masses, ~50–100 m coastline retreat, and ~1 m of vertical erosion (Figure 3.2; Fritz et al., 2009; Tasnim et al., 2015; Besset et al., 2017). In total, >6 200 km^2 were flooded, highlighting the exposure of ~20 % of the delta and ~658 000 people currently living there (~5 % of the entire delta population), of which Labutta, Pyapon and Yangon South show the highest susceptibility with up to ~50 % of the districts' area and ~462 700 people being exposed (Figures 3.2, 3.3 and B15). Properties at risk are more diverse than for the monsoon hazard which is mainly due to the fact that agricultural production is adapted to regular monsoon flooding (that serves for intended flooding in contrast to extreme monsoon floods that will cause damage). A storm surge will largely hit parts of the delta used to produce non-irrigated crops (~67 %), and to lesser extent irrigated crops (~15 %), aquaculture (~5 %), brine ponds and urban areas (~1 %), respectively (Figures 3.3 and B15). While the coincidence of storm surge flooding with water bodies in inland districts reflect the upstream migration of the surge in the river, those LULC types constitute major sources of

income for the delta population and have implications for economic development in the region. The economic sectors show different susceptibilities on district scale, thus calling for local to regional measures to reduce the vulnerability of urban spaces in Yangon West and East, cropland and brine ponds in Pathein, Pyapon, Yangon South and Labutta, as well as aquaculture in Ma-ubin, Yangon North and South (Figure B15).

RSLR constitutes a hazard to coastal lowlands like the Ayeyarwady Delta that is often not considered but is projected to lead to permanent loss of land and consequently challenge sustaining housing and livelihoods of the population. Using 1 m RSLR is a realistic scenario backed up by latest IPCC AR6 projections for 2100 (Fox-Kemper et al., 2021; Garner et al., 2021, 2022). However, as the delta is subsiding up to several centimetres per year (van der Horst et al., 2018; Seeger et al., 2023c), RSLR in sinking areas is higher than projected by the IPCC and impacts may already be noticeable sooner than 2100, i.e. over years to decade(s). We here focus on one of the currently most reliable elevation datasets and document ~30 % of the delta to fall below 1 m RSLR (Figures 3.2 and 3.3; Seeger et al., 2023a; Seeger et al., 2023b). Both coastal and inland areas are exposed, mainly in the districts of Myaungmya (~65 %), Pyapon (~63 %) and Labutta (~57 %; Figures 3.3 and B16). About 14 % of today's delta population (~1.8 million people) will be directly affected; however, population in highly exposed districts already amounts up to ~50 %, respectively (together accounting for >1 million people; Figure B16), and slightly higher RSLR scenarios will pose substantially more people at risk (Seeger et al., 2023a).

The land-use pattern in the low-lying areas at risk of 1 m RSLR differs only slightly from those exposed to storm surge as the spatial extent of both flood types largely overlap (see section 3.3.1.2). About 83 % constitute non-irrigated and irrigated crops (Figure 3.3). In most districts, the lowly-elevated areas prone to RSLR impacts are characterised by more built-up areas than those exposed to Nargis storm surge or monsoon flooding (Figures B14–B16), thereby implying the increasing risk in case urban growth towards small cities in the southern delta continues as observed for the past decades (Vogel et al., 2022).

3.3.1.2 Exposure to multiple flood-type hazards

To generate a holistic understanding of flood hazards in the delta and to characterise the overall exposure of deltaic areas, a synergistic perspective combining individual flood hazards and information about them is required. About 64 % of the area and ~32 % of the population are exposed to multiple, short-term flooding events (Figures 3.4 and 3.5).

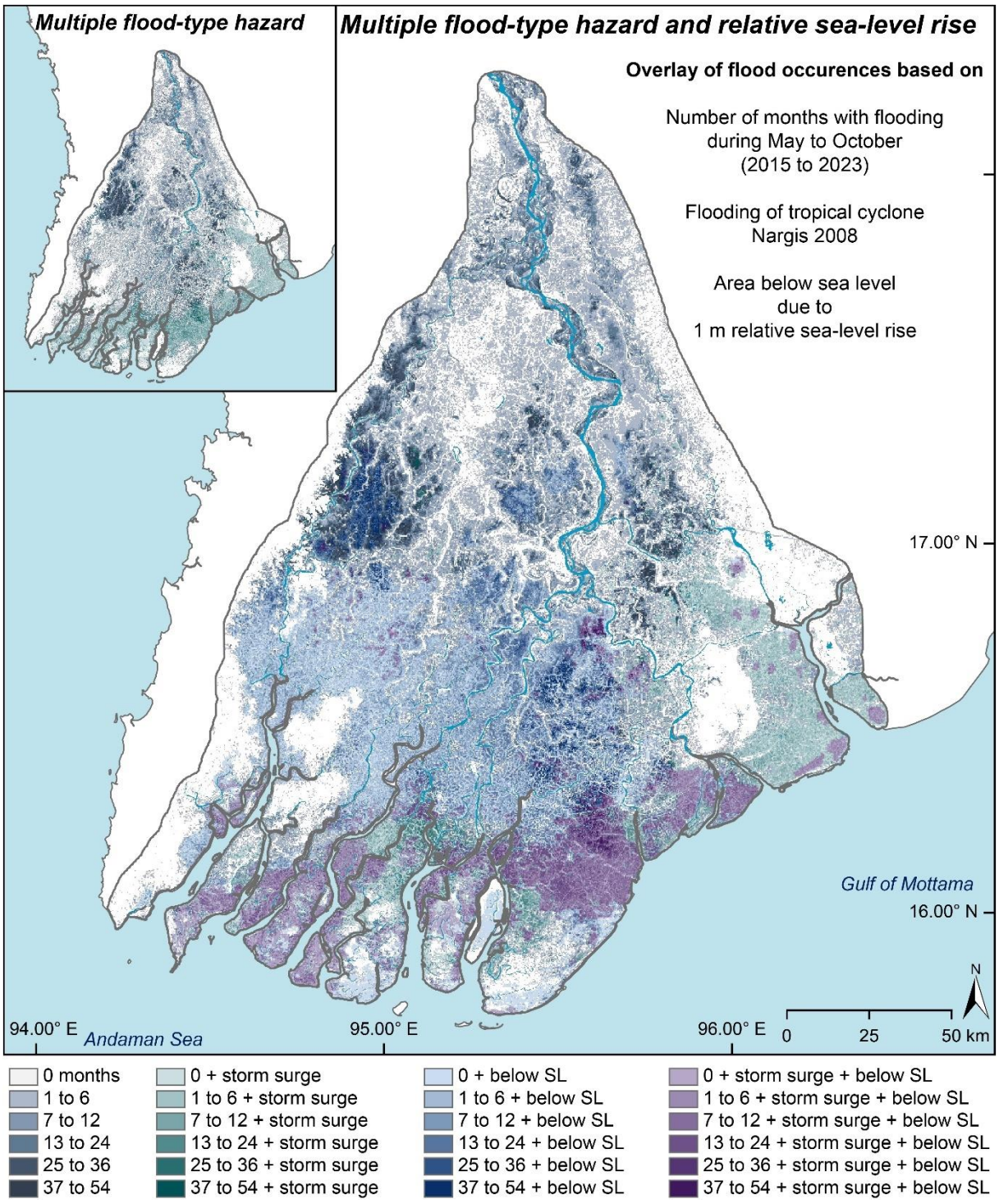


Figure 3.4 *| Exposure of the Ayeyarwady Delta in Myanmar to multiple types of flooding and relative sea-level rise (SL = sea level).*

Approximately 70 % of the area prone to storm surge is regularly flooded during the monsoon season, an area currently inhabited by ~294 400 people (~42 % of the delta population) and mainly used for agricultural production (Figure B17). In relative terms, multiple flood risk is highest for Pyapon, Labutta and Yangon South, of which Yangon South has the highest

population exposed while Pyapon denotes the largest area with land-use properties at risk (Figure B18).

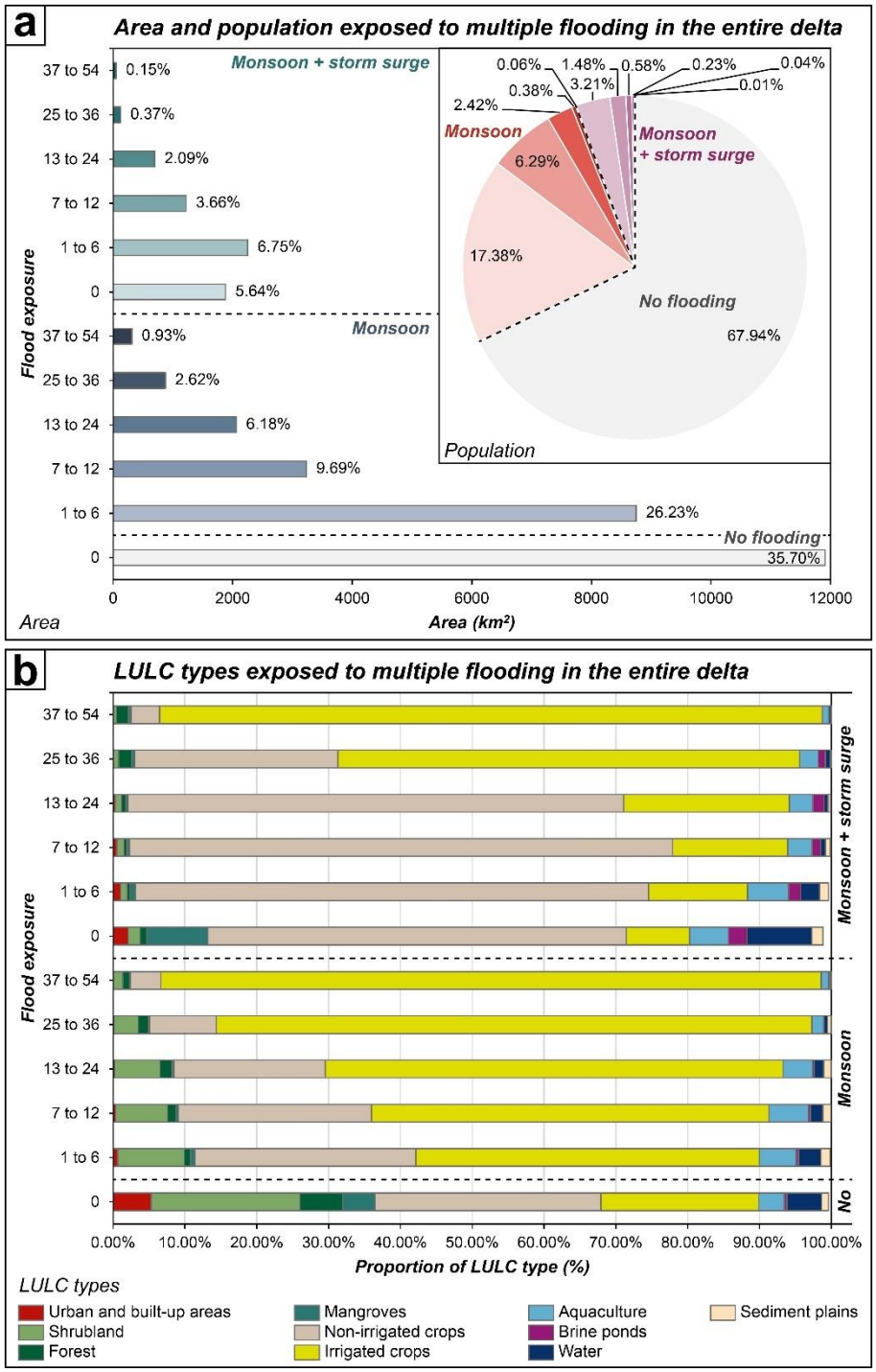


Figure 3.5 | *Exposure of area, population, and land-use properties to multiple flooding from monsoon and storm surge. Note that numbers on the y axis indicate months of monsoon flooding.*

Including 1 m RSLR allows for a rough estimate of mid- to long-term flood exposure towards the future and highlights the susceptibility of >36 % of the deltaic area to both coastal and inland flood hazards, especially in the southernmost districts in the delta (Figures 3.4, 3.6 and B20). From ~2 million people currently living in this zone (~16 % of 2020's total delta population),

~1.4 million live within the highly exposed districts of Pyapon (~53 %; ~498 800), Labutta (~59 %; 335 700), Myaungmya (~47 %; 334 300) and Pathein (~18 %; 241 600).

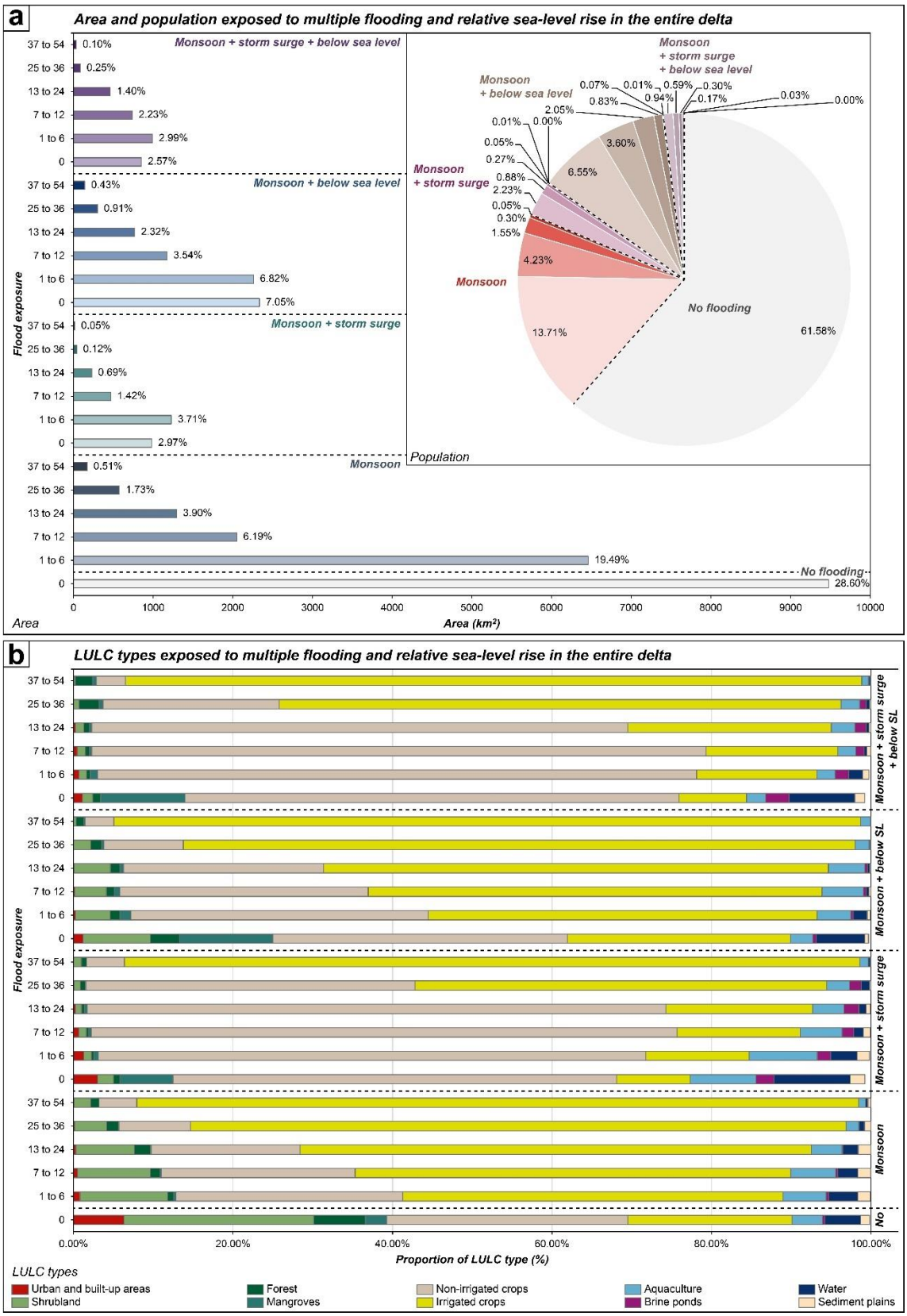


***Figure 3.6** | Exposure of area, population, and land-use properties to multiple flooding and relative sea-level rise. Note that numbers on the y axis indicate months of monsoon flooding (SL = sea level).*

The zone exposed to all three hazard types covers an area of ~7 % in the delta currently inhabited by ~137 600 people (~2 %; Figure 3.6). Pyapon and Labutta would be the most affected districts, both in terms of flood extent (~26 % of Pyapon; ~16 % of Labutta) and exposed population (~57 700 in Pyapon; ~30 900 in Labutta), followed by Pathein and Myaungmya (Figures B19 and B20). Recent studies in the delta revealed between 10 and >30 mm/yr of land subsidence in these parts (2017–2023; Seeger et al., 2023c), thereby implying an increasing risk in the future if not adequately mitigated.

3.3.2 Implications for coping with flood hazards in the Ayeyarwady Delta

Our findings reveal that >70 % of the delta and~40 % of its present population is prone to flooding due to either monsoon precipitation and runoff, storm surge, and RSLR, or their combination (Figures 3.3 and 3.6). As most of the exposed areas are used for the production of agricultural and to lesser extent aquacultural products and mineral (salt) extraction as well as urban and built-up areas (including industrial, commercial and infrastructural branches; Vogel et al., 2022), highlights not only the risk of these assets but also points to potential loss of livelihoods in case of flooding and/or permanent inundation. As such, flooding in the Ayeyarwady Delta poses a serious threat with far-reaching implications for food security in the delta and tremendous consequences for economic production in the region and the country. Our findings highlight the relevance of integrated flood management in the delta that addresses the high exposure of the agricultural production areas but also promotes risk-sensitive construction methods where urban settlements are located or built. Based on more detailed, follow-up investigations, endeavours are recommended to evaluate nature-based solutions to adapt and mitigate the negative impacts of frequent and high-energy flood types as well as RSLR.

To characterise flood-prone areas and specify factors contributing to flood exposure locally, further combination of established datasets, e.g. with information on physical features, and spatially focussed investigations are recommended. By linking flood maps from this study to accurate elevation data on local scale allows for further delineation of areas at risk based on elevation (Figures B21–B24). This may help to rank low-lying areas of a certain elevation threshold into exposure categories and hence priority areas for interventions. However, this investigation only serves on small local scales where the effect of slope on absolute elevation is insignificant. In deltas, for example, flood-affected areas located in the upper delta part (e.g.

near the apex) may have higher absolute elevations than downstream and thus different elevation thresholds are needed to apply an elevation-informed risk zoning. Furthermore, overlays with other datasets such as land use and geomorphology/aerial imagery will provide detailed local information about assets at risk and the physical setting and will consequently help to guide the development of local management strategies to cope with the risk of single and multiple floods (Figures B13 and B21–S24).

3.3.3 Implications for generating first-order flood hazard assessments in data-sparse coastal lowlands of the world

The combination and evaluation of open-access and publicly (free-of-charge) available datasets of Sentinel-1 imagery, global precipitation estimates, satellite-based river discharge measurements, elevation, land use, and population data allowed to identify and characterise in detail flood hazards and exposure of the so far poorly studied and poorly accessible Ayeyarwady Delta in Myanmar. This approach is highly suitable for application in other regions where high-resolution data and information on flood events and flood parameters is limited, unavailable or inaccessible. While global flood hazard maps are becoming increasingly available and were improved recently (e.g. Sampson et al., 2015 and follow-up products), these require quality assessments using accurate data obtained from local measurements and observations of past flood events (Schumann et al., 2018). Similarly, inundation models rely on information about boundary conditions such as precipitation, discharge, water level, and flood defences as well as independent observations for validation (Bates, 2023). These requirements often cannot be fulfilled in data-sparse coastal lowlands and complex modelling environments like river deltas where a dense measurement and monitoring network is missing. Furthermore, those products and software environments often involve a complex application procedure, are only accessible for certain users and institutions, or—in case of setting up hydrodynamic models—require additional expertise and computational resources, all of which may create barriers for users from broad, interdisciplinary research fields and from the so-called Global South. Our approach overcomes these challenges as it only involves basic GIS skills while cloud computing allows for the investigation of large areas up to several tens of thousands km^2, enabling the analysis of entire megadeltas and river basins at their system scale.

Investigating both single and multiple flood-type scenarios provides information to rank flood exposure at different levels and compositions. The use of these multiple flood hazard scenarios

is recommended especially when quantity and quality of available data do not allow for setting up a hydrodynamic model that is able to address compound flooding in large-scale environments at low computational cost (e.g. SFINCS; Leijnse et al., 2021). Our approach faces limitations for assessing compound flooding as the individual flood components addressed by the multiple flood-type scenarios of this study would interact dynamically. Thus, they could lead to different spatial patterns and extents than indicated by the static overlays in Figure 3.4. Yet, both single and multiple flood-type hazard maps allow to attribute flood components, provide a first-order hazard assessment and form the basis for subsequent focus studies and models, for example by serving as validation data. With the flexibility to integrate a diverse array of datasets, e.g. by adding further ones (e.g. geomorphological maps, information on flood protection measures, data on vertical land motion) and/or replacing records from this study (e.g. using global data products in case local ones are not available), this approach is suitable to study flood exposure in a tailor-made fashion in all data-sparse regions in the world.

This approach can also be employed to address societal and environmental vulnerability and risk by including further demographic and socio-economic datasets such as household information and access to infrastructure, qualitative data, as well as information on environmental dynamics and pressures. Hence, it complements previous concepts of coastal vulnerability and delta risk by detailing spatially resolved information (e.g. Bevacqua et al., 2018 and references therein; Hagenlocher et al., 2018; Cremin et al., 2023; Vogel et al., 2024). It thereby allows to attribute different types of flood hazards, provides a profound base for vulnerability assessments and thus enables risk-informed management decisions.

3.4 Conclusions

We presented a standardised, integrative approach to conduct a first-order assessment of flood hazards in data-sparse coastal lowlands. We characterised present-day flood exposure due to monsoon and storm surge flooding as well as RSLR by combining only open and freely available datasets in open-source software, using the megadelta of the Ayeyarwady River in Myanmar, a region marked by data scarcity and restricted accessibility. The flood extent mappings were supplemented with information on precipitation and runoff, elevation, land use, and population, thereby allowing to explain observed flood extents and to characterise flood-prone areas in detail.

While >70 % of the Ayeyarwady Delta and ~40 % of its present population is prone to flooding, we demonstrated that the southernmost districts, especially Pyapon and Labutta, show the highest exposure, and agricultural and aquacultural products range among the most exposed assets, stressing the need for strategies of sustaining food security and livelihoods relying on those economic sectors. Our work underlines the necessity of long-term adaptation measures and risk-sensitive development (which may include the diversification of livelihoods) and overall to strengthen the people's awareness and preparedness (not only) in respect to flood-related risks.

We have shown the general applicability of this approach for data-sparse coastal lowlands in the world in order to generate a first-order flood hazard assessment by highlighting its effectiveness in terms of workflow set up, data availability and collection, as well as computing capacity. The flexibility of the approach to be extended by integrating various available datasets and combining them in manifold ways supports to describe and evaluate flood-prone areas on regional and local scale, thereby allowing for attribution and complementing concepts of vulnerability and risk, and supporting risk-informed decision making and development of effective multi-flooding adaptation strategies.

Data availability statement: The data that support the findings of this study are openly available at the following URL/DOI: https://doi.org/10.5281/zenodo.10889566 (Seeger et al., 2024).

References

Bates, P. (2023). Fundamental limits to flood inundation modelling. *Nature Water*, *1*, 566–567. https://doi.org/10.1038/s44221-023-00106-4

Becker, M., Seeger, K., Paszkowski, A., Marcos, M., Almar, R., Bates, P., France-Lanord, C., Hossain, Md S., Khan, J., Karegar, M., Karpytchev, M., Long, N., Minderhoud, P. S. J., Neal, J., Nicholls, R. J., & Syvitski, J. (2024). Coastal flooding in Asian Megadeltas: Recent advances, persistent challenges, and call for actions admidst local and global changes. *Reviews of Geophysics*, *62*(4), e2024RG00846. https://doi.org/10.1029/2024RG000846

Besset, M., Anthony, E. J., Dussouillez, P., & Goichot, M. (2017). The impact of Cyclone Nargis on the Ayeyarwady (Irrawaddy) River delta shoreline and nearshore zone (Myanmar): Towards degraded delta resilience?. *Comptes Rendus Geoscience*, *349*(6–7), 238–247. https://doi.org/10.1016/j.crte.2017.09.002

Bevacqua, A., Yu, D., Zhang, Y. (2018). Coastal vulnerability: Evolving concepts in understanding vulnerable people and places. *Environmental Science & Policy*, *82*, 19–29. https://doi.org/10.1016/j.envsci.2018.01.006

Bondarenko, M., Kerr, D., Sorichetta, A., & Tatem, A. J. (2020). Census/projection-disaggregated gridded population datasets, adjusted to match the corresponding UNPD 2020 estimates, for 183 countries in 2020 using Built-Settlement Growth Model (BSGM) outputs. WorldPop, University of Southampton, UK. http://dx.doi.org/10.5258/SOTON/WP00685

Brakenridge, G. R., Syvitski, J. P. M., Niebuhr, E., Overeem, I., Higgins, S. A., Kettner, A. J., & Prades, L. (2017). Design with nature: Causation and avoidance of catastrophic flooding, Myanmar. *Earth-Science Reviews*, *165*, 81–109. https://doi.org/10.1016/j.earscirev.2016.12.009

Brakenridge, G. R., Kettner, A. J., Paris, S., Cohen, S. & Nghiem, S. V. (2023a). River and Reservoir Watch Version 4.5, Satellite-based river discharge and reservoir area measurements, DFO Flood Observatory, University of Colorado, USA. https://floodobservatory.colorado.edu/SiteDisplays/29.htm (last access: 20 February 2024)

Brakenridge, G. R., Kettner, A. J., Paris, S., Cohen, S. & Nghiem, S. V. (2023b). River and Reservoir Watch Version 4.5, Satellite-based river discharge and reservoir area measurements, DFO Flood Observatory, University of Colorado, USA. https://floodobservatory.colorado.edu/SiteDisplays/25.htm (last access: 20 February 2024)

Brakenridge, G. R., Kettner, A. J., Paris, S., Cohen, S. & Nghiem, S. V. (2023c). River and Reservoir Watch Version 4.5, Satellite-based river discharge and reservoir area measurements, DFO Flood Observatory, University of Colorado, USA. https://floodobservatory.colorado.edu/SiteDisplays/30.htm (last access: 20 February 2024)

Brill, D., Brückner, H., Jankaew, K., Kelletat, D., Scheffers, A., & Scheffers, S. (2011). Potential predecessors of the 2004 Indian Ocean Tsunami – Sedimentary evidence of extreme wave events at Ban Bang Sak, SW Thailand. *Sedimentary Geology*, *239*(3–4), 146–161. https://doi.org/10.1016/j.sedgeo.2011.06.008

Copernicus Emergency Management Service (© 2015 European Union) (2015). [EMSR130] Irrawaddy Delta: Delineation Map, Monitoring 1

Cosslett, T. L., & Cosslett, P. D. (2014). Major threats to Mekong Delta: Climate Change and Mainstream Dams. In: Cosslett, T. L., & Cosslett, P. D. (2014). *Water Resources and Food Security in the Vietnam Mekong Delta*. Springer, Cham, 75–96. http://dx.doi.org/10.1007/978-3-319-02198-0_3

Cremin, E., O'Connor, J., Banerjee, S., Bui, L. H., Chanda, A., Hua, H. H., Huynh, D. V., Le, H., Murshed, S. B., Mashfiqus, S., Vu, A., Sebesvaris, Z., Large, A., & Renaud, F. (2023). Aligning the Global Delta Risk Index with SDG and SFDRR global frameworks to assess risk to socio-ecological systems in river deltas. *Sustainability Science*, *18*, 1871–1891. https://doi.org/10.1007/s11625-023-01295-3

Davies, G., Griffin, J., Løvholt, F., Glimsdal, S., Harbitz, C., Thio, H. K., Lorito, S., Basili, R., Selva, J., Geist, E., & Baptista, M. A. (2018). A global probabilistic tsunami hazard assessment from earthquake sources. *Geological Society, London, Special Publications*, *456*(1), 219–244. https://doi.org/10.1144/SP456.5

Dottori, F., Salamon, P., Bianchi, A., Alfieri, L., Hirpa, F. A., Feyen, L. (2016). Development and evaluation of a framework for global flood hazard mapping. *Advances in Water Resources*, *94*, 87–102. https://doi.org/10.1016/j.advwatres.2016.05.002

Edmonds, D. A., Caldwell, R. L., Brondizio, E. S., & Siani, S. M. O. (2020). Coastal flooding will disproportionately impact people on river deltas. *Nature Communications*, *11*, 4741. https://doi.org/10.1038/s41467-020-18531-4

Eilander, D., Couasnon, A., Ikeuchi, H., Muis, S., Yamazaki, D., Winsemius, H. C., & Ward, P. (2020). The effect of surge on riverine flood hazard and impact in deltas globally. *Environmental Research Letters*, *15*(10), 104007. https://doi.org/10.1088/1748-9326/ab8ca6

Food and Agriculture Organization of the United Nations (FAO), & United Nations Educational, Scientific and Cultural Organization (UNESCO) (1976). Soil map of the world, 1:5 000 000, Volume IX, Southeast Asia.

Fox-Kemper, B., Hewitt, H. T., Xiao, C., Aðalgeirsdoìttir, G., Drijfhout, S. S., Edwards, T. L., Golledge, N. R., Hemer, M., Kopp, R. E., Krinner, G., Mix, A., Notz, D., Nowicki, S., Nurhati, I. S., Ruiz, L., Salleìe, J.-B., Slangen, A. B. A., & Yu, Y. (2021). Ocean, Cryosphere and Sea Level Change. In: Masson-Delmotte, V., Zhai, P., Pirani, A., Connors, S. L., Peìan, C., Berger, S., Caud, N., Chen, Y., Goldfarb, L., Gomis, M. I., Huang, M., Leitzell, K., Lonnoy, E., Matthews, J. B. R., Maycock, T. K., Waterfield, T., Yelekci¸, O., Yu, R., & Zhou, B. (2021). *Climate Change 2021: The Physical Science Basis. Contribution of Working Group I to the Sixth Assessment Report of the Intergovernmental Panel on Climate Change*. Cambridge University Press, Cambridge, 9-1–9-257,

https://www.ipcc.ch/report/ar6/wg1/downloads/report/IPCC_AR6_WGI_Chapter_09.pdf (last access: 21 February 2024)

Fritz, H., Blount, C., Swe Thwin, Moe Kyaw Thu, & Nyein Chan (2009). Cyclone Nargis storm surge in Myanmar. *Nature Geoscience*, *2*, 448–449. https://doi.org/10.1038/ngeo558

Garner, G. G., Hermans, T., Kopp, R. E., Slangen, A. B. A., Edwards, T. L., Levermann, A., Nowikci, S., Palmer, M. D., Smith, C., Fox-Kemper, B., Hewitt, H. T., Xiao, C., Aðalgeirsdoìttir, G., Drijfhout, S. S., Edwards, T. L., Golledge, N. R., Hemer, M., Kopp, R. E., Krinner, G., Mix, A., Notz, D., Nowicki, S., Nurhati, I. S., Ruiz, L., Salleìe, J.-B., Yu, Y., Hua, L., Palmer, T., & Pearson, B. (2021). IPCC AR6 Sea-Level Rise Projections, Version 20210809, PO.DAAC [data set], CA, USA, https://podaac.jpl.nasa.gov/announcements/2021-08-09-Sealevel-projections-from-the-IPCC-6th-Assessment-Report (last access: 21 February 2024)

Garner, G. G., Kopp, R. E., Hermans, T., Slangen, A. B. A., Koubbe, G., Turilli, M., Jha, S., Edwards, T. L., Levermann, A., Nowikci, S., Palmer, M. D., & Smith, C. (2022). Framework for Assessing Changes To Sea-level (FACTS), Geoscientific Model Development, *Zenodo* [model], https://doi.org/10.5281/zenodo.6419954

Goodbred, S. L., & Saito, Y. (2012). Tide-Dominated Deltas. In: Davis Jr., R. A., & Dalrymple, R. W. (2012). *Principles of Tidal Sedimentology*. Springer, Dordrecht, 129–149. https://doi.org/10.1007/978-94-007-0123-6_7

Gorelick, N., Hancher, M., Dixon, M., Ilyushchenko, S., Thau, D., & Moore, R. (2017). Google Earth Engine: Planetary-scale geospatial analysis for everyone. *Remote Sensing of Environment*, 202, 18–27. https://doi.org/10.1016/j.rse.2017.06.031

Government of the Union of Myanmar (2015). Myanmar – Post-disaster needs assessment of floods and landslides July–September 2015, Government of the Union of Myanmar, https://documents1.worldbank.org/curated/en/646661467990966084/pdf/103631-WP-P157276-PUBLIC-PFLNA-Report-2016.pdf (last access: 22 February 2024)

Hagenlocher, M., Renaud, F. G., Haas, S., & Sebesvari, Z. (2018). Vulnerability and risk of deltaic social-ecological systems exposed to multiple hazards. *Science of the Total Environment*, *631–632*, 71–80. https://doi.org/10.1016/j.scitotenv.2018.03.013

Hansford, M. R., Plink-Björklund, P., & Jones, E. R. (2020). Global quantitative analyses of river discharge variability and hydrograph shape with respect to climate types. *Earth-Science Reviews*, *200*, 102977. https://doi.org/10.1016/j.earscirev.2019.102977

Heinkel, S.-B., Thiebes, B., Zin Mar Than, Toe Aung, Tin Tin Kyi, Win Lei Mar, Saw Sandar Oo, Miller, C., Willkomm, M., Win Maung, Zin Nwe Myint, Khin Khin Soe, Spohner, R., & Kraas, F. (2022). Disaster preparedness and resilience at household level in Yangon, Myanmar. *Natural Hazards*, *112*, 1273–1294. https://doi.org/10.1007/s11069-022-05226-w

Hein Min Htet (2017). Flood Risk Mapping Using Satellite Images and GIS Tools: A study on flood analysis of Thabaung, Kangyidaunt and Pathein Area, Ayeyarwady Region. The First Myanmar National Conference on Earth Sciences (MNCES) 2017, November 27–28, 2017, Monywa, Myanmar, https://cwmd.kumamoto-u.ac.jp/conference/abstract/UDP09_CWMDInternationalConference2019.pdf (last access: 13 June 2023)

Herrera-García, G., Ezquerro, P., Tomás, R., Béjar-Pizarro, M., López-Vinielles, J., Rossi, M., Mateos, R. M., Carreón-Freyre, D., Lambert, J., Teatini, P., Cabral-Cano, E., Erkens, G., Galloway, D., Hung, WC., Kakar, N., Sneed, M., Tosi, L., Wang, H., & Ye, S. (2021). Mapping the global threat of land subsidence. *Science*, *371*(6524), 34–36. https://doi.org/10.1126/science.abb8549

Hill, C., Dunn, F., Haque, A., Amoako-Johnson, F., Nicholls, R. J., Raju, P. V., & Appeaning Addo, K. (2020). Hotspots of Present and Future Risk Within Deltas: Hazards, Exposure and Vulnerability. In: Nicholls, R., Adger, W., Hutton, C., & Hanson, S. (2020). *Deltas in the Anthropocene*. Palgrave Macmillan, Cham, 127–151. https://doi.org/10.1007/978-3-030-23517-8_6

Hooijer, A., & Vernimmen, R. (2021). Global LiDAR land elevation data reveal greatest sea-level rise vulnerability in the tropics. *Nature Communications*, *12*, 3592. https://doi.org/10.1038/s41467-021-23810-9

Huffman, G. J., Stocker, E. F., Bolvin, D. T., Nelkin, E. J., & Jackson Tan (2019). GPM IMERG Final Precipitation L3 1 month 0.1 degree x 0.1 degree V06. Greenbelt, MD, Goddard Earth Sciences Data and Information Services Center (GES DISC). 10.5067/GPM/IMERG/3B-MONTH/06 (last access: 10 February 2023)

ICHARM (International Centre for Water Hazard and Risk Management), Public Works Research Institute (PWRI), CTI Engineering International Co., Ltd., CTI Engineering Co., Ltd, & PASCO CORPORATION (2016a). Republic of the Union of Myanmar: Transformation of Urban Management – Flood Management Component. Asian Development Bank, Tsukuba and Tokyo, Japan, Technical Assistance Consultant's Report, Final Report Part 2, 56 pp. https://www.adb.org/sites/default/files/project-documents/46496/46496-001-tacr-en_9.pdf (last access: 22 February 2024)

ICHARM, PWRI, CTI Engineering International Co., Ltd., CTI Engineering Co., Ltd, & PASCO CORPORATION (2016b). Republic of the Union of Myanmar: Transformation of Urban Management – Flood Management Component. Asian Development Bank, Tsukuba and Tokyo, Japan, Technical Assistance Consultant's Report, Final Report Annexes 1–7, 159 pp. https://www.adb.org/sites/default/files/project-documents/46496/46496-001-tacr-en_1.pdf (last access: 22 February 2024)

ICHARM, PWRI, CTI Engineering International Co., Ltd., CTI Engineering Co., Ltd, & PASCO CORPORATION (2016c). Republic of the Union of Myanmar: Transformation of Urban Management – Flood Management Component. Asian Development Bank, Tsukuba and Tokyo, Japan, Technical Assistance Consultant's Report, Final Report Annex 8.1, 13 pp. https://www.adb.org/sites/default/files/project-documents/46496/46496-001-tacr-en_2.pdf (last access: 22 February 2024)

ICHARM, PWRI, CTI Engineering International Co., Ltd., CTI Engineering Co., Ltd, & PASCO CORPORATION (2016d). Republic of the Union of Myanmar: Transformation of Urban Management – Flood Management Component. Asian Development Bank, Tsukuba and Tokyo, Japan, Technical Assistance Consultant's Report, Final Report Annex 9, 6 pp. https://www.adb.org/sites/default/files/project-documents/46496/46496-001-tacr-en_4.pdf (last access: 22 February 2024)

Ikeuchi, H., Hirabayashi, Y., Yamazaki, D., Muis, S., Ward, P. J., Winsemius, H. C., Verlaan, M., & Kanae, S. (2017). Compound simulation of fluvial floods and storm surges in a global coupled river-coast flood model: Model development and its application to 2007 Cyclone Sidr in Bangladesh. *Journal of Advances in Modeling Earth Systems*, *9*(4), 1847–1862. https://doi.org/10.1002/2017MS000943

Islam, A. S., Haque, A., & Bala, S. K. (2010). Hydrologic characteristics of floods in Ganges–Brahmaputra–Meghna (GBM) delta. *Natural Hazards*, *54*, 797–811. https://doi.org/10.1007/s11069-010-9504-y

ITHACA, WFP, & DLR (2008). Myanmar: Tropical Cyclone Nargis – TerraSAR-X acquisition footprints (scheduled for May, 8th 2008). https://reliefweb.int/attachments/bcdcc378-7f8c-31df-8e66-c1d06be843de/BDA65B02003DDE36C1257442003F3724-ithaca_TC_mmr080507.pdf (last access: 22 February 2024)

Joint Typhoon Warning Center (JTWC) (2023). Best Track Archive, Naval Meteorology and Oceanography Command, Mississippi, USA. https://www.metoc.navy.mil/jtwc/jtwc.html?best-tracks (last access: 4 February 2024)

Jongman, B., Ward, P. J., & Aerts, J. C. J. H. (2012). Global exposure to river and coastal flooding: Long term trends and changes. *Global Environmental Change*, *22*(4), 823–835. https://doi.org/10.1016/j.gloenvcha.2012.07.004

Kittiphong Phongsaphan, Chishtie, F., Poortinga, A., Bhandari, B., Chinaporn Meechaiya, Thannarot Kunlamai, Khun San Aung, Saah, D., Anderson, E., Markert, K., Markert, A., & Peeranan Towashiraporn (2019). Operational Flood Risk Index Mapping for Disaster Risk Reduction Using Earth Observations and Cloud Computing Technologies: A Case Study on Myanmar. *Frontiers in Environmental Science*, *7*, 191. https://doi.org/10.3389/fenvs.2019.00191

Krien, Y., Testut, L., Islam, A. K. M. S., Bertin, X., Durand, F., Mayet, C., Tazkia, A. R., Becker, M., Calmant, S., Papa, F., Ballu, V., Shum, C. K., & Khan, Z. H. (2017). Towards improved storm surge models in the northern Bay of Bengal. *Continental Shelf Research*, *135*, 58–73. https://doi.org/10.1016/j.csr.2017.01.014

Kuenzer, C., Guo, H., Huth, J., Leinenkugel, P., Li, X., & Dech, S. (2013). Flood Mapping and Flood Dynamics of the Mekong Delta: ENVISAT-ASAR-WSM Based Time Series Analyses. *Remote Sensing*, *5*(2), 687–715. https://doi.org/10.3390/rs5020687

Kulp, S. A., & Strauss, B. H. (2019). New elevation data triple estimates of global vulnerability to sea-level rise and coastal flooding. *Nature Communications*, *10*, 4844. https://doi.org/10.1038/s41467-019-12808-z

Leijnse, T., van Ormondt, M., Nederhoff, K., & van Dongeren, A. (2021). Modeling compound flooding in coastal systems using a computationally efficient reduced-physics solver: Including fluvial, pluvial, tidal, wind- and wave-driven processes. *Coastal Engineering*, *163*, 103796. https://doi.org/10.1016/j.coastaleng.2020.103796

Liew, S. C., Gupta, A., Chia, A. S., & Ang, W. C. (2016). The flood of 2011 in the lower Chao Phraya valley, Thailand: Study of a long-duration flood through satellite images. *Geomorphology*, *262*, 112–122. https://doi.org/10.1016/j.geomorph.2016.03.022

Maranzoni, A., D'Oria, M., & Rizzo, C. (2023). Quantitative flood hazard assessment methods: A review. *Journal of Flood Risk Management*, *16*(1), e12855. https://doi.org/10.1111/jfr3.12855

Marfai, M. A., & King, L. (2008). Potential vulnerability implications of coastal inundation due to sea level rise for the coastal zone of Semarang city, Indonesia. *Environmental Geology*, *54*, 1235–1245. https://doi.org/10.1007/s00254-007-0906-4

Myanmar Information Management Unit (MIMU) (2015). Probable Affected Village Tracts in Ayeyarwady Region. MIMU, MIMU1324v01. https://documents.themimu.info/downloads/QhCT0Hd/Map_Flood%20Affected%20Village%20Tracts-Ayeyarwady%20Reg_MIMU1324v01%2007Sep2015%20A1.pdf (last access: 22 February 2024)

Myanmar Information Management Unit (MIMU) (2020). Probable Flood Inundated Ayeyarwady and Bago (West) Region (as of 1st September 2020). MIMU, MIMU1515v01. https://documents.themimu.info/downloads/p1wVEsI/Map_Flood-Area%20in%20Ayeyarwady%20and%20Bago%20(As%20of%2001Sep)%20MIMU1515v01%2002Sep2020%20A3_ENG.pdf (last access: 22 February 2024)

Neumann, B., Vafeidis, A. T., Zimmermann, & Nicholls, R. J. (2015). Future Coastal Population Growth and Exposure to Sea-Level Rise and Coastal Flooding – A Global Assessment. *PLoS ONE*, *10*(3), e0118571. https://doi.org/10.1371/journal.pone.0118571

Nicholls, R. J., Lincke, D., Hinkel, J., Brown, S., Vafeidis, A. T., Meyssignac, B., Hanson, S. E., Merkens, JL., & Fang, J. (2021). A global analysis of subsidence, relative sea-level change and coastal flood exposure, *Nature Climate Change*, *11*, 338–342. https://doi.org/10.1038/s41558-021-00993-z

Pickering, M. D., Horsburgh, K. J., Blundell, J. R., Hirschi, J. JM., Nicholls, R. J., Verlaan, M., & Wells, N. C. (2017). The impact of future sea-level rise on the global tides. *Continental Shelf Research*, *142*, 50–68. https://doi.org/10.1016/j.csr.2017.02.004

Plink-Björklund, P. (2015). Morphodynamics of rivers strongly affected by monsoon precipitation: Review of depositional style and forcing factors. *Sedimentary Geology*, *323*, 110–147. https://doi.org/10.1016/j.sedgeo.2015.04.004

Rahman, S., Islam, A. K. M. S., Saha, P., Tazkia, A. R., Krien, Y., Durand, F., Testut, L., Islam, G. M. T., & Bala, S. K. (2019). Projected changes of inundation of cyclonic storms in the Ganges–Brahmaputra–Meghna

delta of Bangladesh due to SLR by 2100. *Journal of Earth System Science*, *128*, 145. https://doi.org/10.1007/s12040-019-1184-8

Röbke, B. R., & Vött, A. (2017). The tsunami phenomenon. *Progress in Oceanography*, *159*, 296–322. https://doi.org/10.1016/j.pocean.2017.09.003

Sampson, C.C., Smith, A. M., Bates, P. D., Neal, J. C., Alfieri, L., & Freer, J. E. (2015). A high-resolution global flood hazard model. *Water Resources Research*, *51*(9), 7358–7381. https://doi.org/10.1002/2015WR016954

Schmitt, R. J. P., & Minderhoud, P. S. J. (2023). Data, knowledge, and modeling challenges for science-informed management of river deltas. *One Earth*, *6*(3), 216–235. https://doi.org/10.1016/j.oneear.2023.02.010

Schumann, G. JP., Bates, P. D., Apel, H., & Aronica, G. T. (2018). Global Flood Hazard Mappping, Modelling, and Forecasting: Challenges and Perspectives. In: Schumann, G. JP., Bates, P. D., Apel, H., & Aronica, G. T. (2018). *Global Flood Hazard – Applications in Modeling, Mapping, and Forecasting*. American Geophyiscal Union, Washington D.C., 239–244. https://doi.org/10.1002/9781119217886.ch14

Seeger, K., Minderhoud, P. S. J., Peffeköver, A., Vogel, A., Brückner, H., Kraas, F., Nay Win Oo, & Brill, D. (2023a). Assessing land elevation in the Ayeyarwady Delta (Myanmar) and its relevance for studying sea level rise and delta flooding. *Hydrology and Earth System Sciences*, *27*(11), 2257–2281. https://doi.org/10.5194/hess-27-2257-2023

Seeger, K., Minderhoud, P. S. J., Peffeköver, A., Vogel, A., Brückner, H., Kraas, F., Nay Win Oo, & Brill, D. (2023b). FABDEM V1-0 adjusted for the Ayeyarwady Delta in Myanmar by local spot height data from topographic maps. *Zenodo*. https://doi.org/10.5281/zenodo.7875855

Seeger, K., Shirzaei, M., Minderhoud, P. S. J., Brückner, H., & Brill, D. (2023c). How Much is the Ayeyarwady Delta (Myanmar) Affected by Land Subsidence? Insights into Vertical Land Motion Based on a Multitemporal DInSAR Algorithm. Abstract EP23E-1985, American Geophysical Union Fall Meeting 2023, December 11–15, 2023, San Francisco, California, USA. https://agu.confex.com/agu/fm23/meetingapp.cgi/Paper/1311807

Shakti, P. C., Miyamoto, M., Misumi, R., Nakamura, Y., Sriariyawat, A., Visessri, S., & Kakinuma, D. (2020). Assessing Flood Risk of the Chao Phraya River Basin Based on Statistical Rainfall Analysis. *Journal of Disaster Research*, *15*(7), 1025–1039. https://doi.org/10.20965/jdr.2020.p1025

Sriariyawat A., Kimmany, B., Miyamoto, M., Kakinuma, D., Shakti, P. C., & Visessri, S. (2022). An Approach to Flood Hazard Mapping for the Chao Phraya River Basin Using Rainfall-Runoff-Inundation Model. *Journal of Disaster Research*, *17*(6), 864–876. https://doi.org/10.20965/jdr.2022.p0864

Syvitski, J. P. M., & Brakenridge, G. R. (2013). Causation and avoidance of catastrophic flooding along the Indus River, Pakistan. *GsA today*, *23*(1), 4–10. http://dx.doi.org/10.1130/GSATG165A.1

Syvitski, J., Anthony, E., Saito, Y., Zăinescu, F., Day, J., Bhattacharya, J. P., & Giosan, L. (2022). Large deltas, small deltas: Toward a more rigorous understanding of coastal marine deltas. *Global and Planetary Change*, *218*, 103958. https://doi.org/10.1016/j.gloplacha.2022.103958

Tasnim, K. M., Esteban, M., Shibayama, T., & Takagi, H. (2015). Storm Surge Due to 2008 Cyclone Nargis in Myanmar and Post-cyclone Preparedness Activities. In: Esteban, M., Takagi, H., & Shibayama, T. (2015). *Handbook of Coastal Disaster Mitigation for Engineers and Planners*. Butterworth-Heinemann, 55–74. https://doi.org/10.1016/B978-0-12-801060-0.00004-6

Tellman, B., Sullivan, J. A., Kuhn, C., Kettner, A. J., Doyle, C. S., Brakenridge, G. R., Erickson, T. A., & Slayback, D. A. (2021). Satellite imaging reveals increased proportion of population exposed to floods. *Nature*, *596*, 80–86. https://doi.org/10.1038/s41586-021-03695-w

Tessler, Z. D., Vörösmarty, J., Grossberg, M., Gladkova, I., Aizenman, H., Syvitski, J. P. M., & Foufoula-Georgiou, E. (2015). Profiling risk and sustainability in coastal deltas of the world. *Science*, *349*(6248), 638–643. https://doi.org/10.1126/science.aab3574

Tierolf, L., de Moel, H., & van Vliet, J. (2021). Modeling urban development and its exposure to river flood risk in Southeast Asia. *Computers, Environment and Urban Systems*, *87*, 101620. https://doi.org/10.1016/j.compenvurbsys.2021.101620

United Nations Platform for Space-based Information for Disaster Management and Emergency Response (UN-SPIDER) (no date). SAR-Flood mapping using a change detection approach. https://www.un-spider.org/sites/default/files/Code_GEE_flood_mapping.txt (last access: 20 February 2024)

UNOSAT (2015). Flood Waters Near City of Yangon, Myanmar (10 Aug 2015). https://reliefweb.int/attachments/9b42a7be-91b8-39e5-a59f-0e602863dd7a/UNOSAT_A3_20150703MMR_Portrait_Yangon_South.pdf (last access: 22 February 2024)

van der Horst, T., Rutten, M. M., van de Giesen, N. C., & Hanssen, R. F. (2018). Monitoring land subsidence in Yangon, Myanmar using Sentinel-1 persistent scatterer interferometry and assessment of driving mechanisms, *Remote Sensing of Environment*, *217*, 101–110. https://doi.org/10.1016/j.rse.2018.08.004

Vogel, A., Seeger, K., Brill, D., Brückner, H., Khin Khin Soe, Nay Win Oo, Nilar Aung, Zin Nwe Myint, & Kraas, F. (2022). Identifying Land-Use Related Potential Disaster Risk Drivers in the Ayeyarwady Delta (Myanmar) during the Last 50 Years (1974–2021) Using a Hybrid Ensemble Learning Model. *Remote Sensing*, *14*(15), 3568. https://doi.org/10.3390/rs14153568

Vogel, A., Seeger, K., Brill, D., Brückner, H., & Kraas, F. (2024). Towards Integrated Flood Management: Vulnerability and Flood Risk in the Ayeyarwady Delta of Myanmar. *International Journal of Disaster Risk Reduction*, *114*, 104723. https://doi.org/10.1016/j.ijdrr.2024.104723

Ward, P. J., de Perez, E. C., Dottori, F., Jongman, B., Luo, T., Safaie, S., & Uhlemann-Elmer, S. (2018). The Need for Mapping, Modeling, and Predicting Flood Hazard and Risk at the Global Scale. In: Schumann, G. JP., Bates, P. D., Apel, H., & Aronica, G. T. (2018). *Global Flood Hazard – Applications in Modeling,*

Mapping, and Forecasting. American Geophyiscal Union, Washington D.C., 1–18. https://doi.org/10.1002/9781119217886.ch1

Webster, P. J. (2008). Myanmar's deadly daffodil. *Nature Geoscience*, *1*, 488–490. https://doi.org/10.1038/ngeo257

Woodruff, J., Irish, J., & Camargo, S. (2013). Cosatal flooding by tropical cyclones and sea-level rise. *Nature*, *504*, 44–52. https://doi.org/10.1038/nature12855

WorldPop (www.worldpop.org - School of Geography and Environmental Science, University of Southampton; Department of Geography and Geosciences, University of Louisville; Departement de Geographie, Universite de Namur), & Center for International Earth Science Information Network (CIESIN), Columbia University (2018). Global High Resolution Population Denominators Project - Funded by The Bill and Melinda Gates Foundation (OPP1134076). https://dx.doi.org/10.5258/SOTON/WP00647

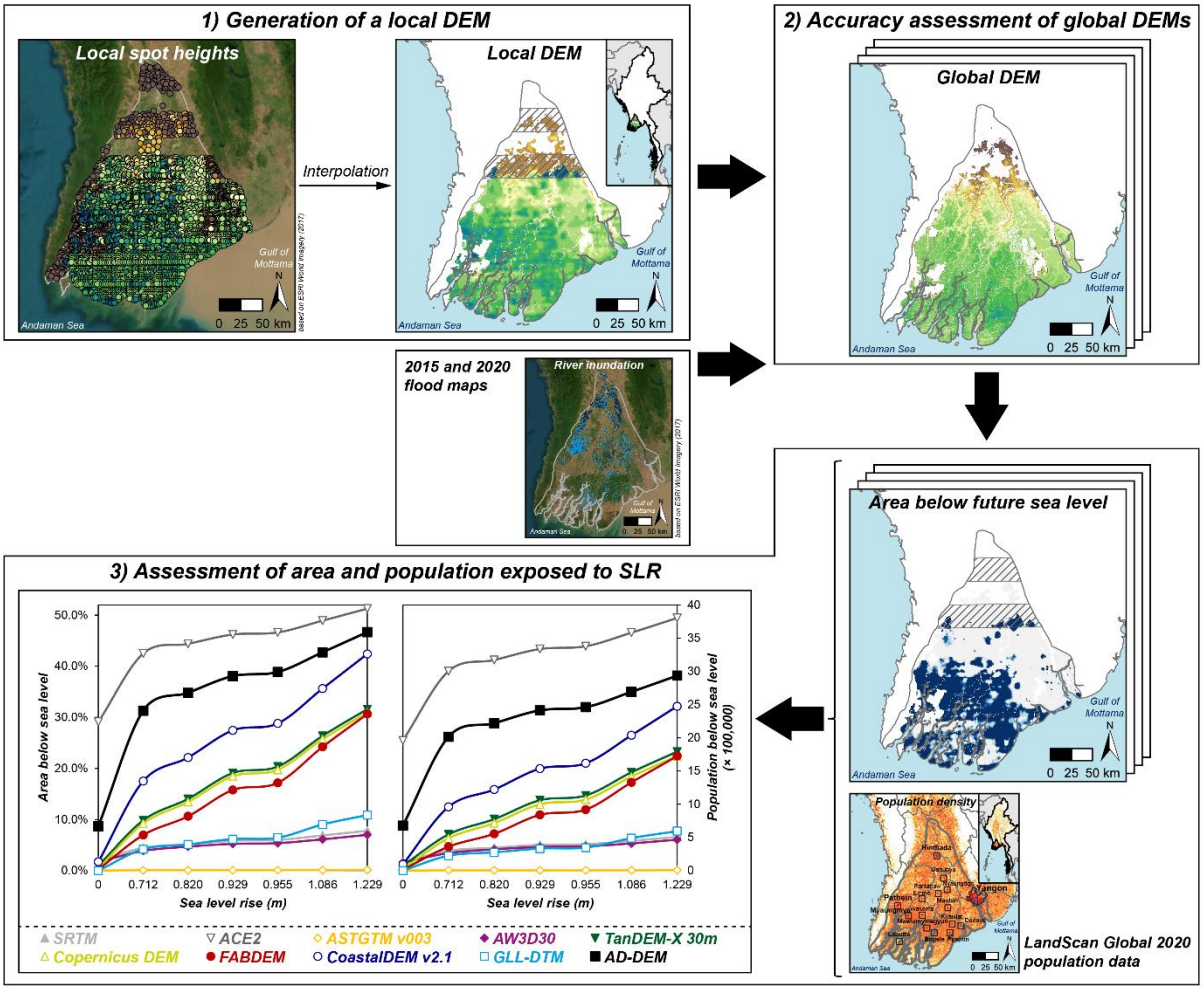
4 Land elevation is key – On the proper handling of elevation and sea-level data for improving assessments of relative sea-level rise impact

4.1 Assessing land elevation in the Ayeyarwady Delta (Myanmar) and its relevance for studying sea level rise and delta flooding

Abstract: With their low lying, flat topography, river deltas and coastal plains are extremely prone to relative sea level rise and other water-related hazards. This calls for accurate elevation data for flood risk assessments, especially in the densely populated Southeast Asian deltas. However, in data-poor countries such as Myanmar, where high accuracy elevation data are not accessible, often only global satellite-based digital elevation models (DEMs), suffering from low vertical accuracy and remote sensing artefacts, can be used by the public and scientific community. As the lack of accurate elevation data hampers the assessment of flood risk, studying available information on land elevation and its reliability is essential, particularly in the context of sea level rise impact. Here, we assess the performance of 10 global DEMs in the Ayeyarwady Delta (Myanmar) against the new, local, so-called AD-DEM, which was generated based on topographical map elevation data. To enable comparison, all DEMs were converted to a common vertical datum tied to local sea level. While both CoastalDEM v2.1 (Kulp and Strauss, 2021) and FABDEM (Hawker et al., 2022) perform comparably well, showing the highest correspondence in comparison with AD-DEM and low-elevation spot heights, FABDEM outperforms CoastalDEM v2.1 by the absence of remote sensing artefacts. The AD-DEM provides a high-accuracy, open and freely available, and independent elevation dataset suitable for evaluating land elevation data in the Ayeyarwady Delta and studying topography and flood risk at large scale, while small-scale investigations may benefit from a FABDEM locally improved with data from the AD-DEM.

Based on the latest Intergovernmental Panel on Climate Change (IPCC) projections of sea level rise, the consequences of DEM selection for assessing the impact of sea level rise in the Ayeyarwady Delta are shown. We highlight the need for addressing particularly low-lying

populated areas within the most seaward districts with risk mitigation and adaptation strategies while also the more inland delta population should be made aware of facing a higher risk of flooding due to relative sea level rise in the next ~100 years.



Graphical abstract

Chapter 4.1 is related to: **Seeger, K.**, Minderhoud, P.S.J., Peffeköver, A., Vogel, A., Brückner, H., Kraas, F., Nay Win Oo, Brill, D., 2023. *Assessing land elevation in the Ayeyarwady Delta (Myanmar) and its relevance for studying sea level rise and delta flooding*. Hydrology and Earth System Sciences, 27 (11), 2257–2281. https://doi.org/10.5194/hess-27-2257-2023.

The scientific article is published under a CC-BY 4.0 Attribution 4.0 International licence (https://creativecommons.org/licenses/by/4.0/). The reader can access the content of this chapter also via the article doi provided above. The article material was not modified; only the thesis layout was adopted.

4.1.1 Introduction

Deltas are hotspots of human settlement and economic production by providing various ecosystem services. Human–environment interactions are particularly dynamic in Southeast Asian deltas where human activities in the form of resource extraction and land use changes are increasing and lead to substantial landscape modifications (e.g. Woodroffe et al., 2006; Myat Myat Thi et al., 2012; Nicholls et al., 2020). At the same time, these low-lying and densely populated coastal areas are among the most vulnerable in facing the risk of sea level rise (SLR), extreme waves such as storm surges and other climate-related extremes (Nicholls and Cazenave, 2010; Williams, 2013; Masson-Delmotte et al., 2021). Against this background, increasing population and land use and land cover change not only challenge the sustainability of deltas to ensure income and food security for societies in coastal areas (e.g. Tran et al., 2015) and maintain their functioning in balance with natural dynamics (Ottinger et al., 2013; Renaud et al., 2013; Loucks, 2019) but also contribute to increasing vulnerability (Syvitski, 2008; Tessler et al., 2015; Vogel et al., 2022). For example, the extraction of groundwater, sediment and other resources as well as the construction of dams and reservoirs have already reduced sediment supply in major Southeast Asian rivers, such as the Mekong or the Red River (e.g. Wang et al., 2011; Van Binh et al., 2020), and accelerated sediment compaction within the deltas significantly (Syvitski, 2008, and references therein; Minderhoud et al., 2017, 2018; Zoccarato et al., 2018). Consequences are enhanced coastal erosion (due to sediment starvation) and accelerated deltaic subsidence (due to accelerated compaction as well as buildings and infrastructural loading), thereby often exacerbating relative sea level change and highlighting the critical role of land elevation for low-lying coastal areas prone to flooding from SLR and other water-related hazards.

Given their multiple informative benefits, digital elevation models (DEMs) have been considered fundamental in concepts of vulnerability and risk indices (e.g. McLaughlin and Cooper, 2010; Furlan et al., 2021) and constitute primary physical input data for vulnerability and risk mapping/models (e.g. Fereshtehpour and Karamouz, 2018; Rincón et al., 2018; Nirwansyah and Braun, 2021). Therefore, when studying natural hazards in a holistic manner, the selection of the DEM is key and significantly shapes the outcome of their assessment (van de Sande et al., 2012; Chen et al., 2021; Xu et al., 2021).

In coastal areas, where the usage of DEMs becomes highly relevant in the context of flood risk assessment, several studies investigated land elevation in the recent past by (i) accuracy

assessments of commonly available DEMs (e.g. Du et al., 2016; Hawker et al., 2019; Zhang et al., 2019) and (ii) the generation of global coastal lowland DEMs from globally available data (Kulp and Strauss, 2018; Vernimmen et al., 2020) or DEMs based on local data (e.g. El-Quilish et al., 2018; Minderhoud et al., 2019). Accurate elevation data are needed to generate realistic assessments of flood exposure and consequently risk and vulnerability (Gesch et al., 2018). This holds particularly true for coastal lowlands and river deltas, where changes in land elevation exacerbate the impact of relative SLR (RSLR) and where subsidence is dominant (e.g. Becker et al., 2020; Nicholls et al., 2021; Shirzaei et al., 2021). Especially for deltas, characterised by high population and socio-economic growth (Hanson et al., 2011; Bucx et al., 2014; Szabo et al., 2016; Loucks, 2019), the increasing flood vulnerability requires a comprehensive flood risk assessment, including the impact of RSLR. In this context, the choice of a DEM, being representative for the physical characteristics of a study area, is not trivial, and different DEMs may lead to significantly different results and implications in view of flood risk and potentially affected coastal population (Kulp and Strauss, 2019). However, although called for in scientific research for several years now (e.g. Gesch, 2009; Schumann and Bates, 2018; Kulp and Strauss, 2019), high-quality (and ideally ground truth) data are often not available to the public, and thus the establishment of local DEMs and corresponding quality assessments often remains challenging in areas with sparse or hardly accessible data.

In countries such as Myanmar, often only global satellite-based DEMs are available to the scientific and public community (cf. GERICS and KfW Development Bank, 2015; Chen et al., 2020; Mulhern, 2020). However, when studying RSLR, the use of such global DEMs is problematic for three reasons. Firstly, their considerably large vertical errors of several metres affect the quality of the SLR impact assessment, particularly in low-lying areas where changes occur on the decimetre scale (cf. Gesch, 2013; Schumann et al., 2014, 2018; Minderhoud et al., 2019). Secondly, the elevation data of these DEMs are given either in height above the global geoid or ellipsoid. However, local sea level often differs from the global geoid reference, and geoid models differ by up to several metres offset from each other (e.g. Üstün et al., 2016). Consequently, the neglection of datum conversion can lead to additional errors and a misjudgement of the flood risk. Thirdly, remote sensing artefacts, such as stripes, speckle noise, voids and other errors (Hirt et al., 2018) not only affect DEM quality itself but also result in erroneous impact assessments (e.g. Wechsler, 2007; Yamazaki et al., 2017; Hirt et al., 2018).

In Myanmar, most flood risk assessments only consider elevation data indirectly (Kittiphong Phongsaphan et al., 2019), do not specify the DEM used (Khin Thandar Win et al., 2014), or

rely on global DEMs such as SRTM (Farr et al., 2007), HydroSHEDS (Lehner et al., 2008), and AW3D (Tadono et al., 2016) to investigate the impact of flooding related to enhanced precipitation (ICHARM et al., 2016; Hein Min Htet, 2017) and storms (Liu et al., 2017). The Coastal Risk Screening tool of Climate Central, Inc. (https://coastal.climatecentral.org/, last access: 31 August 2022) constitutes a convenient, user-friendly interactive map that visualises the impact of future SLR and extreme water levels based on the recently developed and updated CoastalDEM v2.1 (Kulp and Strauss, 2018, 2021) and reanalysed surge and sea levels of Muis et al. (2016). However, the performance of DEMs used in these studies was so far only addressed by Bhagabati et al. (2020), who generated a DEM for the Bago River basin based on geodetic data, supplemented by ALOS (Tadono et al., 2016) data and cross-sectional measurements. When comparing their EnDEM to commonly available SRTM, ASTGTM (Tachikawa et al., 2011) and HydroSHEDS, they concluded that among these only HydroSHEDS, which is a hydrologically improved version of SRTM (Lehner et al., 2008), was to some extent comparable to EnDEM (Bhagabati et al., 2020). However, the lack of documentation on vertical reference does not allow for utilising their findings in view of SLR impact assessment.

As a contribution to improved risk assessment for the Ayeyarwady Delta, where the quality of available elevation data is so far not known, this study aims to assess its elevation in relation to local mean sea level (MSL) by (a) generating a DEM based on geodetic data (called AD-DEM hereafter); (b) using the AD-DEM to evaluate available global DEMs, referenced to local MSL; (c) identifying deltaic areas prone to be effected by RSLR and monsoon flooding in their relation to topography.

Leading research questions that will be addressed are the following:

i. What is the present elevation of the Ayeyarwady Delta with respect to local MSL?
ii. What discrepancies exist between local elevation data and available global DEMs?
iii. Which consequences do different elevation models have when used to assess future RSLR and delta flooding impacts?
iv. Which is – in the absence of ground truthing possibilities – the most trustworthy elevation model when studying RSLR and delta flooding in the Ayeyarwady Delta?
v. How do these implications call for future coping with SLR?

4.1.2 Study area

Originating from the confluence of rivers sourced in the south-eastern Himalaya, Shan Highland, Rakhine Mountains and Central Dry Zone in Myanmar, the Ayeyarwady River forms a north–south-oriented fluvial system with a drainage basin covering more than 414 000 km^2 (Woodroffe et al., 2006), thereby draining ca. 60 % of the country's territory and supplying water to 90 % of the Myanmar population (Chen et al., 2020). From the delta apex close to Myanaung north of Hinthada (Figure 4.1), the Ayeyarwady first branches (from west to east) into its two first-order distributaries Pathein and Myitmakha rivers (further downstream entering the Yangon River) and later into the second-order distributaries Wakema, Ya Zu Daing, Toe and Pan Hlaing rivers (Chen et al., 2020) as well as several smaller river channels. Spanning over an area of ca. 35 000 km^2, the Ayeyarwady Delta is home to more than 15 million people (nearly 30 % of the Myanmar population; Rose et al., 2021), and it provides fertile alluvial soils used for agriculture and increasingly for aquaculture (Frenken, 2012; Torbick et al., 2017; Vogel et al., 2022). Furthermore, the deltaic marshland as well as intertidal flats and islands host several endangered species and highlight the ecological value of the landscape to be protected in the form of key biodiversity areas (Webb et al., 2014; Zöckler and Kottelat, 2017). However, due to increasing population and human impact, which is also expected to continue, perhaps grow in the future, this biodiversity as well as the environmental stability and functioning of the delta is threatened (Webb et al., 2014; Zöckler and Kottelat, 2017; Vogel et al., 2022).

Characterised by the tropical monsoon climate, annual precipitation amounts to 2000–3000 mm in the delta and up to 6000 mm in the mountain ranges (Win Win Zin and Rutten, 2017), with 70 %–90 % falling in the rainy season (Furuichi et al., 2009; Zin Mie Mie Sein et al., 2021). In addition to monsoon precipitation, the region is prone to tropical cyclones that may strike the coast between May and October (e.g. Wang et al., 2013; Brill et al., 2020), causing heavy rainfalls and severe flooding (Brakenridge et al., 2017). As such, the most prominent and devastating disaster was category 4 tropical cyclone Nargis that hit the delta in 2008, causing a storm surge of 5 m and storm waves of 2 m height (Fritz et al., 2009). Its unexpected movement, intensity and timing with respect to tidal constellation led to flooding up to 50 km inland, causing more than 138 000 fatalities (Fritz et al., 2009). After Nargis, severe flooding occurred due to exceptionally intense monsoon precipitation in 2015, affecting more than 1.6 million people (with 132 deaths) and up to 530 000 ha of agricultural and aquacultural production areas (Brakenridge et al., 2017; IFRC, 2017; Government of the Union of Myanmar, 2015).

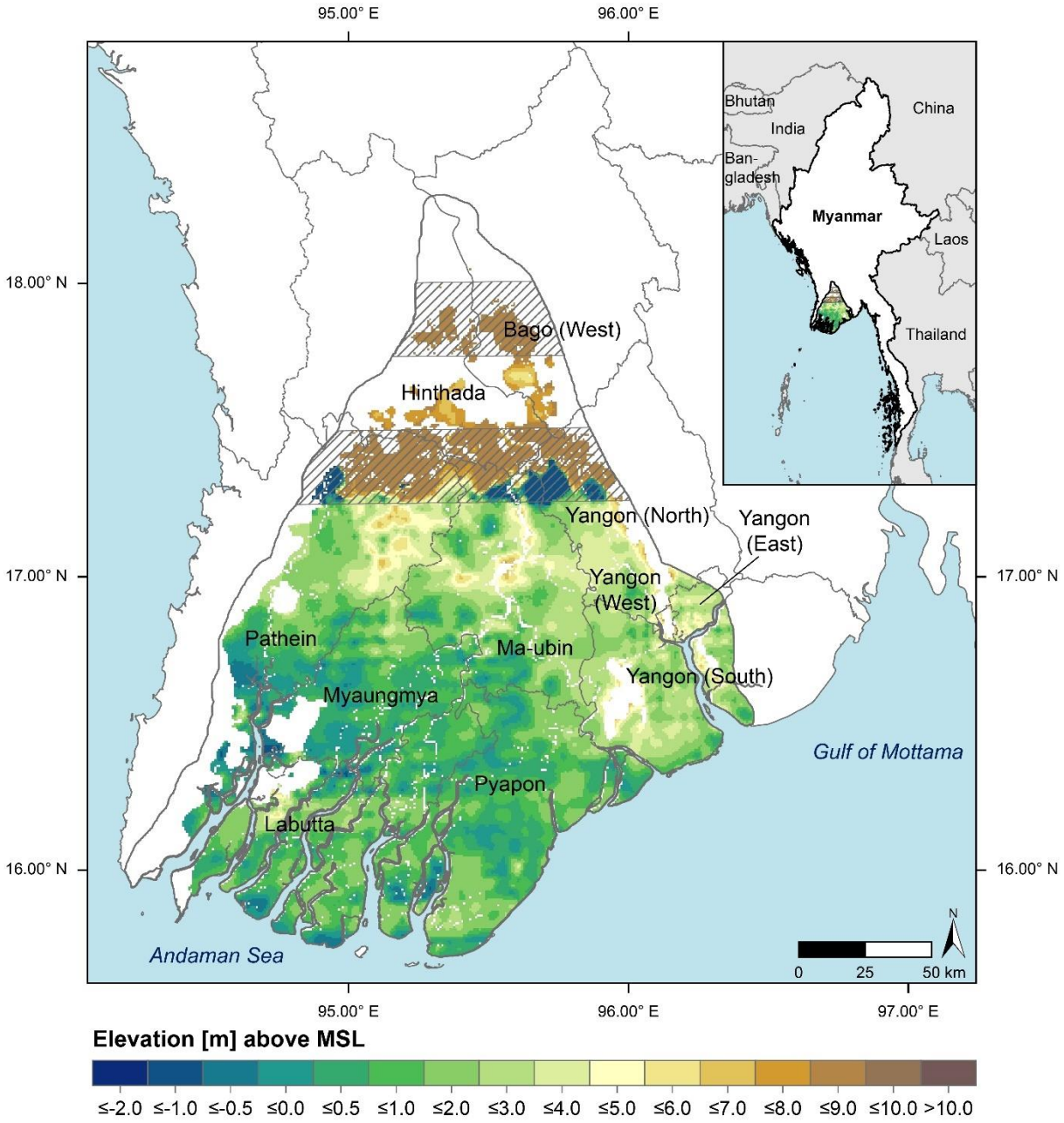


***Figure 4.1** | Local digital elevation model for the Ayeyarwady Delta in Myanmar (AD-DEM; Seeger et al., 2023a) based on the interpolation of digitised spot and contour heights from topographic maps (see also Figure C1). Areas containing interpolation artefacts are marked with hatching. Names and boundaries of administrative districts are shown.*

The Ayeyarwady Delta is a mixed wave-and-tide-dominated system, with particularly the western delta part exposed to waves (Anthony et al., 2019). Tidal range increases towards the Gulf of Mottama in the east, where it may peak at maximum 7 m (Rao et al., 2005). Tidal influence varies spatially and temporally. In the most western delta sector, spring and neap tides are 2.2 and 1.8 m; in the eastern part they are 5.7 and 4.0 m (Kravtsova et al., 2009), while the distributary channels show a mesotidal range of 2–4 m (Ramaswamy et al., 2004; Chen et al., 2020). Together with spring tides reaching up to 300 km inland to the delta apex (Hedley et al.,

2010), tide dynamics and tidal constellation may significantly contribute to amplify the impact of storm surge flooding and SLR.

For the first decade of the 21st century, RSLR has been estimated to be 3.4 $mmyr^{-1}$ (Syvitski et al., 2009) in the Ayeyarwady Delta, but these rates are solely based on discontinuous tide gauge data between 1916 and 1962 (PSMSL, 2021). By including a compaction rate of 2–3 $mmyr^{-1}$,

Syvitski et al. (2009) postulate up to 6 $mmyr^{-1}$ RSLR for the delta. These rates already exceed the global mean (Church et al., 2006; Masson-Delmotte et al., 2021), thus underpinning its status as a "delta in peril" (Syvitski et al., 2009). Considering global and regional influences, other than land subsidence, sea level is projected to rise by 14–56 cm until the 2050s (based on the reference period 2000–2004) and 21–121 cm until the 2080s (Fee et al., 2017; Horton et al., 2017). Projections of the latest Intergovernmental Panel on Climate Change (IPCC) report (Masson-Delmotte et al., 2021) point to future regional sea levels in 2100 up to 96 cm (intermediate greenhouse gas (GHG) emission scenario SSP2-4.5, 83rd percentile) and 123 cm (high GHG emission scenario SSP5-8.5, 83rd percentile) higher than compared to the period of 1995–2014 (Fox-Kemper et al., 2021; Garner et al., 2021, 2022). According to the same scenarios, sea level in the Ayeyarwady Delta will have risen by a further 67 and 98 cm in 2150, respectively (see Appendix C). Since already 0.5 m of the total SLR would lead to a coastline retreat of 10 km (Department of Meteorology and Hydrology and Ministry of Transport, 2012; van Driel and Nauta, 2014), inundation areas are expected to increase both permanently along the actual coastline due to the flat and low-lying topography (Figure 4.1) as well as episodically inland due to high-tide flooding and storm surges reaching further inland (Fee et al., 2017). As flood frequency and magnitude will increase in all coastal districts, so will saltwater intrusion, thus exacerbating the risk of freshwater shortage, especially during a lengthening dry season (Fee et al., 2017), with severe consequences for agricultural production and food security (e.g. Bucx et al., 2014; Schneider and Asch, 2019; Sakai et al., 2021). However, given that the role of topography and subsidence in the Ayeyarwady Delta has been studied only for specific locations so far, e.g. by observing subsidence at rates of 10–20 $mmyr^{-1}$ in Yangon City in the eastern part of the delta (van der Horst et al., 2018), previous estimates on both RSLR that considered lower values of subsidence or even excluded it (Horton et al., 2017) and flood risk assessments may underestimate future RSLR (e.g. ICHARM et al., 2016; Hein Min Htet, 2017; Liu et al., 2017; Kittiphong Phongsaphan et al., 2019).

4.1.3 Material and methods

4.1.3.1 Generation of an elevation model for the Ayeyarwady Delta based on geodetic data

To investigate land elevation in the Ayeyarwady Delta independently of data derived from satellite-based measurements, we used height information from recent topographic maps at a scale of 1 : 50000, which were made and published by the Survey Department, Ministry of Forestry in the Union of Myanmar, in cooperation with the Japan International Cooperation Agency (JICA), and sold by East View Geospatial, Inc. (2014). Map sheets covering the Ayeyarwady Delta were accessed via the Specialised Information Service Cartography and Geodata (SIS Maps) of the Map Department of the Staatsbibliothek zu Berlin funded by the German Research Foundation (SIS Maps, 2021). To create a local DEM for our region of interest (ROI; the spatial extent of the Ayeyarwady Delta as defined by Tessler et al., 2015), 102 topographical map sheets were georeferenced and digitised, covering also the wider surroundings (15°30’ to 18°30’ N and 94°00’ to 97°00’ E) to enhance the performance of DEM interpolation. In total, 9179 elevation points were digitised (5673 lying within the ROI). Point elevations are regularly distributed in the central to southern delta parts, while they are more unsystematically and less densely distributed especially in the northern delta parts. Elevation contours are only present in the upper delta, i.e. north of 17.0° N. As contour lines already constitute indirect elevation information instead of locally precise ground measurements, we considered them only in areas that are not spatially covered by spot height data in order to supplement the input elevation data for DEM interpolations. From these contour data, points were extracted at 250 and 2000 m intervals, respectively, to test whether the spacing has an impact on DEM interpolation. Furthermore, to reduce the potential of height overestimations in the immediate surroundings of outcrops and improve the quality of the DEM in low-lying coastal areas, which are of particular interest in this study, values of elevation higher than a specified threshold are excluded, thereby eliminating outcrops. All data were projected to the Myanmar 2000 datum (JICA et al., 2004).

Interpolation was conducted using the Geostatistical Wizard within the Analysis environment of ArcGIS Pro 2.9.1. Minderhoud et al. (2019) compared 22 interpolation methods for the creation of a DEM in a similar setting, i.e. the Mekong Delta, and found empirical Bayesian with empirical transformation and exponential modelling to provide the most accurate results (i.e. in terms of absolute accuracy). Thus, similar set-up settings were adopted in this study.

The grid cell resolution of 750 m × 750 m was defined as justified by the point density following Aguilar et al. (2006). In total, nine versions of AD-DEM were generated – (i–iii) including digitised spot heights, (iv–vi) including spot heights and contour heights extracted every 250 m, and (vii–ix) including spot heights and contour heights extracted every 2000 m. All of them apply also specific elevation thresholds of 20 and 10 m, respectively (Table C2). Areas – such as outcrops and northernmost delta parts – that are in reality higher than the elevation threshold applied for DEM interpolation were masked. As data collection for generating the topographic maps used for the AD-DEM was conducted between 2002 and 2004, the location of river channels is likely best reflected by the SRTM water body mask created in 2000 as changes in geomorphology following river meandering and channel migration will be less compared to water masks of DEMs generated at a later point in time. Therefore, we used the SRTM water body mask file (NASA JPL, 2013) to exclude all areas marked as water from the final DEMs.

4.1.3.2 Processing of global DEMs and determination of local mean sea level (MSL)

In total, 10 global DEMs were used to assess their performance in the Ayeyarwady Delta. We integrated SRTM, ACE2, ASTGTM v003, AW3D30, TanDEM-X (30 m), TanDEM-X (12 m), Copernicus DEM, FABDEM, CoastalDEM v2.1 and GLL-DTM v1. Both SRTM and TanDEMX are based on radar interferometry, while ASTGTM and AW3D30 were processed from optical imagery (Farr et al., 2007; Tachikawa et al., 2011; Tadono et al., 2016; Wessel, 2018). All these DEMs are digital surface models (DSMs). By including altimetry data, ACE2 (nearly a digital terrain model (DTM)) was generated out of SRTM, whereas CoastalDEM v2.1 (nearly DTM) is a correction of the SRTM-based NASADEM (Crippen et al., 2016), which was trained with ICESat-2 satellite lidar data and further datasets in a neural network (Berry et al., 2010; Kulp and Strauss, 2021). Recently, edits on the TanDEM-X data have led to the release of the Copernicus DEM (DSM; Airbus Defence and Space, 2020). By eliminating the bias of tree and building heights, Hawker et al. (2022) generated the FABDEM (nearly DTM) out of the Copernicus DEM. In contrast, the GLL-DTM v1 constitutes a DTM that was interpolated from ICESat-2 satellite lidar data (Vernimmen et al., 2020). An overview of main characteristics such as coverage, resolution, and accuracy, information on eventual edits that have been made after DEM generation as well as a brief description of each DEM is available in Appendix C. Though elevation data from surface and terrain models may show some systematic offset due to the inclusion of canopy and building heights in the DSMs compared to real ground elevation assessment of DTMs, we include both types of DEMs in the comparison as these DEMs are most often used, sometimes without considering the DEM type and

suitability for its application. Thus, we want to demonstrate the relevance of careful DEM selection, because the outcomes of any geomorphological and hydrological study as well as risk assessment and flood modelling will strongly depend on the underlying elevation data (e.g. Wechsler, 2007; Siart et al., 2009; Gesch et al., 2018; Brosens et al., 2022).

Pre-processing of global DEMs and their respective water mask files included mosaicking of single DEM tiles, reprojection to UTM 46N based on Everest 1830 ellipsoid, clipping to the ROI and referencing to MSL. We used the latest Mean Dynamic Topography (MDT) data, i.e. the CNES-CLS18 dataset of Mulet et al. (2021), accessed via the AVISOC website (https://www.aviso.altimetry.fr/en/data/products/auxiliary-products/mdt/mdt-global-cnes-cls18.html, last access: 22 February 2022) as an estimation of sea surface height in relation to geoid (see Appendix C for details on local MSL in Myanmar and its potential offset to a geoid reference). Furthermore, the MDT may provide a more steady and reliable reference than the sparse and discontinuous tide gauge data as tidal range and mean sea level along the delta coast vary in space and time. The variety of vertical datums used by the array of DEMs together with the complex geoid setting along the Myanmar coast made datum transformation to MSL challenging, and relations between vertical references of MDT and DEM data needed to be considered when converting from geoid to MSL (Figure 4.2).

Processing involved, in total, three datum conversions. First, given that the majority of DEMs is referenced to the EGM96 geoid, the other datasets were transformed to EGM96 as well. Second, the original MDT data (called $MDT_{GOCO05s}$) were transposed to EGM96 (called MDT_{EGM96}). Subsequently, the third datum conversion was conducted by applying the MDT_{EGM96} to correct the DEMs to MSL. An overview of all datum transformation and processing steps is given in Figure 4.2, and all details are provided in Appendix C.

It should be noted that since the GLL-DTM v1 of Vernimmen et al. (2020) was already referenced to MSL, this DEM did not require the processing as outlined in Figure 4.2. However, the GLL-DTM v1 refers to MSL based on an older MDT dataset (Rio et al., 2014), which is referenced to the EGMDIR-R4 geoid, where the potential offset between this geoid and the original geoid reference of DEM data was not considered. Due to the missing integration of geoid offset, the GLL-DTM v1 should be used with caution. Although we are unable to correct this ourselves, we included it in our investigations of the Ayeyarwady Delta as it was generated especially for coastal lowlands and to highlight the importance of carefully dealing with vertical datums of datasets using different geoid models.

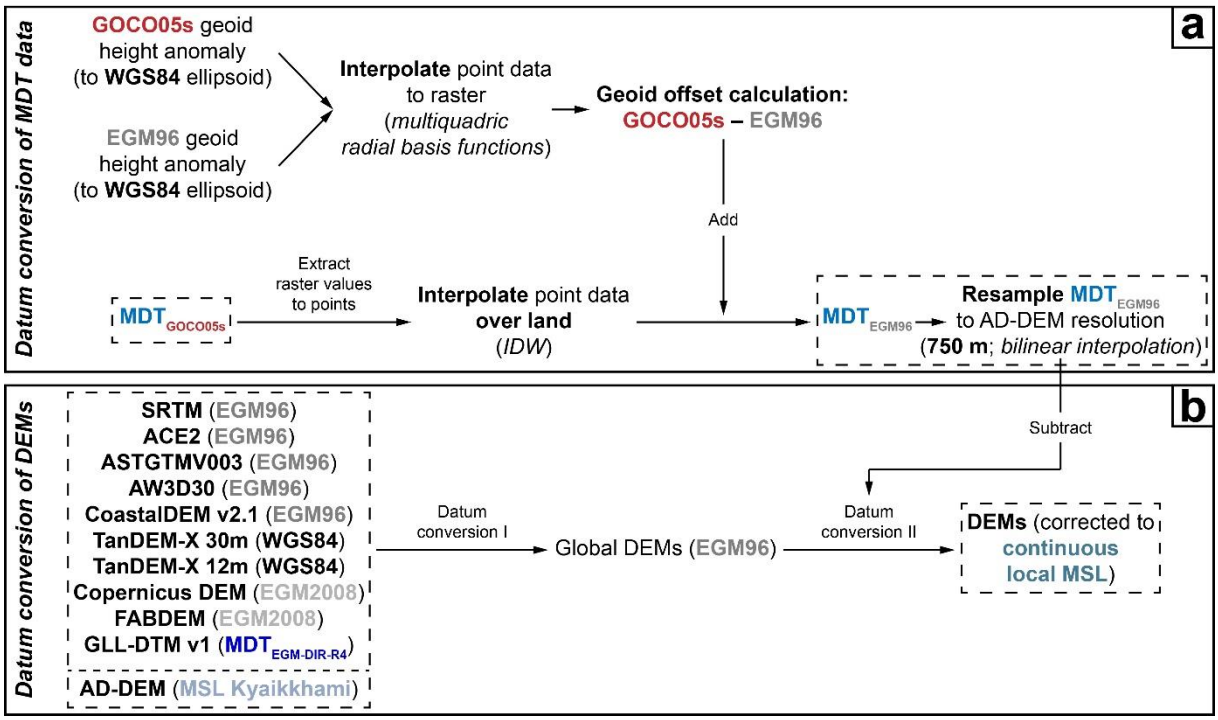


Figure 4.2 *| Workflow of datum conversions conducted in this study to reference the Mean Dynamic Topography (i.e. $MDT_{GOCO05s}$) and digital elevation models to a common reference geoid first (i.e. to the EGM96 geoid (MDT_{EGM96} in a); datum conversion I in b).*
Subsequently, the corrected MDT data (MDT_{EGM96}) were applied to reference all DEMs to the continuous local mean sea level (MSL) of the Myanmar coast (datum conversion II in b). AD-DEM is the newly developed digital elevation model for the Ayeyarwady Delta based on local data presented in this study.

After referencing the DEMs to MSL, inland water bodies were masked using the DEM-specific water mask files. In addition, cell values with an elevation of more than 7 m below MSL were removed as they likely constitute erroneous height estimates, following Vernimmen et al. (2020). Depending on the type of validation, i.e. with spot heights from topographic maps (East View Geospatial, Inc., 2014) or the AD-DEM, the global DEMs were further processed. The spatial resolution of the DEMs was resampled to match the horizontal accuracy of the AD-DEM using the bilinear resampling technique (ESRI, 2023). For validating the GLL-DTM v1, the AD-DEM was resampled to its resolution of 0.05° (Table C1 in Appendix C). Since outcrops and elevation values outside critical lowlands have been excluded to improve the interpolation of the AD-DEM, these areas were also excluded in the global DEMs to ensure comparability among all DEMs of this study.

Given the large number of DEMs included in this study, together with the most used DEMs in the context of studies with a focus on Myanmar as well as the expected similarity between TanDEM-X data and the limited comparability of the GLL-DTM v1, we decided to exclude the TanDEM-X 12 m and the GLL-DTM v1 data from the results in the main text. However, results for these DEMs are provided in Appendix C.

4.1.3.3 Mapping of areas prone to monsoon flooding

Besides direct validation using spot heights and the AD-DEM, we also performed an additional validation of relative elevation for the DEMs by their ability to match observed floods in deltaic areas affected by inland flooding. We adopted the principal approach from Minderhoud et al. (2019), who used the correlation of land elevation and tidal flooding to assess the quality of DEMs indirectly. Here, we use mapping of recent monsoon floods due to increased discharge as this allows for investigating the relation between topography and flood pattern also inland. Therefore, we mapped areas inundated during the monsoon periods of 2015 and 2020, respectively, using an image-rationing change detection approach on Sentinel-1 imagery (10 m spatial resolution) in the environment of Google Earth Engine (GEE; Gorelick et al., 2017). The pre-event imagery was recorded in February during the dry season, while the selection of imagery capturing maximum flood extents was made based on maximum rainfall amounts and river discharge. Monthly accumulated precipitation estimates were obtained from the GPM_3IMERGM v6 product of the NASA Global Precipitation Measurement (GPM) programme (Huffman et al., 2019) for the rainy months from May to October via the NASA Giovanni web environment (NASA, 2021). Discharge estimates from satellite microwave radiometry were accessed via the River and Reservoir Watch Version 4.5 processor of the Dartmouth Flood Observatory (Brakenridge et al., 2022) and were downloaded for River Watch stations 25, 29 and 30. Since an array of GEE scripts has been published in the recent past (e.g. Inman and Lyons, 2020; Moharrami et al., 2021; Tripathy and Malladi, 2022), we adopted the script of United Nations Platform for Space-based Information for Disaster Management and Emergency Response (UN-SPIDER, 2019) and slightly adjusted it, i.e. by setting the difference threshold to 1.3, thereby minimising false positive and false negative detections. For further handling and analysis, the data were vectorised in the ArcGIS Pro environment.

4.1.3.4 Mapping of areas prone to future RSLR

To gain insights into the potential impact of RSLR in the Ayeyarwady Delta, we estimated areas and population at risk of future RSLR. We calculated areas below certain elevation levels to simulate the impact of selected SLR scenarios by using median projections for Yangon from the NASA Sea Level Projection Tool of the IPCC Sixth Assessment Report (Fox-Kemper et al., 2021; Garner et al., 2021, 2022). Estimates of 50th and 83rd percentiles from the intermediate SSP2-4.5, the medium-to-high SSP3-7.0 and the high SSP5-8.5 reference scenarios were used to illustrate the area drowned due to SLR by 2100 and 2150, respectively.

From these, only the medium-confidence projections were included, thereby excluding the highly uncertain behaviour of the Greenland and Antarctic ice sheets and their contribution to SLR which are reflected by the low-confidence projections. To calculate the area below sea level, DEMs were used in their original resolution. The results were intersected with population data from the LandScan Global 2020 dataset (30 arcsec spatial resolution; Rose et al., 2021). To make our outcomes for decision-makers as clear and practicable as possible, results are presented at administrative district level.

4.1.4 Results

4.1.4.1 Performance and accuracy of the AD-DEM

The new, local AD-DEM not only reveals new insights into the topography of the Ayeyarwady Delta but also constitutes an independent source for evaluating the performance of global DEMs as it is based on field surveys and aerial photography. Given the uneven distribution of spot heights in the delta, point density ranges from 0 to 2.85 points km^{-2} with the highest densities in Yangon City. While elevation points in townships in the southernmost delta are regularly distributed at densities of up to 0.2 points km^{-2}, their distribution is highly irregular towards townships in the central and northern parts (~0.05–0.1 points km^{-2}), with profound data gaps at 17.2–17.5 and 17.7–18.0° N. Based on 4792 spot heights located within the ROI, point density within the delta is ~0.14 points km^{-2}. If areas without nearly any elevation points are excluded, the deltaic area is 28 801 km^2 instead of 33 357 km^2. Nevertheless, point density does not substantially improve (~0.17 points km^{-2}). This resulted in an optimal spatial resolution of our AD-DEM of 750 m × 750 m (Figure 4.1; Tables C1 and C2) as a coarser resolution means a downgrade of the best achievable accuracy, while a finer resolution is not justified by the spatially heterogeneous elevation point density.

Among all versions of the AD-DEM, version VI gives the best results with a vertical accuracy of 1.004 m root mean square error (RMSE) and an average standard error of 0.864 m (Table C2). Therefore, we base our investigations of deltaic topography and the comparison with global DEMs on this version of the AD-DEM. Elevation of the delta plain ranges between –1.7 and 8.8 m, with 50 % below 1.3 m (Figures 4.1 and C5; Table C3). While northern deltaic areas are more than 8 m above MSL, the AD-DEM indicates a sharp elevation change of up to 10 m at ~17.37° N with elevations even below –1 m above MSL in the north-eastern delta. As contour data along the river banks are nearly the only existing data in these areas, their dominance in

DEM interpolation may introduce this imperfection of sharp, unrealistic elevation change (Figure 4.1). From the central delta downstream (i.e. ca. 150 km downstream of the apex; Figure 4.5a), topography gradually smoothens to overall maximum elevations of several decimetres to 1 m (Figures 4.1 and 4.5a). At 16.25° N, where a second elevation offset of ~50 cm is visible in the AD-DEM at the boundary between irregularly to regularly distributed spot height data (Figures 4.1 and C1), mean elevation is around 1 m, locally higher in the upper centre of the lowest delta plain and lower at the island of Meinmahla Kyun Wildlife Sanctuary and along the delta shoreline (Figures 4.1 and C26).

4.1.4.2 Performance and accuracy of global satellite-based DEMs

4.1.4.2.1 Performance of global DEMs based on visual inspection

How differently the DEMs represent land elevation of the Ayeyarwady Delta becomes already clear by visual inspection (Figures 4.3 and C4). All DEMs indicate elevations of more than 10 m for the northernmost delta near the apex and lowest elevations in the southern and south-eastern parts, i.e. in Labutta and Pyapon districts. The most striking feature towards the coast is the island of Meinmahla Kyun Wildlife Sanctuary where all DSMs indicate higher elevation compared to the surroundings (Figures 4.3 and C26). For the entire delta plain, SRTM, ASTGTM v003 and AW3D30 document average heights of ~4.36 to 6.99 m (mean) and 3.68 to 6.32 m (median; Table C3). Among these, height distributions of SRTM and AW3D30 are quite similar while ASTGTM v003 reveals increased elevation counts for classes >4 m, showing delta-wide highest elevations for the entire dataset (Figures 4.3 and C5). Both SRTM and AW3D30 suffer from remote sensing artefacts as SW–NE-oriented stripes are visible in the SRTM, whereas topography as represented by AW3D30 is affected by distortions that reflect the sensor swaths of the ALOS PRISM (triplet mode; Tadono et al., 2009; Figure 4.3).

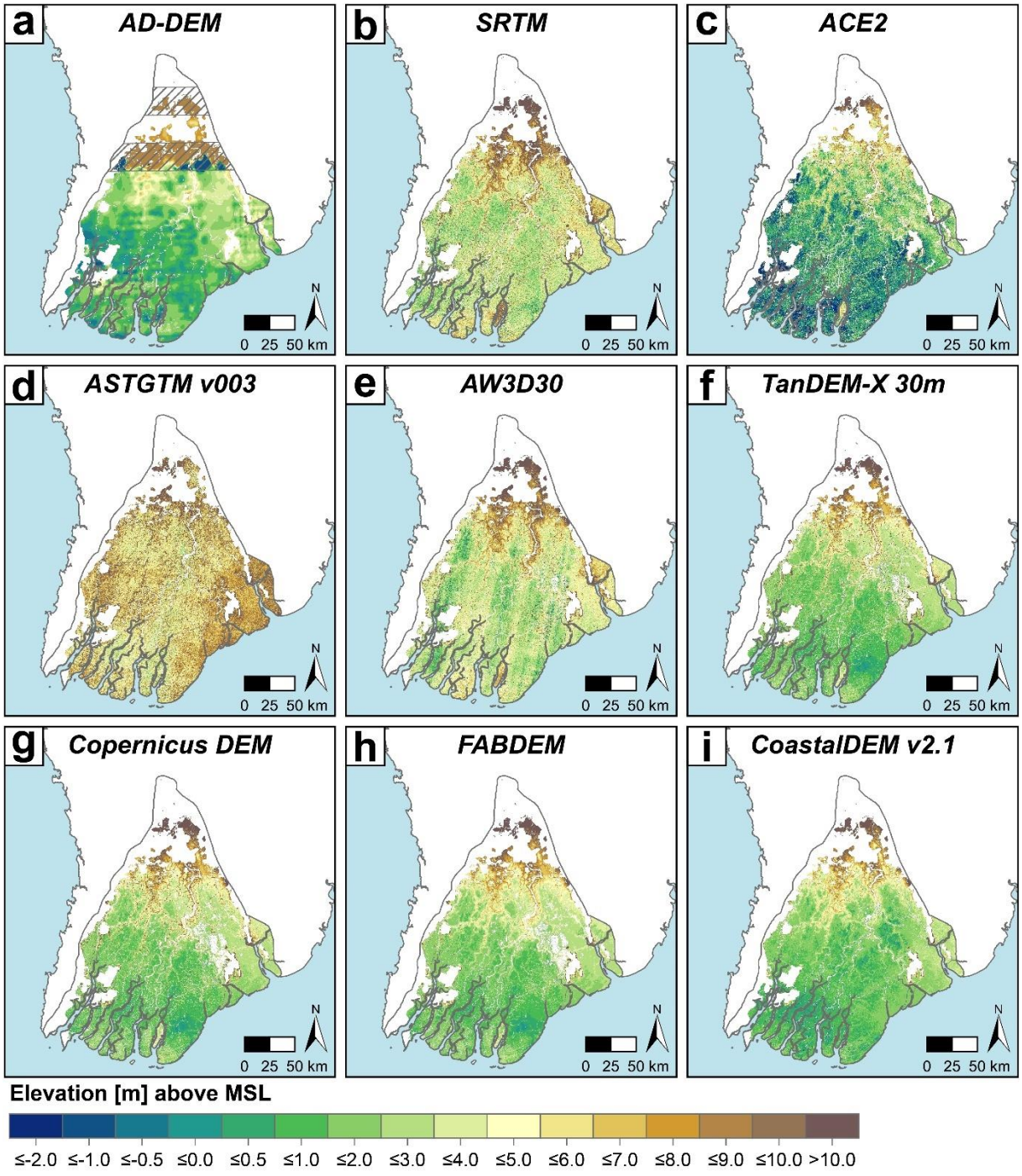


Figure 4.3 | *The new, local AD-DEM (a) in comparison to global digital elevation models in the Ayeyarwady Delta (b–i).*

With average heights of ~1.68 m (mean) and ~0.94 m (median; Table C3), ACE2 indicates the lowest elevation for the delta plain, which is reflected also by the comparably high frequency of counts below MSL (Figure C5). As ACE2 is the product of merging SRTM with altimetry data, it suffers from the same stripe artefacts as SRTM. In contrast, artefacts are not visible in TanDEM-X DEMs and processed versions like Copernicus DEM and FABDEM. As the TanDEM-X 30 m was generated by averaging heights from TanDEM-X 12 m data, both their statistics and rasters are very similar. However, maximum heights of more than 400 m above

MSL point towards the presence of unrealistic elevation values that are likely erroneous as the delta ROI does not include any mountains or elevated terrain (Table C3). Consequently, these values have been corrected in Copernicus DEM and FABDEM. Removing trees and buildings from the Copernicus DEM makes FABDEM (Hawker et al., 2022) deliver a smoother surface with less deviation of elevation data and lower average heights of ~2.75 m (mean) and ~1.83 m (median; Table C3). Though the TanDEM-X, Copernicus DEM, FABDEM and CoastalDEM v2.1 share the general pattern of height distributions, lowest elevations of <2 m are especially frequent in CoastalDEM v2.1 (Figure C5). Mean and median elevation of CoastalDEM v2.1 nearly match the AD-DEM (Table C3); however, visual investigation reveals that the same sensing artefacts as observed for SRTM are present. Hence, this implies that – since CoastalDEM v2.1 used elevation data from the NASADEM, which is an improved SRTM – both processing and corrections of SRTM applied in NASADEM and CoastalDEM v2.1, respectively, could not account for these artefacts adequately. According to the GLL-DTM v1, average heights are higher than observed for CoastalDEM v2.1 and more similar to FABDEM and Copernicus DEM, while there is much less scatter of elevation counts (Table C3; Figure 4.1.3). The latter may be attributed to its comparably coarse resolution that does not capture small-scale topography. However, given that the GLL-DTM v1 refers to a different MDT dataset than the one used in this study, without being corrected for this unknown geoid offset, it remains open whether this vertical bias is responsible for indicating higher elevations than, for example, AD-DEM (Table C3; Figures C4 and C5).

4.1.4.2.2 Direct validation with spot heights from topographic maps

After extracting all 4792 spot heights inside the ROI from the DEMs using bilinear interpolation of values at point location, we included only those containing data in the specific DEM. Spot heights range from –2.31 to 214.99 m above MSL with mean and median elevation of 6.06 and 1.69 m, respectively (Figure C6). Largest inaccuracies are documented for the ASTGTM v003 with average height residuals of 2.75 m (mean) and 4.38 m (median), as well as 6.21 m for absolute error and 9.20 m for RMSE (Tables 4.1 and C4; Figures C7 and C8). Thus, R^2 of 0.75 indicates the lowest quality compared to other DEMs of this study (Tables 4.1 and C4). Though SRTM performs better than ASTGTM v003 in terms of height residuals, it still indicates elevations overall higher than the spot heights. In contrast, while the corrected SRTM version ACE2 has a comparatively high correlation (R^2 = 0.86), it mainly shows negative deviations (Table 4.1; Figure C7). The absolute error is still more than 3 m, and the elevation data show substantial scatter as reflected by the maximum standard deviation, σ, compared to all DEMs.

TanDEM-X and improved versions like Copernicus DEM and FABDEM reveal not only lower height residuals but also point densities that are considerably higher than for the others (Figures C7–C10). Nevertheless, RMSE is in a similar range as for SRTM and ACE2, being 7.23 m minimal for the Copernicus DEM (Table 4.1). The recently published FABDEM shows the lowest absolute error of 2.73 m and median height residual of ~0.24 m, and it performs nearly as well as ACE2 in terms of R^2 (Table 4.1). Being generated for coastal regions in particular, CoastalDEM v2.1 indicates even less uncertainty with median height residuals on the centimetre scale, and median elevation differs by only 0.12 m from median spot height elevation (Table 4.1; Figure C8). In contrast, mean and absolute errors are increased, and RMSE is the second largest, amounting to 7.81 m. R^2 is slightly lower than for Copernicus DEM and FABDEM (Table 4.1). Overall, all DEMs indicate significantly lower elevations for the mountain ranges of the Rakhine Mountains, and so far, we have no explanation for this.

Table 4.1 *| Statistics for DEMs minus spot height elevation at spot height location.*
Best performances are shown in italics. DEMs were used in their original resolution and vertically referenced to the same mean sea level. N – number of spot heights in the ROI, with no data values excluded for each DEM, respectively; HR – height residual; MAE – mean absolute error; RMSE – root mean square error; Min – minimum DEM elevation at spot height location; Max – maximum DEM elevation at spot height location; mean spot – mean elevation of all spot heights included in the comparison; mean DEM – mean DEM elevation at all spot height locations included in the comparison; Median spot – median elevation of all spot heights included in the comparison; Median DEM – median DEM elevation at all spot height locations included in the comparison; σ spot – standard deviation of elevation of all spot heights included in the comparison; σ DEM – standard deviation of DEM elevation at all spot height locations included in the comparison; σ HR – standard deviation of height residuals; R^2 – coefficient of determination.

DEM	*N*	Mean HR	MAE	RMSE	Min DEM	Max DEM	Mean spot	Mean DEM	Median spot	Median DEM	Median HR	*σ* spot	*σ* DEM	*σ* HR	*R^2*
SRTM	4781	1.17	4.05	7.36	-3.31	182.88	6.00	7.17	1.68	4.20	2.09	16.11	11.90	7.26	0.83
ACE2	4358	-1.87	3.32	7.33	-6.41	189.09	6.39	4.52	1.77	1.32	-0.80	16.78	12.44	7.08	*0.86*
ASTGTM v003	4776	2.75	6.21	9.20	-2.31	165.07	6.00	8.75	1.69	6.82	4.38	16.11	10.49	8.77	0.75
AW3D30	4775	0.93	3.79	7.35	-2.74	167.52	6.00	6.94	1.70	4.01	2.01	16.11	11.50	7.29	0.84
TanDEM-X 30 m	4678	*-0.23*	3.09	7.52	-4.97	166.03	6.09	5.86	1.71	2.42	0.54	16.27	11.63	7.52	0.82
Copernicus DEM	4776	-0.52	2.90	*7.23*	-1.12	166.11	6.00	5.48	1.69	2.25	0.41	16.11	11.53	7.21	0.84
FABDEM	4776	-1.01	*2.73*	7.40	-1.12	160.34	6.00	4.99	1.69	2.04	0.24	16.11	10.96	7.34	0.85
CoastalDEM v2.1	4746	-1.65	2.94	7.81	-2.28	192.21	6.00	4.34	1.70	1.58	*-0.06*	16.10	10.81	7.63	0.83

To assess the quality of the DEMs for the low-lying delta parts, we validated them against spot height elevations less than 10 m above MSL (Tables 4.2 and C5). Integrated spot heights (Σ 4112) range from –2.31 to 9.97 m above MSL. As observed for the DEM comparison with all spot heights, similar trends are found for low elevations, with ASTGTM v003 being the least accurate one (Table 4.2). SRTM and AW3D30 are characterised by comparably less deviations; ACE2 and TanDEM-X perform better, showing even lower height residuals and higher point densities (Figures C11 and C12; Tables 4.2 and C5). However, they all show RMSE in the same range of 2.58 to 3.87 m and overall low quality with R^2 of 0.28. Best results are delivered by those DEMs that have been corrected by processing with additional datasets. While CoastalDEM v2.1 shows the best accuracy with average residuals of 0.04 m (mean) and 0.14

m (median), as well as 1.31 m of absolute error and 1.79 m RMSE, FABDEM documents the highest level of agreement with spot height data (R^2 = 0.45; Table 4.2), which is also reflected by maximum point densities (Figure C12). In contrast, the relatively poor performance of the GLL-DTM v1 in terms of R^2 likely results from its spatial resolution being too coarse to give adequate results for the spot height comparison, which adds to the unknown bias of its different vertical datum (Table C5).

Table 4.2 *| Statistics for DEMs minus spot height elevation at spot height location for the low-lying delta plain (spot heights <10 m above MSL).*
DEMs were used in their original resolution and vertically referenced to the same mean sea level. Best performances are shown in italics.

	N	**Mean HR**	**MAE**	**RMSE**	**Min DEM**	**Max DEM**	**Mean spot**	**Mean DEM**	**Median spot**	**Median DEM**	**Median HR**	**σ spot**	**σ DEM**	**σ HR**	***R²***
SRTM	4105	2.50	3.01	3.87	-3.31	34.07	1.82	4.32	1.33	3.75	2.31	2.20	3.28	2.95	0.23
ACE2	3694	-0.42	1.92	2.58	-6.41	19.13	1.87	1.45	1.35	0.85	-0.56	2.26	2.87	2.55	0.28
ASTGTM v003	4100	4.82	5.20	6.08	-2.31	33.91	1.82	6.65	1.33	6.43	4.86	2.20	3.47	3.71	0.04
AW3D30	4099	2.32	2.70	3.39	-2.74	25.03	1.83	4.15	1.33	3.66	2.28	2.20	2.80	2.47	0.29
TanDEM-X 30 m	4002	1.14	1.78	3.01	-4.97	40.66	1.83	2.97	1.34	2.04	0.68	2.21	3.22	2.79	0.28
Copernicus DEM	4100	0.79	1.60	2.39	-1.12	23.62	1.82	2.62	1.33	1.82	0.55	2.20	2.76	2.26	0.37
FABDEM	4100	0.46	1.32	1.84	-1.12	21.27	1.82	2.28	1.33	1.67	0.40	2.20	2.21	*1.79*	*0.45*
CoastalDEM v2.1	4078	*0.04*	*1.31*	*1.79*	-2.28	17.18	1.83	1.87	1.34	1.35	*0.14*	2.20	2.02	*1.79*	0.42
AD-DEM	3616	-0.03	0.53	0.85	-1.26	8.37	1.60	1.56	1.29	1.19	0.03	1.85	1.53	0.85	0.80

In the absence of any additional independent ground truth measurements in the Ayeyarwady Delta, we checked the AD-DEM against the spot heights (<10 m only) used for interpolation to assess the performance of the interpolation algorithm for the AD-DEM. For low-lying elevations, the AD-DEM is accurate at 0.53 m absolute error and 0.85 m RMSE, showing average height residuals of –0.03 m (mean) and 0.03 m (median). The quality of correlation is documented by R^2 of 0.80 (Table 4.2).

Overall, and as the statistics of this comparison with spot heights show, it turns out that relying on individual selected accuracy parameters does not provide a holistic picture of the performance of a DEM. Rather, mean and median residuals, absolute errors, and RMSE and R^2 indicate varying degrees of DEM quality. Therefore, we suggest that the collective of these statistics provides the best answer to which DEM represents the true elevation of the delta best.

4.1.4.2.3 Direct validation of global DEMs with AD-DEM

Validation with the AD-DEM serving as reference allows us to assess and quantify spatial patterns and differences, thereby complementing the comparison of DEMs by visual inspection (Section 4.1.4.2.1) and at spot height locations (Section 4.1.4.2.2). By subtracting resampled DEM versions by the AD-DEM, the resulting maps and their statistics document both similarities and differences between the DEMs (Figures 4.4 and C13; Table C6). Relative to AD-DEM, in general, most DEMs tend to overestimate elevation of the delta plain (Figures 4.4 and C13).

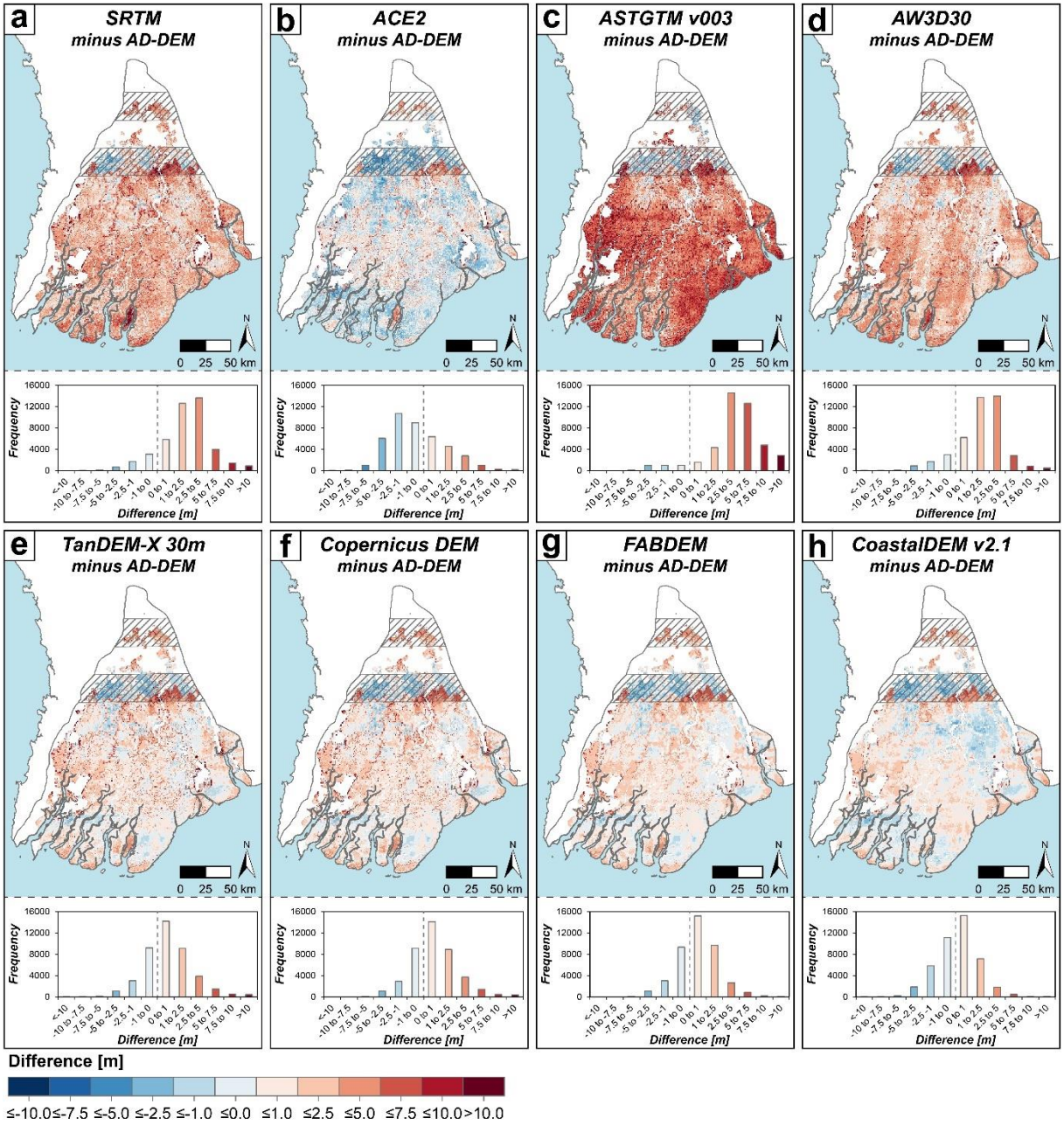


Figure 4.4 *| Differences between global DEMs and the AD-DEM together with frequency distributions of height residuals (in m).*
Areas where AD-DEM has interpolation artefacts are marked with hatching.

SRTM, ASTGTM v003, and AW3D30 show deviations of several metres that are on average 4.87 m (mean) and 4.75 m (median) for ASTGTM v003 and 3.83 m (mean) and 2.22 m (median) for SRTM (Table C6). Since AW3D30 strongly suffers from artefacts (see Section 4.1.4.2.1), these also become visible in the difference map (Figure 4.4d). While ASTGTM v003 indicates maximal positive deviations from AD-DEM, ACE2 documents the most negative ones, i.e. lowest elevation compared to AD-DEM (Figures 4.3 and 4.4; Table C6). The error statistics of ACE2 range between that of the aforementioned DEMs and TanDEM-X data which perform moderately compared to all other DEMs of this study (Figures 4.4 and C13; Table C6). Height

residuals and uncertainties of TanDEM-X are slightly reduced by Copernicus DEM and FABDEM (Figure 4.4e–g; Table C6). FABDEM differs from AD-DEM by 0.63 m (mean) and 0.46 m (median) revealing an uncertainty of 2.00 m RMSE (Figure 4.4g; Table C6). Its quality relative to AD-DEM is further described by an R^2 of 0.53. Besides FABDEM (and the GLL-DTM), CoastalDEM v2.1 shows the greatest similarity to AD-DEM as residuals are mainly present on the decimetre scale (Figure 4.4h; Table C6). Thus, uncertainty is minimal with RMSE = 1.75 m, while correlation to AD-DEM only slightly improves compared to FABDEM, amounting to R^2 = 0.55 (Table C6).

Aside from the central and southern delta plain, all DEMs underestimate delta elevation relative to AD-DEM in the northern part, i.e. where mainly contour data (only present along river banks) could be used to interpolate the AD-DEM. Similarly, all DEMs show higher elevations directly south of this zone, overall reflecting the interpolation artefacts in the AD-DEM.

4.1.4.2.4 Indirect validation of DEMs by comparison with areas drowned during recent flood events

Investigating the topography of areas that have recently been affected by flooding provides an indirect way to detect potential inaccuracies in the DEMs. Though pluvial and fluvial flooding may be less correlated with absolute elevation than, for example, tidal flooding, we expect a correlation of flooded areas with topographic depressions and other low-relief surfaces and use this spatial relation to validate the DEMs in terms of relative elevation. The 2015 and 2020 monsoon flooding events show different spatial extents, with the 2020 flooding affecting more areas in the southern part of the delta than in 2015. These areas are relatively lower in elevation as documented by the DEMs (Figure C18; further details are given in Appendix C). To evaluate the DEMs, we generated several elevation profiles throughout the delta that cross particularly flood-prone areas, thereby including different land surface types as well as typical features of fluvial landscapes (Figures 4.5 and C19).

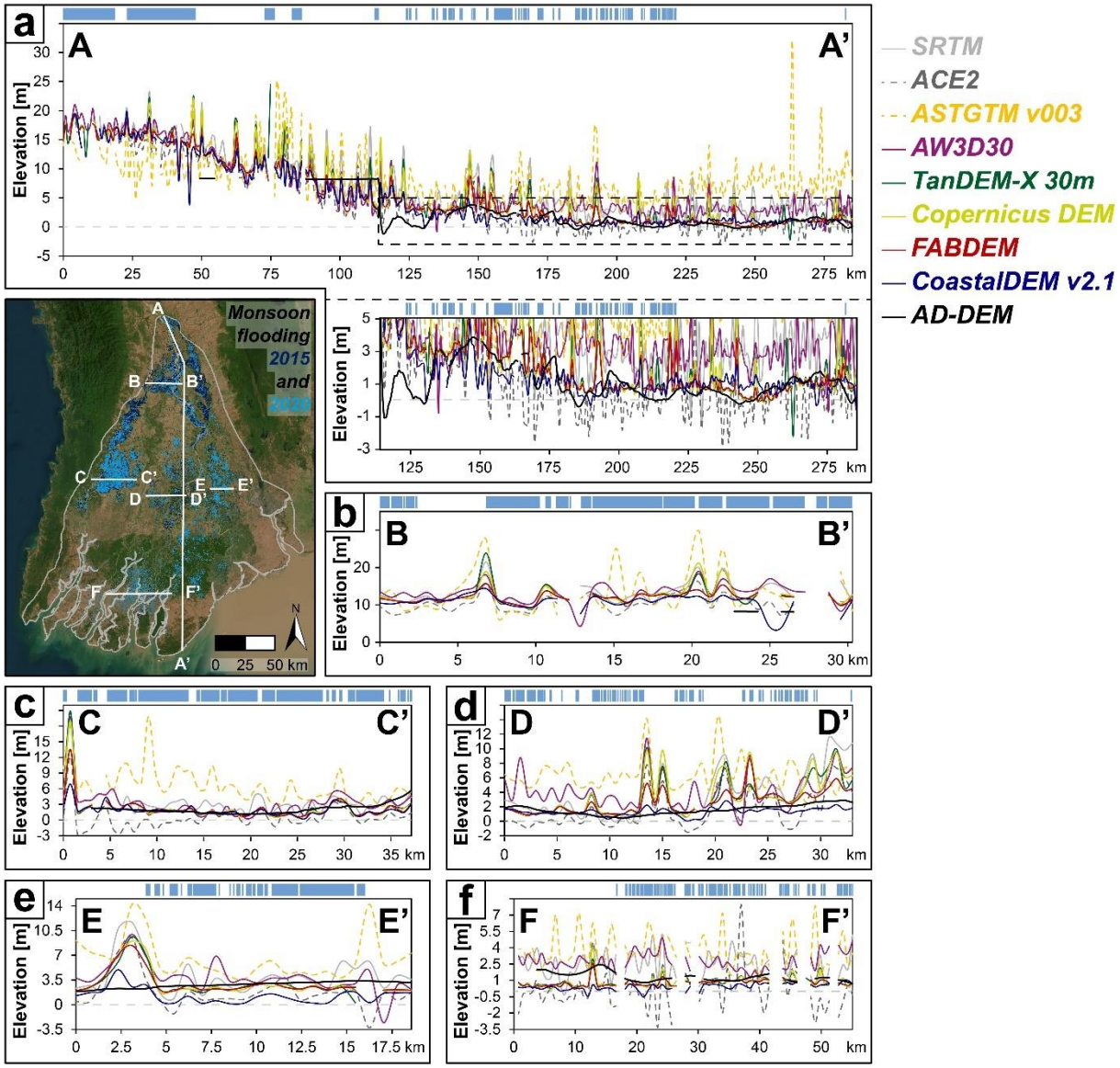


***Figure 4.5** | Delta elevation along longitudinal (a) and cross sections (b–f) in deltaic areas affected by flooding during the monsoon seasons of 2015 and 2020 (Base map: EsriWorld Imagery, 2017).*
Elevation profiles are based on DEMs resampled to 750 m spatial resolution. Blue bars on top of the profiles indicate the location of inundated areas along the profiles. The black dashed rectangle in (a) marks the low-elevation zone along the longitudinal profile that is also shown enlarged.

For the upper delta plain, which is characterised by abandoned river channels, levees, shrubland vegetation and cropping (Vogel et al., 2022), most DEMs show similar cross sections for profile B–B' where depressions coincide with mapped inundation (Figure 4.5b). However, while ASTGTM v003 indicates elevation changes of sometimes more than 20 m over short distance that are likely unrealistic within an individual inundation area, ACE2 performs partly contrary to the other DEMs, particularly in the western part of profile B (Figure 4.5b). Here, according to ACE2, only slopes of a depression would have been affected by flooding while the lowest point would have remained dry. In the most western part of the ROI, profile C–C' documents the transition of the Rakhine Mountains towards the Ayeyarwady basin north of Pathein that is

characterised by shrubland and agricultural land use (Vogel et al., 2022). Since most of the DSMs show abrupt elevation changes within individual inundation zones, only corrected DSMs (or nearly DTMs) such as Copernicus DEM, FABDEM and CoastalDEM v2.1 that show moderate changes seem reasonable (Figure 4.5c). In contrast, GLL-DTM v1 and AD-DEM only reflect the general, large depression of Pathein as small-scale topographic features are either averaged out or not recorded at all due to data paucity. Lying in the central delta, profile D–D' crosses a sequence of silted-up oxbows, which are used for the cultivation of irrigated crops (Vogel et al., 2022), separated by former river banks, covered with shrubs and trees. All TanDEM-X-based DEMs indicate a similar relative topographic setting, with differences in absolute elevation becoming particularly obvious along vegetated former river banks. The TanDEM-X-based DEMs show major differences from ASTGTM v003 and AW3D30 and minor deviations from SRTM (Figure 4.5d). From the high- and mid-resolution DEMs, CoastalDEM v2.1 indicates the smoothest topographic profile, showing the highest correspondence with AD-DEM and also underlying spot heights (Figures 4.5d and C8). Overall, depressions and flat terrains with maximum elevations of 8 m above MSL were the most extensively affected by the monsoon flooding events (Figure 4.5d). However, given that individual inundation areas are small compared to DEM resolution, this does not allow for further conclusions other than already stated above, where ASTGTM v003, ACE2 and AW3D30 show less correspondence with flood mapping.

At profile E–E' in the eastern delta, characterised by a marshy environment used for the cultivation of irrigated crops (Vogel et al., 2022), flooding is more extensive than for the silted-up oxbows, with the largest contiguous inundation areas being located in the flattest topographies (Figure 4.5e). Given that embankments in the Ayeyarwady Delta were designed to protect against floods of up to a 20-year recurrence (e.g. Myat Myat Thi et al., 2012), the dike present in the westernmost part of the cross section has a relative elevation of 4–5 m and is therefore best represented by CoastalDEM v2.1 as most of the other DEMs indicate higher relative dike elevation (Figure 4.5e). However, CoastalDEM v2.1 indicates significantly lower absolute elevations than those of independent elevation data (see also Figure 4.4h) and implies an atypical bimodal profile of the dike. Thus, FABDEM provides the best compromise and best reflects both the relative height of the dike and the smooth topography of the embanked paddy fields. Though the integration of only two events might be insufficient to characterise flood risk in detail, there is an obvious relation between relief and inundation, promoting low-relief and water-logging conditions inside the embanked area. Finally, profile F–F' crosses the lowest

delta plain, once a transition zone towards coastal mangrove marsh, nowadays used for cultivating irrigated and dry crops (Vogel et al., 2022). This area was flooded particularly during the 2020 monsoon season and is characterised by many small individual inundation areas (Figure 4.5f). However, these are not restricted to depressions, which are mainly located distal to the distributary channels and in the centre of deltaic islands, but rather occur also in the surroundings, which most DEMs indicate to have a pronounced relief (Figure 4.5f). As the profile section does not cross any significantly inclined topographical features like steep river banks or beach ridges, which can be found directly along the shore, FABDEM, CoastalDEM v2.1, GLL-DTM v1 and AD-DEM likely reflect the topographic setting more realistically than the others, with FABDEM performing most similar to AD-DEM (Figure 4.5f).

4.1.4.3 Estimation of coastal area at risk of future sea level rise

Combining the DEMs with the latest datasets of SLR projections and actual population (as of 2020) allows us for the first time to quantify both the spatial extent and number of people prone to flooding by SLR in the Ayeyarwady Delta. By 2100, regional sea level will be 0.712 m (50th percentile of SSP24.5 scenario) to 1.229 m (83rd percentile of SSP5-8.5 scenario) higher than in the reference period of 1995 to 2014 (Fox-Kemper et al., 2021). By 2150, which is the maximum of the projection timeline, even delta parts of more than 2.210 m elevation could be drowned (Figures 4.6, C20 and C21; Table C7; Fox-Kemper et al., 2021). However, these future sea levels will be reached even sooner when rates of land subsidence are higher or more dynamic than considered in the vertical land motion rates of the IPCC Sixth Assessment Report.

For the 0.712 m SLR scenario, the range of DEMs indicates in total 18.5 to 11072.0 km^2 (0.1 % to 42.5 %) of the administrative deltaic area to be lost, an area today populated by ~3800 to more than 3 million people (2020 population; Figure C22; Table C7). With 1.229 m SLR under the high SSP5-8.5 scenario, more than 50 % of the delta could fall below sea level, thus affecting an area where ~25 % of the delta's 2020 population is living (Figure C22; Table C7). However, these numbers can be narrowed down when using the DEMs with the most robust performance in Section 4.1.4.2. FABDEM, CoastalDEM v2.1 and AD-DEM indicate 7.0 %, 17.5 % and 31.3 % of land below a 0.712 m raised sea level and even 30.7 %, 42.4 % and 46.7 % if SLR reaches 1.229 m (Table C7). Within these areas, today more than 359 000 (FABDEM; 0.712 m SLR scenario) to nearly 3 million people (AD-DEM; 1.229 m SLR scenario) are living. Sea levels higher than 2.210 m compared to the baseline reference 1995–2014, as projected by the IPCC for 2150, will increase the drowned delta area by a further ~20 %–30 %, i.e. to 53.2

% for FABDEM, 67.5 % for CoastalDEM v2.1 and 65.0 % for AD-DEM (Table C7), while estimates based on lower GHG emission scenarios from 2150 projections are in the range of high GHG emission scenarios for the year 2100. Accordingly, these DEMs indicate a population of 3.6 million to 5 million people living today in areas below 2.210 m above MSL; this is equivalent to one-third of the total delta population (as of 2020). ACE2 even points to nearly 5.2 million people living at risk of SLR, while in contrast ASTGTM v003 reveals the lowest estimate of ~64 500 people (Table C7).

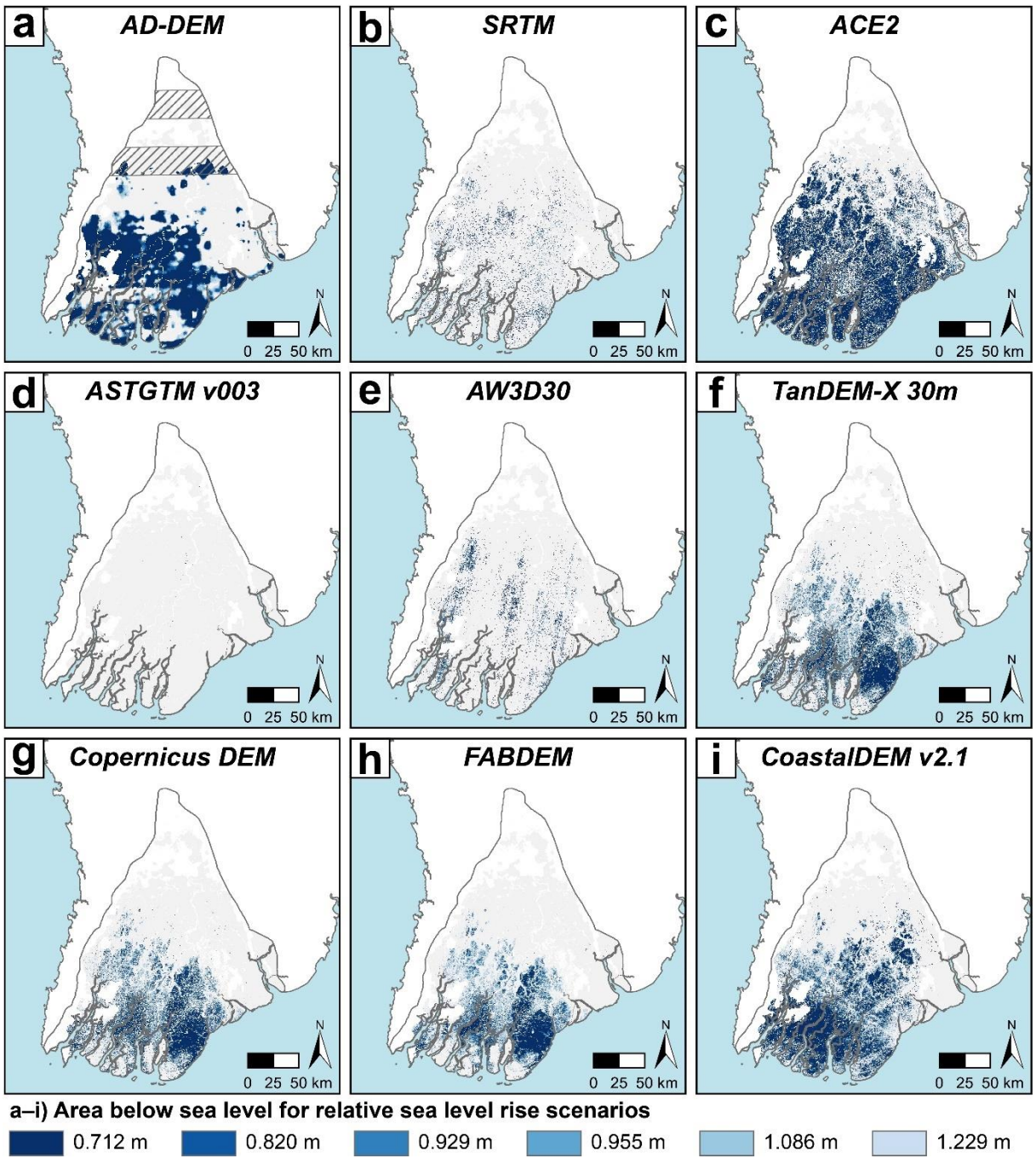


Figure 4.6 *| Area below future mean sea level according to local and global DEMs following median sea level rise projections for Yangon for 2100 (compared to the baseline period 1995–2014) from the Sea Level Projection*

Tool of the IPCC Sixth Assessment Report (Fox-Kemper et al., 2021; Garner et al., 2021, 2022). Note that in case of higher RSLR, these scenarios will be reached sooner than 2100.

Besides those estimates, the DEMs also show different spatial patterns of SLR impact, thereby again reflecting sensing artefacts like stripes as discussed in Section 4.1.4.2.1 (Figures 4.6, C20 and C21). The majority of the DEMs, i.e. all TanDEMX-based DEMs as well as the AD-DEM and GLL-DTM, indicates that moderate SLR will largely impact the southeastern delta, while only ACE2, CoastalDEM v2.1 and AD-DEM also show areas affected more inland (Figures 4.6, C20 and C21). However, all of them point towards the administrative districts of Pyapon, Labutta and Myaungmya, which are particularly vulnerable to SLR as the cities of Pyapon, Dedaye, Bogale, Kyaiklat, Labutta, Mawlamyinegyun, Myaungmya, Einme and Wakema (Figure C26), each of them with more than 5000 inhabitants, are located in those areas that will be drowned by up to ~94 % in the future (Figures 4.7 and C22–S25). The least affected districts will be Hinthada and Thayarwady in the northernmost delta. Besides FABDEM and CoastalDEM v2.1, which revealed a comparably good performance in comparison with independent elevation data, the SLR impact assessments based on these DEMs lead to considerably different estimates of affected district areas and population, thereby highlighting the range of uncertainty for each district (Figures 4.7 and C25). For the SLR scenarios as projected by the IPCC for 2100, largest spatial uncertainties amount to ~30 % for Myaungmya and ~24 % for Labutta districts, equivalent to an absolute range of up to ~348 000 ± 57 000 and ~487 000 ± 119 000 people (2020 population) who live at risk of 1.229 m SLR in Labutta and Myaungmya, respectively (Figure C25). Even higher sea levels as are projected for 2150 further turn out the exposure and vulnerability of the densely populated metropolitan area of Yangon and Ma-ubin district with the smaller cities of Ma-ubin, Pantanaw, Nyaungdon and Danubyu (Figures 4.6, 4.7 and C25–C26). Based on the 2.210 m SLR scenario, between ~322 000 and 682 000 people (2020 population) will be affected in Ma-ubin district, reflecting the largest spatial uncertainty for the best-performing DEMs (i.e. ~35 %, equivalent to >360 000 people; Figures 4.7 and C25). Though spatial uncertainty of SLR impact is less for the Yangon districts (i.e. ~8 %–30 %), the range of affected population increases as population density is magnitudes higher than in other districts (Figure C26). Thus, based on the comparison of AD-DEM, FABDEM and CoastalDEM v2.1, we estimate ~362 000 ± 265 000 people in Yangon North, ~317 000 ± 109 000 in Yangon South, ~368 000 ± 93 000 in Yangon East and ~30 000 ± 29 000 people in Yangon West (2020 population) to be affected by SLR until 2150 (Figures C24 and C25). However, much larger uncertainties of nearly 95 % exist if considering all DEMs of this study, despite their qualitative performance. As these largest uncertainties are obtained for

the district of Pyapon under the projection of 2.210 m SLR, translation into population counts to a range of ~20 000 to ~974 000 people at flood risk due to SLR (Figure C24).

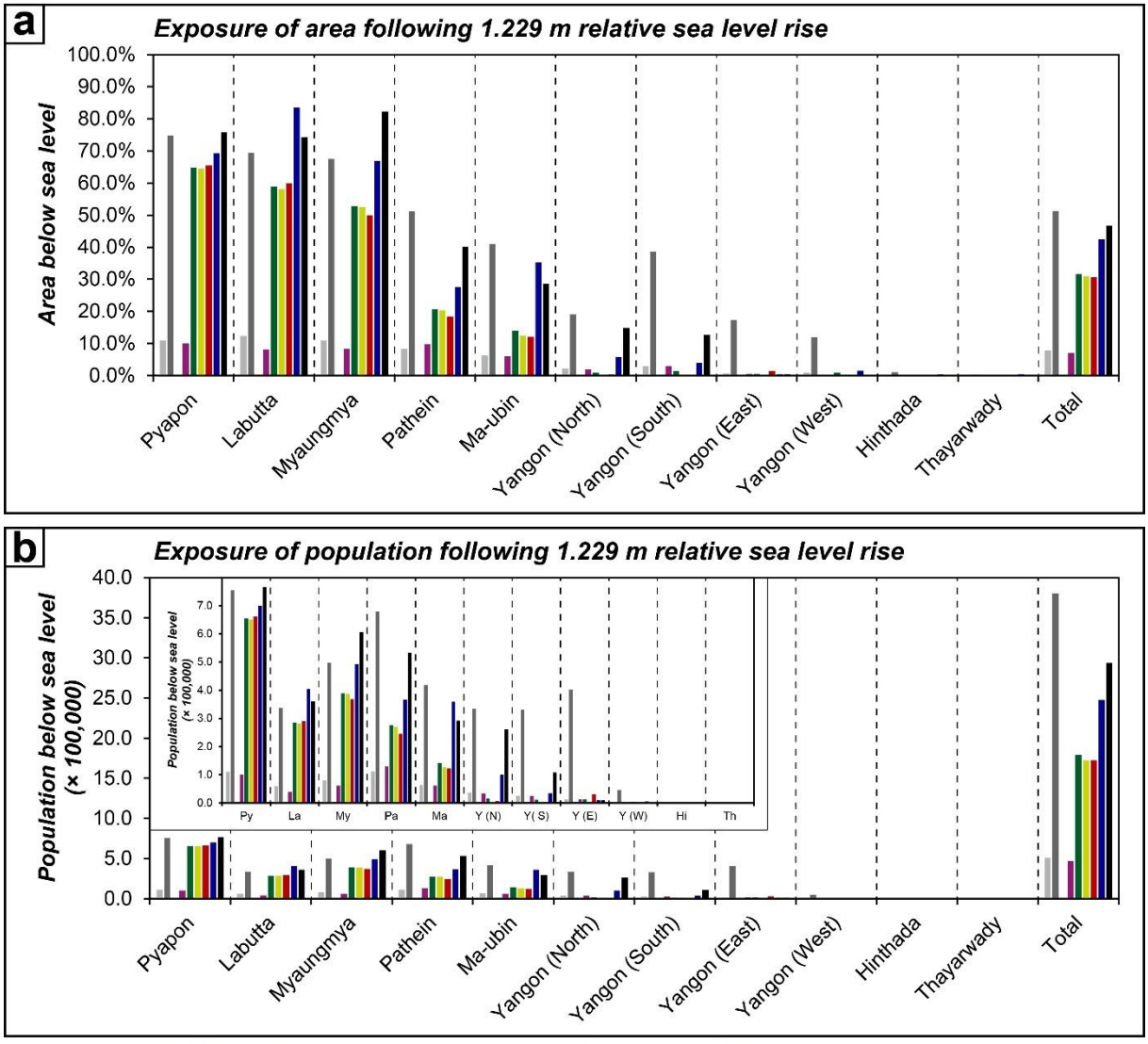


***Figure 4.7** | Area (a) and people (b) affected by sea level rise of 1.229 m as projected by SSP5-8.5 (83rd percentile) for 2100 for each administrative district of the Ayeyarwady Delta and the entire delta.*
Estimates of affected district population are enlarged in the insets. All population estimates are based on the actual population of 2020 (Rose et al., 2021).

Overall, in view of all SLR scenarios considered in this study, the most extensive impact on almost all deltaic districts will occur when SLR exceeds 0.929 and 1.086 m by 2100 as well as 1.939 and 2.210 m by 2150 (Figure C22), pointing towards the impending challenge of potential huge outmigration of the delta. As vertical land motion rates of the IPCC Sixth Assessment Report may not sufficiently capture the contributions of land subsidence and land elevation change, actual RSLR may exceed these IPCC projections, thereby pointing to the uncertainty in timing of SLR impact.

4.1.5 Discussion

4.1.5.1 Suitability of DEMs for studying flood risk in the Ayeyarwady Delta

Based on local geodetic measurements, the here-presented, local AD-DEM reveals unique and highly valuable information on land elevation of the Ayeyarwady Delta at high vertical accuracy of 0.86 m mean average standard error and 1.00 m RMSE. Therefore, it not only serves for evaluating global satellite-based DEMs but also provides new reliable insights into the exposure of the delta to RSLR. Focussing on low elevations of ≤10 m makes it particularly suitable to study the central-to-lower delta plain, which are the most vulnerable parts to RSLR. Though its spatial resolution of 750 m × 750 m may hamper its suitability on a small, local scale (e.g. in terms of identifying single topographical features), AD-DEM proves particularly well for studying larger local/subregional (e.g. at township level) to delta-wide patterns of topography, land elevation and correlated exposure to floods and RSLR.

To evaluate the performance of DEMs in the Ayeyarwady Delta, we assessed 10 global DEMs, firstly based on their visual impression, secondly in relation to independent elevation data in terms of spot heights and the AD-DEM, and thirdly by conducting an indirect validation by analysing the topographies of areas inundated during recent flooding events. While stripes and sensing artefacts constitute obvious qualitative constraints for some DEMs (i.e. SRTM, AW3D30, CoastalDEM v2.1) or turn out in the form of unrealistic elevation values that are likely erroneous (e.g. TanDEM-X), accuracies are specified by an array of error metrics. Overall, none of the DEMs included in this study prove best for each metric and each validation type. Since the datum of the GLL-DTM v1 could not be tied to the same local MSL as all the other DEMs, its statistics calculated in this study may not be reliable. When comparing the DEMs to spot heights (and excluding the GLL-DTM v1), Copernicus DEM shows the smallest RMSE, while FABDEM indicates the smallest MAE, and median height residual is minimal for CoastalDEM v2.1 (Table 4.1). In contrast, ACE2 shows the highest agreement with the spot height data. However, in view of low elevations (<10 m), CoastalDEM v2.1 and FABDEM reveal the best accuracies (Table 4.2). The latter DEMs also show the lowest errors in comparison to AD-DEM (Table C6), where CoastalDEM v2.1 indicates uncertainties of 0.10 to 0.46 m less than FABDEM, while correlation with AD-DEM improves only slightly (Table C6).

However, the lack of evenly distributed spot heights together with the presence of elevation data in the upper delta plain only along the river banks constitutes itself a source of uncertainty

for the AD-DEM, with the elevation of the delta plain potentially not completely represented locally. Since we observe elevation offsets to spot heights in the Rakhine Mountains for all DEMs exceeding up to –2.5σ, these are likely systematic biases we have no explanation for but which may be attributed to inconsistencies during surveying and data collection that may occur over such a large area (i.e. >44 000 km^2; JICA et al., 2004). Still, as these biases are restricted to the mountain ranges, we highlight the value of the AD-DEM for assessing land elevation in the low-lying delta because it represents local elevation with a vertical accuracy at a decimetre to metre scale, being independent of satellite-based measurements, where errors are in the range of several metres.

Furthermore, the systematic offset between DSMs and DTMs needs to be considered as the AD-DEM constitutes a DTM, which is also reflected by overall lower elevations in vegetated areas such as in the mangroves of the Meinmahla KyunWildlife Sanctuary or along former point bars now covered by shrubs and trees (Figures 4.4, 4.5, C13 and C19). Rightfully, the corrected DSMs, namely FABDEM and CoastalDEM v2.1, which are nearly DTMs, show the closest similarity to AD-DEM and also the most realistic setting in comparison with inundation areas. However, their relation to AD-DEM differs depending on the local profile setting. While discrepancies are lowest for smooth, flat terrain characterised by low-growing crops and vegetation, CoastalDEM v2.1 seems to level out relief changes present between former point bars and oxbows or yields an atypical profile for a dike, whereas FABDEM reflects a more pronounced and – at least in terms of the dike – more realistic topography. From the central to the lower delta, absolute elevations of both FABDEM and CoastalDEM v2.1 are mainly consistent with the AD-DEM (Figure 4.4) but with the tendency that CoastalDEM v2.1 is locally 2–3 m lower than AD-DEM, while FABDEM is either in line or slightly below AD-DEM in marshy environments cultivated with irrigated and/or dry crops (Figure 4.5e and f).

In view of studying the impact of flooding in the Ayeyarwady Delta, the large-scale pattern of area at risk mapped based on AD-DEM also serves as reference to evaluate the performance of the other DEMs. However, the relatively coarse resolution of the AD-DEM makes it less suitable to function as benchmark to evaluate the small-scale spatial pattern of the DEMs. FABDEM and its underlying source data, the Copernicus DEM, show similar large-scale patterns of areas at risk of future SLR. On a local scale, in central parts of the lower delta, where vegetation accompanies the channel network (mainly trees), the Copernicus DEM tends to underestimate the potentially drowned area and would also underestimate the impact of a flood with a critical surge height (Figure C27). In contrast, if FABDEM is used to estimate flood

impact, calculations must be taken cautiously when focusing on urban settlements in the delta as building infrastructure constitutes certain resistance against flooding, which is neglected by the DTM (see also Bellos and Tsakiris, 2015). Discrepancies between DSM (Copernicus DEM) and DTM (FABDEM) are most prominent in Yangon City. Here, the delineated area below sea level must not be equalised with the area affected by flooding due to SLR and other mechanisms since built-up infrastructure has been neglected. Indicating the lowest elevations, CoastalDEM v2.1 shows the most extensive area below future sea level. Though considering building infrastructure indirectly via population data, on a local scale, CoastalDEM v2.1 reveals a significantly different pattern for Yangon City than FABDEM (Figure C27). We interpret this discrepancy as reflecting that population data as an indicator for urban development and thus positive error in DEMs (Kulp and Strauss, 2018) does not provide a thoroughly proper approach to improve the correction of vertical error in the underlying NASADEM. However, translating this discrepancy between CoastalDEM v2.1 and FABDEM into population at risk in these areas would require further and detailed investigations on township and ward levels, which would be – in view of the 74 townships in the delta – beyond the scope of this study.

Given the absence of any other independent ground truthing possibilities and no DEM clearly outperforming the others throughout all validations and statistics, we consider FABDEM and CoastalDEM v2.1 as the most consistent ones with respect to elevation indicated by spot heights, and the AD-DEM. Though amongst these, CoastalDEM v2.1 reveals in some places slightly better absolute statistics, they are often in the same range for FABDEM and the latter, in addition, outperforms CoastalDEM v2.1 in terms of spatial resolution and the absence of sensing artefacts. Thus, we suggest FABDEM as the most suitable when it comes to considering the role of topography for flood risk assessment in the Ayeyarwady Delta. To further improve FABDEM for the Ayeyarwady Delta, we suggest supplementing it with the local elevation data used for the AD-DEM, which will complement the large-scale suitability of the AD-DEM by allowing small-scale studies at high vertical accuracy (Seeger et al., 2023b).

4.1.5.2 Implications for assessing flood risk in the Ayeyarwady Delta

By integrating 10 global DEMs in addition to the local AD-DEM to assess the impact of SLR on the Ayeyarwady Delta, we visualise and quantify the range of potential consequences in terms of area and population falling below future sea level. In addition to the uncertainties we quantified related to the topographic data, further uncertainties exist with regard to the population and SLR datasets used and that process dynamics in reality are more complex than

could be captured by our study. Given that our calculations are based on population estimates of 2020, these do not consider any trends such as urbanisation and population growth which have occurred (Vogel et al., 2022) and can also be expected to continue in the future. Thus, the number of people below sea level may be considerably higher in the future than estimated in this study. Furthermore, subsidence will increase the impact of SLR, lowering elevation locally by up to ~2.70 m until 2150 if continuing at rates of 10–20 $mmyr^{-1}$ as observed for Yangon City (van der Horst et al., 2018). However, subsidence rates, especially in deltaic settings, are caused by many different processes that can be highly spatio-temporally variable (Shirzaei et al., 2021), and increased human activities are known to accelerate rates (Minderhoud et al., 2017, 2018; Candela and Koster, 2022), hampering reliable long-term estimations. Therefore, we highlight that the IPCC SLR scenarios – although projected for 2100 and 2150, respectively – could be realised much sooner, and land elevation thus becomes even more critical. The lack of knowledge on the magnitude of subsidence processes in the Ayeyarwady Delta, together with the limited availability of information and high-quality local data related to subsidence drivers like groundwater withdrawal (Viossanges et al., 2017), adds unknown and potentially large uncertainties to our SLR impact assessments. For example, groundwater withdrawal has been monitored only sporadically at artesian irrigation projects and in urban areas (Viossanges et al., 2017). However, some observations indicate falling groundwater levels, and according to the Water Supply System Master Plan (JICA, 2014), up to 3 million people rely on groundwater resources in Yangon City. Recent studies by Hashimoto et al. (2022) document even larger extraction amounts than reported by JICA (2014), which are also very high compared to other Asian cities affected by extraction-induced subsidence (Hashimoto et al., 2022). Though agricultural areas in the lower delta are reported to rely less on groundwater than townships of the upper delta and Yangon City, reliable estimates are absent, while groundwater use for cultivation (horticulture, aquaculture, etc.) is unknown (Viossanges et al., 2017). Thus, rates of RSLR will most likely be even larger than estimated so far. On a global scale, Tay et al. (2022) came to a similar conclusions for several coastal cities, including Yangon City, that the impact of land subsidence is underestimated by recent RSLR assessments like the IPCC Sixth Assessment Report. Consequently, future RSLR may affect substantially more land and inhabitants than we could estimate for the Ayeyarwady Delta so far, especially in the eastern part of the delta. Similarly, the RSLR rates of Nicholls et al. (2021) provide an approximation of future RSLR along the delta coast that is still associated with a range of uncertainties due to the lack of subsidence information covering the entire delta and the use of simplified, linearly extrapolated subsidence rates.

To gain a more complete understanding of flood risk in the delta, it is important to consider the different mechanisms and hydrodynamics that are involved in or add to SLR. Besides land subsidence lowering the elevation of the land and hereby increasing RSLR (Minderhoud et al., 2020; Nicholls et al., 2021), these include interactions with tidal constituents, surge and waves, potential feedbacks on nearshore bathymetry and shoreline morphology (Idier et al., 2019) as well as consideration of coastal squeeze (Luo et al., 2018). Together with local mechanisms such as drainage backflow and groundwater inundation that have been observed especially in urban areas (Habel et al., 2020), those processes will make the flood pattern more complex. In tropical deltas characterised by a monsoonal climate, such as the Ayeyarwady, pluvial flooding and increased river discharge constitute sources of flood risk nearly independent from the coast but rather coming from the hinterland (Figures 4.5 and C14–S19), also affecting higher elevations (Figure C18) and thereby enlarging inundation areas impacted by seaborne flood hazards. Data paucity challenges the simulation of these so-called multi-mechanism or compound flooding events in the Ayeyarwady Delta and would require the acquisition and careful selection of further (available) data. As input elevation data for simulating (compound) flooding at delta scale, we found FABDEM to be the best currently available DEM, in the absence of superior high-resolution DEMs. FABDEM may be further improved by integrating local elevation data from this study (Seeger et al., 2023b). To simulate floods adequately in urban settings such as Yangon City, FABDEM is recommended to be used either with reinserted building heights from the Copernicus DEM or in combination with increased surface roughness (i.e. via increasing the Manning's coefficient or via the friction term within the momentum equations; Schubert and Sanders, 2012; Bellos and Tsakiris, 2015). In the absence of these flood models, we recommend to revise existing flood hazard assessments by integrating validated data (such as accurate DEMs) and mapping of past flood events in order to consider multiple flood risks when designing present and future sustainable development pathways for the Ayeyarwady Delta. In this sense, we also call for the acquisition and accessibility of accurate and high-resolution data, such as lidar data, to the scientific public to reduce uncertainties in flood risk assessments on smaller scales, thereby supporting local risk mitigation and adaptation strategies. Based on the assessment of land elevation in view of SLR and delta flooding in the Ayeyarwady Delta, low-lying and densely populated areas within the most seaward districts should be addressed in particular by developing risk mitigation and adaptation strategies, while also the more inland delta population should be prepared to face a higher risk of flooding due to sea level rise in the next ~100 years.

4.1.6 Conclusions

As flood risk assessments based on high-accuracy elevation data either do not exist or are not publicly accessible for the Ayeyarwady Delta in Myanmar, available risk assessments so far rely at best on global DEMs, suffering from low vertical accuracy and remote sensing artefacts. To investigate their uncertainties and thus their suitability to provide reliable information on flood risk due to the impact of SLR and other water-related hazards, we assessed the land elevation of the Ayeyarwady Delta in relation to continuous local MSL by (a) generating the new, local AD-DEM based on topographical map elevation data and (b) comparing the performance of the new AD-DEM and 10 available global DEMs, referenced to local MSL. Thirdly, (c) we identified deltaic areas prone to SLR and monsoon flooding and interpreted their relation to topography. With respect to our research questions, we conclude the following:

i. The new, local AD-DEM, generated based on digitised spot heights and supplemented by elevation points extracted from contour lines in particularly data sparse regions, indicates a mean delta plain elevation of ~2.1 m (median ~1.3 m) above local MSL and is accurate for elevations ≤10.0 m at 1.0 m RMSE. With a horizontal resolution of 750 m, it is suitable for studying topography on delta scale and provides an independent dataset to validate commonly used global elevation data.

ii. The global DEMs integrated into this comparison show up to several metres deviation from geodetic spot heights and the AD-DEM. ASTGTM v003 reveals the lowest vertical accuracy and significantly overestimates low-lying areas (RMSE of up to 9.20 m), while ACE2 performs comparably well in comparison with spot heights but overall indicates significantly lower elevations than AD-DEM and all other global DEMs (mean height residuals of –0.47 to –1.87 m). FABDEM and CoastalDEM v2.1 show the highest correspondence with AD-DEM and low-elevation spot heights with height residuals at the centimetre to decimetre scale and RMSE of 1.75 to 2.00 m.

iii. Presently available flood risk assessments of Myanmar often either do not refer to underlying elevation data or use global SRTM and ALOS DEMs, which, however, suffer from artefacts, overestimate delta elevation compared to independent elevation data and thus underestimate areas at risk of SLR. As DEMs corrected or trained with additional datasets perform substantially better, they allow for delineating areas at risk of SLR in higher resolution than AD-DEM. Using these

DEMs (i.e. ADDEM, FABDEM, and CoastalDEM v2.1) and assuming high GHG emission scenarios (where vertical land motion is likely underestimated), 30.7 % to 46.7 % of the total delta area with at present 1.7 to 2.9 million people (2020 population) will fall below sea level by 2100, most of them in Pyapon, Labutta and Myaungmya districts. By 2150 (probably sooner), up to 67.5 % of the delta could be drowned, an area with at present 5 million people that also includes more inland districts. As monsoon flooding also affects higher elevations, it has the potential to further enlarge inundation areas impacted by sea-borne flood hazards.

iv. To further investigate the impact of SLR and delta flooding in the Ayeyarwady Delta in the absence of high-resolution DEMs, we recommend the use of FABDEM as it proves to perform comparably well, is of adequate spatial resolution, and does not suffer from stripes or other artefacts. To simulate floods also adequately in urban settings such as Yangon City, FABDEM is recommended to be used either with reinserted building heights from the Copernicus DEM or in combination with increased surface roughness. Further improvement may include supplementing FABDEM with local elevation data from this study. For DEM accuracy assessments in general, we recommend to analyse a given dataset by as many quality standards as possible to gain a holistic picture and to determine the most accurate one based on its overall performance instead of relying on individual selected accuracy parameters.

v. Our findings indicate that water-related hazards in the Ayeyarwady Delta and available risk assessments need to be re-examined by integrating validated elevation data to strengthen their reliability. As SLR may be compounded by other types of flooding and involves numerous mechanisms and process dynamics, which are themselves subject to uncertainties, the overall flood pattern becomes more complex. With our study, we addressed the uncertainties related to DEMs and land elevation (apart from vertical land motion) and stress the need of addressing low-lying and densely populated areas within the most seaward districts in particular by developing risk mitigation and adaptation strategies, while also the more inland delta population should be made aware to face a higher risk of flooding due to SLR in the next ~100 years.

Data availability statement: The AD-DEM is available online (https://doi.org/10.5281/zenodo.7875964, Seeger et al., 2023a). Digitised elevation data from topographical maps will be made available upon request. FABDEM V1-0 adjusted for the Ayeyarwady Delta in Myanmar by local spot height data from topographic maps is available under a Creative Commons Attribution-NonCommercial-ShareAlike 4.0 International (CCBY-NC-SA 4.0) licence (https://doi.org/10.5281/zenodo.7875855, Seeger et al., 2023b).

References

Aguilar, F. J., Aguilar, M. A., Agüera, F., and Sánchez, J.: The accuracy of grid digital elevation models linearly constructed from scattered sample data, *Int. J. Geogr. Inf. Sci.*, *20*:2, 169–192, https://doi.org/10.1080/13658810500399670, 2006.

Anthony, E. J., Besset, M., Dussouillez, P., Goichot, M., and Loisel, H.: Overview of the Monsoon-influenced Ayeyarwady River delta, and delta shoreline mobility in response to changing fluvial sediment supply, *Mar. Geol.*, *417*, 106038, https://doi.org/10.1016/j.margeo.2019.106038, 2019.

Airbus Defence and Space: Copernicus Digital Elevation Model Product Handbook Version 3.0, Airbus, 38 pp., 2020.

Berry, P. A. M., Smith, R. G., and Benveniste, J.: ACE2: The New Global Digital Elevation Model, in: *Gravity, Geoid and Earth Observation, International Association of Geodesy Symposia 135*, edited by Mertiklas, S.P., Springer, Berlin, Heidelberg, Germany, 231–237, https://doi.org/10.1007/978-3-642-10634-7_30, 2010.

Becker, M., Papa, F., Karpytchev, M., Delebecque, C., Krien, Y., Khan, J. U., Ballu, V., Durand, F., Le Cozannet, G., Islam, A. K. M. S., Calmant, S., and Shum, C. K.: Water level changes, subsidence, and sea level rise in the Ganges-Brahmaputra-Meghna delta, *Proc. Natl. Acad. Sci. U.S.A.*, *117*:4, 1867–1876, https://doi.org/10.1073/pnas.1912921117, 2020.

Bellos, V., and Tsakiris, G.: Comparing Various Methods of Building Representation for 2D Flood Modelling In Built-Up Areas, *Water Resour. Manag.*, *29*, 379–397, https://doi.org/10.1007/s11269-014-0702-3, 2015.

Bhagabati, S. S., Kawasaki, A., Takeuchi, W., and Win Win Zin: Improving River Bathymetry and Topography Representation of a Low-Lying Flat River Basin by Integrating Multiple Sourced Datasets, *J. Disaster Res.*, *15*:3, 335–343, https://doi.org/10.20965/jdr.2020.p0335, 2020.

Brakenridge, G. R., Syvitski, J. P. M., Niebuhr, E., Overeem, I., Higgins, S. A., Kettner A. J., and Prades, L.: Design with nature: Causation and avoidance of catastrophic flooding, Myanmar, *Earth Sci. Rev.*, *165*, 81–109, https://doi.org/10.1016/j.earscirev.2016.12.009, 2017.

Brakenridge, G. R., Kettner, A. J., Paris, S., Cohen, S., and Nghiem, S. V.: River and Reservoir Watch Version 4.5, Satellite-based river discharge and reservoir area measurements, 1998-present, DFO Flood Observatory, University of Colorado, USA: https://floodobservatory.colorado.edu/DischargeAccess.html, last access: 8 September 2022.

Brill, D., Seeger, K., Pint, A., Reize, F., Kay Thwe Hlaing, Seeliger, M., Opitz, S., Khin Mi Mi Win, Win Thuzar Nyunt, Nilar Aye, Aung Aung, Kyaw Kyaw, Kraas, F., and Brückner, H.: Modern and historical tropical cyclone and tsunami deposits at the coast of Myanmar: Implications for their identification and preservation in the geological record, *Sedimentology*, *67*, 1431–1459, https://doi.org/10.1111/sed.12586, 2020.

Brosens, L., Campforts, B., Govers, G., Aldana-Jague, E., Razanamahandry, V. F., Razafimbelo, T., Rafolisy, T, and Jacobs, L.: Comparative analysis of the Copernicus, TanDEM-X, and UAV-SfM digital elevation models to estimate lavaka (gully) volumes and mobilization rates in the Lake Alaotra region (Madagascar), *Earth Surf. Dynam.*, *10*, 209–227, https://doi.org/10.5194/esurf-10-209-2022, 2022.

Bucx, T., van Driel, W., de Boer, H., Graas, S., Langenberg, V. T., Marchand, M., and Van de Guchte, C.: *Comparative assessment of the vulnerability and resilience of deltas – extended version with 14 deltas – synthesis report*, Delta Alliance International, Delft-Wageningen, The Netherlands, Delta Alliance report number 7, 145 pp., 2014.

Candela, T., and Koster, K.: The many faces of anthropogenic subsidence, *Science*, *376*:6600, 1381–1382, https://doi.org/10.1126/science.abn3676, 2022.

Chen, D., Li, X., Saito, Y., Liu, J. P., Duan, Y., Liu, S., and Zhang, L.: Recent evolution of the Irrawaddy (Ayeyarwady) Delta and the impacts of anthropogenic activities: A review and remote sensing survey, *Geomorphology*, *365*, 107231, https://doi.org/10.1016/j.geomorph.2020.107231, 2020.

Chen, J., Huang, G., and Chen, E.: Towards better flood risk management: Assessing flood risk and investigating the potential mechanisms based on machine learning models, *J. Environ. Manage.*, *293*, 112810, https://doi.org/10.1016/j.jenvman.2021.112810, 2021.

Church, J. A., White, N. J., Hunter, J. R.: Sea-level rise at tropical Pacific and Indian Ocean islands, *Glob. Planet Change*, *53*, 155–168, https://doi.org/10.1016/j.gloplacha.2006.04.001, 2006.

Climate Service Center Germany (GERICS) and KfW Development Bank: Regional Sea Level Rise South Asia, KfW, Hamburg and Frankfurt am Main, *Climate Focus Paper 2015*, 12 pp., 2015.

Department of Meteorology and Hydrology, and Ministry of Transport: Myanmar's National Adaptation Programme of Action (NAPA) to Climate Change, United Nations Environment Programme (UNEP), 126 pp., 2012.

Du, X., Guo, H., Fan, X., Zhu, J., Yan, Z., and Zhan, Q.: Vertical accuracy assessment of freely available digital elevation models over low-lying coastal plains, *Int. J. Digit. Earth*, *9*:3, 252–271, https://doi.org/10.1080/17538947.2015.1026853, 2016.

East View Geospatial, Inc.: EVMap50-MMR 1:50,000 Scale Topographic Maps, Minnetonka, Minnesota, 2014.

El-Quilish, M., El-Ashquer, M., Dawod, G., and El Fiky, G.: Development and Accuracy Assessment of High-Resolution Digital Elevation Model Using GIS Approaches for the Nile Delta Region, Egypt, *American Journal of Geographic Information System*, *7*:4, 107–117, https://doi.org/10.5923/j.ajgis.20180704.02, 2018.

ESRI: Cell size and resampling in analysis, https://desktop.arcgis.com/en/arcmap/latest/extensions/spatial-analyst/performing-analysis/cell-size-and-resampling-in-analysis.htm, last access: 4 April 2023.

Farr, T. G., Rosen, P. A., Caro, E., Crippen, R., Duren, R., Hensley, S., Kobrick, M., Paller, M., Rodriguez, E., Roth, L., Seal, D., Shaffer, S., Shimada, J., Umland, J., Werner, M., Oskin, M., Burbank, D., and Alsdorf,

D.: The Shuttle Radar Topography Mission, *Rev. Geophys.*, *45*:2, RG2004, https://doi.org/10.1029/2005RG000183, 2007.

Fee, L., Gilbert, M., Bartlett, R., Capizzi, P., Horton, R., and Lesk, C.: Climate Change Vulnerability Assessment of Labutta Township, Myanmar, 2016–2050: scenarios for building resilience, UN-Habitat and UN-Environment, Nairobi, Kenya, 168 pp., 2017.

Fereshtehpour, M., and Karamouz, M.: DEM Resolution Effects on Coastal Flood Vulnerability Assessment: Deterministic and Probabilistic Approach, *Water Resour. Res.*, *54*:7, 4965–4982, https://doi.org/10.1029/2017WR022318, 2018.

Fox-Kemper, B., Hewitt, H. T., Xiao, C., Aðalgeirsdóttir, G., Drijfhout, S. S., Edwards, T. L., Golledge, N. R., Hemer, M., Kopp, R. E., Krinner, G., Mix, A., Notz, D., Nowicki, S., Nurhati, I. S., Ruiz, L., Sallée, J.-B., Slangen, A. B. A., and Yu, Y.: Ocean, Cryosphere and Sea Level Change, in: *Climate Change 2021: The Physical Science Basis. Contribution of Working Group I to the Sixth Assessment Report of the Intergovernmental Panel on Climate Change*, edited by Masson-Delmotte, V., Zhai, P., Pirani, A., Connors, S. L., Péan, C., Berger, S., Caud, N., Chen, Y., Goldfarb, L., Gomis, M. I., Huang, M., Leitzell, K., Lonnoy, E., Matthews, J. B. R., Maycock, T. K., Waterfield, T., Yelekçi, O., Yu, R., and Zhou, B., Cambridge University Press, Cambridge, 9-1–9-257, In press.

Frenken, K.: Irrigation in Southern and Eastern Asia in figures: AQUASTAT Survey – 2011, FAO, Rome, Italy, FAO Water Reports 37, 512 pp., 2012.

Fritz, H. M., Blount, C. D., Swe Thwin, Moe Kyaw Thu, and Nyein Chan: Cyclone Nargis storm surge in Myanmar, *Nat. Geosci.*, *2*, 448–449, https://doi.org/10.1038/ngeo558, 2009.

Furlan, E., Dalla Pozza, P., Michetti, M., Torresan, S., Critto, A., and Marcomini, A.: Development of a Multi-Dimensional Coastal Vulnerability Index: Assessing vulnerability to inundation scenarios in the Italian coast, *Sci. Total Environ.*, *772*, 144650, https://doi.org/10.1016/j.scitotenv.2020.144650, 2021.

Furuichi, T., Win, Z., and Wasson, R. J.: Discharge and suspended sediment transport in the Ayeyarwady River, Myanmar: Centennial and decadal changes, *Hydrol. Process.*, *23*, 1631–1641, https://doi.org/10.1002/hyp.7295, 2009.

Garner, G. G., Hermans, T., Kopp, R. E., Slangen, A. B. A., Edwards, T. L., Levermann, A., Nowikci, S., Palmer, M. D., Smith, C., Fox-Kemper, B., Hewitt, H. T., Xiao, C., Aðalgeirsdóttir, G., Drijfhout, S. S., Edwards, T. L., Golledge, N. R., Hemer, M., Kopp, R. E., Krinner, G., Mix, A., Notz, D., Nowicki, S., Nurhati, I. S., Ruiz, L., Sallée, J.-B., Yu, Y., Hua, L., Palmer, T., and Pearson, B.: IPCC AR6 Sea-Level Rise Projections, Version 20210809, PO.DAAC, CA, USA, Dataset accessed [2022-05-23] at https://podaac.jpl.nasa.gov/announcements/2021-08-09-Sea-level-projections-from-the-IPCC-6th-Assessment-Report, 2021.

Garner, G. G., Kopp, R. E., Hermans, T., Slangen, A. B. A., Koubbe, G., Turilli, M., Jha, S., Edwards, T. L., Levermann, A., Nowikci, S., Palmer, M. D., and Smith, C.: Framework for Assessing Changes To Sea-

level (FACTS), Geoscientific Model Development, *Zenodo* [model], https://zenodo.org/record/6419954, last access: 22 November 2022, 2022.

Gesch, D. B.: Analysis of Lidar Elevation Data for Improved Identification and Delineation of Lands Vulnerable to Sea-Level Rise, *J. Coast. Res.*, *53*, 49–58, https://doi.org/10.2112/SI53-006.1, 2009.

Gesch, D. B.: Consideration of Vertical Uncertainty in Elevation-Based Sea-Level Rise Assessments: Mobile Bay, Alabama Case Study, *J. Coast. Res.*, *63*, 197–210, https://doi.org/10.2112/SI63-016.1, 2013.

Gesch, D. B.: Best Practices for Elevation-Based Assessments of Sea-Level Rise and Coastal Flooding Exposure, *Front. Earth Sci.*, *6*:230, 1–19, https://doi.org/10.3389/feart.2018.00230, 2018.

Gorelick, N., Hancher, M., Dixon, M., Ilyushchenko, S., Thau, D., and Moore, R.: Google Earth Engine: Planetary-scale geospatial analysis for everyone, *Remote Sens. Environ.*, *202*, 18–27, https://doi.org/10.1016/j.rse.2017.06.031, 2017.

Government of the Union of Myanmar: Myanmar – Post-disaster needs assessment of floods and landslides July–September 2015, Government of the Union of Myanmar, 267 pp., 2015.

Habel, S., Fletcher, C. H., Anderson, T. R., and Thompson, P.R.: Sea-Level Rise Induced Multi-Mechanism Flooding and Contribution to Urban Infrastructure Failure, *Sci. Rep.*, *10*, 3796, https://doi.org/10.1038/s41598-020-60762-4, 2020.

Hanh Tran, Thuc Tran, and Kervyn, M.: Dynamics of Land Cover/Land Use Changes in the Mekong Delta, 1973–2011: A Remote Sensing Analysis of the Tran Van Thoi District, Ca Mau Province, Vietnam, *Remote Sens.*, *7*:3, 2899–2925, https://doi.org/10.3390/rs70302899, 2015.

Hanson, S., Nicholls, R., Ranger, N., Hallegatte, S., Corfee-Morlot, J., Herweijer, C., and Chateau, J.: A global ranking of port cities with high exposure to climate extremes, *Clim. Change*, *104*, 89–111, https://doi.org/10.1007/s10584-010-9977-4, 2011.

Hashimoto, R., Kazama, S., Hashimoto, T., Oguma, K., and Takizawa, S.: Planning methods for conjunctive use of urban water resources based on quantitative water demand estimation models and groundwater regulation index in Yangon City, Myanmar, *J. Clean. Prod.*, *367*, 133123, https://doi.org/10.1016/j.jclepro.2022.133123, 2022.

Hawker, L., Neal, J., and Bates, P.: Accuracy assessment of the TanDEM-X 90 Digital Elevation Model for selected floodplain sites, *Remote Sens. Environ.*, *232*, 111319, https://doi.org/10.1016/j.rse.2019.111319, 2019.

Hawker, L., Uhe, P., Paulo, L., Sosa, J., Savage, J., Sampson, C., and Neal, J.: A 30 m global map of elevation with forests and buildings removed, *Environ. Res. Lett.*, *17*:2, 024016, https://doi.org/10.1088/1748-9326/ac4d4f, 2022.

Hedley, P. J., Bird, M. I., and Robinson, R. A. J.: Evolution of the Irrawaddy delta region since 1850, *The Geographical Journal*, *176*:2, 138–149, https://doi.org/10.1111/j.1475-4959.2009.00346.x, 2010.

Hein Min Htet: Flood Risk Mapping Using Satellite Images and GIS Tools: A study on flood analysis of Thabaung, Kangyidaunt and Pathein Area, Ayeyarwady Region, The First Myanmar National Conference on Earth Sciences (MNCES) 2017, University of Monywa, Monywa, Myanmar, 27–28 November 2017, https://mynces.org/download/ProceedingMNCES2017/35HeinMinHtetMNCES2017.pdf, 2017.

Hirt, C.: Artefact detection in global digital elevation models (DEMs): The Maximum Slope Approach and its application for complete screening of the SRTM v4.1 and MERIT DEMs, *Remote Sens. Environ.*, *207*, 27–41, https://doi.org/10.1016/j.rse.2017.12.037, 2018.

Horton, R., De Mel, M., Peters, D., Lesk, C., Bartlett, R., Helsingen, H., Bader, D., Capizzi, P., Martin, S., and Rosenzweig, C.: Assessing Climate Risk in Myanmar: Technical Report, Center for Climate Systems Research at Columbia University, WWF-US and WWF-Myanmar, 88 pp., 2017.

Huffman, G. J., Stocker, E. F., Bolvin, D. T., Nelkin, E. J., Tan, J.: GPM IMERG Final Precipitation L3 1 month 0.1 degree x 0.1 degree V06 [dataset], https://doi.org/10.5067/GPM/IMERGDF/DAY/06, edited by Savtchenko, A., Greenbelt, Maryland, Goddard Earth Sciences Data and Information Services Center (GES DISC), last access: 18 June 2021, 2019.

Idier, D., Bertin, X., Thompson, P., and Pickering, M. D.: Interactions Between Mean Sea Level, Tide, Surge, Waves and Flooding: Mechanisms and Contributions to Sea Level Variations at the Coast, *Surv. Geophys.*, *40*, 1603–1630, https://doi.org/10.1007/s10712-019-09549-5, 2019.

Inman, V. L., and Lyons, M. B.: Automated Inundation Mapping Over Large Areas Using Landsat Data and Google Earth Engine, *Remote Sens.*, *12*:8, 1348, https://doi.org/10.3390/rs12081348, 2020.

International Centre for Water Hazard and Risk Management (ICHARM), Public Works Research Institute (PWRI), CTI Engineering International Co., Ltd., CTI Engineering Co., Ltd, and PASCO CORPORATION: Republic of the Union of Myanmar: Transformation of Urban Management – Flood Management Component, Asian Development Bank, Tsukuba and Tokyo, Japan, Technical Assistance Consultant's Report, Final Report Annexes 1–7, 159 pp., 2016.

International Federation of Red Cross and Red Crescent Societies (IFRC): Final Report Myanmar: Floods, IFRC, 31 pp., 2017.

Japan International Cooperation Agency (JICA), Myanmar Survey Department, and Ministry of Forestry: The study on the establishment of geographic database for national rehabilitation and development programme in the Union of Myanmar – Final Report Volume 1: Main report, JICA, 86 pp., 2004.

Japan International Cooperation Agency (JICA): Preparatory Survey Report on the Project for the Improvement of Water Supply, Sewerage and Drainage System in Yangon City in the Republic of the Union of Myanmar – Volume III: Water Supply System Master Plan, JICA, 275 pp., 2014.

Khin Thandar Win, Nilar Aye, and Kyaw Zaya Htun: Vulnerability of Flood Hazard in Selected Ayeyarwady Delta Region, Myanmar, *International Journal of Science and Engineering Applications*, *3*:3, 44–48, http://dx.doi.org/10.7753/IJSEA0303.1003, 2014.

Kittiphong Phongsaphan, Chishtie, F., Poortinga, A., Bhandari, B., Chinaporn Meechaiya, Thannarot Kunlamai, Khun San Aung, Saah, D., Anderson, E., Markert, K., Markert, A., and Peeranan Towashiraporn: Operational Flood Risk Index Mapping for Disaster Risk Reduction Using Earth Observations and Cloud Computing Technologies: A Case Study on Myanmar, *Front. Environ. Sci.*, *7*, 191, https://doi.org/10.3389/fenvs.2019.00191, 2019.

Kravtsova, V. I., Mikhailov, V. N., and Kidyaeva, V. M.: Hydrological Regime, Morphological Features and Natural Territorial Complexes of the Irrawaddy River Delta (Myanmar), *Water Resour.*, *36*:3, 243–260, https://doi.org/10.1134/S0097807809030014, 2009.

Kulp, S. A., and Strauss, B. H.: CoastalDEM: A global coastal digital elevation model improved from SRTM using a neural network, *Remote Sens. Environ.*, *206* (1), 231–239, https://doi.org/10.1016/j.rse.2017.12.026, 2018.

Kulp, S. A., and Strauss, B. H.: New elevation data triple estimates of global vulnerability to sea-level rise and coastal flooding. *Nat. Commun.*, *10*:4844, 1–12, https://doi.org/10.1038/s41467-019-12808-z, 2019.

Kulp, S. A., and Strauss, B. H.: CoastalDEM v2.1: A high-accuracy and high-resolution global coastal elevation model trained on ICESat-2 satellite lidar, *Climate Central Scientific Report*, 17 pp., 2021.

Lehner, B., Verdin, K., and Jarvis, A.: New Global Hydrography Derived From Spaceborne Elevation Data, *EOS Transa. Am. Geophys. Union*, *89*:10, 93–94, https://doi.org/10.1029/2008EO100001, 2008.

Liu, J., Wang, X., Zhang, B., Li, J., Zhang, J., and Liu, X.: Storm flood risk zoning in the typical regions of Asia using GIS technology, *Nat. Hazards*, *87*, 1691–1707, https://doi.org/10.1007/s11069-017-2843-1, 2017.

Loucks, D. P.: Developed river deltas: are they sustainable?, *Environ. Res. Lett.*, *14*:11, 113004, https://doi.org/10.1088/1748-9326/ab4165, 2019.

Luo, S., Shao, D., Long, W., Liu, Y., Sun, T., and Cui, B.: Assessing 'coastal squeeze' of wetlands at the Yellow River Delta in China: A case study, *Ocean Coast. Manag.*, *153*, 193–202, https://doi.org/10.1016/j.ocecoaman.2017.12.018, 2018.

Masson-Delmotte, V., Zhai, P., Pirani, A., Connors, S. L., Péan, C., Berger, S., Caud, N., Chen, Y., Goldfarb, L., Gomis, M. I., Huang, M., Leitzell, K., Lonnoy, E., Matthews, J. B. R., Maycock, T. K., Waterfield, T., Yelekçi, O., Yu, R., and Zhou, B. (Eds.): *Climate Change 2021: The Physical Science Basis. Contribution of Working Group I to the Sixth Assessment Report of the Intergovernmental Panel on Climate Change*, Cambridge University Press, 2021.

McLaughlin, S., and Cooper, J. A. G.: A multi-scale coastal vulnerability index: A tool for coastal managers?, *Environ. Hazards*, *9*:3, 233–248, https://doi.org/10.3763/ehaz.2010.0052, 2010.

Minderhoud, P. S. J., Erkens, G., Pham, V. H., Bui, V. T., Erban, L., Kooi, H., and Stouthamer, E.: Impacts of 25 years of groundwater extraction on subsidence in the Mekong delta, Vietnam, *Environ. Res. Lett.*, *12*:6, 064006, https://doi.org/10.1088/1748-9326/aa7146, 2017.

Minderhoud, P. S. J., Coumou, L., Erban, L. E., Middelkoop, H., Stouthamer, E., and Addink, E. A.: The relation between land use and subsidence in the Vietnamese Mekong delta, *Sci. Total Environ.*, *634*, 715–726, https://doi.org/10.1016/j.scitotenv.2018.03.372, 2018.

Minderhoud, P. S. J., Coumou, L., Erkens, G., Middelkoop, H., and Stouthamer, E.: Mekong delta much lower than previously assumed in sea-level rise impact assessments, *Nat. Commun.*, *10*:3847, 1–13, https://doi.org/10.1038/s41467-019-11602-1, 2019.

Minderhoud, P. S. J., Middelkoop, H., Erkens, G., and Stouthamer, E.: Groundwater extraction may drown mega-delta: projections of extraction-induced subsidence and elevation of the Mekong delta for the 21st century, *Environ. Res. Commun.*, *2*, 011005, https://doi.org/10.1088/2515-7620/ab5e21, 2020.

Moharrami, M., Javanbakht, M., and Attarchi, S.: Automatic flood detection using sentinel-1 images on the google earth engine, *Environ. Monit. Assess.*, *193*, 248, https://doi.org/10.1007/s10661-021-09037-7, 2021.

Muis, S., Verlaan, M., Winsemius, H. C., Aerts, J. C. J. H., and Ward, P. J.: A global reanalysis of storm surges and extreme sea levels, *Nat. Commun.*, *7*, 11969, https://doi.org/10.1038/ncomms11969, 2016.

Mulet, S., Rio, M.-H., Etienne, H., Artana, C., Cancet, M., Dibarboure, G., Hui Feng, Husson, R., Picot, N., Provost, C., and Strub, P. T.: The new CNES-CLS18 global mean dynamic topography, *Ocean Sci.*, *17*, 789–808, https://doi.org/10.5194/os-17-789-2021, 2021.

Mulhern, O.: Sea Level Rise Projection Map – Rangoon, https://earth.org/data_visualization/sea-level-rise-by-2100-rangoon/, 2020, last access: 31 August 2022.

Myat Myat Thi, Gunawardhana, L. N., and Kazama, S.: A comparison of historical land-use change patterns and recommendations for flood plain developments in three delta regions in Southeast Asia, *Water Int.*, *37*:3, 218–235, http://dx.doi.org/10.1080/02508060.2012.687511, 2012.

National Aeronautics and Space Administration (NASA): Giovanni – The Bridge Between Data and Science v 4.37, https://giovanni.gsfc.nasa.gov/giovanni/, last access: 18 June 2021.

National Aeronautics and Space Administration (NASA) Jet Propulsion Laboratory (JPL): NASA Shuttle Radar Topography Mission Water Body Data Shapefiles & Raster Files, https://doi.org/10.5067/MEaSUREs/SRTM/SRTMSWBD.003, last access: 8 February 2022, 2013.

Nicholls, R. J., and Cazenave, A.: Sea-Level Rise and Its Impact on Coastal Zones, *Science*, *328*:5985, 1517–1520, https://doi.org/10.1126/science.1185782, 2010.

Nicholls, R. J., Adger, W. N., Hutton, C. W., and Hanson, S. E. (Eds.): *Deltas in the Anthropocene*, Palgrave Macmillan, Cham, Switzerland, 282 pp., https://doi.org/10.1007/978-3-030-23517-8, 2020.

Nicholls, R. J., Lincke, D., Hinkel, J., Brown, S., Vafeidis, A. T., Meyssignac, B., Hanson, S. E., Merkens, J-L., and Fang, J.: A global analysis of subsidence, relative sea-level change and coastal flood exposure, *Nat. Clim. Chang.*, *11*, 338–342, https://doi.org/10.1038/s41558-021-00993-z, 2021.

Nirwansyah, A. W., and Braun, B.: Tidal Flood Risk on Salt Farming: Evaluation of Post Events in the Northern Part of Java Using a Parametric Approach, *Geosciences*, *11*:10, 420, https://doi.org/10.3390/geosciences11100420, 2021.

Ottinger, M., Kuenzer, C., Liu, G., Wang, S., and Dech, S.: Monitoring land cover dynamics in the Yellow River Delta from 1995 to 2010 based on Landsat 5 TM, *Appl. Geogr.*, *44*, 53–68, https://doi.org/10.1016/j.apgeog.2013.07.003, 2013.

Permanent Service for Mean Sea Level (PSMSL): Permanent Service for Mean Sea Level – Tide Gauge Data, https://psmsl.org/data/obtaining/, last access: 3 May 2021.

Ramaswamy, V., Rao, P. S., Rao, K. H., Swe Thwin, Srinivasa Rao, N., and Raiker, V.: Tidal influence on suspended sediment distribution and dispersal in the northern Andaman Sea and Gulf of Martaban, *Mar. Geol.*, *208*:1, 33–42, https://doi.org/10.1016/j.margeo.2004.04.019, 2004.

Rao, P. S., Ramaswamy, V., and Swe Thwin: Sediment texture, distribution and transport on the Ayeyarwady continental shelf, Andaman Sea, *Mar. Geol.*, *216*:4, 239–247, https://doi.org/10.1016/j.margeo.2005.02.016, 2005.

Renaud, F. G., Syvitski, J. P. M., Sebesvari, Z., Werners, S. E., Kremer, H., Kuenzer, C., Ramesh, R., Jeuken, A., and Friedrich, J.: Tipping from the Holocene to the Anthropocene: How threatened are major world deltas?, *Curr. Opin. Environ. Sustain.*, *5*:6, 644–654, https://doi.org/10.1016/j.cosust.2013.11.007, 2013.

Rincón, D., Khan, U. T., and Armenakis, C.: Flood Risk Mapping Using GIS and Multi-Criteria Analysis: A Greater Toronto Area Case Study, *Geosciences*, *8*:8, 275, https://doi.org/10.3390/geosciences8080275, 2018.

Rio, M.-H., Mulet, S., and Picot, N.: Beyond GOCE for the ocean circulation estimate: Synergetic use of altimetry, gravimetry, and in situ data provides new insight into geostrophic and Ekman currents, *Geophys. Res. Lett.*, *41*:24, 8918–8925, 2014.

Rose, A., McKee, J., Sims, K., Bright, E., Reith, A., and Urban, M.: LandScan Global 2020 [dataset], Oak Ridge National Laboratory, https://doi.org/10.48690/1523378, 2021.

Sakai, T., Omori, K., Aung Naing Oo, and Yan Zaung Zaw: Monitoring saline intrusion in the Ayeyarwady Delta, Myanmar, using data from the Sentinel-2 satellite mission, *Paddy Water Environ.*, 19, 283–294, https://doi.org/10.1007/s10333-020-00837-0, 2021.

Schneider, P., and Asch, F.: Rice production and food security in Asian Mega deltas – A review on characteristics, vulnerabilities and agricultural adaptation options to cope with climate change, *J. Agron. Crop Sci.*, *206*:4, 491–503, https://doi.org/10.1111/jac.12415, 2019.

Schubert, J. E., and Sanders, B. F.: Building treatments for urban flood inundation models and implications for predictive skill and modeling efficiency, *Adv. Water Resour.*, *41*, 49–64, https://doi.org/10.1016/j.advwatres.2012.02.012, 2012.

Schumann, G. J.-P., Bates, P. D., Neal., J. C., and Andreadis, K. M.: Fight floods on a global scale, *Nature*, *507*, 169, https://doi.org/10.1038/507169e, 2014.

Schumann, G., Bates, P. D., Apel, H., and Aronica, G. T.: Global Flood Hazard Mapping, Modeling, and Forecasting: Challenges and Perspectives, in: *Global Flood Hazard – Applications in Modeling, Mapping, and Forecasting*, edited by: Schumann, G. J.-P., Apel, H., and Aronica, G. T., American Geophysical Union, Washington DC., 239–244, https://doi.org/10.1002/9781119217886.ch14, 2018.

Schumann, G. J.-P., and Bates, P. D.: The Need for a High-Accuracy, Open-Access Global DEM, *Front. Earth Sci.*, *6*, 225, https://doi.org/10.3389/feart.2018.00225, 2018.

Seeger, K., Minderhoud, P. S. J., Peffeköver, A., Vogel, A., Brückner, H., Kraas, F., Nay Win Oo, and Brill, D.: Local digital elevation model for the Ayeyarwady Delta in Myanmar (AD-DEM) derived from digitised spot and contour heights of topographic maps, *Zenodo* [dataset], https://doi.org/10.5281/zenodo.7875964, 2023a.

Seeger, K., Minderhoud, P. S. J., Peffeköver, A., Vogel, A., Brückner, H., Kraas, F., Nay Win Oo, and Brill, D.: FABDEM V1-0 adjusted for the Ayeyarwady Delta in Myanmar by local spot height data from topographic maps, *Zenodo* [dataset], https://doi.org/10.5281/zenodo.7875855, 2023b.

Shirzaei, M., Freymueller, J., Törnqvist, T., Galloway, D. L., Dura, T., and Minderhoud, P. S. J.: Measuring, modelling and projecting coastal land subsidence, *Nat. Rev. Earth Environ.*, *2*, 40–58, https://doi.org/10.1038/s43017-020-00115-x, 2021.

Siart, C., Bubenzer, O., and Eitel, B.: Combining digital elevation data (SRTM/ASTER), high resolution satellite imagery (Quickbird) and GIS for geomorphological mapping: A multi-component case study on Mediterranean karst in Central Crete, *Geomorphology*, *112*:1–2, 106–121, https://doi.org/10.1016/j.geomorph.2009.05.010, 2009.

Specialised Information Service Cartography and Geodata (SIS Maps): Topo List, https://kartographie.staatsbibliothek-berlin.de/en/about-us/map-catalogs/topo-list/, last access: 29 March 2021.

Syvitski, J. P. M.: Deltas at risk, *Sustain. Sci.*, *3*, 23–32, https://doi.org/10.1007/s11625-008-0043-3, 2008.

Syvitski, J. P. M., Kettner, A. J., Overeem, I., Hutton, E. W. H., Hannon, M. T., Brakenridge, G. R., Day, J., Vörösmarty, C., Saito, Y., Giosan, L., and Nicholls, R. J.: Sinking deltas due to human activities, *Nat. Geosci.*, *2*, 681–686, https://doi.org/10.1038/ngeo629, 2009.

Szabo, S., Brondizio, E., Renaud, F. G., Scott, H., Nicholls, R. J., Matthews, Z., Tessler, Z., Tejedor, A., Sebesvari, Z., Foufoula-Georgiou, E., da Coasta, S., and Dearing, J. A.: Population dynamics, delta vulnerability and environmental change: comparison of the Mekong, Ganges-Brahmaputra and Amazon delta regions, *Sustain. Sci.*, *11*, 539–554, https://doi.org/10.1007/s11625-016-0372-6, 2016.

Tachikawa, T., Kaku, M., Iwasaki, A., Gesch, D., Oimoen, M., Zhang, Z., Danielson, J., Krieger, T., Curtis, B., Haase, J., Abrams, M., Crippen, R., and Carabajal, C.: ASTER Global Elevation Model Version 2 –

Summary of Validation Results, National Aeronautics and Space Administration (NASA) Land Processes Distributed Active Archive Center, and Joint Japan-US ASTER Science Team, 26 pp., 2011.

Tadono, T., Nagai, H., Ishida, H., Oda, F., Naito, S., Minakawa, K., and Iwamoto, H.: Generation of the 30 m-mesh global digital surface model by ALOS Prism, in: *Int. Arch. Photogramm. Remote Sens. Spatial Inf. Sci., XLI-B4, XXIII ISPRS Congress*, Prague, Czech Republic, 12–19 July 2016, 157–162, https://doi.org/10.5194/isprs-archives-XLI-B4-157-2016, 2016.

Tay, C., Lindsey, E. O., Shi Tong Chin, McCaughey, J. W., Bekaert, D., Nguyen, M., Hoa, H., Manipon, G., Karim, M., Horton, B. P., Tanghua Li, and Hill, E. M.: Sea-level rise from land subsidence in major coastal cities, *Nat. Sustain.*, *5*, 1049–1057, https://doi.org/10.1038/s41893-022-00947-z, 2022.

Tessler, Z. D., Vörösmarty, C. J., Grossberg, M., Gladkova, I., Aizenman, H., Syvitski, J. P. M., and Foufoula-Georgiou, E.: Profiling risk and sustainability in coastal deltas of the world, *Science*, *349*:6248, 638–643, https://doi.org/10.1126/science.aab3574, 2015.

Torbick, N., Chowdhury, D., Salas, W., and Qi, J.: Monitoring Rice Agriculture across Myanmar Using Time Series Sentinel-1 Assisted by Landsat-8 and PALSAR-2, *Remote Sens.*, *9*:2, 119, https://doi.org/10.3390/rs9020119, 2017.

Tripathy, P., and Malladi, T.: Global Flood Mapper: a novel Google Earth Engine application for rapid flood mapping using Sentinel-1 SAR, *Nat. Hazards*, *114*, 1341–1363, https://doi.org/10.1007/s11069-022-05428-2, 2022.

United Nations Platform for Space-based Information for Disaster Management and Emergency Response (UN-SPIDER): SAR-Flood mapping using a change detection approach, https://www.un-spider.org/sites/default/files/Code_GEE_flood_mapping.txt, last access: 22 June 2021, 2019.

Üstün, A., Abbak, R. A., and Zeray Östürk, E.: Height biases of SRTM DEM related to EGM96: from a global perspective to regional practice, *Surv. Rev.*, *50*, 26–35, https://doi.org/10.1080/00396265.2016.1218159, 2016.

Van Binh, D., Kantoush, S., and Sumi, T.: Changes to long-term discharge and sediment loads in the Vietnamese Mekong Delta caused by upstream dams, *Geomorphology*, *353*, 107011, https://doi.org/10.1016/j.geomorph.2019.107011, 2020.

van de Sande, B., Lansen, J., and Hoyng, C.: Sensitivity of Coastal Flood Risk Assessments to Digital Elevation Models, *Water*, *4*:3, 568–579, https://doi.org/10.3390/w4030568, 2012.

van der Horst, T., Rutten, M. M., van de Giesen, N. C., and Hanssen, R. F.: Monitoring land subsidence in Yangon, Myanmar using Sentinel-1 persistent scatterer interferometry and assessment of driving mechanisms, *Remote Sens. Environ.*, *217*, 101–110, https://doi.org/10.1016/j.rse.2018.08.004, 2018.

van Driel, W. F., and Nauta, T. A.: Vulnerability and Resilience Assessment of the Ayeyarwady Delta in Myanmar, Full assessment phase, Delta Alliance report no. 10, Bay of Bengal Large Marine Ecosystem (BOBLME)

Project, Global Water Partnership (GWP) and Delta Alliance, Delft-Wageningen, The Netherlands, 148 pp., 2014.

Vernimmen, R., Hooijer, A., and Pronk, M.: New ICESat-2 Satellite LiDAR Data Allow First Global Lowland DTM Suitable for Accurate Coastal Flood Risk Assessment, *Remote Sens.*, *12*:17, 2827, https://doi.org/10.3390/rs12172827, 2020.

Viossanges, M., Johnston, R., and Drury, L.: *Groundwater Resources of the Ayeyarwady Basin, Ayeyarwady State of the Basin Assessment (SOBA) Report 2a*, National Water Resources Committee (NWRC), Myanmar, 168 pp., 2017.

Vogel, A., Seeger, K., Brill, D., Brückner, H., Khin Khin Soe, Nay Win Oo, Nilar Aung, Zin Nwe Myint, and Kraas, F.: Identifying Land-Use Related Potential Disaster Risk Drivers in the Ayeyarwady Delta (Myanmar) during the Last 50 Years (1974–2021) Using a Hybrid Ensemble Learning Model, *Remote Sens.*, *14*:15, 3568, https://doi.org/10.3390/rs14153568, 2022.

Wang, H., Saito, Y., Zhang, Y., Bi, N., Sun, X., and Yang, Z.: Recent changes of sediment flux to the western Pacific Ocean from major rivers in East and Southeast Asia, *Earth Sci. Rev.*, *108*:1–2, 80–100, https://doi.org/10.1016/j.earscirev.2011.06.003, 2011.

Wang, S.-Y., Buckley, B. M., Yoon, J.-H., and Fosu, B.: Intensification of premonsoon tropical cyclones in the Bay of Bengal and its impacts on Myanmar, *J. Geophys. Res. Atmos.*, *118*:10, 4373–4384, https://doi.org/10.1002/jgrd.50396, 2013.

Webb, E. L., Jachowski, N. R. A., Phelps, J., Friess, D. A., Maung Maung Than, and Ziegler, A. D.: Deforestation in the Ayeyarwady Delta and the conservation implications of an internationally-engaged Myanmar, *Glob. Environ. Change*, *24*, 321–333, https://doi.org/10.1016/j.gloenvcha.2013.10.007, 2014.

Wechsler, S. P.: Uncertainties associated with digital elevation models for hydrologic applications: a review, *Hydrol. Earth Syst. Sci.*, *11*, 1481–1500, https://doi.org/10.5194/hess-11-1481-2007, 2007.

Wessel, B.: TanDEM-X Ground Segment – DEM Products Specification Document, EOC, DLR, Oberpfaffenhofen, Germany, Public Document TD-GS-PS-0021, Issue 3.2, [Online], Available: https://tandemx-science.dlr.de/, 2018.

Williams, S. J.: Sea-Level Rise Implications for Coastal Regions, *J. Coast. Res.*, *63*, 184–196, https://doi.org/10.2112/SI63-015.1, 2013.

Win Win Zin, and Rutten, M.: Long-term Changes in Annual Precipitation and Monsoon Seasonal Characteristics in Myanmar, *Hydrol. Curr. Res.*, *8*:2, 1–8, http://dx.doi.org/10.4172/2157-7587.1000271, 2017.

Woodroffe, C. D., Nicholls, R. J., Saito, Y., Chen, Z., and Goodbred, S. L.: Landscape variability and the response of Asian megadeltas to environmental change, in: *Global Change and Integrated Coastal Management*, edited by: Harvey, N., Springer, Dordrecht, The Netherlands, 277–314, 2006.

Xu, K., Fang, J., Fang, Y., Sun, Q., Wu, C., and Liu, M.: The Importance of Digital Elevation Model Selection in Flood simulation and a Proposed Method to Reduce DEM Errors: A Case Study in Shanghai, *Int. J. Disaster Risk Sci.*, *12*, 890–902, https://doi.org/10.1007/s13753-021-00377-z, 2021.

Yamazaki, D., Ikeshima, D., Tawatari, R., Yamaguchi, T., O'Loughlin, F., Neal, J. C., Sampson, C. C., Kanae, S., and Bates, P. D.: A high-accuracy map of global terrain elevations, *Geophys. Res. Lett.*, *44*:11, 5844–5853, https://doi.org/10.1002/2017GL072874, 2017.

Zhang, K., Gann, D., Ross, M., Robertson, Q., Sarmiento, J., Santana, S., Rhome, J., and Fritz, C.: Accuracy assessment of ASTER, SRTM, ALOS, and TDX DEMs for Hispaniola and implications for mapping vulnerability to coastal flooding, *Remote Sens. Environ.*, *225*, 290–306, https://doi.org/10.1016/j.rse.2019.02.028, 2019.

Zin Mie Mie Sein, Ullah, I., Saleem, F., Zhi, X., Syed, S., and Azam, K.: Interdecadal Variability in Myanmar Rainfall in the Monsoon Season (May–October) Using Eigen Methods, *Water*, *13*:5, 729, https://doi.org/10.3390/w13050729, 2021.

Zoccarato, C., Minderhoud, P. S. J., and Teatini, P.: The role of sedimentation and natural compaction in a prograding delta: insights from the mega Mekong delta, *Vietnam, Sci. Rep.*, *8*, 11437, https://doi.org/10.1038/s41598-018-29734-7, 2018.

Zöckler, C., and Kottelat, M.: *Biodiversity of the Ayeyarwady Basin, Ayeyarwady State of the Basin Assessment (SOBA) Report 4.5*, National Water Resources Committee (NWRC), Myanmar, 194 pp., 2017.

4.2 Sea level much higher than assumed in most coastal hazard assessments

Abstract: The impacts of sea-level rise and other hazards on the world's coasts are determined by coastal sea-level height and land elevation. Their correct alignment is crucial for reliable impact assessments. Here we reveal shortcomings and errors in this key aspect in the vast majority of contemporary sea-level rise and coastal hazard impact assessments. Over 99 % of the evaluated assessments handled sea-level and land elevation data improperly and substantially misjudged sea level relative to coastal elevation. Consequently, actual sea-level height is underestimated by 0.2–0.5 metres on average in coastal hazard assessments globally, while regionally even exceeding 1 metre in particularly vulnerable regions like Southeast Asia and the Small Island Developing States. With true sea level higher than assumed in existing scientific assessments, which inform policymakers, IPCC impact reports and Loss and Damage negotiations, worldwide 37 % more area and 67 % more people (increase of 88 million to 132 million people) will fall below sea level following 1 metre of relative sea-level rise. Our results underscore the importance of proper use of sea-level and land elevation data and emphasise the need to critically re-evaluate existing coastal hazard and sea-level rise impact studies.

Chapter 4.2 is related to: **Seeger, K.**, Minderhoud, P.S.J., in review. *Sea level much higher than assumed in most coastal hazard assessments*. Nature, 2025-02-05097A.

The scientific article is published under a CC-BY 4.0 Attribution 4.0 International licence (http://creativecommons.org/licenses/by/4.0/). The reader is recommended to refer to the peer-reviewed and published version of the content of this chapter which can be accessed via the article doi provided here (https://doi.org/10.1038/s41586-026-10196-1).

4.2.1 Introduction

Sea-level rise (SLR) poses a major risk to vast coastal lowlands in the world such as large and densely populated river deltas and coastal plains. Impact assessments of SLR and coastal flood hazards heavily depend on correctly referencing local sea-level height to coastal land elevation data. However, for virtually all studies we evaluated we found this is not the case, resulting in

widespread wrongly assessed coastal sea-level height in hazard assessments. Our analysis reveals that coastal sea levels are in reality higher than assumed in the vast majority of local, regional and global hazard assessments. Less than 1 % of the evaluated scientific literature provided thorough documentation and handled coastal sea-level and elevation data properly. This questions the reliability of more than 99 % of the evaluated assessments of coastal impacts, exposure, vulnerability, and risk. In the evaluated studies, more than 98% suffered from vertical datum conversion errors and documentation shortcomings, thereby impinging scientific standards of transparency and reproducibility and making these studies irreproducible.

According to IPCC AR 6 (SSP1-1.9 to SSP5-8.5) (IPCC, 2023), global mean sea level is projected to rise between 0.28 m and 1.01 m by 2100 compared to 1995–2014, driven by human-induced global warming. Including deep uncertainties in the behaviour of the polar ice sheets, these projections could increase by several metres (IPCC, 2023). In addition, negative vertical land motion, i.e. land subsidence (the sinking of the land) is an accelerating/increasing prominent phenomenon in coastal lowlands that contributes to relative sea-level rise (RSLR) (e.g., Ericson et al., 2006). Land subsidence results from natural processes such as sediment loading and compaction or tectonic displacement as well as human-induced infrastructural loading, drainage and underground resource extraction (Shirzaei et al., 2021; Candela and Koster, 2022). Consequently, the impacts of RSLR, coastal and compound flooding are closely related to coastal land elevation and local sea-level height. Assessing the impacts of these hazards on the coasts of the world to evaluate exposure and vulnerability necessitates the use of elevation information, mostly provided by digital elevation models (DEMs). Constituting the fundamental base of any such impact and exposure assessment, the quality (mainly vertical accuracy and spatial resolution) of the DEM(s) is fundamental to the accuracy of the derivatives and widely addressed in scientific literature (e.g., Schumann, 2014; Hinkel et al., 2021). While high-quality elevation information, e.g. acquired through airborne LiDAR, is available in several regions of the Global North (e.g., Schumann et al., 2018), for the vast majority of the coastal areas worldwide, the best available elevation data is satellite-based. While this global available data allowed unprecedented (global) SLR and coastal hazard studies (e.g., Dasgupta et al., 2009; Neumann et al., 2015), it is well-established that these often contain vertical errors up to several metres, sensing or interpolation artefacts, or are outdated, thereby impacting the quality of coastal hazard assessments, especially in flat, subsiding coastal plains (such as densely populated river deltas) (Schumann et al., 2018; Fisher and Tate, 2006; Kulp and Strauss, 2016). However, in addition to considering vertical uncertainty of elevation data, a crucial step

to properly use DEMs in coastal hazard assessments is to correctly tie coastal elevation to local sea-level height and convert all data to a common vertical reference frame (Minderhoud et al., 2019; Seeger et al., 2023). We evaluated a large quantity of contemporary SLR impact and coastal hazard assessments and found that these crucial steps are often not considered or performed properly. Rather than considering actual, local sea-level height, coastal sea level is most often assumed to equal global geoid or even ellipsoid models, to which open-access global DEMs are vertically referenced when provided. However, geoid or ellipsoid height can vary up to several metres from the true local sea-level height, particularly in regions in the Global South which suffer from data paucity in global geoid models (e.g., refs. Üstün et al., 2016; Vu et al., 2020; Fusami et al., 2023). The widespread omission in (global) SLR and coastal hazard assessments to consider and convert to true local sea level leads to errors with magnitudes as large as a century of projected SLR for the most affected regions in the world (Minderhoud et al., 2019; Seeger et al., 2023). Here we evaluate the omnipresence of these issues in contemporary SLR and coastal hazard impact studies and quantify the magnitude of these errors globally and for the different regions in the world.

4.2.2 Methods

4.2.2.1 Conduction of literature research and evaluation

We conducted a guided and reproducible literature research and evaluation adhering to the standards of the Preferred Reporting Items for Systematic Reviews and Meta-Analyses (PRISMA) process. All details of the literature research, selection and evaluation are provided in Tables D1 and D2 in Appendix D. We used the Scopus search engine and employed a search term for titles, abstracts and keywords that covered keywords from low-lying coastal environments, processes and hazards, as well as elevation information and elevation dynamics, impact and/or hazard assessments, projections or evaluations (Table D1). To narrow down the initial amount of 35,001 documents, we focused on the last 15 years (2009 to 2025) and included only peer-reviewed scientific articles, reviews or data papers. Further filters applied refer to the exclusion of certain subject areas, keywords and limiting the search to the English language. This refined search term reduced the amount of literature to 7,241 documents that were subsequently screened in two consecutive rounds following established inclusion and exclusion criteria (Figure D1; Table D1). The first screening was conducted based on title, abstract and keywords, and the second screening was conducted based on in-depth analysis of

the full article and, when needed, its references and supplementary material. The included literature, consisting of 385 publications, underwent an in-depth evaluation, in which we scrutinised them and, where needed, also secondary references to assess all relevant details related to study area, distance to shore, study focus/flood type, number of DEMs, DEM(s) used, actuality of DEM, DEM type, DEM coverage, acquisition and technique, performance of DEM accuracy assessment, DEM accuracy, spatial resolution, DEM availability, horizontal datum used, vertical datum documentation, correctness of vertical datum conversion, vertical datum type, vertical datum used, actuality of sea-level reference, and – where needed – additional comments.

The individual papers were accessed either via the Scopus search engine, or ISI Web of Science, Science Direct, Google Scholar or ResearchGate. The complete evaluation of the selected 385 publications and consequent result analysis following the developed evaluation criteria and coding is provided in Table D2. Only publications that handle all datasets in a consistent vertical reference frame (i.e. performing a correct vertical datum conversion) and refer to the latest available sea-level information at their time (i.e. using an up-to-date sea-level reference and correct vertical datum conversion) were considered as proper.

Finally, we also evaluated >90 publications that were not obtained by the PRISMA-guided literature research conducted on the Scopus search engine. The evaluation of this additional literature was not included into the statistics presented in this study but presents an extended consideration and assessment of literature from the same topical fields (Supplementary Data D1).

4.2.2.2 Vertical datum conversion and processing of digital elevation models

To obtain land elevation above continuous local sea level globally and quantify the discrepancies to land elevation with respect to global geoid and in case of incomplete vertical datum conversion, we processed four of the most recent global DEMs at global scale by converting them from their original vertical reference system to mean sea level as indicated by the mean dynamic topography (MDT) product. The DEMs included were CoastalDEM v2.1 (original vertical reference system: EGM96, spatial resolution: 90 m × 90 m) (Kulp and Strauss, 2021), FABDEM v1.0 (original vertical reference system: EGM2008, spatial resolution: 30 m × 30 m) (Hawker et al., 2021), GLL-DTM v2 (original vertical reference system: MDT (Rio et al., 2014), spatial resolution: 1 deg × 1 deg, i.e. ~1000 m × ~1000 m) (Vernimmen and Hooijer, 2022) and DeltaDTM v1 (original vertical reference system: EGM2008, spatial resolution: 30

m × 30 m) (Pronk, 2024). As geoid offset was not adequately considered during datum conversion of the processed, available GLL-DTM v2, we obtained the pre-converted GLL-DTM v2 (referenced to EGM96) to conduct the vertical datum conversion to mean sea level.

We used the latest available global MDT HYBRID-CNES-CLS2022 dataset (CLS, 2022), which provides sea surface height above geoid across the globe, measured by satellite altimetry and combined with gravitational field information, oceanographic data from drifting buoys, high-frequency radar velocities and hydrological profiles. Several studies confirm the accuracy of MDT data in the range of centimetres (e.g., Knudsen et al., 2011; Hamden et al., 2021), although accuracy decreases towards the very coastal stretches. The MDT dataset (CLS, 2022) provides spatially continuous information of sea surface height above the GOCO06s geoid at a resolution of 0.125 deg averaged over a period from 1993 to 2021. It therefore provides latest available information on global mean sea level and an accurate substitute for local tide gauge information in those regions. It serves as an open-accessible product that – if properly aligned with elevation information – allows to investigate elevation with respect to local sea level continuously along the world's coastlines.

In order to tie land elevation as given by the DEMs to mean sea level as given by MDT, the offsets of the underlying respective vertical reference systems (i.e. EGM96, EGM2008 and GOCO06s) have to be determined first (Figure D5). For all our computations, we used the ArcGIS Pro environment. Geoid information was obtained from the openly accessible calculation service of the International Centre for Global Earth Models (ICGEM) from GFZ Helmholtz Centre for Geosciences (Ince et al., 2019). Point data on geoid height anomaly to the WGS84 ellipsoid was obtained for the entire globe at a resolution of 0.085 deg for the EGM96, EGM2008 and GOCO06s geoids, respectively. For each geoid, the height anomaly points were interpolated into a global raster by using multiquadric radial basis functions which gave the most accurate interpolation results. The choice of this interpolation algorithm is furthermore supported by gravitational field modelling studies such as Doganalp and Selvi (2015) and Li (2018). Subsequently, the global geoid raster files were resampled to a spatial resolution of 90 m × 90 m and 1000 m × 1000 m by using bilinear resampling to be comparable with the DEMs' spatial resolution and to avoid potential artefacts in the entire datum conversion process. Geoid offsets were determined by subtracting the GOCO06s geoid height anomaly raster from the EGM96 and EGM2008 geoid height anomaly rasters.

Using mean sea level as indicated by MDT as a vertical datum for land elevation data requires the extrapolation of MDT over land. We extracted point values from the MDT raster using

bilinear interpolation at point locations and subsequently extrapolated them over land using an inverse distance weighting algorithm and a smooth neighbourhood type. The resulting raster dataset was resampled to a spatial resolution of 90 m × 90 m and 1000 m × 1000 m by using bilinear resampling in order to enable comparability with the DEMs' spatial resolution and to avoid the introduction of potential artefacts in the datum conversion process.

The processing of DEMs involved two main processes (Figure D5d). Firstly, the DEMs were transposed from the EGM96 and EGM2008 geoid to the GOCO06s geoid by adding the beforehand calculated geoid offset. Therewith, the vertical references of DEM-derived land elevation and MDT-derived sea surface height are aligned to a common datum (i.e., GOCO06s). This is a prerequisite in order to obtain land elevation above mean sea level by subtracting the MDT data from the respective DEM (Figure D5d).

To automate the processing of the DEMs' datum conversion, we applied two model workflows to transpose DEM tiles from the EGM geoid to GOCO06s and subsequently to MDT while ensuring to keep their original resolution and properties. The related Python codes are given in Supplementary Data D2 and D3.

We applied a distance threshold for which we deem this approach of DEM vertical datum conversion valid as the performance of MDT extrapolation over land decreases with increasing distance from shore. We considered to transpose all land elevation information within a distance of 500 km from the coast to mean sea level, thereby ensuring for adequate interpolation (extrapolation) performance and full coverage of vast low-lying coastal plains and river deltas such as the Ganges-Brahmaputra-Meghna Delta.

4.2.2.3 Assessment of coastal land elevation and sea-level height, sea-level rise impact and low-elevation coastal zone from global digital elevation models

We investigated coastal land elevation and sea-level height globally by extracting points from the original and vertically transposed DEMs as well as their differences, respectively, every 90 m along the coastline using bilinear interpolation of values at point locations and excluding no data values and water bodies before rasterizing them. As some of the evaluated DEMs showed large negative, unrealistic elevation values which are likely artefacts from the (source) DEM acquisition and generation process itself, we excluded these by applying an elevation threshold of -7m above mean sea level, which represents some of the lowest elevations in the coastal lowlands such as the Netherlands (e.g., Vernimmen and Hooijer, 2023). Calculated statistics include min, max, mean, and median elevation as well as standard deviation, and are given for

global, continental and regional scale. For statistics of the GLL-DTM v2 and for visualisation purposes of all other DEMs, we referred to coastal land elevation and sea-level height at 1000 m resolution. Similarly, we obtained the discrepancies between coastal sea-level height and commonly used EGM96 and EGM2008 geoids.

To show the impacts of neglected conversion to a sea-level datum, we investigated the impact of 1m relative sea-level rise (RSLR) on area and population when simulated for DEMs with their original vertical reference system and transposed to mean sea level. Similarly, we investigated the discrepancies in area and population within the 10 m low-elevation coastal zone (LECZ) when different DEMs with and without proper vertical datum alignment are used. After no data values and large negative values (i.e. ≤-7 m above MSL) were excluded and water bodies masked, we reclassified the DEMs applying thresholds of ≤1 m and ≤ 10m, respectively. Area in km^2 was calculated for global, continental and regional scales (Figure D15) using zonal statistics.

To estimate population falling below 1m RSLR and within the LECZ, we downloaded unconstrained WorldPop data from 2020 at 100 m spatial resolution (WorldPop and CIESIN, 2018). Instead of global WorldPop data, data for individual countries were used as the global dataset provides only aggregated data which would lead to substantial overestimation in population. Population estimates were derived for global, continental and regional scales using zonal statistics.

For coastal elevation values, RSLR impact and LECZ statistics, the respective deviations between estimates for DEMs with and without proper vertical datum conversion were quantified both absolutely as well as discrepancies in percentage of estimates for the DEM with proper vertical datum conversion to mean sea level (Supplementary Data D4 and D5).

4.2.3 Majority of coastal hazard assessments contains errors or is not reproducible

We evaluated 385 scientific publications (all peer-reviewed, >53 % published in the last 5 years) on (R)SLR and coastal flood exposure, vulnerability and risk, presenting both global and regional hazard assessments. We scrutinised each on correctness of DEM usage, vertical datum conversion and proper integration of sea-level height and coastal elevation (see Methods for details; Figures D1–D4; Tables D1–D2; Supplementary Data D1). We documented an ubiquity

of errors and omissions for the vast majority of studies. To assess the impacts on the resulting hazard assessments, we quantified the most frequent errors stemming from incorrect or absent vertical datum conversion in the evaluated studies (see Supplementary Data D2–D5). In most cases, this resulted in an underestimation of actual, present-day sea level with respect to land elevation. Effectively, this means that in reality coastal sea levels are higher than assumed, especially in data-sparse regions of Southeast Asia, Africa, and Small Island Development States (SIDS), leading to severe underestimations in coastal exposure and consequentially people and assets at risk in the majority of the impact assessments.

The evaluated coastal hazard assessment literature investigates coastal settings all over the world and across spatial scales. The impact assessments focused on (R)SLR (14 %), storm surge (8 %), tsunami (8 %), coastal exposure/vulnerability/risk more in general (41 %), or included combinations of different single-type coastal hazards, exposure/vulnerability/risk assessments and technical aspects and methodological advancements (29 %). The evaluated literature includes ample studies from data-sparse coastal lowlands in Africa (14 %) and Asia (58 %) which are severely impacted by RSLR and coastal flooding (Becker et al., 2024), poor data availability and accessibility as well as data inaccuracy due to the comparably poor performance of global earth gravity models (e.g., Nyoka et al., 2022). Moreover, the evaluated literature includes high-impact, global hazard assessments (10 %) which dictate the contemporary scientific understanding of global coastal hazard impacts.

In a large part of the evaluated publications (75 %), documentation of used sea-level height, coastal elevation and vertical datums is either incomplete (15 %), or entirely missing (60 %) (Figure 4.8). While 26 % properly documented the vertical datum used, only 1 % correctly aligned sea-level height to the coastal elevation's vertical datum. For the vast majority of evaluated assessments (99 %), sea level and coastal elevation alignment and datum conversion was either not assessable or demonstrable incorrect. In 63 % of the studies, the vertical datum type was not provided, making it unknown whether vertical reference systems were converted correctly and/or aligned properly to sea level (Figures 4.8 and D3), while 33 % demonstrably did not use a sea-level datum or applied them erroneously. The most prominent error (25 % of studies; Figures 4.8, 4.9 and D3) was the neglection of datum conversion from geoid to a sea-level datum, thereby implicitly assuming a geoid height of 0m to match local sea-level height. The second most frequent error (7 %) was incomplete datum conversion and inadequate alignment of vertical datums of datasets involved (e.g., land elevation, bathymetry, sea level, heights of coastal infrastructure, etc.). Only one (Kulp and Strauss, 2016) out of the 385

evaluated studies (0.3 %) contained no conversion and alignment errors and had complete datum documentation.

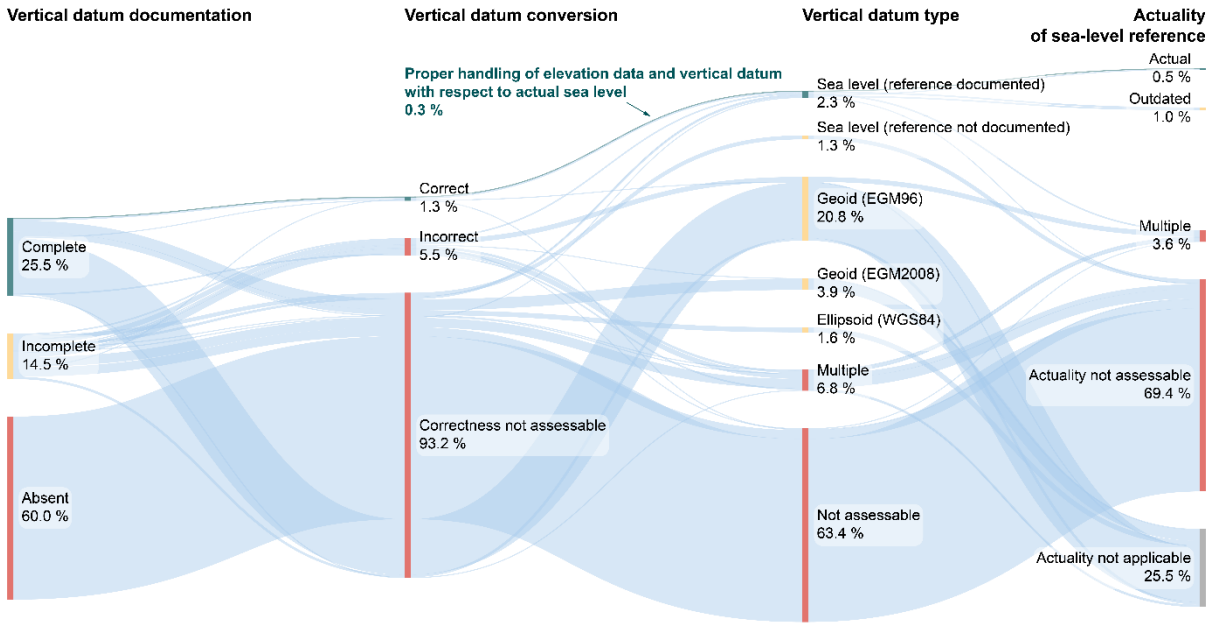


Figure 4.8 *| Evaluation of sea-level and coastal elevation data documentation and their proper use and alignment in coastal hazard assessments.*
Only 0.3 % of the evaluated studies completely documented, converted and properly adjusted coastal elevation data with sea-level information, questioning the reliability of more than 99 % of the evaluated coastal impact, exposure, vulnerability, and risk assessments. 33 % did not use a sea-level datum or applied them erroneously while in 63% the vertical datum type was not specified. In 75% of the studies, vertical datum documentation was incomplete or absent and in more than 98% of the evaluated assessments the proper alignment of sea-level and coastal elevation data was not assessable or demonstratable incorrect, impinging scientific standards of transparency and reproducibility and revealing errors in the sea-level height used in coastal hazard assessments.

To quantify the magnitudes of coastal sea-level height error following the most frequently observed processing errors, we performed meta-analyses on a global scale (see Methods for details, Figure D5). Neglecting (Figures 4.9, D6–D9) datum conversion using geoid-based elevation data resulted in a global average underestimation of sea-level height of respectively 0.5 m (EGM96) and 0.2 m (EGM2008). Regionally however, the errors were much larger up to several metres (2.8–3.4 m for EGM96 and 5.0–7.6 m for EGM 2008) (Figure 4.9). Improper alignment of sea-level datasets due to incomplete datum conversion (Figure D8) resulted in an average global underestimation of 0.02 m, regionally going up to 5.0–6.7 m (Supplementary Data D4). While the global mean values average out the high regional and sub-regional discrepancies, several key regions in the world suffer from substantial underestimations. Largest errors were observed in Southeast Asia, on average amounting to an underestimation of sea level of more than 1 m, as was previously already highlighted in local studies in this region that focused on the Mekong and Ayeyarwady deltas (Minderhoud et al., 2019; Seeger et al., 2023). Large errors were also prevalent in East Africa, Melanesia, Micronesia, Polynesia,

and the Caribbean. The lowest errors and discrepancies between sea level and geoid were found for the United States and other parts of North America, as well as Northern and Western Europe (Supplementary Data D4), reflecting the strong performance of geoid models to approach actual sea-surface height in data-rich regions like the Global North. However, in data-sparse and remote regions of the world where geoid and sea level do not align well, failure to properly convert to a sea-level datum, immediately transfers these discrepancies (Figure 4.9) as errors into hazard and SLR impact assessments (e.g., Muis et al., 2016; Brown et al., 2018; Gebremichael et al., 2018; Merkens et al., 2018; Adegun, 2023; del Campo et al., 2023) or delineation of the low-elevation coastal zone (LECZ) (e.g., Liu et al., 2015; MacManus et al., 2021; Tagtachian and Balk, 2023). Similarly, omitting to convert the vertical datums of elevation (DEM) and sea-level data (e.g., altimetry-based mean dynamic topography (MDT) or mean sea surface (MSS)) to a common datum before combining them, introduces a conversion error (e.g., Muis et al., 2017; Vernimmen et al., 2020; Vousdoukas et al., 2022; Vernimmen and Hooijer, 2023; Zhang et al., 2023; Wu et al., 2024).

In addition, a third source of error stems from the actuality of the sea-level data used. Tide gauges provide locally specific information, but their ability to adequately reflect recent sea level can be severely restricted when time series is too short, incomplete, or outdated. As tidal datums often have been established decades to centuries ago, e.g., the *North American Vertical Datum of 1988* (*NAVD 88*) in 1985 (NOAA, 2018), or the *Normaal Amsterdams Peil* (*NAP*) in the 17th century (NAP, without date), their usage is valid as long as sea-level changes since establishment are correctly taken into account. However, none of the publications to which this applies documents whether past sea-level change since datum establishment is considered, also in regions in the United States, Australia, New Zealand, and Europe, where high-quality elevation and sea-level information is available (e.g., Sheng et al., 2010; Wood et al., 2024; Supplementary Data D1). The incorrect use of sea-level height information e.g., from tide gauges or satellite altimetry (e.g., Vernimmen and Hooijer, 2023; Hooijer and Vernimmen, 2021) without considering past sea-level changes since datum establishment and start of the projection period contradicts the implied actuality of the hazard assessment conducted. Especially in view of the high rates of RSLR outpacing global SLR in many parts of the world, most prominently in densely populated coastal lowlands of Asia (Nicholls et al., 2021), assessments of actual coastal exposure absolutely necessitate to account for relative sea-level changes since tide gauge datum establishment or, in case of MDT/MSS, the average observation period. Similarly, to ensure the actuality of those hazard and impact assessments, we highlight

the urgency of using latest available and most accurate elevation data which, however, is not straightforward yet as only 22 % refer to actual DEMs and only 9 % include DEM accuracy assessments (Figure D4).

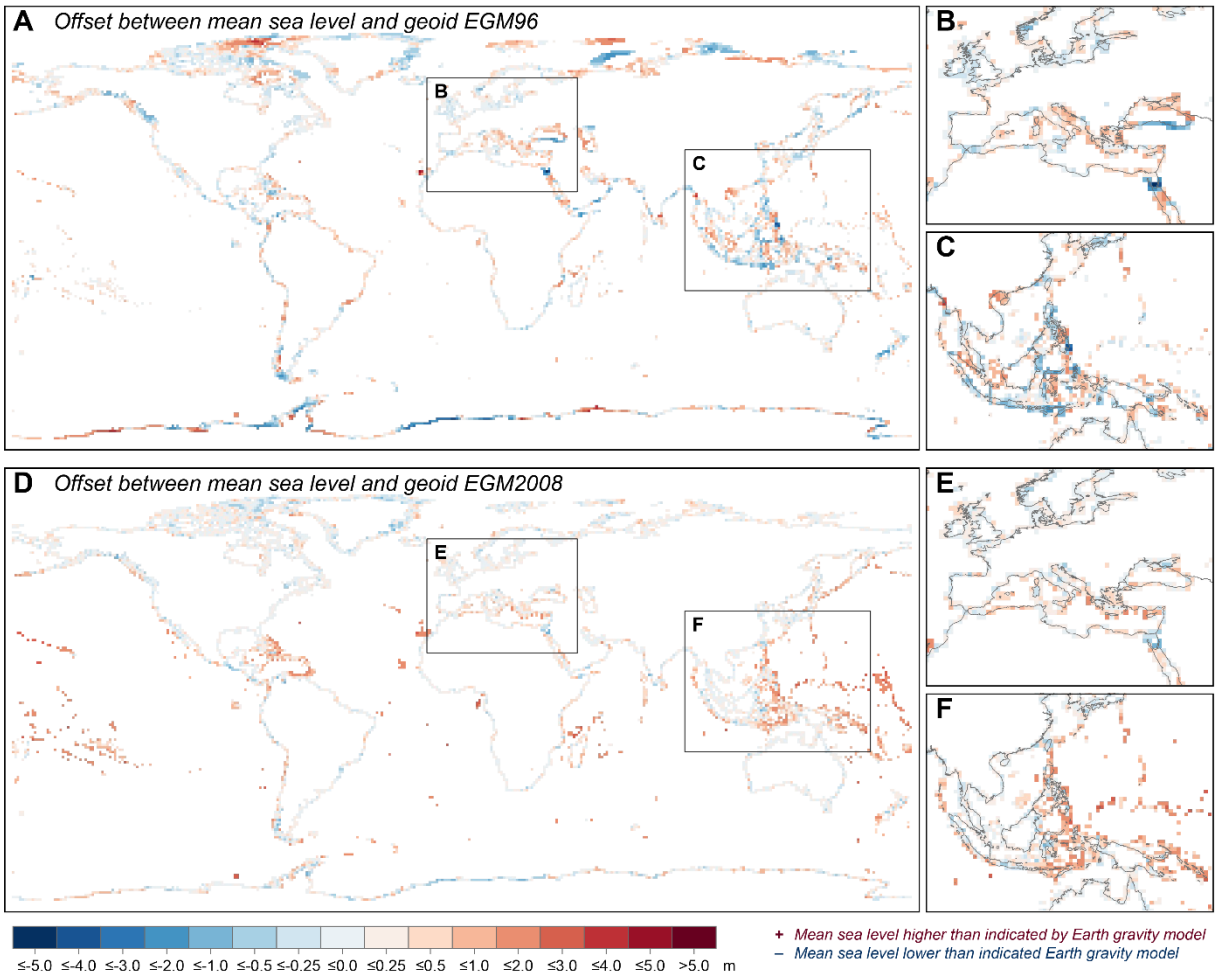


Figure 4.9 *| Discrepancy between coastal sea-level and most-used geoid height across the globe. (A–C) The still widely-used Earth Gravitational Model (EGM96) shows large deviations from actual sea level as indicated by latest available mean dynamic topography (CLS, 2022), especially visible on regional scale. (D–F) The more recent EGM2008 geoid model shows overall improvement over EGM96 and provides globally a better approximation of local sea level. Especially in data-rich countries of the Global North, the global geoids perform well (e.g., USA, Northern and Western Europe). However, several regions like Southeast Asia, Oceania, Micronesia and the Caribbean still suffer from substantial underestimations, ranging from several decimetres up to two metres in the tropical regions. The vast majority of evaluated literature containing demonstratable errors assumed geoid 0m elevation to represent local sea level, thereby introducing the above discrepancy as error into the hazard and SLR impact assessment. For visualisation purposes, the spatial scale of the data shown was resampled to 1 deg using bilinear resampling while all statistics are given at 90 m spatial resolution.*

4.2.4 Sea level higher than previously assumed in most coastal hazard assessments

To demonstrate the potential magnitude of errors present in nearly all coastal hazard assessments (up to 99 % of the evaluated literature), we quantified the impacts of the most

frequently witnessed errors on global RSLR impact assessments. We used four of the currently best-performing global DEMs as supplied in their data repositories (Kulp and Strauss, 2021; Hawker et al., 2021; Vernimmen and Hooijer, 2022; Pronk, 2024) and applied a RSLR scenario of 1 m while omitting the proper inclusion of sea-level datum, mimicking the omnipresent error in assessments (Supplementary Data D5). We compared the results to the same DEMs properly aligned to local mean sea level by using the most recent MDT data (CLS, 2022). Our analysis revealed that coastal sea level is in reality globally on average 0.2–0.5 m higher than assumed in previous coastal hazard assessments (Figure 4.10). Regionally, the largest sea-level height underestimations coincide with vulnerable regions in the Global South like Southeast Asia, hosting large and densely populated river deltas, large parts of Africa and SIDS (often lowly-elevated atolls) of Melanesia, Micronesia and Polynesia (Figures 4.10 and D10–D15; Supplementary Data D5).

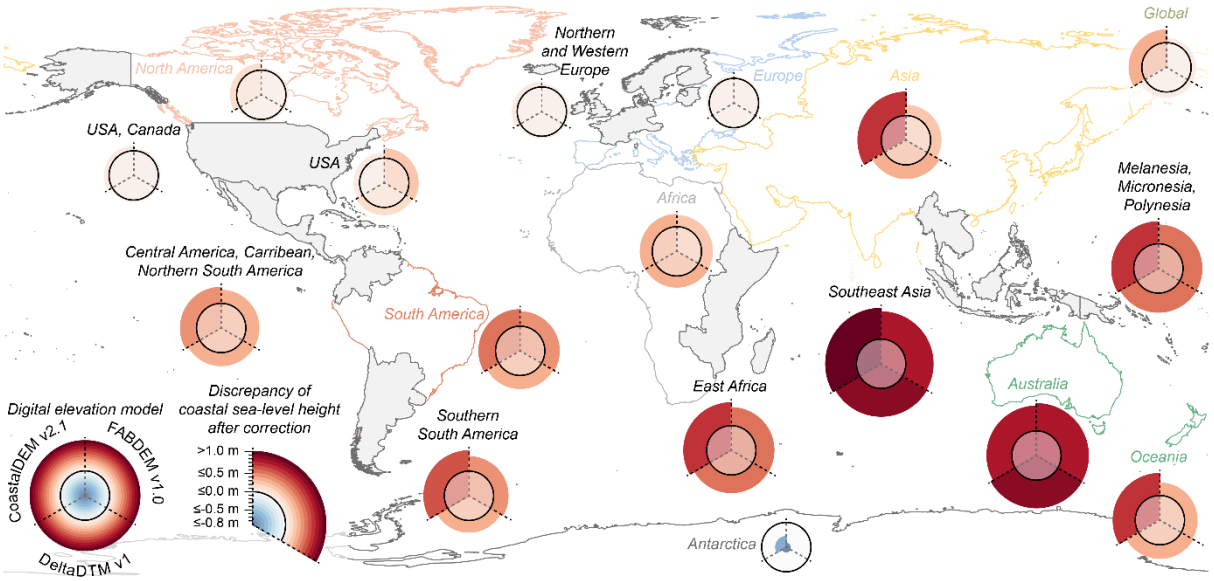


***Figure 4.10** | Discrepancy between commonly assumed coastal sea-level height in hazard assessments with actual local sea-level height.*
Meta-analysis of the most common error in existing coastal hazard assessments, i.e. assuming geoid height to represent local sea-level height, using modern, globally available digital elevation models (CoastalDEM v2.1 (Kulp and Strauss, 2021); FABDEM v1.0 (Hawker et al., 2021); DeltaDTM v1 (Pronk, 2024)). The difference given is the coastal sea-level height discrepancy for each DEM compared to our assessment when properly aligning coastal elevation to sea level. On average, global coastal sea level is underestimated by 0.2 m to 0.5 m, depending on DEM and vertical datum used, while regionally highest median underestimations of 1 m to 1.1 m were observed along the coastlines of Southeast Asia. All statistics are given at 90 m spatial resolution.

Globally, area and population exposed to 1 m RSLR were underestimated respectively by up to 37 % and 67 %, increasing the area exposed by >245,700 km^2 to more than 670,000 km^2 and population by up to 88.3 million to 132.1 million people (Figures 4.11 and D10). In the most effected region, Southeast Asia, which is included by the majority of the evaluated literature, area and population within this 1 m RSLR were underestimated even by up to 94 % and 96 %,

respectively, and include up to 100,300 km^2 and 47.0 million people (Figures 4.11 and D10–D14; Supplementary Data D5).

Neglected and incorrect datum conversion resulted in an underestimation of area and people in the LECZ (first 10 metres of coastal elevation) of respectively 4 % and 5 % globally and increases the global LECZ to >4 million km^2 being inhabited by more than 1 billion people (Supplementary Data D5).

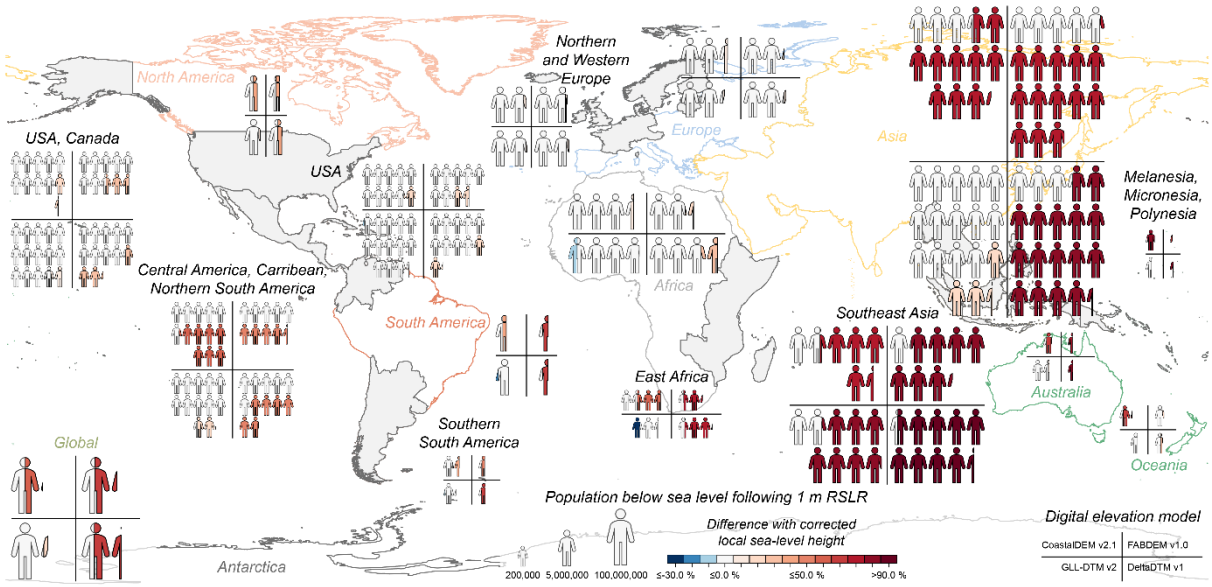


Figure 4.11 *| Differences in population falling below sea level following 1m relative sea-level rise (RSLR) with proper alignment of land and sea-level height.*
Meta-analysis of the impact of the most frequently observed errors in existing coastal hazard assessments, i.e. assuming geoid height to represent local sea-level height and improper alignment of land and sea-level heights, using modern, globally available digital elevation models (CoastalDEM v2.1 (Kulp and Strauss, 2021); FABDEM v1.0 (Hawker et al., 2021); GLL-DTM v2 (Vernimmen and Hooijer, 2022); DeltaDTM v1 (Pronk, 2024)). Due to the widespread omission to tie elevation data to local sea level instead of global geoid models, population estimates relative to local mean sea level are 12 % to 67 % higher globally and amount to 102.8 million to 132.1 million people falling below sea level following 1 m RSLR. Maximum population discrepancies of 74 % to 96 % (i.e. 23.8 million to 44.8 million people) are observed along the coastlines of Southeast Asia where – if properly assessed – 32.1 million to 47.0 million people will fall below sea level following 1 m RSLR. All statistics are given for the DEM's respective spatial resolution.

Our literature evaluation also revealed widespread and persistent propagation of erroneous workflows, e.g. omitting sea-level datum conversion (Muis et al., 2016; MacManus et al., 2021) or introducing datum conversion errors (Muis et al., 2017; Zhang et al., 2023; Wu et al., 2024; Kirezci et al., 2020), to consequently affect follow-up studies which apply the same data and processing approach (Vernimmen et al., 2020; Vernimmen and Hooijer, 2023; Kirezci et al., 2025) (Supplementary Data D1). Similarly, assessments using modelling frameworks that include elevation data in the coastal zone also suffer from the investigated issues such as incomplete or absent vertical datum documentation (e.g., Adegun, 2023; Bolleter et al., 2021), non-assessability of datum conversion (e.g., Lincke and Hinkel, 2018, 2021), and/or lack of a

sea-level datum (e.g., Vafeidis et al., 2019; Adams et al., 2024; Ghomsi et al., 2024; Supplementary Data D1), impeding the assessment of the correctness of their results.

4.2.5 Conclusions and outlook

Our analysis reveals widespread misuse of sea-level and elevation data within a wide scientific community which has led to large errors in the vast majority of coastal hazard and (R)SLR impact assessments. From all evaluated studies, over 99 % either missed crucial documentation and processing information, making it impossible to evaluate their correctness and rendering the studies irreproducible, or made demonstratable errors in sea level datum consideration and/or proper conversion. This questions the validity and correctness of existing coastal hazard assessment literature, with potential far-reaching implications as such studies are used to underpin IPCC SLR impact reports (IPCC, 2023; Muis et al., 2016; Kirezci et al., 2020; IPCC, 2021) and global disaster risk reduction efforts (UNDRR), informing governments and policymakers worldwide, and provide quantitative input for Loss and Damage negotiations.

Our meta-analysis revealed that coastal sea level worldwide is on average 0.2–0.5 m higher than assumed in coastal hazard assessments affected by the most encountered error. This means that a substantially larger area (up to 37 %) and more people (up to 67 % more, 132.1 million people in total) will fall below sea level following 1 m RSLR than previously assessed. Our findings highlight the tremendous need to carefully consider and process sea-level and elevation data in coastal settings, to ensure proper inclusion and datum conversion to a reliable and up-to-date sea-level datum and adequately document data, datum and datum conversion to ensure transparency and reproducibility. One potential explanation for the encountered widespread misuse may be the current constellation that leaves complex geodetic transformations required to use elevation data for coastal hazard assessments in the hands of non-specialist end users unfamiliar to the required post-processing steps. The facts that geoid models are developed and performing well in reflecting local sea-level height in countries of the Global North (e.g., USA, Western Europe) may perhaps explain the overconfidence placed in geoid model performance by Global North-based scientists when performing assessments on global scale or in other regions of the world where geoid models perform less well. In addition, to increase the reliability of coastal hazard assessment results, including DEM accuracy assessments using multiple elevation datasets is recommended (Seeger et al., 2024). While we addressed issues on coastal elevation and sea level, we found indications for similar problems in studies using

bathymetry data which suggests further future research and critical reflection in those domains as well. Aside from scientific publications, our results suggest that many grey literature, like policy-forming documents, governmental reports and other consultancy-based assessments focusing on coastal exposure and risk, will likely suffer from similar errors. Ultimately, the correct use of sea-level and land elevation data is also critical to the emerging integration of vertical land motion and coastal land subsidence into RSLR projections (Shirzaei et al., 2021; Minderhoud et al., 2025).

This study likely reveals only the tip of the iceberg, as our evaluated publications provide a representative selection of the entire volume of coastal hazards assessments publications. This calls for a systemic change on how we deal with sea-level and elevation data in the scientific community and beyond. One solution to avoid future misuse may lie in the hands of the data providers, which could provide readily combined products of digital terrain with sea level to facilitate proper end use. This would especially make sense for DEMs that are specifically developed to target the coastal zone and facilitate coastal hazard assessments, like CoastalDEM and DeltaDTM. In addition, our results show that scientific peer-review fails to withhold these errors from initial publication and propagation through literature, resulting in a vast body of irreplicable scientific literature with unknown and unquantifiable errors. In addition, to avoid future misconduct, journals could introduce a dedicated step in the review process to evaluate proper use of elevation data and vertical datums. This will not only help to spot errors, avoid data misuse, and make studies replicable; it also raises awareness on these prominent issues with the wider scientific community. This is crucial as presently we risk that all global efforts of improving our projections of future sea-level change to mm accuracy (e.g., IPCC, 2023, 2021) become nullified by sea-level and elevation data misuse in coastal hazards and impacts assessments.

Data availability statement: Original digital elevation models, mean dynamic topography, and population data used in this study are available online (Kulp and Strauss, 2021; Hawker et al., 2021; Vernimmen and Hooijer, 2022; Pronk et al., 2024; CLS, 2022; WorldPop and CIESIN, 2018). The processed, global digital elevation models, properly converted to local mean sea level using mean dynamic topography measurements, used in this study are accessible here: [online repository link will follow upon publication]. The results of the in-depth literature evaluation, model workflow codes and coastal impact assessments are available in the Supplementary Data. The processed data of this study is made available in course of the publication of the scientific article to which this chapter is related.

References

K. H. Adams, J. T. Reager, B. A. Buzzanga, C. H. David, A. H. Sawyer, B. D. Hamlington, Climate-Induced Saltwater Intrusion in 2100: Recharge-Driven Severity, Sea Level-Driven Prevalence. *Geophys. Res. Lett. 51*(22), e2024GL110359 (2024). https://doi.org/10.1029/2024GL110359.

O. B. Adegun, Flood-related challenges and impacts within coastal informal settlements: a case from LAGOS, NIGERIA. *Int. J. Urban Sustainable Dev. 15*(1), 1–13 (2023). https://doi.org/10.1080/19463138.2022.2159415.

M. Becker, K. Seeger, A. Paszkowski, M. Marcos, F. Papa, R. Almar, P. Bates, C. France-Lanord, Md. S. Hossain, Md. J. U. Khan, M. A. Karegar, M. Karpytchev, N. Long, P. S. J. Minderhoud, J. Neal, R. J. Nicholls, J. Syvitski, Coastal Flooding in Asian Megadeltas: Recent Advances, Persistent Challenges, and Call for Actions Amidst Local and Global Challenges. *Rev. Geophys. 62*(4), e2024RG000846 (2024). https://doi.org/10.1029/2024RG000846.

J. Bolleter, B. Grace, P. Hooper, S. Foster, Wet-bulb Temperature and Sea-level Rise in the United Arab Emirates – Planning Responses. *Planning Practice & Research 36*(4), 408–429 (2021). https://doi.org/10.1080/02697459.2020.1859199.

S. Brown, R. J. Nicholls, A. N. Lázár, D. D. Hornby, C. Hill, S. Hazra, K. A. Addo, A. Haque, J. Caesar, E. L. Tompkins, What are the implications of sea-level rise for a 1.5, 2 and 3 °C rise in global mean temperatures in the Ganges-Brahmaputra-Meghna and other vulnerable deltas?. *Reg. Environ. Change 18*, 1829–1842 (2018). https://doi.org/10.1007/s10113-018-1311-0.

T. Candela, K. Koster, The many faces of anthropogenic subsidence. *Science 376*(6600), 1381–1382 (2022). https://doi.org/10.1126/science.abn3676.

CLS, Copernicus Marine Service, 2022 Hybrid Mean Dynamic Topography CNES-CLS22-CMEMS2020, CNES (2022); https://doi.org/10.24400/527896/a01-2024.010.

S. Dasgupta, B. Laplante, C. Meisner, D. Wheeler, J. Yan, The impact of sea level rise on developing countries: a comparative analysis. *Clim. Change 93*, 379–388 (2009). https://doi.org/10.1007/s10584-008-9499-5.

F. M. del Campo, S. J. Singh, T. Fishman, A. Thomas, M. Drescher, The Bahamas at risk: Material stocks, sea-level rise, and the implications for development. *J. Ind. Ecol. 27*(4), 1165–1183 (2023). https://doi.org/10.1111/jiec.13402.

S. Doganalp, H. Z. Selvi, Local geoid determination in strip area projects by using polynomials, least-squares collocation and radial basis functions. *Measurement 73*, 429–438 (2015). https://doi.org/10.1016/j.measurement.2015.05.030.

J. P. Ericson, C. J. Vörösmarty, S. L. Dingman, L. G. Ward, M. Meybeck, Effective sea-level rise and deltas: Causes of change and human dimension implications. *Global Planet. Change 50*, 63–82 (2006). https://doi.org/10.1016/j.gloplacha.2005.07.004.

P. F. Fisher, N. J. Tate, Causes and consequences of error in digital elevation models. *Prog. Phys. Geogr. 30*(4), 467–489 (2006). https://doi.org/10.1191/0309133306pp492ra.

A. A. Fusami, J. D. Edan, A. Takana, Local orthometric height based on a combination of GPS-derived ellipsoidal height and geoid model: A review paper. *J. Geodetic Sci. 13*(1), 20220158 (2023). https://doi.org/10.1515/jogs-2022-0158.

E. Gebremichael, M. Sultan, R. Becker, M. El Bastawesy, O. Cherif, M. Emil, Assessing Land Deformation and Sea Encroachment in the Nile Delta: A Radar Interferometric and Inundation Modeling Approach. *J. Geophys. Res. Solid Earth 123*(4), 3208–3224 (2018). https://doi.org/10.1002/2017JB015084.

F. E. K. Ghomsi, B. Nyberg, R. P. Raj, A. Bonaduce, B. J. Abiodun, O. M. Johannessen, Sea level rise and coastal flooding risks in the Gulf of Guinea. *Sci. Rep. 14*, 29551 (2024). https://doi.org/10.1038/s41598-024-80748-w.

M. H. Hamden, A. H. M. Din, D. D. Wijaya, M. Y. M. Yusoff, M. F. Pa'suya, Regional Mean Sea Surface and Mean Dynamic Topography Models Around Malaysian Seas Developed From 27 Years of Along-Track Multi-Mission Satellite Altimetry Data. *Front. Earth Sci. 9*, 665876 (2021). https://doi.org/10.3389/feart.2021.665876.

L. Hawker, J. Neal, P. Uhe, L. Paulo, J. Sosa, J. Savage, C. Sampson, FABDEM, version 1.0, University of Bristol (2021); https://doi.org/10.5523/bris.25wfy0f9ukoge2gs7a5mqpq2j7.

J. Hinkel, L. Feyen, M. Hemer, G. Le Cozannet, D. Lincke, M. Marcos, L. Mentaschi, J. L. Merkens, H. de Moel, S. Muis, R. J. Nicholls, A. T. Vafeidis, R. S. W. van de Wal, M. I. Vousdoukas, T. Wahl, P J. Ward, C. Wolff, Uncertainty and Bias in Global to Regional Scale Assessments of Current and Future Coastal Flood Risk. *Earth's Future 9*(7), e2020EF001882 (2021). https://doi.org/10.1029/2020EF001882.

A. Hooijer, R. Vernimmen, Global LiDAR land elevation data reveal greatest sea-level rise vulnerability in the tropics. *Nat. Commun. 12*, 3592 (2021). https://doi.org/10.1038/s41467-021-23810-9.

E. S. Ince, F. Barthelmes, S. Reißland, K. Elger, C. Förste, F. Flechtner, H. Schuh, ICGEM – 15 years of successful collection and distribution of global gravitational models, associated services, and future plans. *Earth Syst. Sci. Data 11*(2), 647–674 (2019). https://doi.org/10.5194/essd-11-647-2019.

IPCC, "*Climate Change 2021: The Physical Science Basis. Contribution of Working Group I to the Sixth Assessment Report of the Intergovernmental Panel on Climate Change*" (IPCC, 2021); https://doi.org/10.1017/9781009157896.

IPCC, "*Climate Change 2023: Synthesis Report. Contribution of Working Groups I, II and III to the Sixth Assessment Report of the Intergovernmental Panel on Climate Change*" (IPCC, 2023); https://doi.org/10.59327/IPCC/AR6-9789291691647.

E. Kirezci, I. R. Young, R. Ranasinghe, S. Muis, R. J. Nicholls, D. Lincke, J. Hinkel, Projections of global-scale extreme sea levels and resulting episodic coastal flooding over the 21st Century. *Sci. Rep. 10*, 11629 (2020). https://doi.org/10.1038/s41598-020-67736-6.

E. Kirezci, I. Young, R. Ranasinghe, Y. Chen, Y. Zhang, A. Rajabifard, Global Dataset of Extreme Sea Levels and Coastal Flood Impacts over the 21st Century. *Data 10*(2), 15 (2025). https://doi.org/10.3390/data10020015.

P. Knudsen, R. Bingham, O. Andersen, M-H. Rio, A global mean dynamic topography and ocean circulation estimation using a preliminary GOCE gravity model. *J. Geod. 85*, 861–879 (2011). https://doi.org/10.1007/s00190-011-0485-8.

S. Kulp, B. H. Strauss, Global DEM Errors Underpredict Coastal Vulnerability to Sea Level Rise and Flooding. *Front. Earth Sci. 4*, 36 (2016). https://doi.org/10.3389/feart.2016.00036.

S. A. Kulp, B. H. Strauss, CoastalDEM, version 2.1, *Climate Central* (2021); https://go.climatecentral.org/coastaldem.

D. Lincke, J. Hinkel, Economically robust protection against 21st century sea-level rise. *Global Environ. Change 51*, 67–73 (2018). https://doi.org/10.1016/j.gloenvcha.2018.05.003.

D. Lincke, J. Hinkel, Coastal Migration due to 21st Century Sea-Level Rise. *Earth's Future 9*(5), e2020EF001965 (2021). https://doi.org/10.1029/2020EF001965.

X. Li, Using radial basis functions in airborne gravimetry for local geoid improvement. J. *Geod. 92*, 471–485 (2018). https://doi.org/10.1007/s00190-017-1074-2.

J. Liu, J. Wen, Y. Huang, M. Shi, Q. Meng, J. Ding, H. Xu, Human settlement and regional development in the context of climate change: a spatial analysis of low elevation coastal zones in China. *Mitigation Adapt. Strategies Global Change 20*, 527–546 (2015). https://doi.org/10.1007/s11027-013-9506-7.

K. MacManus, D. Balk, Engin, H., G. McGranahan, R. Inman, Estimating population and urban areas at risk of coastal hazards, 1990–2015: how data choices matter. *Earth Syst. Sci. Data 13*, 5747–5801 (2021). https://doi.org/10.5194/essd-13-5747-2021.

J-L. Merkens, D. Lincke, J. Hinkel, S. Brown, A. T. Vafeidis, Regionalisation of population growth projections in coastal exposure analysis. *Clim. Change 151*, 413–426 (2018). https://doi.org/10.1007/s10584-018-2334-8.

P. S. J. Minderhoud, L. Coumou, G. Erkens, H. Middelkoop, E. Stouthamer, Mekong delta much lower than previously assumed in sea-level rise impact assessments. *Nat. Commun. 10*, 3847 (2019). https://doi.org/10.1038/s41467-019-11602-1.

P. S. J. Minderhoud, M. Shirzaei, P. Teatini, From InSAR-Derived Subsidence to Relative Sea-Level Rise – A Call for Rigor. *Earth's Future 13*(1), e2024EF005539 (2025). https://doi.org/10.1029/2024EF005539.

S. Muis, M. Verlaan, H. C. Winsemius, J. C. J. H. Aerts, P. J. Ward, A global reanalysis of storm surges and extreme sea levels. *Nat. Commun. 7*, 11969 (2016). https://doi.org/10.1038/ncomms11969.

S. Muis, M. Verlaan, R. J. Nicholls, S. Brown, J. Hinkel, D. Lincke, A. T. Vafeidis, P. Scussolini, H. C. Winsemius, P. J. Ward, A comparison of two global datasets of extreme sea levels and resulting flood exposure. *Earth's Future 5*(4), 379–392 (2017). https://doi.org/10.1002/2016EF000430.

NAP, "Arise of the NAP" (NAP, without date); https://www.normaalamsterdamspeil.nl/en/nap-geschiedenis/.

B. Neumann, A. T. Vafeidis, J. Zimmermann, R. J. Nicholls, Future Coastal Population Growth and Exposure to Sea-Level Rise and Coastal Flooding – A Global Assessment. *PLoS One 10*(6), e0131375 (2015). https://doi.org/10.1371/journal.pone.0131375.

R. J. Nicholls, D. Lincke, J. Hinkel, S. Brown, A. T. Vafeidis, B. Meyssignac, S. E. Hanson, J-L. Merkens, J. Fang, A global analysis of subsidence, relative sea-level change and coastal flood exposure. *Nat. Clim. Change 11*, 338–342 (2021). https://doi.org/10.1038/s41558-021-00993-z.

NOAA National Geodetic Survey, "North American Vertical Datum of 1988 (NAVD 88)" (NOAA, 2018); https://www.ngs.noaa.gov/datums/vertical/north-american-vertical-datum-1988.shtml.

C. J. Nyoka, A. H. M. Din, M.F. Pa'suya, A. H. Omar, Rigorous evaluation of global geopotential models for geoid modelling: A case study in Kenya. *J. Afr. Earth. Sci. 194*, 104612 (2022). https://doi.org/10.1016/j.jafrearsci.2022.104612.

M. Pronk, DeltaDTM: A global coastal digital terrain model, version 1, *4TU.ResearchData* (2024); https://doi.org/10.4121/21997565.v4.

M-H. Rio, S. Mulet, N. Picot, Beyond GOCE for the ocean circulation estimate: Synergetic use of altimetry, gravimetry, and in situ data provides new insight into geostrophic and Ekman currents. *Geophys. Res. Lett. 41*(24), 8918–8925 (2014). https://doi.org/10.1002/2014GL061773.

G. J-P. Schumann, Fight floods on a global scale. *Nature 507*, 169 (2014). https://doi.org/10.1038/507169e.

G. J-P. Schumann, P. D. Bates, The Need for a High-Accuracy, Open-Access Global DEM. *Front. Earth Sci. 6*, 225 (2018). https://doi.org/10.3389/feart.2018.00225.

K. Seeger, P. S. J. Minderhoud, A. Peffeköver, A. Vogel, H. Brückner, F. Kraas, Nay Win Oo, D. Brill, Assessing land elevation in the Ayeyarwady Delta (Myanmar) and its relevance for studying sea level rise and delta flooding. *Hydrol. Earth Syst. Sci. 27*, 2257–2281 (2023). https://doi.org/10.5194/hess-27-2257-2023.

K. Seeger, P. S. J. Minderhoud, L. T. Hauser, P. Teatini, M-N. Woillez, "How to assess coastal flood risk in data-sparse coastal lowlands? Accurate information on land elevation is key" (A Question of development No. 17, Agence Française Développement, 2024); https://www.afd.fr/en/ressources/how-assess-coastal-flood-risk-data-sparse-coastal-lowlands-accurate-information-land-elevation-key.

Y. P. Sheng, Y. Zhang, V. A. Paramygin, Simulation of storm surge, wave, and coastal inundation in the Northeastern Gulf of Mexico region during Hurricane Ivan in 2004. *Ocean Modell. 35*, 314–331 (2010). https://doi.org/10.1016/j.ocemod.2010.09.004.

M. Shirzaei, J. Freymueller, T. E. Törnqvist, D. L. Galloway, T. Dura, P. S. J. Minderhoud, Measuring, modelling and projecting coastal land subsidence. *Nat. Rev. Earth Environ. 2*, 40–58 (2021). https://doi.org/10.1038/s43017-020-00115-x.

D. Tagtachian, D. Balk, Uneven vulnerability: characterizing population composition and change in the low elevation coastal zone in the United States with a climate justice lens, 1990–2020. *Front. Environ. Sci. 11*, 1111856 (2023). https://doi.org/10.3389/fenvs.2023.1111856.

A. Üstün, R. A. Abbak, E. Zeray Öztürk, Height biases of SRTM DEM related to EGM96: from a global perspective to regional practice. *Surv. Rev. 50*(358), 26–35 (2016). https://doi.org/10.1080/00396265.2016.1218159.

A. T. Vafeidis, M. Schuerch, C. Wolff, T. Spencer, J. L. Merkens, J. Hinkel, D. Lincke, S. Brown, R. J. Nicholls, Water-level attenuation in global-scale assessments of exposure to coastal flooding: a sensitivity analysis. *Nat. Hazards Earth Syst. Sci. 19*(5), 973–984 (2019). https://doi.org/10.5194/nhess-19-973-2019.

R. Vernimmen, A. Hooijer, M. Pronk, New ICESat-2 Satellite LiDAR Data Allow First Global Lowland DTM Suitable for Accurate Coastal Flood Risk Assessment. *Remote Sens. 12*(17), 2827 (2020). https://doi.org/10.3390/rs12172827.

R. Vernimmen, A. Hooijer, GLL_DTM, version 2, *Zenodo* (2022); https://doi.org/10.5281/zenodo.6534526.

R. Vernimmen, A. Hooijer, New LiDAR-Based Elevation Model Shows Greatest Increase in Global Coastal Exposure to Flooding to Be Caused by Early-Stage Sea-Level Rise. *Earth's Future 11*(1), e2022EF002880 (2023). https://doi.org/10.1029/2022EF002880.

M. I. Vousdoukas, J. Clarke, R. Ranasinghe, L. Reimann, N. Khalaf, T. M. Duong, B. Ouweneel, S. Sabour, C. E. Iles, C. H. Trisos, L. Feyen, L. Mentaschi, N. P. Simpson, African heritage sites threatened as sea-level rise accelerates. *Nat. Clim. Change 12*(3), 256–263 (2022). https://doi.org/10.1038/s41558-022-01280-1.

D. T. Vu, S. Bruinsma, S. Bonvalot, D. Remy, G. S. Vergos, A Quasigeoid-Derived Transformation Model Accounting for Land Subsidence in the Mekong Delta towards Height System Unification in Vietnam. *Remote Sens. 12*(5), 817 (2020). https://doi.org/10.3390/rs12050817.

M. Wood, I. D. Haigh, Q. Q. Le, H. N. Nguyen, H. B. Tran, S. E. Darby, R. Marsh, N. Skliris, J. J-M. Hirschi, Risk of compound flooding substantially increases in the future Mekong River delta. *Nat. Hazards Earth Syst. Sci. 24*(10), 3627–3649 (2024). https://doi.org/10.5194/nhess-24-3627-2024.

WorldPop, CIESIN, Population Counts / Unconstrained individual countries 2020 (100m resolution), Global High Resolution Population Denominators Project – Funded by The Bill and Melinda Gates Foundation (OPP1134076) (2018); https://dx.doi.org/10.5258/SOTON/WP00645.

S. Wu, X. Zhou, J. Reyns, D. Yamazaki, J. Lin, X. Li, Climate change and urban sprawl: Unveiling the escalating flood risks in river deltas with a deep dive into the GBM river delta. *Sci. Total Environ. 947*, 174703 (2024). https://doi.org/10.1016/j.scitotenv.2024.174703.

S. Zhang, J. Zhang, X. Li, X. Du, T. Zhao, Q. Hou, X. Jin, Quantitative risk assessment of typhoon storm surge for multi-risk sources. *J. Environ. Manage. 327*, 116860 (2023). https://doi.org/10.1016/j.jenvman.2022.116860.

4.3 Attributing uncertainties in elevation assessments for data-sparse coastal lowlands using global elevation models: A globally applicable approach showcasing the Vietnamese Mekong Delta

Abstract: River deltas and coastal plains are at risk of sea-level rise and other coastal hazard, often exacerbated by land subsidence. The relative elevation of a coastal lowland to local sea level is a crucial determent for its overall exposure, making it key input for coastal hazard assessments However, locally-sources, high-accuracy elevation data, such as LiDAR, is not available for many data-sparse coastal lowlands worldwide, leaving global digital elevation models as only source of information. While these provide an adequate spatial (i.e. horizontal) resolution for regional, delta-wide coastal assessments, their vertical errors in the range of several metres impede investigations of (relative) sea-level rise impact where changes occur on millimetre- to centimetre-scale. Assessing the quality of available elevation datasets is required to identify the best performing model(s) to use for generating reliable coastal impact and exposure assessments. While data-intrinsic inaccuracy has been extensively addressed both in dataset documentation and literature, the relevance and proper vertical datum conversion from global geoid and ellipsoid to local sea level is often still omitted in many applied studies from coastal research. Similarly, the impact of the actuality of elevation data (i.e. time since data acquisition) on assessments in coastal lowlands is so far understudied although elevation models may become quickly outdated, especially where coastal lowlands are facing high rates of elevation change resulting from the interplay of vertical land motion, (vertical) sediment accretion and sea-level change. Particularly for flat, low-lying subsiding coastal landscapes like the Mekong Delta, being in parts only a few decimetres elevated above sea level and experiencing land subsidence of up to several centimetres per year, the reliability of elevation data and adequate representation of elevation relative to local sea level as well as the consideration of factors impacting elevation over time is of utmost importance. We present a globally applicable approach to quantify and attribute uncertainties in elevation assessment for data-sparse coastal lowlands using global elevation models to sources such as inaccuracy, vertical datum offset and actuality. We showcase this approach by revisiting land elevation in the Vietnamese Mekong Delta (i) by vertically referencing 11 commonly used global elevation models and an updated local elevation model to a common actual, local sea-level datum, and (ii) by conducting a thorough assessment of elevation model performance that not only allows

for the quantification of errors and elevation assessment uncertainties but also their attribution to data-intrinsic inaccuracy, vertical datum offset and, tentatively, non-linear impact of elevation change due to vertical land motion (e.g. extraction-induced land subsidence) and sea-level change affecting the actuality of the elevation model. Our approach not only allows to improve the understanding of coastal elevation to further improve relative sea-level rise and flood impact assessments and to substantiate projections of future elevation in the Mekong Delta, but in its design, applying solely open data and commonly used GIS software, facilitates similar assessments of elevation model performance and elevation assessment uncertainties in other (data-sparse) coastal regions in the world.

Key words: Digital elevation model (DEM); land elevation change; land subsidence; relative sea-level rise; sea level; vertical datum

Chapter 4.3 is related to: **Seeger, K.**, Minderhoud, P.S.J., submitted. *Attributing uncertainties in elevation assessments for data-sparse coastal lowlands using global elevation models: A globally applicable approach showcasing the Vietnamese Mekong Delta*. Scientific Reports.

The scientific article is published under a CC-BY 4.0 Attribution 4.0 International licence (http://creativecommons.org/licenses/by/4.0/). The reader is recommended to refer to the peer-reviewed and published version of the content of this chapter which can be accessed via the article doi provided here (https://doi.org/10.1038/s41598-026-38315-y).

4.3.1 Introduction

Coastal lowlands are at risk of sea-level rise (SLR), often exacerbated by coastal subsidence (Shirzaei et al., 2021). Especially densely populated river deltas are prone to suffer from magnitudes of land subsidence that outpace dimensions of absolute sea-level change and together with sediment starvation due to sediment trapping in upstream dams culminate in elevation loss (e.g., Ericson et al., 2006; Syvitski et al., 2009; Nicholls et al., 2021; Chan et al., 2024; Ohenhen et al., 2025). Consequently, these lowlands are also increasingly exposed to other coastal hazards such as storm surge flooding (e.g. Edmonds et al., 2020). The elevation of coastal lowlands above sea level is a critical factor in safeguarding these globally important

landscapes from temporary and permanent inundation, salinity intrusion and other cascading effects on the environment and society, affecting for example socio-economic productivity (see also Renaud et al., 2013). Land elevation data, mostly in form of digital elevation models (DEMs), are necessary for any quantitative coastal hazard impact assessment or projection, and the reliability of these assessments is strongly determined by the quality of the underlying elevation data. Therefore, thorough DEM accuracy assessments are needed to ensure the reliability of flood risk and SLR impact evaluations or at least to quantify ranges of uncertainty, both in terms of area, population and assets at risk (e.g., Kulp and Strauss, 2016; Gesch et al., 2023; Seeger et al., 2023; Hauser et al., 2023).

Information on land elevation is obtained either by direct measurements through topographical levelling surveys and Global Navigation Satellite System (GNSS) measurements, or by exploiting remote sensing data from aircrafts or satellites (optical, radar, laser altimetry) to generate DEMs of the Earth's surface. DEMs are subdivided into models representing a landscape's surface (so-called digital surface models (DSMs)), i.e. including vegetation and building heights, and digital terrain models (DTMs) that represent elevation of the bare earth (e.g., Wilson, 2012; Guth et al., 2021). While the DEM type depends on the acquisition techniques and processing approaches of a given dataset, it is important to select the correct DEM type fitting the purpose of application (Wilson, 2012).

Local ground measurements of land elevation data provide elevation information of high vertical accuracy, but suffer from coarse spatial resolutions and time-consuming data acquisition. Through remote sensing techniques such as aerial photogrammetry, and more recently, airborne Light Detection and Ranging (LiDAR), the quality of DEMs has been improved over the years to reach horizontal resolutions and vertical accuracies on centimetre- to decimetre-scale (e.g. Hodgson and Bresnahan, 2004; Buffington et al., 2016; Ren et al., 2016). While such high-accuracy, locally-source data is publicly available for several coastal regions, for example in the United States, Australia, New Zealand and Europe, it is unfortunately not available for major parts of the Earth's coast, amongst other the vast, densely populated coastal lowlands of Asia and Africa as well as many Small Island Developing States. Here, global, freely available, satellite-based DEMs are commonly used (e.g., as highlighted by Almar et al., 2023; Becker et al., 2024), however often studies do not take limitations of the applicability of these DEMs properly into consideration. Although global DEMs often provide an adequate spatial (i.e. horizontal) resolution (i.e. in the range of ~10 to 90 m), sufficient for setting up regional, delta-wide flood models or estimating coastal population and land-use asset

exposure, their vertical errors in the range of several metres impede investigations of (relative) SLR impact where changes occur on millimetre- to centimetre-scale. Inaccuracies related to the acquisition of elevation data or DEM processing itself (e.g. sensing or interpolation artefacts) have been addressed by post-processing first-order DEMs such as SRTM (Farr et al., 2007), ASTER (Abrams et al., 2010; Tachikawa et al., 2011), AW3D (ALOS) (Tadono et al., 2016) and TanDEM-X (Wessel, 2018), through applying void-filling and smoothing (e.g. ACE2 (Smith and Berry, 2009; Berry et al., 2010; Berry et al., 2019), Copernicus DEM (Airbus Defence and Space, 2020)), filtering elevation data with spatial vegetation, building and/or applying population data in random forest algorithms or neural networks (MERITDEM (Yamazaki et al., 2017), FABDEM (Hawker et al., 2022), Coastal DEM (Kulp and Strauss, 2018; 2021)) or employing recently-available satellite LiDAR measurements (ICESat-2) (GLL-DTM (Vernimmen et al., 2020; Vernimmen and Hooijer, 2023); DeltaDTM (Pronk et al., 2024). These recent DEMs constitute the newest generation with improved vertical accuracy, specifically targeting applications in coastal lowland contexts, with the FathomDEM (Uhe et al., 2025), created using advanced postprocessing of the Copernicus DEM, as the youngest sibling.

The majority of those DEMs is provided with vertical reference to ellipsoid (e.g. WGS84) or a global geoid (e.g. EGM96, EGM2008), the latter often considered to reflect sea level, thus providing elevation information at global scale with respect to sea level. However, the accuracy of these global geoids to represent the actual local sea-level height varies a lot and is dependent on the amount and accuracy of input data used when generated. Offsets with true local sea-level height in several regions worldwide can be more than 1 metre, a bias which is very often not corrected for in impact assessments using global DEMs (Seeger and Minderhoud, in review). Consequently, in these data-sparse regions, local sea level may differ up to more than a metre from the global geoid (e.g., Üstün et al., 2016; Minderhoud et al., 2019a; Seeger et al., 2023; Fusami et al., 2023), thereby introducing systematic errors into SLR impact assessments conducted based on global elevation data whose vertical reference was not properly corrected from geoid/ellipsoid to sea level (Seeger and Minderhoud, in review). Finally, the actuality of elevation data, i.e. referring back to the time of data acquisition, impacts the quality of coastal impact assessments. Especially in rapidly subsiding coastal lowlands such as river deltas, DEMs may become quickly outdated, as these landscapes can experience several centimetres to even decimetres subsidence per year (Minderhoud et al., 2020a; Dörr et al., 2024; Copernicus EMSN091, 2021; Ohenhen et al., 2025). In such areas, using for example the SRTM DEM,

originally acquired in February 2000, or any of its post-processed versions in a heavily subsiding environment results in substantial misjudgements of actual elevation, and this limitation is hardly considered in the majority of coastal impact assessments based on global DEMs.

While several studies have addressed DEM accuracy by comparing different DEMs and investigate their performance in terms of fluvial flood inundation (e.g., Schumann et al., 2008; Cook and Merwade, 2009; Hawker et al., 2018a; Azizian and Brocca, 2019; Xu et al., 2021), only a few focused on the impact of DEM selection on (relative) SLR impact (Minderhoud et al., 2019a; Almar et al., 2021; Seeger et al., 2023; Hauser et al., 2023; Vernimmen and Hooijer, 2023). So far, only Minderhoud et al. (2019a) tentatively attributed the errors associated with a DEM in the Mekong Delta to DEM accuracy and the lack of datum conversion to local sea level. However, due to information paucity on local vertical datums, this was done through a basic transformation, i.e. by lowering the global MERITDEM to equalise the mean elevation of a local DEM (Topo DEM) with sea level datum alignment, rather than systematically converting the vertical reference system from the EGM96 geoid to local sea level as indicated by tide gauge data (i.e. Hon Dau tide gauge). Although tide gauges provide highly local information on sea level, their usage is only recommended if they provide a sufficiently long, continuous and up-to-date monitoring period for small study sites or regions without any significant sea-level variations along the coast (Wöppelmann and Pirazzoli, 2005). Also the absence of any documentation about the position of a tide gauge with respect to a certain geoid/ellipsoid may hamper the proper alignment of a geoid- or ellipsoid-referenced DEM to local sea level. In their DEM accuracy and (relative) SLR impact assessment for the Ayeyarwady Delta (Myanmar), Seeger et al. (2023) employed an open-data vertical datum conversion approach that – in the absence of any suitable tide gauge information – allows for the proper conversion of global DEMs to actual, continuous local mean sea level (MSL) along the Myanmar coast by applying latest, freely available satellite-altimetry-derived mean dynamic topography (MDT). This workflow also includes the beforehand required correction of geoid offset between the different vertical reference systems used by elevation and sea-level datasets and thus improves previous datum conversion workflows that lack this relevant processing step (e.g. Muis et al., 2017; Vernimmen et al., 2020; Vernimmen and Hooijer, 2023).

In this study, we investigate land elevation datasets and their performance in data-sparse coastal lowlands, showing a globally applicable approach to quantify and attribute uncertainties in global DEMs to sources such as inaccuracy, vertical datum offset and actuality, which matters

in terms of relative SLR impact. We highlight the applicability of this approach by revisiting land elevation in the Vietnamese Mekong Delta where Minderhoud et al. (2019a) uncovered the delta's true elevation to be on average only ~0.8 m above local sea level whereas previous assessments using global DEMs (e.g. SRTM and MERITDEM) assumed the average elevation of the delta to be considerably higher (i.e. 2.6 m and 3.3 m above sea level, respectively). The previous overestimations stemmed from a combined effect of vertical datum offset, DEM data inaccuracy, and DEM actuality, however the individual contribution of each uncertainty was not quantified (Minderhoud et al., 2019a), which we will advance upon in this study. Firstly, we update the local Topo DEM of Minderhoud et al. (2019b) (hereafter referred to as Topo DEM v1) to actual, continuous local MSL by applying an updated vertical datum conversion from Seeger et al. (2023) (see also Seeger and Minderhoud, in review) (hereafter referred to as Topo DEM v2; Figure 4.12). Secondly, we extend the spatial coverage of Topo DEM v1 northward by including also Ho Chi Minh City, and neighbouring provinces. Thirdly, we extend the DEM accuracy assessment to evaluate the performance of in total 11 high-resolution, global DEMs, thereby ensuring to include latest available coastal DEMs such as DeltaDTM while also reassessing those DEMs that Minderhoud et al. (2019a) investigated in their study (i.e. SRTM and MERITDEM). Furthermore, we investigate the potential impacts of absent and incomplete, incorrect datum conversion, e.g. by including the GLL-DTM v2 referenced to (outdated) MDT as provided by Vernimmen and Hooijer (2023), using the approach of this study (see also Seeger and Minderhoud, in review). We also consider different versions of recent DEMs and integrate both DeltaDTM v1 and v1.1 as we assume the inclusion of elevations up to 30 m in v1.1 to result in (slight) differences in DEM performance in the flat, low-lying Mekong Delta (see also Pronk et al., 2024). To enable 1:1 comparison to findings from Minderhoud et al. (2019a), we focus on results obtained for the Vietnamese Mekong Delta in the main text while providing also the statistics for the extended area of interest in the supplementary material. Based on this thorough assessment, integrating the DEMs in their original vertical reference and converted to the same vertical datum, our study not only allows to extend and detail previous studies on the Mekong Delta's elevation but also to attribute and quantify the sources causing uncertainties in the global DEMs to adequately represent the delta's local elevation. Therewith, we showcase the considerations to be made when handling elevation models in data-sparse local to regional contexts and derive the best compromise of high accuracy and resolution data recommended for further studies on the Mekong Delta such as sea-level rise impact assessments and flood modelling research.

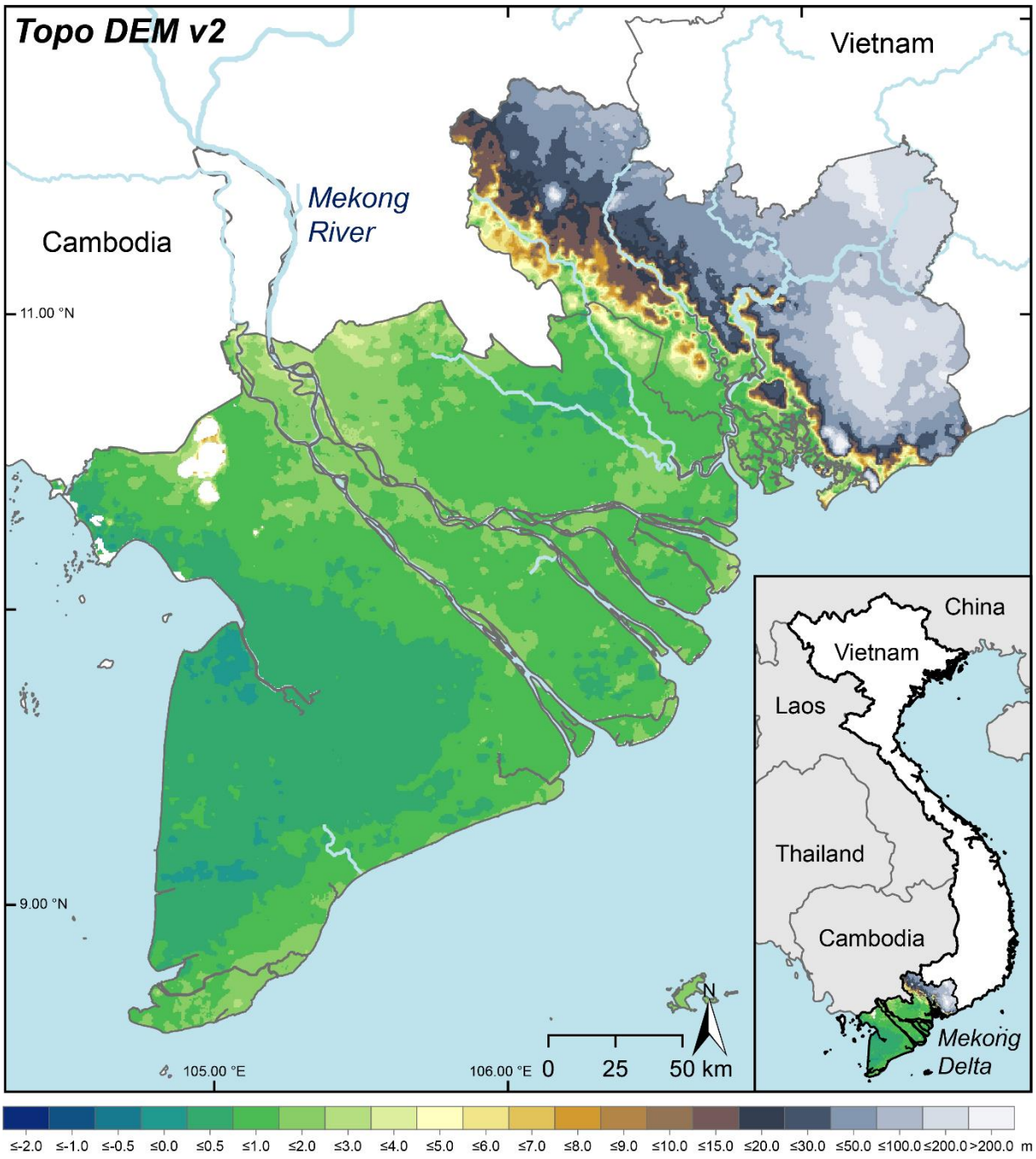


***Figure 4.12** | Local topographical elevation model of the Vietnamese Mekong Delta, updated from Minderhoud et al. (2019a) by referencing to actual local, continuous mean sea level indicated by mean dynamic topography (Jousset et al., 2023).*

4.3.2 Methods

4.3.2.1 Processing of local elevation data: Generation of Topo DEM v2

Topo DEM v2 was processed based on local point elevation measurements throughout the Vietnamese Mekong Delta and its adjacent provinces. These ground measurements were performed as part of the field work conducted for topographic map generation from 2001 to

2003 and are referenced to MSL defined by Hon Dau tide gauge, which is located ca. 1400 km north of the study area (Vu et al., 2020). To transpose the geodetic heights to MSL as defined by latest available MDT (1993–2021; Jousset et al. 2023), they were first adjusted by SLR that occurred at Hon Dau since datum establishment which is MSL over 1950 to 2005 (Vu et al., 2020; 2021). Consequently, MSL for MDT (Jousset et al., 2023) dates around April 2007 while it is 1992 for Hon Dau datum. Tide gauge information of Hon Dau obtained from the Permanent Sea Level Stations repository indicates 1.8 mm/yr of SLR and that sea level has risen by 0.027 m between 1992 (i.e. year for MSL of Hon Dau datum) and 2007 (i.e. year for MSL of MDT time period) (PSMSL, 2025a). By subtracting this amount from the elevation points transpose them to actual MSL at Hon Dau (Figure 4.13). We assume that this determined actual MSL equalises actual MSL as given by MDT (Jousset et al., 2023). However, in order to transpose the local elevation data to continuous MSL along the coast of the Mekong Delta, the offset between Hon Dau MSL and GOCO06s geoid has to be determined first. Geoid information in the form of height anomaly to the WGS84 ellipsoid was obtained from the openly accessible calculation service of the International Centre for Global Earth Models (ICGEM) (Ince et al., 2019) and handled following Seeger and Minderhoud (in review). Given that the quality of satellite altimetry measurements along the coast may be susceptible to land contamination and limitations due to geophysical and environmental corrections (Vignudelli et al., 2011; Vignudelli et al., 2019; Birol et al., 2025), we do not apply an individual MDT value but apply a radius of 100 km and add the average offset of 1.173 m. Consequently, all elevation points are referenced to the GOCO06s geoid. Finally, they were converted to continuous local MSL by subtracting MDT (Jousset et al., 2023) and following the approach of Seeger et al. (2023) and Seeger and Minderhoud (in review). To avoid introducing artefacts due to the differential spatial resolution of MDT and elevation data and to enable datum conversion to MDT not only for the most coastal point elevations but also inland, we resampled the MDT dataset to a resolution of 90 m using bilinear resampling and extrapolated the data up to 500 km inland using Inverse Distance Weighting and applying a smoothing factor of 0.5. The distance threshold was chosen to provide the best compromise in covering vast coastal lowlands (thereby also including the largest delta in the world, i.e. the Ganges-Brahmaputra-Meghna Delta), while also keeping sufficient quality in face of decreasing extrapolation performance with increasing distance. The resampled and extrapolated MDT dataset was subtracted from the pre-processed elevation measurements and therewith concluded the datum conversion process to actual, continuous local MSL along the Mekong Delta coast.

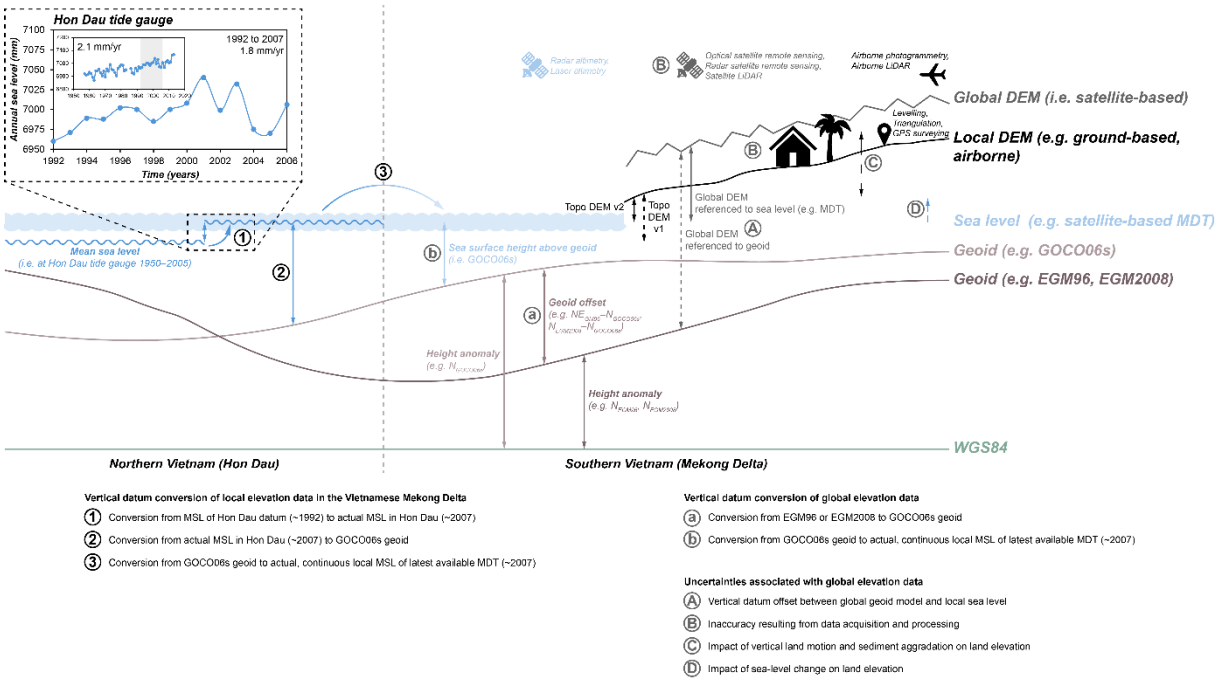


Figure 4.13 *| Vertical datums of elevation and sea-level datasets used for the example of the Mekong Delta together with steps of datum conversion for local (1–3) and global elevation data (a–b) and sources of uncertainty associated with global elevation data (A–E).*
To transpose local geodetic heights from mean sea level (MSL) of Hon Dau datum, which is MSL over 1950 to 2005 (Vu et al., 2020; 2021), to actual, continuous local MSL as defined by latest available mean dynamic topography (MDT) (1993–2021; Jousset et al. 2023), sea-level rise at Hon Dau tide gauge between 1992 (i.e. year for MSL of Hon Dau datum) and 2007 (i.e. year for MSL of MDT time period) had to be considered (step 1) (PSMSL, 2025a). Subsequent steps of converting the local geodetic heights to MDT included the determination of offset to the global GOCO06s geoid (step 2) and subtraction of MDT data (step 3). To transpose global digital elevation models (DEMs) from global geoid models such as EGM96 or EGM2008 to actual, continuous local MSL as defined by MDT, they were first converted to GOCO06s (step a) and then corrected to MDT (step b). Arrows indicate the relations between vertical reference systems that are relevant to transpose elevation and sea-level datasets (solid and short-dashed lines). This figure also illustrates the various sources of uncertainty associated with global DEMs in coastal lowlands, which are vertical datum offset (A), inaccuracy (B), and actuality in terms of impacts due to land elevation change (C) and sea-level change (D).

The local elevation data was interpolated into a DEM based on Empirical Bayesian Kriging with empirical transformation and exponential modelling, which has revealed the most accurate results in former interpolation algorithm tests by Minderhoud et al. (2019a). The interpolation was performed using the Geostatistical Wizard in the ArcGIS Pro Analysis 3.1.3 environment. For the Mekong Delta, we only included elevations ≤10 m into the DEM interpolation in order to ensure high DEM accuracy and minimise the risk of higher elevations from outcrops impacting DEM interpolation in the flat, low-lying surroundings. For the larger study area, i.e. including also Ho Chi Minh City and neighbouring provinces, which are located on higher ground and characterised by hilly terrain, we integrated all local point elevations into DEM generation. As indicated by point density per km^2 (Aguilar et al., 2006), a grid cell resolution of 500 m × 500 m was considered for both interpolations to adequately reflect local elevation.

Subsequently, all elevations >10 m, outcrops and water bodies were masked as in Topo DEM v1 (Minderhoud et al., 2019b) and as indicated by Topo DEM v2 of the larger study area.

For the larger study area, we did not interpolate the provinces outside the delta into a DEM separately but also included the delta as this allows for a smooth interpolation performance at the transition from Ho Chi Minh province towards the delta. However, the resulting DEM shows a lower accuracy in the Mekong Delta than the Topo DEM v2 solely covering the Mekong Delta and including only elevations ≤10 m. Hence, we combine both and replace the elevation of the Mekong Delta in the DEM covering the larger study area (i.e. Topo DEM v2 covering the Mekong Delta plus the surrounding provinces, interpolated by using all elevation points) by the elevation of the Mekong Delta as given by the DEM covering solely the Mekong Delta (i.e. Topo DEM v2 interpolated by using only elevations ≤10 m). However, as this article focuses on the performance of elevation datasets in the Vietnamese Mekong Delta, including comparisons to previous works, we do not address the results for the larger study area in the main text but provide the data and statistics online.

4.3.2.2 Assessment of global elevation model performance

We revisit land elevation in the Vietnamese Mekong Delta by extending the assessment of DEM performance, integrate a lot more elevation datasets than previous works, updating them to latest available MSL, and widening the spatial coverage to include also surrounding provinces. Global DEMs are often used to overcome the limited availability or absence of local elevation data or its coarse spatial resolution impacting the precision of follow-up applications. However, as the low accuracy of global DEMs is often not or only inadequately addressed, we assessed the quality for the majority of open and freely available DEMs in the Vietnamese Mekong Delta and surrounding provinces, quantifying both respective DEM accuracy and the impact of absent or incomplete and incorrect vertical datum conversion.

In total, 11 global DEMs were used for the comparison with Topo DEM v1 and v2, namely SRTM (Farr et al., 2007), ACE2 (Smith and Berry, 2009; Berry et al., 2010; Berry et al., 2019), MERITDEM (Yamazaki et al., 2017), ASTGTM v003 (Abrams et al., 2010; Tachikawa et al., 2011), AW3D30 (Tadono et al., 2016), TanDEM-X 90m (Wessel, 2013), Copernicus DEM (Airbus Defence and Space, 2020), FABDEM v1.0 (Hawker et al., 2022), CoastalDEM v2.1 (Kulp and Strauss, 2018; 2021), GLL-DTM v2 (Vernimmen and Hooijer, 2023), DeltaDTM (Pronk et al., 2024). While both SRTM and MERITDEM have been addressed by studies of Minderhoud et al. (2019a), the quantified uncertainties could only be attributed tentatively.

More recent DEMs such as FABDEM have been applied in the Mekong Delta (e.g. Wood et al., 2024), however without assessing their quality. To quantify also the impacts of incomplete vertical datum conversion and difference in elevation threshold applied in DEM interpolation, we integrate the GLL-DTM v2 referenced to (outdated) MDT as performed by Vernimmen and Hooijer (2023) and using the approach of this study (see also Seeger and Minderhoud, in review) as well as both DeltaDTM v1 and v1.1 (Pronk et al., 2024; Pronk, 2024).

Our quality assessments included both validation with the local Topo DEM v2 to assess and quantify spatial patterns and differences, as well as spot height comparison with elevation at locations of point measurements that fed the local DEM interpolation. Beforehand, the global DEMs were pre-processed. Single DEM tiles covering the area of interest were mosaicked and projected to UTM 48N based on the WGS84 ellipsoid. Subsequently, the vertical datums of the DEMs (i.e. EGM96 and EGM2008) were converted to MSL as defined by MDT (Jousset et al., 2023) and considering to correct for respective geoid offsets (Figure 4.13; Seeger and Minderhoud, in review). Although GLL-DTM v2 is already provided with a reference to MSL (Vernimmen and Hooijer, 2023), we obtained the DEM referenced to EGM96 and could therefore correct for the previously unconsidered geoid offset by applying the same workflow as for the other global DEMs (Figure 4.13). All DEMs, including versions with the vertical reference as provided in the respective data repositories as well as with respect to MSL (this study), were masked by applying their respective water body masks. For ACE2, MERITDEM and CoastalDEM v2.1 and FABDEM v1.0, water bodies were excluded based on masks from the underlying source data, which is SRTM and only in case of FABDEM Copernicus. GLL-DTM v2 and DeltaDTM v1 and v1.1 did not require this processing step as the spatial resolution of GLL-DTM v2 is too coarse to adequately resolve the deltaic river and channel network while in DeltaDTM, these values are already eliminated. Largely negative and therefore likely erroneous elevation values were excluded by applying a threshold of <-7 m above the respective vertical datum (Vernimmen et al., 2020; Vernimmen and Hooijer, 2023; Seeger et al., 2023; Seeger and Minderhoud, in review). As for Topo DEM v 1 and v2, we applied the same outcrop mask to the global DEMs. In addition, all global DEMs were resampled to 500 m × 500 m spatial resolution using bilinear resampling and snapping to Topo DEM. Only for GLL-DTM v2 with a resolution of ~1000 m × ~1000 m, we resampled the local Topo DEM v2 using bilinear resampling to match the same spatial resolution as GLL-DTM v2. All these pre-processing steps enable a proper conduction of DEM comparison in terms of difference mapping with the local Topo DEM v2 and ensure comparability. Only for extracting point

elevations from each DEM and quantifying geoid offset per DEM, the respective spatial resolution of the original DEM was used.

4.3.2.3 Quantification of vertical datum offsets

To quantify the overall discrepancies between geoid models and actual continuous local sea-level height along the coast for the entire Mekong Delta, we used geoid information for EGM96, EGM2008 and GOCO06s obtained in form of height anomaly to the WGS84 ellipsoid from the ICGEM calculation service (Ince et al., 2019). The respective offsets between EGM96 and EGM2008 geoids to GOCO06s were calculated and subsequently subtracted from mean dynamic topography, i.e. MDT – (EGM–GOCO06s). As the processing of the geoid rasters included bilinear resampling to 90 m spatial resolution (Seeger and Minderhoud, in review), all statistics for the respective offsets of EGM96 and EGM2008 to MSL are given at 90 m × 90 m spatial resolution. However, in order to account for an adequate vertical datum conversion of GLL-DTM v2 and compare it to the original GLL-DTM v2 (Vernimmen and Hooijer, 2023), which serves as an example of incomplete vertical datum conversion, we used EGM96 geoid data at 1000 m × 1000 m spatial resolution. Consequently, the resulting statistics are provided at the same resolution.

4.3.3 Results and interpretation

4.3.3.1 Converting vertical datum to actual continuous local sea level

The reliability of elevation data in terms of accuracy (i.e. the absence of uncertainties arising from data acquisition and DEM interpolation) and adequate representation with respect to actual continuous local sea level (i.e. the appropriateness of the vertical reference system to equal actual true sea level experienced along a given coastline) is of utmost importance for flat, low-lying coastal landscapes like the Mekong Delta. Being in parts only a few decimetres elevated above sea level makes elevation-dependent assessments highly sensitive to any uncertainties in the elevation data itself and in the estimation of coastal sea level.

To assess the uncertainties related to vertical reference frames and local sea level for the different assessments and DEMs in the Mekong Delta, we focussed on the most common vertical datums used for global DEMs (i.e. EGM96 and EGM2008), which constitute also the original vertical reference of the DEMs used in previous Mekong Delta assessments. We quantified the differences between EGM96, EGM2008 and local MSL, respectively, and determined a mean geoid offset of 1.26 m (median: 1.29 m) for EGM96 and 1.17 m (median:

1.17 m) for EGM2008. Similarly, the offset range is lower for EGM2008 and constitutes only 0.84 m to 1.46 m, with the showing less variability (σ = 0.11 m) while it ranges from 0.77 m to 1.65 m for EGM96 and showing larger deviation of 0.24 m (Figure 4.14; Table 4.3). This better performance of EGM2008 is probably related to the increased amount of gravitational field data serving as an input and allowing for an improved performance geoid interpolation in the larger data-sparse region.

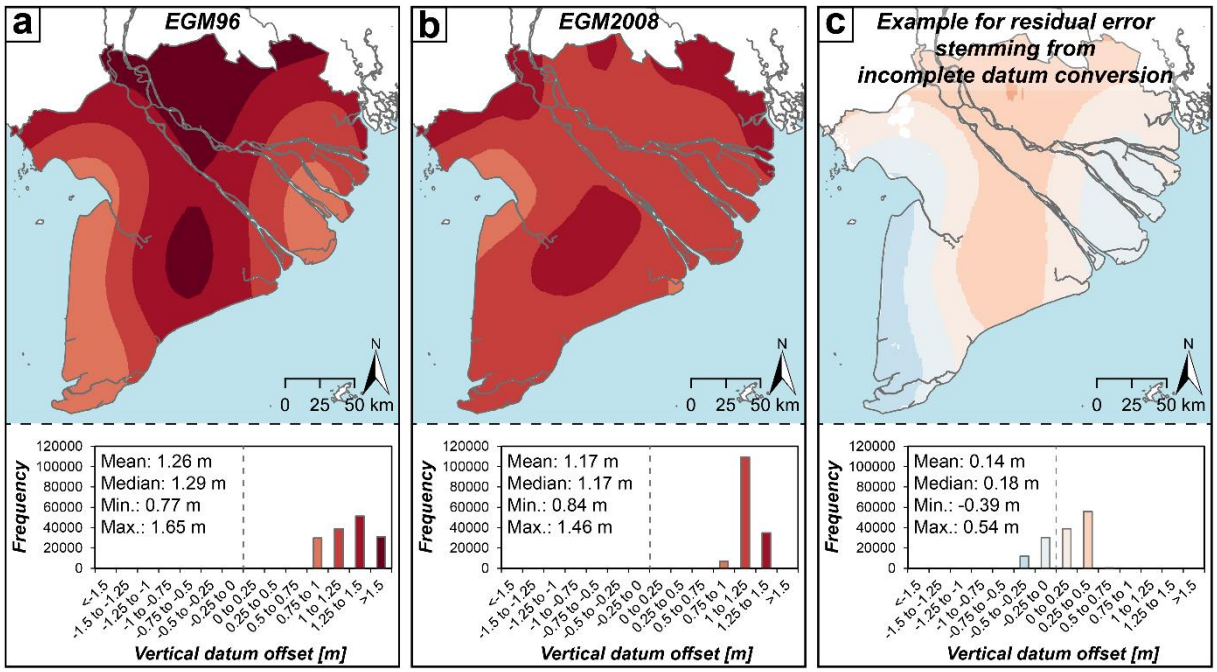


***Figure 4.14** | Offsets between commonly used geoid models (EGM96 (a); EGM2008 (b)) as well as an example of incomplete datum conversion (c) and local mean sea level as indicated by mean dynamic topography of Jousset et al. (2023) in the Vietnamese Mekong Delta.*

***Table 4.3** | Offsets between commonly used geoid models as well as an example of incomplete datum conversion and local mean sea level as indicated by mean dynamic topography of Jousset et al. (2023) in the Vietnamese Mekong Delta.*

Vertical datum	*N*	Mean offset (m)	Median offset (m)	MAE (m)	RMSE (m)	Min. offset (m)	Max. offset (m)	*σ* (m)
EGM96	151369	1.26	1.29	1.26	1.07	0.77	1.65	0.24
EGM2008	151369	1.17	1.17	1.17	1.01	0.84	1.46	0.11
Example of incomplete datum conversion	137689	0.14	0.17	0.25	0.26	-0.39	0.54	0.25

We quantify to what extent the vertical datum offset impacts the reliability of an individual global DEM in the Mekong Delta and compare the respective DEMs both in their original reference and transposed to actual continuous local MSL with Topo DEM v2 as well as its local point elevations. We observe that the respective global DEM errors reduce after converting them to actual continuous local MSL (Table 4.4). Determining the difference between DEM errors before and after datum conversion allows to quantify the impact the vertical datum issue has on the individual DEM reliability. Tendentially, the smaller the overall DEM errors, the

larger the impact of lacking vertical datum conversion is. In a spatially resolved comparison with Topo DEM v2, the discrepancies introduced range from 11.6 % to 147.4 %. Thereby, percentages of more than 100.0 % are obtained in case the uncertainty of the transposed DEM is smaller than the vertical datum offset of the respective original vertical reference system used (Table 4.3) and the difference in DEM error before and after datum conversion exceeds the uncertainty of the transposed DEM (Table 4.4), specifically for the versions of DeltaDTM (i.e. 101.7 % for v1 and 147.4 % for v1.1). Similarly, the impact of vertical datum conversion is also high for other DEMs such as CoastalDEM v2.1 (46.3 %), FABDEM (48.6 %) and MERITDEM (59.7 %), thereby indirectly reflecting the effectiveness of accuracy improvement through post-processing which leads to a relative dominance of the vertical datum issue in the DEM-related uncertainty. Similar patterns, however with slightly different percentages, are documented for the comparison with local point elevations, enabling pointwise DEM uncertainty attribution to vertical datum offset over the entire point elevation range as well as by focusing on particularly low-lying elevations (i.e. ≤10 m above MSL).

Following the most prominent error in handling coastal elevation and sea-level datasets (Seeger and Minderhoud, in review), i.e. the absence of vertical datum conversion from a global geoid or ellipsoid model to actual continuous local sea level, the second most frequent error is partial or incomplete, and therefore incorrect, datum conversion. From the global DEMs used in this study, this error was only encountered with the GLL-DTM for which geoid offset correction between the elevation and sea-level data used was not conducted during the processing of the original GLL-DTM (Vernimmen et al., 2020; Vernimmen and Hooijer, 2023), thereby resulting in artefacts impacting the alignment and consequently applicability of this DEM. Comparing the original GLL-DTM v2 (Vernimmen and Hooijer, 2023) with the GLL-DTM v2 properly converted to actual continuous local MSL reveals only minor average offsets at large regional to global scale, as smaller-scale offsets in both directions average each other out (Seeger and Minderhoud, in review). However at local to smaller-regional scale the variability is large and the impact of the incorrect conversion becomes much more relevant (this study). In the Mekong Delta, the incorrect vertical datum conversion affecting the GLL-DTM v2 resulted in offsets of ca. 0.14 m (mean) and 0.18 m (median), with a standard deviation of 0.25 m and overall ranging from -0.39 m to 0.54 m (Figure 4.14c). RMSE of GLL-DTM v2 improves by ca. 0.12 m (33.3 %) (0.08 m (17.6 %) in comparison with local spot heights) if datum conversion is conducted completely and correctly. Consequently, errors made in vertical datum conversion account for 33.3 % (17.6 % in comparison with local spot height) of the DEM's uncertainty (Table 4.4).

With a higher spatial resolution of GLL-DTM, however, we would expect even much greater discrepancies and effects on the quality of the DEM attributable to improper handling of the elevation and sea-level data.

4.3.3.2 Performance of digital elevation models in the Vietnamese Mekong Delta

4.3.3.2.1 Revisiting local elevation data in the Vietnamese Mekong Delta

We updated the existing Topo DEM v1 (Minderhoud et al., 2019b) by referencing the data to actual, continuous local MSL (Topo DEM v2) which enables for an up-to-date assessment of land elevation in the Vietnamese Mekong Delta. For the entire study area, including the Vietnamese part of the Mekong Delta and northern provinces, the interpolation of Topo DEM v2 is based on a spatial interpolation of point elevations (30,696 in total) from topographical maps. The exclusion of elevations ≥10 m reduced the source dataset to 22,376 point elevations, however still allowing for a point density in the delta that justifies keeping a spatial resolution of 500 m × 500 m. Since we do not have any further independent local elevation data that could be used to validate the interpolated Topo DEM, we assessed its accuracy based on comparison with the local point elevations (i.e. ≤10 m) and determined an overall accuracy of 0.26 m root mean square error (RMSE) for Topo DEM v2 and Topo DEM v1, respectively (Tables E1 and E2 in Appendix E). Based on visual impression, the overall reflection of land surface height changes only slightly (Figures 4.12 and 4.15). The frequency of lower elevations and thus the spatial extent of lowly elevated areas increased. This becomes particularly evident in the Ca Mau peninsula, reflecting more pronounced sea-level variations in this part of the sea (especially in Rach Gia Bay) compared to Hon Dau in northern Vietnam result in higher MSL/lower elevation above MSL. While in comparison the maximum and minimum elevations increased and decreased for Topo DEM v2, the average elevation of the Mekong Delta is updated to 0.77 m (mean) and 0.72 m (median) compared to 0.80 m (mean) and 0.74 m (median) as previously indicated by Topo DEM v1, resulting in an average height residual of 4–5 cm (Figure 4.16). The fact that this amount equals annual sinking rates of land subsidence hotspots in the Mekong Delta (Minderhoud et al., 2020a; Dörr et al., 2024) highlights the enormous sensitivity of the flat, low-lying and sinking landscape to any error and uncertainty in the elevation data, even if high-accuracy local elevation data is used. Consequently, if properly conducted, converting the vertical datum from MSL indicated by a single tide gauge (and established several years ago) to actual, continuous sea-surface height along the deltaic coast makes the characterisation of local elevation with respect to sea level more precise as potential

sea-level variations along the ca. 2000 km long Vietnamese coastline can be accounted for. In the Mekong Delta, this is a crucial step to further narrow down existing uncertainties in the assessment of relative SLR.

4.3.3.2.2 Which one is the best? – On the local validation of global satellite-based digital elevation models

Disentangling DEM uncertainty into DEM-specific accuracy and vertical referencing to actual (continuous) local sea level is crucial to understand the suitability and therefore reliability and applicability of a DEM in a given coastal study area for any coastal hazard or impact assessment. With all elevation data (both DEMs and local point elevations) in the same vertical reference frame, i.e. MSL according to MDT (Jousset et al., 2023), the impact of respective vertical datum offset on the DEMs' quality assessment is excluded. Hence, we can characterise and compare their performance and accuracy against the background of their generation (i.e. including data acquisition, DEM interpolation and further processing).

Visual inspection of the DEMs available for the Mekong Delta reveals the huge differences in their capability to correctly reflect the delta's flat, low-lying terrain (Figure 4.15). Rather, artefacts like stripes from sensing are dominating, especially in SRTM, ASTGTM v003 and AW3D30, and are also preserved in post-processed DEMs such as ACE2, MERITDEM and CoastalDEM v2.1, reflecting that the application of smoothing filters and correction algorithms did not perform well in this coastal lowland (Figure 4.15). Consequently, the elevation frequency distributions of those DEMs show an almost bimodal shape and are characterised by one mode in the range of 1 m to 2 m (i.e. reflecting the delta's average elevation) and a second, minor one at the lower end of the frequency distribution with most values in classes -1 m to -2 m and <-2 m (i.e. including erroneous values resulting from the DEM's artefacts) (Figure 4.15). Stripes related to the SRTM DEM are largely hidden in MERITDEM and likely do not become visible in its elevation frequency distribution as related values are in the same range as the indicated delta elevation. While average elevations of SRTM and MERITDEM prior to vertical datum conversion are corresponding with values determined by Minderhoud et al. (2019a) (only for SRTM, mean delta elevation is ~0.3 m lower, likely resulting from slightly different pre-processing performance), they are 0.45 m and 1.06 m lower after transposing them to MSL, respectively (Figure 4.15; Table 4.4). ASTGTM v003 varies in that from SRTM-based DEMs and AW3D30 as it indicates the highest elevations throughout the entire array of datasets. In contrast, visual comparison of TanDEM-X 90m and its post-processed versions such as Copernicus DEM and FABDEM reveal a similar representation of the delta terrain, which is

also in line with the local DEM, however, indicating higher mean elevations. Developed for improving global DEM performance in coastal lowlands, the global coastal DEMs of CoastalDEM v2.1, GLL-DTM v2, and DeltaDTM v1 and v1.1 show an overall better representation of the Mekong Delta's elevation, both in terms of approaching average elevation and elevation frequency distribution as well as in lower error statistics (Figure 4.15; Table 4.4).

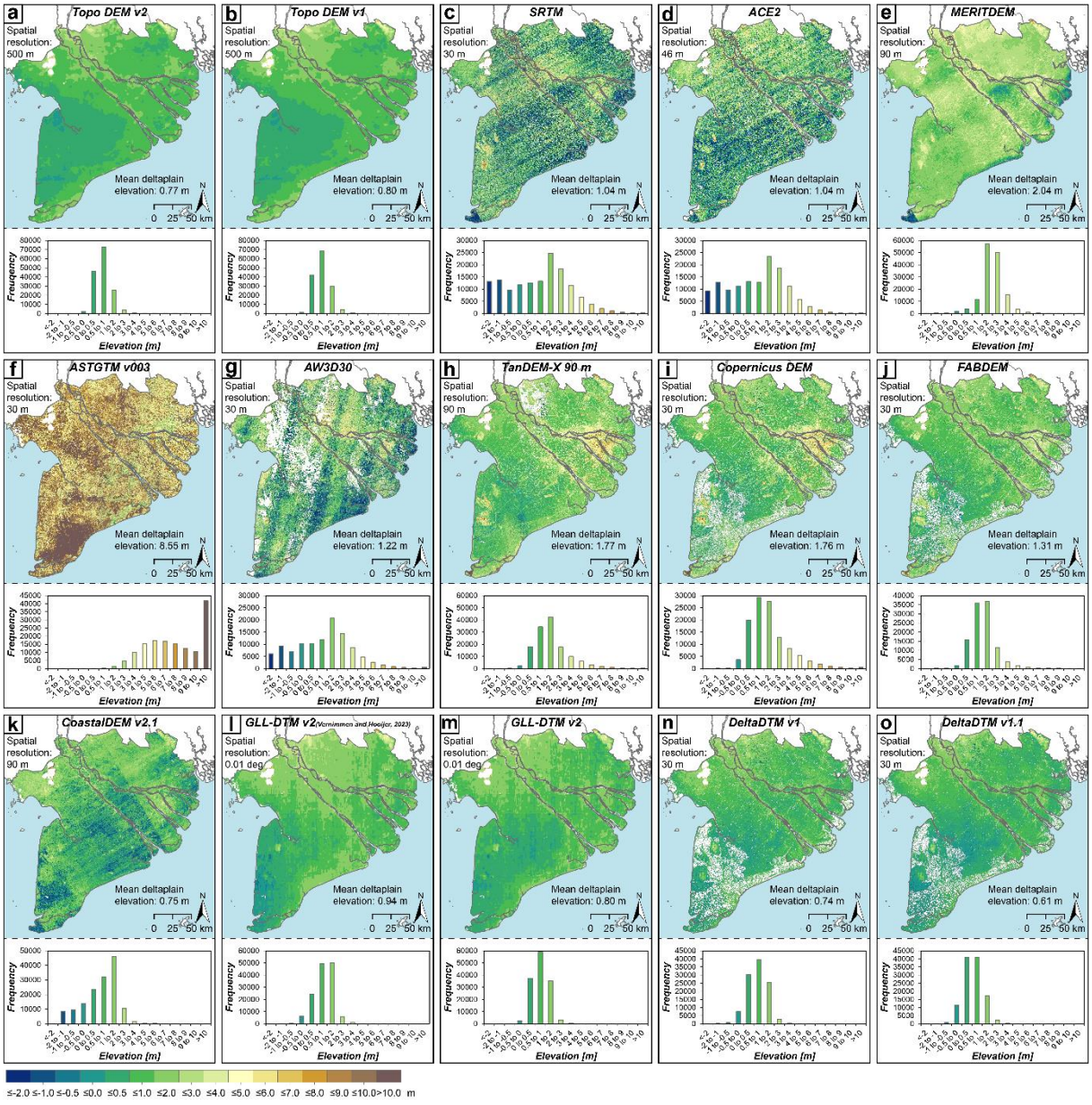


***Figure 4.15** | Digital elevation models included in this study, all referenced to actual, local continuous mean sea level as indicated by mean dynamic topography (Jousset et al., 2023).*

All of these coastal DEMs have been trained on or processed with high-accuracy IceSAT-2 satellite LidAR. However, CoastalDEM v2.1 still suffers from underlying SRTM artefacts (which are transferred via NASADEM that was used as source DEM for generating CoastalDEM v2.1) although it reflects the delta's average elevation well. Consequently,

indicated elevations are characterised by a left-skewed frequency distribution and comparably high standard deviation which is twice as high as for other coastal DEMs (Table 4.4). Both GLL-DTM v2 and DeltaDTM yield a more accurate representation of the delta's terrain. Especially GLL-DTM v2 (converted to MSL by this study) and DeltaDTM v1 reveal the best results, with mean errors less than 0.10 m and RMSE of 0.35 m and 0.49 m, respectively (Table 4.4).

Table 4.4 *| Performance of local and global DEMs in the Vietnamese Mekong Delta validated by the local Topo DEM v2 and DEM-specific vertical datum offsets quantified as differences in RMSE and discrepancies from RMSE of DEMs referenced to mean dynamic topography (MDT).*
N – number of grid cells in the study area, with no-data values excluded for each DEM, respectively; Mean DEM – mean DEM elevation in the study area; Median DEM – median DEM elevation in the study area; Min. DEM – minimum DEM elevation in the study area; Max. DEM – maximum DEM elevation in the study area; σ DEM – standard deviation of DEM elevation in the study area; HR – height residual; MAE – mean absolute error; RMSE – root mean square error.

DEM	*N*	Mean DEM (m)	Median DEM (m)	Min. DEM (m)	Max. DEM (m)	*σ* DEM (m)	Max. negative HR (m)	Max. positive HR (m)	Mean error (m)	MAE (m)	Median error (m)	RMSE (m)	Difference in RMSE (m)	Discrepancy (%)
Topo DEM v2	152028	0.77	0.72	-0.37	8.97	0.57								
Topo DEM v1	147582	0.80	0.74	-0.52	6.98	0.54	-7.03	1.62	0.04	0.06	0.05	0.10		
$SRTM_{MDT}$	144113	1.04	0.91	-6.89	143.06	2.56	-10.12	142.12	0.29	1.87	0.17	2.55		
$SRTM_{EGM96}$	145672	2.27	2.00	-7.00	145.00	2.63	-9.56	144.06	1.52	2.26	1.40	3.00	0.45	17.6
$ACE2_{MDT}$	133927	1.04	0.93	-6.99	140.23	2.32	-8.90	139.29	0.29	1.65	0.17	2.26		
$ACE2_{EGM96}$	134211	2.30	2.20	-7.00	141.70	2.38	-10.02	140.76	1.55	2.09	1.55	2.76	0.50	22.0
$MERITDEM_{MDT}$	146263	2.04	1.96	-6.65	139.47	1.33	-7.89	138.53	1.29	1.40	1.28	1.80		
$MERITDEM_{EGM96}$	146269	3.29	3.26	-6.46	140.94	1.40	-7.44	140.00	2.54	2.57	2.56	2.86	1.06	58.7
ASTGTM $v003_{MDT}$	145981	8.55	7.44	-1.43	152.33	4.99	-3.88	151.39	7.80	7.80	6.68	9.30		
ASTGTM $v003_{EGM96}$	145981	9.80	9.00	0.00	154.00	5.00	-2.60	153.06	9.05	9.05	7.98	10.38	1.08	11.6
$AW3D30_{MDT}$	109349	1.22	1.00	-6.96	111.90	2.46	-8.79	111.36	0.46	1.72	0.29	2.46		
$AW3D30_{EGM96}$	110184	2.46	2.00	-7.00	113.00	2.54	-9.64	112.47	1.70	2.22	1.52	3.00	0.54	22.1
$TanDEM\text{-}X_{MDT}$	138263	1.77	1.24	-6.81	163.51	1.85	-7.81	162.57	1.05	1.15	0.48	2.05		
$TanDEM\text{-}X_{EGM96}$	138313	3.02	2.52	-6.51	164.98	1.86	-7.66	164.04	2.29	2.30	1.75	2.88	0.83	40.6
Copernicus DEM_{MDT}	114885	1.76	1.09	-5.35	138.51	2.03	-6.40	137.57	0.96	1.18	0.24	2.19		
Copernicus $DEM_{EGM2008}$	114887	2.94	2.29	-4.27	139.93	2.02	-5.23	138.99	2.14	2.15	1.42	2.90	0.71	32.4
$FABDEM_{MDT}$	108892	1.31	1.01	-4.09	139.50	1.41	-5.00	138.55	0.50	0.66	0.21	1.43		
$FABDEM_{EGM2008}$	113820	2.48	2.21	-2.55	144.54	1.38	-3.50	143.60	1.68	1.69	1.40	2.12	0.69	48.6
CoastalDEM $v2.1_{MDT}$	145917	0.75	0.77	-5.50	159.20	1.26	-6.80	158.26	-0.00	0.77	0.03	1.20		
CoastalDEM $v2.1_{EGM96}$	146009	2.01	2.01	-4.05	159.96	1.32	-5.35	159.02	1.26	1.38	1.32	1.76	0.56	46.3
GLL-DTM $v2_{MDT}$ (this study)	137689	0.80	0.76	-1.48	8.09	0.51	-5.41	6.86	0.08	0.26	0.08	0.35		
GLL-DTM $v2_{MDT}$ (original)	138749	0.94	0.89	-1.67	8.15	0.64	-5.37	6.93	0.22	0.37	0.26	0.47	0.12	33.3
DeltaDTM $v1_{MDT}$	107553	0.74	0.67	-3.21	7.87	0.63	-5.13	6.56	-0.07	0.35	-0.07	0.49		
DeltaDTM $v1_{EGM2008}$	114856	1.91	1.83	-1.88	9.56	0.63	-3.98	7.98	1.11	1.13	1.11	1.21	0.72	147.4
DeltaDTM $v1.1_{MDT}$	114585	0.61	0.53	-6.08	28.70	0.69	-7.05	27.64	-0.20	0.33	-0.19	0.55		
DeltaDTM $v1.1_{EGM2008}$	114587	1.78	1.69	-4.88	30.00	0.70	-5.84	29.06	0.98	1.00	0.98	1.11	0.56	101.7

By subtracting Topo DEM v2 from each of the other DEMs referenced to MSL, we quantify all differences between local and global elevation datasets. This not only substantiates the inappropriateness of SRTM, ACE2 and AW3D30 to be applied in the Mekong Delta as

inaccuracies are in the range of several metres and are particularly evident from -2.5 m to -1 m and from 1 m to 2.5 m (Figure 4.16). However, given their bimodal character, they do not show up in any average height residual statistics but only standard deviations and RMSE in the range of ≥2 m (Figure 4.16; Table 4.4). Aside from ASTGTM v003, whose elevation is in many parts of the Mekong Delta more than 2.5 m higher than indicated by Topo DEM v2 (with inaccuracies of more than 10 m particularly in the southwestern Ca Mau peninsula), also MERITDEM represents the Mekong Delta on average 1.29 m higher (Figure 4.16; Table 4.4). This is surprising as MERITDEM was created based on SRTM and involved a correction for vegetation heights (Yamazaki et al., 2017). Thus, we would have expected similar or lower offsets to Topo DEM v2. However, it rather seems that vegetation was not effectively eliminated while artefact correction and smoothing was applied. Also the TanDEM-X based elevation models reveal higher elevations than Topo DEM v2. Seeing the sequence of DEM generations from TanDEM-X 90 m to Copernicus DEM to FABDEM, involving corrections such as void filling and vegetation removals, their comparison with local elevation data reveals their improvement in accuracy, particularly in terms of lowered mean errors and average height residuals and especially following vegetation correction in FABDEM (Figure 4.16; Table 4.4). While difference mapping for GLL-DTM v2 (Figure 4.16k and l) resolves how inadequate consideration of geoid offset in vertical datum conversion impacted also coastal inland elevation, DeltaDTM as the most recent coastal DEM, generated by integrating IceSAT-2 satellite LiDAR into Copernicus DEM, reveals the overall best performance, benefiting from some of the lowest inaccuracies, height residuals and standard deviations while yielding high resolution of 30 m × 30 m. To further investigate the performance of DeltaDTM, and see whether the inclusion of elevations up to 30 m in v1.1 has an impact of its performance in the low-lying Mekong Delta, we included both available v1 and v1.1. We find that although both versions perform very similar, they show slight differences as DeltaDTM v1 outperforms v1.1 in overall lower height residuals and slightly higher accuracy (RMSE = 0.49 m (v1), RMSE = 0.55 m (v1.1). However, since DeltaDTM v1.1 included higher elevations, we would expect its height residuals to be similar to or higher than for v1, i.e. indicating elevations also similar to or higher than Topo DEM v2. Instead, DeltaDTM v1.1 is on average 0.20 m lower than Topo DEM v2 and 0.13 m lower than DeltaDTM v1which are considerably larger differences than the minor differences in the range of ~2 cm with the global-scale validation comparison of Pronk (2024).

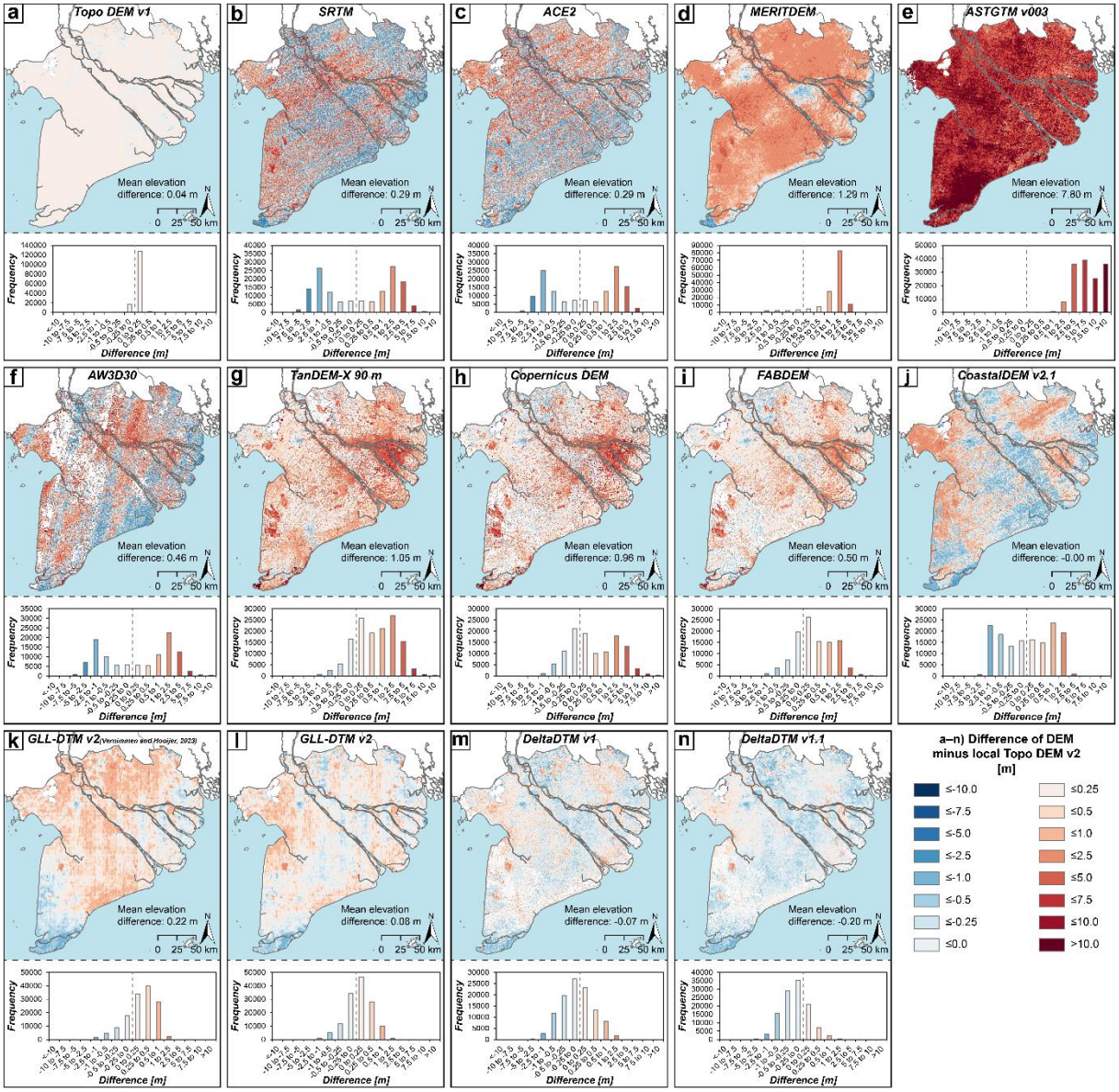


***Figure 4.16** | Height residuals of DEMs referenced to mean sea level compared to Topo DEM v2.*

4.3.4 Discussion, conclusions and outlook

The previous elevation assessment of the Vietnamese Mekong Delta by Minderhoud et al. (2019a) set a benchmark by unravelling the delta's elevation relative to local sea level and its exposure to relative SLR, which had been grossly underestimated in previous SLR impact assessments based on global DEMs, as they overestimated the delta's elevation to sea level by several metres. In addition, this work sensitised the coastal research community for proper converting the vertical datum to local sea level by conducting a tentative vertical datum conversion for one of the two assessed global DEMs. In the recent past years there have been considerable advancements in scientific research on data-sparse coastal lowlands for regions in

the world where high-quality data (e.g. LiDAR) is limited or unavailable. The recent advancements range from the publication of newly processed DEMs specifically targeting global coastal lowlands (Vernimmen et al., 2020; Kulp and Strauss, 2021; Vernimmen and Hooijer, 2023; Pronk et al., 2024), raising awareness on considerations to be made about elevation assessment uncertainty due to DEM inaccuracy and vertical datum offsets (e.g. Gesch, 2018; Seeger et al., 2024) and introducing approaches and showcases how to handle elevation data properly in data-sparse coastal lowlands (Kulp and Strauss, 2016; Seeger et al., 2023; Avornyo et al., 2024). Building on these new DEMs and insights we revisited the land elevation in the Vietnamese Mekong Delta, which provides an excellent test-case being a lowly-elevated coastal lowland with local validation data (i.e. Topo DEM) available, thereby updating and extending the previous elevation assessment of the delta (Minderhoud et al., 2019a).

We took the majority of currently available global DEMs, including the older, most commonly used DEMs and the latest generation of DEMs specifically designed to target coastal lowlands. We compared them against a vertically high-resolution DEM from local origin (i.e. Topo DEM v2), with all DEMs properly referenced to a common vertical datum (Seeger and Minderhoud, in review), in our case to actual local continuous MSL (as indicated by MDT (Jousset et al., 2023). In addition, we also compared all DEMs while omitting the necessary vertical datum conversion (i.e. DEMs are kept in their original reference system, which is mostly a global geoid). This is to mimic and evaluate the impacts of the common, erroneous practice present in almost all global coastal impact assessments published in the last 15 years (highlighted in Minderhoud et al., 2019a; Seeger and Minderhoud, in review). This approach not only allowed us to characterise the presently best performing DEMs but also to attribute and quantify the sources causing uncertainties in a global DEM to adequately represent the delta's local elevation (Figure 4.17). Unravelling and quantifying the specific contributions of these different factors to uncertainties of elevation assessments using global DEMs, has, to our knowledge, not been performed before. We deem such an assessment crucial, not only because it reveals which DEMs perform best for a certain area but also as it pinpoints errors in DEM processing steps (e.g. omitting vertical datum conversion) and indicates how much DEM performance (and its applicability) can be improved if certain processing steps are prioritised and properly applied. For example, the RMSE of ACE2 and MERITDEM are very similar if used in the EGM96 geoid as they are provided (Berry et al., 2019; Yamazaki et al., 2017). However, our assessment highlights that vertical datum conversion to MSL in the Mekong Delta is much more effective to improve the results when using the MERITDEM, while for ACE2 still 80 % of the

documented uncertainties is controlled by inaccuracy in the DEM generation process (i.e. related to acquisition and DEM interpolation), meaning that even after proper referencing to sea level, land elevation will be substantially overestimated by several metres (Figure 4.17; Table 4.4). For global DEMs that included accuracy improvements like vegetation removal or integration of terrain data in their processing (e.g., FABDEM, CoastalDEM v2.1, DeltaDTM v1 and v1.1), vertical datum offset and consequently the need for conversion mount up to 30 % to 60 % uncertainty, reflecting it – at least for DeltaDTM – as an either equal or the most critical factor to consider in order to improve DEM performance. As this attribution highly depends on the magnitude of datum offset to local sea level, which varies around the world (Seeger and Minderhoud, in review), as well as local spatial patterns and landscape features impacting the accuracy of DEM processing and post-processing, this attribution does not allow to be simply transferred to other areas and requires a site-specific evaluation following our presented approach.

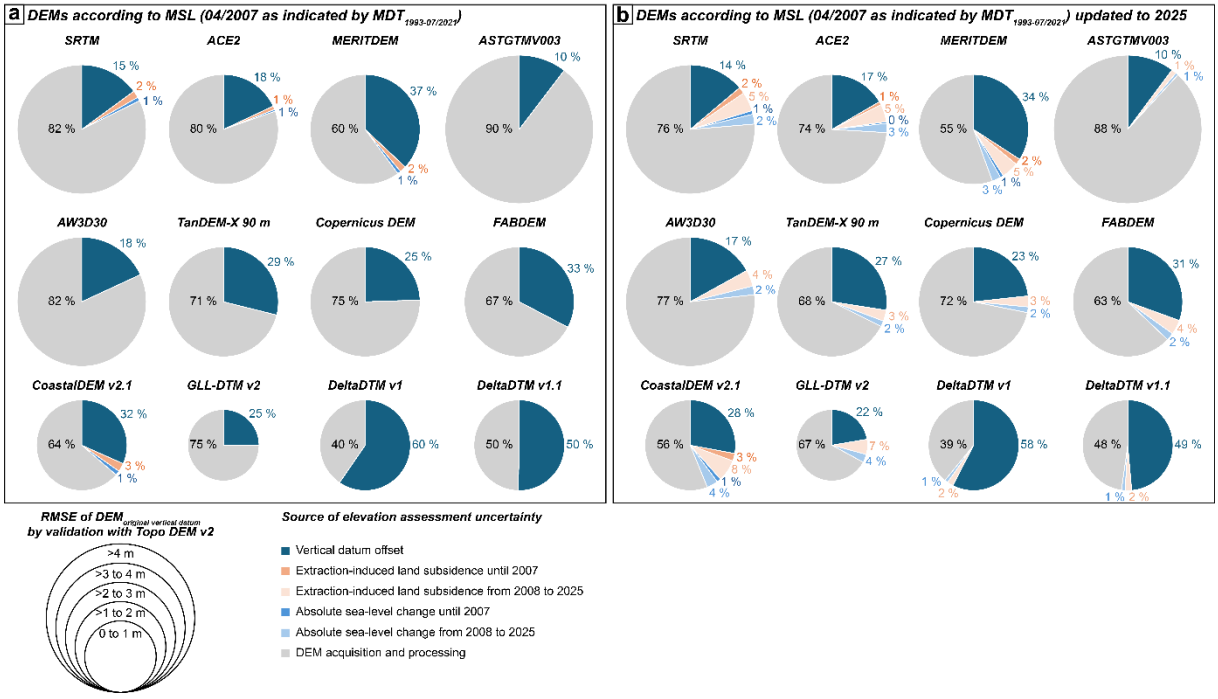


Figure 4.17 *| Quantification and attribution of uncertainties associated with global DEMs in their performance to correctly quantify the elevation of the Vietnamese Mekong Delta.*
Quantifications were conducted relative to root mean square error (RMSE) of DEMs in comparison to Topo DEM v2 based on their original vertical reference. Sources of elevation assessment uncertainty include vertical datum offset, inaccuracy resulting from DEM acquisition and processing, as well as time since DEM generation over which land subsidence and sea-level change have resulted in elevation change. (a) Relative uncertainties for DEMs referenced to mean sea level as indicated by mean dynamic topography (MDT), which provide the local sea level average over the period 1993–07/2021, corresponding to April 2007. (b) Relative uncertainties for DEMs referenced to mean sea level as indicated by mean dynamic topography (MDT), including land subsidence and sea-level rise since April 2007. For these tentative calculations, simulated, non-linear, extraction-induced land subsidence (Minderhoud et al., 2017; Minderhoud et al., 2020b), tide-gauge observations and IPCC-projections of sea-level rise (PSMSL, 2025b; Fox-Kemper et al., 2021; Garner et al., 2021; Garner et al., 2022) were used.

Land elevation is not static but changing over time and the vast majority of coastal lowlands such as river deltas and coastal plains are prone to land subsidence, which may reach several centimetres to locally even decimetres per year (e.g., Erban et al., 2014; Herrera-García et al., 2018; Minderhoud et al., 2018; Ohenhen et al., 2025), together with global SLR resulting in elevated relative SLR (Nicholls et al., 2021). Consequently, the capability of a DEM to adequately represent coastal-deltaic land elevation will change significantly if over years, accumulated subsidence together with SLR exceeds the DEM-inherent uncertainty. Therefore, the actuality of the elevation data used is as crucial as the actuality of sea-level information in order to guarantee up-to-date assessments of coastal hazards and impacts. However, this factor is often overlooked as still a huge number of those assessments applies elevation data more than ten to even 25 years old (e.g., as highlighted in Hawker et al., 2018b; Seeger and Minderhoud, in review). The fact that some of the more recently published DEMs constitute post-processed elevation data such as SRTM, which was acquired in 2000, may cause confusion as users may consider the post-processed DEM to represent more recently acquired elevation data while these DEMs still rely on original, earlier acquired elevation data, leaving the potentials impacts of post-acquisition elevation dynamics unaddressed. We demonstrate the potential impact of outdated elevation on DEM performance using the Mekong Delta and updated the DEMs referenced to continuous local MSL as indicated by MDT (i.e. as of 2007) to MSL 2025. We include both land subsidence and SLR, by using simulated, non-linear extraction-induced land subsidence (Minderhoud et al., 2017; B1 scenario of Minderhoud et al., 2020b) and annual rates of local, delta-average SLR estimated from PSMSL data of Vung Tau tide gauge and IPCC AR6 total rates of sea-level change (PSMSL, 2025b; Fox-Kemper et al., 2021; Garner et al., 2021, Garner et al., 2022; Table E6). For SRTM and its follow-up versions, consideration of extraction-induced land subsidence and absolute SLR since 2000 until MSL of ~2007 already contributes 3–4 % to overall elevation assessment uncertainty, while relative SLR until 2025 increases elevation assessment uncertainty relatively by 9–16 % (Figure 4.17). The impact is less for most recent, TanDEM-X based DEMs (3–6 %) until its dimension approaches that of vertical datum offset and accuracy as GLL-DTM v2 shows a smaller vertical datum offset than DEMs originally referenced to a global geoid and reveals a comparably high accuracy (Figure 4.17; Table 4.4). Only for ASTGTM v003 which suffers from the largest inaccuracies, consideration of land elevation and sea-level change does not result in remarkable performance improvement.

We deem our integration of vertical land motion and sea-level change for the Mekong delta only as a first, preliminary attempt of considering and estimating the effect of elevation dynamics on coastal land elevation datasets. Though we consider the non-linear spatio-temporal behaviour of land subsidence in the Mekong Delta, this assessment only accounts for moderate rates of simulated subsidence induced by groundwater extraction (Minderhoud et al., 2017; Minderhoud et al., 2020b) but does not include contributions from other origins such as natural compaction (Zoccarato et al., 2018; Baldan et al., 2024), other land-use induced shallow processes (Minderhoud et al., 2018), or urban differential compaction (de Wit et al., 2021). The assessment also does not consider the potential contribution of sediment aggradation to elevation gain, whose potential, however, has been shown to be only minor with respect to the current conditions in the delta (Dunn and Minderhoud, 2022). Still, the assessment provides a first demonstration of the entire picture of uncertainties related to elevation data in coastal lowland contexts and how these uncertainties impact the individual DEMs relatively. To further substantiate these quantifications requires to address the limitations mentioned above and consider process- and data-driven spatial variability (Minderhoud et al., 2018; Minderhoud et al., 2020a, 2020b; Figure 4.16). Observational studies reveal that contemporary, total subsidence rates in the Mekong Delta are in places considerably larger than only previously simulated extraction-induced subsidence and delta-wide averages, up to 5–6 cm/yr (Erban et al., 2014; Minderhoud et al., 2020a; Dörr et al., 2024; Ohenhen et al., 2025). Therefore, we expect relative SLR to have a much higher relative impact on elevation assessment uncertainty, especially in case outdated (global) DEMs are used for areas. While some studies handle elevation in the low-lying Mekong Delta more carefully, for example by using the local Topo DEM of Minderhoud et al. (2019a), more recent global DEMs, or addressing vertical datum conversion tentatively (e.g., Eslami et al., 2021; Dang, et al., 2022; Le et al., 2023; Wood et al., 2024), a considerable number of studies still apply outdated and/or inaccurate DEMs that suffer from artefacts (e.g., Dang et al., 2018; Tanaka et al., 2019; Thanh et al., 2020; Wu and Lei, 2020; Chen et al., 2024; Yun et al., 2024), a phenomenon we also observed for coastal hazard and impact assessments in other regions of the world (Seeger and Minderhoud, in review).

With our revisit of land elevation in the Mekong Delta we provide an exemplar showcase of a globally applicable approach to attribute uncertainties in elevation assessment for data-sparse coastal lowlands using global elevation models. Our assessment not only details previous studies on the delta's elevation further, moreover it highlights how to handle coastal elevation and sea-level data properly: (i) by vertically referencing the DEMs to a common actual, local

sea-level datum, and (ii) by conducting a thorough assessment of DEM performance that not only allows for the quantification of errors and elevation assessment uncertainties but also their attribution to DEM inaccuracy, vertical datum offset and, tentatively, non-linear impact of elevation change due to vertical land motion (e.g. extraction-induced land subsidence) and sea-level change affecting DEM actuality. This improved understanding of coastal elevation serves as a starting point to further improve impact assessments of flooding and relative SLR (e.g. Minderhoud et al., 2019a; Wood et al., 2024) and substantiating projections of future elevation in the Mekong Delta (Minderhoud et al., 2020b). With all quantifications of DEM performance and vertical datum offsets based solely on open data and approaches that can be applied in any GIS environment, our demonstrated approach may set a benchmark to initiate similar assessments of DEM performance in other (data-sparse) coastal regions in the world. As elevation forms the basis for any coastal impact assessment, it needs to be handled carefully and with scrutiny, a practice which is currently often lacking in the coastal research community (Seeger and Minderhoud, in review). Similar to sea level, land elevation is not static but dynamic and this should be considered properly in coastal impact assessment, depends on the respective DEM dataset and vertical reference used, as well as the relative SLR and surface elevation change. As new elevation datasets become available, as do vertical reference systems such as geoid models and sea-level datasets, it should be prioritised to provide end users not only with latest available elevation data but also reference them to latest vertical reference systems or sea level, depending on the intended end use (Seeger and Minderhoud, in review). Providing the coastal research community with regular updates of most recent DEMs, already referenced to an actual sea-level datum, such as latest available MDT, will take complex vertical datum conversion steps away from non-specialist end users and thereby reduce overall uncertainties in coastal elevation and elevation-related SLR and other coastal hazard impact assessment.

Data availability statement: The data that support the findings of this study are made available in course of the publication of the scientific article to which this chapter is related.

References

Abrams, M., Bailey, B., Tsu, H., and Hato, M.: The ASTER Global DEM, *Photogramm. Eng. Remote Sensing*, *76*:4, 344–348, 2010.

Aguilar, F. J., Aguilar, M. A., Agüera, F., and Sánchez, J.: The accuracy of grid digital elevation models linearly constructed from scattered sample data, *Int. J. Geogr. Inf. Sci.*, *20*:2, 169–192, https://doi.org/10.1080/13658810500399670, 2006.

Airbus Defence and Space: Copernicus Digital Elevation Model Product Handbook Version 3.0, Airbus, 38 pp., 2020.

Almar, R., Ranasinghe, R., Bergsma, E. W., Diaz, H., Melet, A., Papa, F., Vousdoukas, M., Athanasiou, P., Dada, O., Almeida, L. P., & Kestenare, E. (2021). A global analysis of extreme coastal water levels with implications for potential coastal overtopping. *Nature communications*, *12*(1), 3775. https://doi.org/10.1038/s41467-021-24008-9.

Almar, R., Stieglitz, T., Addo, K. A., Ba, K., Ondoa, G. A., Bergsma, E. W. J., Bonou, F., Dada, O., Angnuureng, D., & Arino, O. (2023). Coastal zone changes in West Africa: Challenges and opportunities for satellite earth observations. *Surveys in Geophysics*, *44*(1), 249–275. https://doi.org/10.1007/s10712-022-09721-4.

Avornyo, S. Y., Minderhoud, P. S. J., Teatini, P., Seeger, K., Hauser, L. T., Woillez, M. N., Jayson-Quashigah, P. N., Mahu, E., Kwame-Biney, M., & Addo, K. A. (2024). The contribution of coastal land subsidence to potential sea-level rise impact in data-sparse settings: The case of Ghana's Volta delta. *Quaternary Science Advances*, *14*, 100175. https://doi.org/10.1016/j.qsa.2024.100175.

Azizian, A., & Brocca, L. (2020). Determining the best remotely sensed DEM for flood inundation mapping in data sparse regions. *International Journal of Remote Sensing*, *41*(5), 1884–1906. https://doi.org/10.1080/01431161.2019.1677968.

Baldan, S., Minderhoud, P. S. J., Xotta, R., Zoccarato, C., & Teatini, P. (2025). Data-driven 3D modelling of long-term Holocene delta evolution and sediment compaction: The Mekong Delta. *Earth Surface Processes and Landforms*, *50*(1), e6046. https://doi.org/10.1002/esp.6046.

Becker, M., Seeger, K., Paszkowski, A., Marcos, M., Almar, R., Bates, P., France-Lanord, C., Hossain, Md S., Khan, J., Karegar, M., Karpytchev, M., Long, N., Minderhoud, P. S. J., Neal, J., Nicholls, R. J., & Syvitski, J. (2024). Coastal flooding in Asian Megadeltas: Recent advances, persistent challenges, and call for actions admidst local and global changes. *Reviews of Geophysics*, *62*(4), e2024RG00846. https://doi.org/10.1029/2024RG000846.

Berry, P. A. M., Smith, R. G., and Benveniste, J.: ACE2: The New Global Digital Elevation Model, in: *Gravity, Geoid and Earth Observation, International Association of Geodesy Symposia 135*, edited by Mertiklas, S.P., Springer, Berlin, Heidelberg, Germany, 231–237, https://doi.org/10.1007/978-3-642-10634-7_30, 2010.

Berry, P. A. M., Smith, R., and Benveniste, J.: Altimeter Corrected Elevations, Version 2 (ACE2) [dataset], Palisades, New York: NASA Socioeconomic Data and Applications Center (SEDAC), https://doi.org/10.7927/H40G3H78, accessed 2022-03-01, 2019.

Birol, F., Bignalet-Cazalet, F., Cancet, M., Daguze, J. A., Fkaier, W., Fouchet, E., Léger, F., Maraldi, C., Niño, F., Pujol, M. I., & Tran, N. (2025). Understanding uncertainties in the satellite altimeter measurement of coastal sea level: insights from a round-robin analysis. *Ocean Science*, *21*(1), 133–150. https://doi.org/10.5194/os-21-133-2025.

Buffington, K. J., Dugger, B. D., Thorne, K. M., & Takekawa, J. Y. (2016). Statistical correction of lidar-derived digital elevation models with multispectral airborne imagery in tidal marshes. *Remote Sensing of Environment*, *186*, 616–625. https://doi.org/10.1016/j.rse.2016.09.020.

Chan, F. K. S., Paszkowski, A., Wang, Z., Lu, X., Mitchell, G., Tran, D. D., Warner, J., Li, J., Chen, Y. D., Li, N., Pal, I., Griffiths, J., Chen, J., Chen, W. Q., & Zhu, Y. G. (2024). Building resilience in Asian mega-deltas. *Nature Reviews Earth & Environment*, *5*(7), 522–537.

Chen, A., Wang, J., Toumi, R., Huang, H., Yang, L., Chen, D., He, B., & Liu, J. (2024). Impact of tropical cyclone precipitation on fluvial discharge in the Lancang–Mekong River Basin. *Geophysical Research Letters*, *52*(8), e2024GL113199. https://doi.org/10.1029/2024GL113199.

Cook, A., & Merwade, V. (2009). Effect of topographic data, geometric configuration and modeling approach on flood inundation mapping. *Journal of Hydrology*, *377*(1-2), 131–142. https://doi.org/10.1016/j.jhydrol.2009.08.015.

Copernicus Emergency Management Service Risk & Recovery Mapping Non-standardised products (FLEX) Lot 1 Final Report (2021). EMSN-091: Assessing changes in subsidence rates in the low Pampanga river basin and Manila area, Philippines. https://mapping.emergency.copernicus.eu/activations/EMSN091/, last access: 26 June 2025.

Dang, T. D., Cochrane, T. A., Arias, M. E., & Tri, V. P. D. (2018). Future hydrological alterations in the Mekong Delta under the impact of water resources development, land subsidence and sea level rise. *Journal of Hydrology: Regional Studies*, *15*, 119–133. https://doi.org/10.1016/j.ejrh.2017.12.002.

Dang, A. T., Reid, M., & Kumar, L. (2022). Assessing potential impacts of sea level rise on mangrove ecosystems in the Mekong Delta, Vietnam. *Regional Environmental Change*, *22*(2), 70. https://doi.org/10.1007/s10113-022-01925-z.

de Wit, K., Lexmond, B. R., Stouthamer, E., Neussner, O., Dörr, N., Schenk, A., & Minderhoud, P. S. J. (2021). Identifying causes of urban differential subsidence in the Vietnamese Mekong Delta by combining InSAR and field observations. *Remote Sensing*, *13*(2), 189. https://doi.org/10.3390/rs13020189.

Dörr, N., Schenk, A., & Hinz, S. (2024). Land subsidence in the Mekong delta derived from advanced persistent scatterer interferometry with an infrastructural reference network. *IEEE Journal of Selected Topics in Applied Earth Observations and Remote Sensing*, *17*, 12077–12091. https://doi.org/10.1109/JSTARS.2024.3420130.

Dunn, F. E., & Minderhoud, P. S. J. (2022). Sedimentation strategies provide effective but limited mitigation of relative sea-level rise in the Mekong delta. *Communications Earth & Environment*, *3*(1), 2. https://doi.org/10.1038/s43247-021-00331-3.

Edmonds, D. A., Caldwell, R. L., Brondizio, E. S., & Siani, S. M. O. (2020). Coastal flooding will disproportionately impact people on river deltas. *Nature Communications*, *11*, 4741. https://doi.org/10.1038/s41467-020-18531-4.

Erban, L. E., Gorelick, S. M., & Zebker, H. A. (2014). Groundwater extraction, land subsidence, and sea-level rise in the Mekong Delta, Vietnam. *Environmental Research Letters*, *9*(8), 084010. https://doi.org/10.1088/1748-9326/9/8/084010.

Ericson, J. P., Vörösmarty, C. J., Dingman, S. L., Ward, L. G., & Meybeck, M. (2006). Effective sea-level rise and deltas: Causes of change and human dimension implications. *Global and Planetary Change*, *50*(1-2), 63–82. https://doi.org/10.1016/j.gloplacha.2005.07.004.

Eslami, S., Hoekstra, P., Kernkamp, H. W. J., Nguyen Trung, N., Do Duc, D., Nguyen Nghia, H., Tran Quang, T., van Dam, A., Darby, S. E., Parsons, D. R., Vasilopoulos, G., Braat, L., & van der Vegt, M. (2021). Dynamics of salt intrusion in the Mekong Delta: results of field observations and integrated coastal–inland modelling. *Earth Surface Dynamics*, *9*(4), 953–976. https://doi.org/10.5194/esurf-9-953-2021.

Farr, T. G., Rosen, P. A., Caro, E., Crippen, R., Duren, R., Hensley, S., Kobrick, M., Paller, M., Rodriguez, E., Roth, L., Seal, D., Shaffer, S., Shimada, J., Umland, J., Werner, M., Oskin, M., Burbank, D., and Alsdorf, D.: The Shuttle Radar Topography Mission, *Rev. Geophys.*, *45*:2, RG2004, https://doi.org/10.1029/2005RG000183, 2007.

Fox-Kemper, B., Hewitt, H. T., Xiao, C., Aðalgeirsdóttir, G., Drijfhout, S. S., Edwards, T. L., Golledge, N. R., Hemer, M., Kopp, R. E., Krinner, G., Mix, A., Notz, D., Nowicki, S., Nurhati, I. S., Ruiz, L., Sallée, J.-B., Slangen, A. B. A., and Yu, Y.: Ocean, Cryosphere and Sea Level Change, in: *Climate Change 2021: The Physical Science Basis. Contribution of Working Group I to the Sixth Assessment Report of the Intergovernmental Panel on Climate Change*, edited by Masson-Delmotte, V., Zhai, P., Pirani, A., Connors, S. L., Péan, C., Berger, S., Caud, N., Chen, Y., Goldfarb, L., Gomis, M. I., Huang, M., Leitzell, K., Lonnoy, E., Matthews, J. B. R., Maycock, T. K., Waterfield, T., Yelekçi, O., Yu, R., and Zhou, B., Cambridge University Press, Cambridge, 9-1–9-257, In press.

Fusami, A. A., Edan, J. D., & Takana, A. (2023). Local orthometric height based on a combination of GPS-derived ellipsoidal height and geoid model: A review paper. *Journal of Geodetic Science*, *13*(1), 20220158. https://doi.org/10.1515/jogs-2022-0158.

Garner, G. G., Hermans, T., Kopp, R. E., Slangen, A. B. A., Edwards, T. L., Levermann, A., Nowikci, S., Palmer, M. D., Smith, C., Fox-Kemper, B., Hewitt, H. T., Xiao, C., Aðalgeirsdóttir, G., Drijfhout, S. S., Edwards, T. L., Golledge, N. R., Hemer, M., Kopp, R. E., Krinner, G., Mix, A., Notz, D., Nowicki, S., Nurhati, I. S., Ruiz, L., Sallée, J.-B., Yu, Y., Hua, L., Palmer, T., and Pearson, B.: IPCC AR6 Sea-Level Rise Projections, Version 20210809, PO.DAAC, CA, USA, Dataset accessed [2022-05-23] at

https://podaac.jpl.nasa.gov/announcements/2021-08-09-Sea-level-projections-from-the-IPCC-6th-Assessment-Report, 2021.

Garner, G. G., Kopp, R. E., Hermans, T., Slangen, A. B. A., Koubbe, G., Turilli, M., Jha, S., Edwards, T. L., Levermann, A., Nowikci, S., Palmer, M. D., and Smith, C.: Framework for Assessing Changes To Sea-level (FACTS), Geoscientific Model Development, *Zenodo* [model], https://zenodo.org/record/6419954, last access: 22 November 2022, 2022.

Gesch, D. B. (2018). Best practices for elevation-based assessments of sea-level rise and coastal flooding exposure. *Frontiers in Earth Science*, *6*, 230. https://doi.org/10.3389/feart.2018.00230.

Gesch, D. (2023). Assessing global elevation models for mapping the low elevation coastal zone. *Geomorphometry* 2023. https://doi.org/10.5281/zenodo.8011577.

Guth, P. L., Van Niekerk, A., Grohmann, C. H., Muller, J. P., Hawker, L., Florinsky, I. V., Gesch, D., Reuter, H. I., Herrera-Cruz, V., Riazanoff, S., López-Vázquez, C., Carabajal, C. C., Albinet, C., & Strobl, P. (2021). Digital elevation models: Terminology and definitions. *Remote Sensing*, *13*(18), 3581. https://doi.org/10.3390/rs13183581.

Hauser, L., Boni, R., Minderhoud, P. S. J., Teatini, P., Woillez, M. N., Almar, R., Avornyo, S. Y., & Addo, K. A. (2023). A scoping study on coastal vulnerability to relative sea-level rise in the Gulf of Guinea. *AFD Research Papers*, (*283*), 1–42. https://www.afd.fr/sites/default/files/2023-08-02-21-15/PR_283_VA_Web.pdf.

Hawker, L., Rougier, J., Neal, J., Bates, P., Archer, L., & Yamazaki, D. (2018a). Implications of simulating global digital elevation models for flood inundation studies. *Water Resources Research*, *54*(10), 7910–7928. https://doi.org/10.1029/2018WR023279.

Hawker, L., Bates, P., Neal, J., & Rougier, J. (2018b). Perspectives on digital elevation model (DEM) simulation for flood modeling in the absence of a high-accuracy open access global DEM. *Frontiers in Earth Science*, *6*, 233. https://doi.org/10.3389/feart.2018.00233.

Hawker, L., Uhe, P., Paulo, L., Sosa, J., Savage, J., Sampson, C., and Neal, J.: A 30 m global map of elevation with forests and buildings removed, *Environ. Res. Lett.*, *17*:2, 024016, https://doi.org/10.1088/1748-9326/ac4d4f, 2022.

Herrera-García, G., Ezquerro, P., Tomás, R., Béjar-Pizarro, M., López-Vinielles, J., Rossi, M., Mateos, R. M., Carreón-Freyre, D., Lambert, J., Teatini, P., Cabral-Cano, E., Erkens, G., Galloway, D., Hung, WC., Kakar, N., Sneed, M., Tosi, L., Wang, H., & Ye, S. (2021). Mapping the global threat of land subsidence. *Science*, *371*(6524), 34–36. https://doi.org/10.1126/science.abb8549.

Hodgson, M. E., & Bresnahan, P. (2004). Accuracy of airborne lidar-derived elevation. *Photogrammetric Engineering & Remote Sensing*, *70*(3), 331–339. https://doi.org/10.14358/PERS.70.3.331.

Ince, E. S., Barthelmes, F., Reißland, S., Elger, K., Förste, C., Flechtner, F., Schuh, H., 2019. ICGEM – 15 years of successful collection and distribution of global gravitational models, associated services and future plans. *Earth Sys. Sci. Data*, *11*, 647–674, https://doi.org/10.5194/essd-11-647-2019.

Jousset, S., Mulet, S., Greiner, E., Wilkin, J., Vidar, L., Dibarboure, G., Picot, N., 2023. New Global Mean Dynamic Topography CNES-CLS-22 Combining Drifters, Hydrological Profiles and High Frequency Radar Data. *ESS Open Archive*, https://doi.org/10.22541/essoar.170158328.85804859/v2.

Kulp, S., & Strauss, B. H. (2016). Global DEM errors underpredict coastal vulnerability to sea level rise and flooding. *Frontiers in Earth Science*, *4*, 36. https://doi.org/10.3389/feart.2016.00036.

Kulp, S. A., and Strauss, B. H.: CoastalDEM: A global coastal digital elevation model improved from SRTM using a neural network, *Remote Sens. Environ.*, *206* (1), 231–239, https://doi.org/10.1016/j.rse.2017.12.026, 2018.

Kulp, S. A., and Strauss, B. H.: CoastalDEM v2.1: A high-accuracy and high-resolution global coastal elevation model trained on ICESat-2 satellite lidar, *Climate Central Scientific Report*, 17 pp., 2021. https://assets.ctfassets.net/cxgxgstp8r5d/3f1LzJSnp7ZjFD4loDYnrA/71eaba2b8f8d642dd9a7e6581dce0c66/CoastalDEM_2.1_Scientific_Report_.pdf.

Le, H. A., Nguyen, T., Gratiot, N., Deleersnijder, E., & Soares-Frazão, S. (2023). The multi-channel system of the Vietnamese Mekong Delta: impacts on the flow dynamics under relative sea-level rise scenarios. *Water*, *15*(20), 3597. https://doi.org/10.3390/w15203597.

Minderhoud, P. S. J., Erkens, G., Pham, V. H., Bui, V. T., Erban, L., Kooi, H., & Stouthamer, E. (2017). Impacts of 25 years of groundwater extraction on subsidence in the Mekong delta, Vietnam. *Environmental research letters*, *12*(6), 064006. https://doi.org/10.1088/1748-9326/aa7146.

Minderhoud, P. S. J., Coumou, L., Erban, L. E., Middelkoop, H., Stouthamer, E., & Addink, E. A. (2018). The relation between land use and subsidence in the Vietnamese Mekong delta. *Science of the Total Environment*, *634*, 715–726. https://doi.org/10.1016/j.scitotenv.2018.03.372.

Minderhoud, P. S. J., Coumou, L., Erkens, G., Middelkoop, H., and Stouthamer, E.: Mekong delta much lower than previously assumed in sea-level rise impact assessments, *Nat. Commun.*, *10*:3847, 1–13, https://doi.org/10.1038/s41467-019-11602-1, 2019a.

Minderhoud, Philip; Coumou, Laura; Erkens, Gilles; Middelkoop, Hans; Stouthamer, Esther (2019b): Digital elevation model of the Vietnamese Mekong delta based on elevation points from a national topographical map [dataset]. *PANGAEA*, https://doi.org/10.1594/PANGAEA.902136.

Minderhoud, P. S. J., Hlavacova, I., Kolomaznik, J., & Neussner, O. (2020a). Towards unraveling total subsidence of a mega-delta–the potential of new PS InSAR data for the Mekong delta. *Proceedings of the International Association of Hydrological Sciences*, *382*, 327–332. https://doi.org/10.5194/piahs-382-327-2020.

Minderhoud, P. S. J., Middelkoop, H., Erkens, G., & Stouthamer, E. J. E. R. C. (2020b). Groundwater extraction may drown mega-delta: projections of extraction-induced subsidence and elevation of the Mekong delta for the 21st century. *Environmental Research Communications*, *2*(1), 011005. https://doi.org/10.1088/2515-7620/ab5e21.

Muis, S., Verlaan, M., Nicholls, R. J., Brown, S., Hinkel, J., Lincke, D., Vafeidis, A. T., Scussolini, P., Winsemius, H. C., & Ward, P. J. (2017). A comparison of two global datasets of extreme sea levels and resulting flood exposure. *Earth's Future*, *5*(4), 379–392. https://doi.org/10.1002/2016EF000430.

Nicholls, R. J., Lincke, D., Hinkel, J., Brown, S., Vafeidis, A. T., Meyssignac, B., Hanson, S. E., Merkens, J. L., & Fang, J. (2021). A global analysis of subsidence, relative sea-level change and coastal flood exposure. *Nature Climate Change*, *11*(4), 338–342. https://doi.org/10.1038/s41558-021-00993-z.

Ohenhen, L., Shirzaei, M., Davis, J.L., Tiwari, A., Nicholls, R.J., Dasho, O., Sadhasivam, N., Seeger, K., Werth, S., Chadwick, A.J., Onyike, F., Lucy, J., Atkins, C., Daramola, S., Ankamah, A., Minderhoud, P.S.J., Yemele, G.C., in review. The Global Threat of Sinking Deltas, 07 April 2025, PREPRINT (Version 1) available at *Research Square* [https://doi.org/10.21203/rs.3.rs-6223150/v1].

Permanent Service for Mean Sea Level (PSMSL), 2025a. Permanent Service for Mean Sea Level – Tide Gauge Data: Hon Dau, https://psmsl.org/data/obtaining/stations/841.php, last access: 7 July 2025.

Permanent Service for Mean Sea Level (PSMSL), 2025b. Permanent Service for Mean Sea Level – Tide Gauge Data: Vung Tau, https://psmsl.org/data/obtaining/stations/1495.php, last access: 4 July 2025.

Pronk, M., Hooijer, A., Eilander, D., Haag, A., de Jong, T., Vousdoukas, M., Vernimmen, R., Ledoux, H., & Eleveld, M. (2024). DeltaDTM: A global coastal digital terrain model. *Scientific Data*, *11*(1), 273. https://doi.org/10.1038/s41597-024-03091-9.

Pronk, M. (2024). DeltaDTM v1.1: A global coastal digital terrain model (Version 4) [Data set]. 4TU.ResearchData. https://doi.org/10.4121/21997565.V4.

Ren, H. C., Yan, Q., Liu, Z. J., Zuo, Z. Q., Xu, Q. Q., Li, F. F., & Song, C. (2016, November). Study on analysis from sources of error for Airborne LIDAR. In *IOP Conference Series: Earth and Environmental Science* (Vol. 46, No. 1, p. 012030). IOP Publishing. https://doi.org/10.1088/1755-1315/46/1/012030.

Renaud, F. G., Syvitski, J. P. M., Sebesvari, Z., Werners, S. E., Kremer, H., Kuenzer, C., Ramesh, R., Jeuken, A., & Friedrich, J. (2013). Tipping from the Holocene to the Anthropocene: How threatened are major world deltas?. *Current Opinion in Environmental Sustainability*, *5*(6), 644–654. https://doi.org/10.1016/j.cosust.2013.11.007.

Schumann, G., Matgen, P., Cutler, M. E. J., Black, A., Hoffmann, L., & Pfister, L. (2008). Comparison of remotely sensed water stages from LiDAR, topographic contours and SRTM. *ISPRS Journal of Photogrammetry and Remote Sensing*, *63*(3), 283–296. https://doi.org/10.1016/j.isprsjprs.2007.09.004.

Seeger, K., Minderhoud, P. S. J., Peffeköver, A., Vogel, A., Brückner, H., Kraas, F., Nay Win Oo & Brill, D. (2023). Assessing land elevation in the Ayeyarwady Delta (Myanmar) and its relevance for studying sea

level rise and delta flooding. *Hydrology and Earth System Sciences*, *27*(11), 2257–2281. https://doi.org/10.5194/hess-27-2257-2023.

Seeger, K., Minderhoud, P. S. J., Hauser, L. T., Teatini, P., Woillez, M.-N., 2024. *How to assess coastal flood risk in data-sparse coastal lowlands? Accurate information on land elevation is key*. A Question of development 71, 1–4. https://www.afd.fr/en/ressources/how-assess-coastal-flood-risk-data-sparse-coastal-lowlands-accurate-information-land-elevation-key. (last access: 7 July 2025)

Seeger, K., Minderhoud, P.S.J., in review. Sea level much higher than assumed in most coastal hazard assessments. *Nature*, 2025-02-05097A.

Shirzaei, M., Freymueller, J., Törnqvist, T. E., Galloway, D. L., Dura, T., & Minderhoud, P. S. J. (2021). Measuring, modelling and projecting coastal land subsidence. *Nature Reviews Earth & Environment*, *2*(1), 40–58. https://doi.org/10.1038/s43017-020-00115-x.

Smith, R. G., and Berry, P. A. M.: ACE2: Global Digital Elevation Model User Guide, 22 pp., 2009.

Syvitski, J. P. M., Kettner, A. J., Overeem, I., Hutton, E. W. H., Hannon, M. T., Brakenridge, G. R., Day, J., Vörösmarty, C., Saito, Y., Giosan, L., and Nicholls, R. J.: Sinking deltas due to human activities, *Nat. Geosci.*, *2*, 681–686, https://doi.org/10.1038/ngeo629, 2009.

Tachikawa, T., Kaku, M., Iwasaki, A., Gesch, D., Oimoen, M., Zhang, Z., Danielson, J., Krieger, T., Curtis, B., Haase, J., Abrams, M., Crippen, R., and Carabajal, C.: ASTER Global Elevation Model Version 2 – Summary of Validation Results, National Aeronautics and Space Administration (NASA) Land Processes Distributed Active Archive Center, and Joint Japan-US ASTER Science Team, 26 pp., 2011.

Tadono, T., Nagai, H., Ishida, H., Oda, F., Naito, S., Minakawa, K., and Iwamoto, H.: Generation of the 30 m-mesh global digital surface model by ALOS Prism, in: *Int. Arch. Photogramm. Remote Sens. Spatial Inf. Sci., XLI-B4, XXIII ISPRS Congress*, Prague, Czech Republic, 12–19 July 2016, 157–162, https://doi.org/10.5194/isprs-archives-XLI-B4-157-2016, 2016.

Tanaka, K., Fujihara, Y., Hoshikawa, K., & Fujii, H. (2019). Development of a flood water level estimation method using satellite images and a digital elevation model for the Mekong floodplain. *Hydrological Sciences Journal*, *64*(2), 241–253. https://doi.org/10.1080/02626667.2019.1578463.

Thanh, V. Q., Roelvink, D., Van Der Wegen, M., Reyns, J., Kernkamp, H., Van Vinh, G., & Linh, V. T. P. (2020). Flooding in the Mekong Delta: the impact of dyke systems on downstream hydrodynamics. *Hydrology and Earth System Sciences*, *24*(1), 189–212. https://doi.org/10.5194/hess-24-189-2020.

Uhe, P., Lucas, C., Hawker, L., Brine, M., Wilkinson, H., Cooper, A., Saoulis, A. A., Savage, J., & Sampson, C. (2025). FathomDEM: an improved global terrain map using a hybrid vision transformer model. *Environmental Research Letters*, *20*(3), 034002. https://doi.org/10.1088/1748-9326/ada972.

Üstün, A., Abbak, R. A., and Zeray Östürk, E.: Height biases of SRTM DEM related to EGM96: from a global perspective to regional practice, *Surv. Rev.*, *50*, 26–35, https://doi.org/10.1080/00396265.2016.1218159, 2016.

Vernimmen, R., Hooijer, A., and Pronk, M.: New ICESat-2 Satellite LiDAR Data Allow First Global Lowland DTM Suitable for Accurate Coastal Flood Risk Assessment, *Remote Sens.*, *12*:17, 2827, https://doi.org/10.3390/rs12172827, 2020.

Vernimmen, R., & Hooijer, A. (2023). New LiDAR-based elevation model shows greatest increase in global coastal exposure to flooding to be caused by early-stage sea-level rise. *Earth's Future*, *11*(1), e2022EF002880. https://doi.org/10.1029/2022EF002880.

Vignudelli S, Vignudelli S, Kostianoy AG, Cipollini P, Benveniste J (eds) (2011) Coastal altimetry. Springer, Berlin. https://doi.org/10.1007/978-3-642-12796-0.

Vignudelli, S., Birol, F., Benveniste, J., Fu, L. L., Picot, N., Raynal, M., & Roinard, H. (2019). Satellite altimetry measurements of sea level in the coastal zone. *Surveys in Geophysics*, *40*, 1319–1349. https://doi.org/10.1007/s10712-019-09569-1.

Vu, D. T., Bruinsma, S., Bonvalot, S., Remy, D., & Vergos, G. S. (2020). A Quasigeoid-derived transformation model accounting for land subsidence in the Mekong delta towards height system unification in Vietnam. *Remote Sensing*, *12*(5), 817. https://doi.org/10.3390/rs12050817.

Vu, D. T., Bruinsma, S., Bonvalot, S., Bui, L. K., & Balmino, G. (2021). Determination of the geopotential value on the permanent GNSS stations in Vietnam based on the Geodetic Boundary Value Problem approach. *Geophysical Journal International*, *226*(2), 1206–1219. https://doi.org/10.1093/gji/ggab166.

Wessel, B. (2013). TanDEM-X Ground Segment – DEM Products Specification Document, EOC, DLR, Oberpfaffenhofen, Germany, Public Document TD-GS-PS-0021, Issue 3.0, [Online]. Available: https://tandemx-science.dlr.de/, 2013.

Wessel, B.: TanDEM-X Ground Segment – DEM Products Specification Document, EOC, DLR, Oberpfaffenhofen, Germany, Public Document TD-GS-PS-0021, Issue 3.2, [Online], Available: https://tandemx-science.dlr.de/, 2018.

Wilson, J. P. (2012). Digital terrain modeling. *Geomorphology*, *137*(1), 107–121. https://doi.org/10.1016/j.geomorph.2011.03.012.

Wood, M., Haigh, I. D., Le, Q. Q., Nguyen, H. N., Tran, H. B., Darby, S. E., Marsh, R., Skliris, N., & Hirschi, J. J. M. (2024). Risk of compound flooding substantially increases in the future Mekong River delta. *Natural Hazards and Earth System Sciences*, *24*(10), 3627–3649. https://doi.org/10.5194/nhess-24-3627-2024.

Wöppelmann, G., & Pirazzoli, P. (2005). Tide gauges (ML Schwartz, ed.), Encyclopedia of Coastal Sciences, 984–986. https://doi.org/10.1007/1-4020-3880-1_322.

Wu, S., & Lei, Y. (2023). Multiscale Flood Disaster Risk Assessment in the Lancang-Mekong River Basin: A Focus on Watershed and Community Levels. *Atmosphere*, *14*(4), 657. https://doi.org/10.3390/atmos14040657.

Xu, K., Fang, J., Fang, Y., Sun, Q., Wu, C., & Liu, M. (2021). The importance of digital elevation model selection in flood simulation and a proposed method to reduce DEM errors: a case study in Shanghai. *International Journal of Disaster Risk Science*, *12*, 890–902. https://doi.org/10.1007/s13753-021-00377-z.

Yamazaki, D., Ikeshima, D., Tawatari, R., Yamaguchi, T., O'Loughlin, F., Neal, J. C., Sampson, C. C., Kanae, S., & Bates, P. D. (2017). A high-accuracy map of global terrain elevations. *Geophysical Research Letters*, *44*(11), 5844–5853. https://doi.org/10.1002/2017GL072874.

Yun, X., Song, J., Wang, J., & Bao, H. (2024). Modelling to assess the suitability of hydrological-hydrodynamic model under the hydropower development impact in the Lancang-Mekong River basin. *Journal of Hydrology*, *637*, 131393. https://doi.org/10.1016/j.jhydrol.2024.131393.

Zoccarato, C., Minderhoud, P. S., & Teatini, P. (2018). The role of sedimentation and natural compaction in a prograding delta: insights from the mega Mekong delta, Vietnam. *Scientific Reports*, *8*(1), 11437. https://doi.org/10.1038/s41598-018-29734-7.

5 Understanding land elevation dynamics for strengthening coastal hazard and impact assessments in the Ayeyarwady Delta (Myanmar)

Abstract: Flat, low-lying river deltas and coastal plains are subject to land subsidence, together with reduced sediment aggradation resulting in net land elevation loss which accelerates relative sea-level rise and increases the exposure to flooding. As deltaic subsidence occurs gradually and over comparably long time scales, it is often not recognised as a hazard itself and consequently hampering effective disaster risk management, which is necessary at a correspondingly early stage. Unravelling land elevation change, especially in form of vertical land movement where deltaic subsidence rates often outpace potential elevation gain through sediment accretion, as well as its drivers is therefore crucial for mitigation of and/or adaptation to suffer from potential impacts of increased inundation exposure. In the Ayeyarwady Delta in Myanmar, land subsidence has only been studied around Yangon City where it could be attributed to the local geology, groundwater extraction and building load. On delta scale, however, land subsidence still constitutes a large unknown that could thus not yet been included in investigations of sea-level rise. Based on a multi-temporal DInSAR algorithm, this study provides the first investigation of land elevation change covering the entire Ayeyarwady Delta where elevation loss occurs at rates of up to several centimetres per year. Besides supporting outcomes from previous studies and extending spatial coverage of existing data, our record also informs about spatio-temporal patterns and gives first insights into driving mechanisms in addition to those of urban subsidence hotspots. This data will support recent research initiatives on relative sea-level rise impact and flood risk in the delta, informing risk management and adaptation efforts to save the delta from drowning.

Chapter 5 is related to: **Seeger, K.**, Shirzaei, M., Werth, S., Minderhoud, P.S.J., Vogel, A., Brückner, H., Kraas, F., Brill, D., in preparation. *Understanding land elevation dynamics for strengthening coastal hazard and impact assessments in the Ayeyarwady Delta (Myanmar)*.

The reader is requested to cite the content of this chapter as indicated above, together with a reference to this PhD thesis, following standards of the CC-BY 4.0 Attribution 4.0 International licence (http://creativecommons.org/licenses/by/4.0/).

5.1 Introduction

Coastal lowlands such as large, densely populated river deltas are among the most vulnerable to impacts of climate change such as sea-level rise (SLR) (Ericson et al., 2006; Nicholls et al., 2021) and coastal flooding (Edmonds et al., 2020), while being also significantly stressed by human activities due to intense land-use land-cover (LULC) change dynamics such as urbanisation, agricultural and aquacultural intensification, upstream damming as well as resource extraction (Renaud et al., 2013). In addition, land subsidence, defined as downward vertical land movement of a specific reference surface and/or subsurface with respect to a fixed vertical datum (Törnqvist and Blum, 2024; Shirzaei et al., 2021), affects these coastal lowlands, contributing to elevation loss and accelerating rates of SLR (e.g., Nicholls et al., 2021). Deltaic land subsidence is a natural phenomenon caused by processes such as tectonics, glacial isostatic adjustment, sediment isostatic adjustment as well as natural sediment compaction and peat oxidation (see also Shirzaei et al., 2021; summary in Becker et al., 2024). However, human activities in the form of resource extraction (e.g. of groundwater and/or hydrocarbon), certain land-use practices, or processes like urbanisation and the associated increasing load from buildings and infrastructure often exacerbate natural rates of subsidence and result in highly non-linear vertical land motion with annual rates of several centimetres to even decimetres per year (Minderhoud et al., 2020; Copernicus EMSN-091, 2021; Becker et al., 2024 and references therein).

With its comparably slow, non-linear and gradual occurrence, behaving time-elapsed and being effective over comparably long time scales, land subsidence constitutes a hidden hazard, which is often not recognised as such although it increases the risk of relative SLR impact and flood exposure. However, missing or inadequate consideration of land subsidence and consequently land elevation loss in hazard and impact assessments of coastal lowlands prone to elevation loss does not provide the full picture but may lead to substantial underestimations in potential relative SLR and flood impacts (Oelsmann et al., 2024). Though sediment delivery to the delta and accretion on the delta plain would help it to keep up with sea level under natural conditions,

therewith potentially leading to elevation gain (i.e. positive elevation change), natural sediment fluxes within the fluvial system are often disrupted due to upstream dams and/or sediment extraction, which result in sediment starvation in the delta and consequently its ability to keep its balance or even prograde (Schmitt et al., 2017; Bussi et al., 2021). In this context, considerations have to be made to properly address and disentangle vertical land motion in form of land subsidence and uplift from land elevation change that includes also the impact of sediment accretion on vertical land motion (Törnqvist and Blum, 2024). Consequently, it requires this awareness also with regard to in situ and remote sensing measurements whether they allow for the unequivocal attribution of elevation change to vertical land motion (Minderhoud et al., 2025). In the absence of both locally resolved sediment aggradation and vertical land motion rates, observations of land elevation change may tentatively be assumed to equal vertical land motion in geomorphologically "static" landscapes such as urban and agricultural areas while sediment deposition and erosion may significantly contribute in coastal, "dynamic" regions such as wetlands and therefore require thorough quantifications aside from vertical land motion (Shirzaei et al., 2021; Törnqvist and Blum, 2024).

As the drivers of deltaic land subsidence and land elevation change act on different spatial and temporal scales, becoming effective also at different vertical depths, make their interplay and thus the overall pattern of land subsidence and land elevation change highly complex and variable across the delta (e.g. de Wit et al., 2021; Candela and Koster, 2022; Minderhoud et al., 2025). To understand land elevation dynamics on local to regional scale, unravelling its magnitudes and intensities over time is as important as of its underlying drivers, helps to gain a thorough understanding of this threat, and complements and strengthens hazard assessments. With the implications that can be deduced for present and future SLR and flood risk, it provides invaluable details for risk mitigation and adaptation strategies (Bucx et al., 2015; Dunn and Minderhoud, 2022; Dunn et al., 2023), and is lastly also highly relevant for future land-use activities and economic production targets set out in delta development and management plans (see also Vo et al., 2025).

For many coastal lowlands such as data-sparse river deltas, land elevation change and the contribution of land subsidence as well as its effects on relative SLR impact and flood exposure are unknown or have been addressed only very recently by global studies focussing on coastal cities, many of which are located in deltas or coastal plains (Wu et al., 2022; Ao et al., 2024), or comparing elevation loss in 40 deltas in the world (Ohenhen et al., 2025). As these studies require the use of a global geodetic velocity frame (such as Hammond et al., 2021) in order to

compare elevation change across the globe, they may suffer from the impact of inaccurate performance of this velocity frame in coastal lowlands of Southeast Asia and Africa where GNSS data is limited due to the comparably low density of GNSS networks. Another limitation of those global studies is that drivers can only be disentangled in a first, tentative manner as they rely on the selection of global datasets and their suitability to reflect regional to local conditions (e.g., Hasan et al., 2023). Local-scale studies addressing land elevation change with respect to a local stable reference point and including local, accurate information – or in its absence quality-assured large-scale/global data – to decipher locally effective drivers and patterns are consequently highly needed to ensure the appropriateness and success of targeted mitigation and adaptation strategies.

In the data-sparse Ayeyarwady Delta in Myanmar, land elevation change so far has only been studied around Yangon City. Here, land subsidence is documented at rates of 10–20 mm/yr (modal value; van der Horst et al., 2018) and max. rates mount to max. 74 mm/yr (Aobpaet et al., 2014), locally exceeding 110 mm/yr (van der Horst et al., 2018), while its spatial pattern has been attributed to the local geological setting (young age of deposits), groundwater extraction and building load. On delta scale, however, land subsidence still constitutes a large unknown that could thus not yet been included in investigations of SLR (Seeger et al., 2023).

Our study provides the first analysis of land elevation change covering the entire Ayeyarwady Delta and provides an overview of potential local drivers as well as a first glimpse on the implications of the observed spatio-temporal patterns with respect to present and future exposure to relative SLR and flooding. Using a multi-temporal Differential Interferometry Synthetic Radar (DInSAR) algorithm on Sentinel-1 satellite data, we determined elevation change rates of up to several centimetres per year which strengthens estimates of land subsidence from previous studies and extends their spatial coverage to observe whether land subsidence also occurs in more rural areas characterised by different types of land use. This data will support recent research initiatives on relative sea-level rise impact and flood risk in the delta, informing risk management and adaptation efforts to save the delta from drowning.

5.2 Methods

5.2.1 SAR interferometric analysis for determining land elevation change

To determine delta-wide changes in land elevation, we used open and freely available Sentinel-1 SAR data and applied a wavelet-based multi-temporal DInSAR algorithm (Shirzaei and Bürgmann, 2012; Shirzaei, 2013; Shirzaei et al., 2019; Lee and Shirzaei, 2023) considering latest available algorithms for pair and pixel selection as well as atmospheric error correction (Lee and Shirzaei, 2023). We investigated Sentinel-1 SLC imagery (IW mode; 10 m spatial resolution) from October 2014 to November 2023 and downloaded data for 5 ascending and 3 descending frames from the Alaska Satellite Facility (ASF) Data Search Vertex (ASF, 2023) for the entire delta (Table 5.1).

Table 5.1 *| Radar satellite data processed to investigate land elevation change in the Ayeyarwady Delta. Satellite data on which the preliminary results of land elevation change investigations in the Ayeyarwady Delta are based on is highlighted in italics.*

Sensor	Mode	Path	Frames	Delta area covered	Time period (final)	Swaths included	Images included (*N*)	Elite pixels (*N*)	Elite pixels in the delta (*N*)
Sentinel-1	ascending	143	55 to 56	Delta apex (N part)	27/10/2014 to 21/11/2023	12	216	883099	877231
Sentinel-1	ascending	143	50 to 51	Delta apex (S part)	24/10/2018 to 21/11/2023	12	250		
Sentinel-1	*ascending*	*143*	*45 to 46*	*Central to NE delta*	*21/03/2017 to 16/10/2023*	*123*	*305*	*845180*	*508165*
Sentinel-1	*ascending*	*143*	*50 to 51*	*Central to SE delta*	*21/03/2017 to 16/10/2023*	*123*	*305*		
Sentinel-1	ascending	41	44	SW delta	14/03/2017 to 02/11/2023	123	200	100662	97494
Sentinel-1	ascending	41	49 to 51	W to NW delta	14/03/2017 to 02/11/2023	123	200		
Sentinel-1	descending	106	533 to 534	Central to NW delta	11/06/2018 to 16/12/2021	123	128	461116	44901
Sentinel-1	descending	106	536 to 537	Central to SW delta	04/11/2017 to 07/09/2023	123	187	182040	180307
Sentinel-1	descending	33	536 to 537	E to SE delta	03/11/2018 to 25/11/2023	23	141	336001	333143

In total, 1932 images were obtained, spanning from October 2014 to November 2023. SLC files were created and concatenated and a multilooking filter applied to reduce the impact of noise, yielding a spatial resolution of ca. 70 m. As the data collection for the time period of 2018–2021 included images of 6-day recurrence, we included only every second image to ensure sufficient storage capacity while keeping the representative character of the dataset. After image concatenation, image pairs were selected based on thresholds set for perpendicular baseline, i.e. the distance between two satellite positions, and temporal baseline, defined as time interval

between satellite information acquired for the same target area at different points in time. As perpendicular baseline depends on the dataset used, it can be adjusted for each separately and in this study was set to 50 m and 60 m. As deltaic landscapes may change substantially within a short time, we kept the temporal baseline within a few months and set it to 120 days. Subsequently, images were co-registered and interferograms generated. To exclude noisy pixels from the analysis of land elevation change, we included only pixels with an average (mean) coherence of ≥0.55 for distributed scatterers and an amplitude dispersion of ≤0.35 for permanent scatterers. Further processing included phase unwrapping to restore original phase information and obtain absolute phase variations of the elite pixel in each interferogram (ESA, 2007). Wavelet-based filters were applied to correct the unwrapped interferograms for long-wavelength contributions, which represent orbital error, and topography-correlated atmospheric delay, following Shirzaei and Walter (2011) and Shirzaei and Bürgmann (2012). The elite pixels were geocoded by using a local reference point with minimal noise which was achieved by calculating the average of 35 pixels within 250 m distance from that point. Finally, the time series was generated and velocity for each elite pixel determined along the satellite's line of sight (LOS) using a re-weighted least squares approach following Shirzaei (2013).

Post-processing included the removal of pixels outside the region of interest and the conversion to the global reference frame of Hammond et al. (2021) to include long-wave deformation of the earth surface beyond the spatial extent of the individual InSAR frame. Consequently, the individual frames need to be concatenated from the various paths before eventually converting the dataset for the entire delta to one single local reference point. As these post-processing steps are still in progress, we here present individually-processed data frames of that satellite path covering the majority of the Ayeyarwady Delta as defined by Tessler et al. (2015) (Table 5.1).

5.2.2 Seasonal signal component filtering for unravelling the impact of water load on spatio-temporal InSAR pattern

To investigate seasonality within the time series of the entire processed InSAR dataset, whether the observed pattern is related to distance from the reference point or whether it arises from the impact of water load and wetting–drying dynamics of the soil during the monsoon season, the InSAR time series amplitude needs to be analysed whether it increases with increasing distance from the reference point. Seasonal amplitude in the InSAR data should not be a function of distance from the reference point. To unravel this, we downloaded monthly water equivalent

thickness information from Gravity Recovery and Climate Experiment (GRACE) and GRACE Follow-On (GRACE-FO) observations (Tapley et al., 2004; Landerer et al., 2020). To identify trends that need to be applied to both the InSAR and the GRACE data, the signal needs to be decomposed. Consequently, the change of water storage per year was decomposed by accounting for annual and semi-annual seasonal signal variations using a harmonic model. Since detrending the InSAR time series for the entire delta requires concatenation beforehand, which turned out to be challenging as the resulting overall time period would only cover years from 2018 to 2021, finding a compromise of a meaningful time period while covering the delta to the largest extent is still work in progress. However, so far decomposition of the InSAR data was done by testing an array of methods on the LOS time series of pixels from individual frames.

5.2.3 Integrating InSAR and existing data to identify local drivers of land elevation change and implications on relative SLR and flood exposure

The attribution of land elevation change to individual drivers and processes requires the availability and completeness of respective information and datasets. However, in data-sparse coastal lowlands such as the Ayeyarwady Delta, this is particularly challenging as the data needed is either not accessible or – in the absence of high-quality local information – global, often inaccurate datasets have to be used. Given these limitations, the status of the processed InSAR data (post-processing in progress) and obtained preliminary results only allowing for tentative implications, we base our investigations of the potential factors controlling land elevation change in the Ayeyarwady Delta on first, visual comparisons with existing datasets such as delta-wide tectonics and geology (Garzanti et al., 2016; Giosan et al., 2018; Jonell et al., 2022), LULC (Vogel et al., 2022), built-up urban area expansion (Fan et al., 2022) and groundwater extraction (van der Horst et al., 2018; Hashimoto et al., 2022), which however, is limited to Yangon City in the eastern part of the delta. We extend this comparison to derive implications in view of present and future relative SLR, flood exposure and vulnerability by taking into account recent studies of Seeger et al. (2023), Seeger et al. (2024) and Vogel et al. (2024).

5.3 Preliminary results, interpretation and discussion

5.3.1 Land elevation change in the Ayeyarwady Delta

This study provides the first delta-wide information on land elevation change for the Ayeyarwady Delta in Myanmar. However, as some post-processing steps of the InSAR-based detections are still work in progress, the results shown here are preliminary findings and constitute displacement velocities along the satellite's line-of-sight (LOS), which we tentatively interpret as elevation change. The results and statistics are based on the data processed for individual data frames covering the majority of the Ayeyarwady Delta as can be seen in Figure 5.1, over a 7-year period from March 2017 to October 2023 (Table 5.1; Figures 5.1 and 5.2).

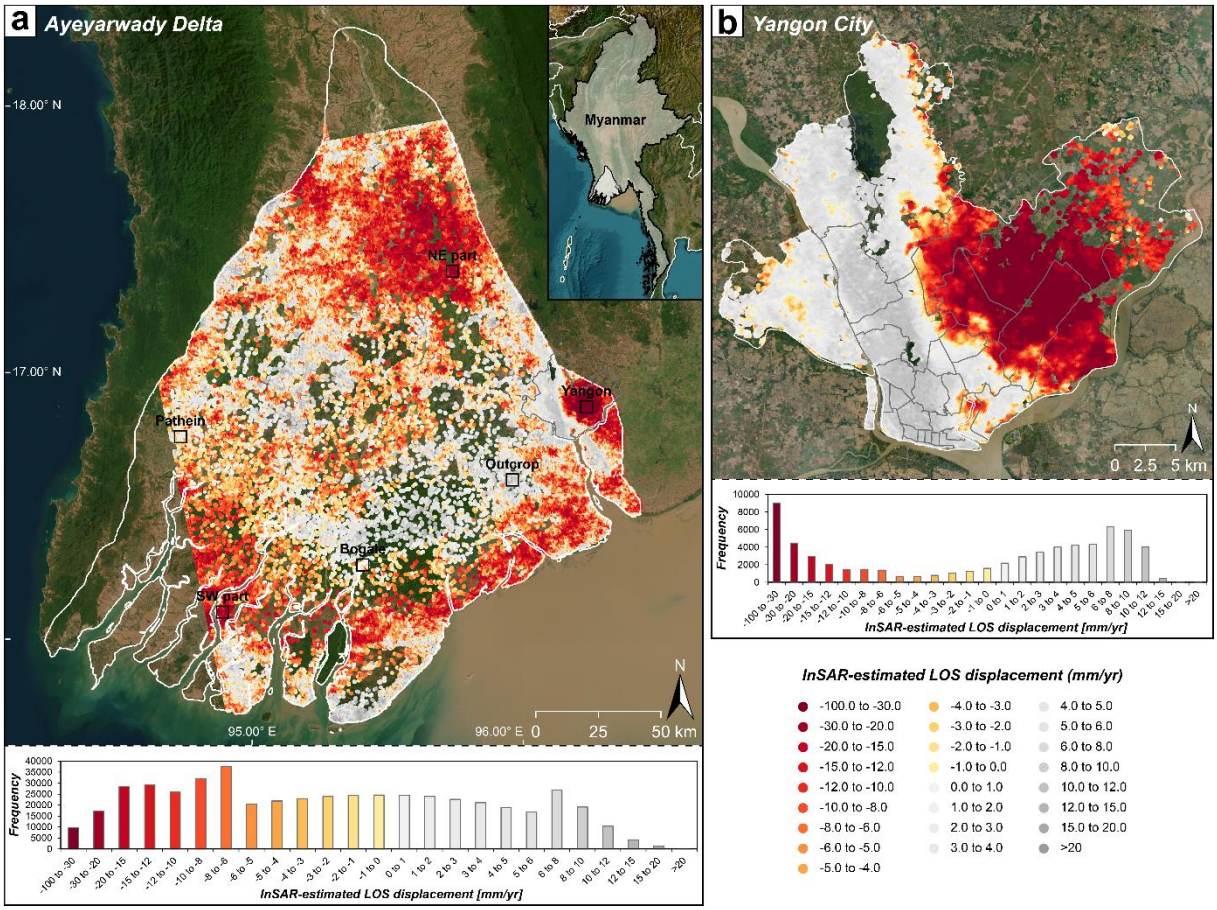


***Figure 5.1** | InSAR-derived displacement velocities along line-of-sight (LOS) for the Ayeyarwady Delta (a) and Yangon City (b).*
Negative values are interpreted as elevation loss, positive values as elevation gain. Annual rates of LOS displacement were determined from Sentinel-1 ascending orbit over the period of March 2017 to October 2023. Small black squares in subfigure (a) indicate locations of timeseries plots shown in Figure 5.2.

In general, land elevation change in the Ayeyarwady Delta reveals a heterogeneous pattern with areas of moderate negative (e.g. elevation loss/subsidence) and positive elevation change (e.g.

elevation gain/uplift) spread over the entire delta and hotspots of elevation loss sticking out especially in the eastern, northern and southern delta parts while elevation gain is observed particularly in some areas of the eastern delta and locally directly at the coastline (Figure 5.1). Consequently, delta-wide elevation change averages at -4 mm/yr (median: -3 mm/yr) with average standard deviations of 0.05 mm/yr (Table 5.2; Figure F1 in Appendix F), and ranges between -99.8 mm/yr and 26.4 mm/yr with standard deviations of 0.05 mm/yr to 1.6 mm/yr (Table 5.2; Figure F1). Areas where elevation loss is most prominent, include the hotspot of Yangon City (Figure 5.1b), as well as the northeastern delta and southern coastal range (Fig. 1a). Overall, the delta loses elevation at rates of -9.3 mm/yr (median: -7.1 mm/yr) while gain rates average at 4.1 mm/yr (median) to 4.8 mm/yr (mean). Local hotspots show annual changes of several centimetres and almost reach a decimetre in Yangon City (Figure 5.1; Table 5.2). Here, maximal negative elevation change rates of the entire delta are documented, reaching up to -99.8 mm/yr. Considering only negative annual changes, Yangon City suffers from average elevation loss of -18.3 mm/yr (median) to -22.7 mm/yr (mean) (Table 5.2). Rates of elevation gain are on average 5.5 mm/yr (median) to 5.8 mm/yr (mean) and reach up to 20.8 mm/yr. The fact that in our dataset for Yangon City less pixels documenting negative elevation change, however at higher magnitudes, and more showing positive elevation change (at lower magnitudes) results in overall negative mean elevation change of -6.5 mm/yr while indicating overall slight median elevation gain of 1.8 mm/yr (Table 5.2). The spatial pattern is however remarkable as areas of maximal positive elevation change are directly next to areas of maximal negative elevation change (Figure 5.1b).

Table 5.2 **|** *Average, minimum and maximum values of land elevation change (LEC), and standard deviation (SD) for the Ayeyarwady Delta and Yangon City based on InSAR-estimated LOS displacement velocities.*

	N **(pixels)**	**Mean LEC (mm/yr)**	**Median LEC (mm/yr)**	**Max. negative LEC (mm/yr)**	**Max. positive LEC (mm/yr)**	**Mean SD (mm/yr)**	**Median SD (mm/yr)**	**Min. SD (mm/yr)**	**Max. SD (mm/yr)**
Ayeyarwady Delta									
Total	508165	-4.0	2.6	-99.8	26.4	0.5	0.5	0.1	1.6
Positive LEC (elevation gain)	189732	4.8	4.1	0.0	26.4	0.5	0.5	0.1	1.5
Negative LEC (elevation loss)	318433	-9.3	-7.1	-99.8	-0.0	0.5	0.5	0.1	1.6
Yangon City									
Total	66633	-6.5	1.8	-99.8	20.8	0.5	0.4	0.2	1.2
Positive LEC (elevation gain)	37828	5.8	5.5	0.0	20.8	0.4	0.4	0.2	0.9
Negative LEC (elevation loss)	28805	-22.7	-18.3	-99.8	-0.0	0.5	0.5	0.2	1.2

Our findings for Yangon City compare well to those of previous studies of Aobpaet et al. (2014) and van der Horst et al. (2018), who determined land elevation changes of 55 mm/yr to -74

mm/yr for the time between April 2012 and April 2014 (Aobpaet et al., 2014) while negative changes increase to -110 mm/yr in December 2014 to April 2017 (van der Horst et al., 2018). Also the overall remarkable spatial pattern is well reflected. However, van der Horst et al. (2018) show more widespread negative elevation change in western Yangon which is less pronounced in studies of Aobpaet et al. (2014) and our work. We so far have no explanation for this but tentatively attribute it to a combination of the respective reference system used and integrating both persistent scatterer- and differential InSAR. Instead, further investigations and direct comparisons with previous studies can only be done after converting to a consistent local reference point and distinguishing between pixels obtained from persistent scatterers and from DInSAR.

Other hotspot areas in the delta are less striking than Yangon City. Nevertheless, further hotspots of negative elevation change also reveal annual rates of several centimetres. This includes, for example, the northern to northeastern delta, mainly located in Thayarwady District, which shows rates of -10 mm/yr to -40 mm/yr. Similarly, the coastal stretch, except of the very coastline, is affected by elevation loss of -10 mm/yr to -30 mm/yr, locally reaching -40 mm/yr or more (Figure 5.1). This pattern of a coastal belt losing elevation behind a coastline showing no or positive elevation change has been observed also in other deltas, such as the Ganges-Brahmaputra-Meghna (Ohenhen et al., 2025), and leaves room for speculating similar, spatially bounded, effective drivers.

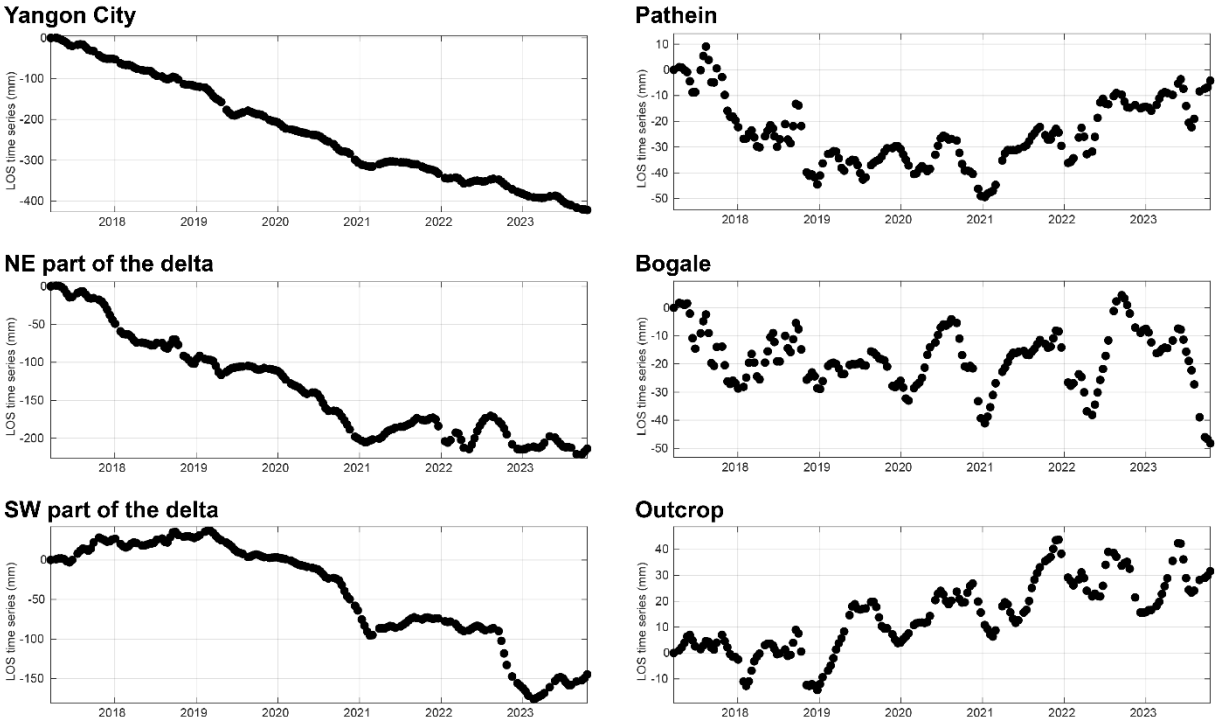


***Figure 5.2** | Timeseries of land elevation change based on InSAR-estimated displacement along line-of-sight (LOS) for selected locations in the Ayeyarwady Delta over the investigation period of March 2017 to October 2023. Pixel locations for which timeseries are shown are indicated in Figure 5.1.*

To unravel spatio-temporal trends of land elevation change in the Ayeyarwady Delta, we investigated time series for locations all over the delta and selected some representative examples, reflecting the different temporal trends in the delta (Figure 5.2). While Yangon City shows an almost linear trend of elevation loss, this is less for areas in the northeastern and southwestern delta, which not only show lower magnitudes but also slight seasonal variations. Furthermore, they differ in that as the northeastern delta suffers from high linear rates of elevation loss until 2021 while then suddenly slowing down until the end of the investigation period. In contrast, changes in the southwestern delta are almost absent or slightly positive but indicating increased elevation losses between 2019 and 2021 and 2022 (Figure 5.2). We also investigated trends for deltaic cities other than Yangon, which are of smaller extent and less inhabitants, however, show substantial urban growth tendencies (e.g. Vogel et al., 2022). The examples of Pathein and Bogale reflect overall slight negative to almost absent land elevation changes, while the respective pattern being dominated by a strong seasonality, where negative changes occur mostly in the second half of the year. We found this seasonal pattern for various locations in the delta and surprisingly also for an area southwest of Yangon we classified as an outcrop (Figure 5.2). Consequently, we expect this seasonality to be related to a large-scale phenomenon affecting the entire delta system. The temporality of this seasonality and its correspondence with that of monsoon (see also Seeger et al., 2024) thus makes comparisons

with spatio-temporal patterns of terrestrial water load and soil wetting–drying cycles highly needed.

5.3.2 Seasonality in water load and signal decomposition

Before investigating seasonality within the time series of the processed InSAR data, the water load information of GRACE needs to be decomposed which was done by using a harmonic model. Over time, water equivalent thickness decreases annually by -0.84 cm/yr while amplitudes reach more than 20 cm/yr and their temporal pattern is in line with seasonal runoff during the monsoon period (Figures 5.3 and 5.4c).

As the current processing status does not allow for comparing seasonal trends in water load with the seasonality in InSAR-derived estimates of land elevation change, we here summarise the analysis steps to be done once data processing is completed, and report on our findings from initial investigations. We tested various methods in order to decompose the InSAR LOS time series. The algorithms tested include fitting a fourier series (to estimate annual signal), singular spectrum analysis and principal component analysis (to investigate other variations), and were conducted for the individual satellite frames separately (Table 5.1). In contrast to our findings on the GRACE data, preliminary visual comparison suggests seasonal variations in the InSAR data to be relatively small while inter-annual variations in the area are, in addition to linear trends, comparably large. However, given the complexity of the entire dataset consisting of pixels processed from six different frames of different orbits and different temporal coverages makes its analysis still complicated. Instead, in addition to the displacement velocities, also LOS time series of each frame needs to be converted into the global reference frame, first, and merged with data from all other frames. This leaves us to the current state with two options: either we will provide information on land elevation change for the entire Ayeyarwady Delta while covering only a limited time period of October 2018 to December 2021, or we will keep the investigation period longer than three years, however missing part of the Ayeyarwady Delta. With either option, LOS time series of the respective frames to be included will be converted to the global vertical reference frame and merged. Subsequently, the data can be shifted to a local stable reference point, for example to the IGL1 GPS station which is outside the delta and shows – apart from seasonal variations – a comparably stable vertical movement component, especially over the investigation period (Figure F2). The time series would then be detrended by applying either a principal component analysis or an independent component analysis which

out of the test runs yielded the most promising results. Once these seasonal signal decompositions are completed, the dataset can be used for further intersectional analyses with information on potential driving mechanisms of land elevation change and subsidence and thus allow for well-grounded interpretations.

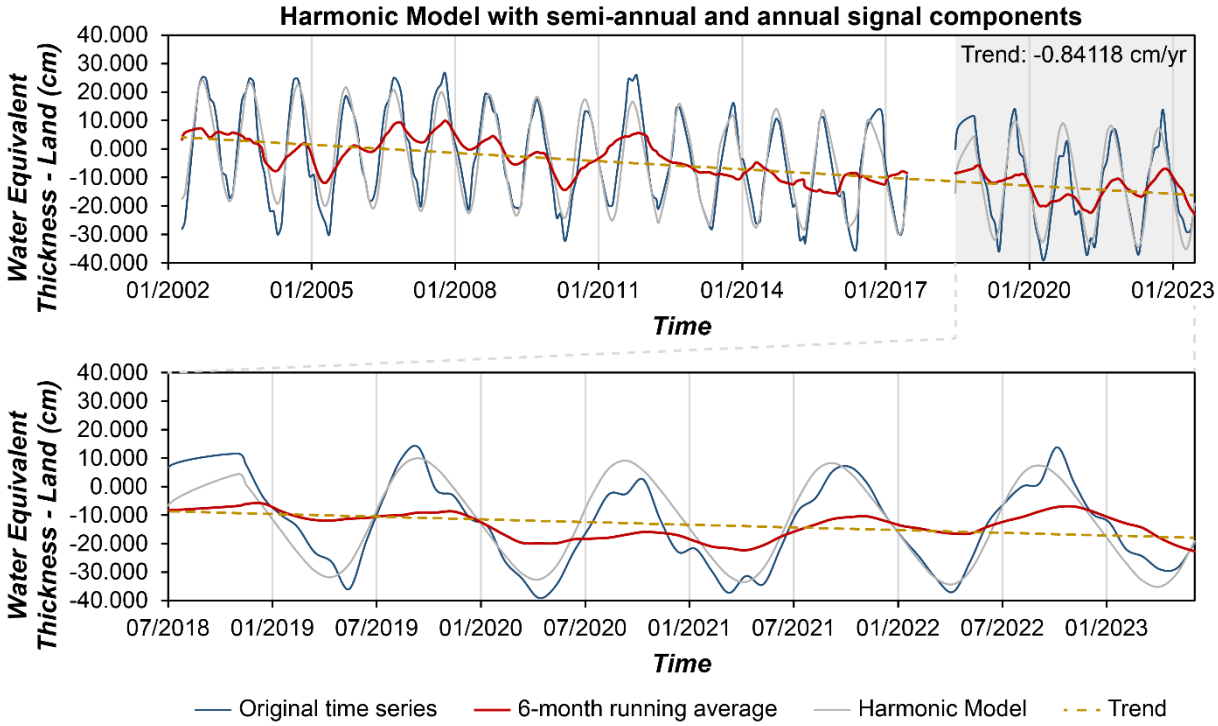


Figure 5.3 *| Monthly measurements of the Earth's surface mass and water changes (blue), 6-month running average (red), as well as the harmonic model (grey) fitted to decompose annual signal components and trend (orange).*
Information on terrestrial water storage was obtained from GRACE, GRACE-FO JPL (300 km × 300 km) imagery (ascending) between 2017 and 2023 (NASA JPL, 2023). The area shaded in light grey highlights the time period covered also by InSAR-based land elevation change and is enlarged in the lower plot.

5.3.3 Unravelling potential drivers of land elevation change based on comparison with existing data

To gain some first, preliminary insights into the relations between land elevation change and its potential drivers in the Ayeyarwady Delta, we conducted comparisons of spatio-temporal patterns the InSAR-based change rates and existing datasets on potential natural and anthropogenic controlling factors based on visual inspection. All findings, however, will be re-investigated after finalisation of post-processing and detrending of the InSAR data and therefore until then do not allow for any quantifications but should be treated as tentative tendencies.

5.3.3.1 Potential natural drivers

To unravel natural drivers of elevation change requires information on the delta's tectonic setting, its geology and sedimentary stratigraphy, of which the latter two allow for insights into sediment compressibility (see for example Zoccarato et al. (2018) for the Vietnamese Mekong Delta). Tectonically, the Ayeyarwady River system is situated in an active thrust-fault system, where the India plate is subducted along the Rakhine Megathrust in the west (Aung et al., 2020), and the Shan Boundary Fault Zone with the Sagaing right lateral strike-slip fault in the east (Bender et al., 1983), forming the 35,000 km^2 large delta classified as bay-head delta in a confined setting between North–South trending mountain ranges (Anthony et al., 2019; Figure 5.4). As the Sagaing strike-slip fault traverses Yangon City where the west side has been documented to move northeastwards at rates of ca. 32 mm/yr while the east side moves southeastwards at rates of ca. 31 mm/yr (Aung et al., 2016), the processed InSAR data needs to be investigated for the potential impact of this lateral movement by separating vertical and horizontal components once data from ascending and descending mode is combined. In order to estimate the contributions of tectonic controls on land elevation change in terms of vertical land motion requires the generation of a model resolving tectonic movements due to strike-slip fault activity and subsequent detrending of the InSAR data. However, the few, very limited available GNSS stations and data, often providing very short or incomplete, discontinuous timeseries, challenge setting up a thorough model that goes beyond simple assumptions.

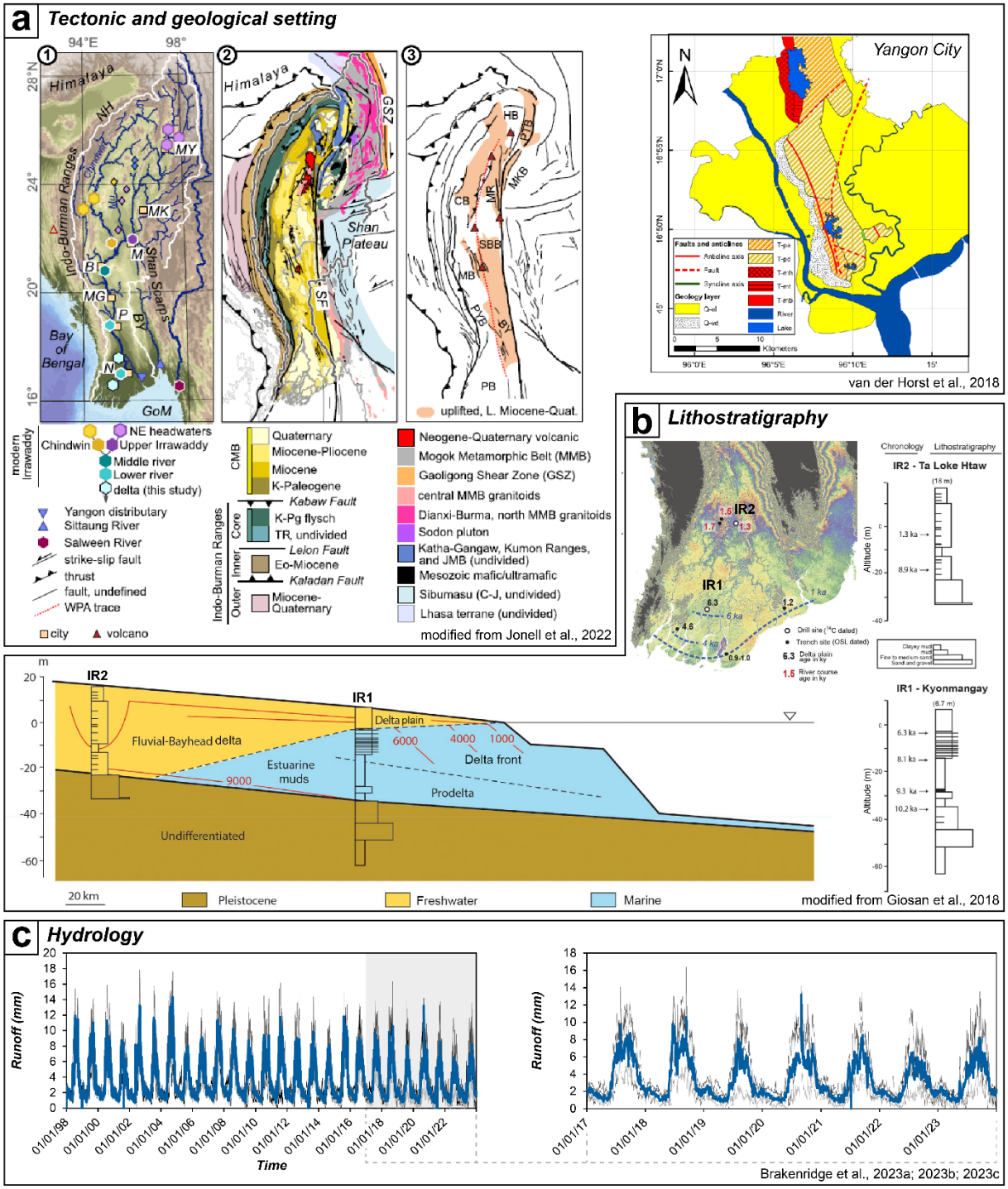


***Figure 5.4** | Overview of potential natural drivers of land elevation change in the Ayeyarwady Delta in Myanmar. The presented compilation of studies on the tectonic and geological (a; Garzanti et al., 2016 and references therein; van der Horst et al., 2018 and references therein; Jonell et al., 2022), stratigraphical (b; Giosan et al., 2018) and hydrological setting (c; Brakenridge et al., 2023a; 2023b; 2023c) provides the most detailed spatial (and temporal) information currently available to unravel natural drivers of delta-wide elevation change. (a) reprinted from van der Horst et al. (2018, p. 107), Copyright (2026), with permission from Elsevier.*

Similar limitations exist for information on the delta's geology which is only described as Quaternary, alluvial deposits, without any further characterisation or vertical differentiation into stratigraphical layers (Figure 5.4; Garzanti et al., 2016; van der Horst et al., 2018; Jonell et al., 2022). Instead, the only available information for the entire delta includes a coarse

stratigraphical cross-section based on two sediment cores (Giosan et al., 2018). This cross-section distinguishes the deltaic stratigraphy into freshwater-dominated sediments on top of Pleistocene sediments for the fluvial-bayhead delta (i.e. the northern delta part, proximate from the apex), which thin out towards the delta plain (i.e. the southern delta part, distal from the apex and proximate from the coast) where they cover marine, estuarine muds (Figure 5.4b; Giosan et al., 2018). Though this lithostratigraphy does not allow for any meaningful comparison with spatio-temporal land elevation change, we can at least expect a tendentially higher natural compaction potential towards the younger, southern delta plain. For Yangon City, the available geological information is more detailed and allows to unequivocally relate areas of larger negative elevation change to young Quaternary alluvial deposits while areas of almost no to positive elevation change coincide with sedimentary deposits of Tertiary age (see also van der Horst et al., 2018 and references therein). Apart from assumptions on delta-wide sediment aggradation and compaction in form of a single value (Syvitski et al., 2009), the absence of any ground-based documentation on local sediment deposition and compaction rates and patterns makes it challenging to estimate the true impact of natural compaction in small-scale, local parts of the northern delta and close to the apex, where sedimentation occurs locally along meandering and anastomosing river arms. Here, we can only suspect that negative elevation change occurs due to high natural compaction of recently deposited sediments or is caused by human activities. In contrast, recent studies of Kuehl et al. (2019) and Glover et al. (2021) on sediment transport in three distributaries and off the delta allow for tentatively attributing elevation change along the deltaic shore (Figure 5.1). Their findings reveal more pronounced sediment transport from the western (comparatively coarse-grained) towards the eastern region (comparatively fine-grained) during the monsoon season, when coastal current and wave energy is high in the western part and estuarine processes are forced towards or onto the shelf (Kuehl et al., 2019; Glover et al., 2021). During the dry season, tidal currents have a relatively higher impact on the distributaries, especially in the eastern delta region. Here, the distributaries turn into partially mixed estuaries where tidal pumping imports shelf sediment from the Gulf of Mottama (Glover et al., 2021). This West–East trending sediment transport theoretically allows for a similar pattern of vertical accretion and matches observations of increasing/decreasing erosion and accretion (Chen et al., 2020). This would be in line with our observations of elevation gain along the very coastline of the southern and eastern part as well as along the Yangon distributary, yielding rates of ~5–10 mm/yr, locally reaching up to 15–20 mm/yr (Figure 5.1). This driving mechanism is likely also responsible that we observe a similar spatial pattern of inland elevation loss and gain along the coastline in other deltas of the world

(Ohenhen et al., 2025). Given the need for thorough ground-based measurements (e.g. by using rod surface elevation tables), we cannot yet disentangle InSAR-detected elevation change into its components of vertical land motion and vertical accretion/erosion, especially along the coastline and close to meandering river arms where morphodynamics are expected to have a comparably larger impact than in more geomorphologically stable areas such as Yangon City.

Other potential influences are long-term contributions of glacial isostatic adjustment (GIA) and sedimentary isostatic adjustment (SIA). Rates of GIA are comparably low and mount to 0.3–0.4 mm/yr (ICE-6G; Peltier et al., 2015; Becker et al., 2024) while a proportion of present-day long-term subsidence can be explained by SIA due to Holocene sedimentation (see also Becker et al. (2024) and references therein). However, isolating SIA from other contributions to vertical land motion in deltaic lowlands remains difficult as shallow compaction and other effects may be dominant (Becker et al., 2024 and references therein).

While the impact of long-term hydro-isostasy due to ocean siphoning and continental levering is mainly limited to deformation of the ocean basins and most coastal regions of deltas (Gehrels and Long, 2008; Polanco et al., 2024), terrestrial water loading can occur on much shorter, seasonal time scales and affect entire delta systems by surface deformation, such as monsoon-related vertical land motion in the Ganges-Brahmaputra-Meghna Delta (Steckler et al., 2010). For the Ayeyarwady Delta, observed seasonal variations in the GRACE, InSAR and available GNSS datasets, even for outcrops that were assumed to be stable, suggest a similar system-wide impact of increased water load during the monsoon season, resulting in seasonal surface deformation (see also Materna et al., 2021). However, detrending of the InSAR data revealed relatively larger inter-annual variations than semi-annual and annual ones, which in view of the current post-processing status cannot be interpreted against the background of multi-annual environmental dynamics or potential issues arising from InSAR processing (e.g. impact of long-wave contributions due to application of a global vertical reference frame).

5.3.3.2 Potential anthropogenic drivers

Unravelling anthropogenic drivers of land elevation change and land subsidence constitutes the ultimate base to mitigate the hazard of land subsidence and relative SLR in coastal lowlands by accounting for adapted land use and resource consumption in coastal development plans and regulations of resource use. Here, we compare the spatio-temporal pattern of determined land elevation change in the Ayeyarwady Delta with local information on LULC (Vogel et al., 2022), highlighting major change dynamics and the impact of built-up urban area expansion (Fan et

al., 2022). In addition, we discuss our findings against locally limited information on groundwater extraction (Figure 5.5; van der Horst et al., 2018; Hashimoto et al., 2022).

Quantifying and attributing rates of land subsidence to LULC change and its dynamics over years to decades is fundamental to unravel the potential influence of land-use practices and 'trajectories' in the course of land transformation on time-lagged behaviour of land elevation change and subsidence (e.g. Minderhoud et al., 2018; Chounna Yemele et al., in review). For the Ayeyarwady Delta, local LULC has been documented over the last 50 years in five-year intervals (Figure 5.5a; Vogel et al., 2022), where major change dynamics include urban growth in low-lying areas, mangrove deforestation and the expansion of irrigated agricultural and aquacultural areas (Vogel et al., 2022). Hotspots of elevation loss coincide with urbanised areas, where maximal negative rates occur in Yangon City while smaller deltaic towns and settlements show less intense elevation loss (Figures 5.1 and 5.5a). Similarly, LOS time series of these towns still reveal the delta-wide observed seasonality while the signal seems to be overprinted by the intensity of human activities in Yangon City (Figures 5.1 and 5.2). Main urban controls of elevation loss (here due to geomorphological stability to be almost equal to land subsidence) include loading by buildings, infrastructure, and large constructions as well as groundwater extraction (e.g., de Wit et al., 2021; Pedretti et al., 2024; Minderhoud et al., 2025). For Yangon City, we can relate most of the elevation loss to the expansion of built-up areas between 2000 and 2020 (Fig. 5b; Fan et al., 2022), the location of industrial zones (van der Horst et al., 2018) and groundwater extraction rates of 1000–2000 mm/yr (Hashimoto et al., 2022), while regions of maximal groundwater extraction (up to 11,000 mm/yr) are located in larger industrial zones in western Yangon, i.e. in sinking areas outside the hotspot (Figure 5.5b and c; van der Horst et al., 2018; Hashimoto et al., 2022). Therewith, our observations are in line with Hashimoto et al. (2022) who document groundwater for industrial use being largely extracted from confined aquifers and thus resulting in net elevation loss while urban households mainly abstract groundwater from unconfined aquifers with less impact on land subsidence. The recently documented groundwater extraction amounts of Yangon City are larger than previously reported and rank very high in comparison to other Asian cities affected by extraction-induced land subsidence (JICA, 2014; Hashimoto et al., 2022). For the entire delta, however, dimensions of groundwater usage by urban settlements, horticultural and aquacultural farms are completely unknown (Viossanges et al., 2017), thereby adding a major uncertainty in understanding the spatio-temporal pattern of land elevation change in terms of subsidence in the delta and developing adequate coping strategies.

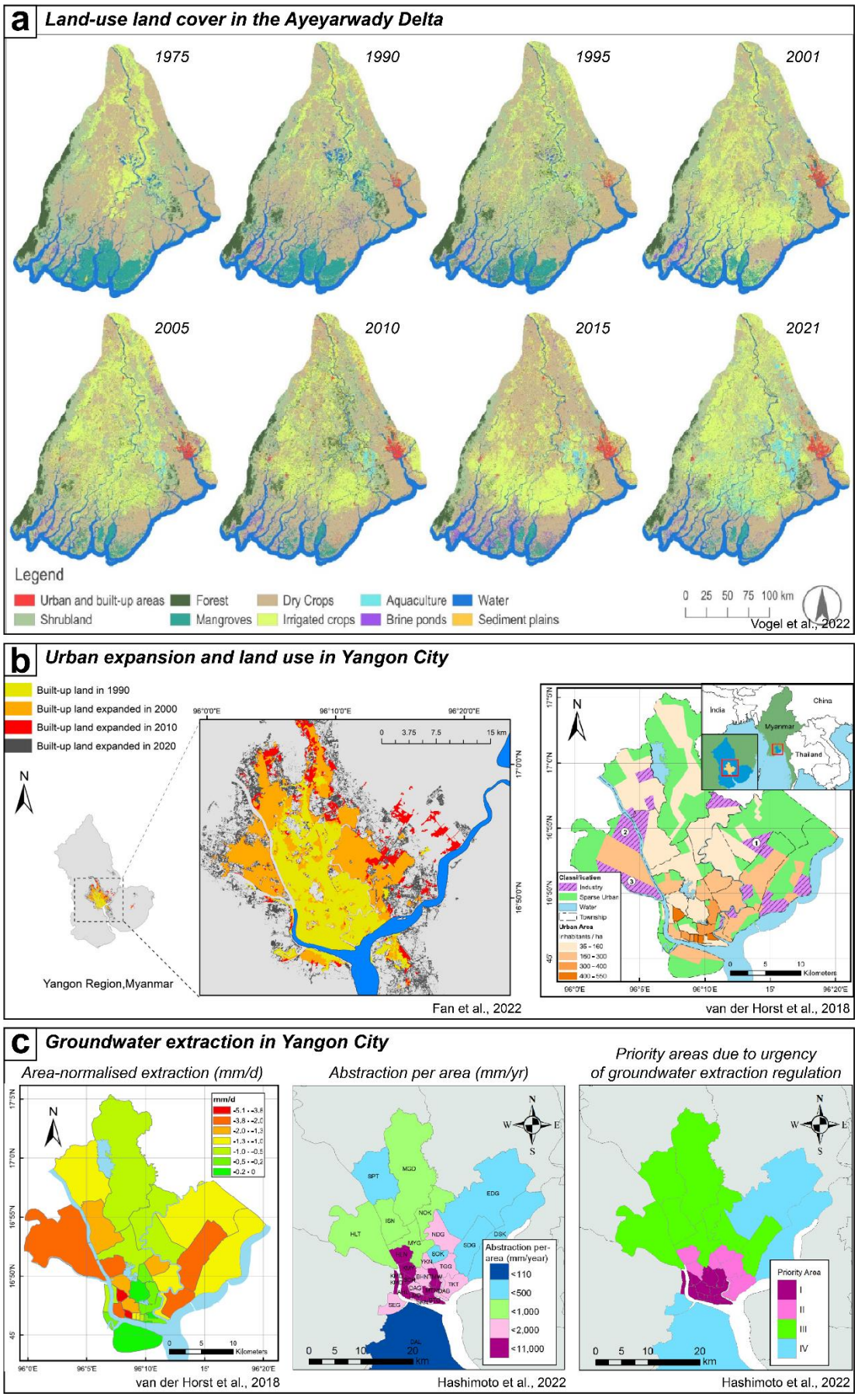


***Figure 5.5** | Overview of potential anthropogenic drivers of land elevation change in the Ayeyarwady Delta in Myanmar.*

Studies on land-use land cover in the delta and its change over the last 50 years (a; Vogel et al., 2022) will allow to unravel delta-wide relations between certain trajectories of land-use land cover change while more detailed investigations of land elevation change will be possible the metropolitan area of Yangon City by comparison with urban expansion and local land-use land cover (b; van der Horst et al., 2018; Fan et al., 2022) as well as groundwater extraction information (c; van der Horst et al., 2018; Hashimoto et al., 2022). (b) and (c) reprinted from van der Horst et al. (2018, pp. 102 and 106) and Hashimoto et al. (2022, p. 6), Copyright (2026), with permission from Elsevier.

Further LULC change dynamics, however with less clear relations to negative land elevation change, include the expansion of agriculture and aquaculture (Figures 5.1 and 5.5a; Vogel et al., 2022). While agriculture already dominates the deltaic landscape before 1974, expansion continues over time and intensification occurs in form of the conversion of non-irrigated to irrigated agriculture (Figures 5.1 and 5.5a; Vogel et al., 2022). We observe the north–northeastern and southern, coastal-range elevation loss hotspots to coincide with agricultural areas. Visual comparison does not allow to identify any clear trend but only to document that elevation loss occurs either in areas of prolonged non-irrigated agriculture or in areas where dynamic shifts between non-irrigated and irrigated land-use practices occur. However, it remains speculative whether the combined effects of soil compaction and drainage cause the non-irrigated fields to lose elevation or whether in areas of high agricultural change dynamics the use of irrigation can be attributed to water sources impacting land subsidence, such as groundwater table lowering in the shallow subsurface or groundwater extraction from deeper aquifers.

To a lesser extent, in the range of a few millimetres to more than 1 cm per year, land elevation loss occurs in the direct vicinity of aquacultural ponds while no relation could be inferred for the expansion of brine ponds along the coast (Figures 5.1 and 5.5a). This is in contrast with findings from the Yellow River Delta, where negative elevation change was documented at similar to even higher rates at both aquacultural sites and brine ponds and attributed to groundwater extraction-induced land subsidence (Higgins et al., 2013; Wang et al., 2022; Zhang et al., 2022). A potential explanation that we do not observe land elevation loss related to brine ponds in the Ayeyarwady Delta could lie in different designs of the ponds where brine resources in the Yellow River Delta are mined from deeper layers (Zhang et al., 2022).

In order to substantiate our tentative findings, we envisage to re-investigate and quantify the relations of land elevation change to both natural and anthropogenic driving mechanisms once InSAR-based datasets on land elevation change are finalised. In particular, trajectories of LULC change will be elaborated to infer and substantiate identified relations over short-term to decadal time steps like dynamically shifting agricultural patterns. As the complete and unequivocal attribution of land elevation change and land subsidence to individual drivers

requires the availability and completeness of respective (local) datasets, which is challenging for data-sparse coastal lowlands such as the Ayeyarwady Delta, it is our goal to provide at least first insights which form a useful initial base for rethinking and strategising risk-sensitive delta development.

5.3.4 Implications of land elevation change on present and future relative sea-level rise and flood exposure

Assessing the hazard of coastal land elevation loss and subsidence includes unravelling its spatio-temporal patterns and drivers while the findings further allow to derive first implications in view of present and future relative SLR, flood exposure and vulnerability. Here, we provide some preliminary implications by taking into account recent studies of delta elevation and SLR impact (Seeger et al., 2023), present flood exposure (Seeger et al., 2024), vulnerability and risk (Vogel et al., 2024; Figure 5.6).

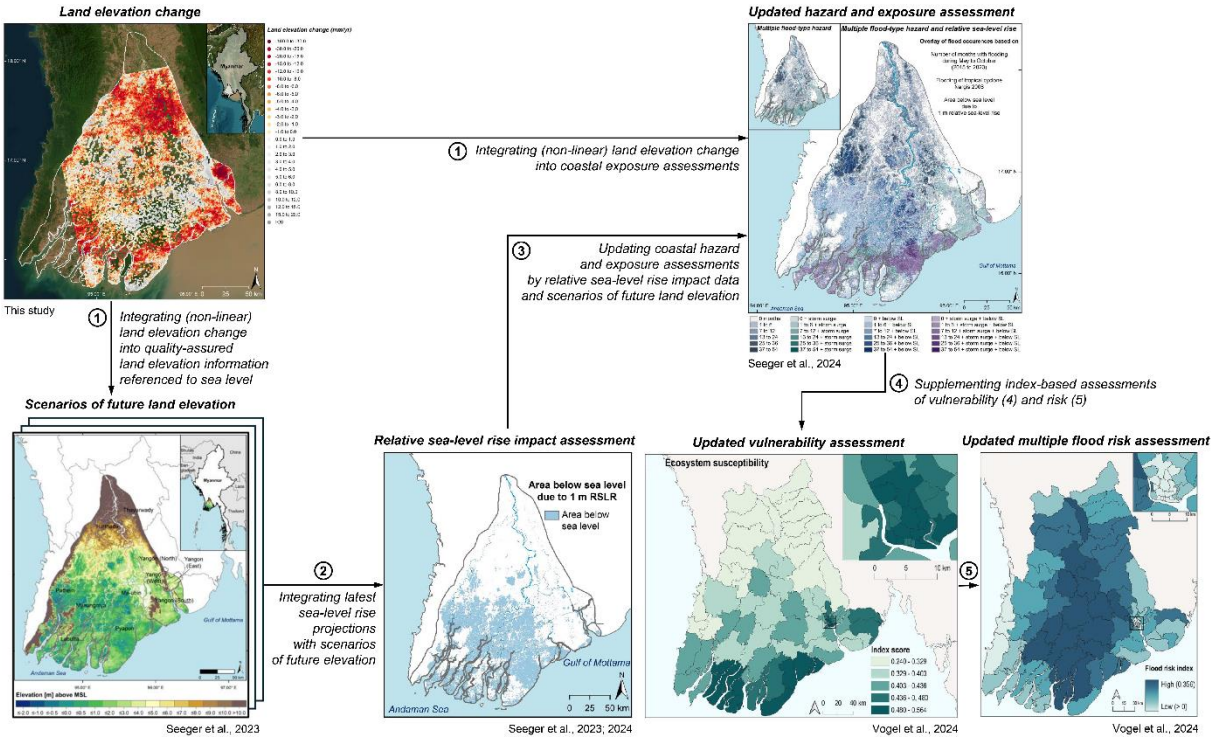


***Figure 5.6** | Outline of how land elevation change information can be used to improve assessments of relative sea-level rise impact (Seeger et al., 2023) and update coastal assessments of coastal exposure, multiple flood hazards (Seeger et al., 2024), vulnerability and risk (Vogel et al., 2024). Land elevation change can be either directly integrated into exposure assessments or used to create scenarios of future land elevation (1) that serve as a basis for relative sea-level rise impact assessment (2) which will then update previous coastal hazard and exposure assessments (3), thereby providing better informed vulnerability (4) and risk assessments (5).*

With an average elevation of only ~1.3 m above mean sea level and lowest elevations already below sea level, the Ayeyarwady Delta is highly prone to land elevation loss and relative SLR

(Seeger et al., 2023). Previous works have shown that up to 47 % of the delta and up to 3 million people will fall below sea level following 1.23 m SLR projected by IPCC AR 6 for 2100 (high SSP5-8.5 scenario; Fox-Kemper et al., 2021; Garner et al., 2021; Garner et al., 2022; Seeger et al., 2023). However, vertical land motion in these assessments has not been adequately considered so far as rates are underestimated, likely due to the strong limitations of the tide gauge used as a reference, i.e. its location at the edge of the delta, unknown benchmark position, outdated and largely discontinuous sea-level measurements between 1916 and 1962 (PSMSL, 2025), as well as GNSS stations located outside the delta.

With an elevation of ca. 2–3 m above mean sea level, Yangon City is on average one metre higher than the vast delta plain, but is maximally losing elevation (30–100 mm/yr; Figure 5.1b), highlighting the urgency of successfully designing and implementing effective coping strategies within the next 20 years. Areas in the delta plain suffering from elevation loss of several centimetres per year are already among the lowest-lying ones in the delta, with only a few decimetres to a metre above mean sea level. Within these areas, many deltaic towns have grown due to urban expansion into the delta at rates of >300 % over the last 25 years (Figures 5.5 and 5.6; Vogel et al., 2022). Consequently, urban growth towards the low-lying coastal delta part represents a major driver of disaster risk and in case, both urban growth and land elevation loss continue at present rates in the coming years to decades, IPCC SLR projections of high emission scenarios for the end of the century may not only become more likely but also become reality decades sooner, impacting substantially more people and assets than estimated so far (Figure 5.6; Seeger et al., 2023).

Similarly, the characterised dimensions of land elevation loss can be integrated into the flexible hazard-assessment workflow of Seeger et al. (2024) and thereby strengthen impact studies of and implications about various single-type and multiple-type flood hazards. While detected land elevation losses in the northern, central delta over time will increase the threat of water logging and more frequent and prolonged flooding during the monsoon season, central to southern deltaic hotspots of land elevation loss will aggravate also impacts of SLR and storm surge. The southern, coastal range of pronounced elevation loss is of fundamental relevance in view of present and future storm surge exposure as well as multiple flooding due to monsoon, storm surge and inundation due to SLR. While it coincides almost completely with delta parts flooded by disastrous Cyclone Nargis 2008 (Fritz et al., 2009; Seeger et al., 2024), over time this coastal belt of pronounced elevation loss will create a large depression like a ‘bathtub’ if elevation loss continues at rates similar to present or accelerates. Since land elevation loss and

land subsidence were not documented in the Ayeyarwady Delta before, and iterated studies on land subsidence in Yangon City did not have any impact on local, national and international agencies to develop concepts of and initiate long-term risk-sensitive delta development, we see the continuation of land elevation loss in a business-as-usual scenario as very likely. Further indications are the absence, limited availability, insufficient quality and low level of detail of local spatial datasets such as detailed geological information or groundwater abstraction monitoring, which hampers to thoroughly unravel driving mechanisms needed to design adaptive coping strategies. And even if land subsidence mitigation and adaptation strategies would exist and be successfully implemented, the response of land subsidence would be delayed with effects lasting up to at least two decades (e.g. Minderhoud et al., 2018). Ongoing deltaic elevation loss is also likely as sediment supply to the delta, which is needed to keep up with relative SLR, is assumed to decrease due to increased human activities in the river basin (Chen et al., 2020 and references therein). Compared to other Asian rivers, sediment load in the Ayeyarwady River is so far less impacted by damming (Latrubesse et al., 2021), which is at present mainly limited to its tributaries while comparably smaller dams for irrigation are located along the lower river to the delta (Chen et al., 2020). However, sediment loads have already been reduced by 30 % (Syvitski et al., 2009), and with the installation of further planned, large hydropower dam projects along the main course of the Ayeyarwady River, sediment loads will be reduced by additional 12 % to 19 % (Tessler et al., 2018; Chen et al., 2020).

With ongoing land elevation loss due to ongoing anthropogenically accelerated subsidence and likely reducing sediment supply (leading to sediment starvation), flood exposure will substantially increase in the future. Consequences of land elevation loss add to the respective impacts of flood hazards. Consequently, land elevation loss not only worsens the impacts directly connected to a certain flood hazard type, i.e. by increasing flood extent, prolonging flood duration and waterlogging, but also leads to a chain of cascading effects, for example infrastructural damages and (prolonged) disruptions, reduced soil fertility of agricultural land due to increased and prolonged saltwater intrusion, leading to harvest losses and production disruptions, affecting livelihoods of the delta's residents, risking food security and resulting in substantial economic productivity losses that not only affect the delta but also the entire country heavily relying on the outputs of primary sector activities in the delta (Schneider and Asch, 2020; Scown et al., 2023; Becker et al., 2024).

Besides its integration into previously conducted spatially detailing flood hazard and exposure assessments (Seeger et al., 2023; Seeger et al., 2024), the finalised data on land elevation change

in the Ayeyarwady Delta will allow for substantiating recent index-based assessments of deltaic vulnerability and risk (Vogel et al., 2024). Yet, we see an increase in susceptibility for deltaic areas most vulnerable to environmental impacts. Northern central to northeastern deltaic townships are expected to show relatively higher index values for pluvial and fluvial flood risk while most coastal townships and Yangon City suffer from relatively higher coastal flood risk (Figure 5.6; Vogel et al., 2024). In this sense, these two hazard and exposure as well as vulnerability and risk assessment approaches allow for the most comprehensive and holistic understanding currently possible for risk-sensitive development in the Ayeyarwady Delta under data scarcity and times of multiple crisis.

5.4 Conclusions and outlook

This study reveals the first delta-wide estimates of land elevation change and land subsidence in the Ayeyarwady Delta in Myanmar. Using a multi-temporal DInSAR algorithm on Sentinel-1 imagery, we documented spatio-temporal patterns, of which preliminary results were presented for a subset of the processed datasets, covering the majority of the delta from March 2017 to October 2023. Post-processing so far included test runs for seasonal signal component filtering, which was already done for terrestrial water storage information from GRACE satellite measurements. Given the fact that post-processing of the InSAR-based elevation change data has not yet been completed, we based our investigations of the potential factors controlling land elevation change in the Ayeyarwady Delta on first, visual comparisons with existing datasets, which was also done to derive first tentative implications on present and future relative SLR, flood exposure and vulnerability.

Land elevation change in the Ayeyarwady Delta reveals a heterogeneous pattern with areas of moderate negative (i.e. elevation loss/subsidence) and positive elevation change (i.e. elevation gain/uplift) spread over the entire delta. Areas of maximal elevation loss include the hotspot of Yangon City, where rates reach -100 mm/yr, as well as the northeastern delta and southern coastal range. Our findings are in line with previous studies for Yangon City, whereas the coastal pattern of elevation loss resembles that of other deltas in the world, suggesting potentially similar driving mechanisms. Limited by data scarcity and the final post-processing of the InSAR data still ongoing, relations between land elevation change and potential drivers were only tentatively determined. Implications on the delta's exposure to relative SLR and

flooding highlighted the increased susceptibility especially in low-lying parts of the southern deltaic area, which already suffers from highest exposure and vulnerability.

To further strengthen existing assessments of relative SLR impact and flooding will require an adequate integration of information on sea level, land elevation and elevation dynamics, considering spatio-temporal heterogeneity and non-linear behaviour of land elevation change. Therefore, establishing and coupling models based on disentangled drivers and processes of land elevation change and land subsidence will facilitate process-specific assessments and projections of non-linear elevation change/subsidence. We can then include these simulated rates into accurate elevation data referenced to actual, local continuous sea level and provide scenarios of future elevation and elevation change as well as improved assessments of coastal exposure. Simulations of process-based land elevation change and subsidence remain challenging for the data-sparse Ayeyarwady Delta. However, previous works on properly aligning land elevation with actual sea level and attempts to unravel land elevation change and natural and anthropogenic drivers constitute the first steps to solve individual pieces of the puzzle.

Data availability statement: The data that support the findings of this study will be made available in course of the publication of this chapter in form of a scientific article.

References

Anthony, E. J., Besset, M., Dussouillez, P., Goichot, M., & Loisel, H. (2019). Overview of the Monsoon-influenced Ayeyarwady River delta, and delta shoreline mobility in response to changing fluvial sediment supply. *Marine Geology*, *417*, 106038. https://doi.org/10.1016/j.margeo.2019.106038.

Ao, Z., Hu, X., Tao, S., Hu, X., Wang, G., Li, M., Wang, F., Hu, L., Liang, X., Xiao, J., Yusup, A., Qi, W., Ran, Q., Fang, J., Chang, J., Zeng, Z., Fu, Y., Xue, B., Wang, P., Zhao, K., Li, L., Li, W., Li, Y., Jiang, M., Yang, Y., Shen, H., Zhao, X., Shi, Y., Wu, B., Yan, Z., Wang, M., Su, Y., Hu, T., Ma, Q., Bai, H., Wang, L., Yang, Z., Feng, Y., Zhang, D., Huang, E., Pan, J., Ye, H., Yang, C., Qin, Y., He, C., Guo, Y., Cheng, K., Ren, Y., Yang, H., Zheng, C., Zhu, J., Wang, S., Ji, C., Zhu, B., Liu, H., Tang, Z., Wang, Z., Zhao, S., Tang, Y., Xing, H., Guo, Q., Liu, Y., & Fang, J. (2024). A national-scale assessment of land subsidence in China's major cities. *Science*, *384*(6693), 301–306. https://doi.org/10.1126/science.adl4366.

Aobpaet, A., Trisirisatayawong, I., Aung, H. H., & Maksin, P. (2014). Yangon surface displacement as detected by insar time series analysis. https://acrs-aars.org/proceeding/ACRS2014/Full%20Papers/Session%20E/Session%20E5/OS-112%20C1_session%20_ACRS14_Anuphao.pdf.

ASF, 2023. ASF Data Search Vertex. https://search.asf.alaska.edu/#/, last access: 21 June 2025.

Aung, L. T., Oo, K. Z., Win, K. M., Moore, G. F., Tun, S. T., & Naing, W. (2020). Active deformation of the Central Myanmar Forearc Basin: insight from post-Pleistocene inversion of the Pyay Fault. *Journal of Asian Earth Sciences: X*, *4*, 100037. https://doi.org/10.1016/j.jaesx.2020.100037.

Aung, P. S., Satirapod, C., & Andrei, C. O. (2016). Sagaing Fault slip and deformation in Myanmar observed by continuous GPS measurements. *Geodesy and Geodynamics*, *7*(1), 56–63. https://doi.org/10.1016/j.geog.2016.03.007.

Becker, M., Seeger, K., Paszkowski, A., Marcos, M., Almar, R., Bates, P., France-Lanord, C., Hossain, Md S., Khan, J., Karegar, M., Karpytchev, M., Long, N., Minderhoud, P. S. J., Neal, J., Nicholls, R. J., & Syvitski, J. (2024). Coastal flooding in Asian Megadeltas: Recent advances, persistent challenges, and call for actions admidst local and global changes. *Reviews of Geophysics*, *62*(4), e2024RG00846. https://doi.org/10.1029/2024RG000846.

Bender, F., Bannert, D., Brinckmann, J., Gramann, F., & Helmcke, D. (1983). Geology of Burma.

Brakenridge, G. R., Kettner, A. J., Paris, S., Cohen, S. & Nghiem, S. V. (2023a). River and Reservoir Watch Version 4.5, Satellite-based river discharge and reservoir area measurements, DFO Flood Observatory, University of Colorado, USA. https://floodobservatory.colorado.edu/SiteDisplays/29.htm (last access: 26 June 2025)

Brakenridge, G. R., Kettner, A. J., Paris, S., Cohen, S. & Nghiem, S. V. (2023b). River and Reservoir Watch Version 4.5, Satellite-based river discharge and reservoir area measurements, DFO Flood Observatory,

University of Colorado, USA. https://floodobservatory.colorado.edu/SiteDisplays/25.htm (last access: 26 June 2025)

Brakenridge, G. R., Kettner, A. J., Paris, S., Cohen, S. & Nghiem, S. V. (2023c). River and Reservoir Watch Version 4.5, Satellite-based river discharge and reservoir area measurements, DFO Flood Observatory, University of Colorado, USA. https://floodobservatory.colorado.edu/SiteDisplays/30.htm (last access: 26 June 2025)

Bucx, T. H. M., Van Ruiten, C. J. M., Erkens, G., & De Lange, G. (2015). An integrated assessment framework for land subsidence in delta cities. *Proceedings of the International Association of Hydrological Sciences*, *372*(372), 485–491. https://doi.org/10.5194/piahs-372-485-2015.

Bussi, G., Darby, S. E., Whitehead, P. G., Jin, L., Dadson, S. J., Voepel, H. E., Vasilopoulos, G., Hackney, C. R., Hutton, C., Berchoux, T., Parsons, D. R., & Nicholas, A. (2021). Impact of dams and climate change on suspended sediment flux to the Mekong delta. *Science of the Total Environment*, *755*, 142468. https://doi.org/10.1016/j.scitotenv.2020.142468.

Candela, T., & Koster, K. (2022). The many faces of anthropogenic subsidence. *Science*, *376*(6600), 1381–1382. https://doi.org/10.1126/science.abn3676.

Chen, D., Li, X., Saito, Y., Liu, J. P., Duan, Y., Liu, S. A., & Zhang, L. (2020). Recent evolution of the Irrawaddy (Ayeyarwady) Delta and the impacts of anthropogenic activities: A review and remote sensing survey. *Geomorphology*, *365*, 107231. https://doi.org/10.1016/j.geomorph.2020.107231.

Chounna Yemele, G., Minderhoud, P. S., Ohenhen, L. O., Seeger, K., Shirzaei, M., & Teatini, P. (2025). Land subsidence dynamics and their interplay with spatial and temporal land-use transitions in the Douala coastland, Cameroon. *EGUsphere*, 2025, 1–29. https://doi.org/10.5194/egusphere-2025-336.

Copernicus Emergency Management Service Risk & Recovery Mapping Non-standardised products (FLEX) Lot 1 Final Report (2021). EMSN-091: Assessing changes in subsidence rates in the low Pampanga river basin and Manila area, Philippines. https://mapping.emergency.copernicus.eu/activations/EMSN091/, last access: 26 June 2025.

de Wit, K., Lexmond, B. R., Stouthamer, E., Neussner, O., Dörr, N., Schenk, A., & Minderhoud, P. S. J. (2021). Identifying causes of urban differential subsidence in the Vietnamese Mekong Delta by combining InSAR and field observations. *Remote Sensing*, *13*(2), 189. https://doi.org/10.3390/rs13020189.

Dunn, F. E., & Minderhoud, P. S. J. (2022). Sedimentation strategies provide effective but limited mitigation of relative sea-level rise in the Mekong delta. *Communications Earth & Environment*, *3*(1), 2. https://doi.org/10.1038/s43247-021-00331-3.

Dunn, F. E., Cox, J. R., Scown, M., Du, H., Triyanti, A., Middelkoop, H., Nienhuis, J. H., & Minderhoud, P. S. J. (2023). Sedimentation-enhancing strategies for sustainable deltas: an integrated socio-biophysical framework. *One Earth*, *6*(12), 1677–1691. https://doi.org/10.1016/j.oneear.2023.11.009.

Edmonds, D. A., Caldwell, R. L., Brondizio, E. S., & Siani, S. M. (2020). Coastal flooding will disproportionately impact people on river deltas. *Nature communications*, *11*(1), 4741. https://doi.org/10.1016/j.oneear.2023.11.009.

Ericson, J. P., Vörösmarty, C. J., Dingman, S. L., Ward, L. G., & Meybeck, M. (2006). Effective sea-level rise and deltas: Causes of change and human dimension implications. *Global and Planetary Change*, *50*(1-2), 63–82. https://doi.org/10.1016/j.gloplacha.2005.07.004.

European Space Agency (ESA), 2007. InSAR Principles: Guidelines for SAR Interferometry Processing and Interpretation. ESA Publications, Noordwijk, The Netherlands. https://earth.esa.int/eogateway/documents/20142/37627/InSAR-Principles-Guidelines-for-SAR-Interferometry-Processing-and-Interpretation.pdf, last access: 26 June 2025.

Fan, P., Chen, J., Fung, C., Naing, Z., Ouyang, Z., Nyunt, K. M., Myint, Z. N., Qi, J., Messina, J. P., Myint, S. W., & Peter, B. G. (2022). Urbanization, economic development, and environmental changes in transitional economies in the global south: A case of Yangon. *Ecological Processes*, *11*(1), 65. https://doi.org/10.1186/s13717-022-00409-6.

Fox-Kemper, B., Hewitt, H. T., Xiao, C., Aðalgeirsdoìttir, G., Drijfhout, S. S., Edwards, T. L., Golledge, N. R., Hemer, M., Kopp, R. E., Krinner, G., Mix, A., Notz, D., Nowicki, S., Nurhati, I. S., Ruiz, L., Salleìe, J.-B., Slangen, A. B. A., and Yu, Y.: Ocean, Cryosphere and Sea Level Change, in: Climate Change 2021: The Physical Science Basis. Contribution of Working Group I to the Sixth Assessment Report of the Intergovernmental Panel on Climate Change, edited by: Masson-Delmotte, V., Zhai, P., Pirani, A., Connors, S. L., Peìan, C., Berger, S., Caud, N., Chen, Y., Goldfarb, L., Gomis, M. I., Huang, M., Leitzell, K., Lonnoy, E., Matthews, J. B. R., Maycock, T. K., Waterfield, T., Yelekci¸, O., Yu, R., and Zhou, B., Cambridge University Press, Cambridge, 9-1–9-257, https://www.ipcc.ch/report/ar6/wg1/downloads/report/IPCC_AR6_WGI_Chapter_09.pdf (last access: 26 June 2025), 2021.

Fritz, H. M., Blount, C. D., Thwin, S., Thu, M. K., & Chan, N. (2009). Cyclone Nargis storm surge in Myanmar. *Nature Geoscience*, *2*(7), 448–449. https://doi.org/10.1038/ngeo558.

Garner, G. G., Hermans, T., Kopp, R. E., Slangen, A. B. A., Edwards, T. L., Levermann, A., Nowikci, S., Palmer, M. D., Smith, C., Fox-Kemper, B., Hewitt, H. T., Xiao, C., Aðalgeirsdoìttir, G., Drijfhout, S. S., Edwards, T. L., Golledge, N. R., Hemer, M., Kopp, R. E., Krinner, G., Mix, A., Notz, D., Nowicki, S., Nurhati, I. S., Ruiz, L., Salleìe, J.-B., Yu, Y., Hua, L., Palmer, T., and Pearson, B.: IPCC AR6 Sea-Level Rise Projections, Version 20210809, PO.DAAC [data set], CA, USA, https://podaac.jpl.nasa.gov/announcements/2021-08-09-Sealevel-projections-from-the-IPCC-6th-Assessment-Report (last access: 26 June 2025), 2021.

Garner, G. G., Kopp, R. E., Hermans, T., Slangen, A. B. A., Koubbe, G., Turilli, M., Jha, S., Edwards, T. L., Levermann, A., Nowikci, S., Palmer, M. D., and Smith, C.: Framework for Assessing Changes To Sea-level (FACTS), Geoscientific Model Development, *Zenodo* [model], https://doi.org/10.5281/zenodo.6419954, 2022.

Garzanti, E., Wang, J. G., Vezzoli, G., & Limonta, M. (2016). Tracing provenance and sediment fluxes in the Irrawaddy River basin (Myanmar). *Chemical Geology*, *440*, 73–90. https://doi.org/10.1016/j.chemgeo.2016.06.010.

Gehrels, R., & Long, A. (2008). Sea level is not level: the case for a new approach to predicting UK sea-level rise. *Geography*, *93*(1), 11–16. https://doi.org/10.1080/00167487.2008.12094214.

Giosan, L., Naing, T., Min Tun, M., Clift, P. D., Filip, F., Constantinescu, S., Khonde, N., Blusztajn, J., Buylaert, J. P., Stevens, T., & Thwin, S. (2018). On the Holocene evolution of the Ayeyawady megadelta. *Earth Surface Dynamics*, *6*(2), 451–466. https://doi.org/10.5194/esurf-6-451-2018.

Glover, H. E., Ogston, A. S., Fricke, A. T., Nittrouer, C. A., Aung, C., Naing, T., Kyu, K. K., & Htike, H. (2021). Connecting sediment retention to distributary-channel hydrodynamics and sediment dynamics in a tide-dominated delta: The Ayeyarwady Delta, Myanmar. *Journal of Geophysical Research: Earth Surface*, *126*(3), e2020JF005882. https://doi.org/10.1029/2020JF005882.

Hammond, W. C., Blewitt, G., Kreemer, C., & Nerem, R. S. (2021). GPS imaging of global vertical land motion for studies of sea level rise. *Journal of Geophysical Research: Solid Earth*, *126*(7), e2021JB022355. https://doi.org/10.1029/2021JB022355.

Hashimoto, R., Kazama, S., Hashimoto, T., Oguma, K., & Takizawa, S. (2022). Planning methods for conjunctive use of urban water resources based on quantitative water demand estimation models and groundwater regulation index in Yangon City, Myanmar. *Journal of Cleaner Production*, *367*, 133123. https://doi.org/10.1016/j.jclepro.2022.133123.

Higgins, S., Overeem, I., Tanaka, A., & Syvitski, J. P. (2013). Land subsidence at aquaculture facilities in the Yellow River delta, China. *Geophysical Research Letters*, *40*(15), 3898–3902. https://doi.org/10.1002/grl.50758.

Japan International Cooperation Agency (JICA): Preparatory Survey Report on the Project for the Improvement of Water Supply, Sewerage and Drainage System in Yangon City in the Republic of the Union of Myanmar – Volume III: Water Supply System Master Plan, JICA, 275 pp., https://openjicareport.jica.go.jp/pdf/12175618_01.pdf (last access: 26 June 2025), 2014.

Jonell, T. N., Giosan, L., Clift, P. D., Carter, A., Bretschneider, L., Hathorne, E. C., Barbarano, M., Garzanti, E., Vezzoli, G., & Naing, T. (2022). No modern Irrawaddy River until the late Miocene-Pliocene. *Earth and Planetary Science Letters*, *584*, 117516. https://doi.org/10.1016/j.epsl.2022.117516.

Kuehl, S. A., Williams, J., Liu, J. P., Harris, C., Aung, D. W., Tarpley, D., Goodwyn, M., & Aye, Y. Y. (2019). Sediment dispersal and accumulation off the Ayeyarwady delta–Tectonic and oceanographic controls. *Marine Geology*, *417*, 106000. https://doi.org/10.1016/j.margeo.2019.106000.

Landerer, F. W., Flechtner, F. M., Save, H., Webb, F. H., Bandikova, T., Bertiger, W. I., Bettadpur, S. V., Byun, S. H., Dahle, C., Dobslaw, H., Fahnestock, E., Harvey, N., Kang, Z., Kruizinga, G. L. H., Loomis, B. D., McCullough, C., Murböck, M., Nagel, P., Paik, M., Pie, N., Poole, S., Strekalov, D., Tamisiea, M. E., Wang, F., Watkins, M. M., Wen, H. Y., Wiese, D. N., & Yuan, D. N. (2020). Extending the global mass

change data record: GRACE Follow-On instrument and science data performance. *Geophysical Research Letters*, *47*(12), e2020GL088306. https://doi.org/10.1029/2020GL088306.

Latrubesse, E. M., Park, E., & Kästner, K. (2021). The Ayeyarwady River (Myanmar): Washload transport and its global role among rivers in the Anthropocene. *PLoS One*, *16*(5), e0251156. https://doi.org/10.1371/journal.pone.0251156.

Lee, J. C., & Shirzaei, M. (2023). Novel algorithms for pair and pixel selection and atmospheric error correction in multitemporal InSAR. *Remote Sensing of Environment*, *286*, 113447. https://doi.org/10.1016/j.rse.2022.113447.

Materna, K., Feng, L., Lindsey, E. O., Hill, E. M., Ahsan, A., Alam, A. K. M. K., Oo, K. M., Than, O., Aung, T., Khaing, S. N., & Bürgmann, R. (2021). GNSS characterization of hydrological loading in South and Southeast Asia. *Geophysical Journal International*, *224*(3), 1742–1752. https://doi.org/10.1093/gji/ggaa500.

Minderhoud, P. S. J., Coumou, L., Erban, L. E., Middelkoop, H., Stouthamer, E., & Addink, E. A. (2018). The relation between land use and subsidence in the Vietnamese Mekong delta. *Science of the Total Environment*, *634*, 715–726. https://doi.org/10.1016/j.scitotenv.2018.03.372.

Minderhoud, P. S. J., Middelkoop, H., Erkens, G., & Stouthamer, E. J. E. R. C. (2020). Groundwater extraction may drown mega-delta: projections of extraction-induced subsidence and elevation of the Mekong delta for the 21st century. *Environmental Research Communications*, *2*(1), 011005. https://doi.org/10.1088/2515-7620/ab5e21.

Minderhoud, P. S. J., Shirzaei, M., & Teatini, P. (2025). From InSAR-derived subsidence to relative sea-level rise—A call for rigor. *Earth's Future*, *13*(1), e2024EF005539. https://doi.org/10.1029/2024EF005539.

National Aeronautics and Space Administration Jet Propulsion Laboratory (NASA JPL), 2023. GRACE Data Analysis Tool. https://grace.jpl.nasa.gov/data-analysis-tool/#b=ESRI_World_Imagery&l=TELLUS_GRAC-GRFO_MASCON_CRI_GRID_RL06.3_V4_LAND(1),OSMCoastlines(1)&vm=2D&ve=-94.81900452488686,-45,94.81900452488686,45&pl=false&pb=false&tr=false&d=2025-03-15&tlr=months, last access: 26 June 2025.

Nevada Geodetic Laboratory (NGL) Station ID : IGL1 Network Operator's Station ID : IGLE. https://geodesy.unr.edu/NGLStationPages/stations/IGL1.sta, last access: 21 June 2025.

Nicholls, R. J., Lincke, D., Hinkel, J., Brown, S., Vafeidis, A. T., Meyssignac, B., Hanson, S. E., Merkens, J. L., & Fang, J. (2021). A global analysis of subsidence, relative sea-level change and coastal flood exposure. *Nature Climate Change*, *11*(4), 338–342. https://doi.org/10.1038/s41558-021-00993-z.

Oelsmann, J., Marcos, M., Passaro, M., Sanchez, L., Dettmering, D., Dangendorf, S., & Seitz, F. (2024). Regional variations in relative sea-level changes influenced by nonlinear vertical land motion. *Nature Geoscience*, *17*(2), 137–144. https://doi.org/10.1038/s41561-023-01357-2.

Ohenhen, L., Shirzaei, M., Davis, J.L., Tiwari, A., Nicholls, R.J., Dasho, O., Sadhasivam, N., Seeger, K., Werth, S., Chadwick, A.J., Onyike, F., Lucy, J., Atkins, C., Daramola, S., Ankamah, A., Minderhoud, P.S.J., Yemele, G.C., in review. The Global Threat of Sinking Deltas, 07 April 2025, PREPRINT (Version 1) available at Research Square [https://doi.org/10.21203/rs.3.rs-6223150/v1].

Pedretti, L., Giarola, A., Korff, M., Lambert, J., & Meisina, C. (2024). Comprehensive database of land subsidence in 143 major coastal cities around the world: overview of issues, causes, and future challenges. *Frontiers in Earth Science*, *12*, 1351581. https://doi.org/10.3389/feart.2024.1351581.

Peltier, W. R., Argus, D. F., & Drummond, R. (2015). Space geodesy constrains ice age terminal deglaciation: The global ICE-6G_C (VM5a) model. *Journal of Geophysical Research: Solid Earth*, *120*(1), 450–487. https://doi.org/10.1002/2014JB011176.

Permanent Service for Mean Sea Level (PSMSL), 2025. Rangoon. https://psmsl.org/data/obtaining/stations/210.php, last access: 26 June 2025.

Polanco, S., Blum, M., Salles, T., Frederick, B. C., Farrington, R., Ding, X., Mather, B., Mallard, C., & Moresi, L. (2024). Flexural isostatic response of continental-scale deltas to climatically driven sea level changes. *Earth Surface Dynamics*, *12*(1), 301–320. https://doi.org/10.5194/esurf-12-301-2024.

Renaud, F. G., Syvitski, J. P. M., Sebesvari, Z., Werners, S. E., Kremer, H., Kuenzer, C., Ramesh, R., Jeuken, A., & Friedrich, J. (2013). Tipping from the Holocene to the Anthropocene: How threatened are major world deltas?. *Current Opinion in Environmental Sustainability*, *5*(6), 644–654. https://doi.org/10.1016/j.cosust.2013.11.007.

Schmitt, R. J. P., Rubin, Z., & Kondolf, G. M. (2017). Losing ground-scenarios of land loss as consequence of shifting sediment budgets in the Mekong Delta. *Geomorphology*, *294*, 58–69. https://doi.org/10.1016/j.geomorph.2017.04.029.

Schneider, P., & Asch, F. (2020). Rice production and food security in Asian Mega deltas—A review on characteristics, vulnerabilities and agricultural adaptation options to cope with climate change. *Journal of Agronomy and Crop Science*, *206*(4), 491–503. https://doi.org/10.1111/jac.12415.

Scown, M. W., Dunn, F. E., Dekker, S. C., van Vuuren, D. P., Karabil, S., Sutanudjaja, E. H., Santos, M.J., Minderhoud, P.S.J., Garmestani, A.S., & Middelkoop, H. (2023). Global change scenarios in coastal river deltas and their sustainable development implications. *Global Environmental Change*, *82*, 102736. https://doi.org/10.1016/j.gloenvcha.2023.102736.

Seeger, K., Minderhoud, P. S. J., Peffeköver, A., Vogel, A., Brückner, H., Kraas, F., Nay Win Oo, & Brill, D. (2023). Assessing land elevation in the Ayeyarwady Delta (Myanmar) and its relevance for studying sea level rise and delta flooding. *Hydrology and Earth System Sciences*, *27*(11), 2257–2281. https://doi.org/10.5194/hess-27-2257-2023.

Seeger, K., Peffeköver, A., Minderhoud, P. S. J., Vogel, A., Brückner, H., Kraas, F., Nay Win Oo, & Brill, D. (2024). Evaluating flood hazards in data-sparse coastal lowlands: highlighting the Ayeyarwady Delta (Myanmar). *Environmental Research Letters*, *19*(8), 084007. https://doi.org/10.1088/1748-9326/ad5b07.

Shirzaei, M., & Walter, T. R. (2011). Estimating the effect of satellite orbital error using wavelet-based robust regression applied to InSAR deformation data. *IEEE Transactions on Geoscience and Remote Sensing*, *49*(11), 4600–4605. https://doi.org/10.1109/TGRS.2011.2143419.

Shirzaei, M., & Bürgmann, R. (2012). Topography correlated atmospheric delay correction in radar interferometry using wavelet transforms. *Geophysical Research Letters*, *39*(1), L01305. https://doi.org/10.1029/2011GL049971.

Shirzaei, M. (2013). A wavelet-based multitemporal DInSAR algorithm for monitoring ground surface motion. *IEEE Geoscience and Remote Sensing Letters*, *10*(3), 456–460. https://doi.org/10.1109/LGRS.2012.2208935.

Shirzaei, M., Manga, M., & Zhai, G. (2019). Hydraulic properties of injection formations constrained by surface deformation. *Earth and Planetary Science Letters*, *515*, 125–134. https://doi.org/10.1016/j.epsl.2019.03.025.

Shirzaei, M., Freymueller, J., Törnqvist, T. E., Galloway, D. L., Dura, T., & Minderhoud, P. S. J. (2021). Measuring, modelling and projecting coastal land subsidence. *Nature Reviews Earth & Environment*, *2*(1), 40–58. https://doi.org/10.1038/s43017-020-00115-x.

Steckler, M. S., Nooner, S. L., Akhter, S. H., Chowdhury, S. K., Bettadpur, S., Seeber, L., & Kogan, M. G. (2010). Modeling Earth deformation from monsoonal flooding in Bangladesh using hydrographic, GPS, and Gravity Recovery and Climate Experiment (GRACE) data. *Journal of Geophysical Research: Solid Earth*, *115*(B8), B08407. https://doi.org/10.1029/2009JB007018.

Syvitski, J. P., Kettner, A. J., Overeem, I., Hutton, E. W., Hannon, M. T., Brakenridge, G. R., Day, J., Vörösmarty, C., Saito, Y., Giosan, L., & Nicholls, R. J. (2009). Sinking deltas due to human activities. *Nature Geoscience*, *2*(10), 681–686. https://doi.org/10.1038/ngeo629.

Tapley, B. D., Bettadpur, S., Watkins, M., & Reigber, C. (2004). The gravity recovery and climate experiment: Mission overview and early results. *Geophysical Research Letters*, *31*(9), L09607. https://doi.org/10.1029/2004GL019920.

Tessler, Z. D., Vörösmarty, C. J., Grossberg, M., Gladkova, I., Aizenman, H., Syvitski, J. P., & Foufoula-Georgiou, E. (2015). Profiling risk and sustainability in coastal deltas of the world. *Science*, *349*(6248), 638–643. https://doi.org/10.1126/science.aab3574.

Tessler, Z. D., Vörösmarty, C. J., Overeem, I., & Syvitski, J. P. (2018). A model of water and sediment balance as determinants of relative sea level rise in contemporary and future deltas. *Geomorphology*, *305*, 209–220. https://doi.org/10.1016/j.geomorph.2017.09.040.

Törnqvist, T. E., & Blum, M. D. (2024). What is coastal subsidence?. *Cambridge Prisms: Coastal Futures*, *2*, e2. https://doi.org/10.1017/cft.2024.1.

van der Horst, T., Rutten, M. M., van de Giesen, N. C., & Hanssen, R. F. (2018). Monitoring land subsidence in Yangon, Myanmar using Sentinel-1 persistent scatterer interferometry and assessment of driving mechanisms. *Remote Sensing of Environment*, *217*, 101–110. https://doi.org/10.1016/j.rse.2018.08.004.

Viossanges, M., Johnston, R., and Drury, L.: Groundwater Resources of the Ayeyarwady Basin, Ayeyarwady State of the Basin Assessment (SOBA) Report 2a, National Water Resources Committee (NWRC), Myanmar, 168 pp., http://themimu.info/sites/themimu.info/files/assessment_file_attachments/SOBA2a_Groundwater_Resources_ARB.pdf (last access: 26 June 2025), 2017.

Vo, T. M. H., Huynh, T. P. L., Tamas, P., Woillez, M. N., Espagne, E., Umans, L., Eslami, S., Nguyen, H. Q., & Minderhoud, P. S. J. (2025). How consistent are adaptation strategies with ongoing climatic and environmental changes in the Vietnamese Mekong Delta: A systematic review. *Environmental Science & Policy*, *168*, 104064. https://doi.org/10.1016/j.envsci.2025.104064.

Vogel, A., Seeger, K., Brill, D., Brückner, H., Soe, K. K., Oo, N. W., Aung, N., Myint, Z. N., & Kraas, F. (2022). Identifying land-use related potential disaster risk drivers in the Ayeyarwady Delta (Myanmar) during the Last 50 years (1974–2021) using a hybrid ensemble learning model. *Remote Sensing*, *14*(15), 3568. https://doi.org/10.3390/rs14153568.

Vogel, A., Seeger, K., Brill, D., Brückner, H., Kyaw, A., Myint, Z. N., & Kraas, F. (2024). Towards integrated flood management: Vulnerability and flood risk in the Ayeyarwady Delta of Myanmar. *International Journal of Disaster Risk Reduction*, *114*, 104723. https://doi.org/10.1016/j.ijdrr.2024.104723.

Wang, G., Li, P., Li, Z., Liang, C., & Wang, H. (2022). Coastal subsidence detection and characterization caused by brine mining over the Yellow River Delta using time series InSAR and PCA. *International Journal of Applied Earth Observation and Geoinformation*, *114*, 103077. https://doi.org/10.1016/j.jag.2022.103077.

Wu, P. C., Wei, M., & D'Hondt, S. (2022). Subsidence in coastal cities throughout the world observed by InSAR. *Geophysical Research Letters*, *49*(7), e2022GL098477. https://doi.org/10.1029/2022GL098477.

Zhang, Y., Luo, Y., Huang, H., Liu, Y., Bi, H., Zhang, X., Zhang, Z., Wang, K., Bai, Z., & Zhou, X. (2022). Correlating severe land subsidence and confined brine aquifer compaction in the Yellow River Delta, China, with Sentinel-1A/1B satellite images. *Marine Georesources & Geotechnology*, *41*(8), 927–934. https://doi.org/10.1080/1064119X.2022.2109537.

Zoccarato, C., Minderhoud, P. S. J., & Teatini, P. (2018). The role of sedimentation and natural compaction in a prograding delta: insights from the mega Mekong delta, Vietnam. *Scientific Reports*, *8*(1), 11437. https://doi.org/10.1038/s41598-018-29734-7.

6 Synthesis

This research aimed to improve the understanding of flood hazards and impacts and solving challenges in their assessments in data-sparse coastal lowlands to guide disaster risk reduction and coping strategies in the view of future flood risk and relative sea-level rise. To achieve this overarching goal, this thesis evaluated three hypotheses by addressing nine subordinate goals. To meet these goals, the conducted research included literature reviews and evaluations to generate state-of-the-art overviews of coastal flood-related hazards and pressures in five Asian megadeltas and to unravel the existence of improper handling of elevation and sea-level data in contemporary sea-level rise and coastal hazard impact assessments. Processing an array of open and freely accessible satellite-derived imagery and datasets of precipitation, river discharge, elevation, land use, and population in geographical information systems allowed for setting up a standardised, integrative and highly flexible open-data workflow to conduct first-order hazard exposure assessments. Integrating elevation data from local ground measurements and satellite observations with satellite-derived geoid, satellite-based and local sea-level information allowed to unravel uncertainties in coastal elevation relative sea level and provide follow-up studies with the most accurate elevation information. First estimates on delta-wide land elevation change in the Ayeyarwady Delta in Myanmar and preliminary investigations of natural and human drivers allowed to derive first implications for future relative sea-level rise and flood exposure and will inform risk-sensitive development pathways.

6.1 Improving the understanding of flood hazards and impacts in data-sparse coastal lowlands

Hypothesis 1 | Coastal hazards, their geophysical drivers and human pressures can be successfully assessed in data-sparse coastal lowlands through using state-of the-art space-borne observation and numerical analyses.

Goal 1.1 | Providing a state-of-the-art understanding of coastal flooding in five selected Asian megadeltas through a systems perspective and learning from state-of-the-art monitoring and modelling approaches.

State-of the-art literature on coastal flood-related hazards, their drivers and pressures was assessed for five Asian megadeltas, namely the Ganges-Brahmaputra-Meghna, Ayeyarwady, Chao Phraya, Mekong and Red River, all of which range among the largest, most densely populated and rapidly growing deltas in Southeast Asia while being highly vulnerable to floods and other climate-induced impacts as well as under stress due to human impacts (*Chapter 2*). Geophysical drivers of coastal flooding include monsoon and river discharge, tides, tropical cyclones, storm surges and wind-waves, as well as sea-level change, vertical land motion and land elevation dynamics, and sediment, shoreline and deltaic landform changes. Main human pressures include population growth and deltaic land-use land cover changes due to urbanisation, mangrove loss due to the expansion of agriculture and aquaculture, groundwater extraction, sand mining and upstream interventions (due to dam construction and impacts on river flow and sediment dynamics). All these drivers are critical in shaping unique flood dynamics in every locality of each delta system but are strongly interconnected. Similarly, coastal flooding in the Asian megadeltas shows various interlinkages between direct and indirect societal, economic, technical, socio-technical, physical and ecological impacts as well as beneficial effects of ecosystem services. Flooding can often cause significant setbacks in socio-economic development and exacerbate poverty in these densely populated and highly resource-dependent lowlands (Figure 2.8; *Chapter 2*). Therefore, taking a systems perspective acknowledges the interplay of natural and anthropogenic drivers and processes as well as the consequential effects and feedbacks of coastal flood impacts and helps to gain a more holistic and complete understanding of the intricate dynamics shaping the Asian megadeltas, including also potential future changes (*Chapter 2*). While the Ayeyarwady and Red River deltas are the least studied deltas out of the five assessed, the findings from

this thesis provide fundamental first steps in assessing the delta's exposure to coastal hazards (*Chapter 3*), land elevation and sea-level rise impact (*Chapter 4.1*) and elevation dynamics (*Chapter 5*). The Ganges-Brahmaputra-Meghna and Mekong deltas constitute the comparably most widely studied deltas, where research occurs already in an iterative phase (e.g. by revisiting land elevation in the Mekong Delta) (*Chapter 4.3*). Still, all deltas require more resources to be allocated towards comprehensive data collection and monitoring in order to systematically address the interacting dynamics in the context of coastal flooding and develop effective risk management strategies (*Chapter 2*).

Goal 1.2 | Defining data and modelling requirements for addressing urgent scientific and policy-relevant questions in the context of coastal flooding in five selected Asian megadeltas.

Following the literature review of the methodological/technical advances in quantifying and understanding driving mechanisms in the investigated Asian deltas, gaps in terms of observations and/or models as well as key challenges to be addressed in the context of these megadeltas were elaborated. There is a need to improve data collection and monitoring systems in all five megadeltas, mainly with regard to (but not limited to) (i) a more complete network of discharge and sediment gauges in deltaic river channels; (ii) a comprehensive network of sea- and water-level monitoring stations and tide gauges; (iii) regular bathymetry measurements in near-shore areas and deltaic channels; (iv) a subsidence monitoring network to understand drivers of elevation loss and the contribution of groundwater extraction; and (v) regular updates of digital elevation models to provide up-to-date elevation information for hazard and impact assessments (*Chapter 2*). Overall, improvements towards better dissemination and sharing of data are needed in order to ensure the data collection is meaningful and relevant (*Chapter 2*). Priorities for transferable methodologies across the five Asian megadeltas were elaborated (Table 2.3), highlighting the particular potential of satellite observations based on open data. As the workflows established in this thesis allow to be transferred to any data-sparse coastal lowland in the world, they contribute to solve requirement (v). The integrative approach for flood hazard exposure assessment (*Chapter 3*) allows for first insights into a variety of flood hazards while being flexible to the study area and the data available (including local, regional and global). The workflow to align vertical datums of coastal elevation and sea-level data (*Chapter 4*) as well as processing steps needed to account for uncertainties in coastal elevation assessment (*Chapter 4.3*) allow for updating elevation information to actual local

sea level in the absence of recently new acquired datasets. In this sense, the data processed during the latest research phase of this thesis already fulfils requirement (v), providing new insights into the elevation of the Vietnamese Mekong Delta (*Chapter 4.3*) and assessing area and population at risk of 1 m relative sea-level rise as well as exposure in the low-elevation coastal zone (*Chapter 4.2*). Works on continuous updates of elevation information are ongoing (see also Section 6.4).

Goal 1.3 | Evaluating flood hazards in data-sparse coastal lowlands.

As the assessment of flood hazard exposure is challenging for data-sparse coastal lowlands, in which high-resolution and high-accuracy data is limited or not accessible and data-scarcity does not allow for setting up hydrodynamic models, a standardised, integrative workflow was developed to perform first-order assessments of flood hazard exposure with respect to single flood types as well as multiple ones at low computational capacities. The approach is highly flexible and allows to evaluate flood-prone areas on regional and local scale, integrating local, high-quality data and, in its absence, regional or global substitutes, while it is independent of index values that are related to a specific unit of area or administrative boundaries (e.g. km^2, townships). Depending on the domain for which data is available and can be integrated, the approach may even allow to address societal and environmental vulnerability and risk if demographic and socio-economic datasets as well as information on environmental dynamics and pressures are included. Therefore, the workflow complements previous concepts of vulnerability and risk by detailing spatially resolved information (*Chapter 3*). Applying this approach in the hardly accessible Ayeyarwady Delta to assess its exposure to frequent (annual) monsoon flooding, episodic (occasional) storm-surge flooding and the rather long-term hazard of relative sea-level rise revealed up to 60 % of the delta (at present 5.4 million people) being at risk of monsoon flooding, 20 % of the delta (at present 658 000 people) at risk of storm surge flooding, and 30 % of the delta (at present 1.8 million people) at risk of relative sea-level rise, while agricultural fields are the most exposed land-use assets, pointing to challenges to sustain food security and livelihoods in case of flooding or permanent inundation (*Chapters 2 and 3*). Combining these single flood types allowed to quantify areas, population and land-use assets at risk of multiple flooding and revealed most exposed areas in the low-lying coastal range, covering >36 % of the deltaic area where at present 2 million people live (*Chapter 3*). Integrating both inland and coastal flood hazards revealed the most complete estimates of deltaic flood exposure (i.e., 70 % of the delta's area and at present 4.9 million people)

and – together with findings from assessments of single flood types – allow to attribute flood components. Moreover, mappings of single and multiple flood-type hazards may serve as validation data for existing global maps of pluvial and fluvial flooding as well as modelling studies (which are in the Ayeyarwady Delta yet to come). With the potential to integrate any further information into such as geomorphology, local elevation and vertical land motion, the workflow of flood hazard exposure assessment offers ways to further detail the characterisation of flood-prone areas. For example, findings of land elevation and elevation change indicate that areas at risk of multiple flooding coincide with the lowest elevated delta parts and southern deltaic hotspots of elevation loss (*Chapter 5*). This highlights the potential interconnectedness of flooding, land elevation and elevation loss in the Ayeyarwady Delta (*Chapters 2, 4.1 and 5*) and therefore provides valuable insights for initiating effective coping strategies, i.e. by taking measures that address drivers of elevation loss and minimise further loss.

6.2 Improving the understanding of coastal land elevation and vertical datums for reliable relative sea-level rise and flood impact and exposure assessments in data-sparse coastal lowlands

As the studies of this thesis have shown, proper integration of data on sea level, coastal land elevation and elevation dynamics is not straightforward yet and requires considerations to be made with respect to elevation assessment uncertainties such as data-inherent inaccuracy, vertical offsets between coastal land elevation and sea-level information, as well as context-related aspects such as coastal-deltaic elevation change (often in form of subsidence-dominated elevation loss) and sea-level rise (Seeger et al., 2023; Seeger and Minderhoud, in review; Seeger and Minderhoud, submitted). Therefore, the following subsections set out how uncertainties related to land elevation can be addressed in data-sparse coastal lowlands.

6.2.1 Bridging from geodesy to geography to overcome vertical reference issues in coastal lowlands

As the studies of this thesis have shown, proper integration of data on sea level, coastal land elevation and elevation dynamics is not straightforward yet and requires considerations to be made with respect to elevation assessment uncertainties such as data-inherent inaccuracy, vertical offsets between coastal land elevation and sea-level information, as well as context-related aspects such as coastal-deltaic elevation change (often in form of elevation loss due to subsidence dominating over vertical accretion) and sea-level rise (Seeger et al., 2023; Seeger and Minderhoud, in review; Seeger and Minderhoud, submitted). The omission of vertical datum alignment of coastal land and sea-level information, and consequently the presence of a vertical datum offset, has been shown to be one major source of uncertainty in elevation-based coastal impact and exposure assessments, and has particular high impacts for coastal lowlands in Southeast Asia (Seeger and Minderhoud, in review; Seeger and Minderhoud, submitted). The encountered widespread misuse of coastal elevation and sea-level data may be explained by the current constellation that leaves complex geodetic transformations required to use elevation data for coastal hazard assessments in the hands of non-specialised end users who are not familiar with the required post-processing steps (see details below; Seeger and Minderhoud, in review). Therefore, linking the coexistence of vertical datums for sea-level and elevation datasets used in coastal hazard and impact assessments together with the relevance of aligning them when combining datasets that use different vertical reference systems to the coastal-deltaic landscape serves as an illustrative concept to bridge between geodetical and geographical disciplines (Figure 6.1). The concept builds on equations and 2D-visualisiations of Seeger et al., (2023); Seeger and Minderhoud (in review) and Seeger and Minderhoud (submitted) and translates mathematical terms of vertical datum conversion steps into a 3D coastal-deltaic landscape view, acknowledging typical landscape features and processes (see also Minderhoud, 2019). Therewith, Figure 6.1 highlights how inadequate consideration of vertical datum alignment affects impact and exposure studies of relative sea-level rise and flooding.

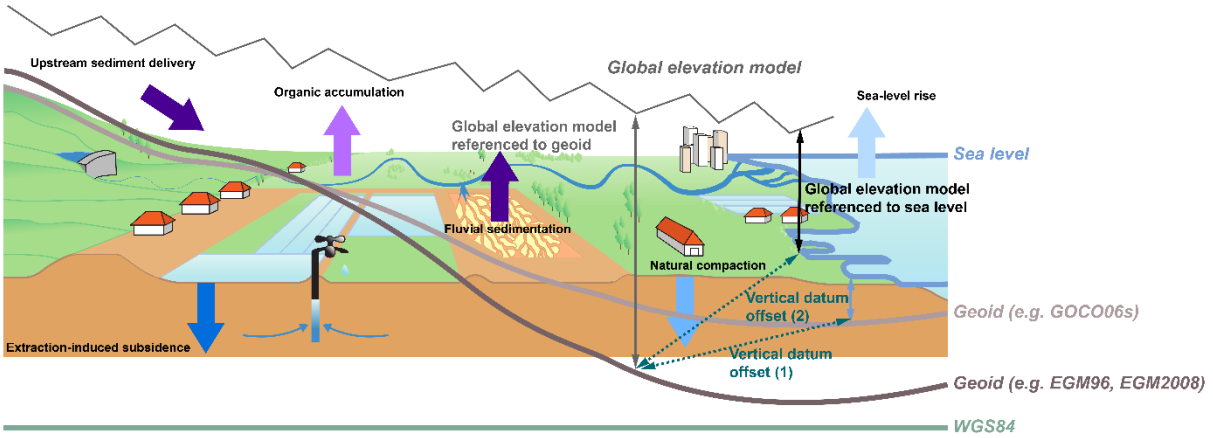


Figure 6.1 *| Relations between vertical reference systems in the coastal landscape. Global elevation models are often referenced to nowadays outdated geoids (such as EGM96 or EGM2008) that in data-sparse coastal lowlands underestimate sea-level height by up to 1 m. Dashed lines show the steps required to conduct vertical datum alignment of elevation and sea-level data, i.e. by aligning their respective vertical reference systems first before transposing elevation to sea level. See also Figure 4.13 for further details on relations between vertical reference systems. Visualisation based on Minderhoud (2019).*

To generate reliable impact and exposure assessments of relative sea-level rise and flooding and to strengthen existing studies where vertical datum alignment has not been considered so far, the puzzle of integrating information on sea level, land elevation and elevation dynamics needs to be solved. This is not trivial, especially for the data-sparse coastal lowlands in Southeast Asia, where global datasets, often suffering from inaccuracy, need to be used in the absence of local high-quality data, and where vertical datum offsets are particularly large (i.e. >1 m), thereby exceeding acceptable uncertainty ranges for those hazard assessments (e.g., Seeger and Minderhoud, in review; Seeger and Minderhoud, submitted). However, limitations in data-sparse coastal lowlands can be overcome. To allow for up-to-date impact and exposure assessments, land elevation needs to be properly referenced to an actual, local sea-level datum. Local tide gauges need to be checked carefully as they may be inadequate in capturing sea level in larger coastal areas under study, or if timeseries is incomplete, too short or outdated (Seeger et al., 2024). Latest available satellite-altimetry-derived products such as mean dynamic topography serve as an open-accessible substitute, performing at accuracies in the range of a few centimetres (e.g., Hamden et al., 2021; Taburet et al., 2022; Jousset et al., 2023; CMEMS, 2025). They allow to account for sea-level variations along the coast which makes them particularly favourable for coastal studies on large, regional to global scale (Seeger et al., 2023; Seeger et al., 2024).

Aligning coastal elevation and sea-level information requires to account for aligning their vertical reference systems first (Figures 4.13, 6.1, C3 and D5). Otherwise, an offset is maintained that yields incorrect outcomes of the conducted vertical datum conversion. Unlike

in the absence of datum conversion, offsets remaining in incorrect datum conversions may average out on global scale but become significant on local to regional scales (Seeger and Minderhoud, in review; Seeger and Minderhoud, submitted). Open-source online services such as the calculation service of the International Centre for Global Earth Models (ICGEM) from GFZ Helmholtz Centre for Geosciences (Ince et al., 2019) provide valuable platforms to obtain data on vertical reference systems, allowing for a variety of models, functional selections and filter applications. Gravitational field data on ellipsoidal grids is calculated based on the application-orientated settings that have been made and consistently maintained for the types of gravitational models needed. Offsets between those models are then calculated by simple subtractions and can be applied to transpose the elevation/sea-level dataset of interest (see also Seeger et al., 2023; Seeger and Minderhoud, in review). Despite the open availability of elevation, sea-level, geoid and ellipsoid data as well as online services, the application of vertical datum conversion in (data-sparse) coastal research contexts is still often not considered or performed properly.

Potential explanations for the encountered widespread omission of vertical datum alignment and the lack of individual processing steps by coastal impact and exposure assessments may lie in the complexity of handling several geodetical datasets in addition to those of land elevation and sea-level which requires to have a full understanding of the metadata in order to solve mathematical terms of datum conversion and alignment. Furthermore, it may be challenging to analyse lengthy data and metadata documentations for vertical datum information that might be hidden or not clearly documented, or when datum information is completely absent. Since large-scale, global land elevation and sea-level data is provided on global repositories in a global geoid or ellipsoid reference frame without informing end users from the coastal research and practice community on the applicability in coastal areas and constraints on vertical datum, obscures the need of post-processing and suggests the data being ready to use. There is the need to agree on a common definition of *sea level* in geodetical and geographical practices. Although theoretical works clearly distinguish between concepts and terms (e.g., Gregory et al., 2019), in practice, land elevation as well as bathymetry datasets referenced to (mean) sea level do not specify the time period, for which sea-level information was averaged, and how this sea-level datum relates to a global reference geoid or ellipsoid (e.g., Hastings and Dunbar, 1999; GEBCO Compilation Group, 2024). Though this research mainly focussed on the relations between coastal land elevation and sea level, indications for similar problems were found in studies using bathymetry data (such as for modelling flood impact), suggesting further future research and

critical reflection in those domains as well (Supplementary Data D1; Seeger and Minderhoud, in review). Disentangling the relations of vertical reference systems constitutes a critical task, particularly where different vertical reference systems of multiple datasets have to be unified. This may play a particular role for coastal-lowland studies that model present and future flood impacts and consider the integration of vertical land motion into relative sea-level rise projections, as they need to integrate land elevation change into elevation, which together with bathymetry needs to be properly aligned with sea-level information.

6.2.2 Accounting for uncertainties in coastal land elevation for reliable relative sea-level rise and flood impact assessments

Hypothesis 2 | Coastal land elevation is one of the main uncertainties in relative sea-level rise and flood impact assessments.

Goal 2.1 | Assessing land elevation in the Ayeyarwady Delta (Myanmar) and quantifying related data-driven uncertainties in sea-level rise impact assessment.

The new, local AD-DEM based on elevation data from topographic maps indicates an average delta plain elevation of ~1.3 m above local mean sea level. 10 commonly used global, space-borne elevation models were referenced to local mean sea level and compared to the local elevation data. Most global elevation datasets overestimate the delta's elevation by several metres. Errors statistics of best performing global elevation models (FABDEM v1.0 and CoastalDEM v2.1) are ~2 m while FABDEM v1.0 outperforms CoastalDEM v2.1 in indirect validation with monsoon flood maps (*Chapter 4.1*). As vertical datums were aligned before comparing local and global data, the determined height residuals can be mainly attributed to inaccuracy of the global elevation data itself, however, the impact of elevation change since data acquisition cannot be entirely excluded (*Chapters 4.1 and 4.3*). To investigate how the discrepancies of global and local elevation translate into sea-level rise impact assessment, IPCC AR6 scenarios for 2100 and 2150 were simulated. This also constitutes the first delta-wide assessment of sea-level rise impact. The 10 elevation datasets give a range of 0.1 % to >50 % of the delta to fall below sea level following 1.23 m sea-level rise by 2100 (i.e. 6200 to 3.8 million people as of 2020). Referring to the best performing global elevation datasets allows to narrow down the range to 30.7 % to 46.7 % of the delta (i.e. 1.7 to 2.9 million people as of 2020)

to fall below sea level. Districts in the lower central to southern delta part, namely Pyapon, Labutta and Myaugmya, are the most exposed. Following sea-level rise of 2.21 m, up to 67.50% of the delta (up to 5 million people as of 2020) could be drowned by 2150, thereby affecting also more inland districts. Highlighting the urgency to properly integrate (relative) sea-level rise into risk mitigation strategies, an improved elevation model is provided for follow-up hazard and impact assessments, which provides the best compromise of the high-accuracy AD-DEM and the best performing, high-resolution global elevation model (FABDEM v1.0) (*Chapter 4.1*).

Goal 2.2 | Evaluating shortcomings and errors in handling of coastal elevation and sea-level data in the vast majority of contemporary sea-level rise and coastal hazard impact assessments.

Inspired by findings from the Ayeyarwady and Mekong deltas (*Chapters 4.1 and 4.3*) where vertical datum offsets between global geoid models used by elevation data and sea level are in the range of ~1 m, together with evidence in the scientific literature of absent or incorrect vertical datum conversion, shortcomings and errors in handling of coastal elevation and sea-level data was systematically assessed. Based on an evaluation of 385 scientific publications (>53 % published in the last 5 years), >99 % of the evaluated assessments handled sea-level and land elevation data improperly and the most prominent error (25 % of the studies) was the neglection of datum conversion, followed by incomplete datum conversion (7 %). Consequently, actual sea-level height is underestimated by 0.2–0.5 m on average in coastal hazard assessments globally, regionally exceeding 1 m such as in Southeast Asia which is in line with findings from the Mekong Delta (*Chapters 4.2 and 4.3*). The use of properly aligned sea-level and elevation data reveals worldwide 37 % more area and 67 % more people (i.e. increase of 88 million to 132 million people) to fall below sea-level following 1 m relative sea-level rise than estimated by existing scientific assessments which have informed policymakers and negotiations up to international, intergovernmental level. The low-elevation coastal zone is 4–5 % larger and inhabited by more than 1 billion people. (*Chapter 4.2*).

Goal 2.3 | Quantifying and attributing uncertainties in land elevation assessment to vertical datum offset, data-inherent inaccuracy and elevation change since data acquisition.

Investigating the performance of elevation data in capturing coastal land elevation reveals vertical errors in the range of several metres that impede assessments of (relative) sea-level rise impact (*Chapter 4*). The uncertainties in coastal land elevation as indicated by elevation models were quantified for the Ayeyarwady Delta in terms of data-intrinsic inaccuracy (i) and, for most global elevation data, is several metres (*Chapter 4.1*). Vertical offsets between commonly used global geoid models and local sea level (ii) are on global average 0.2–0.5 m, locally exceeding 1 m (*Chapter 4.2*). By revisiting land elevation in the Mekong Delta, both sources of uncertainty ((i) and (ii)) were quantified; (i) based on validation with an updated local digital elevation model generated from elevation data from topographic maps (i.e. Topo DEM v2), and (ii) based on comparing the performance of all elevation data (both global elevation models and local elevation data) in the same vertical reference frame (i.e. mean sea level) and by comparing the performance of all elevation data while omitting the necessary vertical datum conversion (i.e. global elevation models are kept in their original reference system). The approach applied in the Mekong Delta allowed to attribute and quantify the sources causing uncertainties in a global elevation model to adequately represent the delta's local elevation. This assessment is not only crucial as it reveals the best performing elevation model for a certain area but also as it pinpoints errors in processing steps and indicates how much model performance (and its applicability) can be improved if certain processing steps are prioritised and properly applied (*Chapter 4.3*). (iii) Elevation change since data acquisition refers to the capability of an elevation model to adequately represent coastal-deltaic land elevation which will change significantly if over years, accumulated subsidence together with sea-level rise exceeds the data-inherent uncertainty. This source of uncertainty was tentatively assessed using non-linear extraction-induced land subsidence rates and available sea-level information from tide gauge. Though this source of uncertainty constitutes comparably the smallest one in the assessment for the Mekong Delta, relative maximum errors are observed for elevation models based on SRTM (i.e. 10–16 %) (*Chapter 4.3*). The more elevation models improve in accuracy, the larger are the relative impacts of neglected or incomplete vertical datum conversion and elevation change since data acquisition. However, as elevation data performance, vertical datum offsets and elevation change over time vary spatially (*Chapter 4*), the demonstrated open-data approach may set a benchmark to initiate similar assessments of DEM performance in other (data-sparse) coastal regions in the world (*Chapter 4.3*).

6.3 Paving the way for risk-sensitive development in the view of future flood risk and relative sea-level rise

Hypothesis 3 | The alignment of coastal land elevation, with integrated vertical land motion, and coastal sea level data is of paramount importance to conduct thorough coastal hazard and impact assessments.

Goal 3.1 | Understanding land elevation dynamics for strengthening coastal hazard and impact assessments in the Ayeyarwady Delta (Myanmar).

First results of delta-wide InSAR-based estimations of land elevation change (03/2017–10/2023) reveal a heterogenous pattern with moderate negative (e.g. elevation loss/subsidence) and positive elevation change (e.g. elevation gain/uplift) spread over the entire delta. Delta-wide average elevation change is -4 mm/yr, while areas of maximal elevation loss include the hotspot of Yangon City, where rates reach -100 mm/yr, as well as the northeastern delta and southern coastal range (*Chapter 5*). Our findings are in line with previous studies for Yangon City, whereas the coastal pattern of elevation loss resembles that of other deltas in the world, suggesting potentially similar driving mechanisms., As post-processing of the InSAR data is not completed yet and information on both potential natural and human drivers is sparse, relations between land elevation change and potential drivers were only tentatively determined. Potential natural drivers include tectonic strike-slip fault activity of the Sagaing Fault, natural compaction of young Quaternary alluvial sediments, local sediment erosion/accretion (contributing to elevation change) as well as seasonal to inter-annual variations due to changes in water load. Potential human drivers are urban expansion leading to increased loading by buildings, infrastructure and large constructions, as well as groundwater extraction (only documented in Yangon City) and, less clear, dynamically shifting agricultural land use as well as non-irrigated agriculture. Limitations induced by data sparsity culminate in this study and challenge to gain a comprehensive understanding of land subsidence for risk-sensitive delta development (*Chapter 5*). It is not possible to disentangle InSAR-estimated land elevation change into vertical land motion and sediment accretion/erosion components, neither to perform thorough investigations of land subsidence drivers such as groundwater extraction which is not monitored in the delta. Therefore, this study is a prime example of the key challenges yet to be overcome in the Asian deltas (Tables 2.1 and 2.2; *Chapter 2*).

Goal 3.2 | Bridging from geodesy to geography to overcome vertical datum issues in coastal lowlands.

Studies of this thesis revealed the significance of vertical datum alignment of coastal elevation and sea-level information as key for reliable coastal exposure and impact assessments (*Chapter 4*). Though all data and software needed to conduct vertical datum conversion properly is openly available, the encountered widespread omission of vertical datum alignment and the lack of individual processing steps by coastal impact and exposure assessments (*Chapter 4.2*) may be explained by the complexity of handling several geodetical datasets in addition to those of land elevation and sea-level which requires to have a full understanding of the metadata in order to solve mathematical terms of datum conversion and alignment. Providing a 3D visualisation that combines the relations between vertical reference systems in the coastal-deltaic landscape with the relevance why vertical reference systems of elevation and sea-level data need to be aligned in order to account for reliable coastal exposure and impact assessments may serve as a powerful step to bridge from geodesy to geography. While the foundation of this bridge has been built by the research and detailed workflow documentations of this thesis, extending this bridge will lie in linking also to other domains such as from oceanography and initiating an interdisciplinary dialogue to achieve a common understanding of sea-level datum and adequate documentation for topographic, bathymetric and sea-level data (*Chapter 6.2.1*).

Goal 3.3 | Paving the way for complementing coastal vulnerability and risk assessments to guide disaster risk reduction and coping strategies in the view of future flood risk and relative sea-level rise.

The research of this thesis forms a basis for assessments of coastal vulnerability and risk by providing fundamental information on flood hazard exposure and (relative) sea-level rise impact in the Ayeyarwady Delta and beyond, providing open-data workflows that allow to conduct these hazard exposure and impact assessments as well as quantifying and attributing uncertainties in elevation assessments.

Elaborating geophysical drivers and human pressures, their interlinkages as well as cascading impacts in the context of coastal flooding, furthermore available, transferable methodologies and key requirements to improve monitoring and modelling reveals a fundamental, comprehensive understanding of the interactions and complexities that deltas face in terms of coastal flooding (*Chapter 2*). Vulnerability and risk studies will benefit

from the informative value, for example by acknowledging these complex human-environmental interactions in their research set-up as well as in delta flood management.

The standardised, integrative workflow developed to perform first-order assessments of flood hazard exposure (*Chapter 3*) provides studies of vulnerability and risk with spatio-temporal information on single- and multiple flood-type hazards as well as spatially detailed information on population and assets at risk. Depending on the input data available, the workflow allows for an extension to supplement vulnerability and risk assessment, for example by the integration of demographic and socio-economic datasets such as household information and access to infrastructure, qualitative data, as well as information on environmental dynamics and pressures (*Chapter 3*).

As coastal elevation is one major determinant of hazard exposure, influencing flood depth and duration, the reliability of the elevation data used also affects the reliability of risk assessments as these often refer to flood depth as a measure of hazard in their calculation. Consequently, risk assessments will benefit from quantifying and attributing uncertainties in elevation assessments of elevation data (*Chapter 4*).

To move from vulnerability and risk assessments to risk-sensitive development, insights from land elevation change studies in the Ayeyarwady Delta (*Chapter 5*) will allow to consider the hazard of subsidence-dominated land elevation loss in the development of dynamic adaptive pathways for future disaster risk management in the delta. This will add to information established on elevation, sea-level rise and flood exposure, as well as disaster-risk driving land-use land cover changes and vulnerability (the latter both being addressed by human-geographical investigations of the research project) and will provide useful input to experts of various spatial scales, organisational structures, sectors, and governmental levels, to identify possible risk-sensitive adaptation strategies. Yet, a thorough understanding of drivers and processes in the context of land elevation change in the Ayeyarwady Delta is challenged by data sparsity (*Chapters 2 and 5*). However, previous works on properly aligning land elevation with actual sea level (Chapter 4), conducting first-order hazard assessments by integrating available data (*Chapter 3*), allow to include findings from land elevation change studies into updated hazard and exposure assessments, consequently updating assessments of environmental susceptibility and multiple flood risk. Generating scenarios of future elevation that integrate simulations of non-linear projections of vertical land motion and related elevation change into actual land elevation information relative to local sea level remains challenging for the Ayeyarwady

Delta (and likely will if data sparsity regarding potential drivers of vertical land motion and elevation change will remain) (*Chapter 5*).

Yet, the works of this research (*Chapters 2–5*) constitute first steps to solve individual pieces of the puzzle, revealing fundamental insights into the exposure of the Ayeyarwady Delta, while providing globally applicable workflows of flood hazard exposure and elevation uncertainty assessment that contribute to unravel the unknowns of flooding and relative sea-level rise and to solve challenges in their assessment in the world's data-sparse coastal lowlands.

6.4 Recommendations for further research

Based on the outcomes of this thesis, the following recommendations for further research are highlighted.

General needs:

- **Improvements in data collection and monitoring systems** in coastal-deltaic systems
  → e.g., including (but not limited to) establishment of groundwater monitoring in the Ayeyarwady Delta to unravel potential impacts on land subsidence
- **Improvements towards better dissemination and sharing of data** to ensure the data collection is meaningful and relevant
  → e.g., including (but not limited to) local (detailed) information on potential natural and anthropogenic drivers of vertical land motion/elevation change in the Ayeyarwady Delta in order to unravel root causes and processes of deltaic land subsidence and elevation loss

Prospects of future research in the context of improving the reliability of coastal exposure and impact assessments by accounting for uncertainties in land elevation assessment

- **Upscaling quantification and attribution of uncertainties in land elevation assessment** to global scale
  → the impact of vertical datum offset has already been assessed (*Chapter 4.2*)

→ recently published probabilistic vertical land motion reconstructions (Oelsmann et al., 2024) offer the potential for integration with quantifications of elevation uncertainty in order to estimate elevation change since data acquisition on global scale

- **Integrating land elevation dynamics into coastal land elevation information**
  → thereby accounting for linking spatio-temporal variability of vertical land motion and related elevation change with actual elevation relative to local sea level
  → thereby facilitating the projection of future elevation and elevation change and accounting for uncertainties in the elevation data
- **Providing continuous updates of elevation information with respect to actual local continuous sea level**
  → thereby ensuring that coastal elevation information is actual and properly aligned with actual sea-level information
  → thereby account for the widespread misuse of sea-level and elevation data within the wide scientific community
- **Continuing initiatives to bridge between geodesy and geography**
  → Raising awareness of the need to adequately document vertical (sea-level) datum for topographic, bathymetric and sea-level data (including specifications of time, location, datasets and further contextual metadata information that might be relevant)
  → Providing a guide of considerations to be made when handling coastal elevation and sea-level data as well as criteria to be checked when performing elevation-based coastal assessments (some of these considerations have been addressed for policymakers by Seeger et al., 2024; however, this policy brief does not include point-by-point instructions nor a checklist which will be done for the coastal research and practice community)
  → Promoting an interdisciplinary dialogue to achieve a common understanding of sea-level datum(s) with respect to the dissemination and application of topographic, bathymetric and sea-level data

References

Copernicus Marine Environment Monitoring Service (CMEMS), 2025. Sea Level TAC – DUACS products. https://documentation.marine.copernicus.eu/QUID/CMEMS-SL-QUID-008-032-068.pdf (last access: 7 July 2025)

GEBCO Compilation Group, 2024. GEBCO‘s global gridded bathymetric data sets. https://www.gebco.net/sites/default/files/documents/GEBCO_grid_2024.pdf (last access: 7 July 2025)

Gregory, J. M., Griffies, S. M., Hughes, C. W., Lowe, J. A., Church, J. A., Fukimori, I., Gomez, N., Kopp, R. E., Landerer, F., Le Cozannet, G., Ponte, R. M., Stammer, D., Tamisiea, M. E., & van de Wal, R. S. W., 2019. Concepts and terminology for sea level: Mean, variability and change, both local and global. *Surveys in Geophysics*, *40*, 1251–1289. https://doi.org/10.1007/s10712-019-09525-z.

Hamden, M. H., Din, A. H. M., Wijaya, D. D., Yusoff, M. Y. M., Pa'suya, M. F., 2021. Regional mean sea surface and mean dynamic topography models around Malaysian seas developed from 27 years of along-track multi-mission satellite altimetry data. *Frontiers in Earth Science*, 9, 665876. https://doi.org/10.3389/feart.2021.665876.

Hastings, D.A., Dunbar, P.K., 1999. Global Land One-kilometer Base Elevation (GLOBE) Digital Elevation Model, Documentation, Volume 1.0. Key to Geophysical Records Documentation (KGRD) 34. National Oceanic and Atmospheric Administration, National Geophysical Data Center, 325 Broadway, Boulder, Colorado 80303, U.S.A. https://repository.library.noaa.gov/view/noaa/13424/noaa_13424_DS1.pdf (last access: 7 July 2025)

Ince, E. S., Barthelmes, F., Reißland, S., Elger, K., Förste, C., Flechtner, F., Schuh, H., 2019. ICGEM – 15 years of successful collection and distribution of global gravitational models, associated services and future plans. *Earth Sys. Sci. Data*, 11, 647–674, https://doi.org/10.5194/essd-11-647-2019.

Jousset, S., Mulet, S., Greiner, E., Wilkin, J., Vidar, L., Dibarboure, G., Picot, N., 2023. New Global Mean Dynamic Topography CNES-CLS-22 Combining Drifters, Hydrological Profiles and High Frequency Radar Data. *ESS Open Archive*, https://doi.org/10.22541/essoar.170158328.85804859/v2.

Minderhoud, P. S. J., Coumou, L., Erkens, G., Middelkoop, H., Stouthamer, E., 2019. Mekong delta much lower than previously assumed in sea-level rise impact assessments, *Nature Communications*, 10 (3847), 1–13, https://doi.org/10.1038/s41467-019-11602-1.

Oelsmann, J., Marcos, M., Passaro, M., Sanchez, L., Dettmering, D., Dangendorf, S., Seitz, F., 2024. Regional variations in relative sea-level changes influenced by nonlinear vertical land motion. *Nature Geoscience*, *17*(2), 137–144. https://doi.org/10.1038/s41561-023-01357-2.

Seeger, K., Minderhoud, P.S.J., Peffeköver, A., Vogel, A., Brückner, H., Kraas, F., Nay Win Oo, Brill, D., 2023. Assessing land elevation in the Ayeyarwady Delta (Myanmar) and its relevance for studying sea level rise and delta flooding. *Hydrology and Earth System Sciences*, 27 (11), 2257–2281. https://doi.org/10.5194/hess-27-2257-2023.

Seeger, K., Minderhoud, P.S.J., Hauser, L.T., Teatini, P., Woillez, M.-N., 2024. How to assess coastal flood risk in data-sparse coastal lowlands? Accurate information on land elevation is key. *A Question of development*, 71, 1–4. https://www.afd.fr/en/ressources/how-assess-coastal-flood-risk-data-sparse-coastal-lowlands-accurate-information-land-elevation-key.

Seeger, K., Minderhoud, P.S.J., in review. Sea level much higher than assumed in most coastal hazard assessments. *Nature*, 2025-02-05097A.

Seeger, K., Minderhoud, P.S.J., submitted. Attributing uncertainties in elevation assessments for data-sparse coastal lowlands using global elevation models: A globally applicable approach showcasing the Vietnamese Mekong Delta. *Scientific Reports*.

Taburet, G., Ballarotta, M., Pujol, M-I., Legeais, J-F., Maillard, G., Durand, C., Dagneaux, Q., Lievin, M., Faugère, Y., Dibarboure, G., 2022. 28 Years of Reprocessed Sea Level Altimetry Products. 2022 Ocean Surface Topography Science Team (OSTST) meeting, October 31 – November 4, 2022, Venice, Italia. https://doi.org/10.24400/527896/a03-2022.3257.

Appendix A – Supplement to Chapter 2

This Supplement is related to: Becker, M., **Seeger, K.**, Paszkowski, A., Marcos, M., Papa, F., Almar, R., Bates, P., France-Lanord, C., Hossain, Md S., Khan, Md J.U., Karegar, M.A., Karpytchev, M., Long, N., Minderhoud, P.S.J., Neal, J., Nicholls, R.J., Syvitski, J., 2024. *Coastal Flooding in Asian Megadeltas: Recent Advances, Persistent Challenges, and Call for Actions Amidst Local and Global Changes*. Reviews of Geophysics, 62 (4), e2024RG000846. https://doi.org/10.1029/2024RG000846.

The supplementary material is published along with the scientific article under a CC-BY-NC-ND 4.0 Attribution-NonCommercial-NoDerivatives 4.0 International licence (https://creativecommons.org/licenses/by-nc-nd/4.0/) and is therefore not included as a supplement in the thesis publication. The reader is referred to access the content of this supplement via the article doi provided above. Throughout this thesis, any references to supplementary material of this chapter/article are prefixed with ‘A’.

Appendix B – Supplement to Chapter 3

This Supplement is related to: **Seeger, K.**, Peffeköver, A., Minderhoud, P.S.J., Vogel, A., Brückner, H., Kraas, F., Nay Win Oo, Brill, D., 2024. *Evaluating flood hazards in data-sparse coastal lowlands: highlighting the Ayeyarwady Delta (Myanmar)*. Environmental Research Letters, 19 (8), 084007. https://doi.org/10.1088/1748-9326/ad5b07.

The supplementary material is published along with the scientific article under a CC-BY 4.0 Attribution 4.0 International licence (http://creativecommons.org/licenses/by/4.0/). The reader can access the content of this supplement here (https://iopscience.iop.org/article/10.1088/1748-9326/ad5b07/data) and also via the article doi provided above. The supplementary material was not modified; only the thesis layout was adopted.

B1. Further contextual and methodological information

Table B1 *| Overview of flood events that impacted Myanmar in the last ~20 years.*
Data are based on MODIS data and were taken from the Global Flood Database of Tellman et al. (2021). Note that population estimates refer to the total population affected by individual flood events and therefore include also people of neighbouring countries.

Flood	Exposed	Displaced	Killed	Duration (d)	Cause
21/06/2002	7,191,176	15,000,000	503	68	Heavy rain
17/08/2002	332,167	5,000	0	18	Heavy rain
18/08/2002	5,200,419	400,000	65	101	Heavy rain
17/09/2002	1,997,756	3,000	1	77	Heavy rain
20/01/2003	469,893	1,500	1	21	Heavy rain
11/06/2003	16,822,143	9,500,000	600	121	Heavy rain
19/06/2003	231,399	20,000	55	14	Heavy rain
02/07/2003	1,112,750	0	0	61	Heavy rain
12/09/2003	385,965	10,000	7	30	Heavy rain
17/10/2003	590,850	3,000	3	19	Heavy rain
14/04/2004	1,543,959	50,000	12	19	Heavy rain
20/06/2004	19,855,086	40,000,000	3,000	109	Heavy rain
06/08/2004	815,647	60,000	11	58	Heavy rain
10/12/2004	117,937	20,000	15	8	Heavy rain
07/07/2005	5,365,759	3,000,000	40	20	Heavy rain
13/08/2005	9,186,959	119,270	11	44	Heavy rain
26/09/2005	857,249	470,000	104	10	Tropical storm/surge
23/11/2005	161,585	700,000	69	50	Heavy rain
10/02/2006	82,804	7,000	3	8	Heavy rain
29/04/2006	156,341	800	21	6	Tropical storm/surge

31/05/2006	4,485,860	600,000	21	54	Heavy rain
20/08/2006	2,041,812	2,000,000	195	116	Heavy rain
04/05/2007	76,856	0	5	5	Heavy rain
11/06/2007	4,536,692	80,000	126	13	Heavy rain
06/07/2007	588,181	3,000	0	26	Heavy rain
12/07/2007	21,488,636	11,100,000	96	90	Heavy rain
18/07/2007	844,212	10,000	170	26	Heavy rain
21/07/2007	27,712,991	5,000,000	1,071	86	Heavy rain
14/08/2007	1,326,841	40,000	2	51	Heavy rain
05/09/2007	999,066	17,000	10	67	Heavy rain
17/10/2007	4,006,102	30,000	2	7	Heavy rain
15/11/2007	5,454,831	3,000,000	3,447	16	Tropical storm/surge
03/05/2008	999,917	1,500,000	100,000[1]	19	Tropical storm/surge
24/05/2008	487,789	0	0	4	Heavy rain
05/07/2008	6,736,689	70,000	350	9	Heavy rain
11/08/2008	234,027	4,000	130	9	Tropical storm/surge
30/08/2008	5,622,068	1,000,000	900	9	Heavy rain
11/09/2008	336,537	0	0	23	Heavy rain
18/08/2009	2,078,688	300,000	0	9	Heavy rain
15/06/2010	2,199,055	0	60	11	Heavy rain
01/07/2010	5,396,863	600,000	0	12	Heavy rain
20/09/2010	212,350	0	2	10	Heavy rain
01/10/2010	19,362,985	500,000	15	11	Tropical storm/surge
23/03/2011	183,922	84,000	59	18	Heavy rain
01/01/2012	493,124	1,000	0	8	Heavy rain
12/09/2012	2,618,604	3,000	0	14	Heavy rain
30/09/2013	996,671	982,799	42	14	Heavy rain
11/07/2014	1,723	500	0	3	Heavy rain
07/11/2014	89,353	1,000	0	9	Heavy rain
20/12/2014	100,896	215,000	34	12	Heavy rain
15/07/2015	536,753	85,400	88	35	Heavy rain
20/04/2016	1,695,401	3,000	18	11	Heavy rain
01/06/2016	1,387,481	25,000	16	76	Heavy rain
18/07/2016	24,903	441	0	1	Heavy rain
25/07/2016	18,456,496	25,000	42	32	Heavy rain
15/08/2016	54,322	0	0	11	Heavy rain
01/12/2016	175,143	0	11	6	Heavy rain
31/12/2016	254,312	1,000,000	96	38	Heavy rain
02/06/2017	1,050,681	113	6	31	Heavy rain
10/08/2017	13,271,467	300,000	117	16	Heavy rain
15/06/2018	1,207,989	1,000	1	5	Heavy rain
15/07/2018	1,209,418	120,000	11	26	Heavy rain

Processing details on flood mapping in Google Earth Engine

The extents of recent flood events were mapped using Synthetic Aperture Radar (SAR) data from the Sentinel-1 mission. The mission provides free-available SAR data (since October 2014) at high temporal (6–12 days) and spatial resolution (10 m) and therefore offers favourable

[1] Note that according to other studies, death toll due to tropical cyclone Nargis exceeded estimates of Tellman et al. (2021) and report more than 138,000 fatalities (Webster., 2008; Fritz et al., 2009).

datasets to investigate flood dynamics at high spatio-temporal resolution. The radar satellite actively transmits radio pulses at long wavelengths (mostly in the microwave range of the electromagnetic spectrum) which enables data acquisition independent of daylight and weather conditions, making it highly proficient to capture flood events that occur under cloud cover such as during the monsoon season or storm events associated with rain bands and/or a dense cirrus shield (e.g. Lin et al. 2016; Notti et al., 2018; Shen et al., 2019).

The flood events in the Ayeyarwady Delta during the last ~10 years were mainly associated with monsoon precipitation and river discharge. For this reason, our investigations focused on months of the monsoon season, i.e. from May to October. Monthly flood extents were mapped for the years of 2015 to 2023 using the cloud computing platform of Google Earth Engine (GEE; Gorelick et al., 2017). Given the vast array of flood mapping and change detection approaches and scripts that have been published since the breakthrough of GEE (e.g. Moharrami et al., 2021; Tripathy and Malladi, 2022; Hamidi et al., 2023), we used the open accessible GEE script of the United Nations Platform for Space-based Information for Disaster Management and Emergency Response (UN-SPIDER) program for delineating flooding extents (UN-SPIDER, no date). By applying a pixel-based image rationing approach of Sentinel-1 imagery before and during flooding, monthly flood extents were estimated for the delta area as defined by Tessler et al. (2015). To retrieve images for time periods without flood occurrence, all imagery within February was selected for each year as – being in the middle of the dry season – natural flood probability in February is very low (Figures B1–B9). For collecting images during months of the monsoon season (i.e., May to October), first and last days of each month were selected to define the respective time frame (Table B2). From the Interferometric Wide (IW) swath mode of Sentinel 1, we used high resolution Ground Range Detected (GRD) images (10 m spatial resolution) with VH polarisation that reveals higher accuracy in capturing flood events (also related to precipitation) than VV polarisation (e.g. Clement et al., 2017; Conde and De Mata Muñoz, 2019; Bekele et al., 2022). We included images recorded from the descending track. The GRD images in GEE were already pre-processed in terms of applying orbit file, removing GRD border noise and thermal noise, applying a radiometric calibration and orthorectification. In addition, pre-processing included the conversion of the backscatter coefficient (0σ) to decibels (Gorelick et al., 2017). After mosaicking and clipping scenes to the region of interest, speckle noise was reduced by applying a smoothing filter using a focal mean of 50 m radius. Subsequently, an image rationing approach was applied to determine the changes between imagery from individual months during the monsoon season relative to the imagery from the

dry season. By reclassifying the resulting difference image using a pixel threshold, monthly flooded areas were delineated. Image ratios exceeding a value of 1 indicate a change detected between the two considered time periods. Different pixel thresholds were tested by comparing the resulting flood delineations with results from emergency mappings (e.g. Copernicus Emergency Management Service, 2015). A pixel threshold value of 1.3 provided the best results and compromise in solving the challenge of defining a single threshold for the large size of the study area extending over five Sentinel frames (Shen et al., 2019). The pixel-based delineated flood extent was refined by additional datasets such as the Global Surface Water layer (Pekel et al., 2016) to exclude permanent and nearly permanent water bodies, i.e., areas covered by water for >10 months per year. To reduce noise effects in the output, all pixels connected to 8 or less neighbouring pixels were removed. Finally, slopes inclined by more than 5 % as indicated by the HydroSHEDS digital elevation model (Lehner et al., 2008) were eliminated to remove false pixels resulting from fore slopes of hills and the Rakhine Mountains starting to rise in the westernmost part of the Ayeyarwady Delta (Hess et al., 1990; Long et al., 2014).

Table B2 *| Time frames of Sentinel-1 data acquired for determining monthly flood extents during the monsoon season from 2015 to 2023.*
Before = reference month from the dry season. After = investigated month from the monsoon season. Start and End refer to the timing of the first and last Sentinel dataset acquired and included into flood mapping. As images were not always available throughout the investigation period due to discontinuous sensing of the Sentinel satellite, comments on spatial coverage are provided.

2015

Before (Start)	*Before (End)*	*After (Start)*	*After (End)*	*Coverage*
09/02/2015	16/02/2015	11/05/2015	16/05/2015	Western and Eastern tracks
09/02/2015	16/02/2015	04/06/2015	09/06/2015	Western and Eastern tracks
09/02/2015	16/02/2015	03/07/2015	22/07/2015	Western and Eastern tracks
09/02/2015	16/02/2015	15/08/2015	15/08/2015	only Eastern track
09/02/2015	16/02/2015	08/09/2015	13/09/2015	Western and Eastern tracks
09/02/2015	16/02/2015	02/10/2015	31/10/2015	Western and Eastern tracks

2016

Before (Start)	*Before (End)*	*After (Start)*	*After (End)*	*Coverage*
04/02/2016	23/02/2016	05/05/2016	29/05/2016	Western and Eastern tracks
04/02/2016	23/02/2016	03/06/2016	27/06/2016	only Western track
04/02/2016	23/02/2016	04/07/2016	28/07/2016	Western and Eastern tracks
04/02/2016	23/02/2016	09/08/2016	21/08/2016	Western and Eastern tracks
04/02/2016	23/02/2016	02/09/2016	26/09/2016	Western and Eastern tracks
04/02/2016	23/02/2016	01/10/2016	25/10/2016	Western and Eastern tracks

2017

Before (Start)	*Before (End)*	*After (Start)*	*After (End)*	*Coverage*
05/02/2017	22/02/2017	05/05/2017	29/05/2017	only Western track
05/02/2017	22/02/2017	10/06/2017	22/06/2017	only Western track
05/02/2017	22/02/2017	04/07/2017	28/07/2017	only Western track

05/02/2017	22/02/2017	09/08/2017	21/08/2017	only Western track
05/02/2017	22/02/2017	02/09/2017	14/09/2017	only Western track
05/02/2017	22/02/2017	08/10/2017	20/10/2017	only Western track

2018

Before (Start)	*Before (End)*	*After (Start)*	*After (End)*	*Coverage*
05/02/2018	17/02/2018	12/05/2018	24/05/2018	only Western track
05/02/2018	17/02/2018	05/06/2018	30/06/2018	only Western track
05/02/2018	17/02/2018	05/07/2018	29/07/2018	only Western track
05/02/2018	17/02/2018	04/08/2018	29/08/2018	only Western track
05/02/2018	17/02/2018	03/09/2018	27/09/2018	only Western track
05/02/2018	17/02/2018	03/10/2018	28/10/2018	only Western track

2019

Before (Start)	*Before (End)*	*After (Start)*	*After (End)*	*Coverage*
01/02/2019	25/02/2019	01/05/2019	25/05/2019	Western and Eastern tracks
01/02/2019	25/02/2019	01/06/2019	30/06/2019	Western and Eastern tracks
01/02/2019	25/02/2019	06/07/2019	31/07/2019	Western and Eastern tracks
01/02/2019	25/02/2019	05/08/2019	29/08/2019	Western and Eastern tracks
01/02/2019	25/02/2019	04/09/2019	29/09/2019	Western and Eastern tracks
01/02/2019	25/02/2019	04/10/2019	29/10/2019	Western and Eastern tracks

2020

Before (Start)	*Before (End)*	*After (Start)*	*After (End)*	*Coverage*
01/02/2020	25/02/2020	01/05/2020	31/05/2020	only Western track
01/02/2020	25/02/2020	07/06/2020	30/06/2020	Western and Eastern tracks
01/02/2020	25/02/2020	06/07/2020	31/07/2020	Western and Eastern tracks
01/02/2020	25/02/2020	05/08/2020	30/08/2020	Western and Eastern tracks
01/02/2020	25/02/2020	04/09/2020	29/09/2020	Western and Eastern tracks
01/02/2020	25/02/2020	04/10/2020	29/10/2020	Western and Eastern tracks

2021

Before (Start)	*Before (End)*	*After (Start)*	*After (End)*	*Coverage*
01/02/2021	26/02/2021	02/05/2021	26/05/2021	Western and Eastern tracks
01/02/2021	26/02/2021	01/06/2021	26/06/2021	Western and Eastern tracks
01/02/2021	26/02/2021	01/07/2021	31/07/2021	Western and Eastern tracks
01/02/2021	26/02/2021	01/08/2021	31/08/2021	Western and Eastern tracks
01/02/2021	26/02/2021	05/09/2021	30/09/2021	Western and Eastern tracks
01/02/2021	26/02/2021	05/10/2021	30/10/2021	Western and Eastern tracks

2022

Before (Start)	*Before (End)*	*After (Start)*	*After (End)*	*Coverage*
03/02/2022	27/02/2022	03/05/2022	27/05/2022	Western and Eastern tracks
03/02/2022	27/02/2022	03/06/2022	27/06/2022	Western and Eastern tracks
03/02/2022	27/02/2022	02/07/2022	26/07/2022	Western and Eastern tracks
03/02/2022	27/02/2022	02/08/2022	31/08/2022	Western and Eastern tracks
03/02/2022	27/02/2022	07/09/2022	24/09/2022	Western and Eastern tracks
03/02/2022	27/02/2022	01/10/2022	30/10/2022	Western and Eastern tracks

2023

Before (Start)	*Before (End)*	*After (Start)*	*After (End)*	*Coverage*
03/02/2023	27/02/2023	05/05/2023	29/05/2023	only Eastern track
03/02/2023	27/02/2023	22/06/2023	22/06/2023	only Eastern track

03/02/2023	27/02/2023	16/07/2023	16/07/2023	only Eastern track
03/02/2023	27/02/2023	09/08/2023	21/08/2023	Western and Eastern tracks
03/02/2023	27/02/2023	02/09/2023	26/09/2023	Western and Eastern tracks
03/02/2023	27/02/2023	08/10/2023	20/10/2023	only Eastern track

B2. Results and discussion

B2.1 Precipitation and runoff patterns from 2015 to 2023

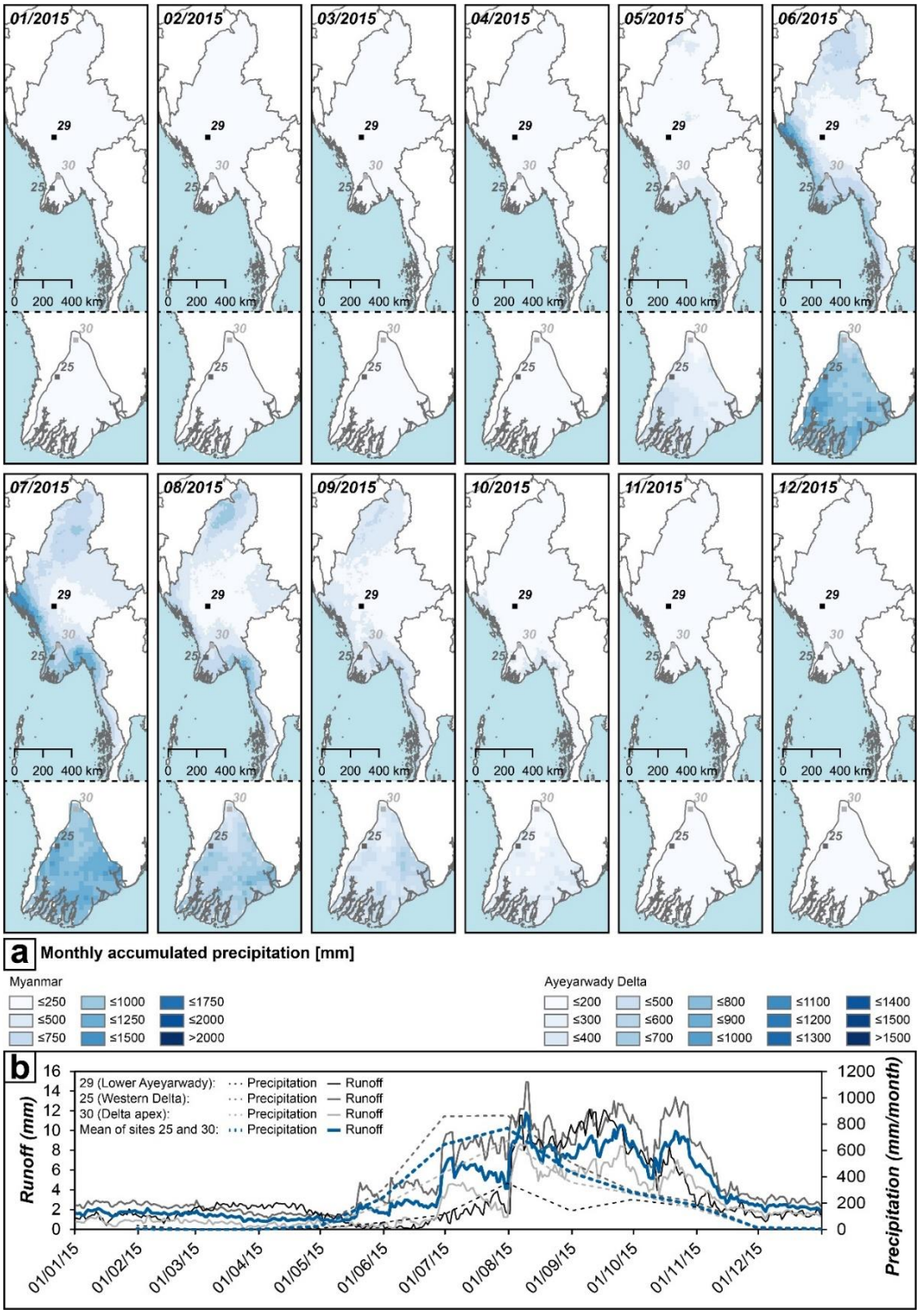


***Figure B1** | Precipitation (a) and runoff patterns (b) in Myanmar and the Ayeyarwady Delta in 2015 based on the GPM_3IMERGM_ v06 product (0.1°; Huffman et al., 2019) and River and Reservoir Watch Version 4.5 (Brakenridge et al., 2023a, 2023b, 2023c). Locations of RiverWatch 4.5 sites 25, 29, and 30 are shown in (a).*

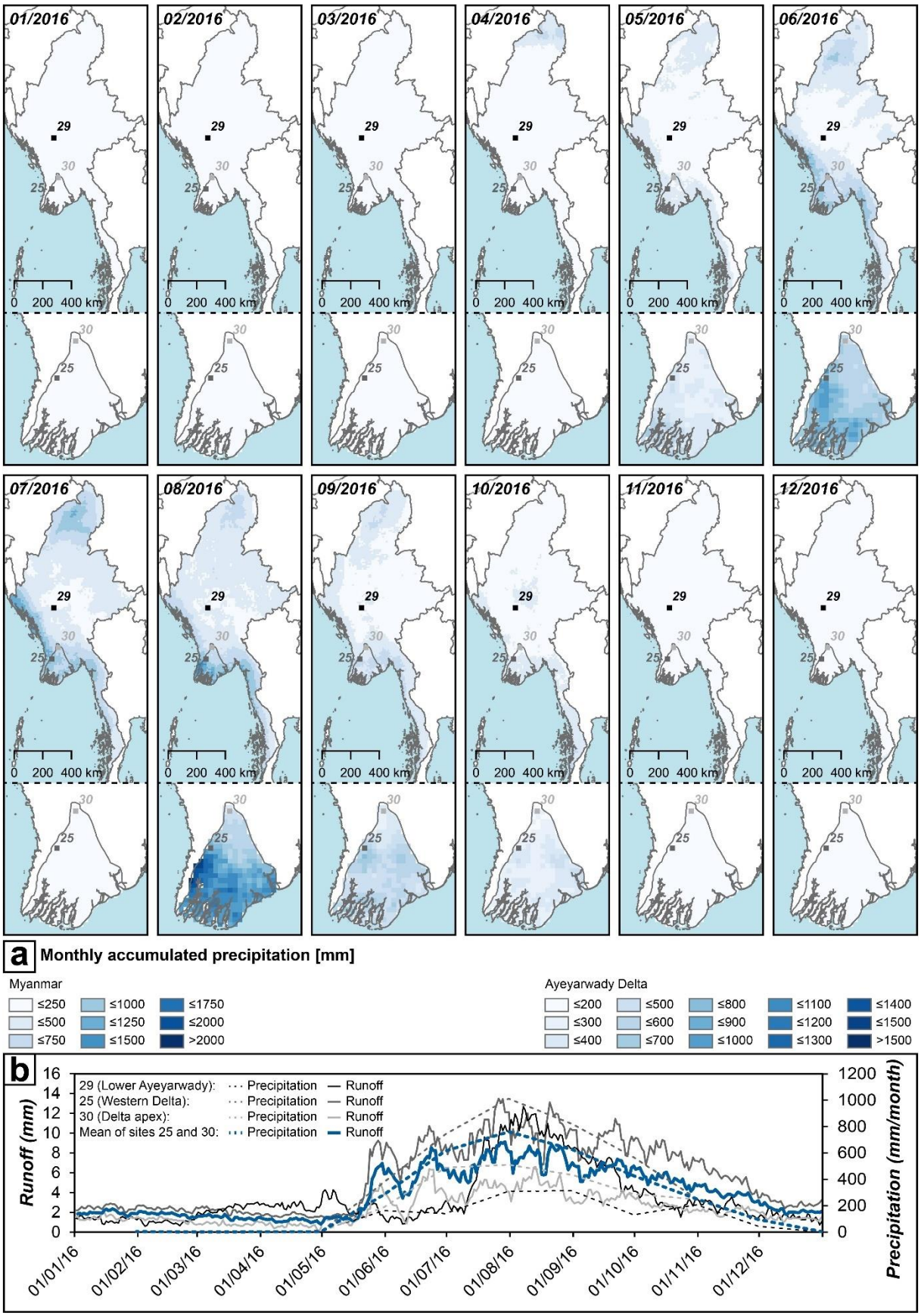


***Figure B2** | Precipitation (a) and runoff patterns (b) in Myanmar and the Ayeyarwady Delta in 2016 based on the GPM_3IMERGM_ v06 product (0.1°; Huffman et al., 2019) and River and Reservoir Watch Version 4.5 (Brakenridge et al., 2023a, 2023b, 2023c). Locations of RiverWatch 4.5 sites 25, 29, and 30 are shown in (a).*

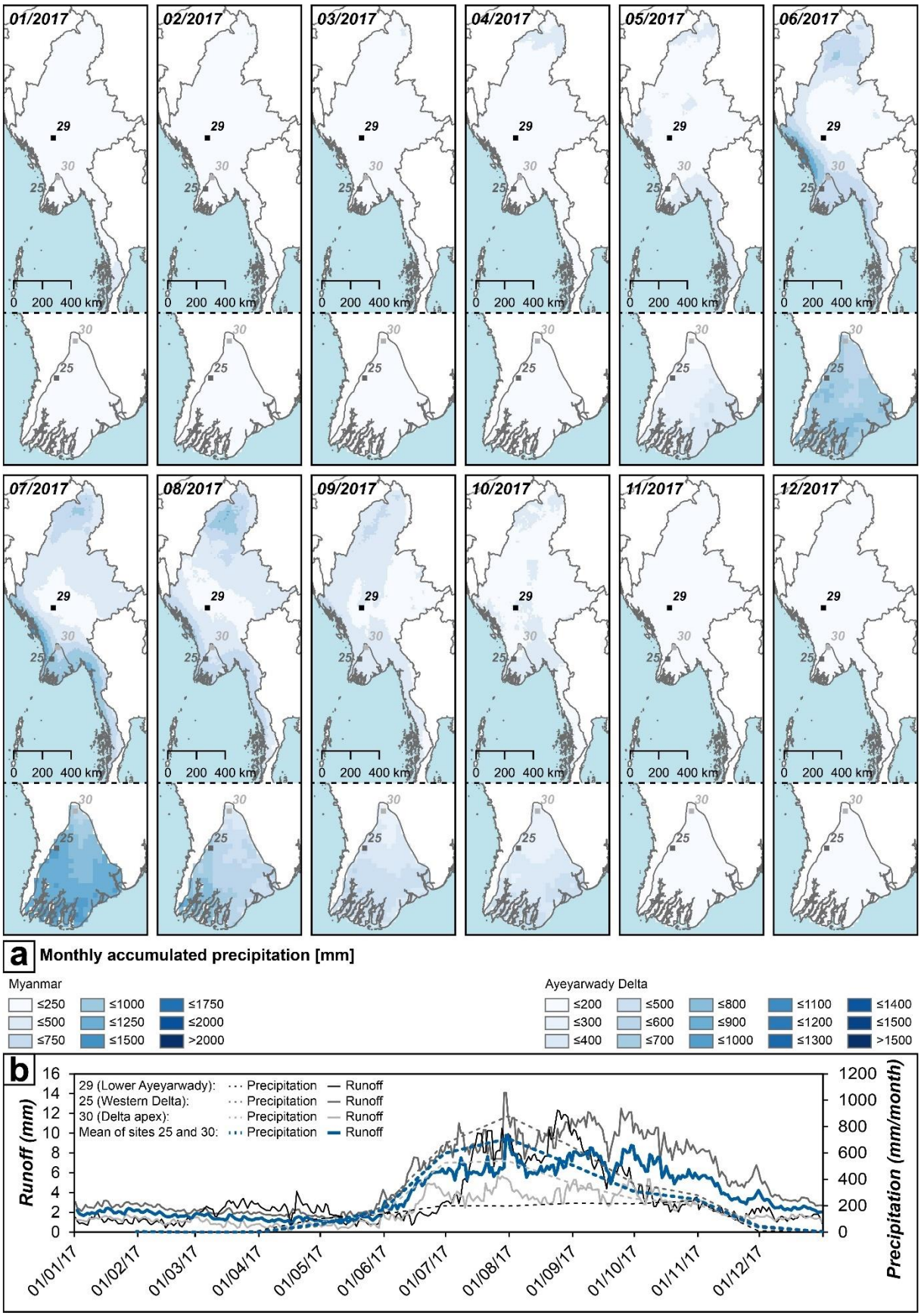


***Figure B3** | Precipitation (a) and runoff patterns (b) in Myanmar and the Ayeyarwady Delta in 2017 based on the GPM_3IMERGM_ v06 product (0.1°; Huffman et al., 2019) and River and Reservoir Watch Version 4.5 (Brakenridge et al., 2023a, 2023b, 2023c). Locations of RiverWatch 4.5 sites 25, 29, and 30 are shown in (a).*

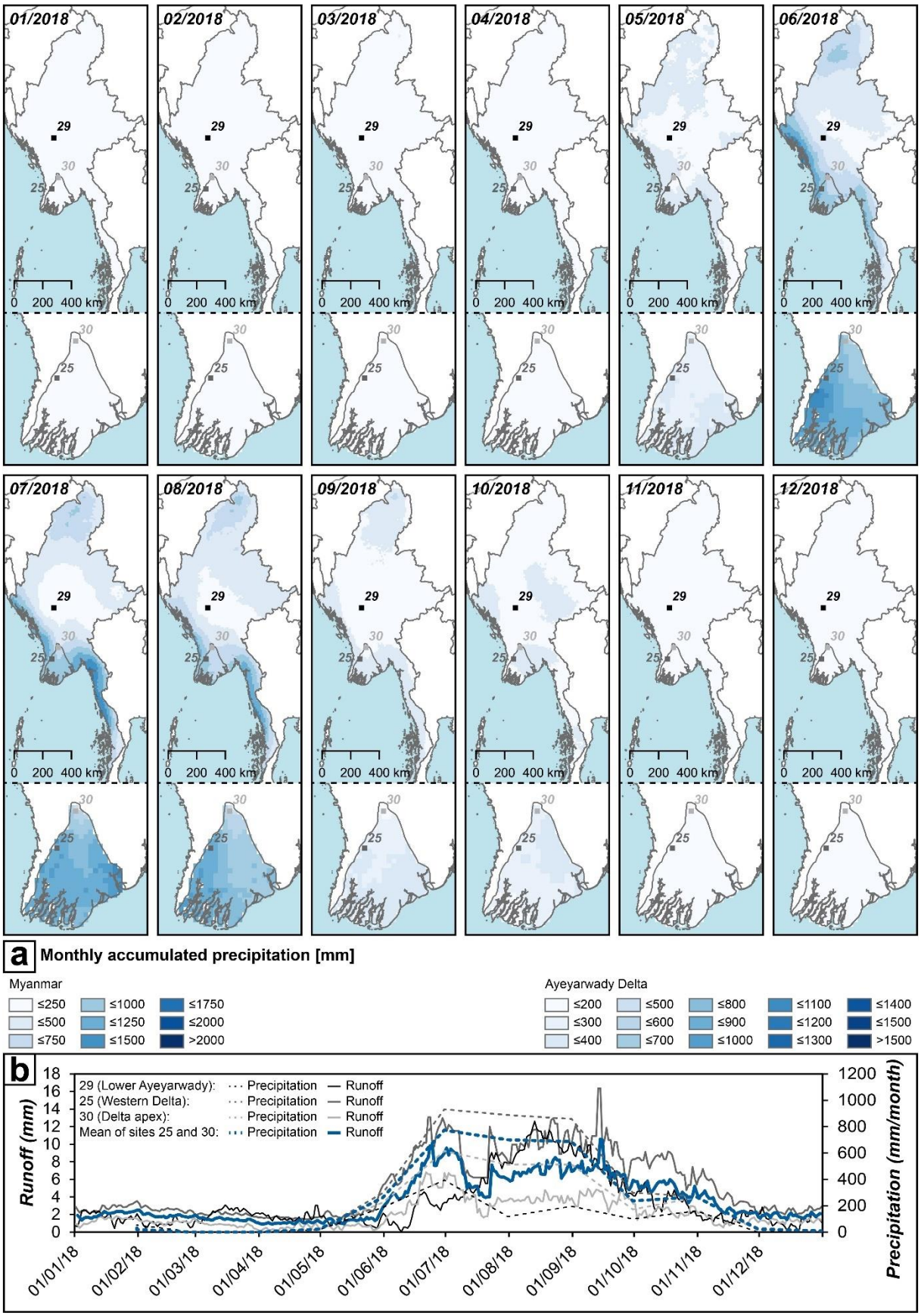


***Figure B4** | Precipitation (a) and runoff patterns (b) in Myanmar and the Ayeyarwady Delta in 2018 based on the GPM_3IMERGM_ v06 product (0.1°; Huffman et al., 2019) and River and Reservoir Watch Version 4.5 (Brakenridge et al., 2023a, 2023b, 2023c). Locations of RiverWatch 4.5 sites 25, 29, and 30 are shown in (a).*

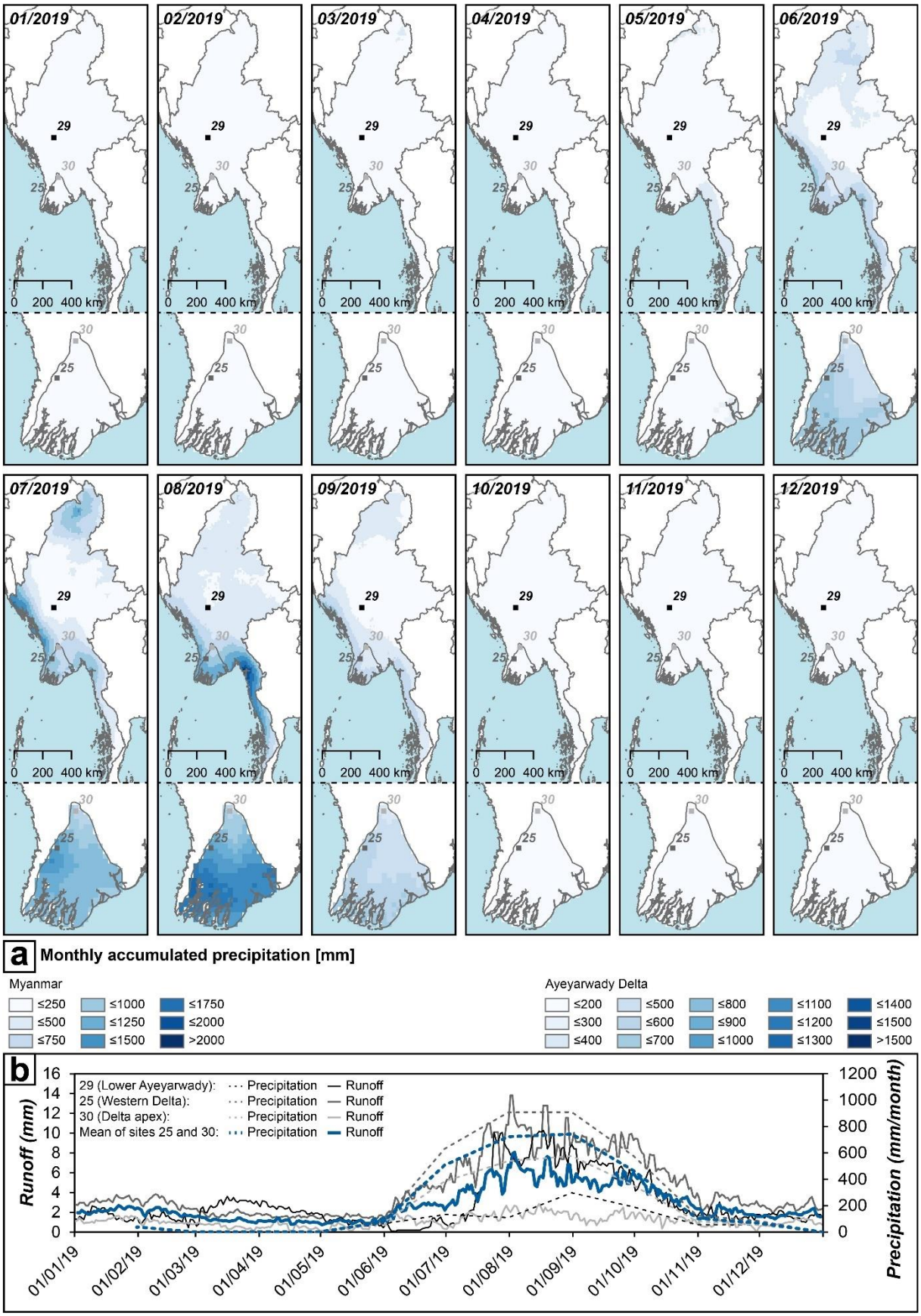


***Figure B5** | Precipitation (a) and runoff patterns (b) in Myanmar and the Ayeyarwady Delta in 2019 based on the GPM_3IMERGM_ v06 product (0.1°; Huffman et al., 2019) and River and Reservoir Watch Version 4.5 (Brakenridge et al., 2023a, 2023b, 2023c). Locations of RiverWatch 4.5 sites 25, 29, and 30 are shown in (a).*

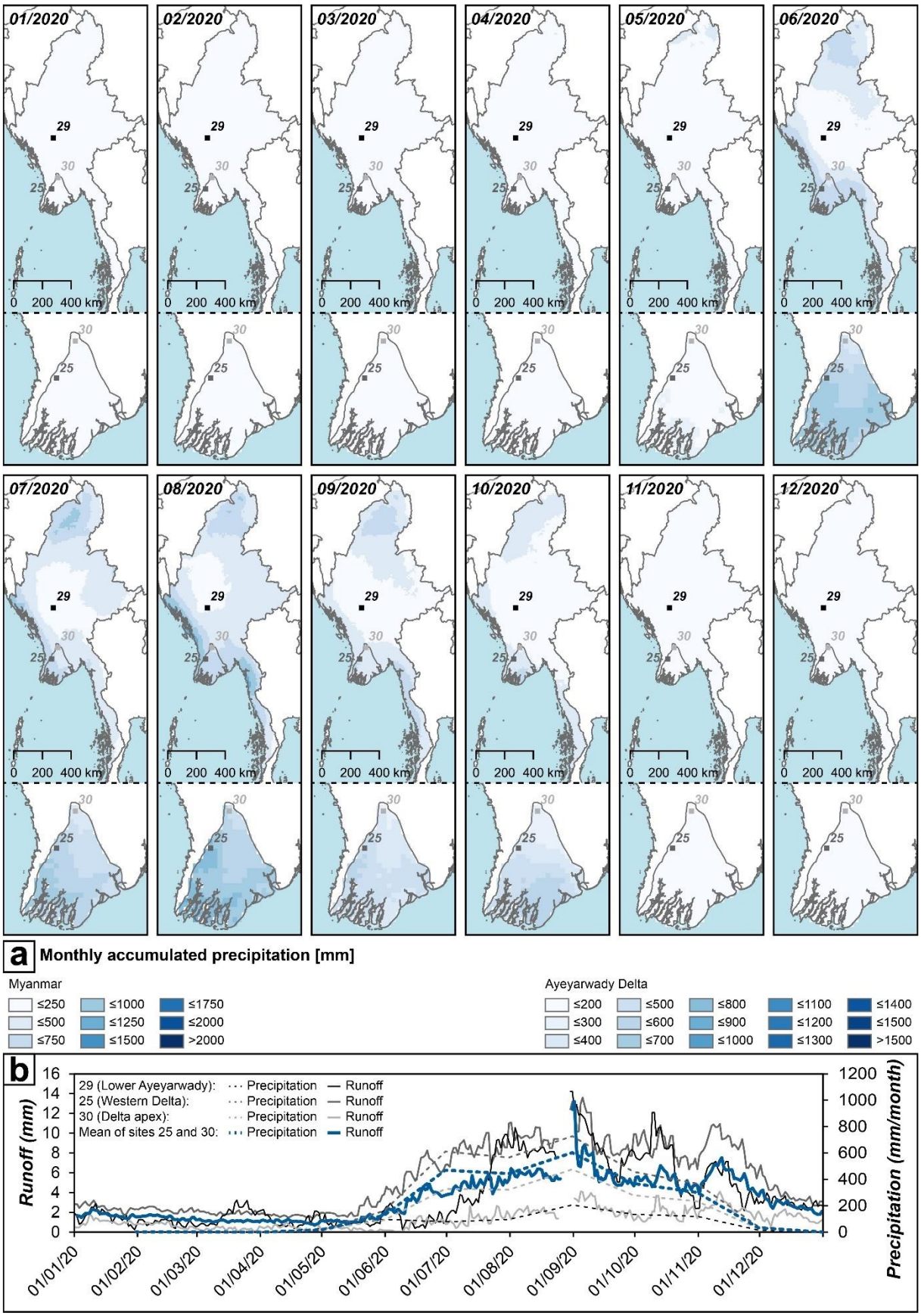


***Figure B6** | Precipitation (a) and runoff patterns (b) in Myanmar and the Ayeyarwady Delta in 2020 based on the GPM_3IMERGM_ v06 product (0.1°; Huffman et al., 2019) and River and Reservoir Watch Version 4.5 (Brakenridge et al., 2023a, 2023b, 2023c). Locations of RiverWatch 4.5 sites 25, 29, and 30 are shown in (a).*

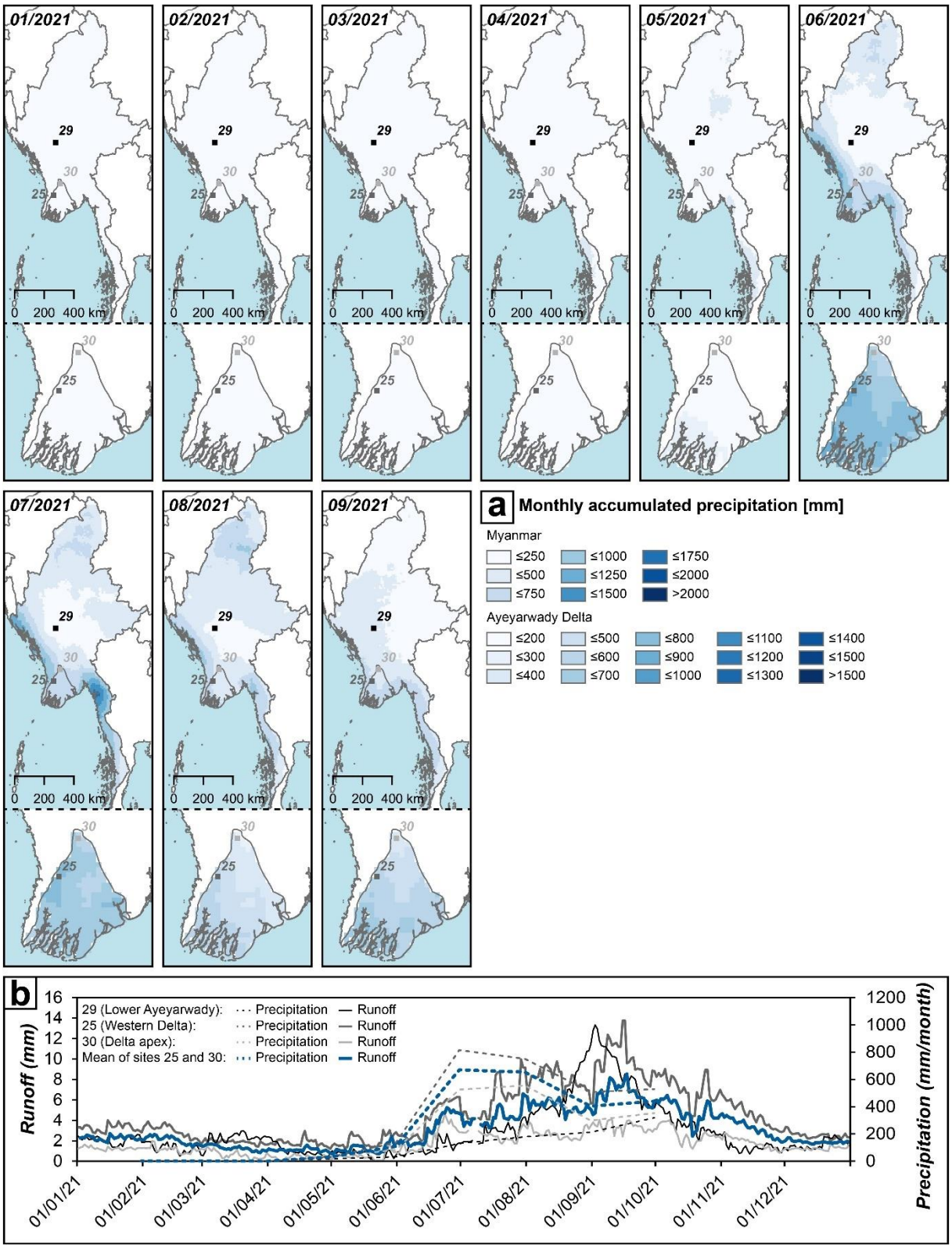


***Figure B7** | Precipitation (a) and runoff patterns (b) in Myanmar and the Ayeyarwady Delta in 2021 based on the GPM_3IMERGM_ v06 product (0.1°; Huffman et al., 2019) and River and Reservoir Watch Version 4.5 (Brakenridge et al., 2023a, 2023b, 2023c). Locations of RiverWatch 4.5 sites 25, 29, and 30 are shown in (a).*

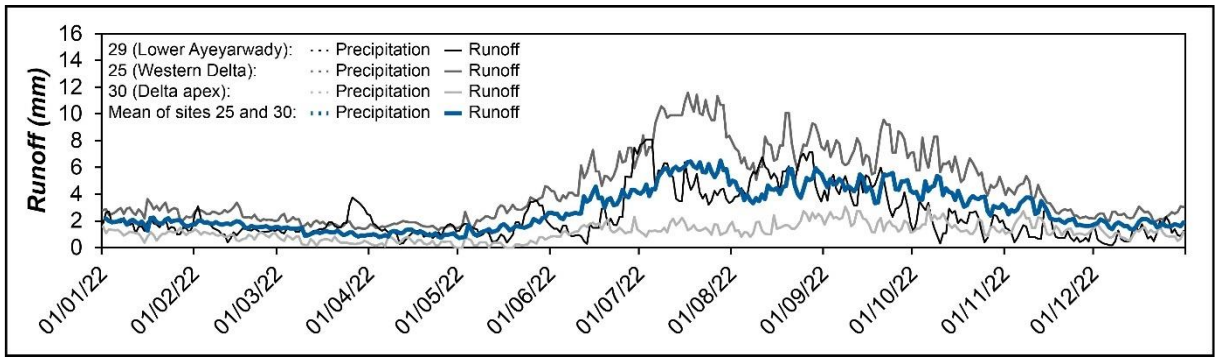


Figure B8 | *Runoff patterns in the lower Ayeyarwady River and the delta for the year 2022 based on River and Reservoir Watch Version 4.5 (Brakenridge et al., 2023a, 2023b, 2023c).*
Locations of RiverWatch 4.0 sites 25, 29, and 30 are shown in previous figures.

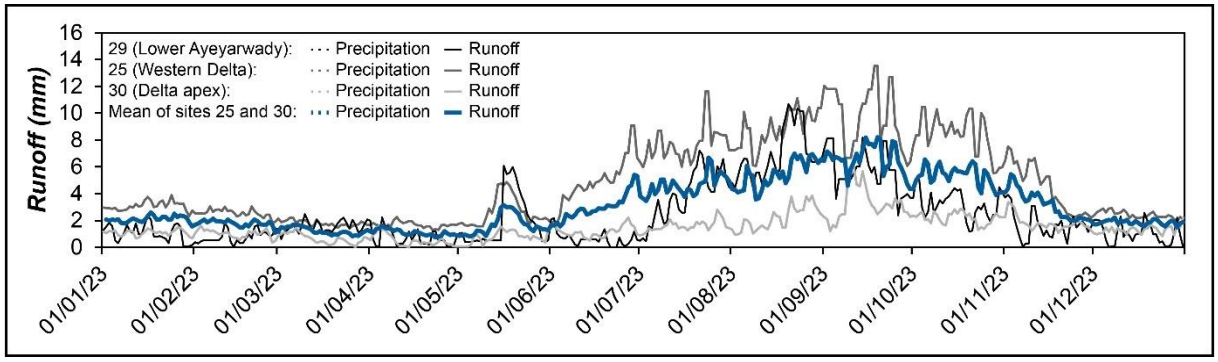


Figure B9 | *Runoff patterns in the lower Ayeyarwady River and the delta for the year 2023 based on River and Reservoir Watch Version 4.5 (Brakenridge et al., 2023a, 2023b, 2023c).*
Locations of RiverWatch 4.5 sites 25, 29, and 30 are shown in previous figures.

B2.2 Spatio-temporal trends of and exposure to monsoon flooding

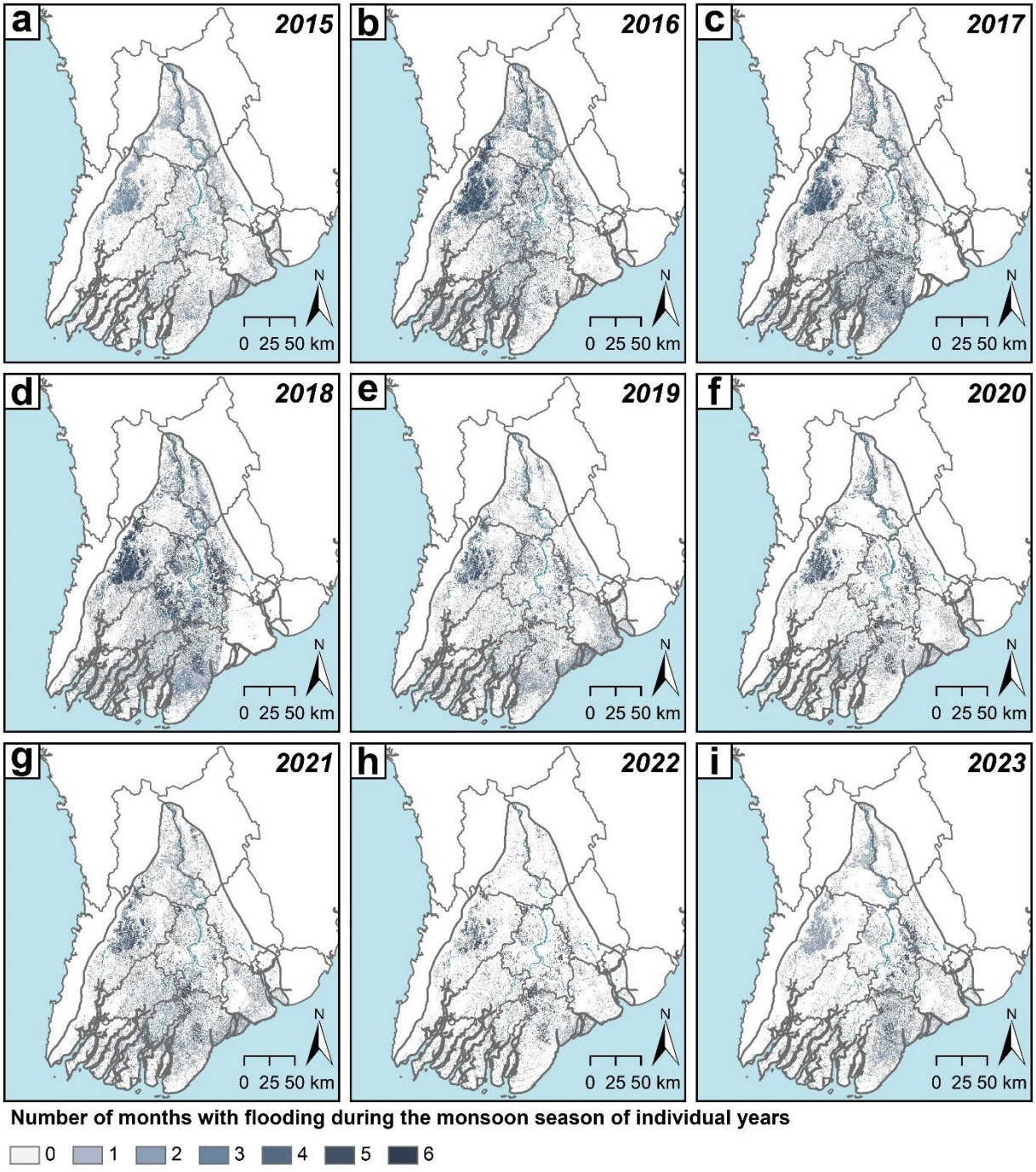


***Figure B10** | Flood frequency pattern during the monsoon season for every year of the investigated time period 2015–2023.*

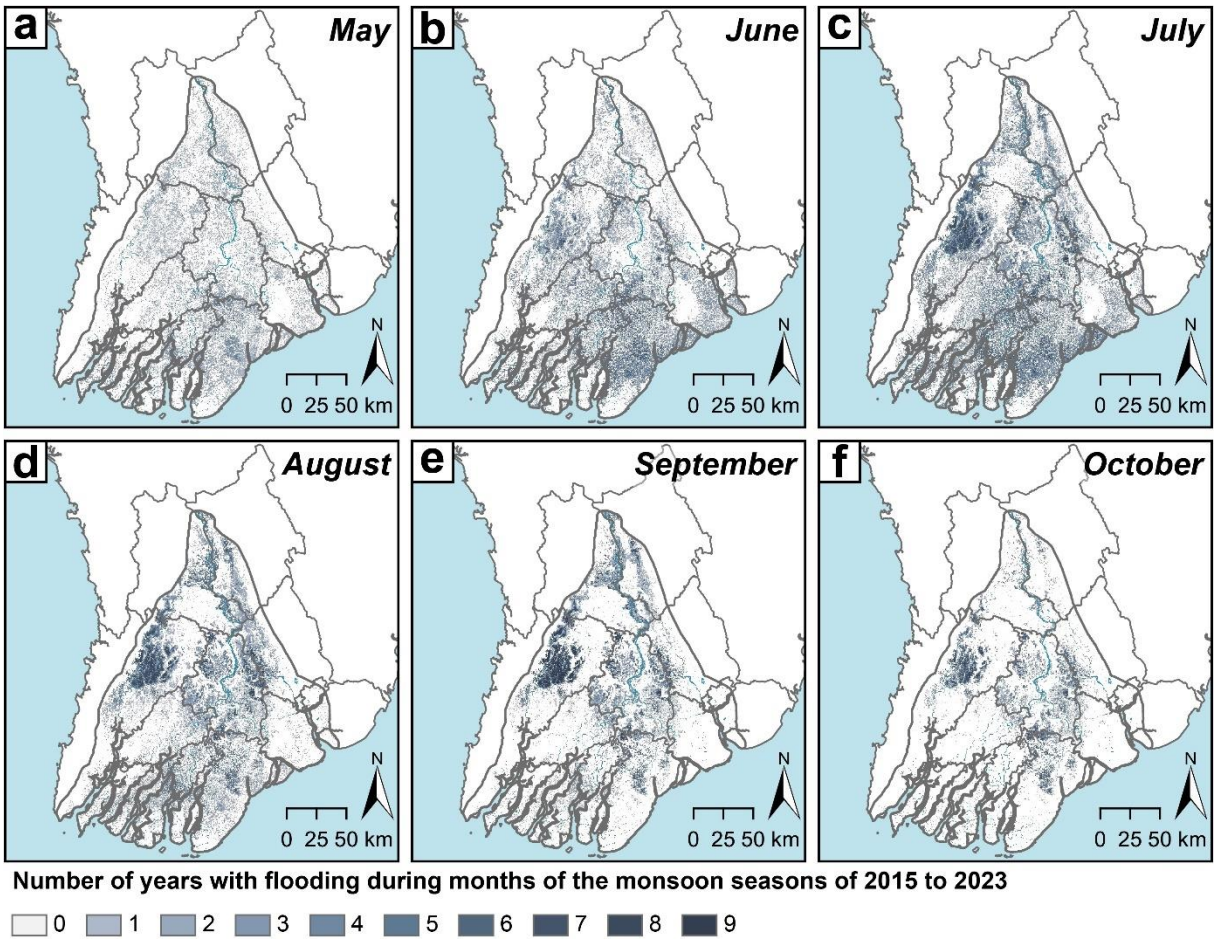


***Figure B11** | Flood frequency pattern for every month of the monsoon season of the investigated time period 2015–2023.*

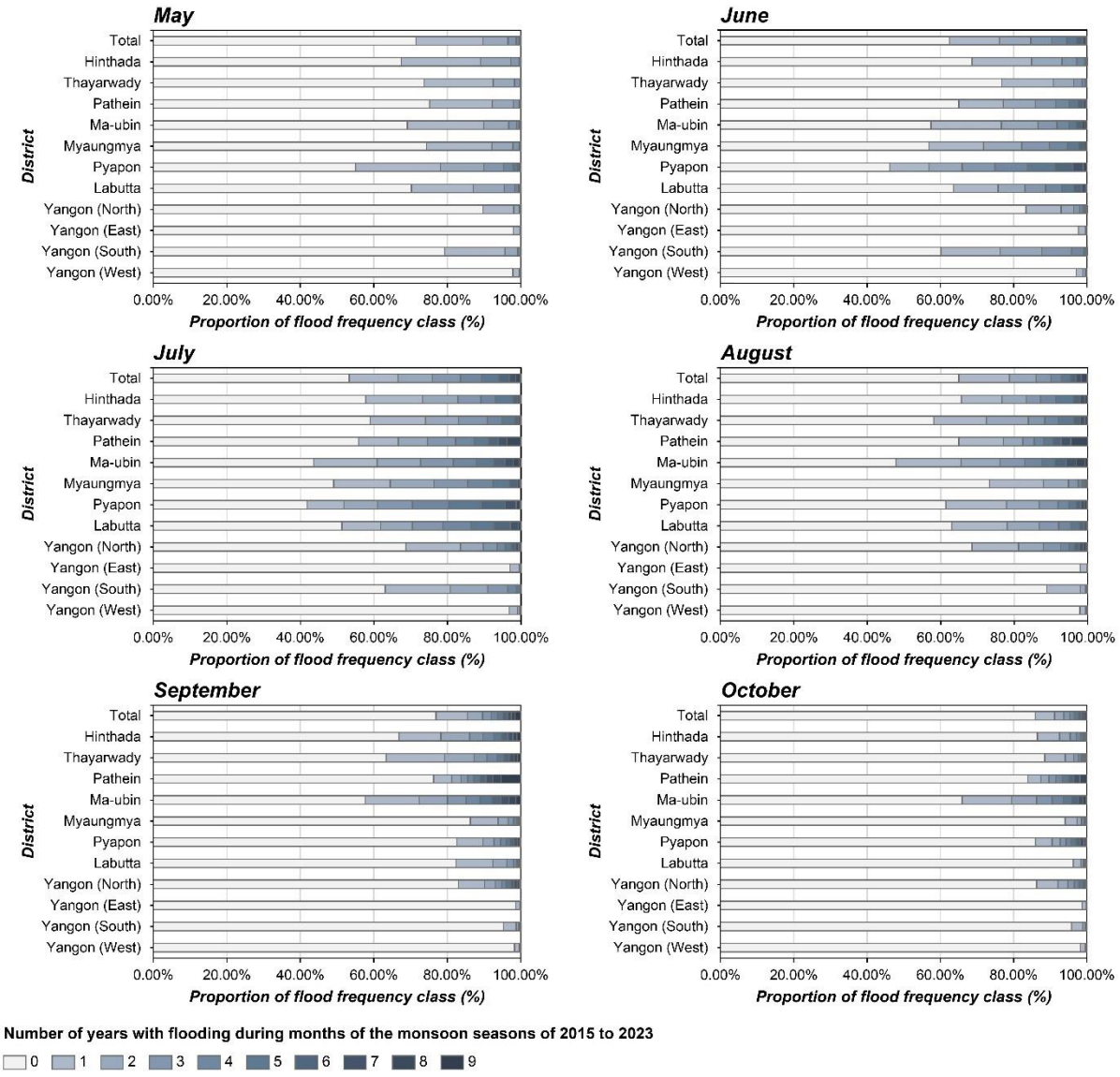


***Figure B12** | Flood frequency pattern for each administrative district for every month of the monsoon season of the investigated time period 2015–2023.*

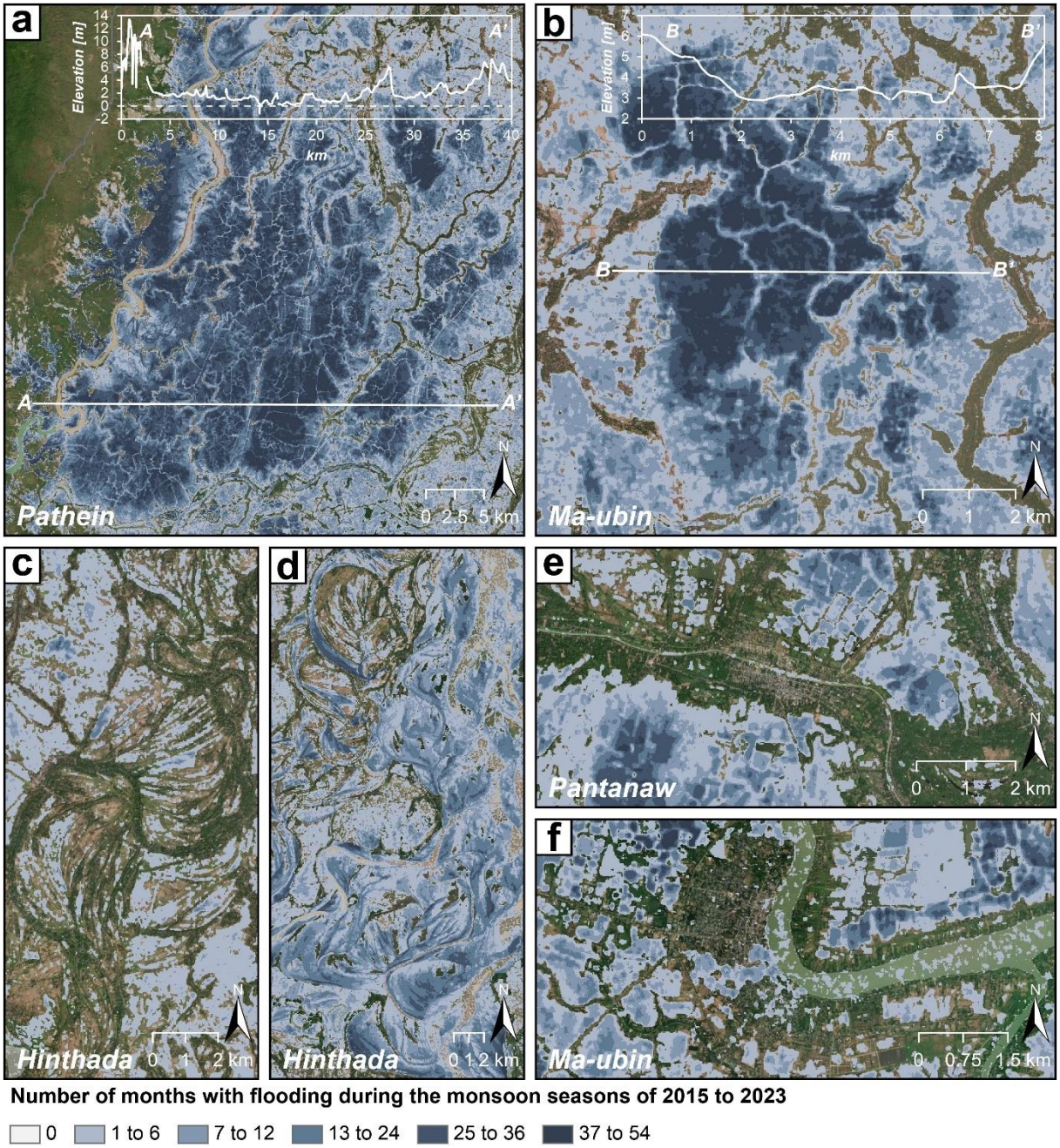


***Figure B13** | Monsoon flooding in selected areas of the Ayeyarwady Delta.*
These include topographic depressions like in Pathein and Ma-ubin districts (a and b) as well as reactivated cut-off meanders in the northern delta (c and d). Some settlements like Pantanaw in the central delta (e) are located outside areas affected by monsoon flooding while others like the city of Ma-ubin are frequently flooded during the monsoon season (f).

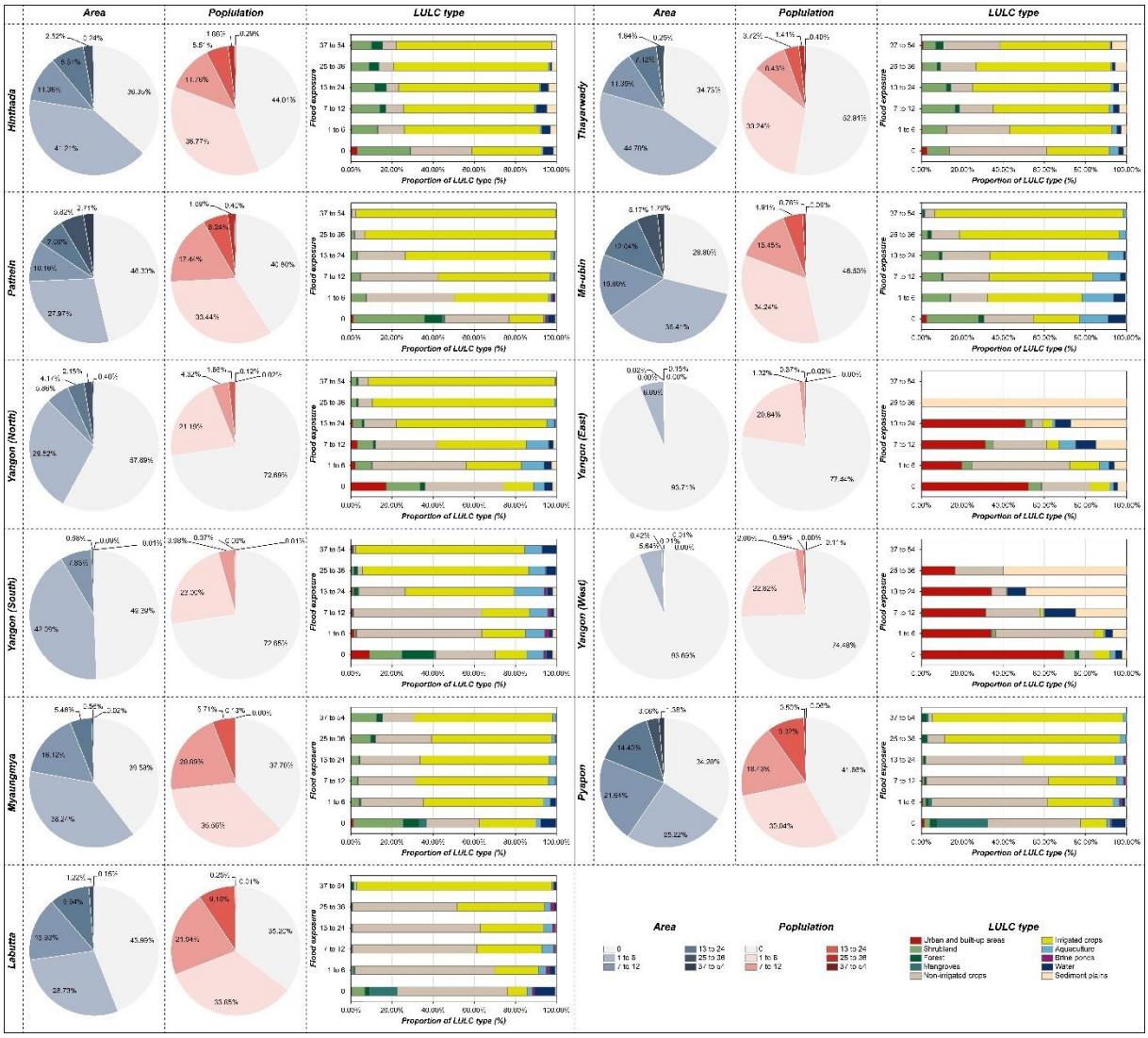


***Figure B14** | Exposure of delta districts to monsoon flooding.*
Note that all percentages per flood frequency class are given relative to the district shares in the delta.

B2.3 Exposure to storm-surge flooding

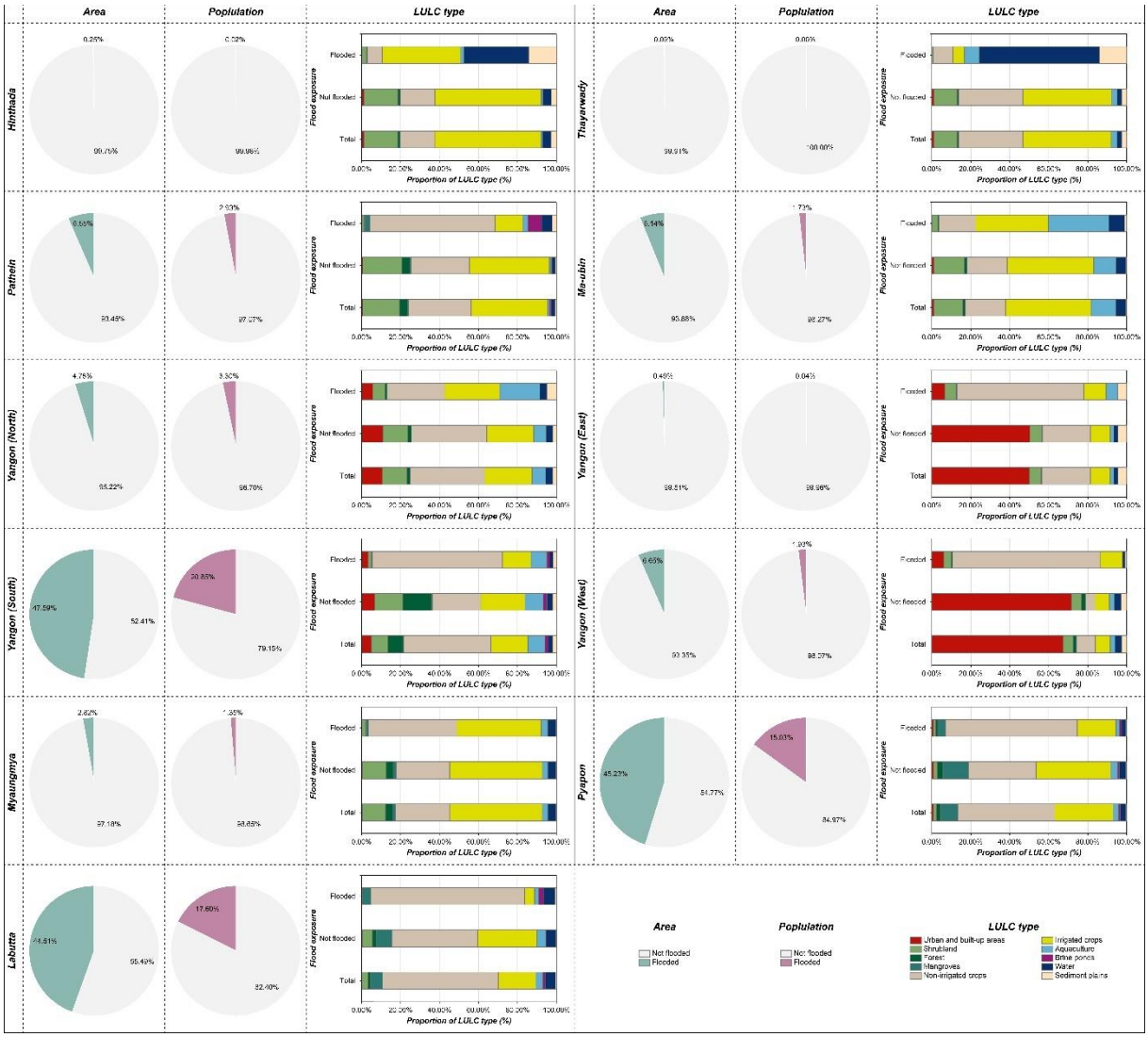


***Figure B15** | Exposure of delta districts to storm surge flooding based on the flood extent of TC Nargis 2008. Note that all percentages per class are given relative to the district shares in the delta.*

B2.4 Exposure to 1 m relative sea-level rise

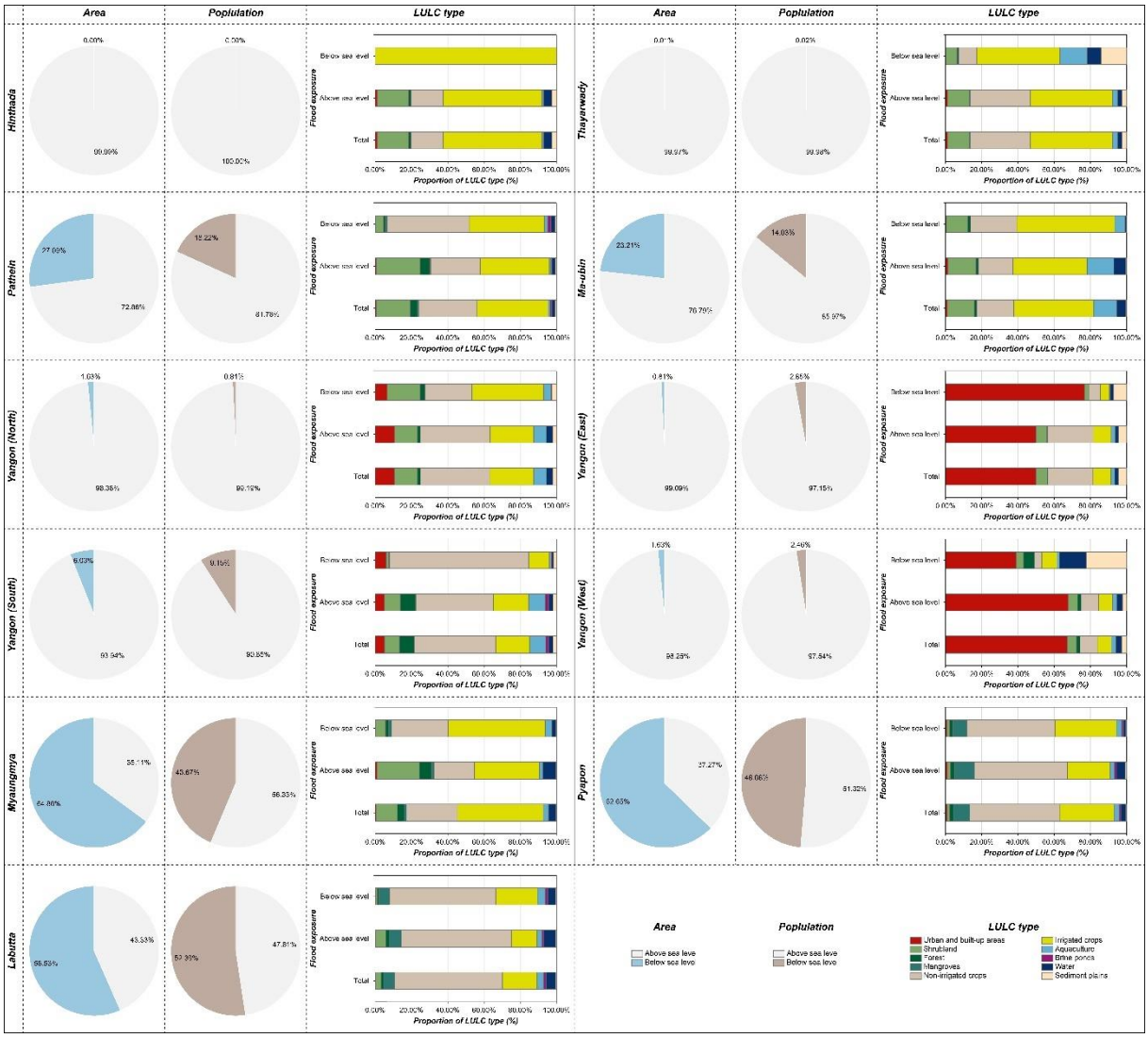


***Figure B16** | Exposure of delta districts to relative sea-level rise based on area falling below sea level assuming relative sea-level rise of 1 m.*
Estimates are based on elevations from the locally adjusted FABDEM of Seeger et al. (2023). Note that all percentages per class are given relative to the district shares in the delta.

B2.5 Exposure to multiple flooding due to monsoon and storm surge

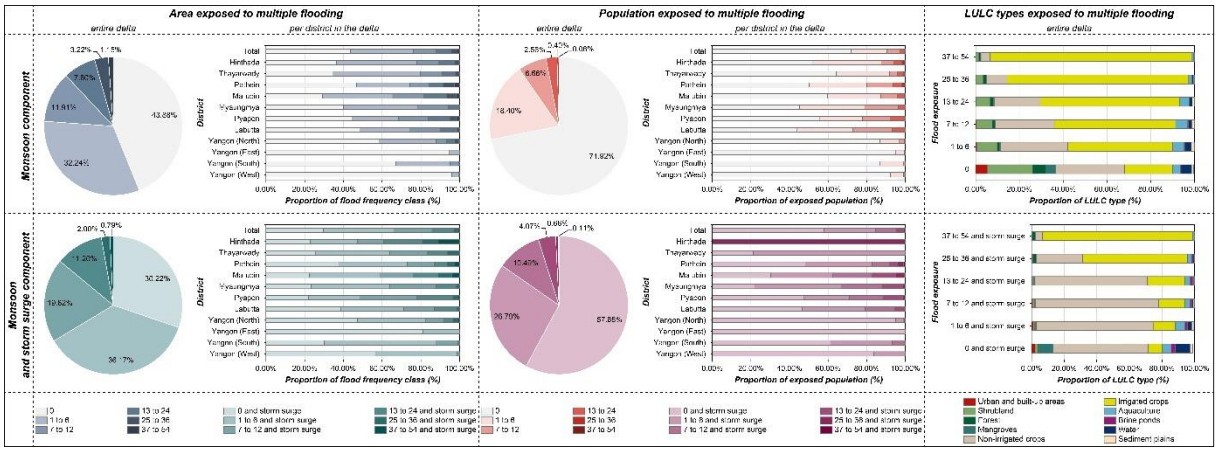


***Figure B17** | Exposure to multiple flooding differentiated into individual components.*

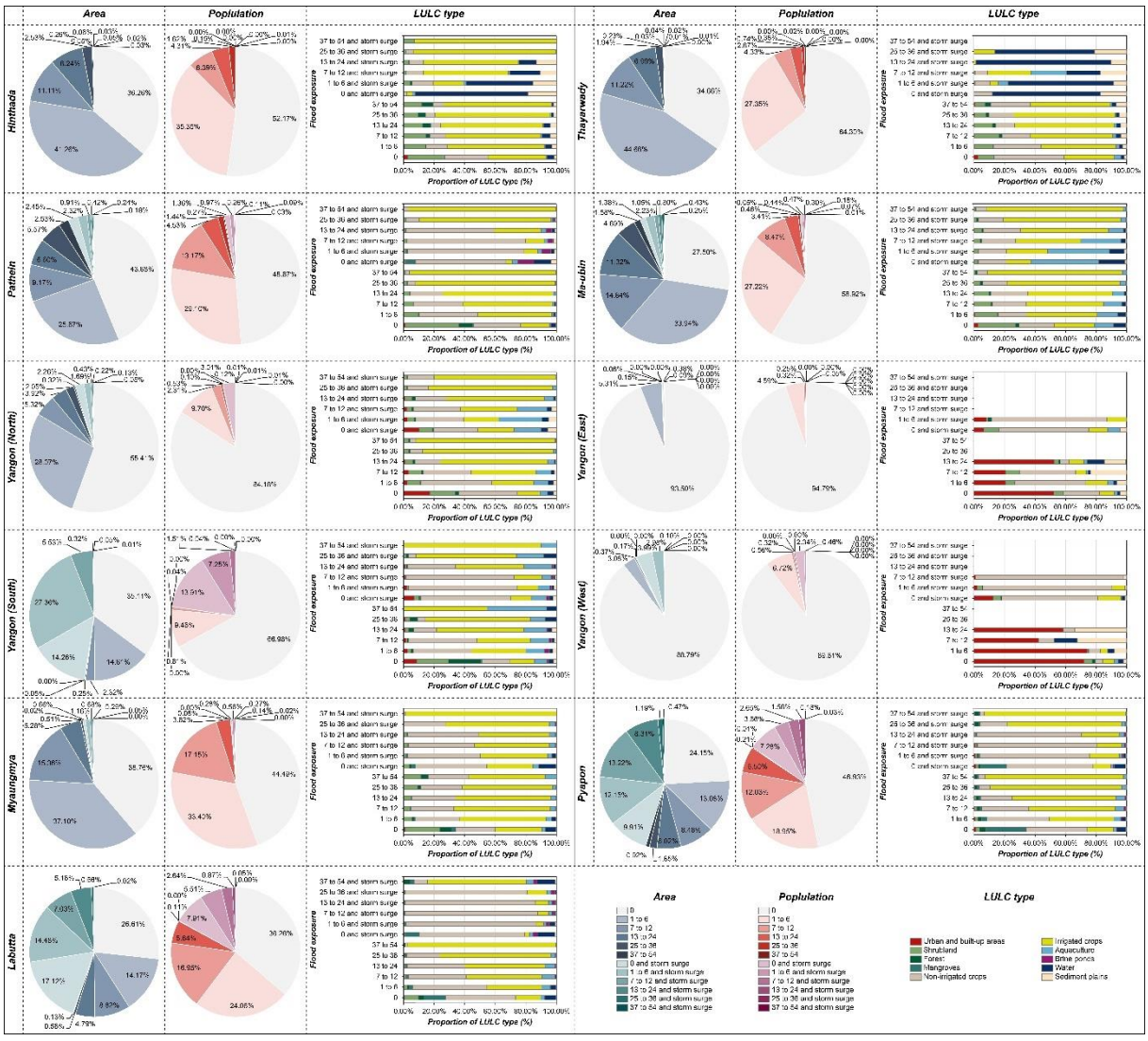


***Figure B18** | Exposure of delta districts to both monsoon and storm surge flooding.*
For the storm surge component, the flood extent of TC Nargis 2008 was used. Note that all percentages per class are given relative to the district shares in the delta.

B2.6 Exposure to multiple flooding due to monsoon and storm surge as well as relative sea-level rise

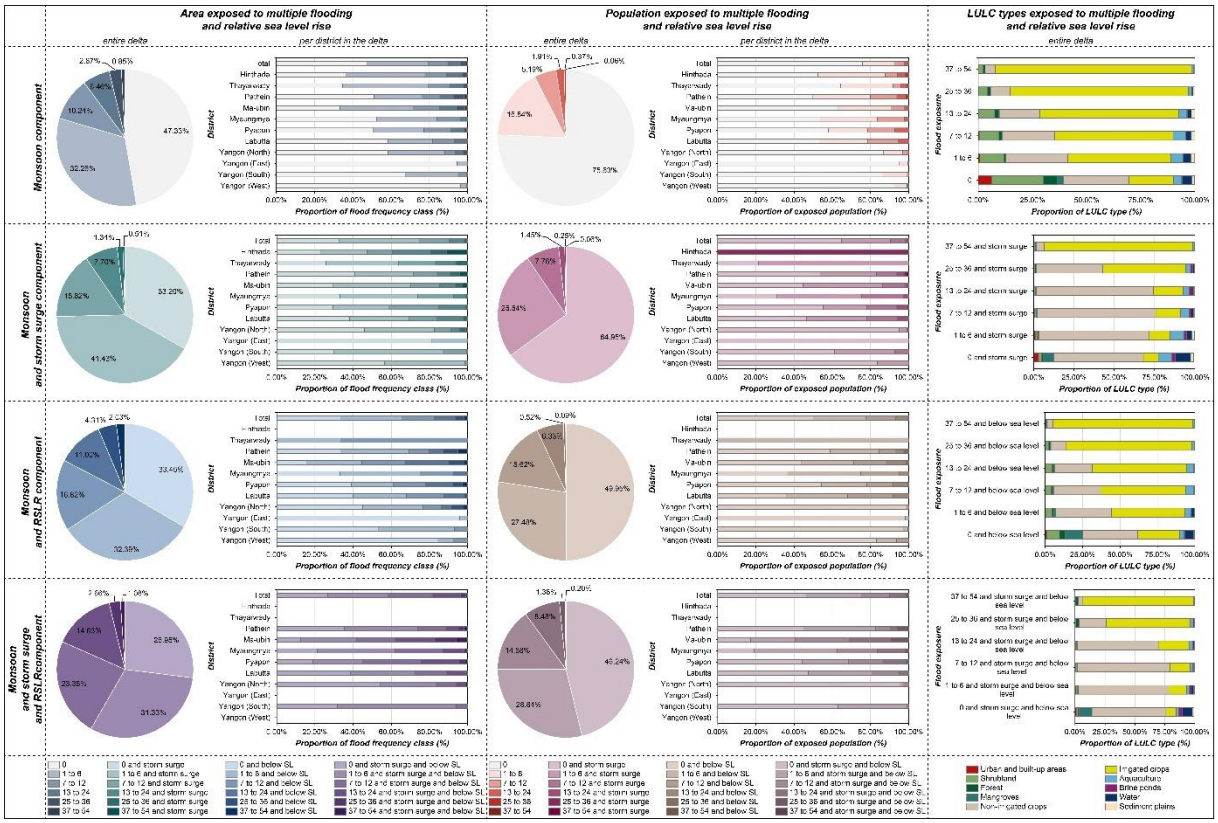


***Figure B19** | Exposure to multiple flooding and relative sea-level rise differentiated into individual components. RSLR = relative sea-level rise, SL = sea level.*

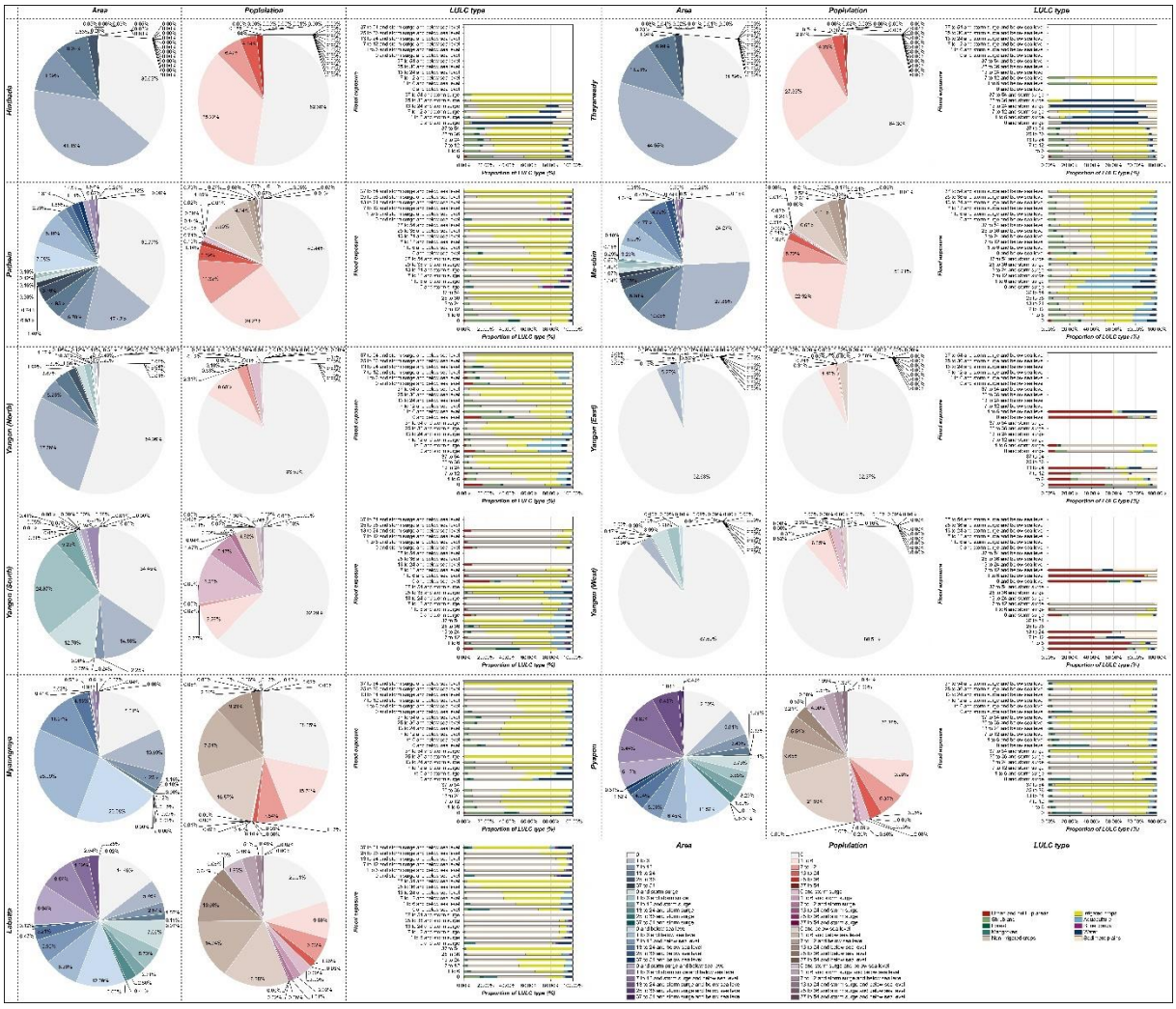


***Figure B20** | Exposure of delta districts to both monsoon and storm surge flooding as well as relative sea-level rise.*
For the storm surge component, the flood extent of TC Nargis 2008 was used. Note that all percentages per class are given relative to the district shares in the delta.

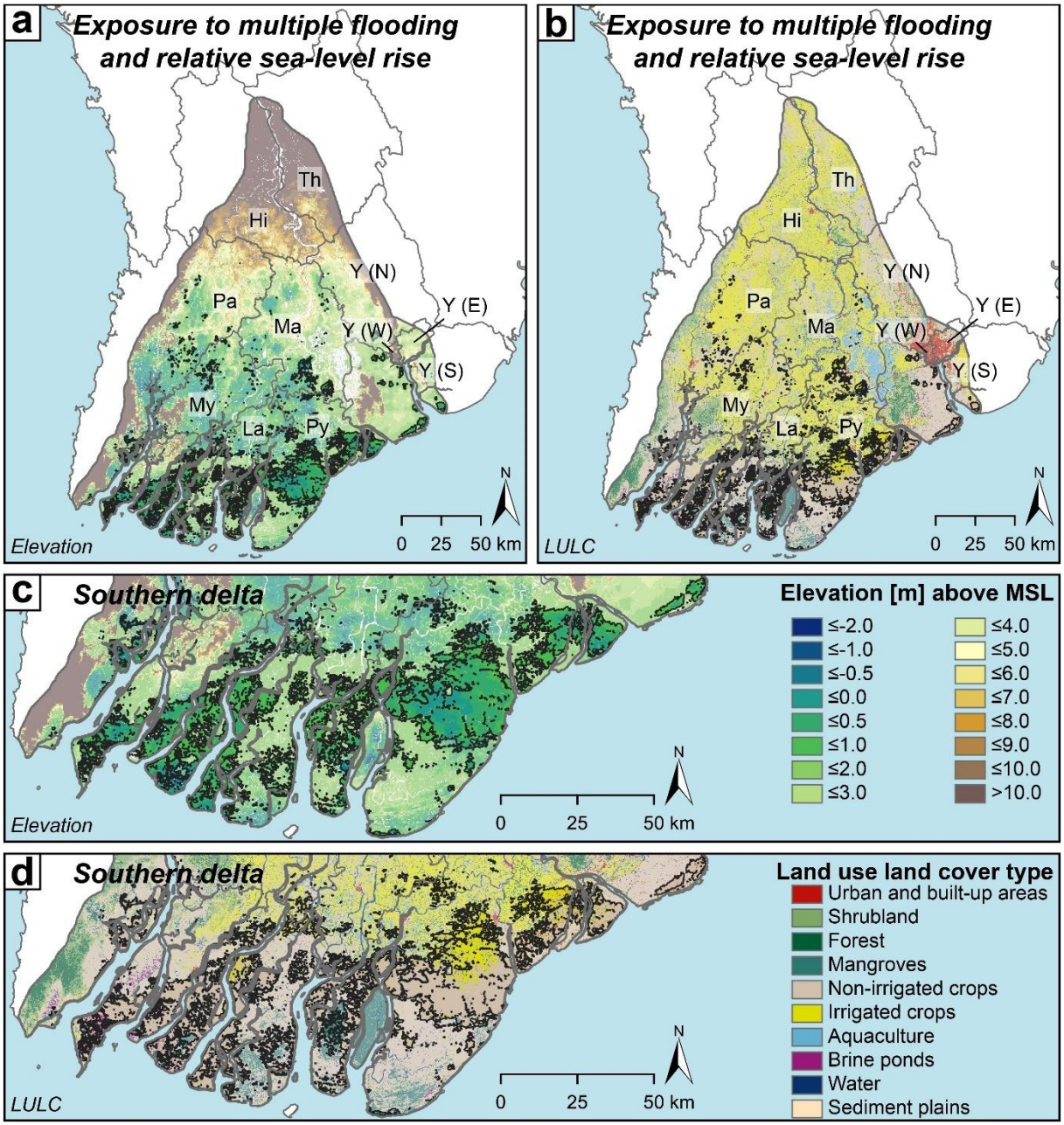


***Figure B21** | Linkages between zones exposed to multiple flooding and relative sea-level rise, elevation and land-use land cover.*

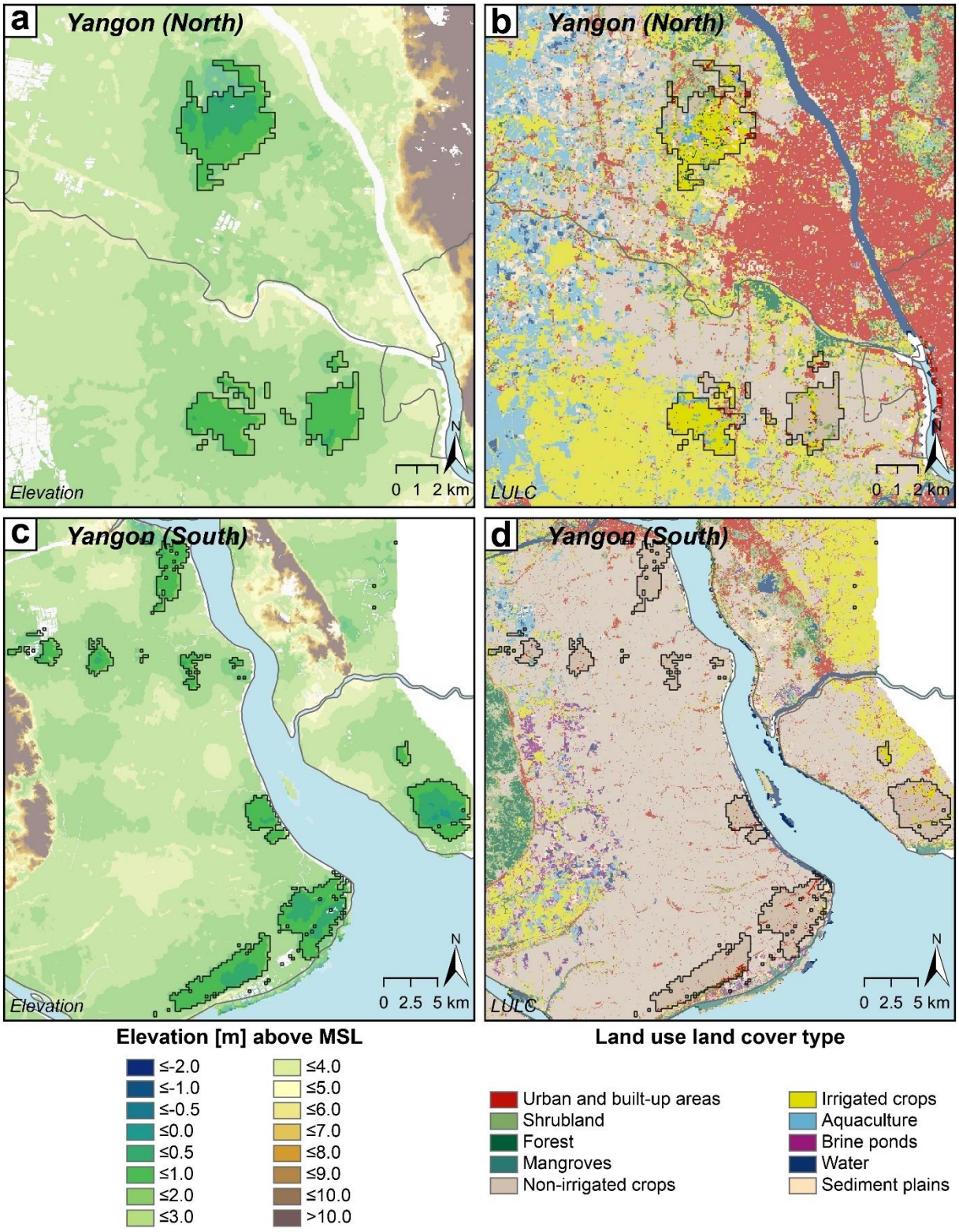


***Figure B22** | Linkages between zones exposed to multiple flooding and relative sea-level rise, elevation and land-use land cover.*

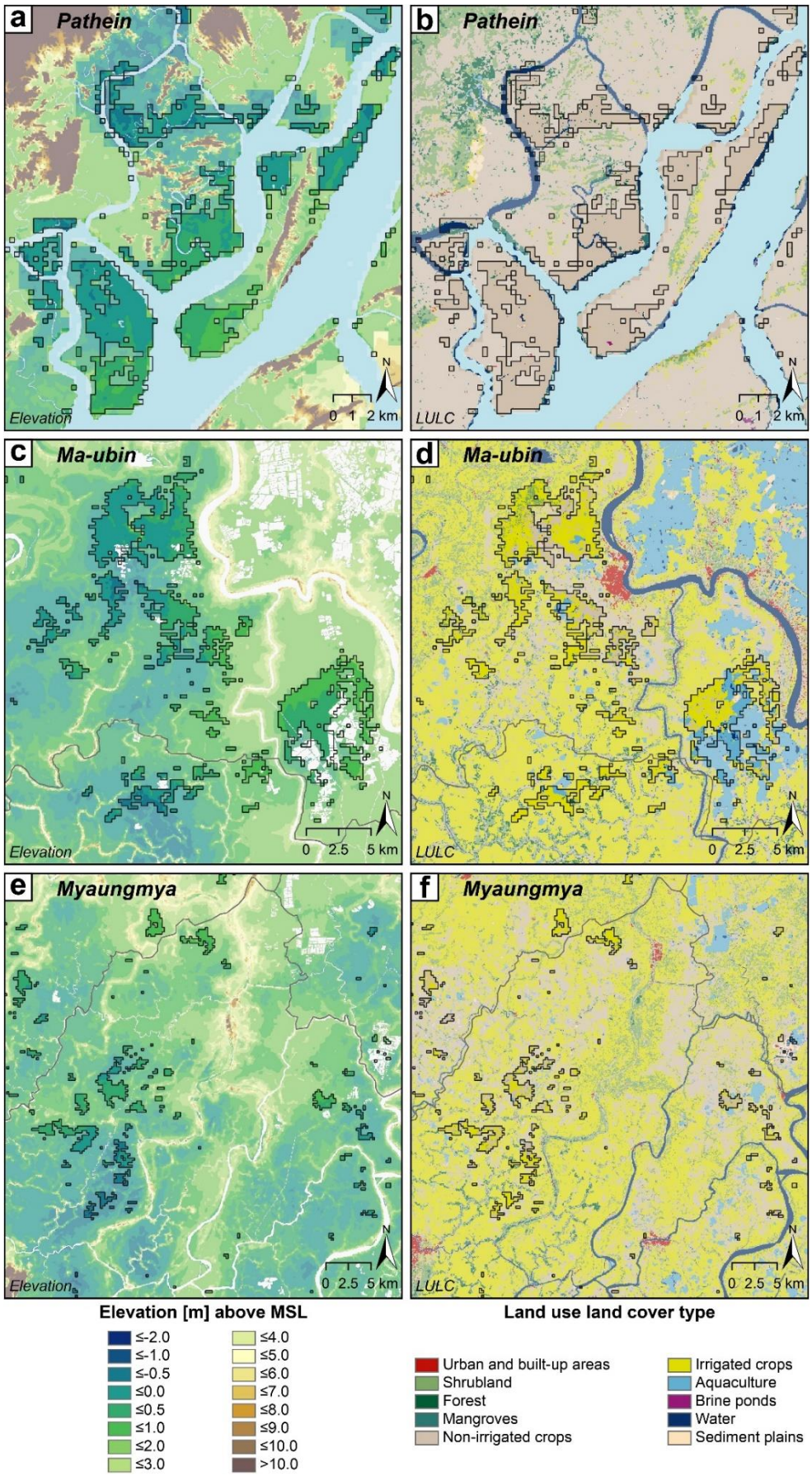


***Figure B23** | Linkages between zones exposed to multiple flooding and relative sea-level rise, elevation and land-use land cover.*

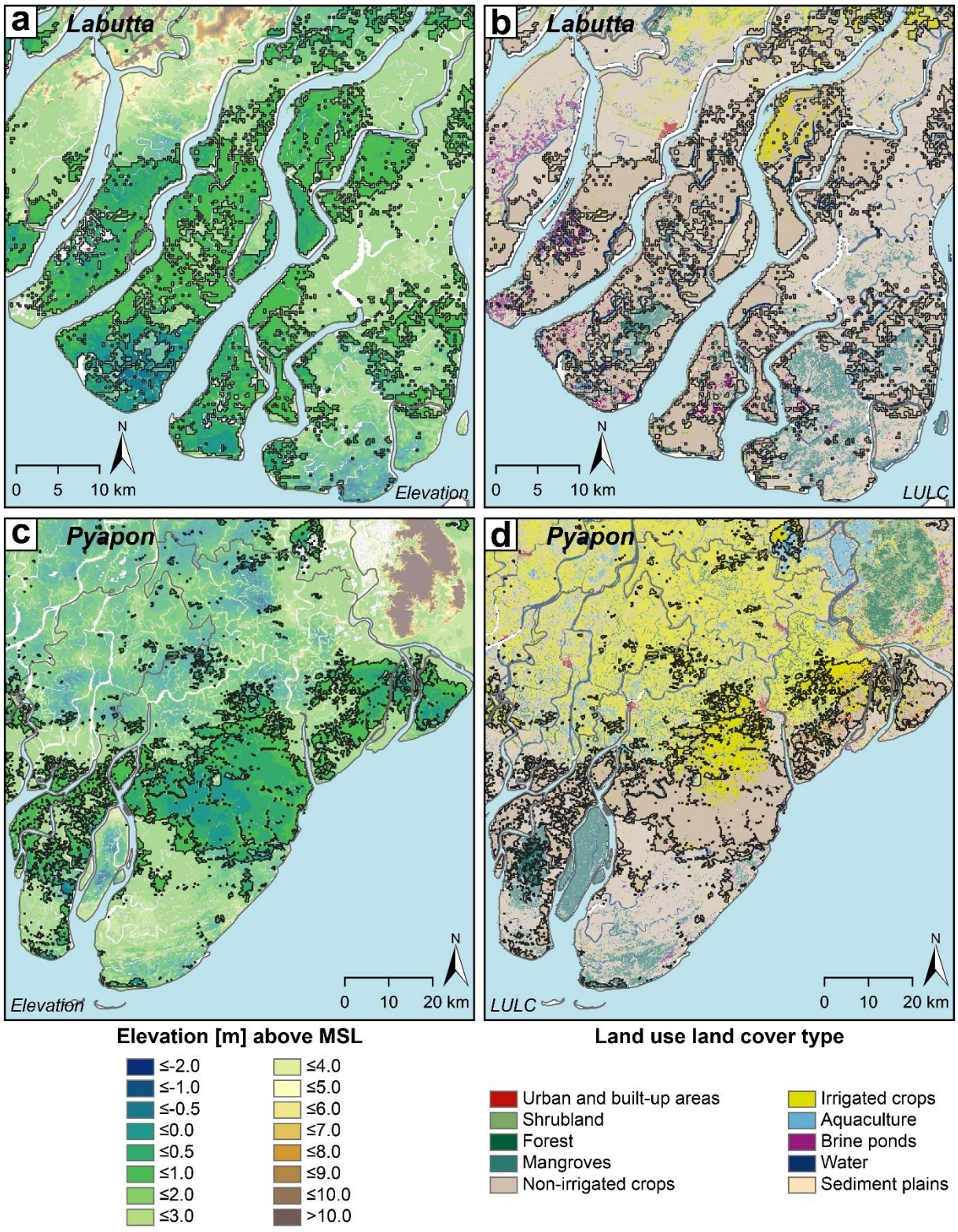


***Figure B24** | Linkages between zones exposed to multiple flooding and relative sea-level rise, elevation and land-use land cover.*

References

Bekele, T. W., Haile, A. T., Trigg, M. A., & Walsh, C. L. (2022). Evaluating a new method of remote sensing for flood mapping in the urban and peri-urban areas: Applied to Addis Abeba and the Akaki catchment in Ethopia. *Natural Hazards Research*, *2*(2), 97–110. https://doi.org/10.1016/j.nhres.2022.03.001

Brakenridge, G. R., Kettner, A. J., Paris, S., Cohen, S. & Nghiem, S. V. (2023a). River and Reservoir Watch Version 4.5, Satellite-based river discharge and reservoir area measurements, DFO Flood Observatory, University of Colorado, USA. https://floodobservatory.colorado.edu/SiteDisplays/29.htm (last access: 20 February 2024)

Brakenridge, G. R., Kettner, A. J., Paris, S., Cohen, S. & Nghiem, S. V. (2023b). River and Reservoir Watch Version 4.5, Satellite-based river discharge and reservoir area measurements, DFO Flood Observatory, University of Colorado, USA. https://floodobservatory.colorado.edu/SiteDisplays/25.htm (last access: 20 February 2024)

Brakenridge, G. R., Kettner, A. J., Paris, S., Cohen, S. & Nghiem, S. V. (2023c). River and Reservoir Watch Version 4.5, Satellite-based river discharge and reservoir area measurements, DFO Flood Observatory, University of Colorado, USA. https://floodobservatory.colorado.edu/SiteDisplays/30.htm (last access: 20 February 2024)

Clement, M. A., Kilsby, C. G., & Moore, P. (2017). Multi-temporal synthetic aperture radar flood mapping using change detection. *Journal of Flood Risk Management*, *11*(2), 152–168. https://doi.org/10.1111/jfr3.12303

Conde, F. C., & De Mata Muñoz, M. (2019). Flood Monitoring Based on the Study of Sentinel-1 SAR Images: The Ebro River Case Study. *Water*, *11*(12), 2454. https://doi.org/10.3390/w11122454

Copernicus Emergency Management Service (© 2015 European Union) (2015). [EMSR130] Irrawaddy Delta: Delineation Map, Monitoring 1

Fritz, H., Blount, C., Swe Thwin, Moe Kyaw Thu, & Nyein Chan (2009). Cyclone Nargis storm surge in Myanmar. *Nature Geoscience*, *2*, 448–449. https://doi.org/10.1038/ngeo558

Gorelick, N., Hancher, M., Dixon, M., Ilyushchenko, S., Thau, D., & Moore, R. (2017). Google Earth Engine: Planetary-scale geospatial analysis for everyone. *Remote Sensing of Environment*, *202*, 18–27. https://doi.org/10.1016/j.rse.2017.06.031

Hamidi, E., Peter, B. G., Muñoz, D. F., Moftakhari, H., & Moradkhani, H. (2023). Fast Flood Extent Monitoring With SAR Change Detection Using Google Earth Engine. *IEEE Transactions on Geoscience and Remote Sensing*, *61*, 1–19. https://doi.org/10.1109/TGRS.2023.3240097

Hess, L. L., Melack, J. M., & Simonett, D. S. (1990). Radar detection of flooding beneath the forest canopy: a review. *International Journal of Remote Sensing*, *11*(7), 1313–1325. https://doi.org/10.1080/01431169008955095

Huffman, G. J., Stocker, E. F., Bolvin, D. T., Nelkin, E. J., & Jackson Tan (2019). GPM IMERG Final Precipitation L3 1 month 0.1 degree x 0.1 degree V06. Greenbelt, MD, Goddard Earth Sciences Data and Information Services Center (GES DISC). 10.5067/GPM/IMERG/3B-MONTH/06 (last access: 10 February 2023)

Lehner, B. Verdin, K., & Jarvis, A. (2008). New Global Hydrography Derived From Spaceborne Elevation Data. *Eos, Transactions American Geophysical Union*, *89*(10), 93–94. https://doi.org/10.1029/2008EO100001

Lin, L., Di, L., Yu, E. G., Kang, L., Shrestha, R., Rahman, Md. Sh., Tang, J., Deng, M., Sun, Z., Zhang, C., & Hu, L. (2016). A Review of Remote Sensing in Flood Assessment. *2016 Fifth International Conference on Agro-Geoinformatics (Agro-Geoinformatics)*, 1–4. https://doi.org/10.1109/Agro-Geoinformatics.2016.7577655

Long, S., Fatoyinbo, T. E., & Policelli, F., (2014). Flood extent mapping for Namibia using change detection and thresholding with SAR. *Environmental Research Letters*, *9*(3), 035002. http://dx.doi.org/10.1088/1748-9326/9/3/035002

Moharrami, M., Javanbakht, M., & Attarchi, S. (2021). Automatic flood detection using sentinel-1 images on the google earth engine. *Environmental Monitoring and Assessment*, *193*, 248. https://doi.org/10.1007/s10661-021-09037-7

Notti, D., Giordan, D., Caló, F., Pepe, A., Zucca, F., & Galve, J. P. (2018). Potential and Limitations of Open Satellite Data for Flood Mapping. *Remote Sensing*, *10*(11), 1673. https://doi.org/10.3390/rs10111673

Pekel, JF., Cottam, A., & Gorelick, N. (2016). High-resolution mapping of global surface water and its long-term changes. *Nature*, *540*, 418–422. https://doi.org/10.1038/nature20584

Seeger, K., Minderhoud, P. S. J., Peffeköver, A., Vogel, A., Brückner, H., Kraas, F., Nay Win Oo, & Brill, D. (2023). FABDEM V1-0 adjusted for the Ayeyarwady Delta in Myanmar by local spot height data from topographic maps. *Zenodo*. https://doi.org/10.5281/zenodo.7875855

Shen, X., Wang, D., Mao, K., Anagnostou, E., & Hong, Y. (2019). Inundation Extent Mapping by Synthetic Aperture Radar: A Review. *Remote Sensing*, *11*(7), 879. https://doi.org/10.3390/rs11070879

Tellman, B., Sullivan, J. A., Kuhn, C., Kettner, A. J., Doyle, C. S., Brakenridge, G. R., Erickson, T. A., & Slayback, D. A. (2021). Satellite imaging reveals increased proportion of population exposed to floods. *Nature*, *596*, 80–86. https://doi.org/10.1038/s41586-021-03695-w

Tessler, Z. D., Vörösmarty, J., Grossberg, M., Gladkova, I., Aizenman, H., Syvitski, J. P. M., & Foufoula-Georgiou, E. (2015). Profiling risk and sustainability in coastal deltas of the world. *Science*, *349*(6248), 638–643. https://doi.org/10.1126/science.aab3574

Tripathy, P., & Malladi, T. (2022). Global Flood Mapper: a novel Google Earth Engine application for rapid flood mapping using Sentinel-1 SAR. *Natural Hazards*, *114*, 1341–1363. https://doi.org/10.1007/s11069-022-05428-2

United Nations Platform for Space-based Information for Disaster Management and Emergency Response (UN-SPIDER) (no date). SAR-Flood mapping using a change detection approach. https://www.un-spider.org/sites/default/files/Code_GEE_flood_mapping.txt (last access: 20 February 2024)

Webster, P. J. (2008). Myanmar's deadly daffodil. *Nature Geoscience*, *1*, 488–490. https://doi.org/10.1038/ngeo257

Appendix C – Supplement to Chapter 4.1

This Supplement is related to: **Seeger, K.**, Minderhoud, P.S.J., Peffeköver, A., Vogel, A., Brückner, H., Kraas, F., Nay Win Oo, Brill, D., 2023. *Assessing land elevation in the Ayeyarwady Delta (Myanmar) and its relevance for studying sea level rise and delta flooding*. Hydrology and Earth System Sciences, 27 (11), 2257–2281. https://doi.org/10.5194/hess-27-2257-2023.

The supplementary material is published along with the scientific article under a CC-BY 4.0 Attribution 4.0 International licence (https://creativecommons.org/licenses/by/4.0/). The reader can access the content of this supplement here (https://hess.copernicus.org/articles/27/2257/2023/hess-27-2257-2023-supplement.pdf) and also via the article doi provided above. The supplementary material was not modified; only the thesis layout was adopted.

C1. Detailed information on material and methods

C1.1 Data

C1.1.1 Elevation data from topographic maps

To investigate land elevation in the Ayeyarwady Delta independently of data derived from global satellite-based measurements, we used height information from topographic maps. Beside the series of mappings conducted since the British colonial times that are available to the public, the most recent topographic maps of Myanmar were made and published by the Survey Department, Ministry of Forestry in the Union of Myanmar, in cooperation with the Japan International Cooperation Agency (JICA), and sold by East View Geospatial, Inc. (2014). The maps are at scale of 1:50,000. Map sheets covering the Ayeyarwady Delta were accessed via the Specialised Information Service Cartography and Geodata (SIS Maps) of the Map Department of the Staatsbibliothek zu Berlin funded by the German Research Foundation (SIS Maps, 2021). Depending on their location, the data are projected to UTM 46 N or 47 N (based on the WGS84 ellipsoid) while mean sea level (MSL) is used as vertical datum. However,

documentation on the date and location of MSL establishment is missing and East View Geospatial, Inc. (2014) only states that source information is "Compiled from best available sources". Further research on cartographic work and vertical datums in Myanmar turned out Kyaikkhami tide observatory (formerly: Amherst) in eastern Myanmar as reference site (JICA et al., 2004a). As the establishment of the Myanmar 2000 datum involved extensive field surveys, aerial signalisation and photography, levelling, GPS observations and aerial triangulation that were conducted between 2000 and 2004, these data not only constitute source data of topographic maps published by JICA et al. (2004b) but very likely also constitute the source data of topographic maps sold by East View Geospatial, Inc. (2014), which were used in this study. Horizontal accuracy is one-third of contour interval for spot heights and one-half for lines (JICA et al., 2004c). Index contour lines are given in 20 m intervals for elevations higher than 200 m and in 10 m intervals for elevations lower than 200 m (JICA et al., 2004c). Ground control points are accurate at standard deviations of 0.5 m horizontally and 0.3 m vertically (JICA et al., 2004c).

C1.1.2 Global and coastal digital elevation models

In total, 10 DEMs were used to assess their performance in the Ayeyarwady Delta. Table C1 provides an overview of main characteristics such as coverage, resolution, and accuracy as well as information on eventual edits that have been made after DEM generation. Though elevation data from surface and terrain models may show some systematic offset due to the inclusion of canopy and building heights in the digital surface models (DSMs) compared to real ground elevation assessment of digital terrain models (DTMs), we include both types of DEMs into the comparison as these DEMs are the most often used, sometimes without considering that the DEM type should suit the application purpose. Thus, we want to demonstrate the relevance of careful DEM selection as the outcomes of any geomorphological and hydrological study as well as risk assessment and flood modelling will strongly depend on the underlying elevation data (e.g., Wechsler et al., 2007; Siart et al., 2009; Gesch et al., 2018; Brosens et al., 2022).

***Table C1** | Overview of all elevation models used in this study.*
DEM = digital elevation model, DSM = digital surface model, DTM = digital terrain model, H = horizontal, V = vertical.

DEM	Type	Coverage	Acquisition	Technique	Datum	Accuracy	References	Availability
SRTM	DSM	60° N to 56° S	11/02/2000 to 22/02/2000	Synthetic Aperture Radar interferometry (dual antennas)	H: WGS84 V: EGM96	H: 1 arc sec × 1 arc sec (~30 m × 30 m) V: 16 m (LE90), 9.73 m (RMSE)	Farr et al. (2007)	Free
ACE2	nearly DTM	60° N to 60° S	03/1994 to 08/2002 (Topex Ku band)	Correction of SRTM (and GLOBE for regions south of 56° S) by multi-mission	H: WGS84 V: EGM96	H: 3 arc sec × 3 arc sec (~90 m × 90 m) V: > 10 m	Smith and Berry (2009); Berry et al.	Free

			04/1994 to 03/1995 (ERS-1) 08/2002 to 07/2005 (Envisat RA-2 Ku band) 08/2002 to 03/2004 (Jason-1 Ku band)	satellite radar altimetry; canopy heights replaced by altimetry heights			(2010); Berry et al. (2019)	
ASTER GDEM	DSM	83° N to 83° S	01/03/2000 to 30/11/2013	Correlation of optical stereo near infrared imagery	H: WGS84 V: EGM96	H: 1 arc sec × 1 arc sec (~30 m × 30 m) V: 20 m (LE95), 10.20 m RMSE	Abrams et al. (2010); Tachikawa et al. (2011)	Free
AW3D30 (ALOS)	DSM	80° N to 80° S	24/01/2006 to 12/05/2011	Resampling AW3D (5 m resolution, based on optical stereo panchromatic imagery) by applying average and medium methods	H: WGS84 V: EGM96	H: 1 arc sec × 1 arc sec (~30 m × 30 m) V: 4.38 m (σ), 4.40 m RMSE	Tadono et al. (2016)	Partially free
TanDEM-X 30 m	DSM	90° N to 90° S	12/12/2010 to 16/01/2015	Bi-static Synthetic Aperture Radar interferometry (twin satellites)	H: WGS84 V: WGS84	H: 1 arc sec × 1 arc sec (~30 m × 30 m) V: < 10 m (LE90)	Wessel (2018)	Free for scientific use
TanDEM-X 12 m	DSM	90° N to 90° S	12/12/2010 to 16/01/2015	Bi-static Synthetic Aperture Radar interferometry (twin satellites)	H: WGS84 V: WGS84	H: 0.4 arc sec × 0.4 arc sec (~12 m × 12 m; between 0° and 50° N/S) V: < 10 (2–4) m (LE90), up to 6.78 m RMSE	Wessel (2018); Wessel et al. (2018)	Free for scientific use
Copernicus DEM GLO-30	DSM	90° N to 90° S	12/12/2010 to 16/01/2015 (source DEM)	Correction of WorldDEM™ (based on TanDEM-X 12 m) by filling voids with ASTER, SRTM90, SRTM30; GMTED2010, SRTM30plus, TerraSAR-X Radargrammetric DEM, AW3D30, and Norway DEM	H: WGS84 V: EGM2008	H: 1 arc sec × 1 arc sec (~30 m × 30 m; between 0° and 50° N/S) V: < 4 (2–4) m (LE90)	Airbus Defence and Space (2020)	Free for registered users
FABDEM	nearly DTM	90° N to 90° S	12/12/2010 to 16/01/2015 (source DEM)	Correction of Copernicus DEM GLO-30 by removing buildings and forest height bias through machine learning techniques	H: WGS84 V: EGM2008	H: 1 arc sec × 1 arc sec (~30 m × 30 m; between 0° and 50° N/S) V: 2.39–6.67 m (LE90); 2.33–6.66 m (RMSE)	Hawker et al. (2022)	Free
CoastalDEM v2.1	nearly DTM	60° N to 56° S; input elevation between -10 and 120 m	11/02/2000 to 22/02/2000 (source DEM)	Correction of NASADEM by training with ICESat 2 satellite LiDAR data and using additional population and vegetation datasets in a neural network	H: WGS84 V: EGM96	H: 3 arc sec × 3 arc sec (~90 m × 90 m) V: 2.99–3.75 m (LE90; for maximum elevations of 5 to 20 m); 2.63–3.23 m (RMSE; for maximum elevations of 5 to 20 m)	Kulp and Strauss (2021)	Free for scientific use
GLL-DTM v1	DTM	90° N to 90° S; input elevation < 10 m	14/10/2018 to 13/05/2020	Inverse distance interpolation of ICESat 2 satellite LiDAR data	H: WGS84 V: MSL	H: 0.05° × 0.05° (~5 km × 5 km) V: 0.50–0.54 m (RMSE; for maximum elevations of 2 to 10 m)	Vernimmen et al. (2020)	Free
AD-DEM	DTM	Ayeyarwady Delta; input elevation ≤ 10 m	26/01/2002 to 10/04/2004 (first order geodetic framework was conducted in 08/2000)	Aerial photography, levelling, GPS observations and aerial triangulation	H: Everest 1830; Adjustment 1937 V: MSL	H: 750 m × 750 m (~0.007 × 0.07°)	This study	Free

Shuttle Radar Topography Mission (SRTM) was a joint venture of NASA, the National Geospatial-Intelligence Agency and the German and Italian Space Agencies (Farr et al., 2007) that provides the first dataset of land elevation covering ca. 80 % of the Earth's land surfaces

(NASA JPL, 2016). In February 2000, the data was acquired by two antennas mounted on the shuttle and an extendable mast in 60 m distance. Since the radar signal could not sufficiently penetrate canopies, the SRTM DEM constitutes a digital surface model (DSM). The envisaged vertical accuracy of 16 m (linear error at 90 % confidence (LE90)) was achieved and is equivalent to <10 m root mean square error (RMSE) (Rabus et al., 2003; Rodríguez et al., 2005; Farr et al., 2007; Mukul et al., 2017). However, as global and regional comparisons against ground truth data turned out spatially varying vertical accuracy, it was decided to improve the quality of the SRTM globally by integrating satellite radar altimetry data from multiple missions to generate the Altimetry Corrected Elevations, Version 2, dataset (ACE2) (Table C1; Berry et al., 2010). In addition, GLOBE data was included to extend the original coverage area of SRTM to 60° S. After analysing waveforms of the entire geodetic mission, all accepted ones were retracked and fused with orbit data and the EGM96 geoid model (Lemoine et al., 1997) to refer to orthometric heights (Berry et al., 2010). From available spatial resolutions of 3, 9 and 30 arc seconds, we obtained data at the highest resolution of 3 arc sec (~90 m). While vertical errors still exceed 10 m (Table C1; Smith and Berry, 2009), the effective penetration of canopies by the altimeter signal, which is reflected by the ground, is responsible for the significant differences between the SRTM and ACE2 that have been documented particularly for tropical rain forests (Smith and Berry, 2009). However, being merged with the SRTM dataset, the ACE2 should not be regarded as a thorough DTM. While water body data is available for the SRTM, distinguishing water from land by two classes, additional datasets for ACE2 include a source, quality, and confidence matrices (Smith and Berry, 2009).

In contrast to these DEMs, the Advanced Spaceborne Thermal Emission and Reflection Radiometer (ASTER) Global Digital Elevation Model (GDEM) Version 3 (ASTGTM) is based on optical stereo imagery acquired by the ASTER instrument (Yamaguchi et al., 1998) mounted on NASA's Terra satellite which was launched in 1999 (Abrams et al., 2020). Version 3 (published in 2019; Abrams et al., 2020) includes 200,000 additional scenes to supplement and fill data gaps of previous versions and has been processed by applying anomaly corrections and void filling with data from ASTER GDEM version 2, SRTM (processed for NASADEM), and ALOS World 3D-30 m (AW3D30) (Abrams and Crippen, 2019). Both datums and resolutions are similar to SRTM. Vertical accuracy, which is 20 m (LE95) and 10.20 m RMSE for version 1 (Ministry of Economy, Trade and Industry (METI) of Japan et al., 2009), has been documented to improve significantly towards version 2 while only minor further improvements have been observed towards version 3 (e.g., Tachikawa et al., 2011; Abrams and Crippen, 2019;

Talchabhadel et al., 2021; Altunel et al., 2022). Along with the ASTER GDEM version 3 (ASTGTM), the ASTER Water Body Dataset (ASTWBD) was published, subdividing water bodies into ocean, river, and lake classes (Abrams et al., 2020).

Similar to ASTER, the ALOS World 3D 30 m mesh (AW3D30) constitutes a DSM originating from optical data, that was acquired by using the Panchromatic Remote sensing Instrument for Stereo Mapping (PRISM) of the Advanced Land Observing Satellite (ALOS) operated by the Japan Aerospace Exploration Agency (JAXA) (Tadono et al., 2016). Using ortho-rectified PRISM imagery of 2.5 m spatial resolution, the AW3D DSM (5 m spatial resolution) was generated (Takaku et al., 2014) and subsequently resampled by applying averaging and selecting medium heights, respectively (Tadono et al., 2016). Absolute vertical accuracy was determined for more than 5,000 ground control points spread over 127 DEM tiles and revealed errors of ~4.40 m, which is below the targeted 5 m mark (Table C1; Tadono et al., 2016). Available additional datasets related to the AW3D30 include a mask file, distinguishing between sea and inland water bodies (JAXA, 2019), a stacking number file, header, and quality assurance information files, as well as a list file for versions 2.1 and 2.2 (JAXA, 2019).

Covering more than 150 million km^2 (German Aerospace Centre (DLR), 2013), the TanDEM-X provides elevation data for the entire land surface of the Earth (Table C1). The DEM was generated based on interferometric synthetic aperture radar (SAR) data acquired by the twin satellite constellation of TerraSAR-X and TanDEM-X (Krieger et al., 2007; Wessel, 2018). DEM tiles of 12 m and 30 m spatial resolution can be accessed via the DLR website after submitting a proposal and are free of charge for scientific use. In contrast to the DEMs mentioned before, elevations of the TanDEM-X are given in ellipsoidal heights. Absolute vertical accuracy is less than 10 m (LE90; Wessel, 2018) while relative accuracy has been estimated at least for the TanDEM-X 12 m data and ranges from 2 m (for slopes ≤20 %) to 4 m (for slopes >20 %; Rizzoli et al., 2017; Wessel, 2018). In addition, investigations on the terrain of selected test sites revealed RMSEs of up to 6.78 m (Wessel et al., 2018). To ensure transparency and enable detailed investigations of the dataset by the user, each TanDEM-X tile is provided in conjunction with a set of information layers, including, amongst others, a height error map, a water indication mask based on amplitude and coherence information (Wendleder et al., 2012), a coverage map as well as a layover and shadow mask (Wessel, 2018). Moreover, the TanDEM-X 12 m data of DLR were edited by Airbus Defence and Space to provide the so called WorldDEM in different versions to commercial users, including, amongst other improvements, the transformation from ellipsoidal to orthometric heights (Airbus Defence and

Space, 2018). To further improve the performance of the DEM, Airbus used the WorldDEM^{TM} version, where implausible terrain features and water bodies have been edited and controlled by a quality check (Airbus Defence and Space, 2018). Based on the WorldDEM^{TM}, Airbus Defence and Space (2020) generated several quality layers that provide auxiliary information and were published together with the DEM as the Copernicus DEM in 2021 (Airbus Defence and Space, 2020). Improvements include, for example, void filling with elevation data of ASTER, different versions of SRTM, GMTED2010, TerraSAR-X Radargrammetric DEM, AW3D30, and Norway DEM (Airbus Defence and Space, 2020). Thus, absolute vertical accuracy improved to <4 m compared to the TanDEM-X 12 m (Table C1) and recent publications recommend its use over previous global DEMs (Guth and Geoffroy, 2021; Marešová et al., 2021). From available 10 m, 30 m, and 90 m spatial resolutions of Copernicus DEM, we used the 30 m version. The water body mask that is provided by Airbus Defence and Space (2020) allows for separating ocean, lakes, and rivers.

The most recently published global DEM is the so-called Forest And Buildings removed Copernicus DEM (FABDEM) of Hawker et al. (2022). Using a three-step correction workflow including forest and building predictor data, random forest machine learning models, and post-processing, they eliminated the bias of tree and building heights in the Copernicus DEM GLO-30 (Hawker et al., 2022), thereby providing nearly terrain elevation. Vertical errors of the Copernicus DEM were reduced from 2.87 to 2.33 m RMSE (1.61 to 1.12 m mean absolute error (MAE)) for urban areas and from 7.98 to 4.96 m RMSE (5.15 to 2.88 m MAE) for forest areas (Hawker et al., 2022).

In contrast to these global DEMs generated for being used in various applications, the CoastalDEM (Kulp and Strauss, 2018; Kulp and Strauss, 2021) and the Global LiDAR lowland DTM (GLL-DTM v1; Vernimmen et al., 2020) aim at improving studies of SLR, flooding, and vulnerability in coastal settings (Kulp and Strauss, 2018; Kulp and Strauss, 2019; Vernimmen et al., 2020; Hooijer and Vernimmen, 2021; Kulp and Strauss, 2021). In 2018, Kulp and Strauss (2018) published their first version of the CoastalDEM, which included 23 variables and is based on SRTM elevation data trained with airborne LiDAR elevation data from the United States and Australia in a multilayer perceptron neural network. Though elevation bias could be reduced for test sites in the United States and Australia, the CoastalDEM v1.1 was likely overfitted as comparisons with other global and local DEMs for study areas like the Mekong Delta show (Vernimmen et al., 2020). Therefore, Kulp and Strauss (2021) revised the CoastalDEM by updating source elevation data with the recently published NASADEM (i.e.,

an improved SRTM; Buckley et al., 2020), using global ICESat 2 satellite LiDAR data for training, and including new and updated input variables in a convolutional neural network (Table C1; Kulp and Strauss, 2021). Thus, for maximum elevations of 5 m (20 m), LE90 improved from 4.24 m (5.73 m) of CoastalDEM v1.1 to 2.99 m (3.75 m) of CoastalDEM v2.1, which is equivalent to reduced RMSE of 4.02 m (4.83 m) in v1.1 and 2.63 m (3.23 m) in v2.1 (Kulp and Strauss, 2021).

Instead of using ICESat 2 data for training, Vernimmen et al. (2020) interpolated the ground track data themselves into a DEM (Table C1). However, due to the setup of the satellite LiDAR with ~90 m across-track distance within beam pairs and along-track distance of ~ 2.5 km (Neuenschwander et al., 2021), horizontal accuracy of the GLL-DTM is much less than for other global DEMs (Table C1) but will likely be improved in future versions as the number of ICESat 2 recordings increases (Vernimmen et al., 2020). The dataset is referenced to MSL based on Mean Dynamic Topography (MDT) data of Rio et al. (2014) and yields vertical accuracies of 0.54 m RMSE for coastal lowland <10 m (Table C1; Vernimmen et al., 2020).

C1.1.3 Mean dynamic topography

In the absence of available information on local MSL in Myanmar and its potential offset to a geoid reference, we used MDT data as an estimation of sea surface height in relation to geoid. Furthermore, it may provide a more steady and reliable reference given the spatial and temporal variability of tidal range.

The latest MDT, i.e. the CNES-CLS18 dataset of Mulet et al. (2021), was used and accessed via the AVISO+ website (https://www.aviso.altimetry.fr/en/data/products/auxiliary-products/mdt/mdt-global-cnes-cls18.html, last access: 22 February 2022). Compared to previous MDT data, the MDT CNES-CLS18 dataset (from now on referred to only as MDT) combines extended records of altimetry and gravitational field measurements as well as in situ oceanographic data from drifting buoys and hydrological profiles and thereby provides estimates on mean sea surface heights at higher spatial resolution (i.e., 0.125°) with improvements particularly for coastal areas and ocean surface currents (Mulet et al., 2021; AVISO+, 2022). As the MDT is a global dataset covering all ocean surfaces of the Earth, it allows us to account for potential sea level variations along the Myanmar coast, especially from the delta towards Kyaikkhami at the Tanintharyi coast in the east and thus to apply a continuous MSL correction instead of using one single reference tide gauge. However, since the MDT is referenced to GOCO05s geoid (Mayer-Gürr et al., 2015), thereby differing from vertical datums

of the DEMs, requires investigations of geoid/ellipsoid height anomalies prior to converting the DEMs to MSL.

C1.2 Processing

C1.2.1 Generation of an elevation model for the Ayeyarwady Delta based on geodetic data

To create a local DEM for our region of interest (ROI; the spatial extent of the Ayeyarwady Delta as defined by Tessler et al. (2015)), 102 map sheets were georeferenced and digitised, covering also the wider surroundings (15°30’ N to 18°30’ N and 94°00’ E to 97°00’ E) to enhance the performance of DEM interpolation. In total, 9179 elevation points were digitised (5,673 lying within the ROI). These include also relative heights (e.g., in case of dam slopes) and benchmarks but given the absence of any documentation on their absolute elevation reduced the dataset to 8,145 spot heights (4,792 within the ROI). Albeit there are no significant differences between horizontal datums of the WGS84 and Everest 1830 ellipsoids, the digitised elevation data were projected to UTM 46 N based on the Everest 1830 ellipsoid to refer, besides the vertical reference, also to a common horizontal datum and UTM zone, consistent with the Myanmar 2000 datum (JICA et al., 2004b). Given unsystematically distributed point elevations and data gaps especially in the northern delta parts (Figure C1), contour lines of these areas were digitised with points extracted at 250 m and 2000 m intervals, respectively, to supplement the input elevation data for DEM interpolations and testing the impact of considering contour data in DEM interpolation. Furthermore, to reduce the potential of height overestimations in the immediate surroundings of outcrops and improve the quality of the DEM in low lying coastal areas, which are of particular interest in this study, values of elevation higher than a specific threshold are excluded, thereby eliminating outcrops.

Interpolation was conducted using the Geostatistical Wizard within the Analysis environment of ArcGIS Pro 2.9.1. Minderhoud et al. (2019) compared 22 interpolation methods for the creation of a DEM in a similar setting, i.e., the Mekong Delta, and found Empirical Bayesian Kriging with empirical transformation and exponential modelling providing the most accurate results (i.e., in terms of absolute accuracy), similar set-up settings were adopted in this study. The grid cell resolution was defined as justified by the point density following Aguilar et al. (2006). In total, nine versions of AD-DEM were generated – (i–iii) including digitised spot heights, (iv–vi) including spot heights and contour heights extracted every 250 m, and (vii–ix) including spot heights and contour heights extracted every 2000 m. All of them apply also specific elevation thresholds of 20 m and 10 m, respectively (Table C2).

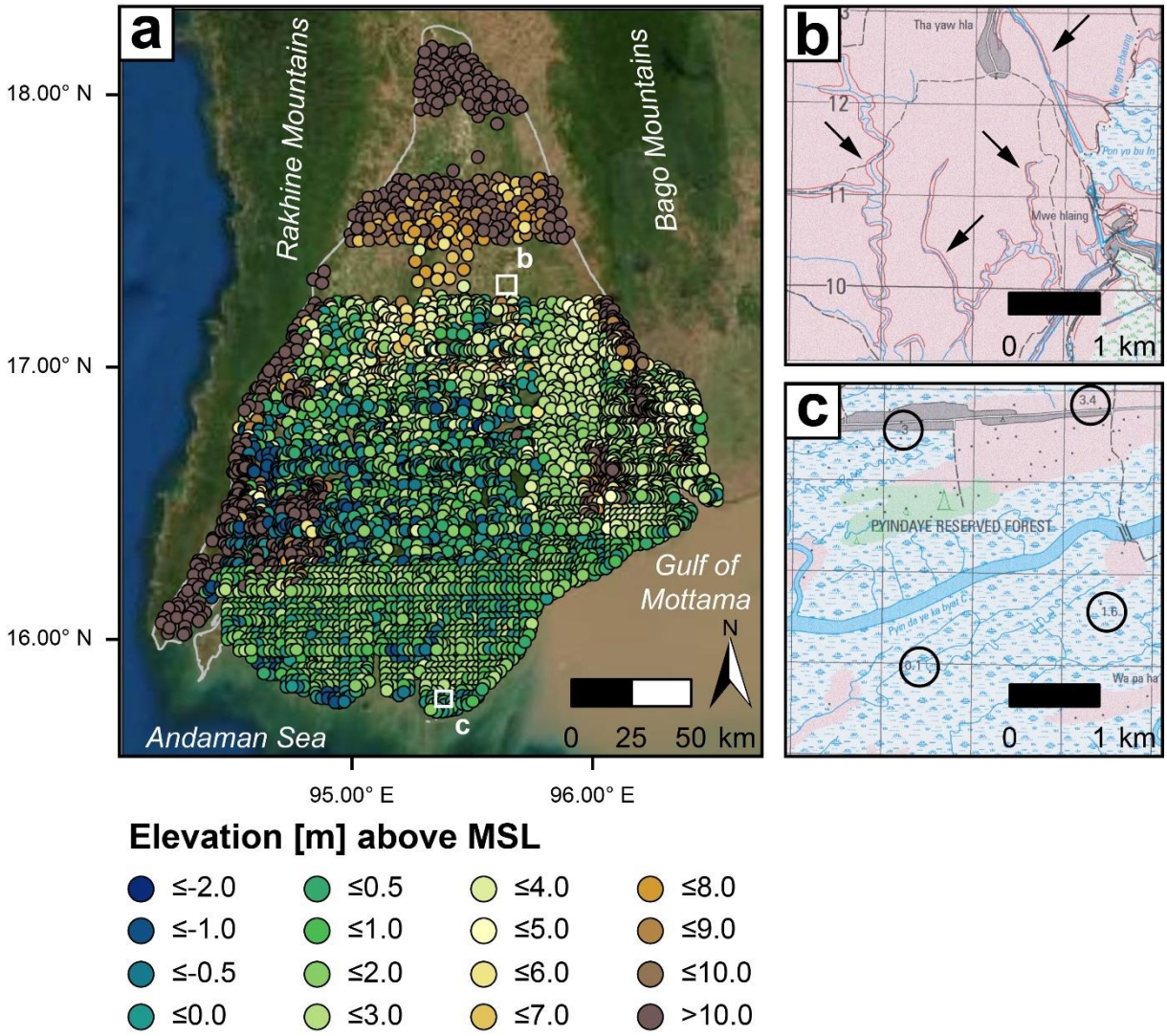


***Figure C1** | Spot heights from topographic maps used for interpolation of the AD-DEM (a; contour data are not shown).*
The spot heights in the north of the delta are irregularly distributed and do not provide full spatial coverage. In these parts, topographic information is only provided by contour lines along the river banks (marked with black arrows; b). The spot heights (marked with black circles; c) provide full spatial coverage and a more regular pattern in the southern, central part of the delta. a) is based on Esri World Imagery (2017); b) and c) are based on topographical map sheets 4143-4 (b) and 4040-1 (c) from East View Geospatial, Inc. (2014).

Areas – such as outcrops and northernmost delta parts – that are in reality higher than the elevation threshold applied for DEM interpolation were masked. As data collection for generating the topographic maps used for the AD-DEM was conducted between 2002 and 2004, the location of river channels is most likely best reflected by the SRTM water body mask created in 2000 as changes in geomorphology following river meandering and channel migration will be less compared to water masks of DEMs generated at a later point in time. Therefore, we used the SRTM water body mask file (NASA JPL, 2013) to exclude all areas marked as water from the final DEMs.

C1.2.2 Processing of global DEMs and determination of local mean sea level (MSL)

Pre-processing of global DEMs and their respective water mask files included mosaicking of single DEM tiles, re-projection to UTM 46 N based on Everest 1830 ellipsoid, and clipping to the ROI. The variety of vertical datums used by the array of DEMs together with the complex geoid setting along the Myanmar coast made datum transformation to MSL challenging as relations between vertical references of MDT and DEM data need to be considered when correcting from geoid to MSL (Figure 4.2). Processing involved in total three datum conversions. First, given that the majority of DEMs is referenced to the EGM96 geoid, the other datasets were transformed to EGM96 as well. Second, the original MDT data (called $MDT_{GOCO05s}$) was transposed to EGM96 (called MDT_{EGM96}). Given the general relationship of geoid and sea level according to Equation (1):

$$N_{GOCO05s} + MDT_{GOCO05s} = N_{EGM96} + MDT_{EGM96} \quad \text{Equation (1)}$$

where N_{EGM96} and $N_{GOCO05s}$ are the respective height anomalies in relation to the reference ellipsoid WGS84, $MDT_{GOCO05s}$ is the original MDT data that needs to be transposed to EGM96, hereafter referred to as MDT_{EGM96}, Equation (2) denotes the term of datum conversion of the MDT from GOCO05s to EGM96:

$$MDT_{EGM96} = MDT_{GOCO05s} + (N_{GOCO05s} - N_{EGM96}) \quad \text{Equation (2)}$$

Subsequently, the third datum conversion was conducted by applying the MDT_{EGM96} to correct the DEMs to MSL.

To transform the MDT of Mulet et al. (2021) from GOCO05s to EGM96, the offset between these two geoids was determined by using height anomaly to the reference ellipsoid WGS84. Height anomalies at 0.2° spatial resolution were obtained from the online ICGEM calculation service provided by the German Research Centre for Geosciences (GFZ; Ince et al., 2019). Compared to all other interpolation methods available in the geostatistical wizard of ArcGIS Pro, multiquadric radial basis functions revealed smallest RMSE, have been recommended also by other studies focussing on gravitational field modelling (Doganalp and Selvi, 2015; Li, 2018 and references therein), and were thus chosen to interpolate geoid height anomalies from point to raster. Overall negative height anomalies indicate the location of both geoids below the WGS84 ellipsoid and show repeated crossings along the Ayeyarwady Delta and Tanintharyi coasts, thus underpinning the use of a continuous MSL correction instead of referring to a single reference site (Figure C2). The offset between the two geoids was determined by subtracting the EGM96 from the GOCO05s data (Figure 4.2; Equation (1)).

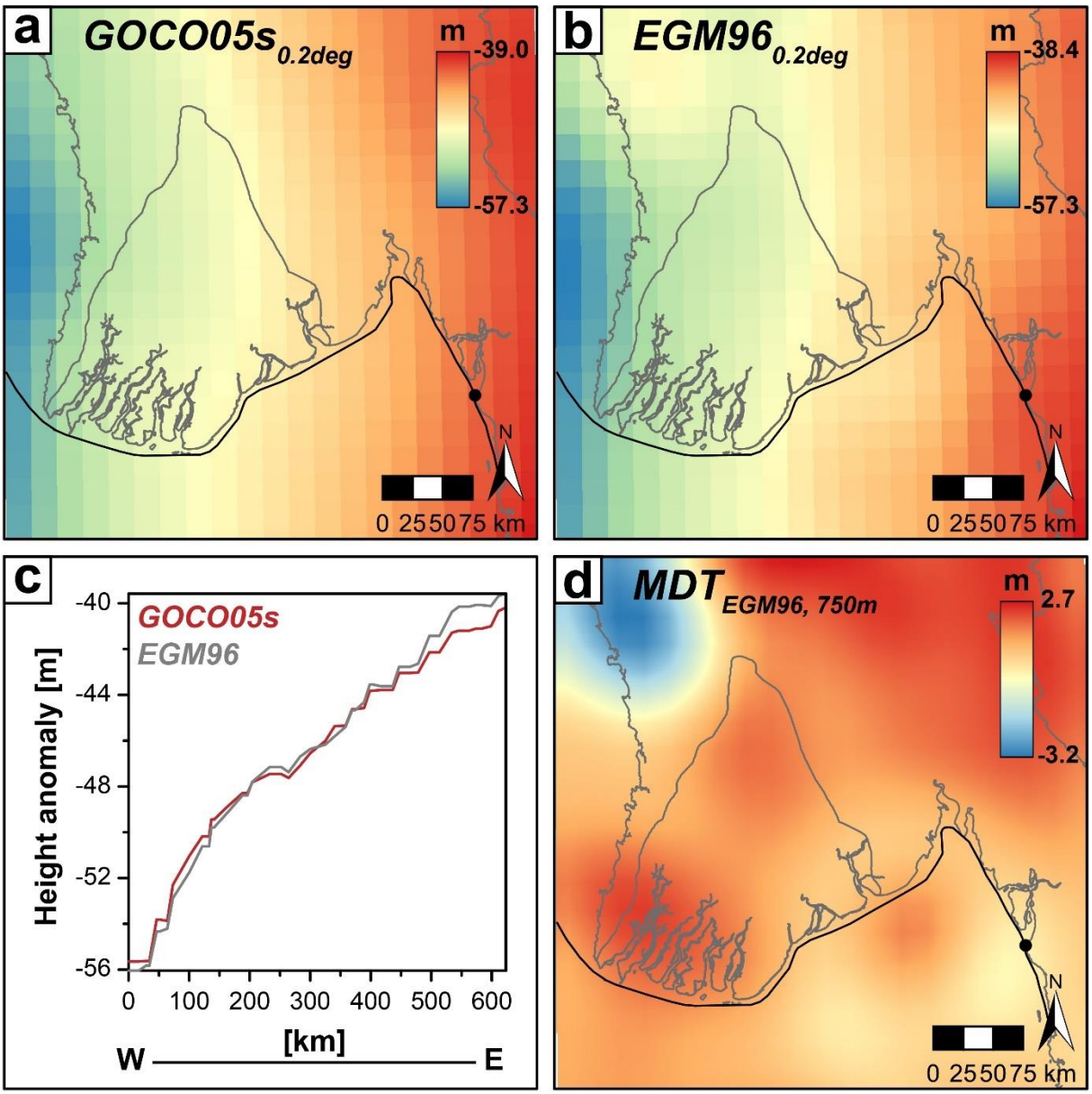


Figure C2 *| Regional setting of geoids (a–c) relevant to transpose MDT data from GOCO05s to EGM96 geoid (d). Height anomalies of GOCO05s and EGM96 compared to WGS84 ellipsoid (a and b) and compared to each other along a shoreline profile (black line; a–c). Processing of the MDT resulted in a MDT dataset, which is referenced to EGM96 geoid and resampled to a spatial resolution of 750 m (d). The black dot at the Tanintharyi coast shows the location of Kyaikkhami, where the original vertical basis of Myanmar elevation data is located.*

Before adding the offset to the $MDT_{GOCO05s}$ data to transpose it to EGM96 according to Equation (2), extrapolation over land is required to enable calculation of MDT with elevation data. For this, points were created from the $MDT_{GOCO05s}$ raster and interpolated over land. The decision whether to use IDW interpolation or Empirical Bayesian Kriging was made based on the point comparison of input and output data at identical locations. Residuals are almost absent for both interpolation algorithms. Finally, inverse distance weighting (IDW, with a power of 2) was used for interpolating the MDT data as it takes the closest value along the coast for extrapolation over land (see also Vernimmen et al., 2020). Finally, the resolution of the

processed MDT_{EGM96} was resampled to match the resolution of the AD-DEM using bilinear interpolation.

For converting vertical datums of the DEMs, we first transformed tiles of TanDEM-X, Copernicus DEM, and FABDEM to EGM96 geoid (15 min resolution) prior to mosaicking using the elevation recalculation raster function in ERDAS Imagine 2020 software environment. It should be noted that since the GLL-DTM v1 of Vernimmen et al. (2020) was already referenced to MSL, this DEM did not require the processing as outlined in Figure 4.2. However, the GLL-DTM v1 refers to MSL based on an older MDT dataset (Rio et al., 2014), which is referenced to the EGM-DIR-R4 geoid, where the potential offset between this geoid and the original geoid reference of DEM data was not considered. Without the MDT interpolation over land of Vernimmen et al. (2020), undoing their MSL referencing to MDT of Rio et al. (2014) and applying our MDT correction would introduce additional bias and thus seems not meaningful. Due to the missing integration of geoid offset, the GLL-DTM v1 should be used with caution. Although we are unable to correct the GLL-DTM v1 ourselves, we included it into our investigations of the Ayeyarwady Delta as it was generated especially for coastal lowlands and to highlight the importance of carefully dealing with vertical datums of datasets using different geoid models.

Prior to transformation of the AD-DEM from its original reference (i.e., local MSL at Kyaikkhami) to the continuous MSL of the MDT_{EGM96}, the offset of MSL Kyaikkhami to EGM96 was determined. According to MDT_{EGM96}, MSL at Kyaikkhami is nearly identical with the EGM96 geoid height with offsets of ~0.02 m (0.125° resolution) and ~0.01 m (750 m resolution; Figure C3). Though the accuracy of MDT data has been improved to centimetre scale since the launch of the GOCE satellite in 2009 (Knudsen et al., 2011), comparisons of latest MDT datasets with independent MDT data and tide gauges document regional deviations of up to ~10 cm (Hamden et al., 2021), thus exceeding the offset of Kyaikkhami MSL to EGM96. Therefore, we did not correct for the local geoid offset in Kyaikkhami but converted the vertical reference of the AD-DEM to MSL in the delta directly by subtracting MDT_{EGM96}, without prior transposition of elevation data to EGM96. Against the background that geoid omission errors and commission errors of both geoid and mean sea surface data constitute the total error of satellite-based MDT data (Bingham et al., 2014; Andersen et al., 2018), it should be kept in mind that uncertainties remain particularly for coastal zones as altimetric monitoring and geoid mapping are influenced by the more pronounced coastal topography/bathymetry

compared to off-shore as well as coastal MDT dynamics (Andersen et al., 2018; Filmer et al., 2018).

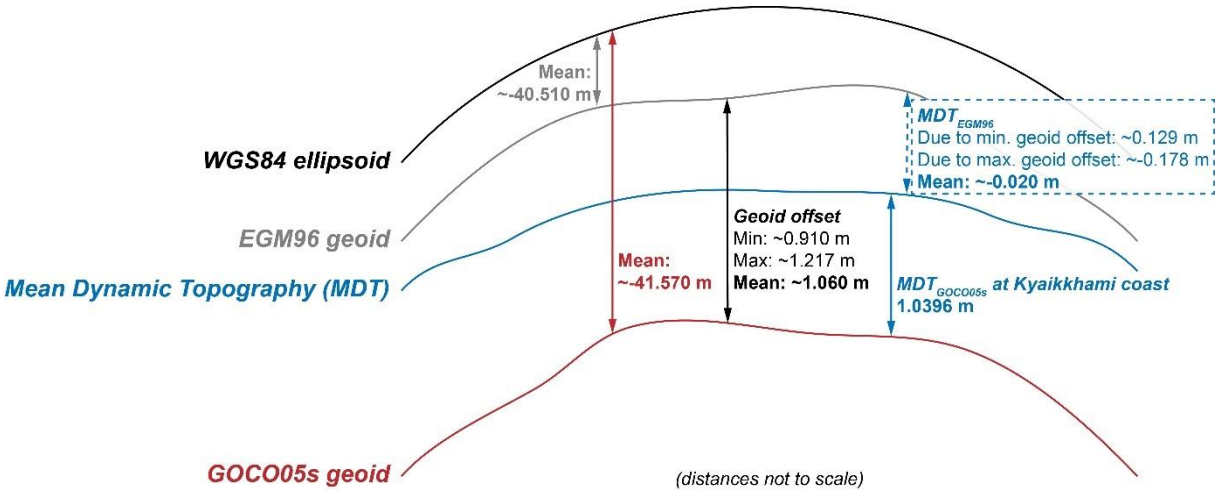


***Figure C3** | Relations between Mean Dynamic Topography (MDT) and EGM96 and GOCO05s geoids with respect to WGS84 ellipsoid for the coastal area of Kyaikkhami in Myanmar (distances are not to scale).*
To transpose the AD-DEM from local MSL at Kyaikkhami to a continuous local MSL (based on MDT_{EGM96}), first the difference between the vertical reference of the AD-DEM (i.e., MSL at Kyaikkhami) and EGM96 needs to be determined. Based on the original resolution of the MDT data (0.125°), this offset is only ~0.02 m and hardly ~0.01 m if the resampled MDT (750 m spatial resolution) is used. Therefore, the vertical reference of the AD-DEM can be converted to the continuous sea level directly, without prior transposition of the elevation data to EGM96.

After referencing the DEMs to MSL, inland water bodies were masked using the DEM-specific water mask files. In addition, cell values with an elevation of more than 7 m below MSL were removed as they likely constitute erroneous height estimates, following Vernimmen et al. (2020) who refer to the lowest point of the Netherlands located in the Zuidplaspolder (e.g., de Groot-Reichwein et al., 2014). Depending on the type of validation, i.e., with spot heights from topographic maps (East View Geospatial, Inc., 2014) or the AD-DEM, the global DEMs were further processed. The spatial resolution of the DEMs was resampled to match comparably the horizontal accuracy of the AD-DEM using the bilinear resampling technique. For validating the GLL-DTM v1, the AD-DEM was resampled to its resolution of 0.05° (Table C1). Since outcrops and elevation values outside critical lowlands have been excluded to improve the interpolation of the AD-DEM, these areas were also excluded in the global DEMs to ensure comparability among all DEMs of this study.

C1.2.3 Mapping of areas prone to monsoon flooding

Besides direct validation using spot heights and the AD-DEM, we also performed an additional validation of relative elevation for the DEMs by their ability to match observed floods in deltaic areas affected by inland flooding. We adopted the principal approach from Minderhoud et al. (2019) who used the correlation of land elevation and tidal flooding to assess the quality of

DEMs indirectly. Here, we use mappings of recent monsoon floods due to increased discharge as this allows for investigating the relation between topography and flood pattern also inland. Therefore, we mapped areas inundated during the monsoon periods of 2015 and 2020, respectively, using an image rationing change detection approach on Sentinel 1 imagery (10 m spatial resolution) in the environment of Google Earth Engine (GEE; Gorelick et al., 2017). The pre-event imagery was recorded in February during the dry season while the selection of imagery capturing maximum flood extents was made based on investigations of rainfall amounts and river discharge. Monthly accumulated precipitation estimates were obtained from the GPM_3IMERGM v6 product of NASA Global Precipitation Measurement (GPM) program (Huffman et al., 2019) for the rainy months from May to October via the NASA Giovanni web environment (NASA, 2021). Discharge estimates from satellite microwave radiometry were accessed via the River and Reservoir Watch Version 4.5 processor of the Dartmouth Flood Observatory (Brakenridge et al., 2022) and were downloaded for River Watch stations 25, 29, and 30. Since an array of GEE scripts has been published in the recent past (e.g., Inman and Lyons, 2020; Peter et al., 2020; Mehmood et al., 2021; Moharrami et al., 2021; Tripathy and Malladi, 2022), we adopted the script of United Nations Platform for Space-based Information for Disaster Management and Emergency Response (UN-SPIDER 2019) and slightly adjusted it, i.e., by setting the difference threshold to 1.3, thereby minimising false positive and false negative detections. For further handling and analysis, the data was vectorised in the ArcGIS Pro environment.

C2. Results and interpretation

C2.1 Performance and accuracy of the AD-DEM

Table C2 *| Summary of cross validation measures for all nine versions of the AD-DEM from the Empirical Bayesian Kriging algorithm.*
To ensure data accuracy as good as possible, especially in data sparse and low-lying delta parts, DEM interpolation was conducted by integrating spot heights and points extracted from contour lines in 250 m and 2000 m intervals, respectively, as well as by excluding elevations >20 m and >10 m. Since the AD-DEM, which was generated based on spot heights and points taken from contour lines in a 250 m interval, both ≤10 m, reveals the lowest error statistics, this version (in italics) was used for assessing the performance of common global and coastal DEMs.

	AD-DEM$_{i}$	**AD-DEM$_{ii}$**	**AD-DEM$_{iii}$**	**AD-DEM$_{iv}$**	**AD-DEM$_{v}$**	***AD-DEM$_{vi}$***	**AD-DEM$_{vii}$**	**AD-DEM$_{viii}$**	**AD-DEM$_{ix}$**
Contour points interval	-	-	-	250 m	250 m	*250 m*	2000 m	2000 m	2000 m
Integrated elevation threshold	-	≤ 20 m	≤ 10 m	-	≤ 20 m	*≤ 10 m*	-	≤ 20 m	≤ 10 m
N (spot heights)	8145	5666	5108	8145	5666	*5108*	8145	5666	5108
N (contour points)	-	-	-	22791	20580	*13582*	2068	1841	1205
Mean (prediction error)	0.110	-0.028	-0.008	-0.044	0.040	*0.025*	0.017	-0.003	0.005
Mean (prediction error) standardised	0.015	0.003	-0.003	Not a number	Not a number	*Not a number*	0.008	0.003	Not a number
RMSE	41.682	2.104	1.221	21.749	1.454	*1.004*	38.040	2.013	1.226
RMSE standardised	0.936	0.970	0.987	Not a number	Not a number	*Not a number*	1.129	1.037	Not a number
Average standard error	39.260	2.174	1.221	20.125	1.352	*0.864*	36.475	2.015	1.177
Inside 90 % interval	91.381	91.264	90.290	95.009	96.079	*96.426*	91.687	91.45	91.589
Inside 95 % interval	95.838	95.747	95.419	97.062	97.706	*97.790*	95.457	95.19	95.121
Average CRPS	9.519	0.882	0.619	2.923	0.353	*0.251*	8.017	0.783	0.547

C2.2 Performance and accuracy of global satellite-based DEMs

C2.2.1 Performance of global DEMs based on visual impression

Table C3 *| Raster statistics for DEMs of this study.*
All DEMs were referenced to MSL. Elevations <-7.00 m above MSL and outcrops were excluded. Note that the GLL-DTM v1 refers to a different MDT dataset than used in this study, and without being corrected for geoid offset.

DEM	**Resolution (m)**	***N***	**Min (m)**	**Max (m)**	**Mean (m)**	**Median (m)**	**σ (m)**
SRTM	30	27134565	-7.00	72.18	4.69	3.90	3.36
ACE2	90	11306350	-7.00	43.91	1.68	0.94	3.13
ASTGTM v003	30	27098350	-2.21	90.88	6.99	6.32	3.50
AW3D30	30	27152171	-7.00	158.10	4.36	3.68	3.05
TanDEM-X 30 m	30	26808299	-7.00	402.91	3.06	2.01	3.17
TanDEM-X 12 m	12	167583275	-7.00	469.41	3.08	2.00	3.29
Copernicus DEM	30	26193614	-6.88	48.65	3.04	1.99	3.06
FABDEM	30	26193621	-1.84	45.59	2.75	1.83	2.59
CoastalDEM v2.1	90	3032777	-7.00	36.05	2.24	1.38	2.40
GLL-DTM v1	~5889	633	0.31	9.88	2.62	2.07	1.75
AD-DEM	~5889	713	-1.62	8.69	2.07	1.33	2.39
AD-DEM	750	45075	-1.72	8.80	2.08	1.28	2.42

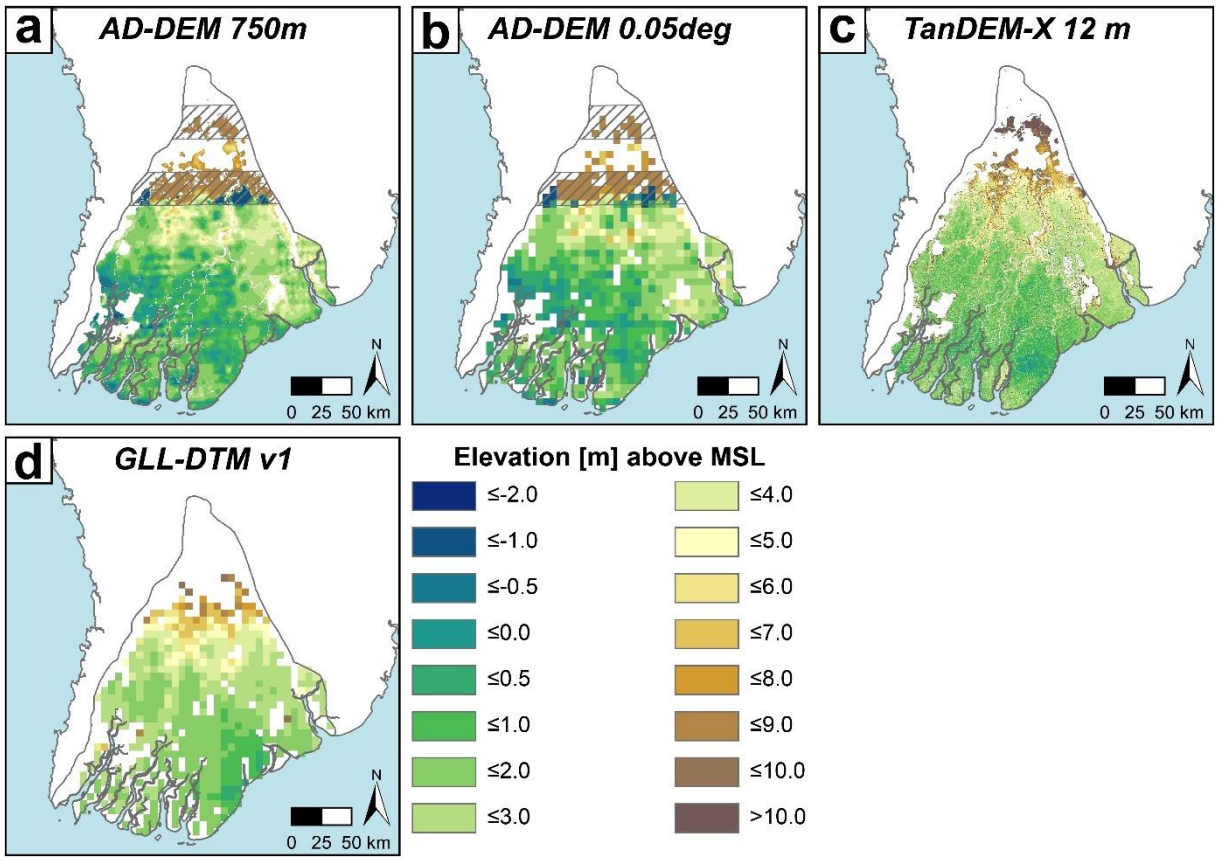


***Figure C4** | The new local AD-DEM (a and b) in comparison to global digital elevation models in the Ayeyarwady Delta, which were excluded from the main text (c and d).*
Areas where AD-DEM has interpolation artefacts are hatched.

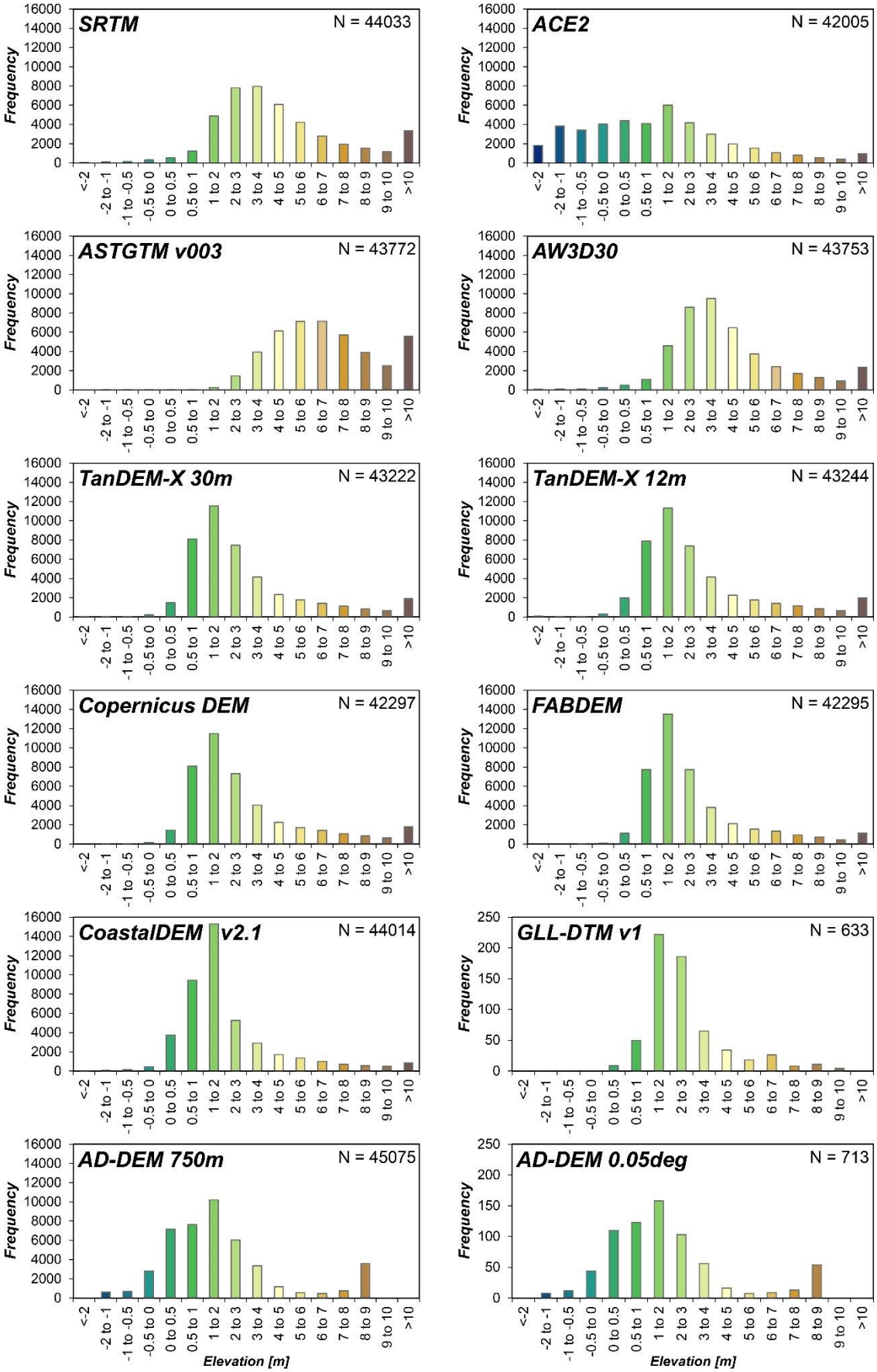


***Figure C5** | Frequency distribution of elevation counts (in m) for each DEM (based on versions resampled to 750 m).*

C2.2.2 Direct validation with spot heights from topographic maps

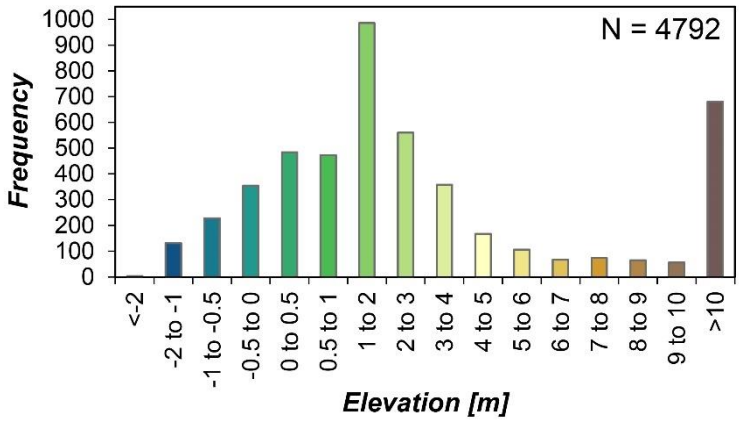


Figure C6 | *Frequency distribution of elevation counts (in m) for spot heights inside the ROI of the Ayeyarwady Delta.*

Table C4 | *Statistics for DEMs minus spot height elevation at spot height location.*
Best performances are shown in italics. DEMs were used in their original resolution. Since the GLL-DTM v1 is only valid for the low elevation coastal zone, it is excluded from validation with all spot heights. All DEMs were referenced to the same mean sea level. N – Number of spot heights in the ROI, with no data values excluded for each DEM respectively; HR – Height residual; MAE – Mean absolute error; RMSE – Root mean square error; Min – minimum DEM elevation at spot height location; Max – maximum DEM elevation at spot height location; Mean spot – mean elevation of all spot heights included in the comparison; Mean DEM – mean DEM elevation at all spot height locations included in the comparison; Median spot – median elevation of all spot heights included in the comparison; Median DEM – median DEM elevation at all spot height locations included in the comparison; σ spot – standard deviation of elevation of all spot heights included in the comparison; σ DEM – standard deviation of DEM elevation at all spot height locations included in the comparison; σ HR – standard deviation of height residuals; R^2 – Coefficient of determination.

DEM	N	Mean HR	MAE	RMSE	Min DEM	Max DEM	Mean spot	Mean DEM	Median spot	Median DEM	Median HR	σ spot	σ DEM	σ HR	R^2
TanDEM-X 12 m	4654	-0.19	3.16	7.61	-4.74	161.44	6.12	5.93	1.72	2.38	0.52	16.30	11.76	7.61	0.82

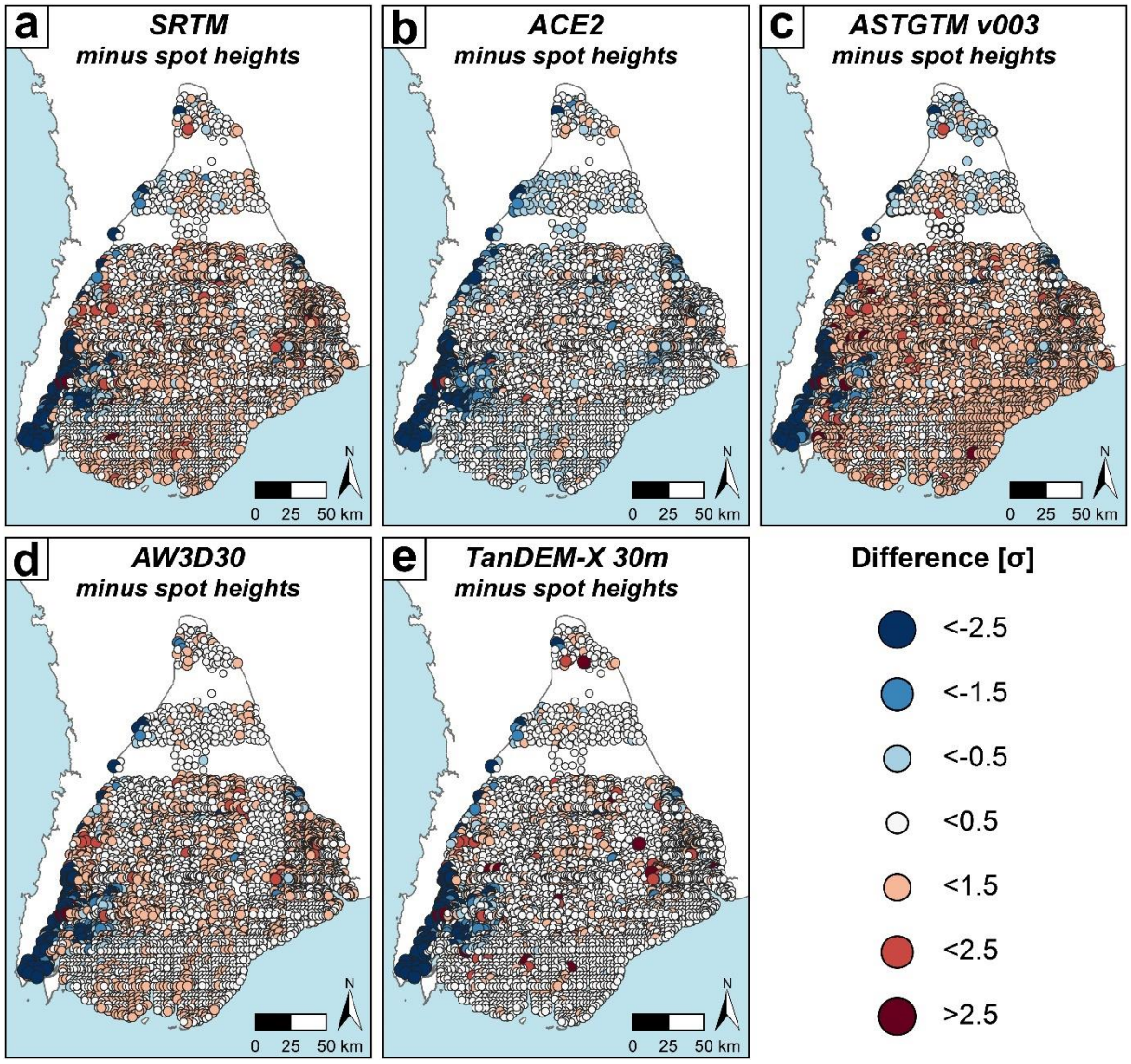


***Figure C7** | Spot height residuals for global DEMs classified by standard deviation.*

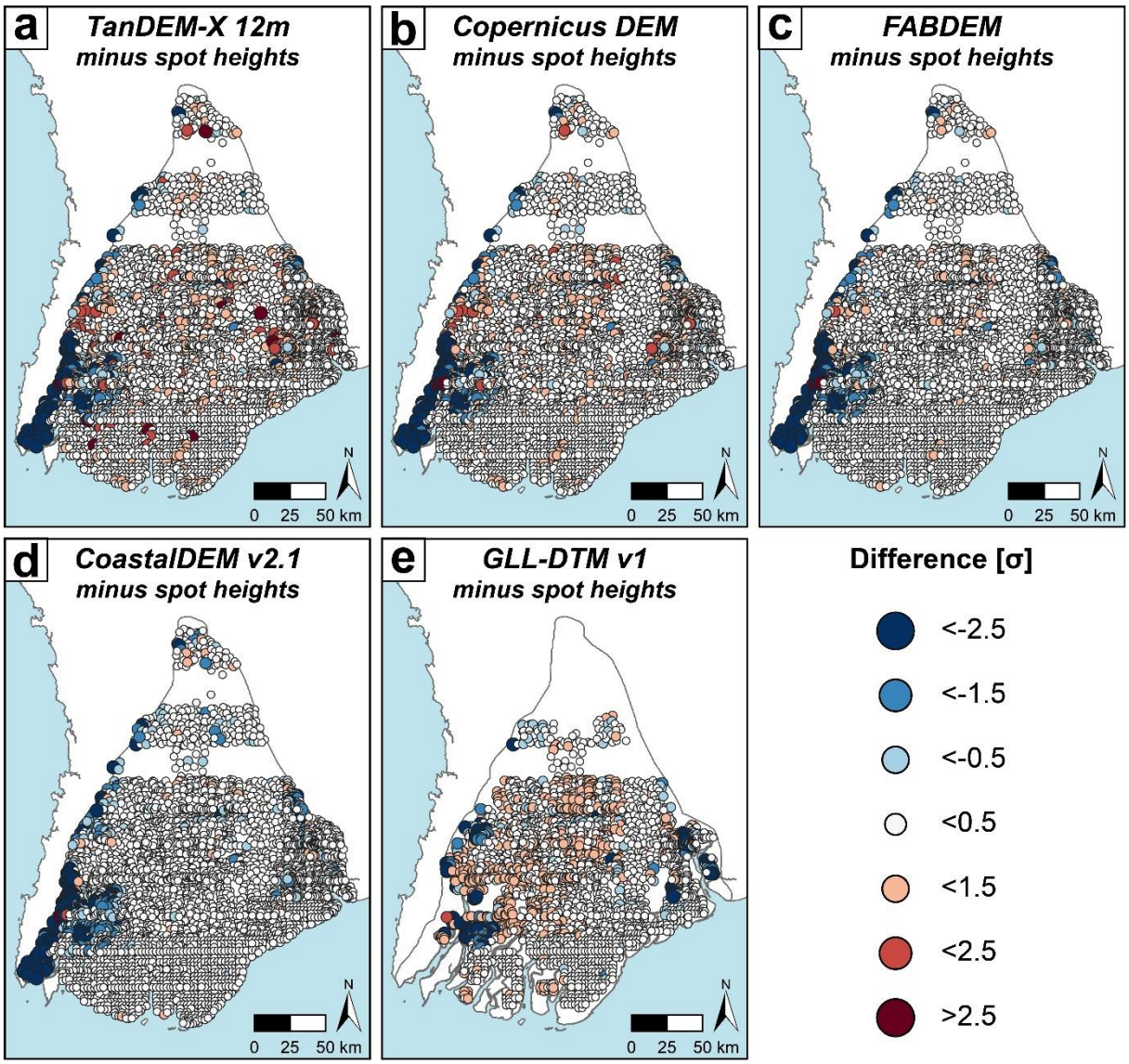


***Figure C8** | Spot height residuals for global DEMs classified by standard deviation.*

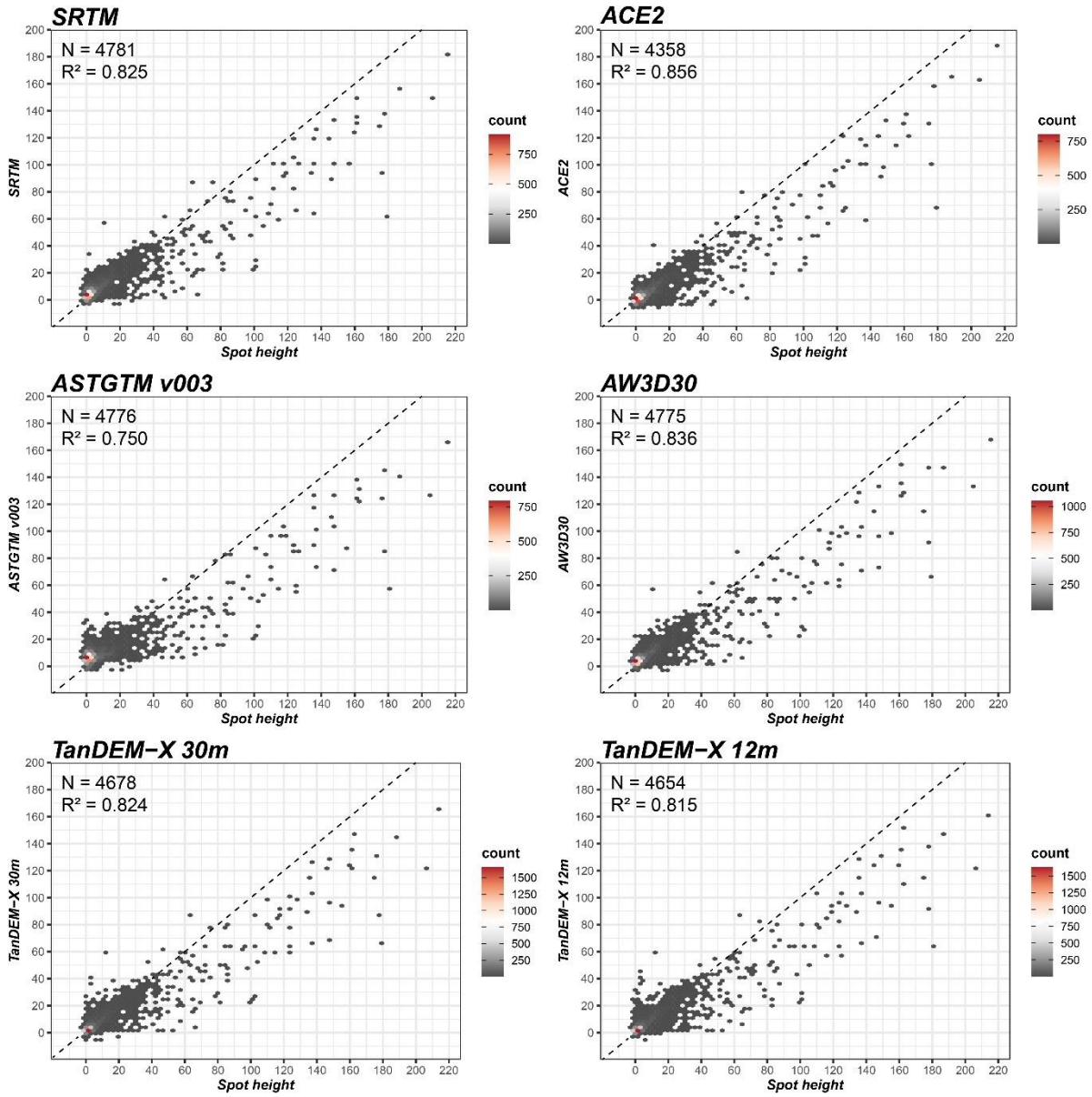


***Figure C9** | 2D density plots for global DEMs in comparison with spot heights in relation to the 1:1 line.*

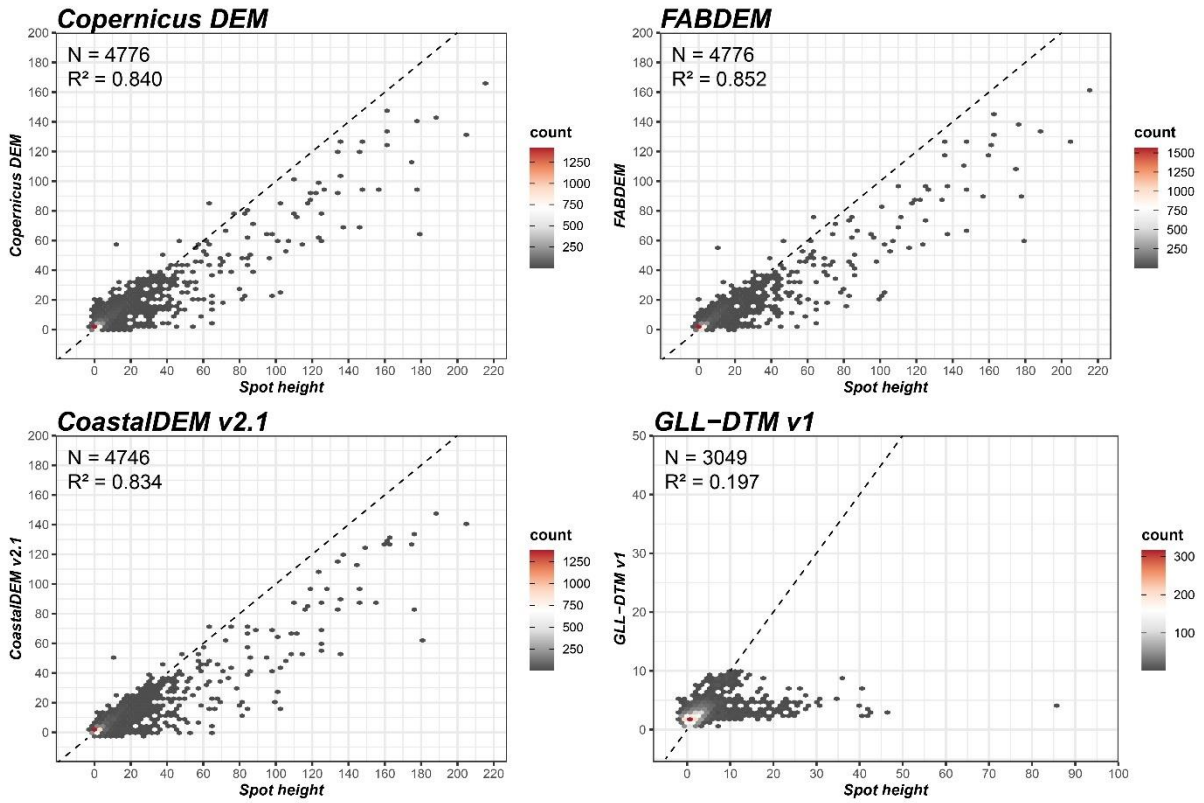


***Figure C10** | 2D density plots for global DEMs in comparison with spot heights in relation to the 1:1 line.*

***Table C5** | Statistics for DEMs minus spot height elevation at spot height location for the low-lying delta plain (spot heights <10 m above MSL).*
DEMs were used in their original resolution and vertically referenced to the same mean sea level. Note that the GLL-DTM v1 refers to a different MDT dataset than used in this study, and without being corrected for geoid offset.

DEM	*N*	Mean HR	MAE	RMSE	Min DEM	Max DEM	Mean spot	Mean DEM	Median spot	Median DEM	Median HR	σ spot	σ DEM	σ HR	R^2
TanDEM-X 12 m	3977	1.18	1.85	3.26	-4.74	46.60	1.83	3.02	1.33	2.05	0.67	2.21	3.44	3.04	0.24
GLL-DTM v1	2893	0.58	1.38	1.79	0.36	9.60	1.78	2.36	1.35	2.04	0.62	2.11	1.37	1.70	0.35

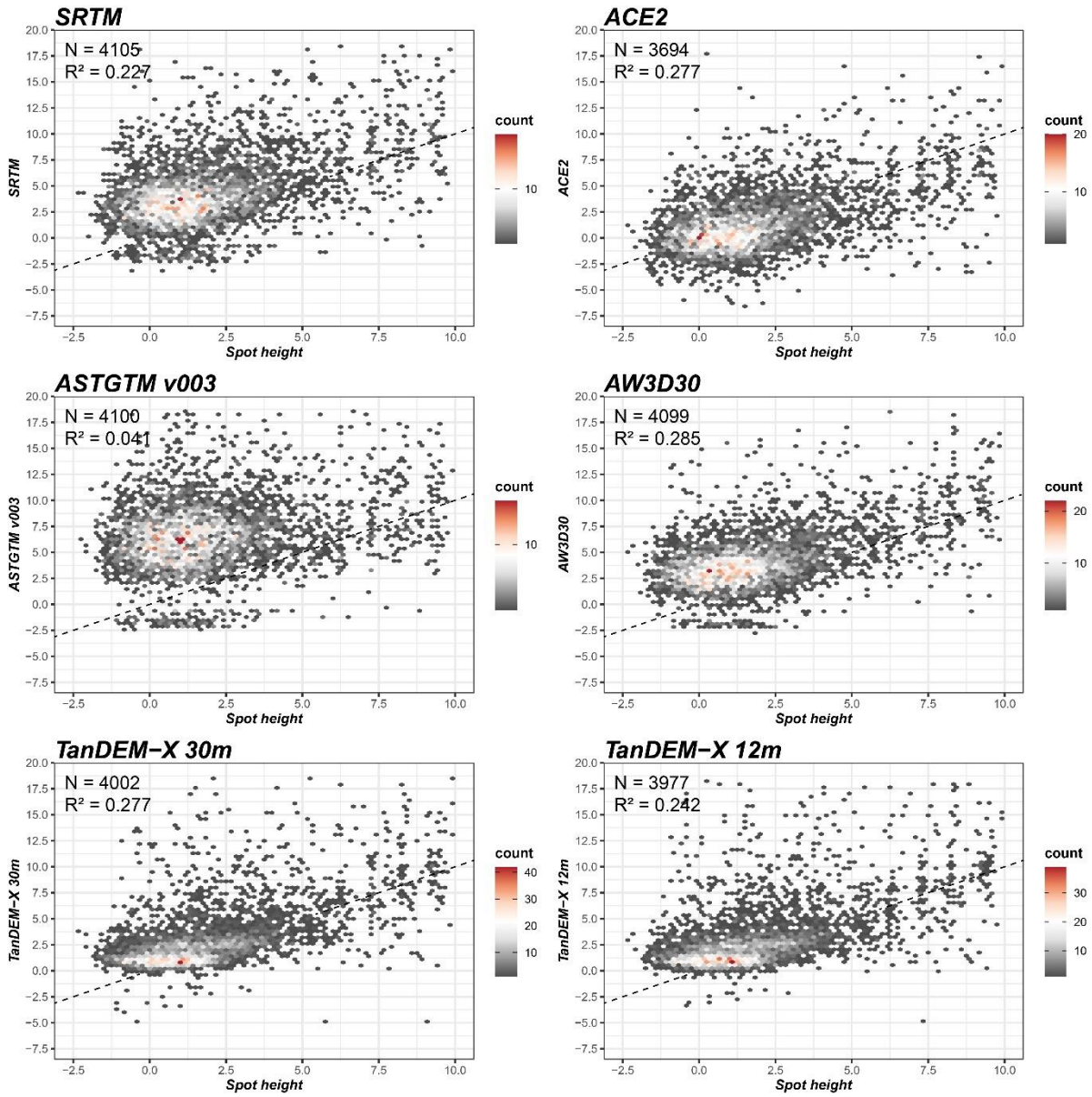


***Figure C11** | 2D density plots for global DEMs in comparison with spot heights of less than 10 m above MSL in relation to the 1:1 line.*
For better visualisation, the maximum of the y axis was limited to 20 m and higher DEM elevations are not shown.

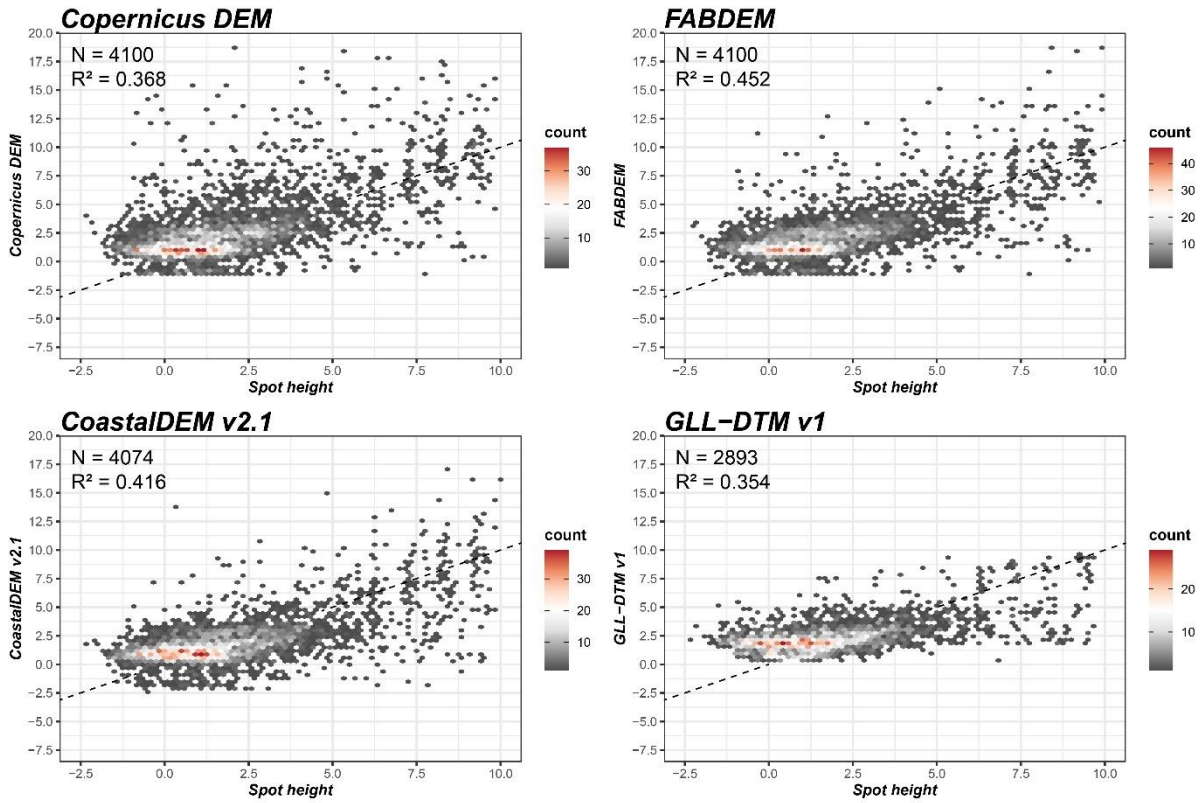


***Figure C12** | 2D density plots for global DEMs in comparison with spot heights of less than 10 m above MSL in relation to the 1:1 line.*
For better visualisation, the maximum of the y axis was limited to 20 m and higher DEM elevations are not shown.

C2.2.3 Direct validation of global DEMs with AD-DEM

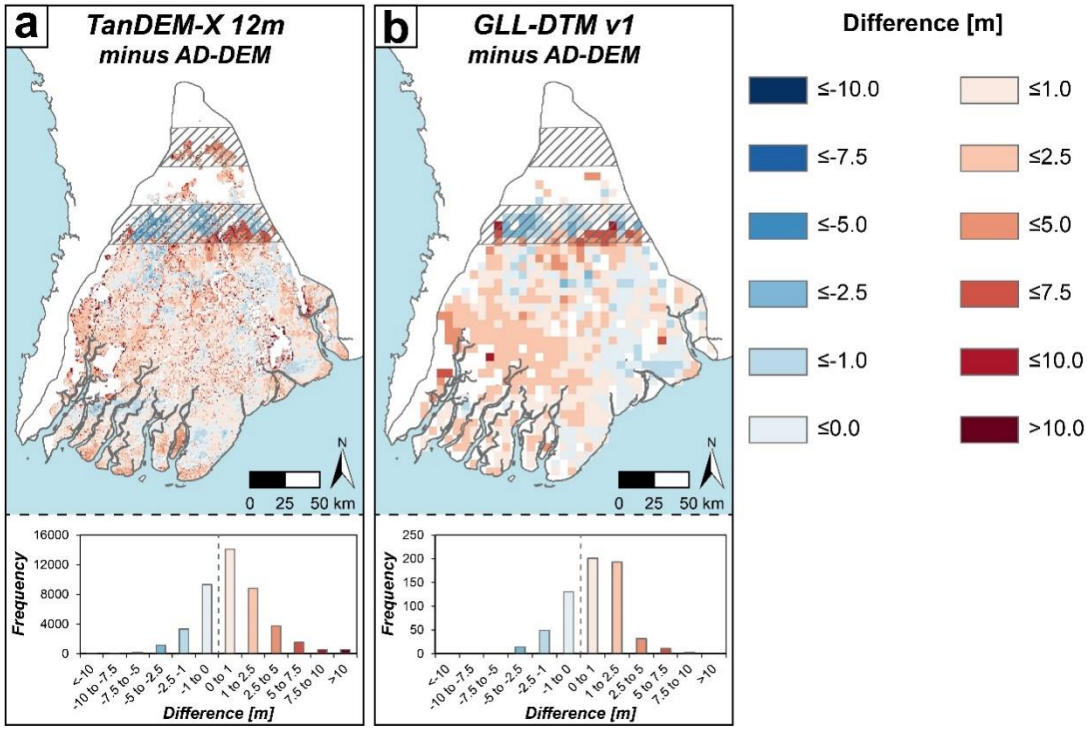


***Figure C13** | Differences between global DEMs and the AD-DEM together with frequency distributions of height residuals (in m).*

Note that for calculating differences between GLL-DTM v1 and AD-DEM, the AD-DEM was used with a resolution of 0.05°. Areas where AD-DEM has interpolation artefacts are hatched.

***Table C6** | Statistics for DEM minus AD-DEM. Best performances are shown in italics.*
Elevations located in the centre of individual raster cells of AD-DEM were subtracted from those extracted from all other DEMs, respectively. DEMs were resampled to 750 m to match the horizontal resolution of the AD-DEM. All DEMs were referenced to mean sea level. Elevations <-7.00 m above sea level and outcrops were excluded and water masks applied.

DEM	*N*	Mean HR	MAE	RMSE	Min DEM	Max DEM	Mean AD-DEM	Mean DEM	Median AD-DEM	Median DEM	Median HR	σ AD-DEM	σ DEM	σ HR	R^2
SRTM	40043	2.55	2.89	3.83	-5.73	39.01	2.13	4.68	1.31	3.86	2.22	2.44	3.27	2.86	0.28
ACE2	36398	-0.47	-1.94	2.68	-6.40	31.86	2.18	1.71	1.34	0.94	-0.67	2.50	3.07	2.64	0.32
ASTGTM v003	39303	4.87	5.17	6.10	-0.37	47.23	2.13	7.00	1.32	6.41	4.75	2.45	3.24	3.67	0.04
AW3D30	39313	2.23	2.62	3.43	-6.97	51.61	2.16	4.38	1.30	3.68	2.07	2.48	2.99	2.62	0.31
TanDEM-X 30 m	37989	0.94	1.61	2.74	-6.72	43.31	2.15	3.09	1.29	2.03	0.49	2.48	3.18	2.57	0.38
TanDEM-X 12 m	37961	0.93	1.58	2.62	-6.16	29.68	2.15	3.08	1.29	2.05	0.51	2.48	3.09	2.45	0.40
Copernicus DEM	35854	0.91	1.55	2.57	-1.15	32.46	2.17	3.08	1.29	2.05	0.50	2.50	3.05	2.40	0.41
FABDEM	35843	0.63	1.27	2.00	-0.85	31.18	2.17	2.80	1.29	1.89	0.46	2.50	2.61	1.90	0.53
CoastalDEM v2.1	40015	*0.17*	*1.17*	*1.75*	-4.71	27.61	2.12	2.29	1.31	1.41	*0.19*	2.44	2.38	*1.74*	*0.55*
GLL-DTM v1	30724	0.674	1.15	1.57	0.32	9.71	1.98	2.66	1.30	2.13	0.66	2.24	1.70	1.41	0.60

C2.2.4 Recent flood events in the Ayeyarwady Delta and indirect validation of DEMs with flood mappings/flood-prone areas

Recent precipitation and flood events in the Ayeyarwady Delta: The Indian monsoon seasons 2015 and 2020

Aside the long-term risk of SLR and coastal storm surges due to tropical cyclones that make landfall in the region (e.g., Brakenridge et al., 2017; Brill et al., 2020), climatological hazards in Myanmar and the Ayeyarwady Delta are heat waves, droughts, as well as extreme precipitation, subsequent floods, and landslides, all of them related to the spatiotemporal variability of the monsoon regime (e.g., Horton et al., 2017; Masson-Delmotte et al., 2021; Zin Mie Mie Sein et al., 2022 and references therein). Flood events in the delta after cyclone Nargis 2008 were mainly induced by heavy rains and increased discharges during the Indian Monsoon season (e.g., Brakenridge et al., 2017; Myanmar Information Management Unit (MIMU), 2017, 2020; UN Office for the Coordination of Humanitarian Affairs (OCHA), 2017, 2018, 2020). In 2015, country-wide flooding occurred due to exceptionally intense monsoon precipitation, which can be related to phases 5 and 6 of a strong Madden–Julian Oscillation (Brakenridge et al., 2017; Da Silva and Matthews, 2021), and that was accompanied by additional rainfalls of tropical cyclone Komen that made landfall in Bangladesh (Government of the Union of Myanmar, 2015). Precipitation amounts exceeded average monsoonal rainfalls by up to 400 % (Brakenridge et al., 2017), and resulted in flooding of unprecedented extent, affecting more than 1.6 million people (with 132 deaths), and up to 530,000 ha of agricultural and aquacultural production areas (Brakenridge et al., 2017; IFRC, 2017; Government of the Union of Myanmar, 2015).

Within the defined delta ROI, rainfalls occurred throughout the monsoonal period, especially from June to August. Precipitation peaked at maximum 987 mm accumulated in July, whereas the maximum countrywide was more than 1,800 mm (Figure C14). River discharge behaves slightly time-elapsed to precipitation, showing maximum discharges in July, August, September, and October (Figure C15). Thereby, the discharge amounts nicely reflect how the distributaries buffer upstream runoff. Flooding occurred already by mid of August (Copernicus Emergency Management Service, 2015), but was most extensive in deltaic districts in September (i.e., Pathein, Hinthada, Bago West and Ma-ubin) with more than 3250 km^2 of the ROI being flooded (Figures 4.5 and C19).

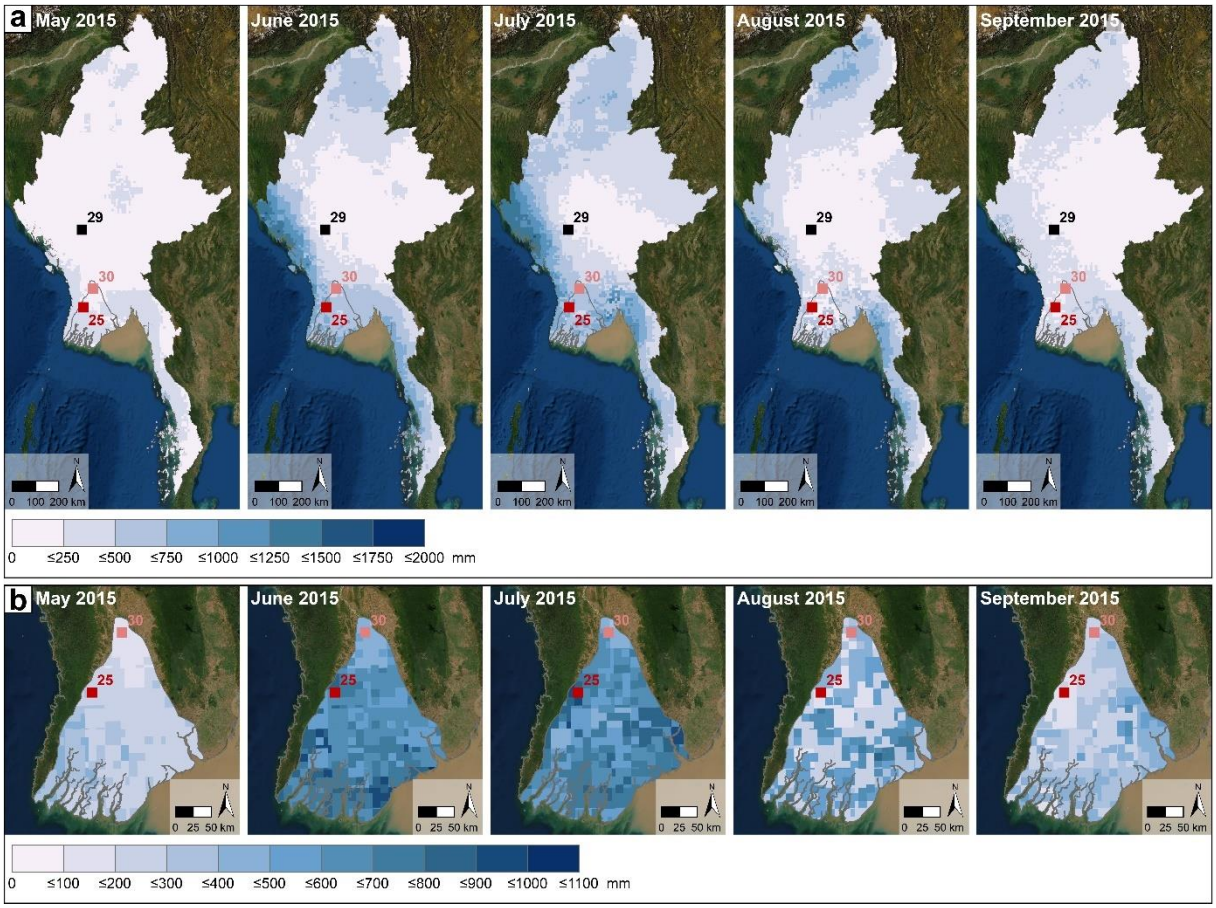


***Figure C14** | Monthly accumulated precipitation in Myanmar (a) and the Ayeyarwady Delta (b) for the monsoon season 2015 together with locations of microwave discharge measurement sites (Brakenridge et al., 2022) based on Esri World Imagery (2017).*

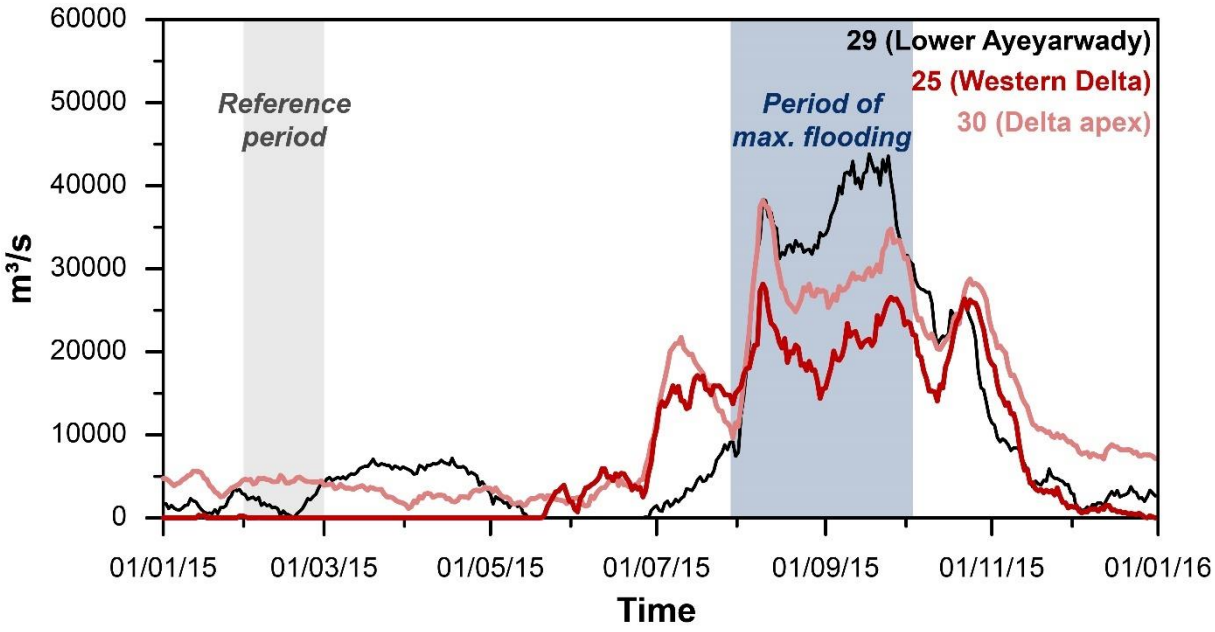


***Figure C15** | Discharge pattern of the monsoon season 2015.*
10-day average discharges are shown for River Watch stations 25, 29, and 30 located at the Ayeyarwady River. Data were accessed via the River and Reservoir Watch Version 4.5 processor of the Dartmouth Flood Observatory (Brakenridge et al., 2022).

In contrast, the 2020 monsoon season was moderate (Department of Meteorology and Hydrology (DMH), 2020). Monsoonal precipitation was accompanied by additional rainfalls of tropical storm Noul that made landfall in Vietnam (ECHO, 2020). 4 deaths were reported due to a landslide event in Mandalay Region (OCHA, 2020), and at least 21,500 people were affected by overflow of the Ayeyarwady and Thanlyin Rivers (Mi Mi Tun, 2020). However, since ca. 1,950 km^2 were inundated in the Ayeyarwady and Bago (West) Regions by 1st September, probably up to 267,277 people were exposed to flooded areas (MIMU, 2020).

From the GPM data, we reveal maximum rainfall in Myanmar of more than 1600 mm accumulated in Myingun Island south of Sittwe in August, whereas in the delta, monthly accumulated precipitation peaked at 833 mm (Figure C16). Generally, the 2020 rainfalls reflect stronger intra-seasonal variability than 2015, which is also reflected by the discharge period. While flooding occurred from June to September, it was most extensive by the end of August, following maximum discharge and amounting to more than 2,700 km^2 (Figures 4.5, C17 and C19). In line with the 2020 precipitation pattern, where highest rainfall amounts were accumulated in the most seaward delta parts as compared to 2015, also the flooded areas of 2020 extend further south than in 2015 (Figures 4.5 and C19). It is therefore likely that these delineated areas not only become flooded due to river and channel overflow but also because of water saturation of the soils.

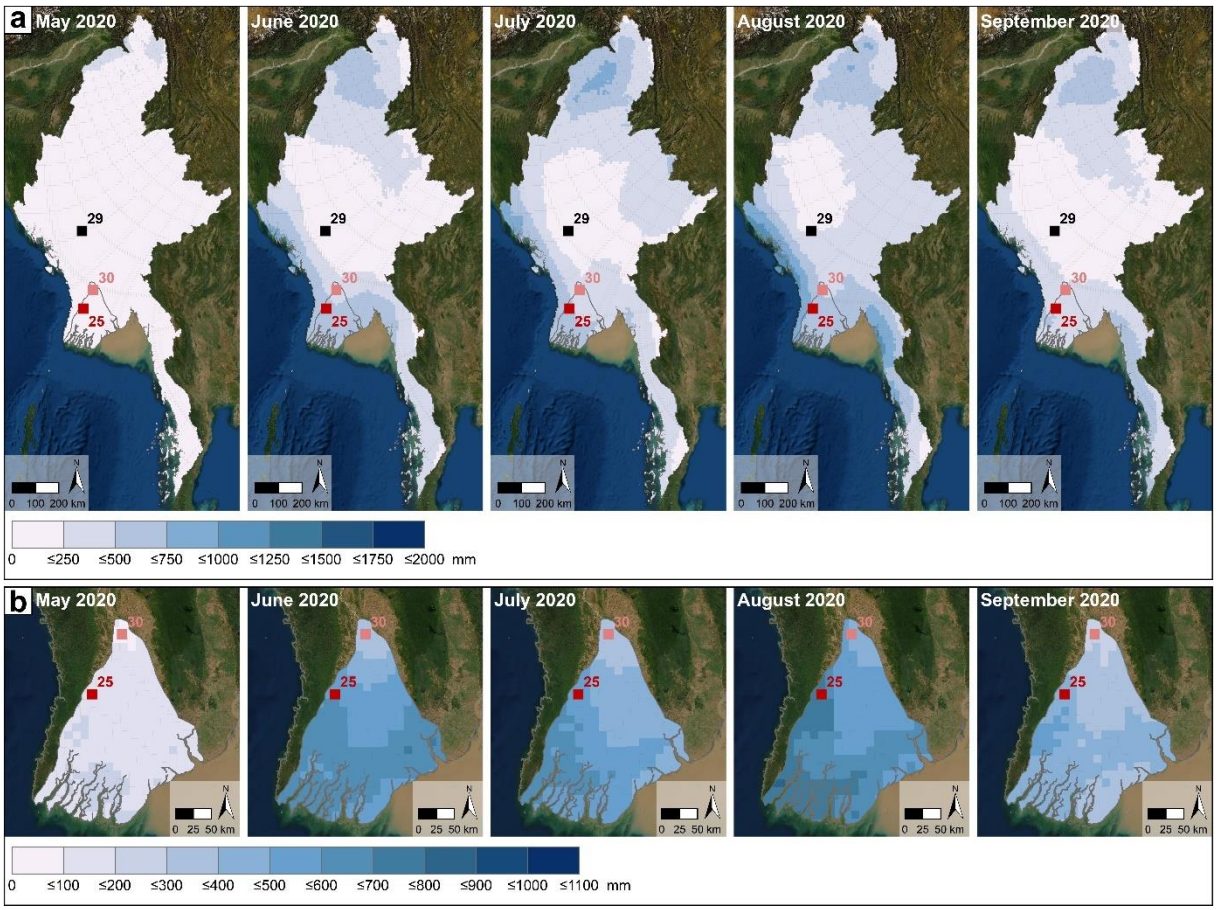


***Figure C16** | Monthly accumulated precipitation in Myanmar (a) and the Ayeyarwady Delta (b) for the monsoon season 2020 together with locations of microwave discharge measurement sites (Brakenridge et al., 2022) based on Esri World Imagery (2017).*

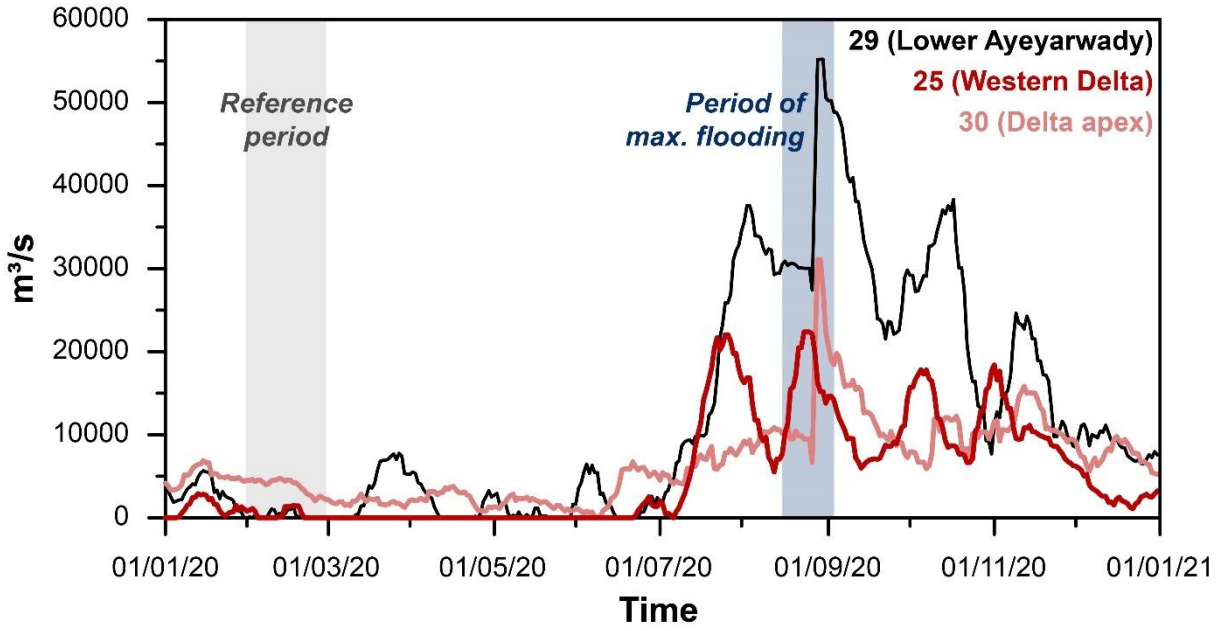


***Figure C17** | Discharge pattern of the monsoon season 2020.*

10-day average discharges are shown for River Watch stations 25, 29, and 30 located at the Ayeyarwady River. Data were accessed via the River and Reservoir Watch Version 4.5 processor of the Dartmouth Flood Observatory (Brakenridge et al., 2022).

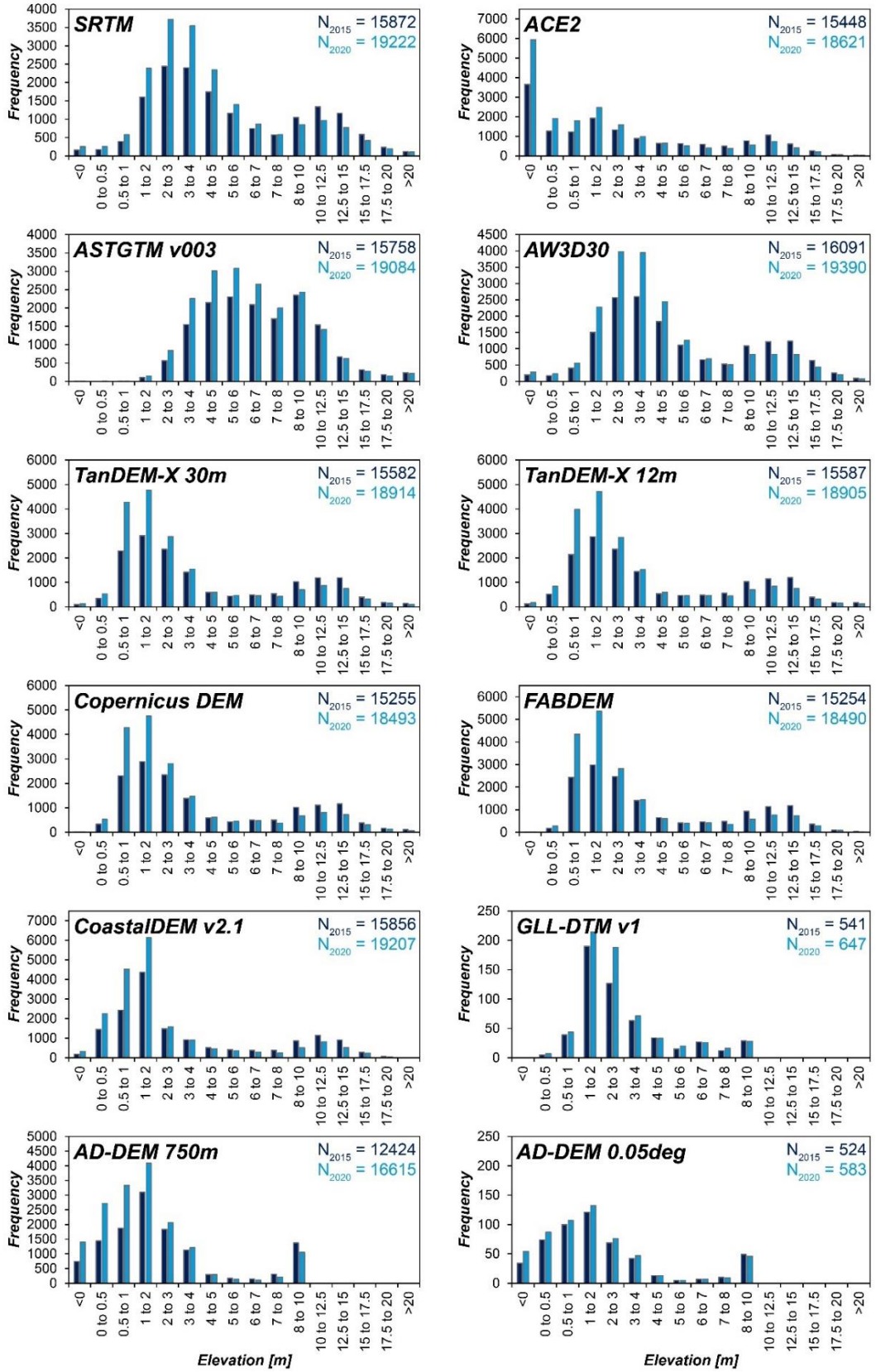


***Figure C18** | Frequency distribution of elevation counts (in m) for DEMs inside areas affected by flooding during the monsoon season of 2015 (dark blue) and 2020 (light blue).*

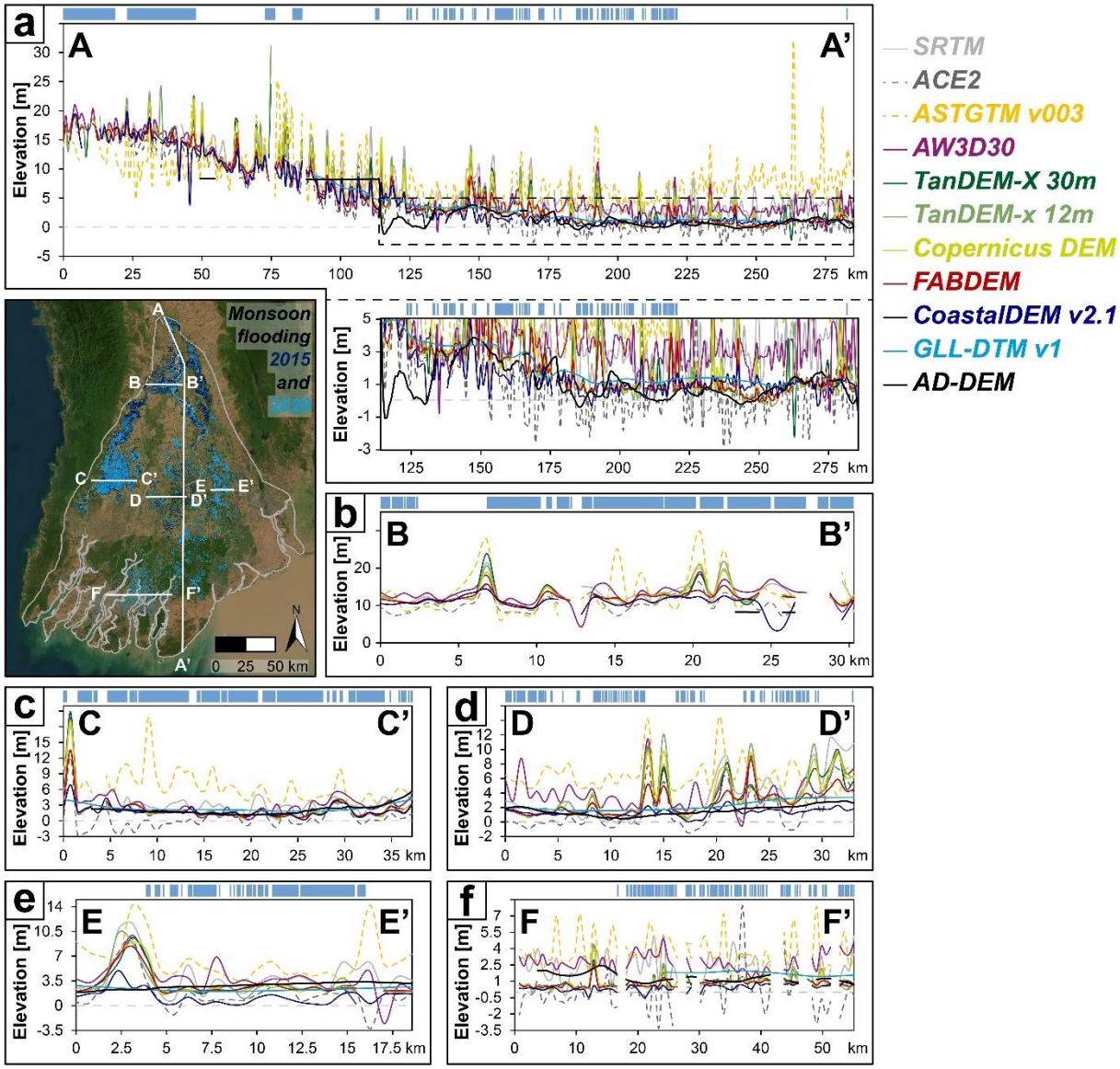


***Figure C19** | Delta elevation along longitudinal (a) and cross sections (b–f) in deltaic areas affected by flooding during the monsoon seasons 2015 and 2020 (Base map: Esri World Imagery, 2017).*
Elevation profiles are based on DEMs resampled to 750 m spatial resolution, except of the GLL-DTM v1, which was used in its original resolution of 0.05°. Blue bars on top of the profiles indicate the location of inundated areas along the profiles. The black-dashed rectangle in (a) marks the low elevation zone along the longitudinal profile that is also shown enlarged.

C2.3 Estimation of low-lying coastal area at risk of future sea-level rise

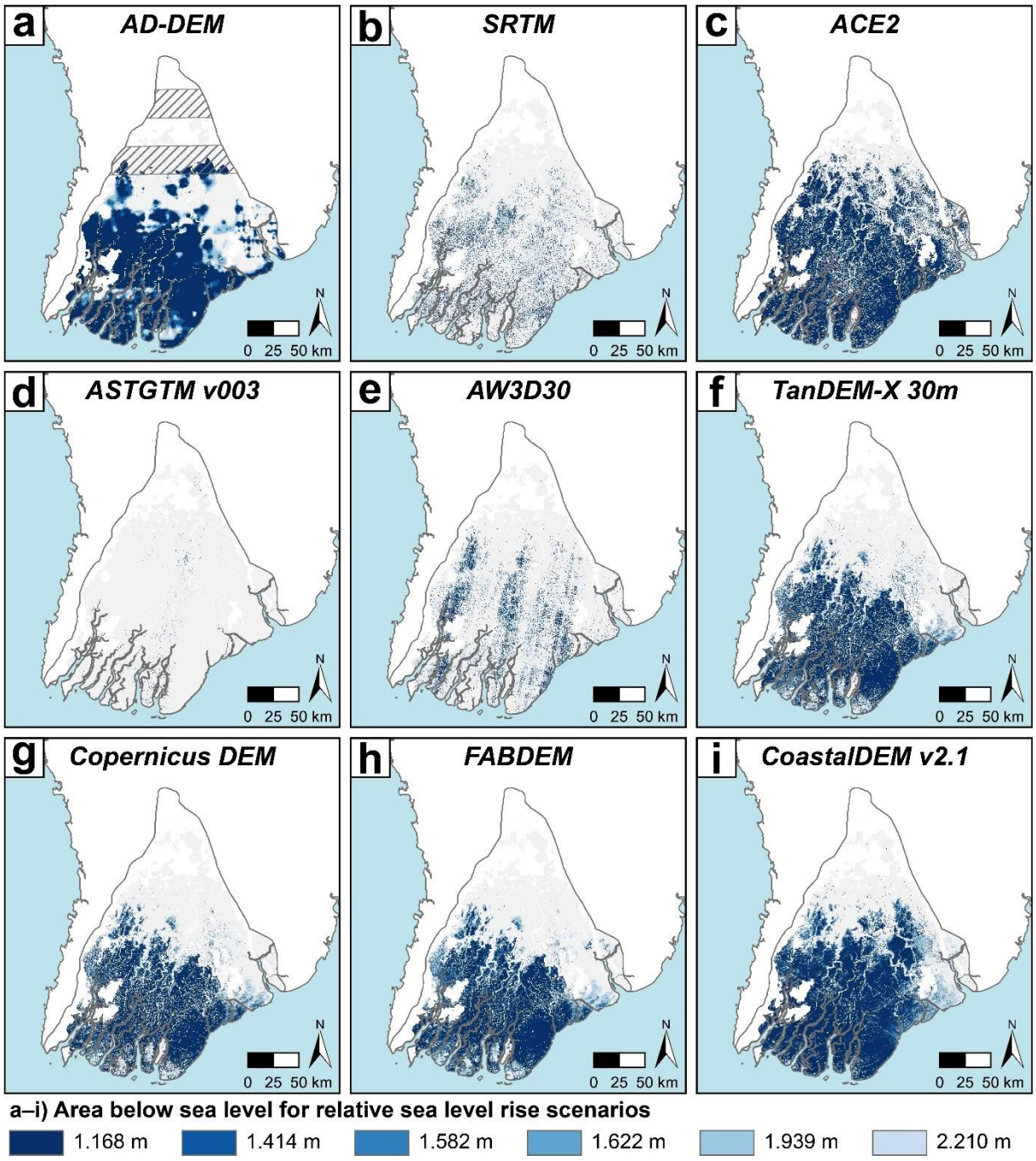


***Figure C20** | Area below future mean sea level according to local and global DEMs following median sea level rise projections for Yangon for 2150 (compared to the baseline period 1995–2014) from the Sea Level Projection Tool of the IPCC 6th Assessment Report (Fox-Kemper et al., 2021; Garner et al., 2021, 2022).*
Note that in case of higher RSLR, these scenarios will be reached sooner than 2150.

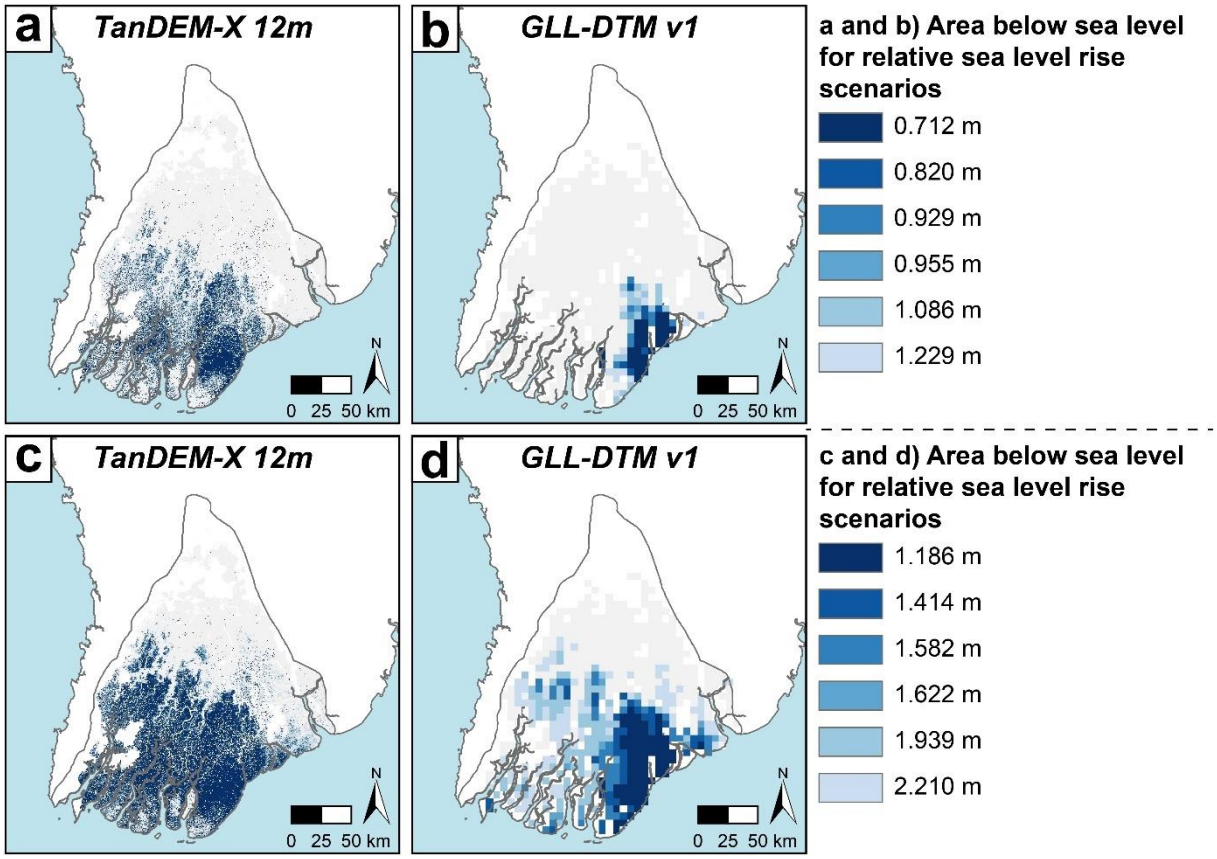


***Figure C21** | Area below future mean sea level according to global DEMs, which were excluded from the main text, following median sea level rise projections for Yangon for 2100 (a and b) and 2150 (c and d) (compared to the baseline period 1995–2014) from the Sea Level Projection Tool of the IPCC 6th Assessment Report (Fox-Kemper et al., 2021; Garner et al., 2021, 2022).*
Note that in case of higher RSLR, these scenarios will be reached sooner than 2100 and 2150, respectively.

***Table C7** | Area and population below sea level for selected relative sea level rise scenarios taken from projections of the IPCC 6th Assessment Report for the years of 2100 and 2150, respectively.*
Estimates of the 50th percentile from the intermediate SSP2-4.5 reference scenario and 83rd percentile from the high SSP5-8.5 reference scenario are given as they constitute lower and upper boundaries of pathway probability. Note that the category of 0 m sea level rise includes areas that are already below sea level. DEMs were used in their original resolution, with water and outcrop masks applied and erroneous elevation data (<-7.00 m) excluded. Area and population estimates are based on administrative districts in the delta ROI that have been masked for outcrops. Note that the outline of administrative units slightly differs from the ROI along the coast and some river channels, likely related to different dates of data generation and underlying source data, together with the impact of coastal and fluvial dynamics (see also Figure C28).

Present				
	0 m SLR			
	Area in km^2	Area in %	Population (as of 2020) as a number (×100,000)	Population (as of 2020) in %
SRTM	501.00	1.92	1.26	0.83
ACE2	7586.13	29.12	19.59	12.90
ASTGTM v003	4.55	0.02	0.01	0.01
AW3D30	439.65	1.69	1.20	0.79
TanDEM-X 30 m	251.01	0.96	0.73	0.48
Copernicus DEM	115.04	0.44	0.24	0.16
FABDEM	60.83	0.23	0.13	0.08

CoastalDEM v2.1	449.97	1.73	0.95	0.63
GLL-DTM v1	0.00	0.00	0.00	0.00
AD-DEM	2268.15	8.71	6.75	4.45

As projected for 2100 (but may be reached sooner)

	0.712 m SLR (SSP2-4.5 50th Percentile)				**1.229 m SLR (SSP5-8.5 83rd Percentile)**			
	Area in km^2	Area in %	Population (as of 2020) as a number (×100,000)	Population (as of 2020) in %	Area in km^2	Area in %	Population (as of 2020) as a number (×100,000)	Population (as of 2020) in %
SRTM	1156.78	4.44	2.98	1.97	2030.60	7.79	5.06	3.33
ACE2	11071.96	42.49	30.02	19.78	13359.58	51.27	38.03	25.05
ASTGTM v003	18.54	0.07	0.04	0.03	32.44	0.13	0.062	0.04
AW3D30	1004.13	3.85	2.64	1.74	1829.36	7.02	4.67	3.07
TanDEM-X 30 m	2559.90	9.83	5.45	3.59	8233.78	31.60	17.91	11.80
Copernicus DEM	2402.78	9.22	4.87	3.21	8059.50	30.93	17.24	11.35
FABDEM	1814.61	6.96	3.59	2.37	7989.57	30.66	17.25	11.37
CoastalDEM v2.1	4561.33	17.51	9.60	6.33	11049.32	42.41	24.74	16.30
GLL-DTM v1	1088.12	4.18	2.24	1.47	2832.93	10.87	5.94	3.91
AD-DEM	8152.00	31.29	20.14	13.27	12160.47	46.67	29.35	19.33

As projected for 2150 (but may be reached sooner)

	1.168 m SLR (SSP2-4.5 50th Percentile)				**2.210 m SLR (SSP5-8.5 83rd Percentile)**			
	Area in km^2	Area in %	Population (as of 2020) as a number (×100,000)	Population (as of 2020) in %	Area in km^2	Area in %	Population (as of 2020) as a number (×100,000)	Population (as of 2020) in %
SRTM	1923.39	7.38	4.79	3.12	5085.83	19.52	12.93	8.52
ACE2	13108.30	50.31	37.18	24.49	16369.05	62.82	51.81	34.13
ASTGTM v003	27.10	0.10	0.05	0.03	330.24	1.27	0.65	0.43
AW3D30	1717.65	6.59	4.39	2.89	4890.86	18.77	12.34	8.13
TanDEM-X 30 m	7697.12	29.54	16.67	10.99	13304.21	51.06	31.39	20.68
Copernicus DEM	7525.81	28.88	16.02	10.55	13069.53	50.16	30.52	20.11
FABDEM	7316.11	28.08	15.64	10.30	13866.88	53.22	36.42	23.99
CoastalDEM v2.1	10330.23	39.65	22.94	15.11	17597.88	67.54	50.00	32.94
GLL-DTM v1	2626.11	10.08	5.51	3.63	11926.35	45.77	28.45	18.74
AD-DEM	11720.23	44.98	28.28	18.63	16931.31	64.98	45.95	30.27

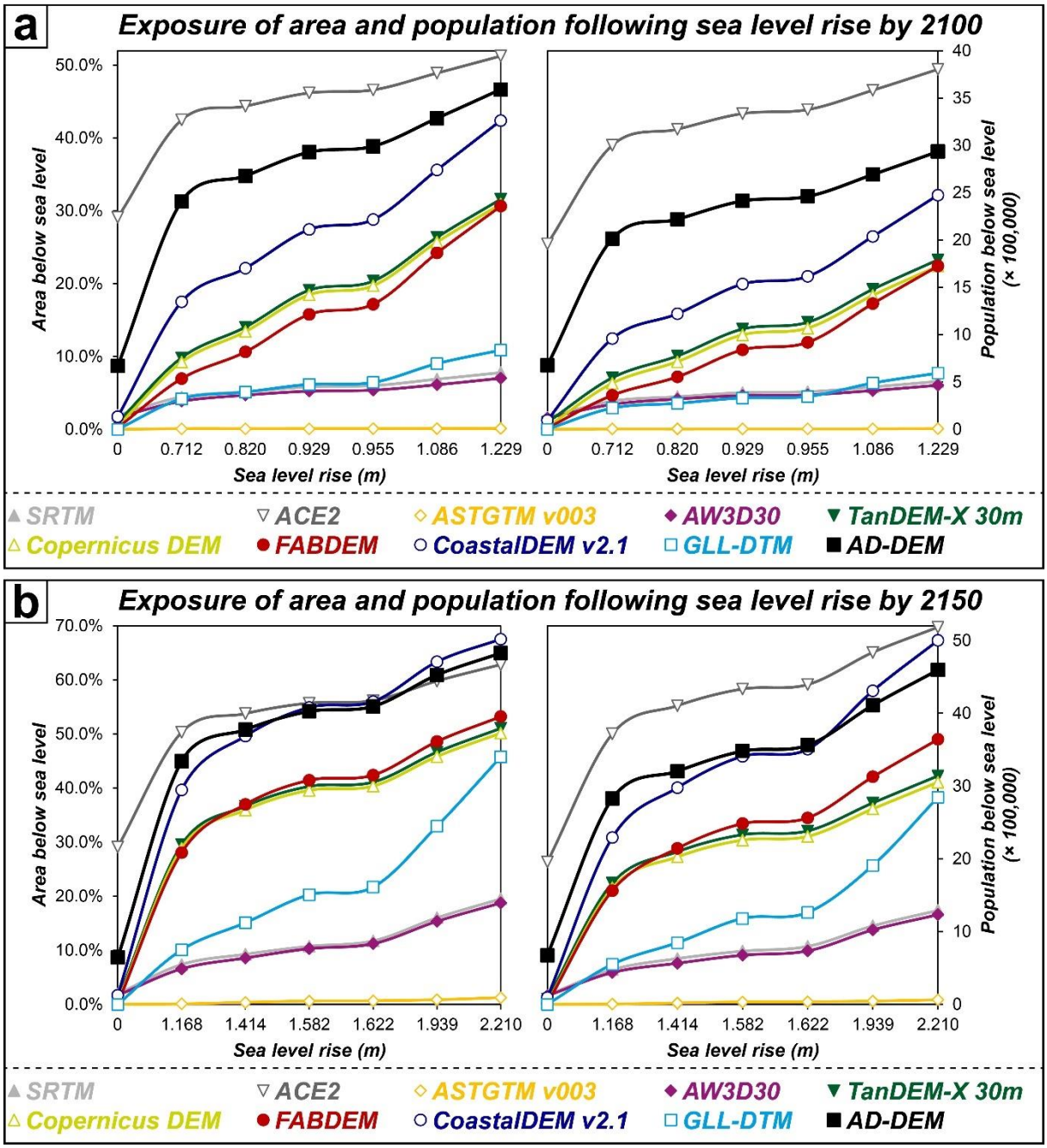


***Figure C22** | Area and people that will fall below future sea level by 2100 (a) and 2150 (b) following median sea level rise projections for Yangon (compared to the baseline period 1995–2014) from the Sea Level Projection Tool of the IPCC 6th Assessment Report (Fox-Kemper et al., 2021; Garner et al., 2021, 2022).*
Estimates on affected people are based on LandScan Global 2020 data (Rose et al., 2021).

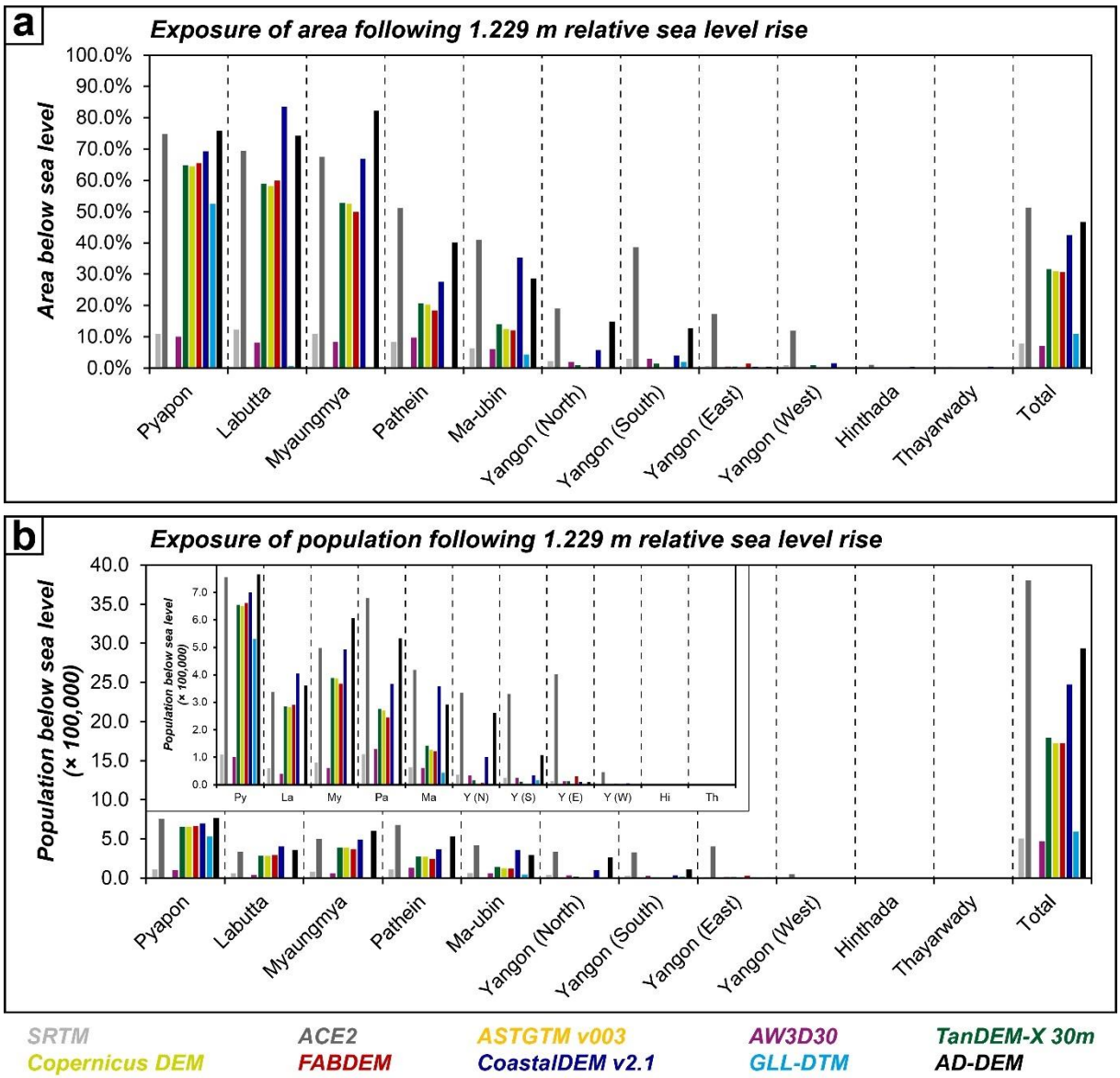


Figure C23 | *Area (a) and people (b) affected by sea level rise of 1.229 m as projected by SSP5-8.5 (83rd percentile) for 2100 for each administrative district of the Ayeyarwady Delta and the entire delta.*
Estimates of affected district population are enlarged in the insets. All population estimates are based on the actual population of 2020 (Rose et al., 2021).

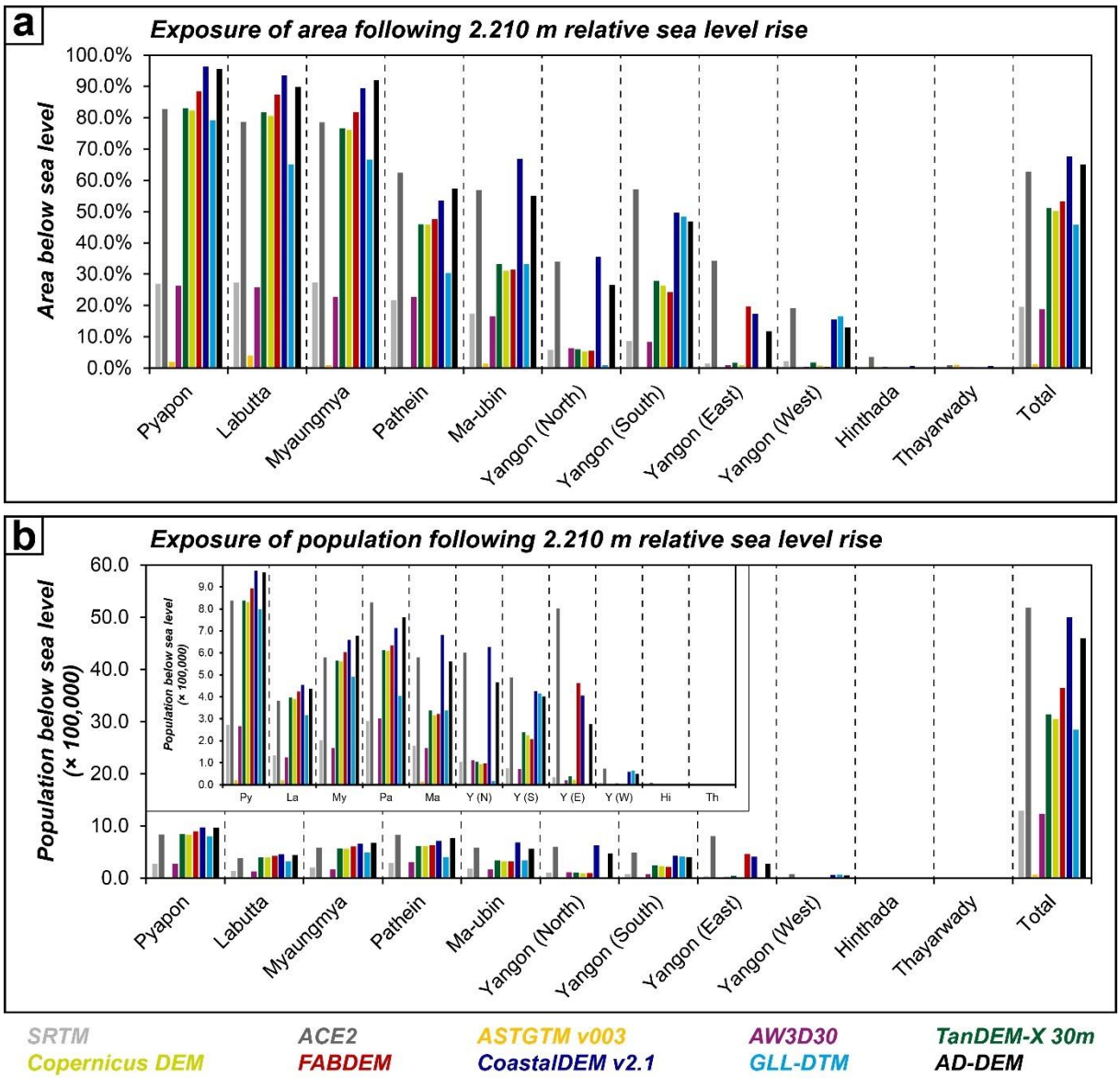


Figure C24 *| Area (a) and people (b) affected by sea level rise of 2.210 m as projected by SSP5-8.5 (83rd percentile) for 2150 for each administrative district of the Ayeyarwady Delta and the entire delta.*
Estimates of affected district population are enlarged in the insets. All population estimates are based on the actual population of 2020 (Rose et al., 2021).

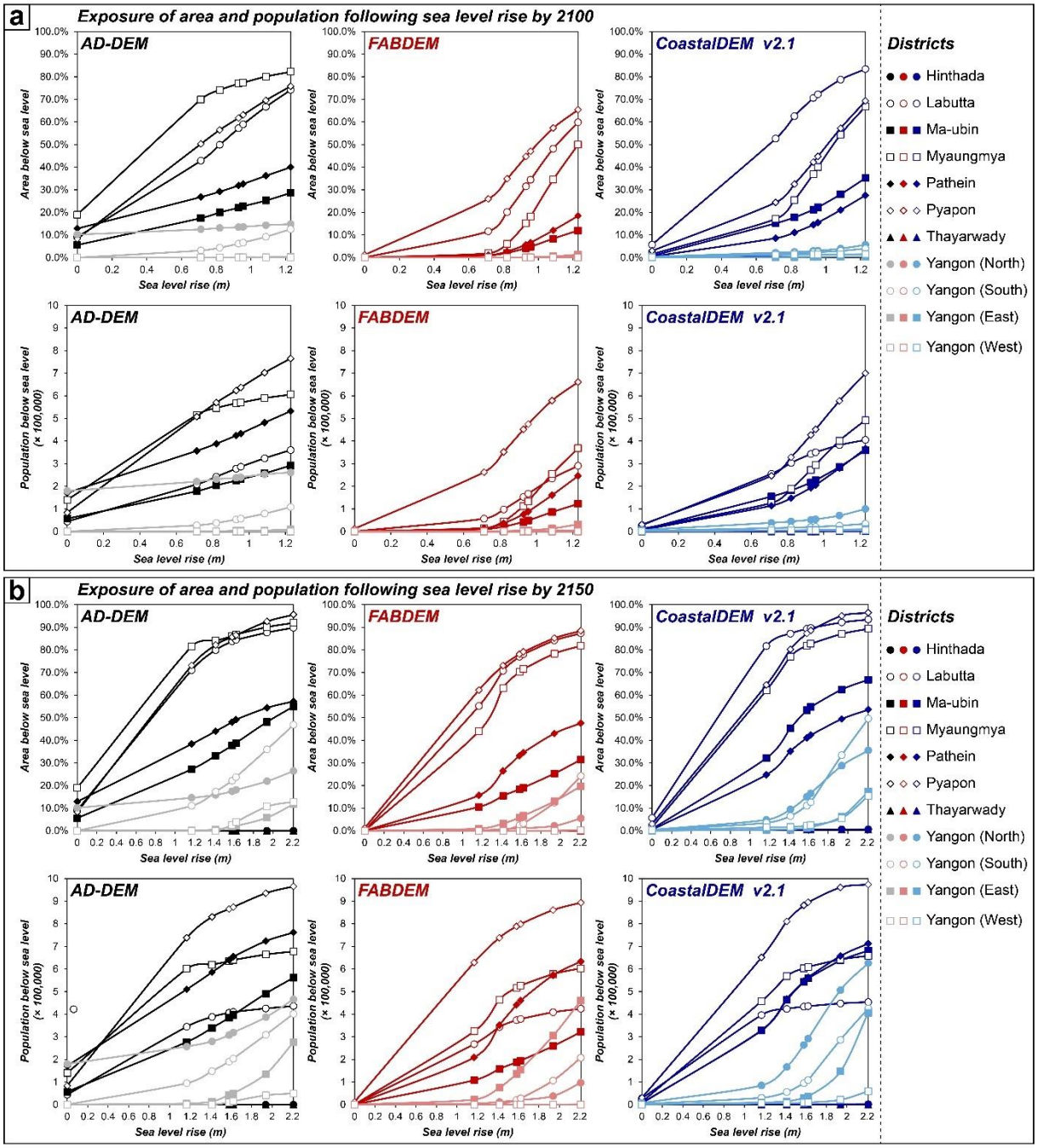


***Figure C25** | Estimated percentage of administrative district area and inhabitants affected by sea level rise according to projections of the IPCC 6th Assessment Report for the years 2100 (a) and 2150 (b) based on AD-DEM, FABDEM, and CoastalDEM v2.1, respectively.*
DEMs were used in their original resolution, with water and outcrop masks applied and erroneous elevation data (<-7.00 m) excluded. Area and population estimates are based on administrative districts in the delta ROI that have been masked for outcrops. All population estimates are based on the actual population of 2020 (Rose et al., 2021).

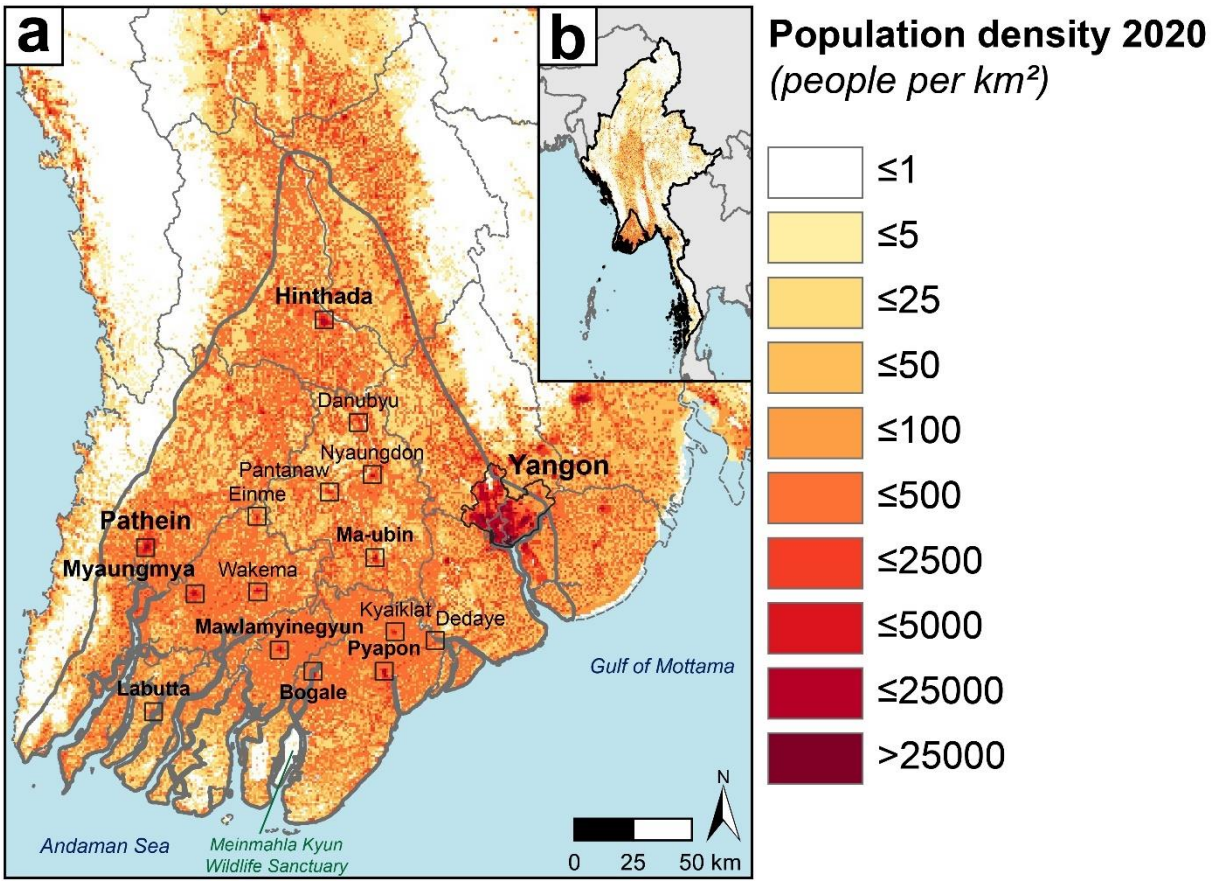


Figure C26 *| Population density in the Ayeyarwady Delta (a) and in Myanmar (b; based on LandScan Global 2020 population data (Rose et al., 2021)) together with the location of major cities and urban settlements that will be most affected by future sea level rise.*
The location of the Meinmahla Kyun Wildlife Sanctuary is shown as well.

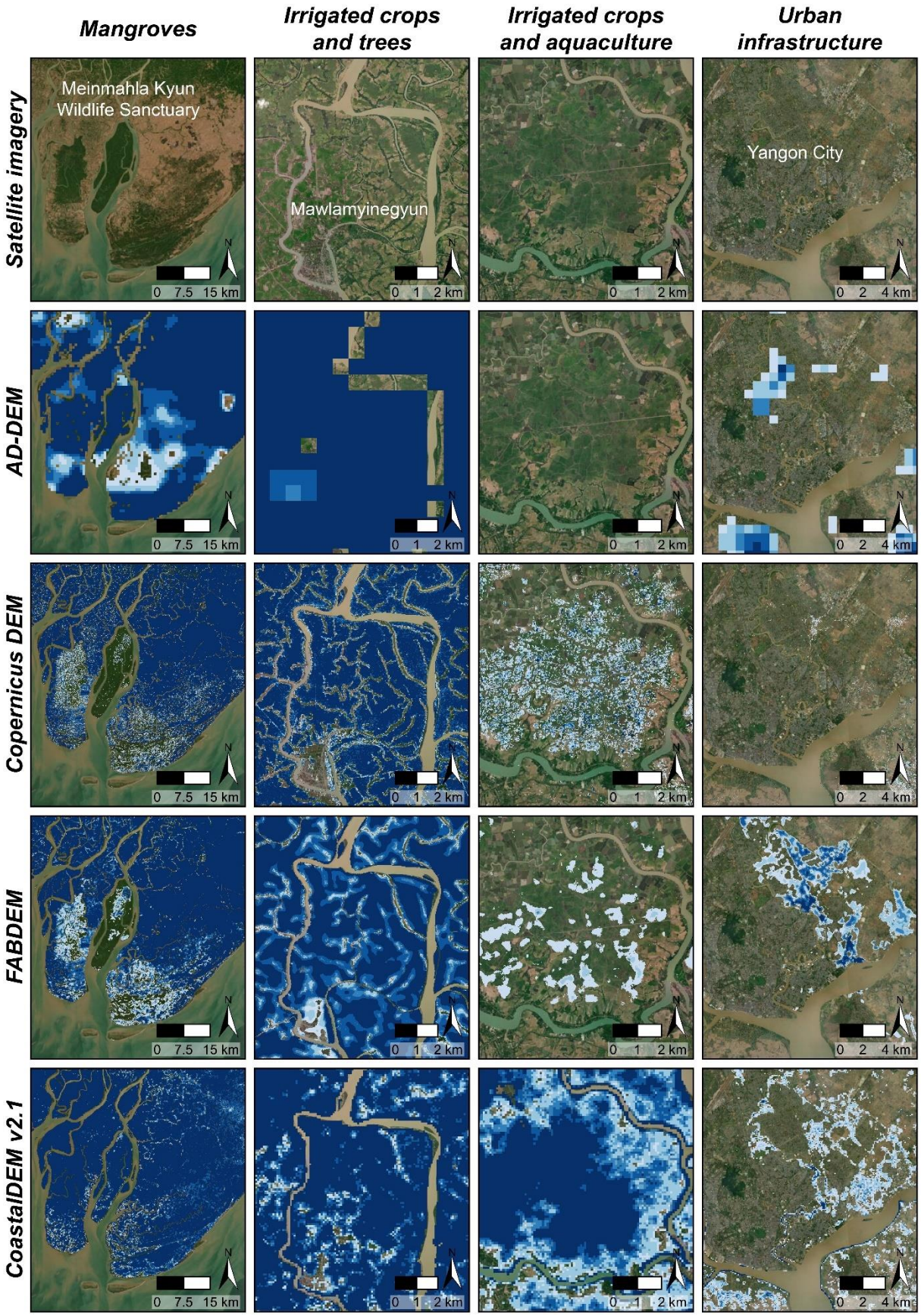


***Figure C27** | Performance of selected DEMs in sea level rise impact assessments for 2150 in relation to land cover based on Esri World Imagery (2017).*

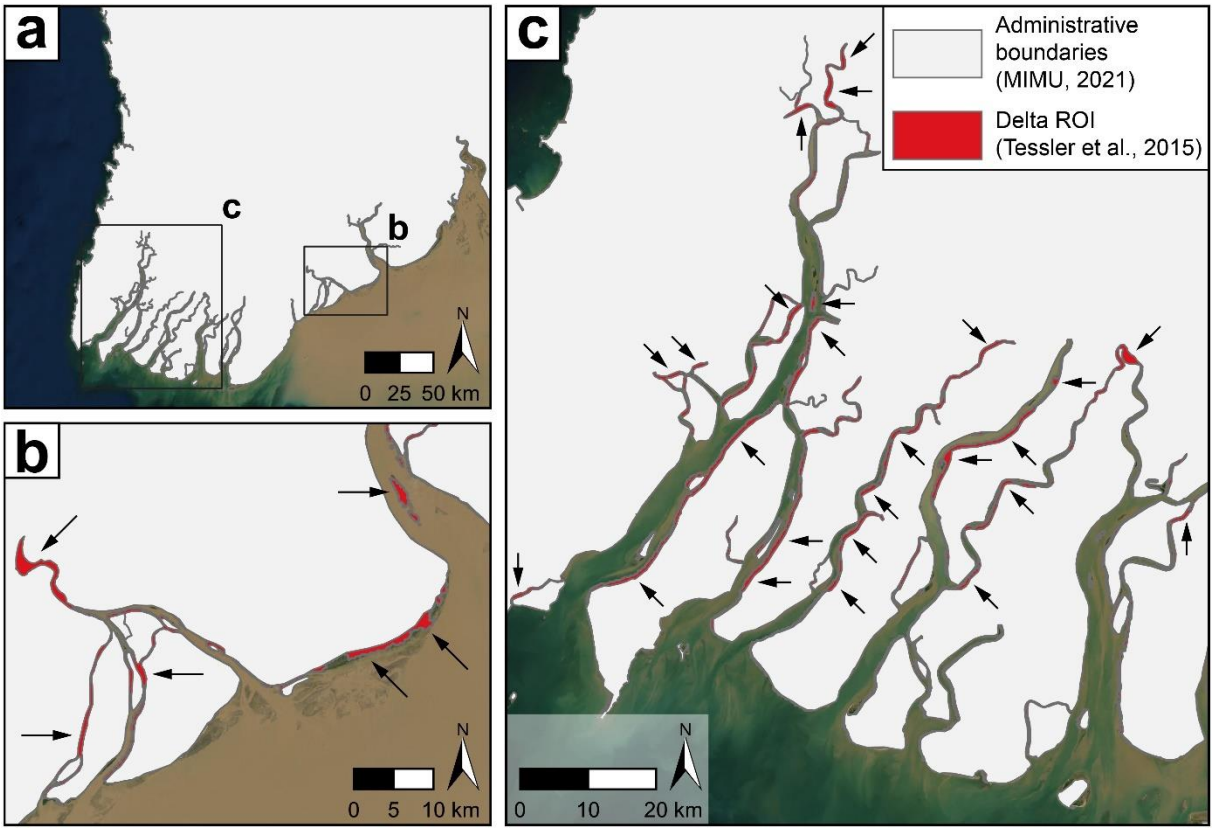


***Figure C28** | Discrepancies in delta shape between boundaries of administrative units (MIMU, 2021) and the ROI used in this study (Tessler et al., 2015).*
Differences along the shore (b) and in river channels (b and c) are indicated by arrows and are ascribed to coastal and fluvial morphodynamics together with different timings of data production. To estimate the impact of SLR on area and population within each administrative district, we used the dataset of MIMU (2021). a), b) and c) are based on Esri World Imagery (2017).

References

Abrams, M., Bailey, B., Tsu, H., and Hato, M.: The ASTER Global DEM, *Photogramm. Eng. Remote Sensing*, *76*:4, 344–348, 2010.

Abrams, M., and Crippen, R.: ASTER GDEM V3 (ASTER Global DEM) User Guide Version 1, Japan's Ministry of Economy, Trade, and Industry (METI), and National Aeronautics and Space Administration (NASA) Jet Propulsion Laboratory/California Institute of Technology, 10 pp., 2019.

Abrams, M., Crippen, R., and Fujisada, H.: ASTER Global Digital Elevation Model (GDEM) and ASTER Global Water Body Dataset (ASTWBD), *Remote Sens.*, *12*:7, 1156, https://doi.org/10.3390/rs12071156, 2020.

Aguilar, F. J., Aguilar, M. A., Agüera, F., and Sánchez, J.: The accuracy of grid digital elevation models linearly constructed from scattered sample data, *Int. J. Geogr. Inf. Sci.*, *20*:2, 169–192, https://doi.org/10.1080/13658810500399670, 2006.

Airbus Defence and Space: WorldDEM^{TM} Technical Product Specification Version 2.4, Airbus, 38 pp., 2018.

Airbus Defence and Space: Copernicus Digital Elevation Model Product Handbook Version 3.0, Airbus, 38 pp., 2020.

Altunel, A. O., Okolie, C. J., and Kurtipek, A.: Capturing the level of progress in vertical accuracy achieved by ASTER GDEM since the beginning: Turkish and Nigerian examples, *Geocarto Int.*, https://doi.org/10.1080/10106049.2022.2063409, 2022.

Andersen, O. B., Nielsen, K., Knudsen, P., Hughes, C. W., Bingham, R., Fenoglio-Marc, L., Gravelle, M., Kern, M., and Polo, S. P.: Improving the Coastal Mean Dynamic Topography by Geodetic Combination of Tide Gauge and Satellite Altimetry, *Mar. Geodesy*, *41*:6, 517–545, https://doi.org/10.1080/01490419.2018.1530320, 2018.

AVISO+: The combined mean dynamic topography MDT CNES-CLS18, https://www.aviso.altimetry.fr/en/data/products/auxiliary-products/mdt/mdt-description.html, last access: 7 September 2022.

Berry, P. A. M., Smith, R. G., and Benveniste, J.: ACE2: The New Global Digital Elevation Model, in: *Gravity, Geoid and Earth Observation, International Association of Geodesy Symposia 135*, edited by Mertiklas, S.P., Springer, Berlin, Heidelberg, Germany, 231–237, https://doi.org/10.1007/978-3-642-10634-7_30, 2010.

Berry, P. A. M., Smith, R., and Benveniste, J.: Altimeter Corrected Elevations, Version 2 (ACE2) [dataset], Palisades, New York: NASA Socioeconomic Data and Applications Center (SEDAC), https://doi.org/10.7927/H40G3H78, accessed 2022-03-01, 2019.

Bingham, R. J., Haines, K., and Lea, D. J.: How well can we measure the ocean's mean dynamic topography from space?, J. *Geophys. Res. Oceans*, *119*:6, 3336–3356, https://doi.org/10.1002/2013JC009354, 2014.

Brakenridge, G. R., Syvitski, J. P. M., Niebuhr, E., Overeem, I., Higgins, S. A., Kettner A. J., and Prades, L.: Design with nature: Causation and avoidance of catastrophic flooding, Myanmar, *Earth Sci. Rev.*, *165*, 81–109, https://doi.org/10.1016/j.earscirev.2016.12.009, 2017.

Brakenridge, G. R., Kettner, A. J., Paris, S., Cohen, S., and Nghiem, S. V.: River and Reservoir Watch Version 4.5, Satellite-based river discharge and reservoir area measurements, 1998-present, DFO Flood Observatory, University of Colorado, USA: https://floodobservatory.colorado.edu/DischargeAccess.html, last access: 8 September 2022.

Brill, D., Seeger, K., Pint, A., Reize, F., Kay Thwe Hlaing, Seeliger, M., Opitz, S., Khin Mi Mi Win, Win Thuzar Nyunt, Nilar Aye, Aung Aung, Kyaw Kyaw, Kraas, F., and Brückner, H.: Modern and historical tropical cyclone and tsunami deposits at the coast of Myanmar: Implications for their identification and preservation in the geological record, *Sedimentology*, *67*, 1431–1459, https://doi.org/10.1111/sed.12586, 2020.

Brosens, L., Campforts, B., Govers, G., Aldana-Jague, E., Razanamahandry, V. F., Razafimbelo, T., Rafolisy, T, and Jacobs, L.: Comparative analysis of the Copernicus, TanDEM-X, and UAV-SfM digital elevation models to estimate lavaka (gully) volumes and mobilization rates in the Lake Alaotra region (Madagascar), *Earth Surf. Dynam.*, *10*, 209–227, https://doi.org/10.5194/esurf-10-209-2022, 2022.

Buckley, S. M., Agram, P. S., Belz, J. E., Crippen, R. E., Gurrola, E. M., Hensley, S., Kobrick, M., Lavalle, M., Martin, J. M., Neumann, M., Nguyen, Q. D., Rosen, P. A., Shimada, J. G., Simard, M., and Tung, W. W.: NASADEM User Guide, National Aeronautics and Space Administration (NASA) Jet Propulsion Laboratory/California Institute of Technology, Pasadena, California, 48 pp., 2020.

Copernicus Emergency Management Service (© 2015 European Union), [EMSR130] Irrawaddy Delta: Delineation Map, Monitoring 1, 2015.

Da Silva, N. A., and Matthews, A. J.: Impact of the Madden–Julian Oscillation on extreme precipitation over the western Maritime Continent and Southeast Asia, *Quaterly Journal of the Royal Meteorological Society*, *147*:739, 3434–3453, https://doi.org/10.1002/qj.4136, 2021.

de Groot-Reichwein, M. A. M., Goosen, H., and van Steekelenburg, M. G. N.: Climate proofing the Zuidsplaspolder: a guiding model approach to climate adaptation, *Reg. Environ. Change*, *14*, 909–918, http://dx.doi.org/10.1007/s10113-013-0509-4, 2014.

Department of Meteorology and Hydrology (DMH): General Weather Forecast for 2020 Rainy Season, https://www.moezala.gov.mm/general-weather-forecast-2020-rainy-season, last access: 24 August 2022.

Doganalp, S., and Selvi, H. Z.: Local geoid determination in strip area projects by using polynomials, least-squares collocation and radial basis functions, *Measurement*, *73*, 429–438, https://doi.org/10.1016/j.measurement.2015.05.030, 2015.

East View Geospatial, Inc.: EVMap50-MMR 1:50,000 Scale Topographic Maps, Minnetonka, Minnesota, 2014.

European Commissions's Directorate-General for European Civil Protection and Humanitarian Aid Operations (ECHO): Vietnam, Laos, Thailand, Myanmar – Tropical Storm NOUL (DG ECHO partners, governments, media), https://reliefweb.int/report/viet-nam/vietnam-laos-thailand-myanmar-tropical-storm-noul-dg-echo-partners-governments-media, last access: 24 August 2022, 2020.

Farr, T. G., Rosen, P. A., Caro, E., Crippen, R., Duren, R., Hensley, S., Kobrick, M., Paller, M., Rodriguez, E., Roth, L., Seal, D., Shaffer, S., Shimada, J., Umland, J., Werner, M., Oskin, M., Burbank, D., and Alsdorf, D.: The Shuttle Radar Topography Mission, *Rev. Geophys.*, *45*:2, RG2004, https://doi.org/10.1029/2005RG000183, 2007.

Filmer, M. S., Hughes, C. W., Woodworth, P. L., Featherstone, W. E., and Bingham, R. J.: Comparison between geodetic and oceanographic approaches to estimate mean dynamic topography for vertical datum unification: evaluation at Australian tide gauges, *J. Geod.*, *92*, 1413–1437, https://doi.org/10.1007/s00190-018-1131-5, 2018.

Fox-Kemper, B., Hewitt, H. T., Xiao, C., Aðalgeirsdóttir, G., Drijfhout, S. S., Edwards, T. L., Golledge, N. R., Hemer, M., Kopp, R. E., Krinner, G., Mix, A., Notz, D., Nowicki, S., Nurhati, I. S., Ruiz, L., Sallée, J.-B., Slangen, A. B. A., and Yu, Y.: Ocean, Cryosphere and Sea Level Change, in: *Climate Change 2021: The Physical Science Basis. Contribution of Working Group I to the Sixth Assessment Report of the Intergovernmental Panel on Climate Change*, edited by Masson-Delmotte, V., Zhai, P., Pirani, A., Connors, S. L., Péan, C., Berger, S., Caud, N., Chen, Y., Goldfarb, L., Gomis, M. I., Huang, M., Leitzell, K., Lonnoy, E., Matthews, J. B. R., Maycock, T. K., Waterfield, T., Yelekçi, O., Yu, R., and Zhou, B., Cambridge University Press, Cambridge, 9-1–9-257, In press.

Garner, G. G., Hermans, T., Kopp, R. E., Slangen, A. B. A., Edwards, T. L., Levermann, A., Nowikci, S., Palmer, M. D., Smith, C., Fox-Kemper, B., Hewitt, H. T., Xiao, C., Aðalgeirsdóttir, G., Drijfhout, S. S., Edwards, T. L., Golledge, N. R., Hemer, M., Kopp, R. E., Krinner, G., Mix, A., Notz, D., Nowicki, S., Nurhati, I. S., Ruiz, L., Sallée, J.-B., Yu, Y., Hua, L., Palmer, T., and Pearson, B.: IPCC AR6 Sea-Level Rise Projections, Version 20210809, PO.DAAC, CA, USA, Dataset accessed [2022-05-23] at https://podaac.jpl.nasa.gov/announcements/2021-08-09-Sea-level-projections-from-the-IPCC-6th-Assessment-Report, 2021.

Garner, G. G., Kopp, R. E., Hermans, T., Slangen, A. B. A., Koubbe, G., Turilli, M., Jha, S., Edwards, T. L., Levermann, A., Nowikci, S., Palmer, M. D., and Smith, C.: Framework for Assessing Changes To Sea-level (FACTS), Geoscientific Model Development, *Zenodo* [model], https://zenodo.org/record/6419954, last access: 22 November 2022, 2022.

German Aerospace Centre (DLR): Earth Observation – Discovering, Surveying, and Understanding Our Planet, DLR, 71 pp., 2013.

Gesch, D. B.: Best Practices for Elevation-Based Assessments of Sea-Level Rise and Coastal Flooding Exposure, *Front. Earth Sci.*, *6*:230, 1–19, https://doi.org/10.3389/feart.2018.00230, 2018.

Gorelick, N., Hancher, M., Dixon, M., Ilyushchenko, S., Thau, D., and Moore, R.: Google Earth Engine: Planetary-scale geospatial analysis for everyone, *Remote Sens. Environ.*, *202*, 18–27, https://doi.org/10.1016/j.rse.2017.06.031, 2017.

Government of the Union of Myanmar: Myanmar – Post-disaster needs assessment of floods and landslides July–September 2015, Government of the Union of Myanmar, 267 pp., 2015.

Guth, P. L., and Geoffroy, T. E.: LiDAR point cloud and ICESat-2 evaluation of 1 second global digital elevation models: Copernicus wins, *Trans. GIS*, *25*:5, 2245–2261, https://doi.org/10.1111/tgis.12825, 2021.

Hamden, M. H., Din, A. H. M., Wijaya, D. D., Yusoff, M. Y. M., and Pa'suya, M. F.: Regional Mean Sea Surface and Mean Dynamic Topography Models Around Malaysian Seas Developed From 27 Years of Along-Track Multi-Mission Satellite Altimetry Data, *Front. Earth Sci.*, *9*, 665876, https://doi.org/10.3389/feart.2021.665876, 2021.

Hawker, L., Uhe, P., Paulo, L., Sosa, J., Savage, J., Sampson, C., and Neal, J.: A 30 m global map of elevation with forests and buildings removed, *Environ. Res. Lett.*, *17*:2, 024016, https://doi.org/10.1088/1748-9326/ac4d4f, 2022.

Hooijer, A., and Vernimmen, R.: Global LiDAR land elevation data reveal greatest sea-level rise vulnerability in the tropics, *Nat. Commun.*, *12*:3592, 1–7, https://doi.org/10.1038/s41467-021-23810-9, 2021.

Horton, R., De Mel, M., Peters, D., Lesk, C., Bartlett, R., Helsingen, H., Bader, D., Capizzi, P., Martin, S., and Rosenzweig, C.: Assessing Climate Risk in Myanmar: Technical Report, Center for Climate Systems Research at Columbia University, WWF-US and WWF-Myanmar, 88 pp., 2017.

Huffman, G. J., Stocker, E. F., Bolvin, D. T., Nelkin, E. J., Tan, J.: GPM IMERG Final Precipitation L3 1 month 0.1 degree x 0.1 degree V06 [dataset], https://doi.org/10.5067/GPM/IMERGDF/DAY/06, edited by Savtchenko, A., Greenbelt, Maryland, Goddard Earth Sciences Data and Information Services Center (GES DISC), last access: 18 June 2021, 2019.

Ince, E. S., Barthelmes, F., Reißland, S., Elger, K., Förste, C., Flechtner, F., and Schuh, H.: ICGEM – 15 years of successful collection and distribution of global gravitational models, associated services and future plans, *Earth Sys. Sci. Data*, *11*, 647–674, https://doi.org/10.5194/essd-11-647-2019, 2019.

Inman, V. L., and Lyons, M. B.: Automated Inundation Mapping Over Large Areas Using Landsat Data and Google Earth Engine, *Remote Sens.*, *12*:8, 1348, https://doi.org/10.3390/rs12081348, 2020.

International Federation of Red Cross and Red Crescent Societies (IFRC): Final Report Myanmar: Floods, IFRC, 31 pp., 2017.

Japan Aerospace Exploration Agency (JAXA): ALOS Global Digital Surface Model "ALOS World 3D – 30m (AW3D30)", https://www.eorc.jaxa.jp/ALOS/en/dataset/aw3d30/aw3d30_e.htm, last access: 28 October 2022, 2019.

Japan International Cooperation Agency (JICA), Myanmar Survey Department, and Ministry of Forestry: The study on the establishment of geographic database for national rehabilitation and development programme in the Union of Myanmar – Executive Summary, JICA, 86 pp., 2004a.

Japan International Cooperation Agency (JICA), Myanmar Survey Department, and Ministry of Forestry: The study on the establishment of geographic database for national rehabilitation and development programme in the Union of Myanmar – Final Report Volume 1: Main report, JICA, 86 pp., 2004b.

Japan International Cooperation Agency (JICA), Myanmar Survey Department, and Ministry of Forestry: The study on the establishment of geographic database for national rehabilitation and development programme in the Union of Myanmar – Final Report Volume 2: Documents, JICA, 86 pp., 2004c.

Knudsen, P., Bingham, R., Andersen, O., and Rio, M.-H.: A global mean dynamic topography and ocean circulation estimation using a preliminary GOCE gravity model, *J. Geod.*, *85*, 861–879, https://doi.org/10.1007/s00190-011-0485-8, 2011.

Krieger, G., Moreira, A., Fiedler, H., Hajnsek, I., Werner, M., Younis, M., and Zink, M.: TanDEM-X: A Satellite Formation for High-Resolution SAR Interferometry, *IEEE Trans. Geosci. Remote Sens.*, *45*:11, 3317–3341, https://doi.org/10.1109/TGRS.2007.900693, 2007.

Kulp, S. A., and Strauss, B. H.: CoastalDEM: A global coastal digital elevation model improved from SRTM using a neural network, *Remote Sens. Environ.*, *206* (1), 231–239, https://doi.org/10.1016/j.rse.2017.12.026, 2018.

Kulp, S. A., and Strauss, B. H.: New elevation data triple estimates of global vulnerability to sea-level rise and coastal flooding. *Nat. Commun.*, *10*:4844, 1–12, https://doi.org/10.1038/s41467-019-12808-z, 2019.

Kulp, S. A., and Strauss, B. H.: CoastalDEM v2.1: A high-accuracy and high-resolution global coastal elevation model trained on ICESat-2 satellite lidar, *Climate Central Scientific Report*, 17 pp., 2021.

Lemoine, F. G., Smith, D. E., Kunz, L., Smith, R., Pavlis, E. C., Pavlis, N. K., Klosko, S. M., Chinn, D. S., Torrence, M. H., Williamson, R. G., Cox, C. M., Rachlin, K. E., Wang, Y. M., Kenyon, S. C., Salmon, R., Trimmer, R., Rapp, R. H., and Nerem, R. S.: The development of the NASA GSFC and NIMA joint geopotential model, in: *Gravity, Geoid and Marine Geodesy*, International Association of Geodesy Symposia 117, edited by: Segawa, J., Fujimoto, H., and Okubo, S., Springer, Berlin, Heidelberg, https://doi.org/10.1007/978-3-662-03482-8_62, 1997.

Marešová, J., Gdulová, K., Pracná, P., Moravec, D., Gábor, L., Prošek, J., Barták, V., and Moudrý, V.: Applicability of Data Acquisition Characteristics to the Identification of Local Artefacts in Global Digital Elevation Models: Comparison of the Copernicus and TanDEM-X DEMs, *Remote Sens.*, *13*:19, 3931, https://doi.org/10.3390/rs13193931, 2021.

Masson-Delmotte, V., Zhai, P., Pirani, A., Connors, S. L., Péan, C., Berger, S., Caud, N., Chen, Y., Goldfarb, L., Gomis, M. I., Huang, M., Leitzell, K., Lonnoy, E., Matthews, J. B. R., Maycock, T. K., Waterfield, T., Yelekçi, O., Yu, R., and Zhou, B. (Eds.): *Climate Change 2021: The Physical Science Basis. Contribution*

of Working Group I to the Sixth Assessment Report of the Intergovernmental Panel on Climate Change, Cambridge University Press, 2021.

Mayer-Gürr, T., Kvas, A., Klinger, B., Rieser, D., Zehentner, N., Pail, R., Gruber, T., Fecher, T., Rexer, M., Schuh, W.-D., Kusche, J., Brockmann, J., Loth, I., Müller, S., Eicker, A., Schall, J., Baur, O., Höck, E., Krauss, S., and Maier, A.: The new combined satellite only model GOCO05s, EGU General Assembly 2015, Vienna, Austria, 12–17 April 2015, EGU2015-12364, http://dx.doi.org/10.13140/RG.2.1.4688.6807, 2015.

Mehmood, H., Conway, C., and Perera, D.: Mapping of Flood Areas Using Landsat with Google Earth Engine Cloud Platform, *Atmosphere*, *12*:7, 866, https://doi.org/10.3390/atmos12070866, 2021.

Mi Mi Tun: Country Report of Myanmar, Department of Disaster Management, Ministry of Social welfare, Relief and Resettlement, 8 pp., 2020.

Minderhoud, P. S. J., Coumou, L., Erkens, G., Middelkoop, H., and Stouthamer, E.: Mekong delta much lower than previously assumed in sea-level rise impact assessments, *Nat. Commun.*, *10*:3847, 1–13, https://doi.org/10.1038/s41467-019-11602-1, 2019.

Myanmar Information Management Unit (MIMU): Seasonal Flooding as of 26th July 2017, MIMU, MIMU1515v01, 2017.

Myanmar Information Management Unit (MIMU): Probable Flood Inundated Ayeyarwady and Bago (West) Region (as of 1st September 2020), MIMU, MIMU1515v01, 2020.

Myanmar Information Management Unit (MIMU): MIMU Geospatial Data, http://geonode.themimu.info/layers/?limit=100&offset=0, last access: 28 October 2022, 2021.

Ministry of Economy, Trade and Industry (METI) of Japan, National Aeronautics and Space Administration (NASA), and United States Geological Survey: ASTER Global DEM Validation Summary Report, 28 pp., 2009.

Moharrami, M., Javanbakht, M., and Attarchi, S.: Automatic flood detection using sentinel-1 images on the google earth engine, *Environ. Monit. Assess.*, *193*, 248, https://doi.org/10.1007/s10661-021-09037-7, 2021.

Mukul, M., Srivastava, V., Jade, S., and Mukul, M.: Uncertainties in the Shuttle Radar Topography Mission (SRTM) Heights: Insights from the Indian Himalaya and Peninsula, *Sci. Rep.*, *7*, 41672, https://doi.org/10.1038/srep41672, 2017.

Mulet, S., Rio, M.-H., Etienne, H., Artana, C., Cancet, M., Dibarboure, G., Hui Feng, Husson, R., Picot, N., Provost, C., and Strub, P. T.: The new CNES-CLS18 global mean dynamic topography, *Ocean Sci.*, *17*, 789–808, https://doi.org/10.5194/os-17-789-2021, 2021.

National Aeronautics and Space Administration (NASA): Giovanni – The Bridge Between Data and Science v 4.37, https://giovanni.gsfc.nasa.gov/giovanni/, last access: 18 June 2021.

National Aeronautics and Space Administration (NASA) Jet Propulsion Laboratory (JPL): NASA Shuttle Radar Topography Mission Water Body Data Shapefiles & Raster Files, https://doi.org/10.5067/MEaSUREs/SRTM/SRTMSWBD.003, last access: 8 February 2022, 2013.

National Aeronautics and Space Administration (NASA) Jet Propulsion Laboratory (JPL), Shuttle Radar Topography Mission, https://www2.jpl.nasa.gov/srtm/mission.htm, last access: 26 August 2022, 2016.

Neuenschwander, A. L., Pitts, K. L., Jelley, B. P., Robbins, J., Klotz, B., Popescu, S. C., Nelson, R. F., Harding, D., Pederson, D., and Sheridan, R.: ATLAS/ICESat-2 L3A Land and Vegetation Height, Version 4, NASA National Snow and Ice Data Center, Boulder, Colorado, USA, 18 pp., https://doi.org/10.5067/ATLAS/ATL08.004, 2021.

Peter, B. G., Cohen, S., Lucey, R., Munasinghe, D., Raney, A., and Brakenridge, G. R.: Google Earth Engine Implementation of the Floodwater Depth Estimation Tool (FwDET-GEE) for Rapid and Large Scale Flood Analysis, *IEEE Geosci. Remote. Sens. Lett.*, *19*, 1–5, https://doi.org/10.1109/LGRS.2020.3031190, 2020.

Rabus, B., Eineder, M., Roth, A., and Bamler, R.: The shuttle radar topography mission – a new class of digital elevation models acquired by spaceborne radar, *ISPRS J. Photogramm. Remote Sens.*, *57*:4, 241–262, https://doi.org/10.1016/S0924-2716(02)00124-7, 2003.

Rio, M.-H., Mulet, S., and Picot, N.: Beyond GOCE for the ocean circulation estimate: Synergetic use of altimetry, gravimetry, and in situ data provides new insight into geostrophic and Ekman currents, *Geophys. Res. Lett.*, *41*:24, 8918–8925, 2014.

Rizzoli, P., Martone, M., Gonzalez, C., Wecklich, C., Tridon, D. B., Bräutigam, B., Bachmann, M., Schulze, D., Fritz, T., Huber, M., Wessel, B., Krieger, G., Zink, M., and Moreira, A.: Generation and performance assessment of the global TanDEM-X elevation model, *ISPRS J. Photogramm. Remote Sens.*, *132*, 119–139, https://doi.org/10.1016/j.isprsjprs.2017.08.008, 2017.

Rodríguez, E., Morris, C. S., Belz, J. E., Chapin, E. C., Martin, J. M., Daffer, W., and Hensley, S.: An Assessment of the SRTM Topographic Products, National Aeronautics and Space Administration (NASA) Jet Propulsion Laboratory (JPL), Technical Report JPL D-31639, 143 pp., 2005.

Rose, A., McKee, J., Sims, K., Bright, E., Reith, A., and Urban, M.: LandSCan Global 2020 [dataset], Oak Ridge National Laboratory, https://doi.org/10.48690/1523378, 2021.

Siart, C., Bubenzer, O., and Eitel, B.: Combining digital elevation data (SRTM/ASTER), high resolution satellite imagery (Quickbird) and GIS for geomorphological mapping: A multi-component case study on Mediterranean karst in Central Crete, *Geomorphology*, *112*:1–2, 106–121, https://doi.org/10.1016/j.geomorph.2009.05.010, 2009.

Smith, R. G., and Berry, P. A. M.: ACE2: Global Digital Elevation Model User Guide, 22 pp., 2009.

Specialised Information Service Cartography and Geodata (SIS Maps): Topo List, https://kartographie.staatsbibliothek-berlin.de/en/about-us/map-catalogs/topo-list/, last access: 29 March 2021.

Tachikawa, T., Kaku, M., Iwasaki, A., Gesch, D., Oimoen, M., Zhang, Z., Danielson, J., Krieger, T., Curtis, B., Haase, J., Abrams, M., Crippen, R., and Carabajal, C.: ASTER Global Elevation Model Version 2 – Summary of Validation Results, National Aeronautics and Space Administration (NASA) Land Processes Distributed Active Archive Center, and Joint Japan-US ASTER Science Team, 26 pp., 2011.

Tadono, T., Nagai, H., Ishida, H., Oda, F., Naito, S., Minakawa, K., and Iwamoto, H.: Generation of the 30 m-mesh global digital surface model by ALOS Prism, in: *Int. Arch. Photogramm. Remote Sens. Spatial Inf. Sci., XLI-B4, XXIII ISPRS Congress*, Prague, Czech Republic, 12–19 July 2016, 157–162, https://doi.org/10.5194/isprs-archives-XLI-B4-157-2016, 2016.

Takaku, J., Tadono, T., and Tsutsui, K.: Generation of high resolution global DSM from ALOS Prism, in *Int. Arch. Photogramm. Remote Sens. Spatial Inf. Sci., XL-4, ISPRS Technical Commission IV Symposium*, Suzhou, China, 14–16 May 2014, 243–248, https://doi.org/10.5194/isprsarchives-XL-4-243-2014, 2014.

Talchabhadel, R., Nakagawa, H., Kawaike, K., Yamanoi, K., and Thapa, B. R.: Assessment of vertical accuracy of open source 30m resolution space-borne digital elevation models, Geomatics, *Nat. Hazards Risk*, *12*:1, 939–960, https://doi.org/10.1080/19475705.2021.1910575, 2021.

Tessler, Z. D., Vörösmarty, C. J., Grossberg, M., Gladkova, I., Aizenman, H., Syvitski, J. P. M., and Foufoula-Georgiou, E.: Profiling risk and sustainability in coastal deltas of the world, *Science*, *349*:6248, 638–643, https://doi.org/10.1126/science.aab3574, 2015.

Tripathy, P., and Malladi, T.: Global Flood Mapper: a novel Google Earth Engine application for rapid flood mapping using Sentinel-1 SAR, *Nat. Hazards*, *114*, 1341–1363, https://doi.org/10.1007/s11069-022-05428-2, 2022.

United Nations Platform for Space-based Information for Disaster Management and Emergency Response (UN-SPIDER): SAR-Flood mapping using a change detection approach, https://www.un-spider.org/sites/default/files/Code_GEE_flood_mapping.txt, last access: 22 June 2021, 2019.

UN Office for the Coordination of Humanitarian Affairs (OCHA): Myanmar: Humanitarian Update on Monsoon Season Floods, 21 July 2017, OCHA, Situation Report, https://reliefweb.int/report/myanmar/myanmar-humanitarian-update-monsoon-season-floods-21-july-2017, 2017.

UN Office for the Coordination of Humanitarian Affairs (OCHA): Myanmar: Floods and Landsclides – Jun 2018, https://reliefweb.int/disaster/fl-2018-000124-mmr, last access: 24 August 2022, 2018.

UN Office for the Coordination of Humanitarian Affairs (OCHA): Myanmar: Floods and Landslides – Jun 2020, https://reliefweb.int/disaster/fl-2020-000172-mmr, last access. 24 August 2022, 2020.

Vernimmen, R., Hooijer, A., and Pronk, M.: New ICESat-2 Satellite LiDAR Data Allow First Global Lowland DTM Suitable for Accurate Coastal Flood Risk Assessment, *Remote Sens.*, *12*:17, 2827, https://doi.org/10.3390/rs12172827, 2020.

Wechsler, S. P.: Uncertainties associated with digital elevation models for hydrologic applications: a review, *Hydrol. Earth Syst. Sci.*, *11*, 1481–1500, https://doi.org/10.5194/hess-11-1481-2007, 2007.

Wendleder, A., Wessel, B., Roth, A., Breunig, M., Martin, K., and Wagenbrenner, S.: TanDEM-X Water Indication Mask: Generation and First Evaluation Results, *IEEE J. Sel. Top. Appl. Earth Obs. Remote Sens.*, *6*:1, 171–179, https://doi.org/10.1109/JSTARS.2012.2210999, 2012.

Wessel, B.: TanDEM-X Ground Segment – DEM Products Specification Document, EOC, DLR, Oberpfaffenhofen, Germany, Public Document TD-GS-PS-0021, Issue 3.2, [Online], Available: https://tandemx-science.dlr.de/, 2018.

Wessel, B., Huber, M., Wohlfahrt, C., Marschalk, U., Kosmann, D., and Roth, A.: Accuracy assessment of the global TanDEM-X Digital Elevation Model with GPS data, *ISPRS J. Photogramm. Remote Sens.*, *139*, 171–182, https://doi.org/10.1016/j.isprsjprs.2018.02.017, 2018.

Li, X.: Using radial basis functions in airborne gravimetry for local geoid improvement, *J. Geod.*, *92*, 471–485, https://doi.org/10.1007/s00190-017-1074-2, 2018.

Yamaguchi, Y., Kahle, A. B., Tsu, H., Kawakami, T., and Pniel, M.: Overview of Advanced Spaceborne Thermal Emission and Reflection Radiometer (ASTER), *IEEE Trans. Geosci. Remote Sens.*, *36*:4, 1062–1071, https://doi.org/10.1109/36.700991, 1998.

Zin Mie Mie Sein, Zhi, X., Ullah, I., Azam, K., Ngoma, H., Saleem, F., Yun Xing, Iyakaremye, V., Syed, S., Hina, S., and Nkunzimana, A.: recent variability of sub-seasonal monsoon precipitation and its potential drivers in Myanmar using in-situ observation during 1981–2020, *Int. J. Climatol.*, *42*:6, 3341–3359, https://doi.org/10.1002/joc.7419, 2022.

Appendix D – Supplement to Chapter 4.2

This Supplement is related to: **Seeger, K.**, Minderhoud, P.S.J., in review. *Sea level much higher than assumed in most coastal hazard assessments*. Nature, 2025-02-05097A.

The supplementary material is published along with the scientific article under a CC-BY 4.0 Attribution 4.0 International licence (http://creativecommons.org/licenses/by/4.0/). The reader is recommended to refer to the peer-reviewed and published version of the content of this supplement which can be accessed here (https://media.springernature.com/original/springer-static/esm/art%3A10.1038%2Fs41586-026-10196-1/MediaObjects/41586_2026_10196_MOESM1_ESM.pdf) and also via the doi of the published article provided here (https://doi.org/10.1038/s41586-026-10196-1).

D1. Supplementary figures

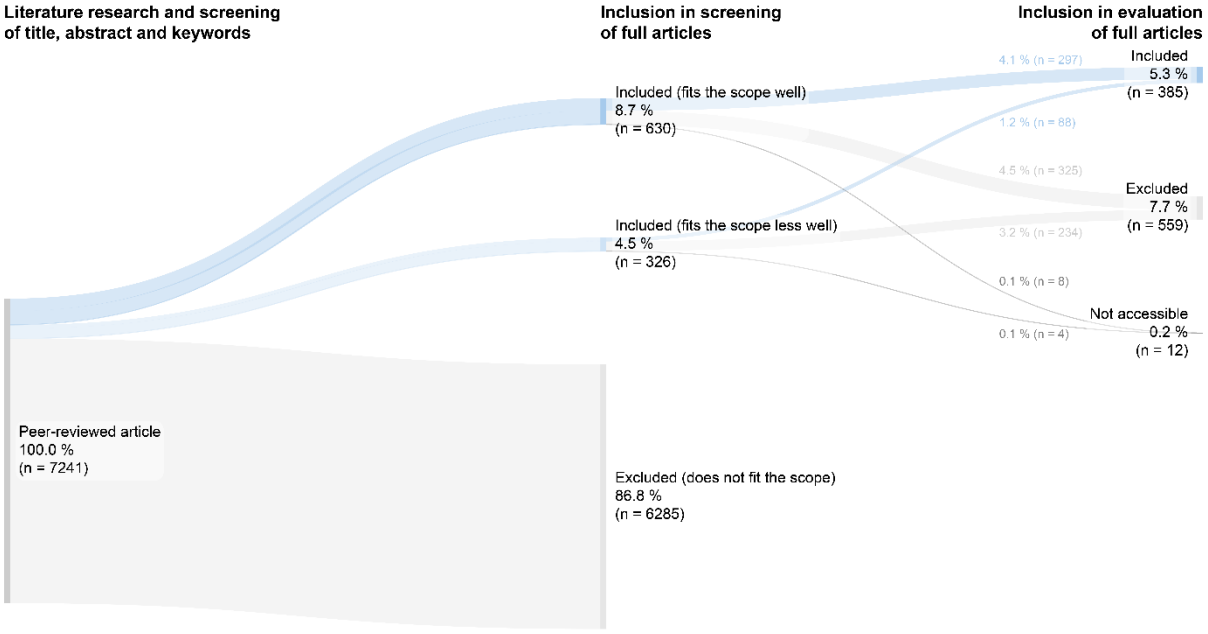


Figure D1 *| Overview of publications searched and screened for their suitability to be included in the literature evaluation of this study.*

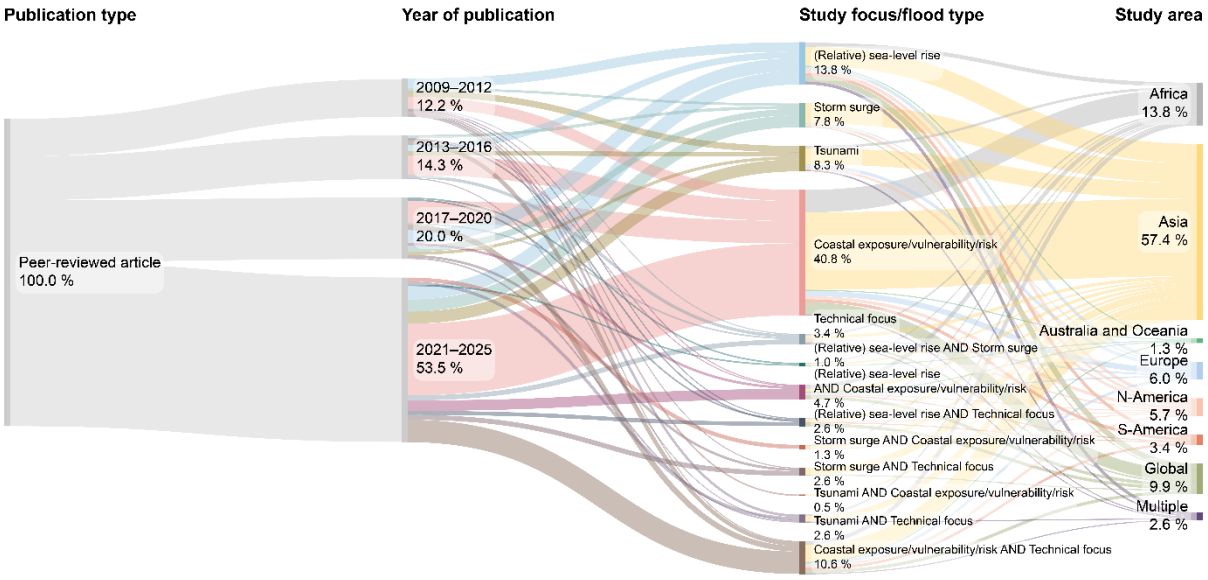


***Figure D2** | Overview of publications included in the literature evaluation of this study. Characteristics of the literature considered in the literature evaluation of this study, including differentiation into publication type, year of publication, study focus and area of interest.*

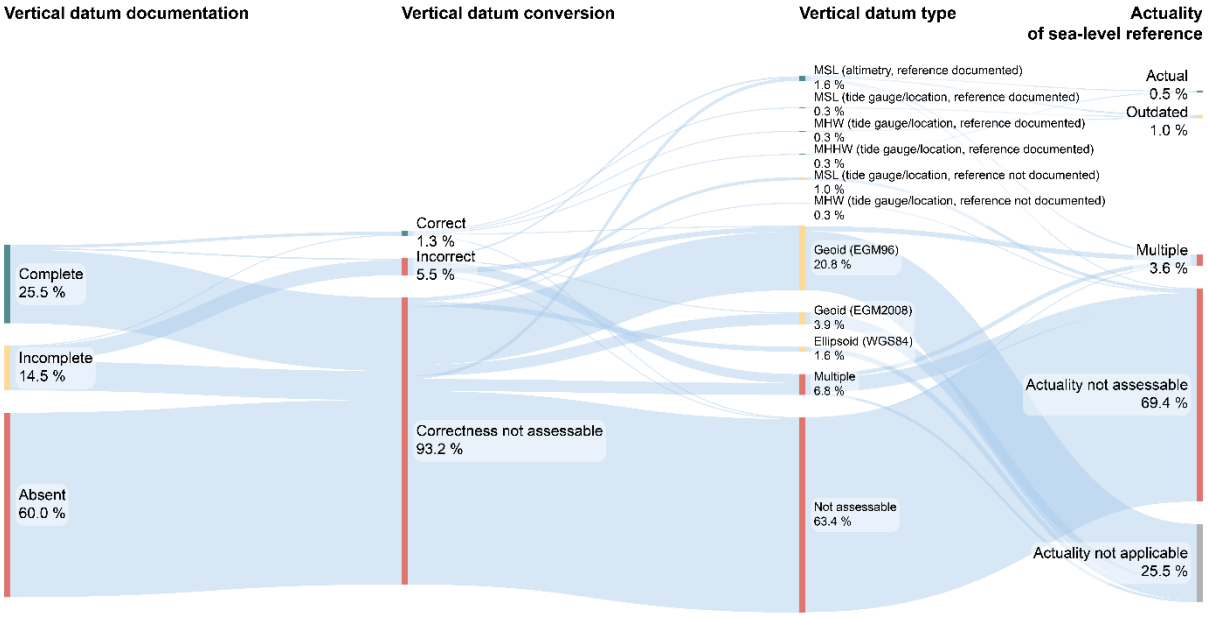


***Figure D3** | Vertical datum types used by the literature evaluated.*

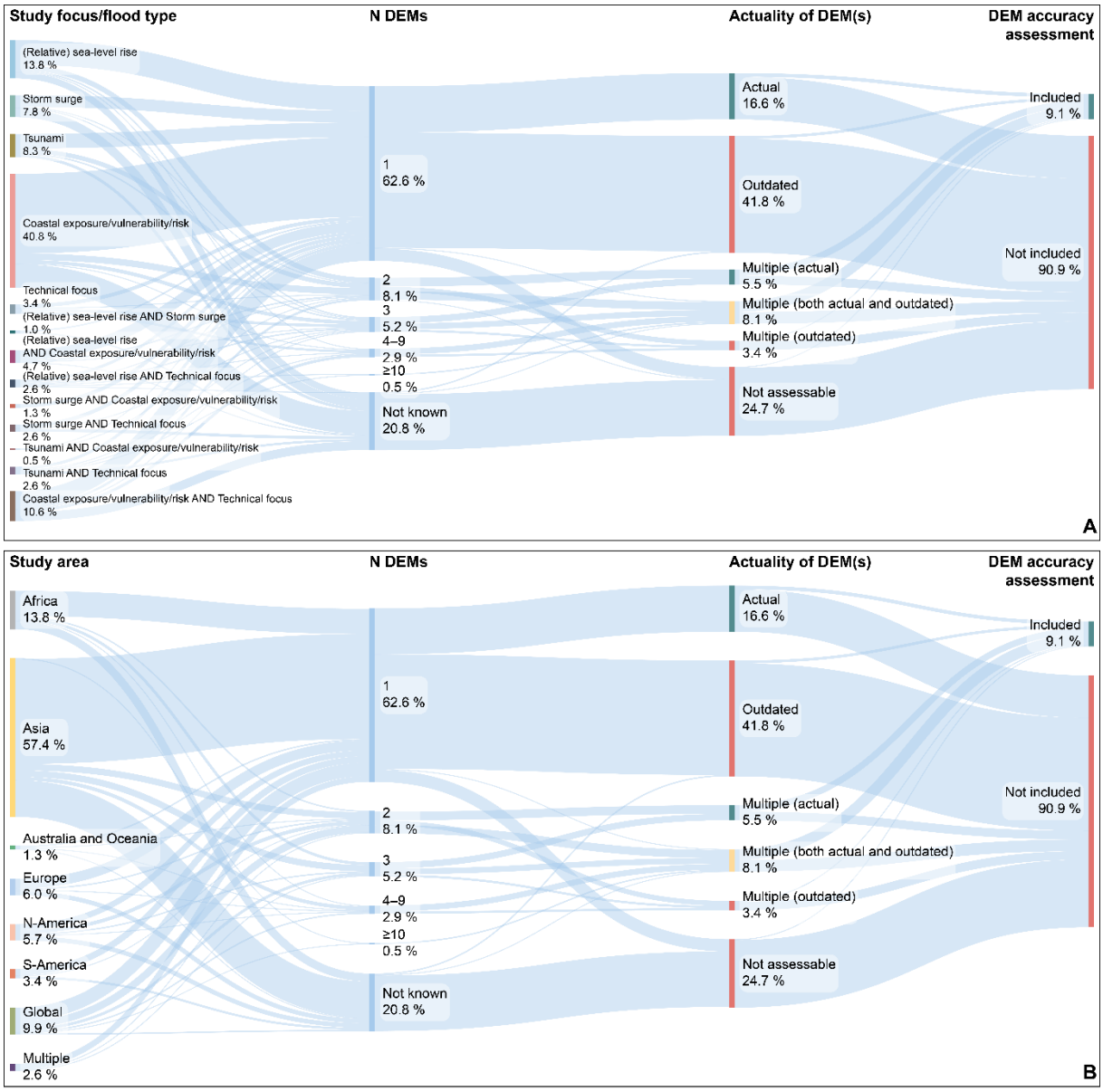


***Figure D4** | Evaluation of the usage of digital elevation models (DEMs) in the literature investigated in this study. Use of DEMs based on (A) study focus/flood type and (B) study area.*

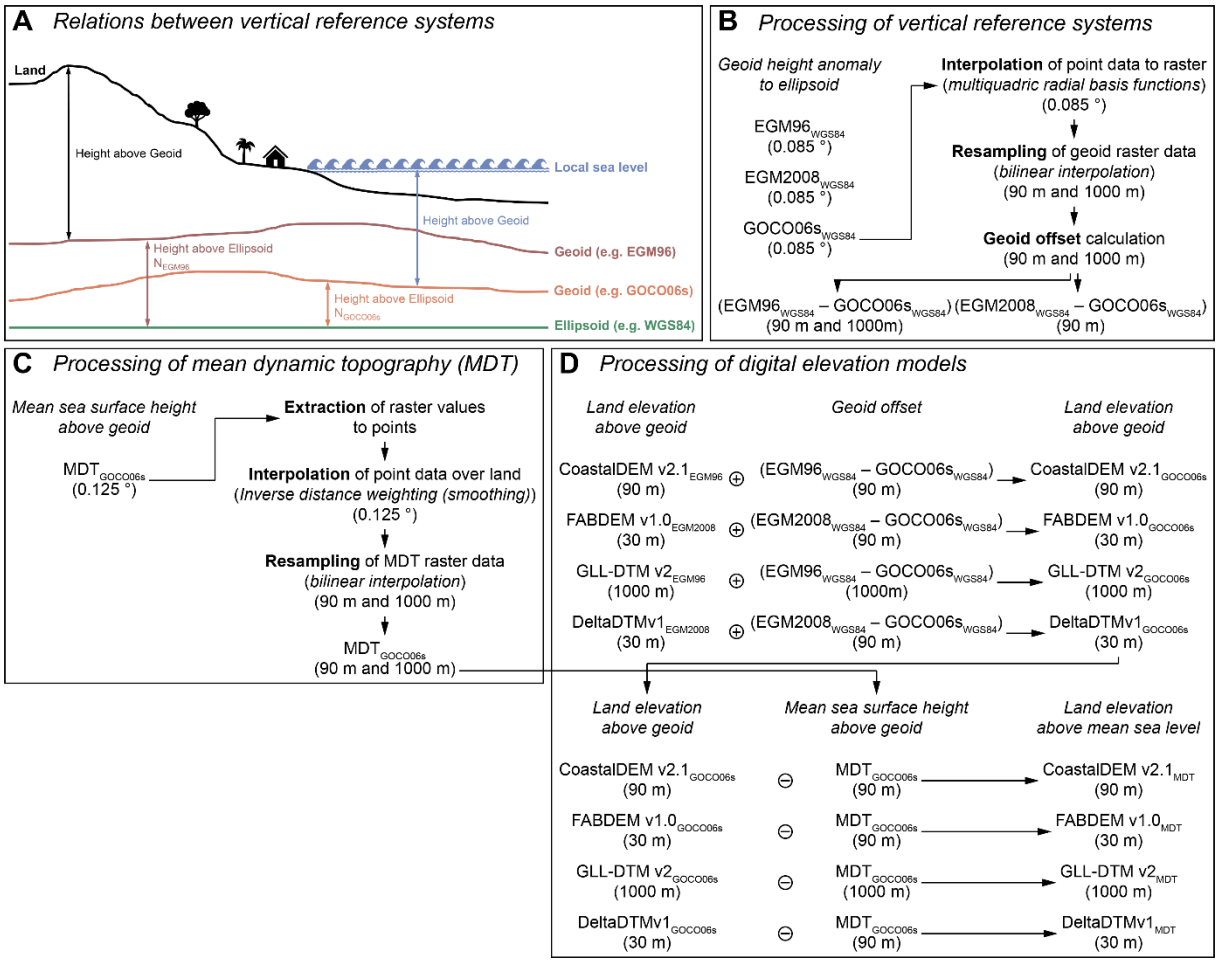


Figure D5 *| Relations between vertical reference systems and processing workflow of vertical datum conversion of elevation data.*
(A) Schematic overview of vertical datums. (B) Calculation of offsets between vertical reference systems as prerequisite for vertical datum conversion of elevation data. (C) Preparation of mean dynamic topography (MDT) data as prerequisite for vertical datum conversion of elevation data. (D) Vertical datum conversion of elevation data from their original vertical reference system to the latest earth gravity model GOCO06s and to mean sea level as indicated by MDT.

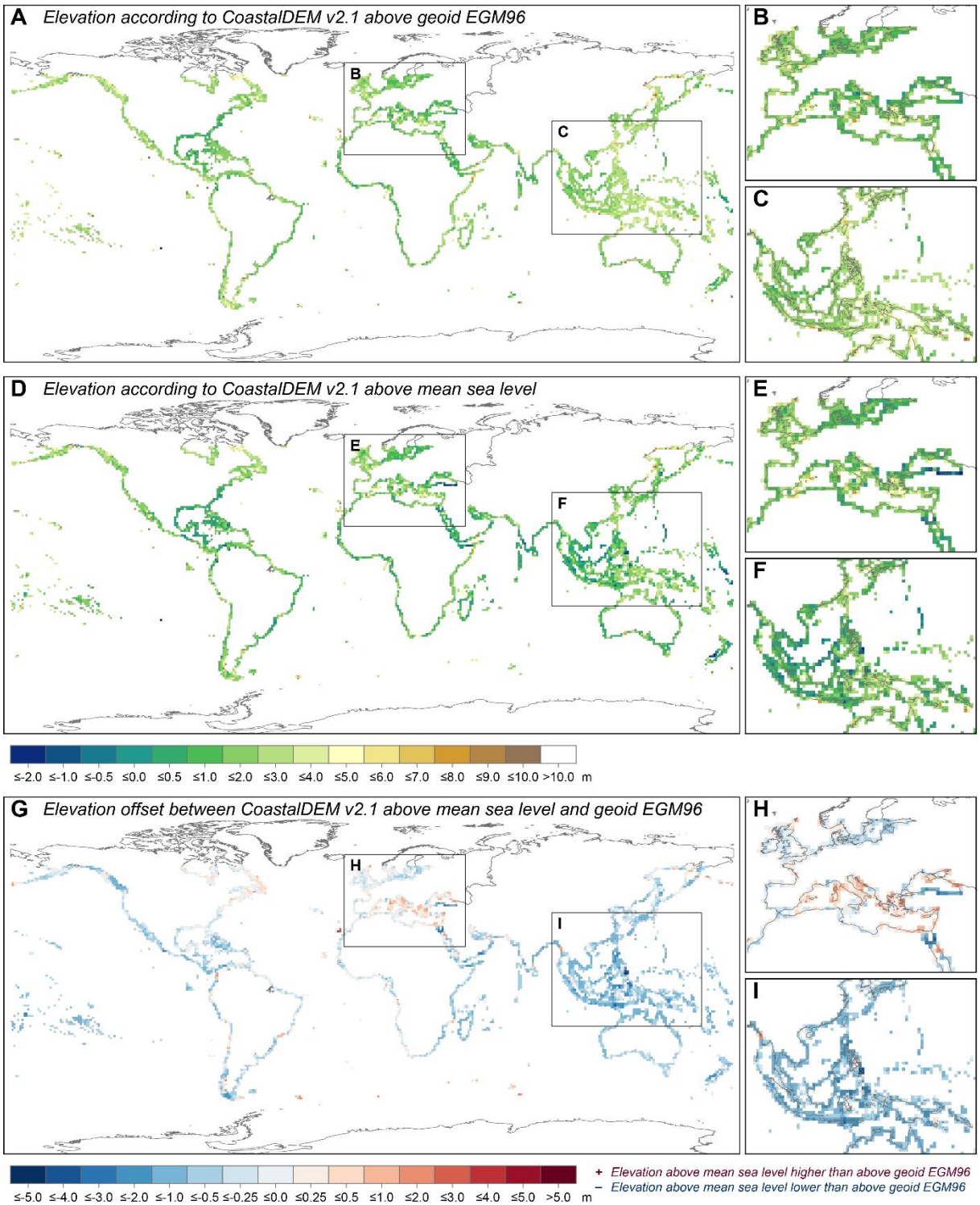


Figure D6 *| Global coastal elevation and discrepancy between geoid-based and sea-level-based elevation for CoastalDEM v2.1.*
Global coastal elevation according to CoastalDEM v2.1 above (A–C) geoid EGM96 and (D–F) mean sea level, as well as (G–I) the offset between both versions. For visualisation purposes, the spatial scale of the data shown was resampled to 1 deg using bilinear resampling while all statistics are given at 90 m spatial resolution.

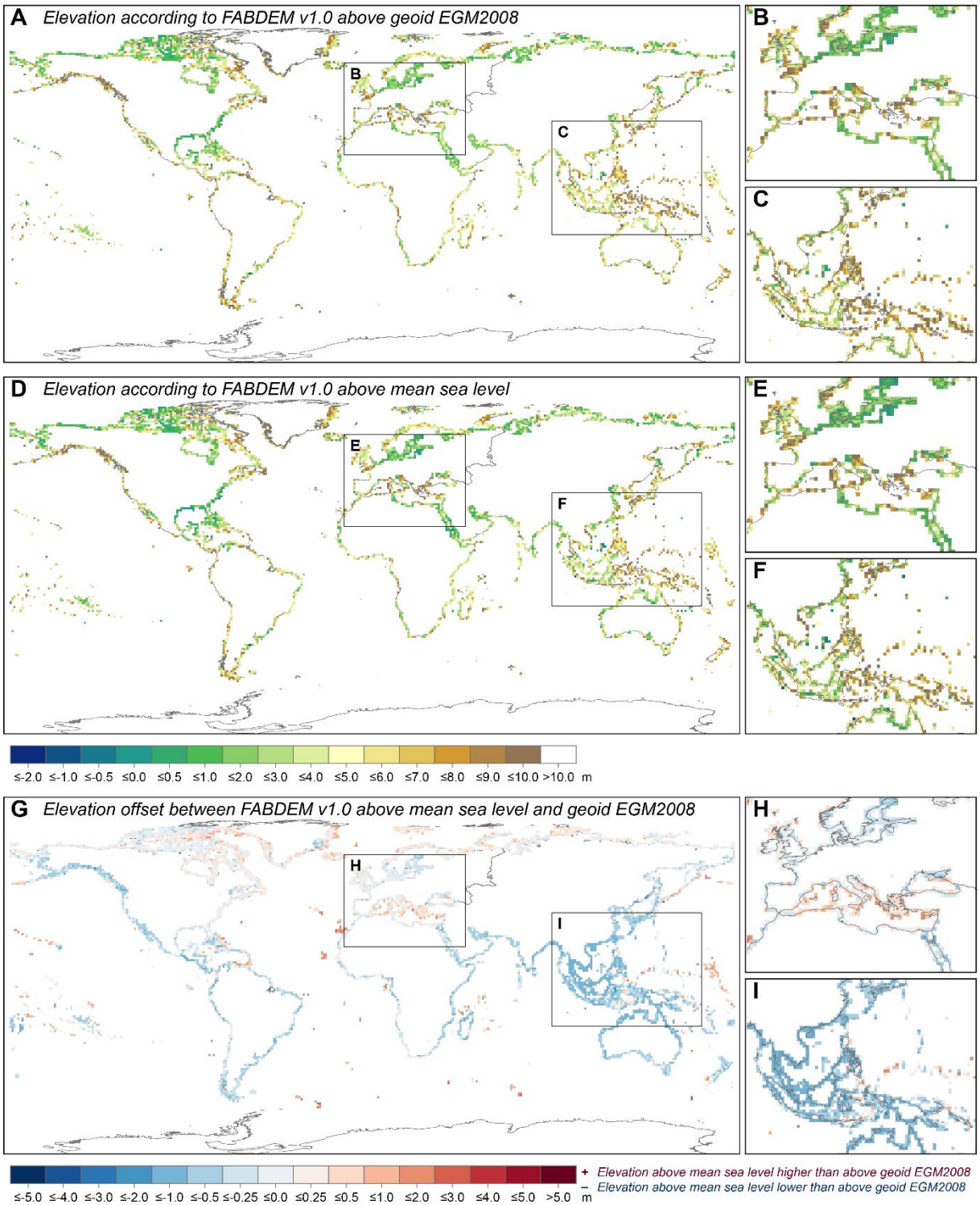


***Figure D7** | Global coastal elevation and discrepancy between geoid-based and sea-level-based elevation for FABDEM v1.0.*
Global coastal elevation according to FABDEM v1.0 above (A–C) geoid EGM2008 and (D–F) mean sea level, as well as (G–I) the offset between both versions. For visualisation purposes, the spatial scale of the data shown was resampled to 1 deg using bilinear resampling while all statistics are given at 90 m spatial resolution.

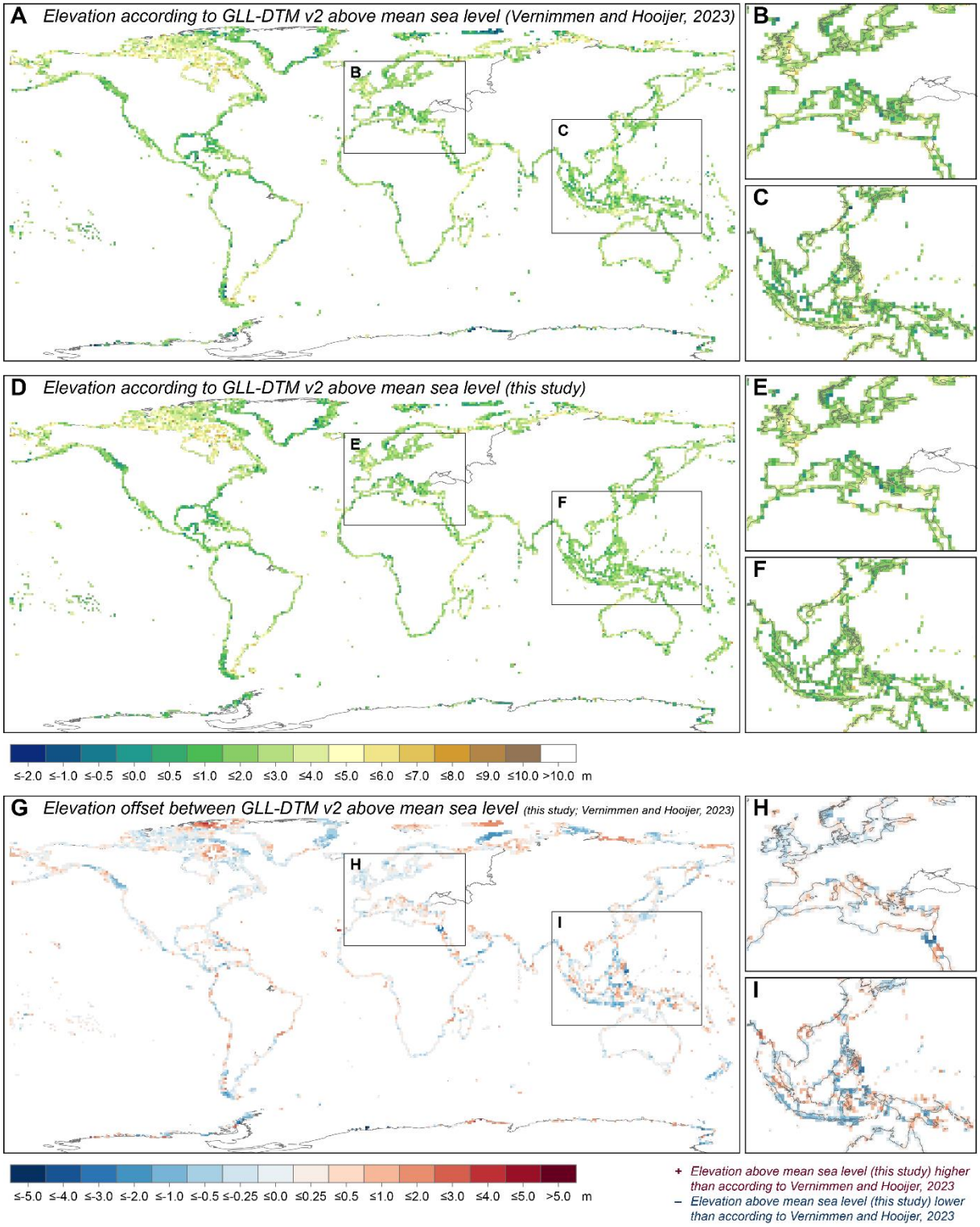


Figure D8 *| Global coastal elevation and discrepancy between sea-level-based elevation for GLL-DTM v2 after Vernimmen and Hooijer (2023), Vernimmen and Hooijer (2022), Rio et al. (2014) and following this study. Global coastal elevation according to GLL-DTM v2 above (A–C) mean sea level after Vernimmen and Hooijer (2023), Vernimmen and Hooijer (2022), Rio et al. (2014) and (D–F) mean sea level following this study, as well as (G–I) the offset between both versions.*

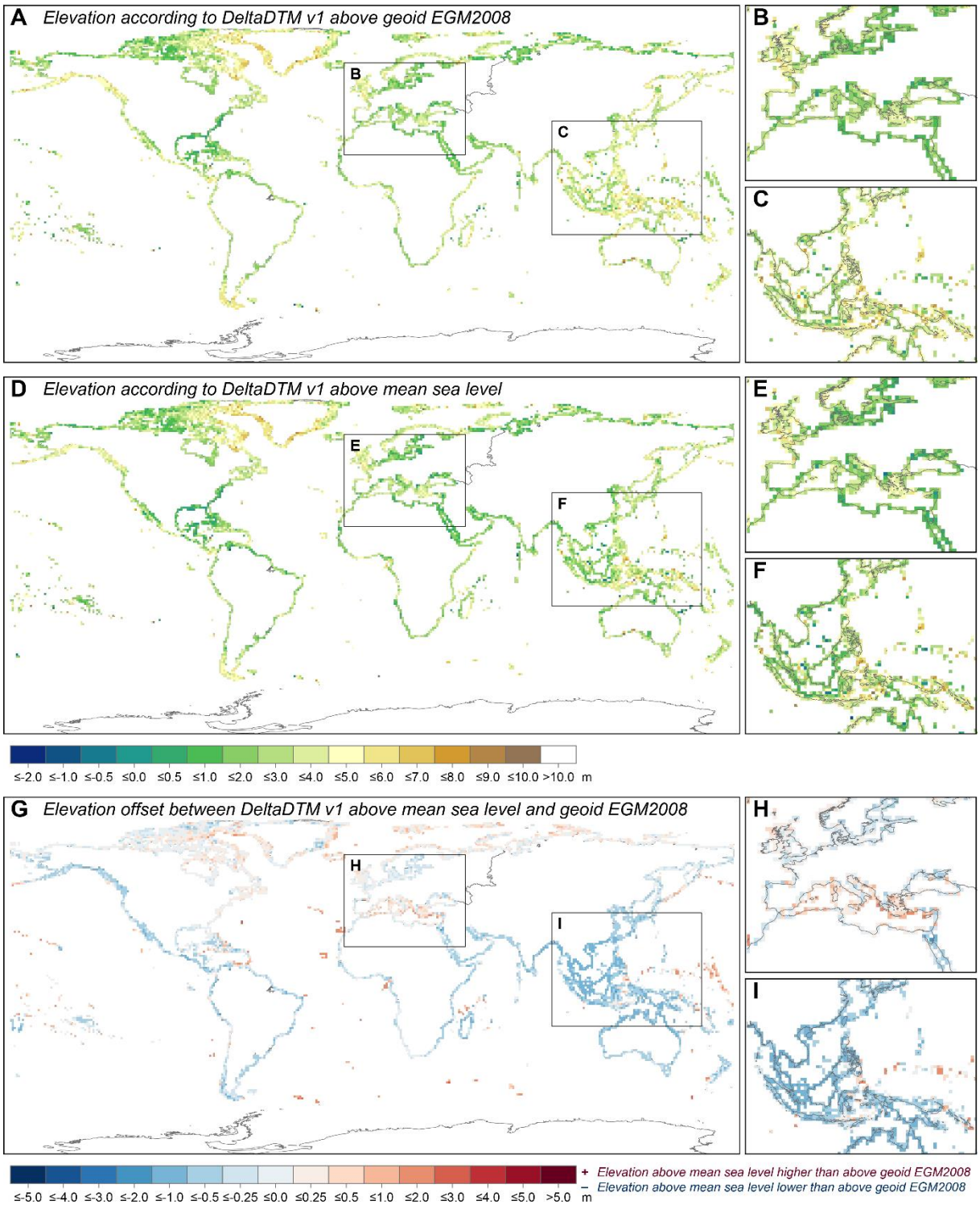


Figure D9 *| Global coastal elevation and discrepancy between geoid-based and sea-level-based elevation for DeltaDTM v1.*
Global coastal elevation according to DeltaDTM v1 above (A–C) geoid EGM2008 and (D–F) mean sea level, as well as (G–I) the offset between both versions. For visualisation purposes, the spatial scale of the data shown was resampled to 1 deg using bilinear resampling while all statistics are given at 90 m spatial resolution.

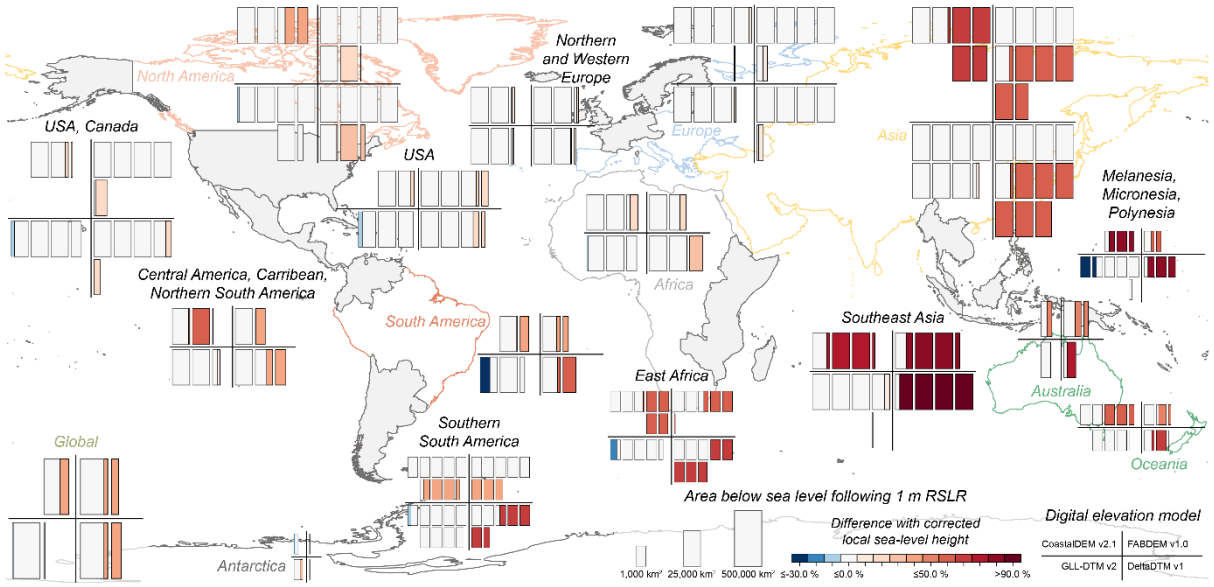
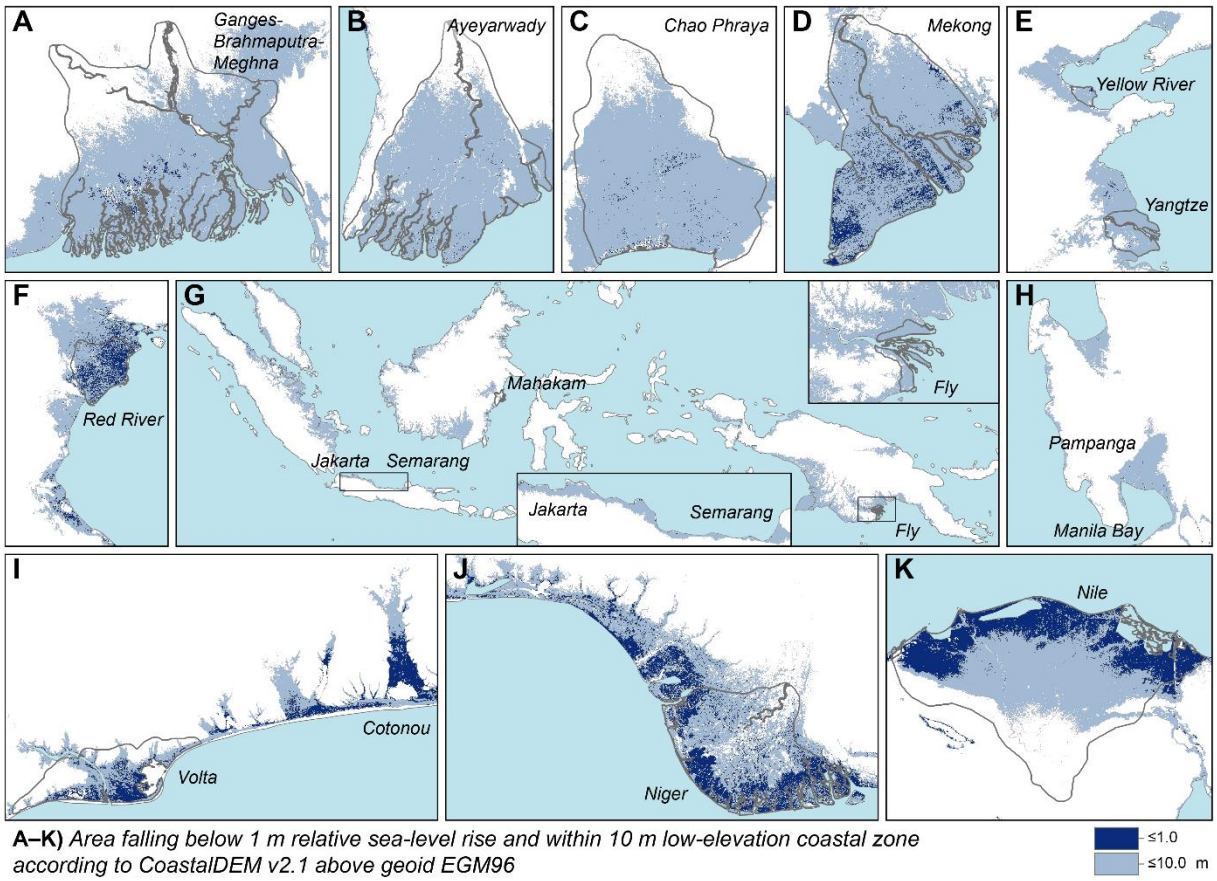
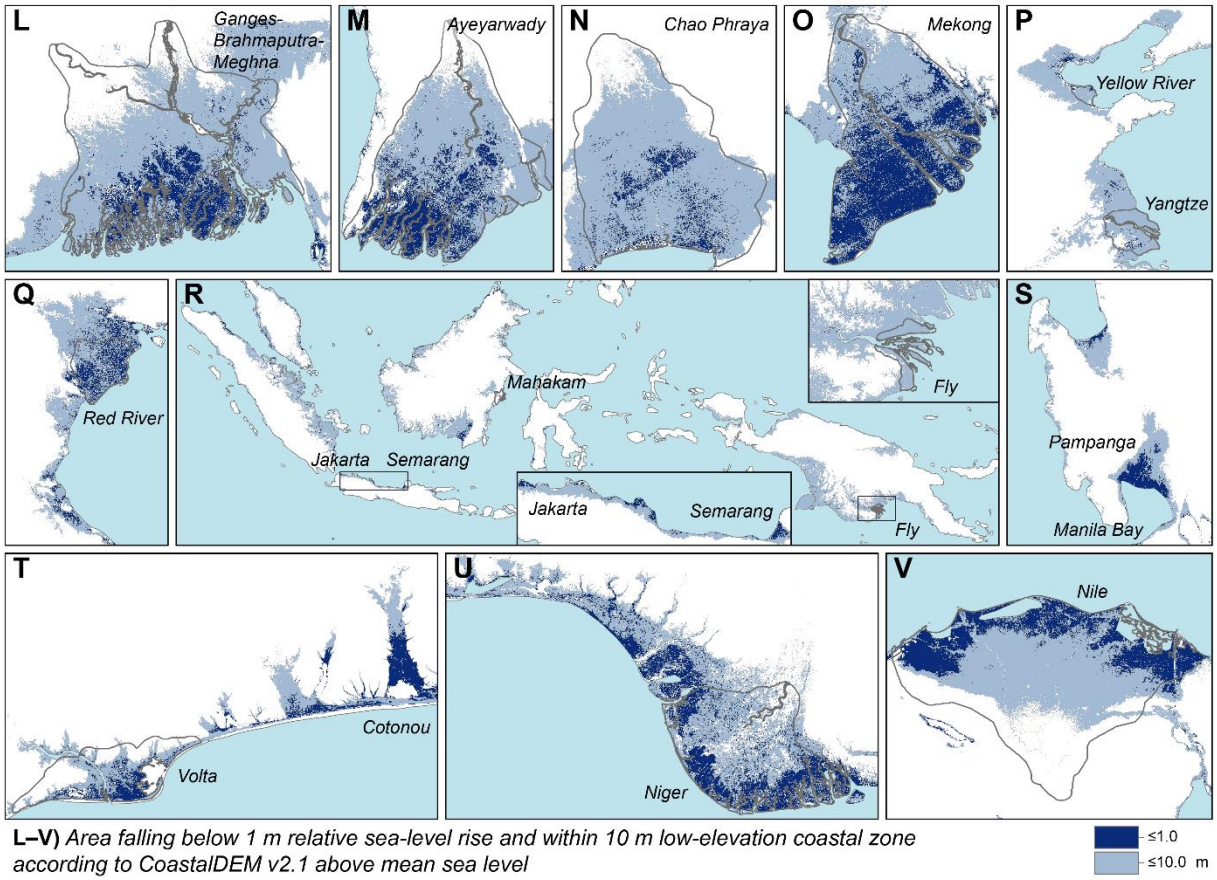


***Figure D10** | Differences in area falling below sea level following 1m relative sea-level rise (RSLR) with proper alignment of land and sea-level height.*
Meta-analysis of the impact of the most frequently observed errors in existing coastal hazard assessments, i.e. assuming geoid height to represent local sea-level height and improper alignment of land and sea-level heights, using modern, globally available digital elevation models (CoastalDEM v2.1 (Kulp and Strauss, 2021); FABDEM v1.0 (Hawker et al., 2021); GLL-DTM v2 (Vernimmen and Hooijer, 2022); DeltaDTM v1 (Pronk, 2024)). Due to the widespread omission to tie elevation data to local sea level instead of global geoid models, area impacted by 1 m RSLR is 31 % to 37 % larger globally. Maximum discrepancies of up to 94 % (i.e. up to 93,800 km^2) are observed along the coastlines of Southeast Asia where – if properly assessed – up to 100,000 km^2 will fall below sea level following 1 m RSLR. All statistics are given for the DEM's respective spatial resolution.

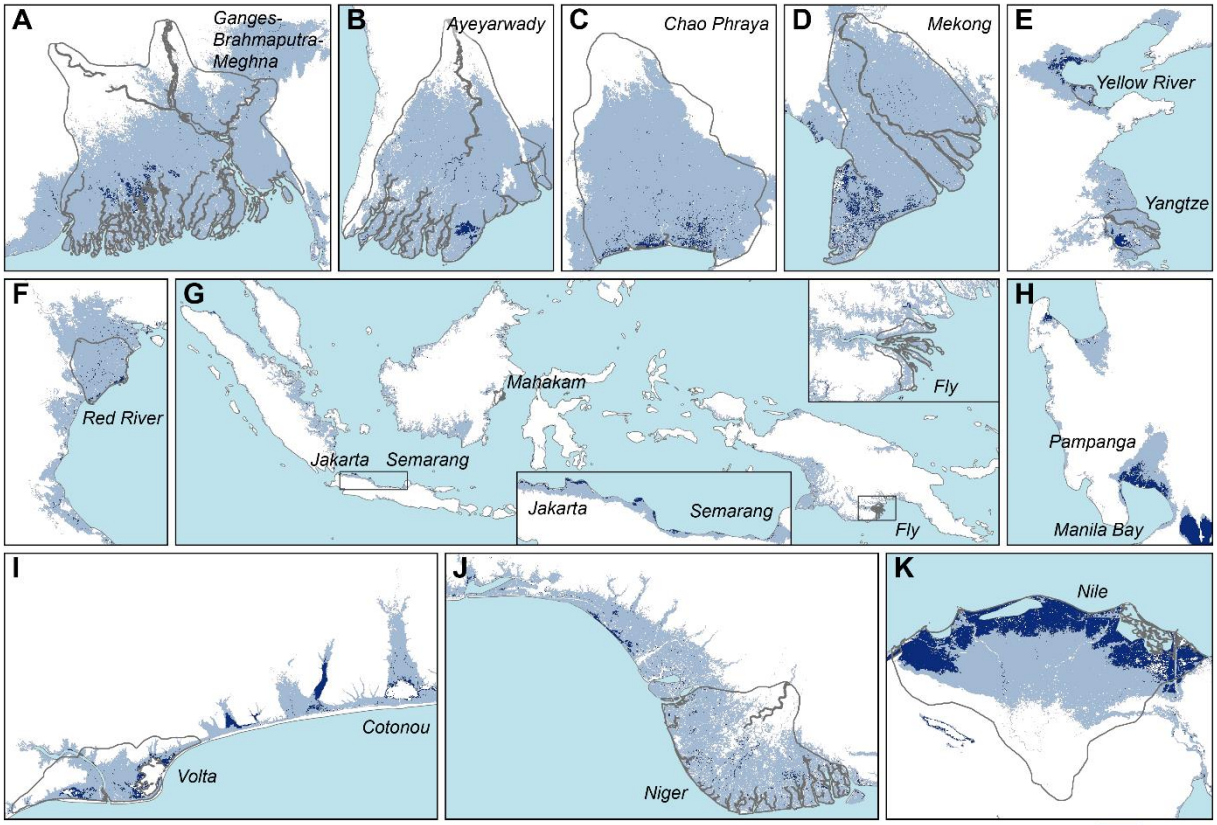


A–K) *Area falling below 1 m relative sea-level rise and within 10 m low-elevation coastal zone according to CoastalDEM v2.1 above geoid EGM96*

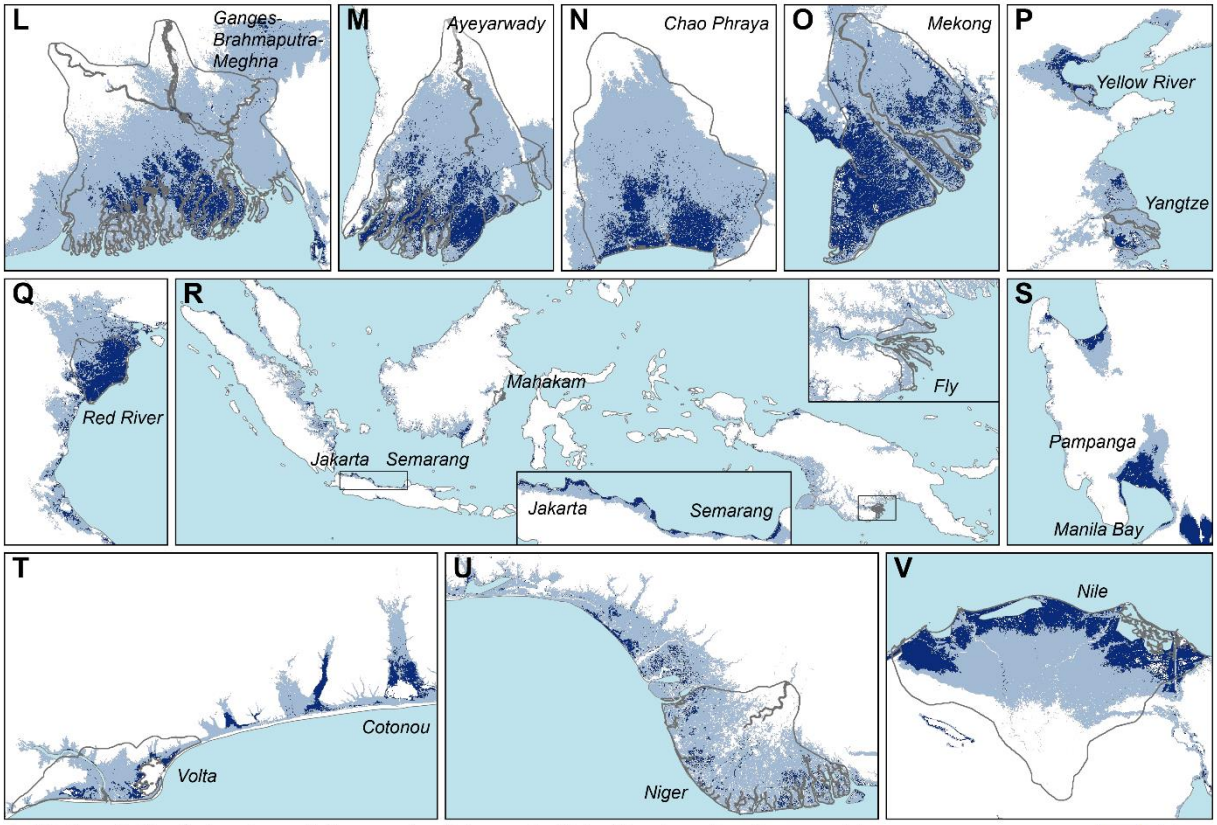


L–V) *Area falling below 1 m relative sea-level rise and within 10 m low-elevation coastal zone according to CoastalDEM v2.1 above mean sea level*

***Figure D11** | Area impacted by 1 m RSLR and within the LECZ for CoastalDEM v2.1. Impact of 1 m RSLR and LECZ based on CoastalDEM v2.1 referenced to (A–K) EGM96 and (L–V) mean sea level.*

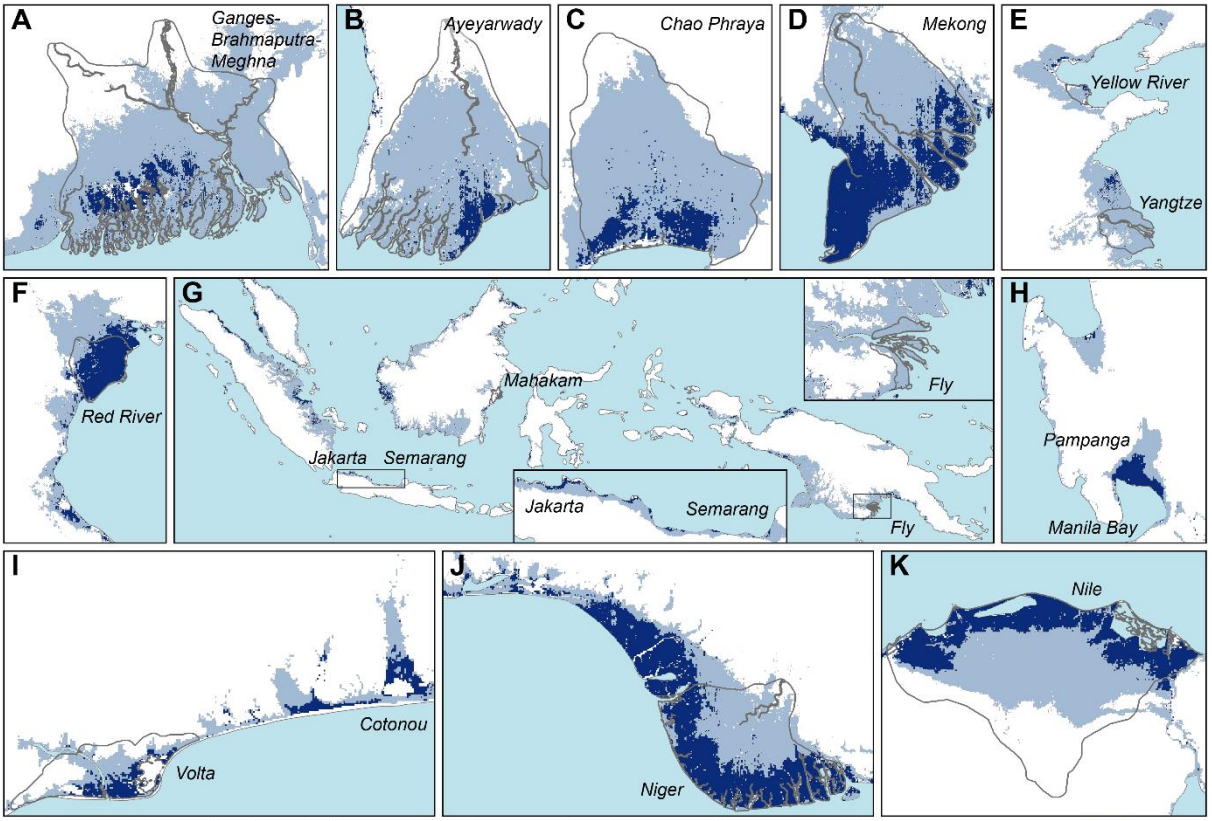


A–K) *Area falling below 1 m relative sea-level rise and within 10 m low-elevation coastal zone according to FABDEM v1.0 above geoid EGM2008*

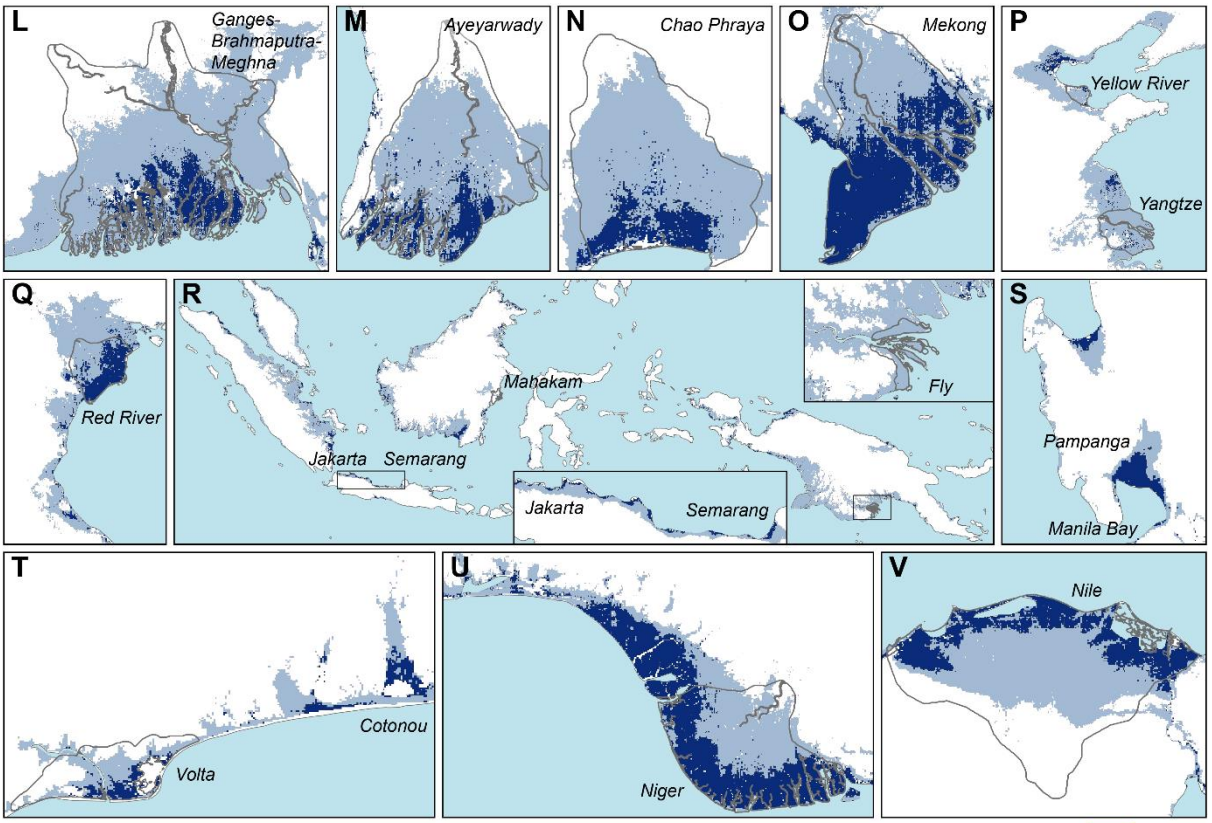


L–V) *Area falling below 1 m relative sea-level rise and within 10 m low-elevation coastal zone according to FABDEM v1.0 above mean sea level*

***Figure D12** | Area impacted by 1 m RSLR and within the LECZ for FABDEM v1.0.*
Impact of 1 m RSLR and LECZ based on FABDEM v1.0 referenced to (A–K) EGM2008 and (L–V) mean sea level.



A–K) *Area falling below 1 m relative sea-level rise and within 10 m low-elevation coastal zone according to GLL-DTM v2 above mean sea level (Vernimmen and Hooijer, 2023)*



L–V) *Area falling below 1 m relative sea-level rise and within 10 m low-elevation coastal zone according to GLL-DTM v2 above mean sea level (this study)*

***Figure D13** | Area impacted by 1m RSLR and within the LECZ for GLL-DTM v2.*
Impact of 1 m RSLR and LECZ based on GLL-DTM v2 referenced to (A–K) mean sea level after Vernimmen and Hooijer (2023), Vernimmen and Hooijer (2022), Rio et al. (2014) and (L–V) mean sea level following this study.

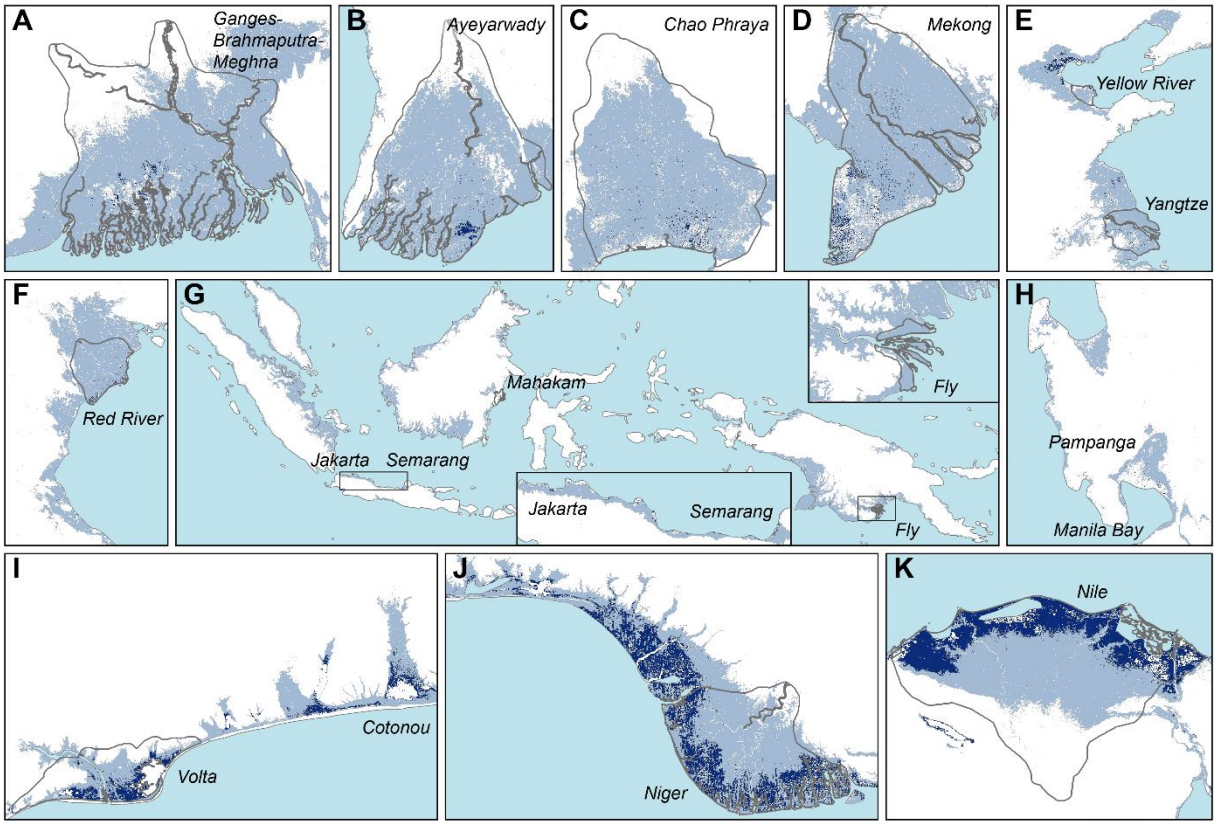


***Figure D14** | Area impacted by 1 m RSLR and within the LECZ for DeltaDTM v1.*
Impact of 1 m RSLR and LECZ based on DeltaDTM v1 referenced to (A–K) EGM2008 and (L–V) mean sea level.

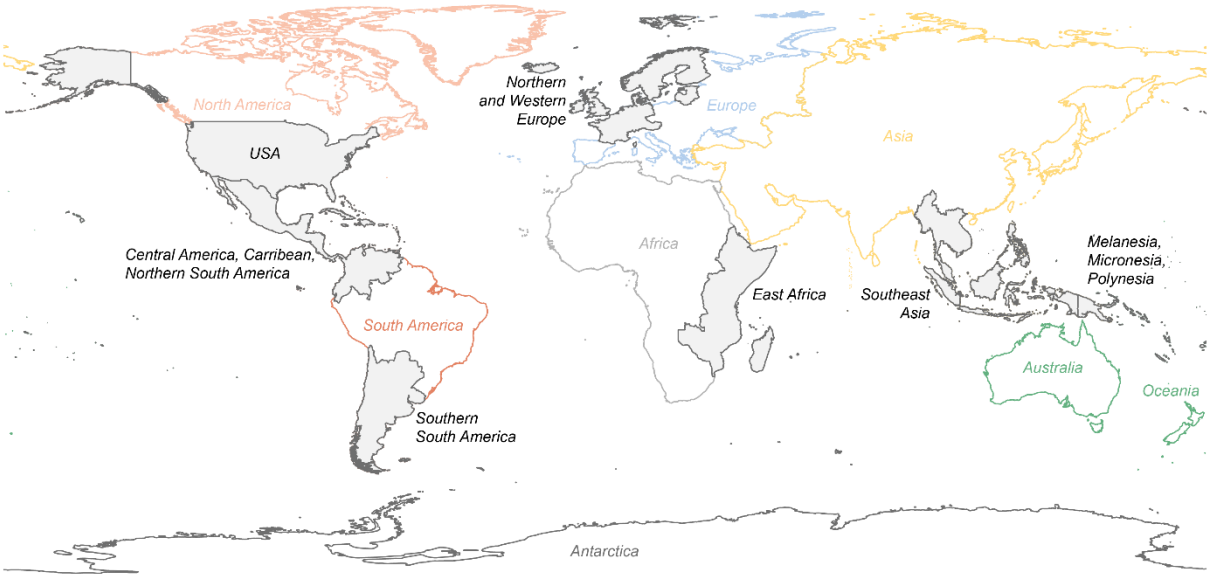


***Figure D15** | Study areas referred to in this study.*
Regions and subregions used to obtain more regional statistics for assessments of coastal elevation, relative sea-level rise impact, and low-elevation coastal zone.

D2. Supplementary tables

***Table D1** | Search term and screening used to collect and select scientific literature for evaluation.*

Scopus search term
TITLE-ABS-KEY ((delta* OR coastal-area* OR coastal-zone* OR coastal-elevation* OR coastal-lowland* OR low-elevation-coastal-zone* OR estuar* OR small-island-developing-states OR sids OR digital-elevation-model* OR dem OR digital-terrain-model* OR dtm OR digital-surface-model* OR dsm) AND (sea-level-rise OR slr OR relative-sea-level OR vertical-land-motion OR vlm OR subsidence OR inundat* OR storm-surge OR submersion OR flood* OR rising-sea*) AND (impact* OR hazard* OR assess* OR project* OR forecast* OR model* OR scenario* OR evalu* OR investig* OR future OR expos* OR risk* OR vulnera*)) AND PUBYEAR > 2008 AND PUBYEAR < 2026 AND PUBYEAR > 2008 AND PUBYEAR < 2026 AND (LIMIT-TO (DOCTYPE , "ar") OR LIMIT-TO (DOCTYPE , "re") OR LIMIT-TO (DOCTYPE , "dp")) AND (EXCLUDE (SUBJAREA , "ENER") OR EXCLUDE (SUBJAREA , "BIOC") OR EXCLUDE (SUBJAREA , "MEDI") OR EXCLUDE (SUBJAREA , "ARTS") OR EXCLUDE (SUBJAREA , "CENG") OR EXCLUDE (SUBJAREA , "CHEM") OR EXCLUDE (SUBJAREA , "IMMU") OR EXCLUDE (SUBJAREA , "PHAR") OR EXCLUDE (SUBJAREA , "VETE") OR EXCLUDE (SUBJAREA , "NEUR") OR EXCLUDE (SUBJAREA , "PSYC") OR EXCLUDE (SUBJAREA , "NURS") OR EXCLUDE (SUBJAREA , "HEAL") OR EXCLUDE (SUBJAREA , "AGRI") OR EXCLUDE (SUBJAREA , "MATE") OR EXCLUDE (SUBJAREA , "ENGI")) AND (LIMIT-TO (LANGUAGE , "English")) AND (EXCLUDE (EXACTKEYWORD , "Sediment Transport") OR EXCLUDE (EXACTKEYWORD , "Holocene") OR EXCLUDE (EXACTKEYWORD , "Seasonal Variation") OR EXCLUDE (EXACTKEYWORD , "Sedimentation") OR EXCLUDE (EXACTKEYWORD , "Sedimentology") OR EXCLUDE (EXACTKEYWORD , "Sediments") OR EXCLUDE (EXACTKEYWORD , "Stratigraphy") OR EXCLUDE (EXACTKEYWORD , "Sediment") OR EXCLUDE (EXACTKEYWORD , "Water Quality") OR EXCLUDE (EXACTKEYWORD , "River Discharge") OR EXCLUDE (EXACTKEYWORD , "Deposition") OR EXCLUDE (EXACTKEYWORD , "Depositional Environment") OR EXCLUDE (EXACTKEYWORD , "Rain") OR EXCLUDE (EXACTKEYWORD , "Runoff") OR EXCLUDE (EXACTKEYWORD , "Sequence Stratigraphy") OR EXCLUDE (EXACTKEYWORD , "Concentration (composition)") OR EXCLUDE (EXACTKEYWORD , "Paleoenvironment") OR

EXCLUDE (EXACTKEYWORD , "Animals") OR EXCLUDE (EXACTKEYWORD , "Fluvial Deposit") OR EXCLUDE (EXACTKEYWORD , "Deposits") OR EXCLUDE (EXACTKEYWORD , "Rainfall") OR EXCLUDE (EXACTKEYWORD , "Drought") OR EXCLUDE (EXACTKEYWORD , "Rhizophoraceae") OR EXCLUDE (EXACTKEYWORD , "Forestry") OR EXCLUDE (EXACTKEYWORD , "Catchments") OR EXCLUDE (EXACTKEYWORD , "Ecology") OR EXCLUDE (EXACTKEYWORD , "Animal"))

Explanation of the Scopus search term	
Search in title, abstract and keywords	delta* OR coastal-area* OR coastal-zone* OR coastal-elevation* OR coastal-lowland* OR low-elevation-coastal-zone* OR estuar* OR small-island-developing-states OR sids OR digital-elevation-model* OR digital-terrain-model* OR dtm OR digital-surface-model* OR dsm **AND** sea-level-rise OR slr OR relative-sea-level OR vertical-land-motion OR vlm OR subsidence OR inundat* OR storm-surge OR submersion OR flood* OR rising-sea* **AND** impact* OR hazard* OR assess* OR project* OR forecast* OR model* OR scenario* OR evalu* OR investig* OR future OR expos* OR risk* OR vulnera*
Filter search for time range of publication, document type, subject area, language and keywords	**AND** PUBYEAR > 2008 AND PUBYEAR < 2026 **AND** **LIMIT-TO** DOCTYPE Article OR Review OR Data paper **AND** **EXCLUDE** SUBJAREA Energy OR Biochemistry, Genetics and Molecular Biology OR Medicine OR Arts and Humanities OR Chemical Engineering OR Chemistry OR Immunology and Microbiology OR Pharmacology, Toxicology and Pharmaceutics OR Veterinary OR Neuroscience OR Psychology OR Nursing OR Health Professions OR Agricultural and Biological Sciences OR Materials Science OR Engineering **AND** **LIMIT-TO** LANGUAGE English

	AND **EXCLUDE** EXACTKEYWORD Sediment Transport OR Holocene OR Seasonal Variation OR Sedimentation OR Sedimentology OR Sediments OR Stratigraphy OR Sediment OR Water Quality OR River Discharge OR Deposition OR Depositional Environment OR Rain OR Runoff OR Sequence Stratigraphy OR Concentration (composition) OR Paleoenvironment OR Animals OR Fluvial Deposit OR Deposits OR Rainfall OR Drought OR Rhizophoraceae OR Forestry OR Catchments OR Ecology OR Animal
Literature obtained *(search conducted on 2025-03-27)*	*Total: n = 7241 (100.0%)*
Literature screening	
Criteria	INCLUSION ▪ Focus on coastal land and coastal sea level ▪ Focus on coastal hazard and impact assessment ▪ Focus on coastal lowlands ▪ Use of satellite-borne elevation information ▪ Methodological/technical articles but with application included ▪ Use of keywords included in the Scopus search term EXCLUSION ▪ Focus on coastal land and coastal sea level ▪ Use of airborne LiDAR without combination with satellite-borne elevation data ▪ Methodological/technical articles without application ▪ Perspective/Discussion articles without application ▪ Focus on secondary hazards (cascading effects) ▪ Assessment of historical events (i.e. not recent past) ▪ Focus on ecology and biodiversity ▪ Focus on (Palaeo)Geomorphology – erosion, periglacial and glacial landforms and processes, basins, watersheds ▪ Focus on (Geo-)Chemistry ▪ Focus on (Hyper-)arid environments ▪ Focus on Hydrodynamics – rivers, waves, dams and drainage and other infrastructural aspects ▪ Focus on Engineering – infrastructure ▪ Focus on Meteorology – pluvial flooding, atmospheric components, etc. ▪ Focus on extraterrestrial environments ▪ Use of languages other than English ▪ Exclusive use of slope information obtained from elevation data ▪ Exclusive use of local elevation data ▪ Articles referring to elevation data cited in tertiary source or beyond (only primary or secondary sourced studies included) ▪ Non-accessible articles ▪ Articles (co-)authored by Minderhoud and/or Seeger (to remove self-inclusion bias)
Literature obtained	*Included (fits the scope well): n = 630 (8.7%)* *Included (fits the scope less well): n = 326 (4.5%)*

(after screening I: title, abstract, keywords)	*Excluded (does not fit the scope): n = 6285 (86.8%)*
Literature obtained (after screening II: full article)	*Included: n = 385 (5.3%)* *Excluded: n = 559 (7.7%)* *Not accessible: n = 12 (0.2%)*

Table D2 **|** *Code description of evaluation categories used to evaluate scientific literature.*

Code category	Code	Definition
Authors	------	List of authors.
Publication type		
Peer-reviewed article	1	Publication in an international, scientific peer-reviewed journal.
Report	2	Publication entailing systematic documentation of scientific findings, detailing practical measures and/or programs (such as development directives), or documenting technical details.
Preprint	3	Publication of a scientific manuscript prior to peer-review process.
Conference paper	4	Publication of a scientific conference contribution.
Non-peer reviewed article	5	Publication in a non-peer-reviewed journal or publication series with articles similarly structured as in peer-reviewed journals.
Book chapter	6	Publication as section in a monography or book series.
Year of publication		
2009	1	Publication in 2009 CE.
2010	2	Publication in 2010 CE.
2011	3	Publication in 2011 CE.
2012	4	Publication in 2012 CE.
2013	5	Publication in 2013 CE.
2014	6	Publication in 2014 CE.
2015	7	Publication in 2015 CE.
2016	8	Publication in 2016 CE.
2017	9	Publication in 2017 CE.
2018	10	Publication in 2018 CE.
2019	11	Publication in 2019 CE.
2020	12	Publication in 2020 CE.
2021	13	Publication in 2021 CE.
2022	14	Publication in 2022 CE.
2023	15	Publication in 2023 CE.
2024	16	Publication in 2024 CE.
Study focus/Flood type		

(Relative) sea-level rise	1	Focus on sea-level rise or sea-level rise impact from either absolute or relative sea-level rise (i.e. with or without including vertical land motion).
Storm surge	2	Focus on storm surge hazard or storm surge impact.
Tsunami	3	Focus on tsunami hazard or tsunami impact.
Coastal exposure/vulnerability/risk	4	Focus on the assessment of coastal exposure, vulnerability, or risk, including also hazard or impact assessments without referring to specific flood types, or referring to extreme water levels resulting from multiple causes. Publications referring to assessments of low-elevation coastal zones (LECZ) belong to this category as well.
Technical focus	5	Focus on technical aspects or methodological setups/workflows in terms of data handling and/or modelling(s).
(Relative) sea-level rise AND Storm surge	6	Focus including topics of both categories *(Relative) sea-level rise* and *Storm surge*.
(Relative) sea-level rise AND Tsunami	7	Focus including topics of both categories *(Relative) sea-level rise* and *Tsunami*.
(Relative) sea-level rise AND Coastal exposure/vulnerability/risk	8	Focus including topics of both categories *(Relative) sea-level rise* and *Coastal exposure/vulnerability/risk*.
(Relative) sea-level rise AND Technical focus	9	Focus including topics of both categories *(Relative) sea-level rise* and *Technical focus*.
Storm surge AND Tsunami	10	Focus including topics of both categories *Storm surge* and *Tsunami*.
Storm surge AND Coastal exposure/vulnerability/risk	11	Focus including topics of both categories *Storm surge* and *Coastal exposure/vulnerability/risk*.
Storm surge AND Technical focus	12	Focus including topics of both categories *Storm surge* and *Technical focus*.
Tsunami AND Coastal exposure/vulnerability/risk	13	Focus including topics of both categories *Tsunami* and *Coastal exposure/vulnerability/risk*.
Tsunami AND Technical focus	14	Focus including topics of both categories *Tsunami* and *Technical focus*.
Coastal exposure/vulnerability/risk AND Technical focus	15	Focus including topics of both categories *Coastal exposure/vulnerability/risk* and *Technical focus*.
Study area		
Africa	1	Study area located on the continent of Africa.
Antarctica	2	Study area located on the continent of Antarctica.
Asia	3	Study area located on the continent of Asia.
Australia and Oceania	4	Study area located on the continent of Australia and Oceania.
Europe	5	Study area located on the continent of Europe.
North America	6	Study area located on the continent of North America.
South America	7	Study area located on the continent of South America.
Global	8	Study area includes the global scale.
Multiple	9	Study area includes locations on several continents.
N DEMs		

1	1	1 DEM considered in the publication.
2	2	2 DEMs considered in the publication.
3	3	3 DEMs considered in the publication.
4	4	4 DEMs considered in the publication.
5	5	5 DEMs considered in the publication.
6	6	6 DEMs considered in the publication.
7	7	7 DEMs considered in the publication.
8	8	8 DEMs considered in the publication.
9	9	9 DEMs considered in the publication.
10	10	10 DEMs considered in the publication.
11	11	11 DEMs considered in the publication.
12	12	12 DEMs considered in the publication.
13	13	13 DEMs considered in the publication.
14	14	14 DEMs considered in the publication.
Not known	100	Number of DEMs considered in the publication is not known/cannot be assessed.
Actuality of DEM(s)		
Actual	1	The evaluated publication refers to the latest available elevation dataset at the time of submission/conference (publication in case of non-peer-reviewed publication). If local elevation data was used, it was considered to be the latest available information.
Outdated	2	The evaluated publication refers to an elevation dataset that is already outdated at the time of submission/conference (publication in case of non-peer-reviewed publication).
Multiple DEMs (both actual and outdated)	3	The evaluated publication refers to min. 2 elevation datasets including both actual and outdated datasets at the time of submission/conference (publication in case of non-peer-reviewed publication). If local elevation data was used, it was considered to be the latest available information.
Multiple DEMs (actual)	4	The evaluated publication refers to min. 2 elevation datasets that are the latest available ones at the time of submission/conference (publication in case of non-peer-reviewed publication). If local elevation data was used, it was considered to be the latest available information.
Multiple DEMs (outdated)	5	The evaluated publication refers to min. 2 elevation datasets that are already outdated at the time of submission/conference (publication in case of non-peer-reviewed publication).
N/A	100	The evaluated publication does not provide any documentation or reference on the elevation data used so its actuality cannot be assessed.
DEM accuracy assessment		
Included	1	The evaluated publication includes an accuracy assessment of the elevation data used for the area under study.
Not included	2	The evaluated publication does not include an accuracy assessment of the elevation data used for the area under study.

Vertical datum documentation		
Complete	1	Documentation on the vertical datum is complete if full documentation is provided by the evaluated publication itself or if a reference to another paper or repository is made that has all the documentation.
Incomplete	2	Documentation on the vertical datum is incomplete if part of the vertical datum documentation is missing. This also holds true if a reference is cited which does not provide complete documentation.
Absent	3	No documentation about the vertical datum by the evaluated publication itself nor by providing any reference.
Vertical datum conversion		
Correct	1	All datasets used (including topography, bathymetry and sea-level datasets) are in the same vertical reference frame (e.g. EGM96, NAVD88) and datum conversion was conducted correctly.
Incorrect	2	Vertical datum conversion is either incomplete (i.e. part of datum conversion is missing) or was incorrectly conducted before elevating water level to simulate flooding (as applied for example in the bathtub approach).
Correctness not assessable	3	The evaluated publication does not provide any documentation about vertical datum conversion and is thus likely incorrect. This category includes also datasets that are referenced to a global vertical datum (such as global geoid or ellipsoid) and where no datum conversion was documented before elevating water level to simulate flooding (as applied for example in the bathtub approach).
N/A	4	The correctness of vertical datum conversion is not applicable as the evaluated publication by purpose included datasets referenced to different vertical datums in order to highlight the discrepancies that exist when using a local, tidal datum and a global geoid or ellipsoid.
Vertical datum type		
Geoid (EGM96)	1	Global EGM96 geoid.
Geoid (EGM2008)	2	Global EGM2008 geoid.
Ellipsoid (WGS84)	3	Global WGS84 ellipsoid.
Tidal (MSL, altimetry, reference documented)	4	Mean sea level estimated from altimetry data, with reference provided.
Tidal (MSL, altimetry, reference not documented)	5	Mean sea level estimated from altimetry data, no reference provided.
Tidal (MHHW, altimetry, reference documented)	6	Mean higher high water estimated from altimetry data, with reference provided.
Tidal (MHHW, altimetry, reference not documented)	7	Mean higher high water estimated from altimetry data, no reference provided.
Tidal (MSL, tide gauge or location, reference documented)	8	Mean sea level estimated from tide gauge data or location, with reference provided.
Tidal (MSL, tide gauge or location, reference not documented)	9	Mean sea level estimated from tide gauge data or location, no reference provided.

Tidal (MHW, tide gauge or location, reference documented)	10	Mean high water estimated from tide gauge data or location, with reference provided.
Tidal (MHW, tide gauge or location, reference not documented)	11	Mean high water estimated from tide gauge data or location, no reference provided.
Tidal (MHHW, tide gauge or location, reference documented)	12	Mean higher high water estimated from tide gauge data or location, with reference provided.
Tidal (MHHW, tide gauge or location, reference not documented)	13	Mean higher high water estimated from tide gauge data or location, no reference provided.
Tidal (MLLW, tide gauge or location, reference documented)	14	Mean lower low water estimated from tide gauge data or location, with reference provided.
Tidal (MLLW, tide gauge or location, reference not documented)	15	Mean lower low water estimated from tide gauge data or location, no reference provided.
Multiple	16	The datasets used are referenced to different vertical reference systems. This category also includes incorrectly conducted vertical datum conversions as these include errors (i.e. artificial offsets) to the targeted vertical datum.
Not documented/ not assessable	17	The evaluated publication does not provide any documentation or reference about the vertical datum type used.
Actuality of sea-level reference		
Actual	1	The evaluated publication refers to the latest available sea-level information at the time of submission/conference (publication in case of non-peer-reviewed publication), or – in case an outdated sea-level reference was used – includes a correction for sea-level change for the time between datum establishment and time of submission/conference (publication in case of non-peer-reviewed publication).
Outdated	2	The evaluated publication refers to sea-level information that is already outdated at the time of submission/conference (publication in case of non-peer-reviewed publication), or – in case an outdated sea-level reference was used – does not include a correction for sea-level change for the time between datum establishment and time of submission/conference (publication in case of non-peer-reviewed publication).
Multiple	3	The evaluated publication refers to different sea-level datasets. This category also includes incorrectly conducted vertical datum conversions as these include errors (i.e. artificial offsets) to the targeted sea-level datum.
Not assessable	4	The evaluated publication does not provide any documentation or reference about the sea-level dataset(s) used or where information about the establishment of the sea-level datum is not available. This category also includes evaluated publications that do not provide unequivocal information about the vertical datum type used as it remains unclear whether a sea-level datum was used or not.

N/A	5	The evaluated publication does not apply sea-level data but, for example, refers to a global geoid or ellipsoid model.

Appendix E – Supplement to Chapter 4.3

This Supplement is related to: **Seeger, K.**, Minderhoud, P.S.J., submitted. *Attributing uncertainties in elevation assessments for data-sparse coastal lowlands using global elevation models: A globally applicable approach showcasing the Vietnamese Mekong Delta*. Scientific Reports.

The supplementary material is published along with the scientific article under a CC-BY 4.0 Attribution 4.0 International licence (http://creativecommons.org/licenses/by/4.0/). The reader is recommended to refer to the peer-reviewed and published version of the content of this supplement which can be accessed here (https://media.springernature.com/original/springer-static/esm/art%3A10.1038%2Fs41598-026-38315-y/MediaObjects/41598_2026_38315_MOESM1_ESM.pdf) and also via the doi of the published article provided here (https://doi.org/10.1038/s41598-026-38315-y).

E1. Performance of digital elevation models in the Vietnamese Mekong Delta

E1.1 Which one is the best? – On the local validation of global digital elevation models: Comparison with local point elevations

Extracting local point elevations from the respective global DEMs in form of a spot height comparison reveals similar results as the spatial comparison with Topo DEM v2 and yields only slight changes in the error and height residual statistics. For most of the DEMs which are comparably higher than indicated by local elevation, error metrics lower by ca. 2–5 cm compared to the statistics of the comparison to Topo DEM v2 (Tables 4.4 and E1). For those DEMs that perform already well in comparison with Topo DEM v2 (i.e. DeltaDTM) or are on average consistent with the local data (i.e. CoastalDEM v2.1), pointwise determined average errors slightly increase and height residuals become (more) negative while for GLL-DTM v2, at least mean error reduces further. This pattern holds true for the comparison with low-lying spot heights (i.e. ≤10 m) as well (Tables 4.4 and E2). Probably the most remarkable difference

between DEM spatial comparison and validation by local point elevations is the decrease of median height residual for SRTM by 13–14 cm to 0.04 m for point elevation comparison with all and only low-elevation spot heights, respectively (Tables E1 and E2). However, we do not consider these slight changes as significant but rather explain them by respective capacities and limitations to resolve local point settings. Instead, we interpret the results of this point elevation comparison being similar to outcomes of the spatial comparison with Topo DEM v2 and to strengthen our overall finding that among the assessed DEMs, most recently processed coastal elevation data provides the most accurate results, of which we strongly recommend the usage of DeltaDTM v1 referenced to local continuous, actual MSL, which shows the overall best agreement with local elevation data in the Vietnamese Mekong Delta.

***Table E1** | Performance of local and global DEMs in the Vietnamese Mekong Delta validated by local point elevations for versions referenced to mean dynamic topography (MDT) and their original vertical reference. N – number of spot heights in the study area, with no-data values excluded for each DEM, respectively; Mean spot – mean point elevation in the study area; Median spot – median point elevation in the study area; Min. spot – minimum point elevation in the study area; Max. spot – maximum point elevation in the study area; Mean DEM – mean DEM elevation in the study area; Median DEM – median DEM elevation in the study area; Min. DEM – minimum DEM elevation in the study area; Max. DEM – maximum DEM elevation in the study area; σ DEM – standard deviation of DEM elevation in the study area; HR – height residual; MAE – mean absolute error; RMSE – root mean square error.*

DEM	*N*	Mean spot (m)	Median spot (m)	Min. spot (m)	Max. spot (m)	Mean DEM (m)	Median DEM (m)	Min. DEM (m)	Max. DEM (m)	σ DEM (m)	Max. negative HR (m)	Max. positive HR (m)	Mean error (m)	MAE (m)	Median error (m)	RMSE (m)
Topo DEM v2	18447	0.79	0.66	-1.06	9.95	0.77	0.70	-0.34	7.58	0.60	2.46	-4.76	-0.03	0.13	0.01	0.26
Topo DEM v1	18685	0.80	0.67	-1.06	9.95	0.82	0.74	-0.49	6.91	0.60	-9.25	1.10	-0.03	0.13	0.01	0.26
$SRTM_{MDT}$	18865	0.83	0.67	-1.06	99.95	0.98	0.83	-6.75	72.99	2.55	-52.76	54.18	0.15	1.85	0.04	2.52
$SRTM_{EGM96}$	18997	0.83	0.67	-1.06	99.95	2.21	2.04	-6.72	74.46	2.60	-51.63	55.24	1.38	2.17	1.28	2.89
$ACE2_{MDT}$	16809	0.80	0.66	-1.06	99.95	0.97	0.86	-5.98	80.84	1.87	-26.38	24.26	0.17	1.24	0.11	1.65
$ACE2_{EGM96}$	16853	0.80	0.66	-1.06	99.95	2.23	2.12	-5.11	82.31	1.94	-25.23	25.19	1.44	1.75	1.38	2.21
$MERITDEM_{MDT}$	18365	0.80	0.66	-1.06	99.95	2.02	1.94	-3.32	79.04	1.26	-24.13	26.85	1.22	1.35	1.24	1.60
$MERITDEM_{EGM96}$	18367	0.80	0.66	-1.06	99.95	3.29	3.25	-5.15	80.51	1.35	28.09	-22.98	2.49	2.52	2.52	2.72
$ASTGTM\ v003_{MDT}$	19028	0.83	0.67	-0.45	99.95	8.60	7.46	-1.23	80.07	5.08	-53.20	80.22	7.78	7.80	6.63	9.36
$ASTGTM\ v003_{EGM96}$	19028	0.83	0.67	-0.45	99.95	9.87	8.76	0.00	80.89	5.08	-52.07	81.04	9.04	9.05	7.91	10.42
$AW3D30_{MDT}$	15977	0.84	0.68	-1.06	61.95	1.27	1.02	-6.27	43.07	2.43	-51.17	41.13	0.43	1.73	0.25	2.48
$AW3D30_{EGM96}$	16055	0.84	0.68	-1.06	61.95	2.50	2.22	-6.97	44.14	2.50	-50.04	42.19	1.66	2.19	1.50	2.99
$TanDEM\text{-}X_{MDT}$	18162	0.81	0.66	-1.06	99.95	1.69	1.17	-5.40	81.73	1.82	26.80	-59.40	0.89	1.06	0.41	1.92
$TanDEM\text{-}X_{EGM96}$	18167	0.81	0.66	-1.06	99.95	2.94	2.47	-3.79	83.20	1.84	-58.28	28.05	2.14	2.17	1.68	2.72
$Copernicus\ DEM_{MDT}$	16479	0.88	0.75	-0.45	99.95	1.68	1.07	-4.15	62.50	1.98	-48.42	60.56	0.80	1.09	0.22	2.07
$Copernicus\ DEM_{EGM2008}$	16479	0.88	0.75	-0.45	99.95	2.87	2.26	-2.92	63.55	1.98	-47.32	61.61	1.98	2.01	1.40	2.74
$FABDEM_{MDT}$	14605	0.87	0.75	-0.45	99.95	1.28	1.03	-1.51	80.92	1.30	-19.02	28.25	0.41	0.62	0.23	1.10
$FABDEM_{EGM2008}$	16341	0.88	0.75	-0.45	99.95	2.45	2.18	-0.92	67.74	1.37	-52.92	43.62	1.57	1.60	1.37	2.00
$CoastalDEM\ v2.1_{MDT}$	18961	0.83	0.67	-1.06	99.95	0.75	0.78	-2.46	69.86	1.26	-60.23	36.45	-0.08	0.82	-0.02	1.25
$CoastalDEM\ v2.1_{EGM96}$	18940	0.83	0.67	-1.06	99.95	2.02	2.00	-1.15	53.92	1.29	-58.87	51.47	1.20	1.37	1.20	1.78
$GLL\text{-}DTM\ v2_{MDT}$ (this study)	17346	0.76	0.66	-0.45	9.95	0.81	0.75	-0.51	7.02	0.55	-8.47	4.12	0.05	0.33	0.09	0.46
$GLL\text{-}DTM\ v2_{MDT}$ (original)	17354	0.76	0.66	-0.45	7.98	0.95	0.89	-0.75	7.19	0.68	-7.51	4.19	0.19	0.42	0.26	0.55
$DeltaDTM\ v1_{MDT}$	14055	0.86	0.75	-0.45	7.98	0.75	0.68	-1.88	6.77	0.61	-7.35	4.71	-0.11	0.36	-0.11	0.52
$DeltaDTM\ v1_{EGM2008}$	16479	0.86	0.75	-0.45	9.95	1.94	1.84	-0.98	9.77	0.70	-7.09	7.20	1.07	1.11	1.11	1.21
$DeltaDTM\ v1.1_{MDT}$	16462	0.87	0.75	-0.45	25.95	0.63	0.53	-3.55	28.95	0.77	-25.09	27.01	-0.24	0.40	-0.19	0.67

DeltaDTM v1.1$_{EGM2008}$	16462	0.87	0.75	-0.45	25.95	1.81	1.70	-2.32	30.00	0.79	-23.98	28.06	0.94	0.99	1.00	1.13

Table E2 *| Performance of local and global DEMs in the Vietnamese Mekong Delta validated by local point elevations ≤10 m for versions referenced to mean dynamic topography (MDT) and their original vertical reference. N – number of spot heights in the study area, with no-data values excluded for each DEM, respectively; Mean spot – mean point elevation in the study area; Median spot – median point elevation in the study area; Min. spot – minimum point elevation in the study area; Max. spot – maximum point elevation in the study area; Mean DEM – mean DEM elevation in the study area; Median DEM – median DEM elevation in the study area; Min. DEM – minimum DEM elevation in the study area; Max. DEM – maximum DEM elevation in the study area; σ DEM – standard deviation of DEM elevation in the study area; HR – height residual; MAE – mean absolute error; RMSE – root mean square error.*

DEM	*N*	Mean spot (m)	Median spot (m)	Min. spot (m)	Max. spot (m)	Mean DEM (m)	Median DEM (m)	Min. DEM (m)	Max. DEM (m)	*σ* DEM (m)	Max. negative HR (m)	Max. positive HR (m)	Mean error (m)	MAE (m)	Median error (m)	RMSE (m)
Topo DEM v2	18447	0.79	0.66	-1.06	9.95	0.77	0.70	-0.34	7.58	0.60	-4.76	2.46	-0.03	0.13	0.01	0.26
Topo DEM v1	18685	0.80	0.67	-1.06	9.95	0.82	0.74	-0.49	6.91	0.60	-9.25	1.10	-0.03	0.13	0.01	0.26
$SRTM_{MDT}$	18858	0.82	0.67	-1.06	9.95	0.98	0.82	-6.75	56.12	2.49	-9.83	54.18	0.16	1.84	0.04	2.48
$SRTM_{EGM96}$	18990	0.82	0.67	-1.06	9.95	2.20	2.04	-6.72	57.19	2.55	-8.33	55.24	1.39	2.16	1.28	2.83
$ACE2_{MDT}$	16806	0.79	0.66	-1.06	9.95	0.96	0.86	-5.98	25.10	1.76	-6.98	24.26	0.17	1.24	0.11	1.63
$ACE2_{EGM96}$	16850	0.79	0.66	-1.06	9.95	2.23	2.12	-5.11	26.04	1.83	-5.42	25.19	1.44	1.75	1.38	2.20
$MERITDEM_{MDT}$	18362	0.79	0.66	-1.06	9.95	2.02	1.94	-3.32	30.80	1.10	-5.37	26.85	1.22	1.34	1.25	1.58
$MERITDEM_{EGM96}$	18364	0.79	0.66	-1.06	9.95	3.28	3.25	-5.15	32.04	1.20	-6.12	28.09	2.49	2.52	2.52	2.70
$ASTGTM\ v003_{MDT}$	19023	0.82	0.67	-0.45	9.95	8.60	7.46	-1.23	80.07	5.06	-4.44	80.22	7.79	7.79	6.63	9.35
$ASTGTM\ v003_{EGM96}$	19023	0.82	0.67	-0.45	9.95	9.86	8.76	0.00	80.89	5.06	-3.25	81.04	9.05	9.05	7.91	10.41
$AW3D30_{MDT}$	15971	0.83	0.68	-1.06	9.95	1.26	1.02	-6.27	43.07	2.42	-7.74	41.13	0.44	1.72	0.25	2.41
$AW3D30_{EGM96}$	16049	0.83	0.68	-1.06	9.95	2.50	2.22	-6.97	44.14	2.49	-7.65	42.19	1.67	2.19	1.50	2.95
$TanDEM\text{-}X_{MDT}$	18155	0.79	0.66	-1.06	9.95	1.69	1.17	-5.40	29.25	1.72	-6.35	26.80	0.90	1.05	0.41	1.81
$TanDEM\text{-}X_{EGM96}$	18160	0.79	0.66	-1.06	9.95	2.94	2.47	-3.79	30.49	1.73	-4.74	28.05	2.15	2.16	1.68	2.65
$Copernicus\ DEM_{MDT}$	16474	0.87	0.75	-0.45	9.95	1.67	1.07	-4.15	62.50	1.93	-5.17	60.56	0.81	1.08	0.22	2.00
$Copernicus\ DEM_{EGM2008}$	16474	0.87	0.75	-0.45	9.95	2.86	2.26	-2.92	63.55	1.93	-3.92	61.61	1.99	2.01	1.40	2.69
$FABDEM_{MDT}$	14603	0.86	0.75	-0.45	9.95	1.27	1.03	-1.51	32.19	1.10	-5.92	28.25	0.41	0.61	0.23	1.08
$FABDEM_{EGM2008}$	16336	0.86	0.75	-0.45	9.95	2.44	2.18	-0.92	45.56	1.26	-4.00	43.62	1.58	1.59	1.37	1.93
$CoastalDEM\ v2.1_{MDT}$	18954	0.81	0.67	-1.06	9.95	0.75	0.78	-2.46	38.90	1.15	-5.89	36.45	-0.07	0.82	-0.02	1.08
$CoastalDEM\ v2.1_{EGM96}$	18933	0.81	0.67	-1.06	9.95	2.02	2.00	-1.15	53.92	1.23	-6.66	51.47	1.21	1.36	1.28	1.64
$GLL\text{-}DTM\ v2_{MDT}$ (this study)	17346	0.76	0.66	-0.45	9.95	0.81	0.75	-0.51	7.02	0.55	-8.47	4.12	0.05	0.33	0.09	0.46
$GLL\text{-}DTM\ v2_{MDT}$ (original)	17354	0.76	0.66	-0.45	7.98	0.95	0.89	-0.75	7.19	0.68	-7.51	4.19	0.19	0.42	0.26	0.55
$DeltaDTM\ v1_{MDT}$	14055	0.86	0.75	-0.45	7.98	0.75	0.68	-1.88	6.77	0.61	-7.35	4.71	-0.11	0.36	-0.07	0.52
$DeltaDTM\ v1_{EGM2008}$	16479	0.86	0.75	-0.45	9.95	1.93	1.84	-0.98	9.77	0.70	-7.09	7.20	1.07	1.11	1.11	1.21
$DeltaDTM\ v1.1_{MDT}$	16459	0.86	0.75	-0.45	9.95	0.63	0.53	-3.55	28.95	0.76	-8.60	27.01	-0.24	0.40	-0.19	0.64
$DeltaDTM\ v1.1_{EGM2008}$	16459	0.86	0.75	-0.45	9.95	1.81	1.70	-2.32	30.00	0.77	-7.50	28.06	0.94	0.99	1.00	1.11

E2. Converting vertical datum to actual continuous local sea level

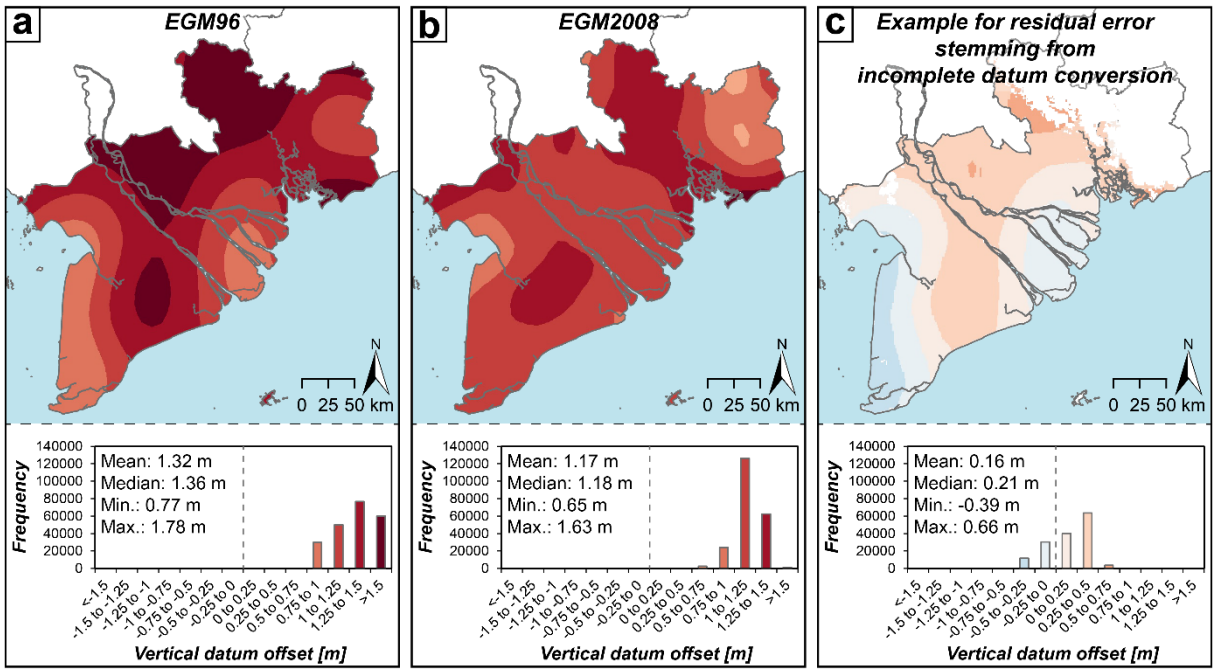


***Figure E1** | Offsets between commonly used geoid models and local mean sea level as indicated by mean dynamic topography of Jousset et al. (2023) in the Vietnamese Mekong Delta and its adjacent provinces.*

***Table E3** | Offsets between commonly used geoid models and local mean sea level as indicated by mean dynamic topography of Jousset et al. (2023) in the Vietnamese Mekong Delta and its adjacent provinces.*

Vertical datum	*N*	Mean offset (m)	Median offset (m)	MAE (m)	RMSE (m)	Min. offset (m)	Max. offset (m)	σ (m)
EGM96	216050	1.32	1.36	1.32	1.34	0.77	1.78	0.25
EGM2008	216050	1.17	1.18	1.17	1.18	0.65	1.63	0.16
Example of incomplete datum conversion	149890	0.16	0.21	0.26	0.30	-0.39	0.66	0.25

E3. Performance of digital elevation models in the Vietnamese Mekong Delta and its adjacent provinces

E3.1 Which one is the best? – On the local validation of global satellite-based digital elevation models

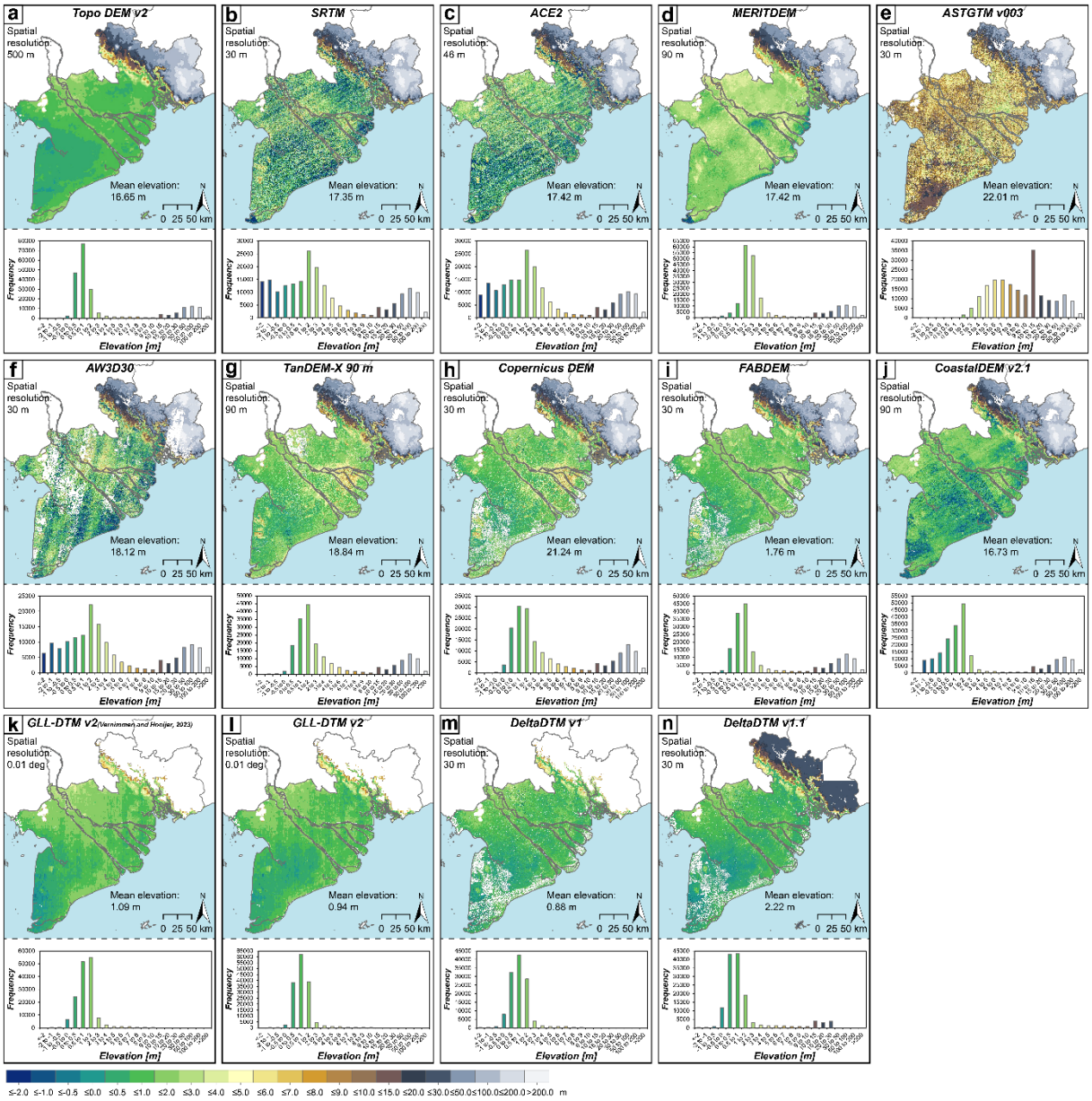


***Figure E2** | Digital elevation models for the Vietnamese Mekong Delta and its adjacent provinces, all referenced to actual, local continuous mean sea level as indicated by mean dynamic topography (Jousset et al., 2023).*

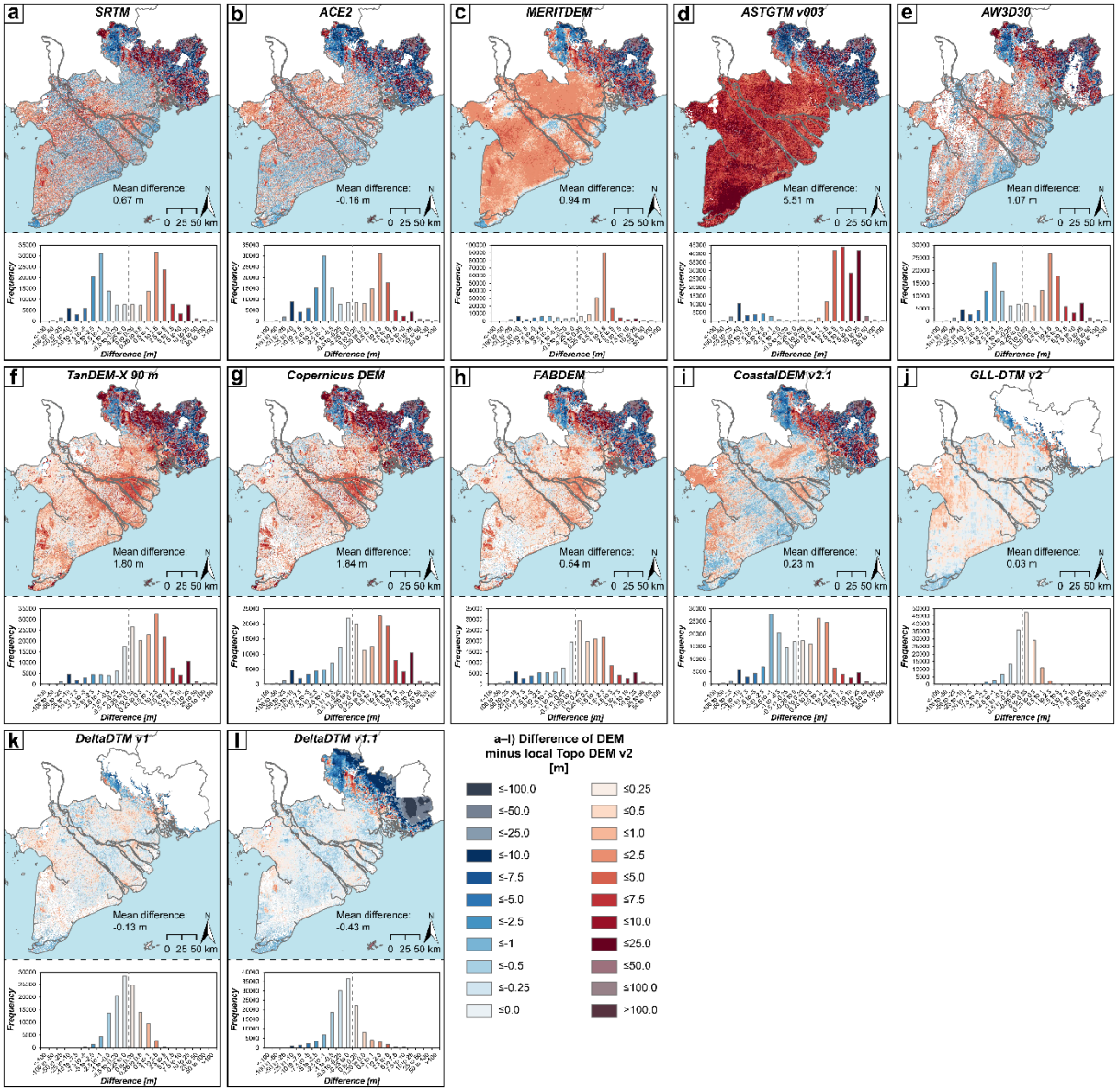


Figure E3 *| Height residuals of DEMs referenced to mean sea level compared to Topo DEM v2 for the Vietnamese Mekong Delta and its adjacent provinces.*

Table E4 *| Performance of local and global DEMs in the Vietnamese Mekong Delta and its adjacent provinces validated by the local Topo DEM v2 and DEM-specific vertical datum offsets quantified as differences in RMSE and discrepancies from RMSE of DEMs referenced to mean dynamic topography (MDT).*
N – number of grid cells in the study area, with no-data values excluded for each DEM, respectively; Mean DEM – mean DEM elevation in the study area; Median DEM – median DEM elevation in the study area; Min. DEM – minimum DEM elevation in the study area; Max. DEM – maximum DEM elevation in the study area; σ DEM – standard deviation of DEM elevation in the study area; HR – height residual; MAE – mean absolute error; RMSE – root mean square error.

DEM	*N*	Mean DEM (m)	Median DEM (m)	Min. DEM (m)	Max. DEM (m)	*σ* DEM (m)	Max. negative HR (m)	Max. positive HR (m)	Mean error (m)	MAE (m)	Median error (m)	RMSE (m)	Difference in RMSE (m)	Discrepancy (%)
Topo DEM v2	219365	16.65	0.91	-0.65	268.65	38.64								
$SRTM_{MDT}$	203572	17.35	1.86	-6.95	922.24	42.75	-192.81	665.65	0.67	4.34	0.14	12.16	0.11	0.9
$SRTM_{EGM96}$	205265	18.51	3.00	-7.00	924.00	42.63	-190.72	667.41	1.97	4.63	1.39	12.27		
$ACE2_{MDT}$	192353	17.42	1.77	-6.96	869.17	42.86	-166.59	620.86	-0.16	4.22	-0.06	12.28	0.04	0.4

$ACE2_{EGM96}$	192702	18.71	3.10	-7.00	870.88	42.84	-164.94	622.57	1.16	4.47	1.21	12.32			
$MERITDEM_{MDT}$	205967	17.42	2.35	-5.13	936.53	40.99	-183.97	679.93	0.94	3.57	1.20	11.42			
$MERITDEM_{EGM96}$	205968	18.74	3.70	-3.87	938.24	41.01	-182.30	681.64	2.26	4.46	2.48	11.60	0.19	1.6	
$ASTGTM\ v003_{MDT}$	205492	22.01	8.74	-1.46	916.55	39.57	-202.94	659.95	5.51	9.05	5.80	14.60			
$ASTGTM\ v003_{EGM96}$	205492	23.33	10.00	0.00	918.00	39.58	-201.72	661.41	6.82	9.96	7.09	15.12	0.53	3.5	
$AW3D30_{MDT}$	159639	18.12	2.00	-6.97	715.51	42.40	-158.80	467.18	1.07	4.33	0.29	11.11			
$AW3D30_{EGM96}$	160522	19.34	3.00	-7.00	717.00	42.33	-157.11	468.67	2.38	4.73	1.58	11.30	0.20	1.7	
$TanDEM\text{-}X_{MDT}$	197363	18.84	1.92	-6.12	1112.77	43.04	-189.93	1039.27	1.80	3.93	0.56	12.52			
$TanDEM\text{-}X_{EGM96}$	197403	20.15	3.24	-6.53	1113.96	43.06	-188.27	1040.46	3.12	4.88	1.84	12.78	0.27	2.1	
$Copernicus\ DEM_{MDT}$	171963	21.40	2.10	-5.05	909.07	45.62	-186.97	652.48	1.84	4.38	0.33	13.20			
$Copernicus\ DEM_{EGM2008}$	171963	22.41	3.32	-3.85	910.38	45.54	-185.36	653.79	3.01	5.15	1.53	13.41	0.21	1.6	
$FABDEM_{MDT}$	172376	19.95	1.51	-2.28	868.39	44.04	-186.92	611.79	0.54	3.54	0.24	12.09			
$FABDEM_{EGM2008}$	171087	21.21	2.71	-1.72	922.47	44.21	-202.82	665.87	1.72	4.46	1.39	12.68	0.59	4.7	
$CoastalDEM\ v2.1_{MDT}$	205653	16.73	1.19	-4.76	937.95	42.32	-208.22	681.36	0.23	3.31	0.01	11.85			
$CoastalDEM\ v2.1_{EGM96}$	205655	18.05	2.45	-6.33	939.66	42.34	-206.56	683.07	1.55	3.77	1.31	11.96	0.10	0.9	
$GLL\text{-}DTM\ v2_{MDT}$ (this study)	150580	0.94	0.79	-1.62	9.61	0.88	-9.29	6.29	0.03	0.34	0.08	0.63			
$GLL\text{-}DTM\ v2_{MDT}$ (original)	150982	1.09	0.94	-1.55	9.90	0.99	-8.80	6.36	0.18	0.44	0.25	0.68	0.04	6.1	
$DeltaDTM\ v1_{MDT}$	120367	0.88	0.78	-3.11	8.91	0.97	-9.44	7.43	-0.13	0.45	-0.08	0.79			
$DeltaDTM\ v1_{EGM2008}$	125276	2.06	1.88	-1.55	9.99	0.99	-8.10	9.03	1.06	1.17	1.11	1.30	0.52	39.7	
$DeltaDTM\ v1.1_{MDT}$	139211	2.22	0.62	-5.11	29.15	5.00	-24.95	28.45	-0.43	0.79	-0.21	1.88			
$DeltaDTM\ v1.1_{EGM2008}$	139211	3.42	1.79	-4.44	30.00	5.03	-23.87	29.30	0.78	1.33	0.99	1.99	0.10	5.2	

E3.2 Which one is the best? – On the local validation of global digital elevation models: Comparison with local point elevations

Table E5 | *Performance of local and global DEMs in the Vietnamese Mekong Delta and its adjacent provinces validated by local point elevations for versions referenced to mean dynamic topography (MDT) and their original vertical reference.*
N – number of spot heights in the study area, with no-data values excluded for each DEM, respectively; Mean spot – mean point elevation in the study area; Median spot – median point elevation in the study area; Min. spot – minimum point elevation in the study area; Max. spot – maximum point elevation in the study area; Mean DEM – mean DEM elevation in the study area; Median DEM – median DEM elevation in the study area; Min. DEM – minimum DEM elevation in the study area; Max. DEM – maximum DEM elevation in the study area; σ DEM – standard deviation of DEM elevation in the study area; HR – height residual; MAE – mean absolute error; RMSE – root mean square error.

DEM	***N***	**Mean spot (m)**	**Median spot (m)**	**Min. spot (m)**	**Max. spot (m)**	**Mean DEM (m)**	**Median DEM (m)**	**Min. DEM (m)**	**Max. DEM (m)**	**σ DEM (m)**	**Max. negative HR (m)**	**Max. positive HR (m)**	**Mean error (m)**	**MAE (m)**	**Median error (m)**	**RMSE (m)**
Topo DEM v2	27032	14.51	0.95	-1.06	250.00	14.34	0.92	-0.32	254.65	34.73	-124.55	84.10	-0.17	1.35	0.01	5.08
$SRTM_{MDT}$	27242	14.44	0.95	-1.06	250.00	14.86	1.75	-6.75	771.08	38.51	-211.19	521.10	0.42	3.66	0.07	11.63
$SRTM_{EGM96}$	27385	14.37	0.95	-1.06	250.00	16.08	3.00	-6.72	772.78	38.45	-209.52	522.81	1.71	3.93	1.34	11.73
$ACE2_{MDT}$	26129	15.00	0.95	-1.06	250.00	14.72	1.57	-6.85	775.88	38.87	-172.74	525.90	-0.28	3.27	-0.25	11.49
$ACE2_{EGM96}$	26165	14.98	0.95	-1.06	250.00	16.03	2.89	-6.70	777.59	38.86	-171.08	527.61	1.05	3.44	1.03	11.53
$MERITDEM_{MDT}$	27283	14.35	0.95	-1.06	250.00	15.14	2.31	-5.50	786.97	37.28	-210.40	537.00	0.79	2.95	1.14	11.45
$MERITDEM_{EGM96}$	27284	14.35	0.95	-1.06	250.00	16.47	3.68	-4.17	788.68	37.29	-208.73	538.70	2.12	3.86	2.42	11.61
$ASTGTM\ v003_{MDT}$	27393	14.34	0.95	-0.45	250.00	19.81	8.62	-1.23	789.84	35.95	-226.02	539.87	5.47	8.40	5.69	14.34
$ASTGTM\ v003_{EGM96}$	27393	14.34	0.95	-0.45	250.00	21.14	9.95	0.00	791.55	35.95	-224.35	541.57	6.80	9.33	7.00	14.87
$AW3D30_{MDT}$	23189	13.56	0.95	-1.06	250.00	14.23	1.89	-6.27	721.66	35.27	-115.68	471.68	0.67	3.43	0.30	9.27
$AW3D30_{EGM96}$	23272	13.52	0.95	-1.06	250.00	15.50	3.15	-6.97	723.36	35.25	-113.91	473.39	1.98	3.84	1.59	9.45
$TanDEM\text{-}X_{MDT}$	26439	14.74	0.95	-1.06	250.00	16.41	1.82	-5.40	779.34	39.11	-209.26	529.36	1.66	3.25	0.51	11.94

TanDEM-X_{EGM96}	26444	14.74	0.95	-1.06	250.00	17.73	3.16	-3.79	781.05	39.13	-207.60	531.07	2.98	4.23	1.81	12.20
Copernicus DEM_{MDT}	24642	15.81	0.95	-0.45	250.00	17.38	1.87	-4.15	770.62	40.13	-216.94	520.65	1.57	3.47	0.32	12.37
Copernicus $DEM_{EGM2008}$	24642	15.81	0.95	-0.45	250.00	18.56	3.08	-2.92	771.93	40.06	-215.33	521.95	2.75	4.25	1.52	12.58
$FABDEM_{MDT}$	22263	16.91	0.96	-0.45	250.00	17.17	1.48	-0.97	743.02	39.55	-205.50	493.04	0.26	2.87	0.23	11.74
$FABDEM_{EGM2008}$	24489	15.91	0.95	-0.45	250.00	17.49	2.65	-0.92	781.64	39.01	-220.48	531.67	1.58	3.61	1.37	12.22
CoastalDEM $v2.1_{MDT}$	27262	14.36	0.95	-1.06	250.00	14.29	1.21	-4.08	782.29	38.07	-226.40	532.32	-0.07	2.78	-0.00	11.77
CoastalDEM $v2.1_{EGM96}$	27262	14.36	0.95	-1.06	250.00	15.62	2.48	-2.39	784.00	38.08	-224.74	534.02	1.26	3.22	1.31	11.84
GLL-DTM $v2_{MDT}$ (this study)	19250	1.00	0.68	-0.45	9.99	0.97	0.79	-1.78	9.61	0.96	-9.39	6.10	-0.02	0.45	0.08	0.83
GLL-DTM $v2_{MDT}$ (original)	19311	0.99	0.68	-0.45	9.99	1.14	0.95	-1.40	9.88	1.07	-8.90	6.55	0.14	0.53	0.25	0.84
DeltaDTM $v1_{MDT}$	15681	1.12	0.78	-0.45	9.99	0.93	0.72	-1.43	8.44	1.02	-8.94	4.99	-0.18	0.48	-0.07	0.86
DeltaDTM $v1_{EGM2008}$	18704	1.13	0.78	-0.45	9.99	2.15	1.90	.0.98	9.87	1.16	-7.58	7.65	1.02	1.18	1.10	1.35
DeltaDTM $v1.1_{MDT}$	20674	2.79	0.87	-0.45	29.99	2.31	0.64	-3.55	29.09	5.06	-27.47	26.45	-0.48	0.83	-0.22	1.84
DeltaDTM $v1.1_{EGM2008}$	20674	2.79	0.87	-0.45	29.99	3.51	1.82	-2.32	30.00	5.09	-26.39	28.02	0.73	1.30	0.98	1.91

E3. Performance of digital elevation models in the Vietnamese Mekong Delta and its adjacent provinces

Table E6 | *Simulated, non-linear, extraction-induced land subsidence (Minderhoud et al., 2017; B1 scenario of Minderhoud et al., 2020), and annual rates of local, delta-average sea-level rise estimated from PSMSL data of Vung Tau tide-gauge observations (1979–2010) and IPCC AR6 total rates of sea-level change (PSMSL, 2025; Fox-Kemper et al., 2021; Garner et al., 2021; Garner et al., 2022) used to obtain tentative estimates of non-linear impact of elevation change due to vertical land motion (e.g. extraction-induced land subsidence) and sea-level change affecting DEM actuality.*

Year	Extraction-induced land subsidence (cm/yr)	Sea-level change (cm/yr)
2000	0.56	0.36
2001	0.58	0.36
2002	0.62	0.36
2003	0.68	0.36
2004	0.70	0.36
2005	0.73	0.36
2006	0.74	0.36
2007	0.76	0.36
Total (2000–2007)	*5.36*	*2.88*
2008	0.78	0.36
2009	0.79	0.36
2010	0.84	0.36
2011	0.84	0.45
2012	0.85	0.45
2013	0.86	0.45
2014	0.86	0.45
2015	0.87	0.45
2016	0.88	0.45
2017	0.88	0.45
2018	0.89	0.45
2019	0.89	0.45
2020	0.89	0.45
2021	0.89	0.49
2022	0.89	0.49

2023	0.89	0.49
2024	0.89	0.49
2025	0.89	0.49
Total (2008–2025)	*15.59*	*8.03*

References

Fox-Kemper, B., Hewitt, H. T., Xiao, C., Aðalgeirsdóttir, G., Drijfhout, S. S., Edwards, T. L., Golledge, N. R., Hemer, M., Kopp, R. E., Krinner, G., Mix, A., Notz, D., Nowicki, S., Nurhati, I. S., Ruiz, L., Sallée, J.-B., Slangen, A. B. A., and Yu, Y.: Ocean, Cryosphere and Sea Level Change, in: *Climate Change 2021: The Physical Science Basis. Contribution of Working Group I to the Sixth Assessment Report of the Intergovernmental Panel on Climate Change*, edited by Masson-Delmotte, V., Zhai, P., Pirani, A., Connors, S. L., Péan, C., Berger, S., Caud, N., Chen, Y., Goldfarb, L., Gomis, M. I., Huang, M., Leitzell, K., Lonnoy, E., Matthews, J. B. R., Maycock, T. K., Waterfield, T., Yelekçi, O., Yu, R., and Zhou, B., Cambridge University Press, Cambridge, 9-1–9-257, In press.

Garner, G. G., Hermans, T., Kopp, R. E., Slangen, A. B. A., Edwards, T. L., Levermann, A., Nowikci, S., Palmer, M. D., Smith, C., Fox-Kemper, B., Hewitt, H. T., Xiao, C., Aðalgeirsdóttir, G., Drijfhout, S. S., Edwards, T. L., Golledge, N. R., Hemer, M., Kopp, R. E., Krinner, G., Mix, A., Notz, D., Nowicki, S., Nurhati, I. S., Ruiz, L., Sallée, J.-B., Yu, Y., Hua, L., Palmer, T., and Pearson, B.: IPCC AR6 Sea-Level Rise Projections, Version 20210809, PO.DAAC, CA, USA, Dataset accessed [2022-05-23] at https://podaac.jpl.nasa.gov/announcements/2021-08-09-Sea-level-projections-from-the-IPCC-6th-Assessment-Report, 2021.

Garner, G. G., Kopp, R. E., Hermans, T., Slangen, A. B. A., Koubbe, G., Turilli, M., Jha, S., Edwards, T. L., Levermann, A., Nowikci, S., Palmer, M. D., and Smith, C.: Framework for Assessing Changes To Sea-level (FACTS), Geoscientific Model Development, *Zenodo* [model], https://zenodo.org/record/6419954, last access: 22 November 2022, 2022.

Jousset, S., Mulet, S., Greiner, E., Wilkin, J., Vidar, L., Dibarboure, G., and Picot, N.: New Global Mean Dynamic Topography CNES-CLS-22 Combining Drifters, Hydrological Profiles and High Frequency Radar Data, ESS Open Archive, https://doi.org/10.22541/essoar.170158328.85804859/v2, 2023.

Minderhoud, P. S. J., Erkens, G., Pham, V. H., Bui, V. T., Erban, L., Kooi, H., and Stouthamer, E.: Impacts of 25 years of groundwater extraction on subsidence in the Mekong delta, Vietnam, *Environ. Res. Lett.*, *12*:6, 064006, https://doi.org/10.1088/1748-9326/aa7146, 2017.

Minderhoud, P. S. J., Hlavacova, I., Kolomaznik, J., and Neussner, O.: Towards unraveling total subsidence of a mega-delta – the potential of new PS InSAR data for the Mekong delta, Proc. IAHS, 382, 327–332, https://doi.org/10.5194/piahs-382-327-2020, 2020.

Permanent Service for Mean Sea Level (PSMSL), 2025. Permanent Service for Mean Sea Level – Tide Gauge Data: Vung Tau, https://psmsl.org/data/obtaining/stations/1495.php, last access: 4 July 2025.

Appendix F – Supplement to Chapter 5

This Supplement is related to: **Seeger, K.**, Shirzaei, M., Werth, S., Minderhoud, P.S.J., Vogel, A., Brückner, H., Kraas, F., Brill, D., in preparation. *Understanding land elevation dynamics for strengthening coastal hazard and impact assessments in the Ayeyarwady Delta (Myanmar)*.

The reader is requested to cite the content of this supplementary material as indicated above, together with a reference to this PhD thesis, following standards of the CC-BY 4.0 Attribution 4.0 International licence (http://creativecommons.org/licenses/by/4.0/).

F1. Supplementary figures

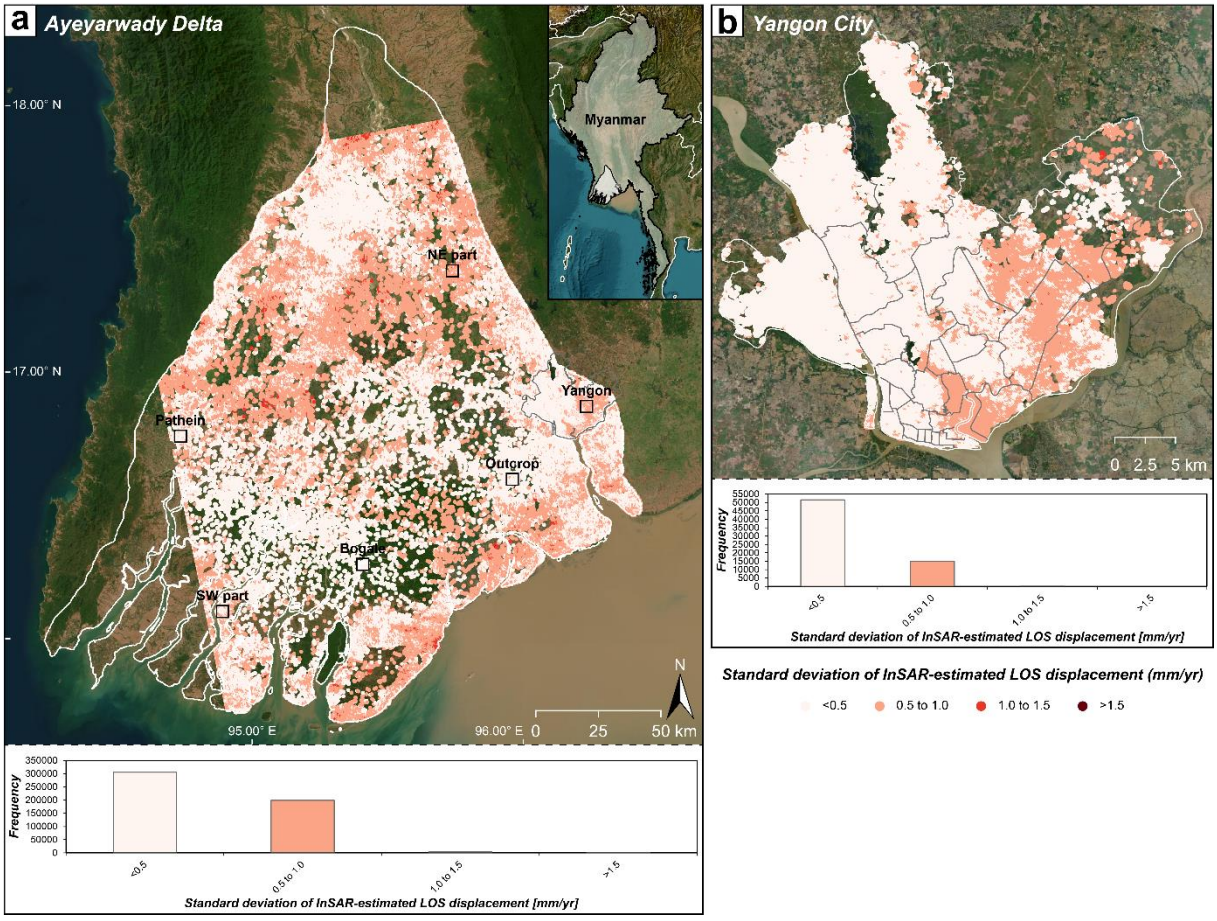


Figure F1 *| Standard deviations for InSAR-derived displacement velocities along line-of-sight (LOS) for the Ayeyarwady Delta (a) and Yangon City (b).*

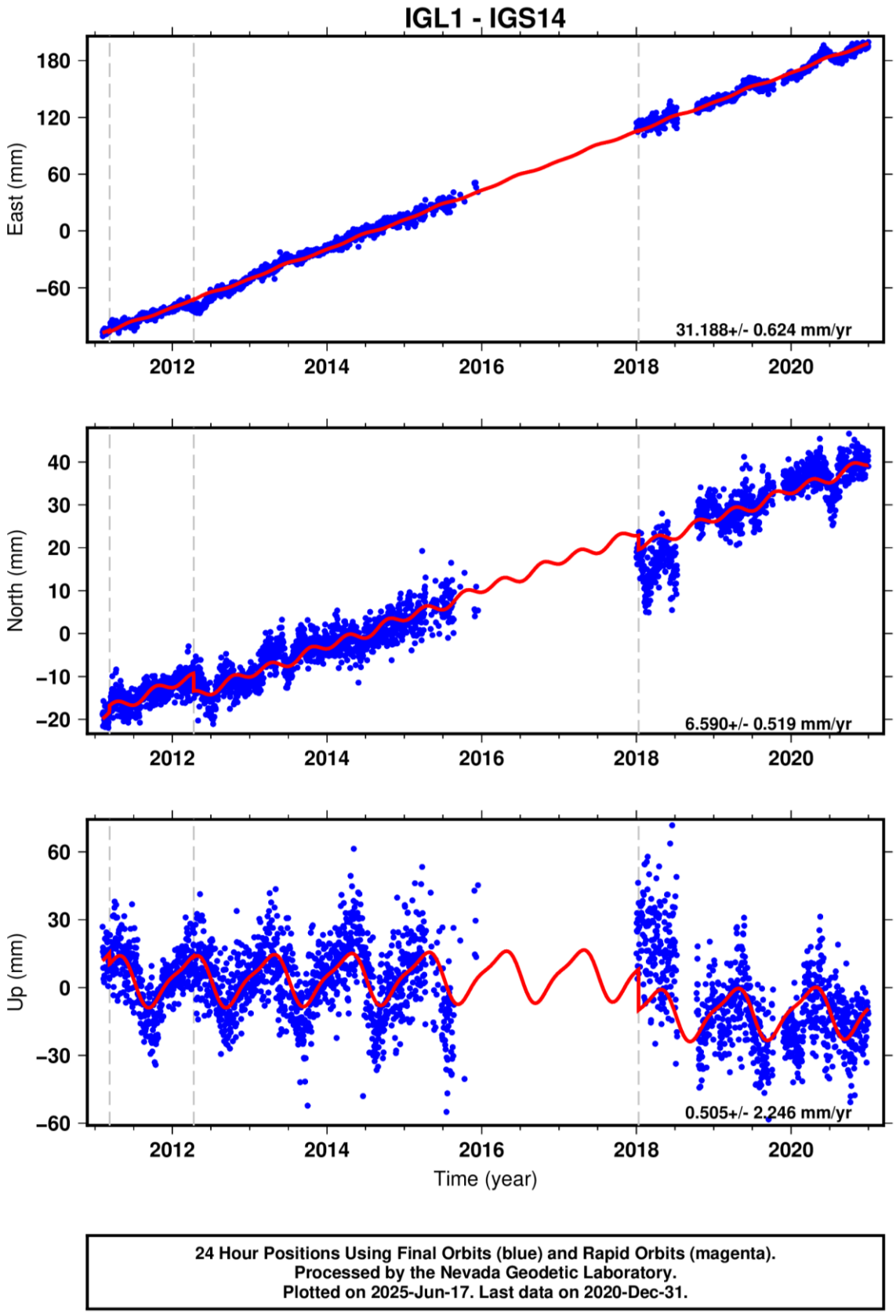


Figure F2 | *Data record of GPS station IGL1 (network operator's station ID: IGLE) situated outside the Ayeyarwady Delta but providing the highest data density and showing – apart from seasonal variations – a comparably stable vertical movement component, especially over the investigation period from March 2017 to October 2023 (Blewitt et al., 2018; Nevada Geodetic Laboratory, without date). Note that last data of IGL1 was obtained on 31st December 2020.*

References

Blewitt, G., Hammond, W.C., Kreemer, C., 2018. Harnessing the GPS data explosion for interdisciplinary science. Eos, 99. https://doi.org/10.1029/2018EO104623.

Nevada Geodetic Laboratory, without date. Station IGL1. https://geodesy.unr.edu/NGLStationPages/stations/IGL1.sta (last access: 5 July 2025)

Own contribution

Chapter 2 is related to: Becker, M., **Seeger, K.**, Paszkowski, A., Marcos, M., Papa, F., Almar, R., Bates, P., France-Lanord, C., Hossain, Md S., Khan, Md J.U., Karegar, M.A., Karpytchev, M., Long, N., Minderhoud, P.S.J., Neal, J., Nicholls, R.J., Syvitski, J., 2024. *Coastal Flooding in Asian Megadeltas: Recent Advances, Persistent Challenges, and Call for Actions Amidst Local and Global Changes*. Reviews of Geophysics, 62 (4), e2024RG000846. https://doi.org/10.1029/2024RG000846.

Author contributions (only detailing own contributions): The study was conceptualised by all authors; KS drafted Section 2 (large parts of the draft were moved to Section 3 in the course of review & editing), Section 3.1.5 (Land elevation and elevation dynamics), Section 4.2.1, and contributed to drafting of Section 3.2; KS visualised Figures 1, 2, 6 and co-created Figures 8 and 9; all authors reviewed and edited the manuscript

Chapter 3 is related to: **Seeger, K.**, Peffeköver, A., Minderhoud, P.S.J., Vogel, A., Brückner, H., Kraas, F., Nay Win Oo, Brill, D., 2024. *Evaluating flood hazards in data-sparse coastal lowlands: highlighting the Ayeyarwady Delta (Myanmar)*. Environmental Research Letters, 19 (8), 084007. https://doi.org/10.1088/1748-9326/ad5b07.

Author contributions: Conceptualisation: KS; Methodology: KS; Investigation: KS, AP; Visualisation: KS; Funding acquisition: DB, HB, FK; Project administration: DB, HB, FK; Supervision: DB, HB, PSJM; Writing – original draft: KS; Writing – review & editing: KS, PSJM, DB, AV, AP, HB, FK, NWO

Chapter 4.1 is related to: **Seeger, K.**, Minderhoud, P.S.J., Peffeköver, A., Vogel, A., Brückner, H., Kraas, F., Nay Win Oo, Brill, D., 2023. *Assessing land elevation in the Ayeyarwady Delta (Myanmar) and its relevance for studying sea level rise and delta flooding*. Hydrology and Earth System Sciences, 27 (11), 2257–2281. https://doi.org/10.5194/hess-27-2257-2023.

Author contributions: KS, PSJM and DB conceptualised the study. KS acquired the elevation data and topographic maps. KS and AP conducted digitisation. KS performed processing, data analyses and visualisation. KS and PSJM discussed intermediate and final results. DB, HB and FK acquired funding and are responsible for supervision and project administration. KS

prepared the original draft of the manuscript. All co-authors reviewed and edited the manuscript.

Chapter 4.2 is related to: **Seeger, K.**, Minderhoud, P.S.J., in review. *Sea level much higher than assumed in most coastal hazard assessments*. Nature, 2025-02-05097A.

Author contributions: Conceptualisation: PSJM, KS; Methodology: KS, PSJM; Investigation: KS; Visualisation: KS, PSJM; Funding acquisition: PSJM; Project administration: PSJM, KS; Supervision: PSJM; Writing – original draft: KS, PSJM; Writing – review & editing: KS, PSJM

Chapter 4.3 is related to: **Seeger, K.**, Minderhoud, P.S.J., submitted. *Attributing uncertainties in elevation assessments for data-sparse coastal lowlands using global elevation models: A globally applicable approach showcasing the Vietnamese Mekong Delta*. Scientific Reports.

Author contributions: KS and PSJM jointly conceptualised this study. KS designed the methodology (DEM assessment), performed the analyses, created the figures and wrote the initial draft. PSJM acquired funding and supervised the investigation. Both authors managed project administration, assessed the results and wrote the final manuscript.

Chapter 5 is related to: **Seeger, K.**, Shirzaei, M., Werth, S., Minderhoud, P.S.J., Vogel, A., Brückner, H., Kraas, F., Brill, D., in preparation. *Understanding land elevation dynamics for strengthening coastal hazard and impact assessments in the Ayeyarwady Delta (Myanmar)*.

Author contributions (preliminary): Conceptualisation: KS, PSJM, DB; Methodology: MS, SW; Investigation: KS, MS, SW; Visualisation: KS; Funding acquisition: DB, HB, FK; Project administration: DB, HB, FK; Supervision: DB, HB, PSJM; Writing – original draft: KS; Writing – review & editing: KS, PSJM